

Title	Development of microelectrode arrays for real-time monitoring of alkaline phosphatase release from cells in clinical analysis
Authors	Balbaied, Thanih
Publication date	2020-12-18
Original Citation	Balbaied, T. A. 2020. Development of microelectrode arrays for real-time monitoring of alkaline phosphatase release from cells in clinical analysis. PhD Thesis, University College Cork.
Type of publication	Doctoral thesis
Rights	© 2020, Thanih A. Balbaied. - https://creativecommons.org/licenses/by-nc-nd/4.0/
Download date	2025-08-17 21:39:19
Item downloaded from	https://hdl.handle.net/10468/11452

Ollscoil na hÉireann, Corcaigh
National University of Ireland, Cork



UCC

Coláiste na hOllscoile Corcaigh, Éire
University College Cork, Ireland

Development of microelectrode arrays for real-time monitoring of Alkaline Phosphatase release from cells in clinical analysis

Thesis presented by
Thanih A. Balbaied
for the degree of
Doctor of Philosophy
2020

University College Cork
Tyndall National Institute Cork
School of Chemistry
Supervisor: Dr Eric Moore



Table of content

Table of content.....	i
List of figure	viii
List of tables	xii
Abstract.....	xiii
Declaration.....	xvi
Acknowledgements.....	xviii
Chapter 1	1
1.1 Motivation.....	2
1.1.1 Aims and objectives	2
1.1.2 Chapter 1.....	2
1.1.3 Chapter 2.....	2
1.1.4 Chapter 3.....	3
1.1.5 Chapter 4.....	3
1.1.7 Chapter 5.....	3
1.1.6 Chapter 6.....	3
1.1.8 Chapter 7.....	4
1.2 Alkaline phosphatase (ALP).....	4
1.3 ALP isoenzyme and tests.....	5
1.4 Traditional ALP methods.....	7
1.5 Chemical sensors for clinical analysis	8
1.5.1 Electrochemical cells.....	9
1.5.2. Nernst-Planck equation	11
1.5.3. Cyclic voltammetry.....	12
1.5.4. Linear Sweep Voltammetry (LSV)	13
1.6 ALP secretion system	14
1.7 Living cells	15
1.7.1 The cell	15
1.7.2 Cell parts	17
1.8 Cell culture system.....	22

Table of content

1.8.1 Important	22
1.8.3 Cell division	23
1.8.4 Culture types	24
1.8.5 Culture condition	24
1.8.6 Culture techniques	26
1.8.7 Cell lines:	28
1.9 Viability assay	31
1.9.1 Metabolic based assay	31
1.9.2 Impedance based assay	33
1.10 Microarrays technology	38
1.10.1 History	38
1.10.2 Microelectrode array	39
1.11 Summary	41
1.11.1 The research strategy:	41
1.11.2 The research method	42
1.11.3 The research techniques	43
1.11.5 Future contribution	43
1.12 Reference	43
Chapter 2	61
2.1 Aim and objectives	62
2.2 Introduction	62
2.1.1 Principle	62
2.1.2 Literature review	63
2.1.3 The Problem statement	64
2.1.4 Summary	64
2.3 Methodology	64
2.3.1 Reagents	64
2.3.2. Instrumentation	65
2.3.3 Cell Culture	65
2.3.4 Determining the optimal concentration of resazurin	66
2.3.5 Determining the optimal time of incubation with resazurin	67
2.3.6 Determining the calibration curve of resazurin and cell numbers	67

Table of content

2.3.7 Determining the optimal density of cell lines.....	67
2.3.8 Determining cell number based resazurin assay.....	67
2.3.9 Microscope images	68
2.3.10 Hemocytometer assay	68
2.3.11 Cell viability at post-confluence culture	69
2.3.12 Data analysis:	69
2.4 Results and Discussion	69
2.4.1 Determining the optimal concentration of resazurin	69
2.4.2 Determining the optimal time of incubation with Resazurin	70
2.4.3 Determining the standard curve of Resazurin and cell numbers	72
2.4.4 Determining the optimal density of cell lines.....	73
2.4.5 Microscope images	75
2.4.6 Determining cell number and comparing to hemocytometer assay.....	77
2.4.7 Cell viability at post-confluence culture	78
2.5 Conclusions	79
2.6 Reference	80
Chapter 3	83
3.1. Aim and objectives.....	84
3.2 Introduction	84
3.2.1 Principle	84
3.2.2 Background	85
3.2.3 Literature review.....	86
3.2.4 The problem statement	87
3.2.5 Summary	87
3.3 Methodology.....	88
3.3.1 Reagents.....	88
3.3.2 Instrumentation	88
3.3.3 ALP release and cell culture	88
3.3.6 Optimization of absorbance measurement.....	91
3.3.7 Linearity performance of ALP release vs cell number	92
3.3.8 Concentration of the substrate pNPP form adhesion cells.....	93
3.3.9 Real-time monitoring of ALP release from cells at post-confluence culture.....	93

Table of content

3.3.10 Statistics analysis.....	93
3.4 Results and Discussion	93
3.4.1 ALP release optimization	93
3.4.2 Optimization of absorbance measurement	97
3.4.3 Linearity performance of ALP release vs cell number	99
3.4.4 Concentration of the substrate pNPP from adhesion cells.....	100
3.4.5 Real-time monitoring of ALP release from cells at post-confluence culture.....	102
3.5 Conclusion	102
3.6 Reference	104
Chapter 4	111
4.1. Aim and Objectives	112
4.2. Introduction	112
4.2.1. Principle	112
4.2.2. Background	114
4.2.3. Literature review.....	114
4.2.4. The problem statement	117
4.2.5. Summary	118
4.3. Methodology.....	118
4.3.1. Chemicals and Instruments.....	118
4.3.2. ALP Release and Cell Culture	119
4.3.3. Stabilization of Graphite Screen-Printed Electrodes	120
4.3.4. Optimization of Electrochemical Measurement.....	120
4.3.5. Linearity Performance of ALP Release vs. Cell Number.....	120
4.3.6. Concentration of the Substrate pAPP from Adhesion Cells.....	121
4.3.7 Real-time monitoring of ALP release from cells at post-confluence culture.....	121
4.3.8 Statistics analysis.....	121
4.4. Results and Discussion	122
4.4.1. Stabilization of Graphite Screen-Printed Electrodes	122
4.4.2. Optimization of Electrochemical Measurement.....	123
4.4.3. Linearity Performance of ALP Release vs. Cell Number.....	125
4.4.4. Concentration of the Substrate pAPP from Adhesion Cells.....	126
4.4.5 Real-time monitoring of ALP release from cells at post-confluence culture.....	128

Table of content

4.5 Conclusions	128
4.6 References	129
Chapter 5	134
5.1 Aim and objectives	135
5.2 Introduction	135
5.2.1 Principle	135
5.2.2 Background	136
5.2.3 Literature review	137
5.2.4 The Problem statement	139
5.2.5 Summary	140
5.3 Methodology	140
5.3.1 Reagents and instruments	140
5.3.2 ALP release and cell culture	140
5.3.3 Capillary electrophoresis experiment (standard curve)	142
5.3.4 Absorbance experiment (standard curve)	142
5.3.5 Absorbance experiment (calibration curve)	143
5.3.6 Electrochemical experiment (calibration curve)	143
5.4 Results and discussion	143
5.4.1 Comparison between capillary electrophoresis and colorimetric analysis for ALP release from living cells	143
5.4.2 Comparison between absorbance and electrochemical analysis for ALP release from living cells	145
5.5 Conclusion	146
5.6 Reference	146
Chapter 6	151
6.1. Aims and objectives of the novelty of the thesis	152
1. To obtain the optimal frequency of each cell line mentioned above	152
2. To allow linearity performance using different cell number	152
3. To investigate real-time monitoring of cell viability for the optimal density	152
4. To proof real-time monitoring of ALP release using differentiation including post-confluence culture and sodium butyrate (NaBt).	152
6.2. Introduction	152

Table of content

6.2.1 Principle	152
6.2.2 Background and literature review	154
6.2.3 The Problem statement	154
6.2.4 Summary	155
6.3. Methodology:.....	155
6.3.1. Reagent	155
6.3.2. Instruments	155
6.3.3. Cell culture	156
6.3.4. Pretreatment and characterization of microelectrodes	156
6.3.5. Real-time impedance measurement of cell viability	157
6.3.6 Real-time monitoring of ALP release using impedance spectroscopy.....	159
6.3.7. Microscope images	160
6.3.8 Cell viability	160
6.4 Results and discussion	160
6.4.1. Electrochemical impedance spectroscopy.....	160
6.4.3. Impedance responses to various concentrations of cells.....	161
6.4.4. Cell monolayer monitoring by impedance.....	163
6.4.5. Cellular morphology on MEAs	163
6.4.6. Impedance responses during alkalinity buffer.....	165
6.4.7. Real-time monitoring of ALP release	167
6.5. Future tests	168
6.6. Conclusion.....	169
6.6. References	170
Chapter 7	177
7.1. Conclusion.....	178
7.2 Future work.....	179
7.2.1 Experiments of interests	179
7.2.2 Cells models and three-dimension cell culture:.....	180
7.2.3 Nanomaterials.....	181
7.2.4 Microelectrode arrays.....	181
7.2.5 Lab on chip	182
7.3 References	183

Table of content

Appendix.....	184
A.1 Modules	185
A.2 Publication and conference attendance.....	185
A.3 Workshops.....	186

List of figure

Figure 1.1: illustrates the 3D structure of ALP shaped in two monomers (A&B). The central core of ALP (Active sites) is formed by the link of the two monomers. The metals positioned on the edges of both monomers are responsible for the catalysis. In the licorice representation, the inorganic phosphate and metal ions are presented [16].....	5
Figure 1.2: ALP isoenzyme with common names, place and function limitation [19].	6
Figure 1.3: The Electrical Double Layer [38].	10
Figure 1.4: The three-electrode system of electrochemical cells showing the diagram of linking the three electrodes with the ampere (A) and the volte (V). They are symbolled as WE RE and CE for working electrode, reference electrode, and counter electrode, , respectively [40].	11
Figure 1.5: The Typical Voltammogram of Cyclic Voltammetry for a Reversible Reaction [41].....	12
Figure 1.6: The Typical Voltammogarm of LSV [42]	14
Figure 1.7: ALP produced in each stage in cells [45].	15
Figure 1.8: organelles of animal cells [51].	17
Figure 1.9: mechanism of ALP release	18
Figure 1.10: The cell membrane [63].	20
Figure 1.11: The cell life cycle [76].	24
Figure 1.12: the change of red phenol over range of pH [86].	26
Figure 1.13: sub culturing techniques [87].	27
Figure 1.14: Schematic of 48-well plate; A the treatment edge and B non-treatment edge. Blue is autoclaved water and pink is the media [88].	27
Figure 1.15: Typical curve of cell growth [90].	28
Figure 1.16: Statistics of cancer first ranked due to incidence or mortality [91].	29
Figure 1.17: The reversible reaction of resazurin and the irreversible reaction of resorufin [117].....	32
Figure 1.18: Generalized scheme representing an optimization protocol of in vitro cytotoxicity assay. ..	33
Figure 1.19: Electric cell-substrate impedance sensing (ECIS) culturware. In the licorice representation, the current pathways: low frequency causes current passes through cell-cell junction and underneath the cells, whereas high frequency allow current passes through cell membrane [136].	38
Figure 1.20: The development stages of recording electrical activity of cultured cells [150].....	39
Figure 2.1: reduction of resazurin into resorufin during metabolism activity of cells.	63
Figure 2.2: Typical equipment of cell culture lab.	65
Figure 2.3: Schematic of sub-culturing cells three times before seeding.	66
Figure 2.4: Actual accounting of cell number using hemocytometer.	68
Figure 2.5: Optimization of the concentration of resazurin at various cell lines. (A) Balbc/3T3 cell lines; (B) A549 cell lines; (C) MCF-7 cell lines; (D) Ht-29 cell lines; (E) coefficient variance % of resazurin concentration of vs cells numbers. Data are expressed as the mean \pm SD of measurements of three independent experiments.....	70
Figure 2.6: Effect of incubation time on fluorescence intensity measured during resazurin reduction. (A) Balbc/3T3 cell lines; (B) A549 cell lines; (C) MCF-7 cell lines; (D) Ht-29 cell lines; (E) Coefficient variance % of incubation time vs. cells numbers. Data are expressed as the mean \pm SD of the measurements of three independent experiments.....	71

Figure 2.7: Experimental and theoretical standard curves of resazurin at various cell lines. (A) Balbc/3T3 cell lines; (B) A549 cell lines; (C) MCF-7 cell lines; (D) Ht-29 cell lines; (E) Coefficient variance % of experimental curves vs. cells numbers. (F) Errors % of theoretical and experimental curves vs. cell number. Data are expressed as mean \pm SD of measurements of three independent experiments.....	73
Figure 2.8: Logistic growth curves of the different cell densities at various cell lines over five days. (A) Balbc/3T3 cell lines; (B) A549 cell lines; (C) MCF-7 cell lines; (D) Ht-29 cell lines; (E) coefficient variance % of growth curves vs. cells numbers. Data are expressed as the mean \pm SD of measurements of three independent experiments.....	75
Figure 2.9: Microscope images of the four cells over five days.	76
Figure 2.10: Logistic growth curves of (A) Balbc/3T3 cell lines; (B) A549 cell lines; (C) MCF-7 cell lines; and (D) Ht-29 cell lines, over five days. (•) estimated cell number using linear equation of standard curve and, (○) accounted cell number using hemocytometer; all compared versus incubation time over five days. Data are expressed as the mean \pm SD of measurements of three independent experiments.	78
Figure 3.1: schematic of the colorimetric reaction of ALP release.....	85
Figure 3.2: A schematic diagram of ALP release. Plate A describes the methods of determination of ALP release from detached cells, where cells were washed with HBSS and then exposed to steps involving trypsinizing, washing and centrifugation and then exposed to the buffer assay. Plate B describes the methods of determination of ALP release from attached cells, where cells were only washed and then directly exposed to the buffer assay. The buffer assay involves 5 mM MgCl ₂ , 30 mM NaCl, and 5 mM pNPP and adjusted to 9.5 pH.....	90
Figure 3.3: Effect of buffer type on pNP concentrations using absorbance detection at 405 nm. All measurements were made at pH 9.5.	94
Figure 3.4: Optimization of factors affected ALP release from Balb/c 3T3 cells (250×10 ³ cells/mL) using absorbance detection (405 nm) and DEA buffer. (A) Effect of Trypsin on ALP release at different incubation times. ALP release remains constant if trypsin is incubated with sample for up to 15 minutes. In the inset, the microscope images of cells exposed to trypsin. (B) The influence of concentration of MgCl ₂ on the ALP release. (C) The influence of increasing concentration of NaCl on the ALP release. (D) The influence of pH of DEA buffer on the ALP release. ALP release has the highest value if the buffer pH is 9.5	97
Figure 3.5: Absorbance optimization of ALP release applied at 405 nm and pH 9.5. (A) standard curve of concentration of pNP (0.16-5 mM) relating to absorbance response (R ² = 0.98). (B) Optimization of reaction time for the enzymatic assay of ALP release. (C) Optimization of pNPP concentrations (0.2-5 mM pAPP) at 30 minutes incubation time. (D) The calibration curve of ALP activity ranging from 1.5-1500 U/L fitted by Lineweaver-Burk model (R ² = 0.99).	99
Figure 3.6: The linearity of the ALP release from the given cells was determined by linear regression analysis of the A ₄₀₅ absorbance values opposite different number of cells.....	100
Figure 3.7: Optimization of pNPP substrate for adhesion cells fitted to the Michaelis-Menten model with R ² less than 0.9 for all cells. In the inset, the Lineweaver-Burk model of enzyme release and pNPP concentration with linear regression R ² higher than 0.9 for all cells.	101
Figure 4.1: Schematic of the electrochemical reaction of ALP release [8].	114
Figure 4.2: A schematic diagram of ALP release. Plate A describes the methods of determination of ALP release from detached cells, where cells are washed with Hank's balanced salt solution (HBSS) and	

List of figure

undergo trypsinization, washing and centrifugation before being exposed to the buffer assay. Plate B describes the methods of determination of ALP release from attached cells, where cells are only washed before being directly exposed to the buffer assay. 119

Figure 4.3: Cyclic voltammograms of 1 mM $[\text{Fe}(\text{CN})_6]^{3-/4-}$ on non-cleaned electrodes (A), cleaned electrodes (10 min) (B), and cleaned electrodes (20 min) (C). The inset demonstrates the curves of reduction peaks' current (ipc) and oxidation peaks' current (ipa) versus the square root of the scan rate $((\text{mV/S})^{1/2})$. The cyclic voltammograms were carried out at an initial potential of -0.2 V and final potential of 0.6 V vs. the Ag/AgCl reference electrode..... 122

Figure 4.4: Linear sweep voltammograms of electrochemical optimization of ALP release applied at a potential of -1.2 V to -1.5 V, and a scan rate of 100 mV/S. (A) The linear sweep voltammograms of a concentration of pAP of 0.16 – 5 mM and in the insert is the standard curve of the current response. (B) Optimization of the reaction time for the enzymatic assay of ALP release and in the inset is current response versus time. (C) Optimization of pAPP concentrations 0.2 – 5 mM pAPP and in the insert is the current response versus concentrations of pAPP. (D) The calibration curve of ALP activity ranging from 1.5 – 1500 U/L fitted by the Lineweaver-Burk model. 125

Figure 4.5: Linear sweep voltammograms of ALP release for each cell range from 2 – 250×10^3 cells/mL at a scan rate of 100 mV/S, incubation time of 10 min and potential range from -1.2 – 1.5 V. In the insert, the linearity performance of the ALP release from the given cells versus the current responses with linear regression analysis is outlined. All the measurements were applied in triplicate in separate graphite-SPE in the presence of 9.7 mM pAPP and at final volume of 70 μL 126

Figure 5.1: Schematic of Capillary Electrophoresis Principle [15]. 136

Figure 5.2: A schematic diagram of ALP release from non-adhesion cells..... 141

Figure 5.3: A schematic diagram of ALP release from attached cells. Cells were washed with Hank's balanced salt solution (HBSS) before being exposed to the buffer assay. 142

Figure 5.4: Comparative studies of capillary electrophoresis and colorimetry toward ALP release from living cells. (A) Electropherograms of pNP concentration formed by ALP release from living cells. (B) Electropherograms of standard pNP concentration (15 – 500 μM) and in the insert is the linear trend of peak areas. (C) The linear trend of absorbance to pNP concentration (15 – 500 μM). (D) Histograms of ALP release from living cells measured by capillary electrophoresis and colorimetry..... 144

Figure 5.5: Comparative studies of absorbance and electrochemical analysis toward ALP release from living cells. (A) Calibration curve of current to concentration of ALP and in the insert is the Lineweaver-Burke plot. (B) Calibration curve of absorbance to concentration of ALP and in the insert is the Lineweaver-Burke plot. (C) Histograms of ALP release from living cells measured by absorbance and electrochemistry. 146

Figure 6.1: shows a schematic of the impedance characteristics of adhesion cells. 153

Figure 6.2: The commercial ECIS 8W10E+ cultureware. In the licorice representation, microelectrode arrays. 157

Figure 6.3: The work station during ALP release monitoring. 157

Figure 6.4: The schematic of the cell growth on microelectrodes (A) and the typical curve (B). 158

Figure 6.5: The workstation of detection amperometry measurement. 159

Figure 6.6: Bode plots of the impedance spectra of experimental data in frequency range of between 1 KHz and 1000 KHz. The spectrum was obtained for 20×10 ³ cells/ mL of the cells of (Balb/c 3T3, A549, MCF-7 and Ht-29) proliferated for over 4 days in the presence of routine media.	161
Figure 6.7: (Left curves) Resistance responses of microelectrode array to various concentrations of the Balb/c 3T3, A549, MCF-7 and Ht-29 cells in monoculture for 10 hours. (Right curves) Calibration curve represents the correlation between cell density and cell index value.	162
Figure 6.8: Logistic growth curves of Balb/c 3T3 cells; A549 cells; MCF-7 cells; and Ht-29 cells, over six days. The normalised CI values of resistance changes at optimal frequency in the case of each cell line.	163
Figure 6.9: Microscope images of the four cell types over a 5-day incubation on microelectrode array.	164
Figure 6.10: EIS results of the four cell types grew on the working electrode before and after exposure to DEA buffer. (Left) Bode plots, and (Right) Nyquist plots.	166
Figure 6.11: (A) Relative impedance changes of Ht-29 cells during ALP release. (B) Microscope images of cells adhesion on 48-well plate and microelectrode array after exposure to NaBt. (C) Resazurin-based assay for cells attached on microelectrode array after differentiation. (D) Amperometric current-time response curve of ALP release. Measurement was applied at a potential of 0.15 V and at assay buffer of DEA (9.5) in the presence of 10 mM pAPP.	168
Figure 7.1: Expression vector of alkaline phosphatase (pSF-CMV-PGK-SEAP) predicting the location of the promoter CMV and the gene of interest ALP.	179
Figure 7.2: steps of Aloe vera extraction (AVE).	180
Figure 7.3: Electric cell-substrate impedance sensing cultureware (1.96 mm ² electrode surface/ well).	182

List of tables

Table 1.1: Microscope picture of attached cells lines and their characteristics and their tissue type.	30
Table 1.2: summarizes the main dispersion regions: α -, β - and γ -dispersions corresponding to correlated biological events.	35
Table 1.3: Basic blots of impedance.	36
Table 2.1: The media and serum of each cell line used for cell culture.	66
Table 2.2: Summary of resazurin data of each cell line versus target days at post-confluence.	79
Table 3.1: Linearity parameters for pNP concentrations vs different buffers using absorbance detection at 405 nm.	94
Table 3.2: effect of solubilisation methods of ALP release.	95
Table 3.3: A summary of the performance analysis of pNPP from different cells.	101
Table 3.4: Summary of ALP release from each cell line versus target days at post-confluence culture..	102
Table 4.1: The research contributed to the development of ALP biosensors.	113
Table 4.2: A summary of the cell number and the composition of media used in this study.....	120
Table 4.3: A summary of the influence of the scan rate on the half peak potential (E_{mid} vs. Ag/AgCl) and peak-to-peak separation (ΔE_p) of anodic and cathodic peaks.	123
Table 4.4: Summary of ALP release from each cell line versus target days at post-confluence culture..	128
Table 5.1: A summary of the cell number and the composition of media used in this study.....	140
Table 6.1: The media and serum of each cell line used for cell culture.	156

Abstract

The alkaline phosphatase (ALP) biomarker is a membrane-bound enzyme widely distributed in the tissues of living organisms, which can instigate particular chemical processes, such as hydrolyses, to provide inorganic phosphate in the human body. ALP activity is routinely used as an indicator in point-of-care applications for some diseases. However, there is mystery about its biological role in terms of regulation during pathogenesis, due to the limitations of real-time monitoring detection tools. The current methods, although sensitive, are costly processes, are time consuming and are based on optical detection, which is hard to miniaturize. There is thus a demand for a reliable technique that addresses these issues and therefore enhances ALP detection in living systems. Our approach in the research is to develop an electrochemical method that will pave the way for performing direct, cost effective and simple monitoring of the ALP biomarker from release in cells for the purposes of clinical analysis.

The thesis discusses a novel strategy that integrates cell culture and electrochemical techniques to develop a real-time detection method for monitoring ALP release from cells using an electric cell-substrate impedance sensing (ECIS) system. The integration of these techniques can enhance the detection of biological targets based on electrochemical changes in electrode interfaces. Our integrative approach took advantage of microelectrode arrays technology, facilitating the yield of recordings, signal shape, and signal-to-noise ratio. For the purposes of the research, electrochemical impedance devices had 40 electrodes distributed in 8 wells that facilitated continuous visualization of cell adhesion, spreading, proliferation, and detachment. Amperometric sensors used three-electrode systems to monitor cellular signal transduction under a monolayer of cell culture conditions. The amperometric sensor application offers solutions that can be used in screening cellular ALP expression detected by electroactive species. This helps to avoid radioactivity, antibodies and mRNA tools that are presently used in clinics. The experimental optimization of the target sample was performed by using resazurin assay. The standard method for ALP detection was used for optimizing the conditions of the enzymatic assay during ALP release.

Balb/c 3T3, A549 and MCF-7 cells displayed an optimal initial density of 40×10^3 cell/mL, whereas the Ht20 cells displayed an optimal density of 80×10^3 cell/mL. This was compatible with the hemocytometer and microscope images. The kinetic enzyme assay of ALP release based on the absorbance analysis showed the optimum activity at 30 minutes incubation time and at 6 mM pNPP concentration. Electrochemical analysis allowed the highest activity after 10 minutes incubation with concentration of pAPP of 9.6 mM. Activity of ALP during the proposed differentiation strategy showed a significant difference in the values of electrochemistry compared to the values of absorbance. The analysis produced findings that were compatible with capillary electrophoresis, which was used as a comparative study. The frequencies required for the target monolayers were optimized on the ECIS system, illustrating a linear relationship between concentration of cells and impedance magnitude. Cellular behaviour was investigated during ALP release, which corresponded to the resazurin-based assay. Real-time ALP release monitoring was proven during differentiation of the colon cancer cell line. A concentration of sodium butyrate of 0.5mM and 1 mM allowed impedance of 550 Ω and 400 Ω compared to the control and to 600 Ω for untreated cells. This indicated a correlation between the cell response and the concentration of sodium butyrate, which suggested that more investigation was necessary to determine the LOD of the developed methodology.

Abstract

Relevant findings were also produced during an investigation of cell morphology and cells viability. This was also proven by amperometry in order to obtain sufficient real-time monitoring of ALP under cellular conditions.

In conclusion, this PhD thesis presents and describes the real-time monitoring for the detection of the ALP biomarker in living cells, with suitable detection results. It contributes to the development of microfluidic testing that would facilitate work on small scale techniques.

Declaration

I, Thanih Balbaied, hereby declare that this thesis is my own work, in partial fulfilment of the requirements of the Doctor of Philosophy degree. It is based on research carried out in Tyndall National Institute and the School of Chemistry, University College Cork, Ireland between October 2015 and October 2021.

Thanih Balbaied



Declaration

Dedicated to my beloved husband Mr Hasan Ban Farag, my loving boy Master Yazan, my parents, Mrs Safyah and Mr Ali Balbaied, and to all my siblings without whom none of my success would be possible.

Acknowledgements

First of all, I would like to thank Allah the Almighty for giving me the opportunity, determination and strength to do my research. My sincere thanks to the custodian of the two Holy Mosques Overseas Scholarship Program.

Now I would like to thank and express my deep and sincere gratitude to my supervisor Dr. Eric Moore for his continuous support, guidance and encouragement. In addition to being an excellent supervisor, he is a man of principles and has immense knowledge of research in general and his subject in particular. I want you to know how much I appreciate the positive influence that you have had on my life. Thank you for your concern and useful advice! I'll be forever grateful.

I would like to acknowledge members of the Tyndall National Institute Dr. Paul Galvin and Dr Walter Messina for their advice, which helped to improve my research skills. I would like to thank Eileen Hurley, leader of the Life Science Interface Laboratory for the wonderful help - thank you for being there for me when I really needed you. Similarly, I would like to acknowledge the former leader of the cell culture laboratory, Michelle Fitzgerald, who helped me with all technical aspects of my work, particularly cell culture techniques. Thanks to Dr Pierre Lovera for allowing me to work in the nanotechnology lab. Also, thanks to Caoimhe Robinson who trained me on the spectrophotometric device in the same lab.

A special thanks to Dr Anna Hogan from the school of Chemistry in UCC for the help with capillary electrophoresis measurements. A big thanks to Dr Gerard O'Keeffe, Senior Lecturer in Anatomy and Neuroscience, and his student Dr Amnah Al Singh who both inspired me during a difficult time when I needed words of encouragement. You cannot imagine how much strength your support has given me during this difficult time. Thank you for your thoughtfulness and your words of encouragement. Thanks to Prof. Colin Hill, professor in the school of microbiology for giving me permission to work in bioscience lab. Also, thanks to Dr Lorraine Draper, project manager microbes to molecules & gut phageomics who supervised me during working in same lab.

Thanks to Patricia Vazquez who supported me whenever I needed it. Special thanks is to my friend Dr Shifa Felemban with whom I shared unforgettable moments during the PhD. Sincere thanks also to Dr Niall Savage and Dr Gerard Duffy for their generosity in giving me knowledge and training in electrochemistry. Thanks also to Dr Yuan Hu who helped me to draw the figures for my thesis. They are truly teachers. Thanks to all past and present who share my office - Suzanne, Vuslat, Julia, Andrea, Paul, Rayn, Colm, Ardeshir, and Fjodor. Thank you for being positive influencers.

Thanks also to my colleagues in the Sensing and Separation group for being reliable and supportive people. Justina Ugwah, Edel Whelton, and Kawther Almosa, please accept my thanks for everything that you've done to help me in the impedance measurements. Samia Alsefri, Ibtiha Albalawi, Hanan Alatawi, and Emma O'Sullivan-words cannot express how grateful I am for your kindness. You are wonderful friends, and I appreciate your love, support, and generosity.

Finally, my deepest gratitude goes to my entire family, to whom this thesis is dedicated. I owe everything to my parents who encouraged and helped me at every stage of my personal and academic life. My heartfelt thanks to you and my brothers and sisters for always picking up the phone when I called, stopping what you were doing and making time to talk. I felt that you were right there with me in my struggles. I owe the warmest thanks to a very special person, my husband, for his continued and unfailing love, support and understanding during my pursuit of a Ph.D degree and which has made the completion of this thesis possible. I greatly value your contribution and deeply appreciate your belief in me. I appreciate my baby, my little boy, for keeping my spirit up with his innocence. Words can never say how grateful I am to both of you. I consider myself the luckiest person in the world to have such a lovely and caring family standing beside me with their love and unconditional support.

Acknowledgements

Chapter 1

General Introduction

Note: some part of this chapter has been published in Journal of Biosensors. Please refer to Appendix A for paper.

1.1 Motivation

Future technologies like sensors or lab-on-a-chip nowadays dominated many fields in the point-of-care applications due to their low cost, fast detection and simple use. Developing methodologies on these devices can enhance the reliability of clinical tests. Alkaline phosphatase (ALP) is one of the most commonly assayed enzymes in routine clinical practice. Due to its close relation to a variety of pathological processes, an abnormal level of ALP in blood serum is an important diagnostic biomarker of many human diseases, such as liver dysfunction, bone diseases, kidney acute injury, and cancer. On the other hand, ALP release has a quantitative indicator of gene reporter in mammalian cells. ALP which catalyzes the dephosphorylation process of proteins, nucleic acids, and small molecules, can be found in a variety of tissues (intestine, liver, bone, kidney, and placenta) of almost all living organisms and therefore have many isoenzymes. However, many sides of ALP isoenzymes' functions are still unknown. For example, the role of ALP regulation in the diseases still unknown, which makes huge challenges in the industry of drug delivery. In order to improve the understanding of the basis of diseases and effectiveness of pharmaceuticals, a real-time detection technique has to be improved.

1.1.1 Aims and objectives

The aim of this thesis was to develop a methodology of real-time monitoring for ALP release from living cells based on microelectrode arrays for clinical analysis. The available methods for ALP monitoring are the label-based assays that have been extensively used in enzyme immunoassays. This method has expensive reagents, which limits the extensive practice in laboratories. Therefore, ensuring convenient and reliable assay methods for real-time monitoring ALP activity is extremely important and valuable, not only for clinical diagnoses but also in the area of biomedical research.

1.1.2 Chapter 1

Chapter 1 has a discussion of general introduction and some of the background for this study. It presents an introduction to the analyte of interest, its isoforms and traditional methods as well as the secretion systems. This was followed by a discussion of chemical sensors for clinical analysis and outlining the properties of living cells and cell culture system. The viability assays used in this thesis was described and compared with others. Furthermore, the theory and technology including microelectrode arrays that enable impedance-based assays were covered.

1.1.3 Chapter 2

Chapter 2 focuses on the optimization of the resazurin assay conditions of the cells of Balb/c 3T3, A549, MCF-7 and Ht-29 in 48-well plate for obtaining the calibration curve of cell viability. First of all, the concentration of resazurin reagent was optimised, then the time of incubation of resazurin with the cells was optimized and then the relationship between the cell concentrations against the fluorescent measurement was found. This was followed by optimizing the cells density with the purpose of simultaneously reach the inhibitive growth contact. The optimal density of each cell line was used for the other assays in this thesis. Then the assay based fluorescent measurement was compared in a similar

Chapter 1

manner with hemocytometer assay and microscope images. The results of resazurin were determined for all cells in the differentiation stage.

1.1.4 Chapter 3

Chapter 3 is concerned with optimization of ALP release from cells using absorbance detection technique. The first part of the chapter was to optimize the reagent components for the best expression of ALP from cells. This was performed by applying several buffers, solubilisation methods, investigation of trypsin effects, pH range, and concentrations of $MgCl_2$ and NaCl. This was followed by conducting of kinetic enzyme assay including determination of standard curve of pNP, time of incubation with substrate (pNPP). Then that allowed to reach the optimal concentration of the substrate (pNPP) producing the calibration curve of ALP that is identified in the Units per Litre (U/L). The kinetic enzyme assay and linearity performance were applied and compared for all cells and the quantity of ALP was determined in the differentiation stage.

1.1.5 Chapter 4

Chapter 4 describes the electrochemical measurement of ALP release by applying linear sweep voltammetry detection technique and using graphite screen printed electrode. The graphite electrodes were characterized in potassium Ferri/Ferrocyanide solution by applying cyclic voltammetry in order to meet the stabilization condition of electrode surface. This was followed by conducting of kinetic enzyme assay including determination of standard curve of pAP, optimal time of incubation with substrate (pAPP), optimal concentration of the substrate (pAPP) all of which allow for producing the calibration curve of ALP that is identified in the Units per Litre (U/L). The kinetic enzyme assay and linearity performance were also applied and compared for all cells and the quantity of ALP was determined in the differentiation stage.

1.1.7 Chapter 5

Chapter 5 is concerned in illustrating the comparative study, which was capillary electrophoresis. This method was performed for all given cells in this thesis. The obtained calibration curve of (pNP) equation from this method was used to determine the quantity of ALP at the stage of inhibitive growth contact of each cell line and compare it with absorbance finding in chapter 3. By the end of this chapter, the experimental findings of absorbance and electrochemical was compared as well. The findings in this chapter can be used for future work. For example, designing experiments for monitoring isoenzyme of ALP inside the capillary.

1.1.6 Chapter 6

Chapter 6 describes the using of impedance-based assay for real time monitoring of ALP release during differentiation. Electric cell-substrate impedance sensing (ECIS) based microelectrode array was selected to measure the cellular responses. Pre-treatment was applied and optimal frequency of each cell line was observed. That was followed by linearity performance in order to examine the constant condition of the electrodes during the assay. Then it was proved the concept of real-time monitoring ALP using two ways

of differentiation; post-confluence culture and applying sodium butyrate for colon cancer cells. ALP activity was determined by amperometric method.

1.1.8 Chapter 7

Chapter 7 outlines the conclusions of the experiments carried out in this thesis and illustrates the future work. Finally, the publications, oral and poster presentation given while doing the thesis was arranged in appendix.

1.2 Alkaline phosphatase (ALP)

The detection of alkaline phosphatase (ALP) occurred in the late 19th century, and it was recognized as an enzyme family after Robison's contributions in 1932 [1]. McComb et al. (1979) summarized many scientific attempts to detect ALP and outlined many topics that are of significance for multidisciplinary researchers [1]. The primary importance of detecting ALP is to identify the possibility of diseases and carry out immediate preventive or treatment procedures [2]. In point of care applications, ALP is known to be measured in routine blood tests, with high levels of serum considered as indications of bone disease, liver disease, or bile duct obstruction. Recently, it appears to be a significant independent prognostic biomarker to indicate cancers [3]–[12]. ALP levels have various reference ranges depending on age, gender and patient history. ALP can be defined as an enzyme that liberates phosphate under alkaline conditions and is made in the liver, bone, and other tissues [13].

X-ray crystallography technique characterizes ALP by obtaining a three-dimensional structure of the enzyme under study through diffracting its crystallized form [14]. Fersht et al. (1999) argue that the threedimensional structure is crucial in determining the functionality of the molecules. On the other hand, nuclear magnetic resonance technique uses energy transitions through a range of wavelengths. This technique characterizes enzymes by creating a difference in the spectrum. This appears in the strength of the electromagnetic field around the nucleus [14]. The approach thus provides more efficiency, allowing for the identification of atoms or particles and their specific functions. Figure 1.1 illustrates that ALP is a homodimeric enzyme shaped in two monomers (A&B), where the central core of ALP (Active sites) is formed by the link of the two monomers. Millán (2006) notes that this property allows it to have a stable heating capacity with a maximum capacity at very high pH. Similarly, an active site found on the enzyme, where one magnesium and two zinc ions are located, has the function of acting as a catalyst site. This occurs when Mg^{2+} and Zn^{2+} activate and inhibit, respectively, protein tyrosine phosphatase 1B (PTP1B). Millan (2010) identifies these occurrences as molecular dynamics simulations. Millan found that Mg^{2+} and Zn^{2+} compete for the same binding site in the active site only when the enzyme is in the closed conformation in its phosphorylated state [15]. At this point, the cations have different effects on hydrolysis, resulting in a difference in the establishment of the structural enzymology PTP1B.

Details of ALP isoenzymes and tests regarding their physical and chemical properties are discussed below. Furthermore, we have discussed some other points, taking into account the methods of discriminating between those isoenzymes.

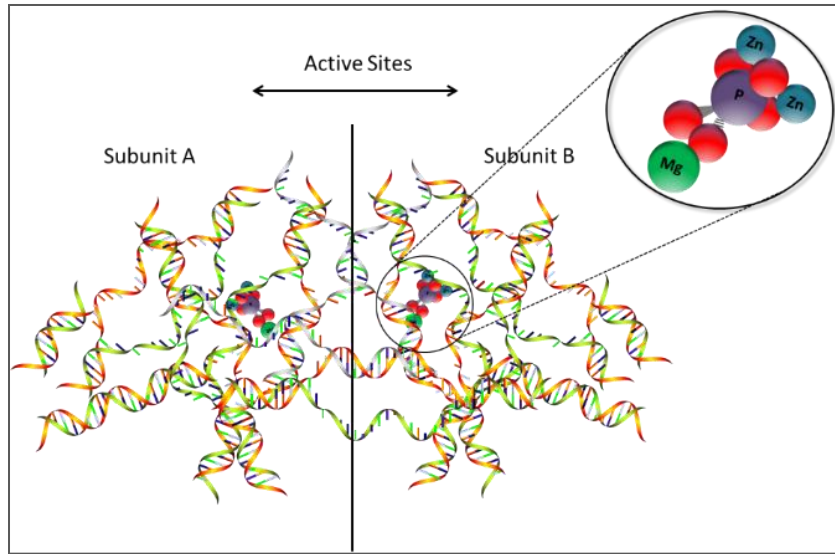


Figure 1.1: illustrates the 3D structure of ALP shaped in two monomers (A&B). The central core of ALP (Active sites) is formed by the link of the two monomers. The metals positioned on the edges of both monomers are responsible for the catalysis. In the licorice representation, the inorganic phosphate and metal ions are presented [16].

1.3 ALP isoenzyme and tests

Mammalian ALPs are present as different isoenzymes. Figure 1.2 shows the four main isoenzymes of ALP, which are germ cell alkaline phosphatase (GCAP), intestinal alkaline phosphatase (IAP), placental alkaline phosphatase (PLAP) and tissue-nonspecific alkaline phosphatase (TNAP). GCAP, IAP and PALP, are located in chromosome 2, whereas TNAP is located in chromosome 1. None of their precise physiological and neoplastic functions are known. However, TNAP is found to be responsible for calcification in bone, and for regulating the secretory activities in the liver. However, their main function is still unidentified. ALP isoenzyme can be referred to as a biomarker for cancer before tumors form. Fishman (1980) contends that PLAP is sometimes found in individuals with ulcerative colitis or polyposis of the colon, and it is through this that they increase the probability of contracting cancer [17]. Bukowczan et al. (2014) also found that PLAP has a relationship with different tumors, for example, renal cell carcinoma (RCC) [18].

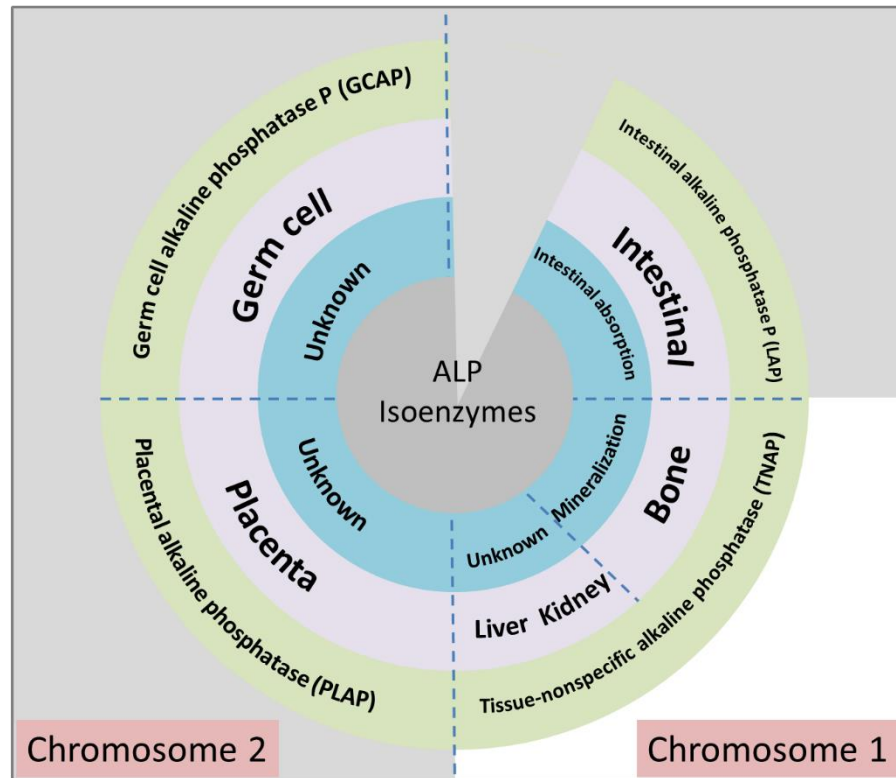


Figure 0.2: ALP isoenzyme with common names, place and function limitation [19].

Some physical and chemical properties are considered when discriminating between isoenzymes. Webster (2008) points out that the concentration of cysteine and histidine that inhibits alkaline phosphatase activity, and the phosphotransferase activity of different isoenzyme preparations are similar [13]. Other physical and chemical properties include heat stability at 56 °C and electrophoretic mobility. The concentrations of Zn ions, L-phenylalanine, and L-tryptophan required to inhibit enzyme activity by 50% are different. This variety was exploited to discriminate ALP isoenzyme. Some traditional methods depend on deactivate ALP, including the use of selective inhibitors (e.g. L-phenylalanine, L-homoarginine, levamisole), or the use of heat treatment. This classic way is to heat up the ALP serum at 56°C for 10 minutes. This would facilitate distinguishing between liver and bone ALP, for instance. Other methods that used such as gel electrophoresis and lectin, rely on sieving media or non-sieving media. They use polyacrylamide, agarose gel, or the wheat-germ lectin for limiting the mobility of ALP isoenzymes in buffers. Moreover, separation-based methods, which are conducted to distinguish ALP isoenzymes, are sometimes coupled with other techniques to give quantity of ALP. For example, chromatography methods, such as affinity chromatography [20], have been applied to distinguish ALP isoenzymes. They are sometimes associated with solid-phase immunoassay and provide data about ALP levels. However, although optimized by using wheat germ agglutinin (WGA) conjugates to the silica particle [21], this method is still insufficient. Liquid chromatography is applied instead with different anion exchange [22]. Per et al. (1992) used weak anion exchange to determine and separate ALP isoenzymes [23]. This assay has improved sensitivity and selectivity compared to electrophoresis methods. However, the temperature for the analytical column must be strictly controlled; otherwise retention times and peak heights will be

affected. These separation methods, although useful as research tools, have limited applications in the routine clinical laboratory.

A number of approaches have been extensively developed to understand the gene expression of ALP in *in vitro* diagnostic tests, which identify the causes of disease, as well as tracking the effectiveness of pharmaceuticals. Therefore, accurate quantification of ALP levels provides a signature of ALP function and gives a better understanding about the prognostic level of ALP in different cancers.

1.4 Traditional ALP methods

Three main traditional methods have been adopted to achieve better quantification of ALP levels. Firstly, the fluorescence-based methods include flow cytometry, histochemical and immunohistochemical techniques. The sample forms precipitate with substrates such as enzyme-labeled fluorescence-97 (ELF97) phosphatase, naphthol phosphate, and menadiol diphosphate, which are coupled with salts and dyes, such as azo dye, diazonium salts and tetrazolium salts, to produce insoluble colored products detected by fluorescence. These methods allow high sensitivity and fast detection because they measure the intensity of light without comparing with a reference. However, their expensive instrumentations hinder their convenience. In addition, they require highly skilled personnel [15], [24], [25].

Secondly, mRNA-based methods, such as a northern blot [26] and a reverse transcriptase-polymerase chain reaction (RT-PCR) [27], can detect real-time ALP levels. The northern blot method detects a specific isoform of ALP [26]. The RT-PCR approach is also based on RNA expression, however; it combines with a single nucleotide primer extension assay in order to discriminate ALP isoenzymes [26].

Thirdly, immunoreaction-based methods, including western blot, radioimmunoassay (RIA), and enzyme-linked immune-sorbent assay (ELISA) have been conducted to gain more selectivity and sensitivity [28]. Western blot involves electrophoretic sieving, which allows ALP to be separated by size and the results transferred to a membrane producing band. The membrane is incubated with labels of specific antibodies. This method, although sensitive, is time-consuming and has a high demand in terms of the experience of the experimenter. Additionally, it requires multiple optimization of the experimental conditions. In RIA, polyclonal are optimized to monoclonal antibodies to eliminate the cross reactivity. Thus, RIA is considered a method valid to detect ALP. RIA requires radioactive isotopes of iodine to act as an indicator. In such assay, beads, such as polystyrene coated with polyclonal rabbit anti-ALP, are incubated with test samples and iodinated by Chloramine, a radioactive compound. The radioactivity is then counted by a gamma counter [29]. Although RIA is a sensitive method, it requires frequent preparation of radioactive antibodies, as well as exposure to radiation hazards. Additionally, it requires multiple steps for handling, storage, and disposal of radioactive materials.

An alternative option that offers a sensitivity similar to that of radioassay but with no radiohazard is ELISA. In this technique enzyme conjugate and monoclonal antibodies are used. Colorimetric assay is then used in the presence of an appropriate chromophore (e.g., p-nitrophenyl phosphate) [30]. Although simple, this technique is a lab-based application [31]. In point-of-care application, ELISA-based antibodies may cause false results [32]. For example, the human body can continue producing antibodies, even though

the person may have previously had the disease and recovered. In addition, some people are poor producers of an antibody or have some interfering substance in their blood. Thus, the amount of antibody may be too low to measure accurately or may go undetected. Cross reactivity is highly likely to occur as a consequence of unrelated antibody. This would cause non-specific binding, thus resulting in positive signals for false reactions [33]. Another limitation with monoclonal antibodies is that immunoassays cannot identify the isoenzyme ALP [34], [35].

Traditional methods mentioned earlier have some advantages. However, they require multiple external controls for quantitative analysis, as well as sequencing experiments to ensure reliability. Additionally, large sample volume, expensive instruments, and costly reagents are generally needed. In addition, clinical ramifications need simpler and more sensitive technique for testing of ALP expression.

Enabling high throughput technologies, such as biosensors in point of care applications requires features that include portability, simplicity, and cost effectiveness. All of these can be achieved through electrochemical methods.

1.5 Chemical sensors for clinical analysis

The number of diagnosis requirements for infectious diseases and cancers are ever increasing, and traditional tools that are usually expensive and hard to access barely meet the large demand. Therefore, it is important to develop effective devices for point of care application that provides sensitive and selective results for early detection, hence improving prognosis. One of these devices is the biosensor, which is defined as a systematic gadget that can be utilized for identifying analytes, by combining a biological component with that of a physicochemical detecting transducer, with the aim of acquiring a quantifiable signal [36] [165]. Biosensors have two parts. One is the biological recognition elements, and they are either natural (e.g., antibody, enzyme, and cell), semisynthetic (e.g., peptide nucleic acid), or synthetic (e.g., imprinted polymer). In living cells, growth inhibition and cell viability, for instance, are the parameter signals. Through this, there are many types of living cells derived from microsystems, such as bacteria, fungi, yeast, mammalian cells. Of these, the mammalian cells are the most commonly used in many fields, particularly in medical diagnostics and cytotoxicity testing, because they allow physiologically relevant studies. In addition, they allow for the probing of pathogenic or toxigenic substances in relevant samples. Living cells are more likely than other elements to have specific reactions (e.g., redox reactions, changes of ionic composition and concentration) that can be used as sensing elements in electrochemical biosensors.

The second major component of biosensors after biological recognition are transducers, which play an important role in conveying the biological parameters to measurable signals. Biosensors can also be divided according to transducer principles. For example, piezo-electric transducer can measure the resonant frequency of the reaction that occurs between the target analyte and the biological recognition elements as a result of applying mechanical stress. Another type of transducer is one that measures precisely optical signals. Essentially, they sense the biological recognition elements when the incident light interacts with the target analyte and produce optical signals, such as polarization or frequency, which can then be optically detected [37], [172]. Electrochemical transducers measure electrical properties, such as

current or voltage, which make them desirable in redox reaction measurements. Electrochemical transducers directly convert the biological events into electrical signals according to the method used. For example, if the amperometric method is used, then the current would be measured and the voltage would be measured through the potentiometric method and so on [37], [172]. Transducers, on the other hand, generally have to be portable, simple, easy to use, disposable and low cost in order to be applicable. Therefore, research is now concerned with miniaturizing them and on utilizing nanotechnology. Electrochemical transducers are more favorable, as they can be downsized, and their signals are highly accurate, compared to other transducers. In accordance, more details are given for techniques for measuring electrochemical reactions.

1.5.1 Electrochemical cells

Electrochemical detection takes place when redox reaction occurs. The redox reaction has two parts: oxidation and reduction. Oxidation refers to the loss of electrons, while reduction refers to the addition of electrons to a chemical species. Oxidation and reduction reactions occur at the same time, because when an electron is lost, it is gained elsewhere – this causes current to generate.

The electrochemical reaction can be spontaneous if the electron naturally transfers in relation to the standard reduction potential (Galvanic). The higher the potential, the stronger the pull for electrons. In addition, the reaction can be electrolytic, where the electricity is used in the electrochemical cell and permits chemical reactions to occur that would not otherwise take place.

The molecule that loses electrons is called the oxidized or reductant agent; the molecule that gains electrons is called the reduced or oxidant agent. The loss and gain of electrons takes place on surfaces called electrodes, which dipped in a solution. This solution is called an electrolyte, and it is important for the flow of ions in oxidation and reduction reactions. The oxidation and reduction reactions occur on anodic and cathodic electrodes, in which electrons flow from anode to cathode.

The current that flows in an electrochemical cell is either Faradaic or non-Faradaic. Faradaic current indicates the redox reactions, while non-Faradaic current is caused by the electrode double layer and nonFaradaic can be avoided by increasing signal to noise ratios [38].

The electrical double layer is established between the electrode and the solution in the time of applying potential in the cell. The surface of the electrode becomes charged, which attracts ions dissolved in the solution. The ions attracted to the surface of electrode has opposite charge thus forming inner and outer layers as shown in Figure 1.3.

The inner layer is the one that is located near the electrode surface and is called the inner Helmholtz plane. It consists of solvent molecules and specifically adsorbed ions. The outer layer is located slightly further from the surface and is called the outer Helmholtz plane. It consists of solvated ions [39].

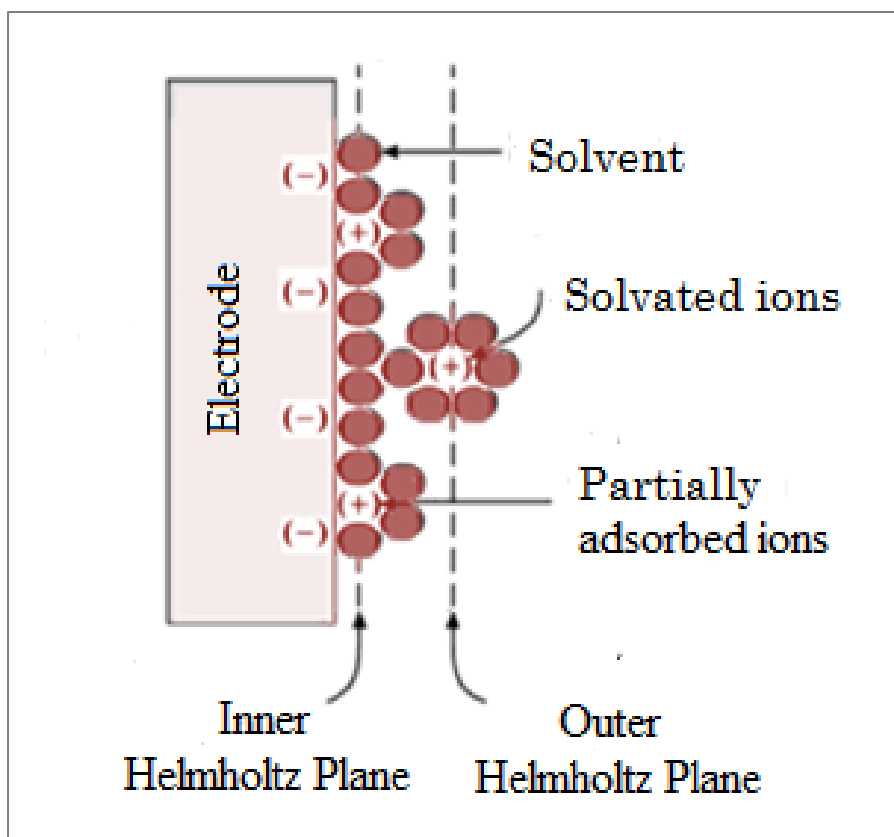


Figure 0.3: The Electrical Double Layer [38].

When measuring current, the 3-electrode system is mostly used for electrochemical experimentation. The parts of the electrochemical setup is shown in Figure 1.4. The potential is linked between two electrodes; working electrode (WE) and reference electrode (RE). Whereas the current is linked between WE and counter electrode (CE). The potential and current can be measured by voltammetry methods, such as cyclic voltammetry, linear sweep voltammetry and amperometry [40].

The working electrode is the one that directly impacts the performance of electrochemical assays in transferring electrons to or from the analyte. [39]. Therefore, the materials that it is made from can be conductive, e.g., metals, semiconductors, or graphite. Additionally, the materials that a working electrode are made from will mainly depend upon the reaction indicated. On the other hand, the reference electrode (e.g. Ag/AgCl) is the second main electrode as its role in electrochemical cell is to maintain the potential. The third important electrode probably is the counter electrode. Its surface area must be much larger than the working electrode in order to avoid reaching the kinetic limits of the process. As the reaction occurs in a solution, then the ionic strength of the solution will be supported. This will reduce the resistance of the solution, which is defined in this case as an electrolyte.

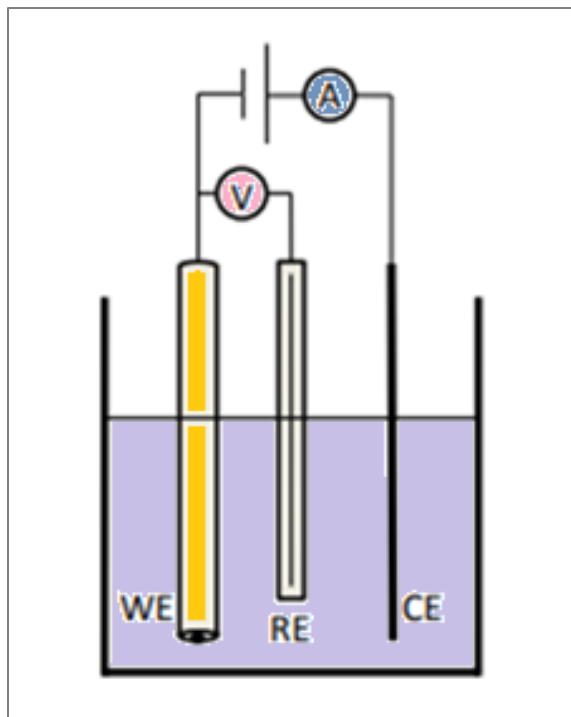


Figure 1.4: The three-electrode system of electrochemical cells showing the diagram of linking the three electrodes with the ampere (A) and the voltmeter (V). They are symbolized as WE RE and CE for working electrode, reference electrode, and counter electrode, respectively [40].

1.5.2. Nernst-Planck equation

The measurable signal produced from electrodes is distance-dependent on transfer electron reaction: the smaller the distance, the faster the rate of electron transfer. This allows for sensitive detection. Moreover, the reaction rate is affected by the mass transport of particles. This has three different forms: migration; diffusion; and convection. Mass transport by diffusion is caused by the gradient in concentration. Migration occurs due to the movement of ions in the solution that are driven by electrostatic force. This can be controlled by increasing the concentration of the electrolyte. Mass transport by convection is caused by the mechanical motion of the solution (e.g. stirring). These three terms are expressed in the Nernst-Planck equation [38].

$$J_j(x) = \underbrace{-D_j \frac{\partial C_j(x)}{\partial x}}_{1^{\text{st}} \text{ term}} - \underbrace{\frac{z_j F}{RT} D_j C_j \frac{\partial \phi(x)}{\partial x}}_{2^{\text{nd}} \text{ term}} + \underbrace{C_j v(x)}_{3^{\text{rd}} \text{ term}}$$

The mass transport represented in the equation is for one dimension to the electrode, which is defined as $J_j(x)$ ($\text{mol cm}^{-1}\text{sec}^{-1}$). The first term is referred to the diffusion, which also refers to Fick's law. The

negative sign shows that the material moves from high concentration to low concentration. The elements affecting mass transport in this term defined as the diffusion coefficient D_j ($\text{cm}^2\text{cm}^{-1}$), and the concentration gradient $\partial C_j(x)/\partial x$. The second term is referred for the migration. It shows the effect of mass transport by the charged species, which can be reduced by increasing the background of the electrolyte. The elements in this term influenced the equation defined as the charge z_j , the-diffusion coefficient, concentration for the species j C_j (mol cm^{-3}) and potential gradient $\partial\phi(x)/\partial x$. The last term is referred the convection of the solution and illustrates the effect of mass transport by velocity of solution [38]. It has two elements affected the equation, which are the rate of concentration for the species j and its rate of moving in the solution $v(x)(\text{cm sec}^{-1})$.

1.5.3. Cyclic voltammetry

Cyclic voltammetry is important in characterizing electrodes as it provides kinetics information relating to the electrochemical reactions occurred at the surface of the electrodes [41].

Cyclic voltammetry is used in order to observe the redox reaction, thus providing information about redox species, reduction and oxidation potentials, reversibility reactions, and stability of systems [265]. This data can be represented in a voltammogram (figure 1.5) where the pre-defined range of potential swept and then return to initial potential in an opposite direction. Maintaining the constant rate of sweep of potential with time is called the scan rate.

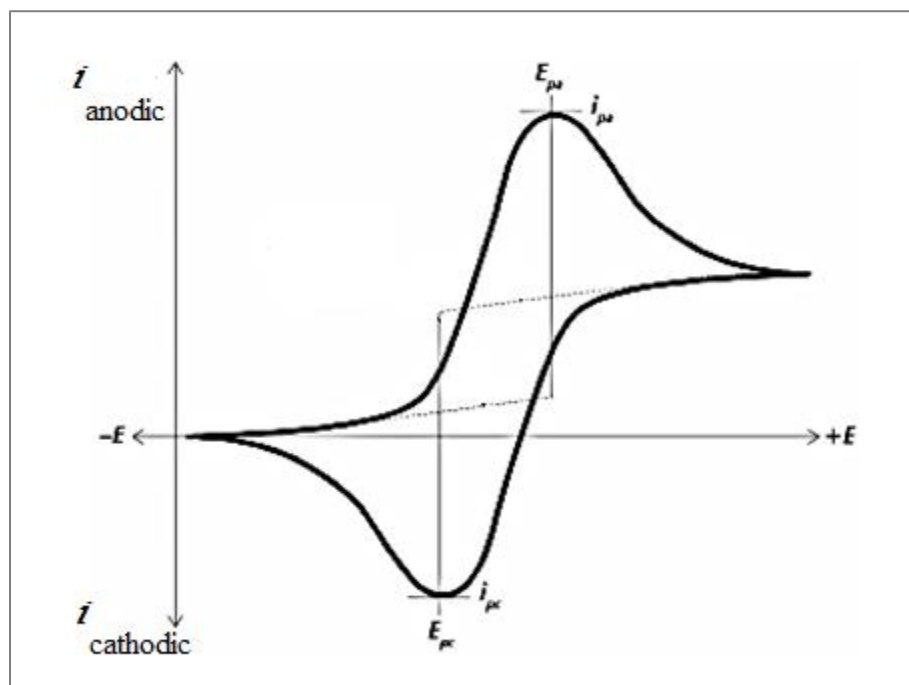


Figure 0.5: The typical voltammogram of cyclic voltammetry for a reversible reaction [41].

The voltammogram can measure different types of current as a result of its ability to apply a wide range of potentials., e.g., peak cathodic current (i_{pc}), in which current flows when rate of reduction is maximum, and peak anodic current (i_{pa}), in which current flows when rate of oxidation is maximum.

The voltammogram can also be used to investigate different type of potentials, such as peak cathodic potential (E_{pc}), which is the potential at which rate of reduction is maximum, and peak anodic potential (E_{pa}), the potential at which rate of oxidation is maximum. These peaks are parameters of cyclic voltammetry. If the difference between potentials is high this means that the reaction irreversible. If it is small, this means that the reaction is reversible, therefore, the electron transfer is higher than the diffusion process [41]. The following equation can describe the reversibility of the reaction with respect of the potential of separation peaks:

$$\Delta E_p = E_{pa} - E_{pc} = 2.303 \frac{RT}{nF}$$

In this equation, the gas constant (R), the temperature in Kelvin (T), the number of electrons (n), and F the Faraday's constant (F) are important factors affecting the difference of potential (ΔE_p). Therefore, by applying these constants at 25 °C with one electron, ΔE_p is expressed as 0.059 V. If the measurement is higher than this, then the reaction will be irreversible.

The following equation is used to calculate the formal reduction potential (E°) and to determine the reversibility of a reaction:

$$E^\circ = \frac{E_{pc} - E_{pa}}{2}$$

1.5.4. Linear Sweep Voltammetry (LSV)

Linear sweep voltammetry is equivalent to a one-segment cyclic voltammetry, where a fixed potential range sweeps linearly from a lower to an upper value, and current is measured as a function of time. LSV has many useful applications. For example, it is used to study electron transfer kinetics reactions in evaluating biological systems. Likewise, LSV produces voltammograms that transform their aspect depending on factors that include: rate of the voltage scan; electron transfer reaction rate; and chemical reactivity of the electroactive species [42]. If LSV is applied then the system (electrode and electrolyte) should be stationary. Changes to the voltage cause the reactants in the electrolyte to react and produce more products. The accumulation of products at interface will change the current. The Nernst equation reveals how the electrode potential is dependent on the concentration in the electrolyte:

$$E = E^\circ - \frac{RT}{nF} \ln \frac{C_{Red}}{C_{Ox}}$$

In this equation E is the potential at working electrode and E° is the formal potential of redox reaction. Reduction occurs when $E < E^\circ$. Figure 1.6 shows the typical voltammogram of LSV.

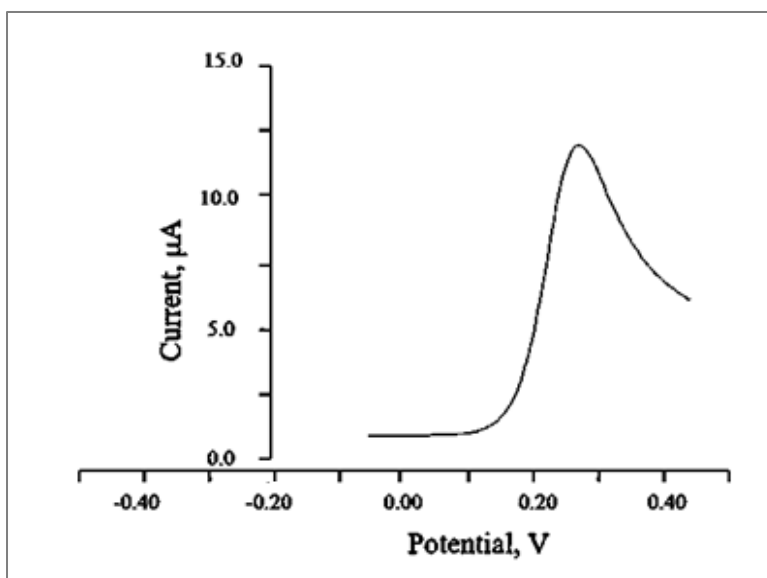


Figure 0.6: The Typical Voltammogram of LSV [42]

The corresponding peak current (i_p) to the potential can be calculated digitally using the current instruments. This can be demonstrated using the Randles-Sevcik equation (at 25 °C):

$$i_p = (2.69 \times 10^5) n^{3/2} A D^{1/2} C_i v^{1/2}$$

Randles-Sevcik equation has some elements affected the peak current i_p . These elements are the number of electron (n), the electrode area A (cm^2), the diffusion coefficient D ($\text{cm}^2 \text{s}^{-1}$), the concentration of redox species C (mol cm^{-3}) and the scan rate v (V s^{-1}). The important of measuring the current is to quantify the amount of the concentration as they have a proportional relationship.

1.6 ALP secretion system

Due to the complicated nature of ALP in terms of its physical and chemical properties and the fact that it has various levels between people and isoenzymes that indicate related diseases, particular expression systems are required to express ALP and makes it detectable *in vitro* assays, which will be expanded upon in the next section.

There are many expression systems for proteins, including mammalian cells, bacteria and yeast. Of these, mammalian cells help in the folding of proteins, post-translational modifications and product assembly. These are all important when harnessing mammalian cells for protein production [43]. In addition, mammalian cells have proved to be well suited to *in vitro* studies, with efficient expression systems that lead to good productivity, because they contain glycosylation, which is required for secretion and stability. However, mammalian cells are more complex and more expensive than other expression systems, such as bacteria and yeast. ALP is located in the membrane of mammalian cells and found to be in the periplasmic space of *E. coli* bacteria [2]. Figure 1.7 shows that ALP is made in the nucleus then formed into protein in the endoplasmic reticulum (ER). Then formed as an isoenzymes in the Golgi body. All these

processes are under natural pH. ALP then bonds to the cell membrane, where the pH is 7.5. This pH doesn't allow ALP to induce, unless the environment surrounding it rises to alkaline pH. An example of this can be seen during cell metabolism, or necrosis inflammation, where HCO_3^- rises cause increased alkalinity in the cell membrane, thus activating ALP [44]. This is discussed more in the cellular process section.

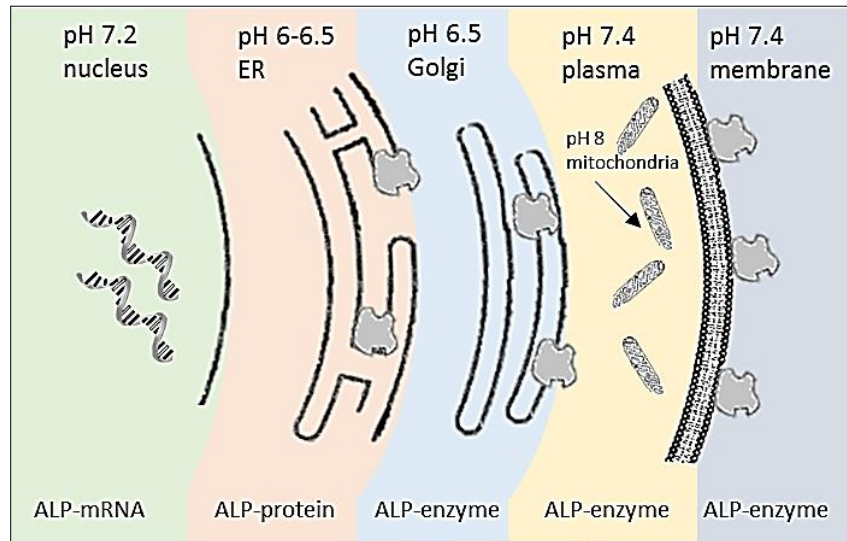


Figure 0.7: ALP produced in each stage in cells [45].

Details of a living cell as an expression system of the enzyme ALP are discussed below. Cell parts that include organelles, the cell membrane, the cytoskeleton, and the extracellular matrix (ECM) are also discussed. Particular attention is given to the cellular processes that were exploited for cell viability in terms of metabolic activity and cell adhesion.

1.7 Living cells

1.7.1 The cell

A cell is a biological term that refers to the basic unit that carries the fundamental molecule where life processes are composed. In cell theory, the historic scientific theory that all living organisms are composed of cells is universally accepted [46]. Cell theory has three basic principles. The first principle is that living organisms are made up of a single cell or more. The second principle is that some cells are formed through the replication of an existing cell. The third principle states that cells are the basic organizational unit of all organisms. Cells vary in size, organization, and shape. Even cells that are within the same organism exhibit different features in terms of organization, size, and shape. Cells are small in size, since they are made up of a nucleus that only controls a specific volume of the cytoplasm. Moreover, the cell's surface area to volume ratio limits its size. However, many small cells grouped together may have a bigger surface area than one large cell with the same volume. A big surface area is crucial, because oxygen, nutrients, and other materials needed by the cell enter through the cell's surface [46]. As the cell enlarges, its surface area diminishes, hindering the intake of the much-needed nutrients. Additionally, cells are

Chapter 1

shaped differently based on their functions. For instance, the neurons are thin and long, while the white blood cells are round to allow for smooth movement.

Additionally, the cell performs many processes that include cell division, growth, metabolism, motility, and protein synthesis. All these processes are important in carrying out bodily functions. For example, cell division ensures that the cells are renewed and reproduced to increase in number in a process called the life cell cycle. This process will be discussed in detail later in this chapter.

Similarly, protein synthesis is an essential process, whereby cells generate new proteins, while some cellular proteins are lost through degradation. The process produces amino acids that act as the building blocks of information. For example, RNA strands are synthesized from the DNA template. The RNA is then transcribed into mRNA. The mRNA is free to move in the cell through complex processes resulting in a three-dimension protein molecule [47]. This happens in two main processes called transcription and translation.

After successful cell division, more cells grow through the cellular metabolism function. Metabolism is a set of chemical reactions that are life-sustaining in the organism [48]. It takes place in two steps: catabolism and anabolism. In catabolism, the cell breaks down compound molecules into smaller molecules that are then oxidized to produce energy. Anabolism is a constructive process that involves the formation of complex molecules from smaller units using energy [49]. The complex sugars that are present inside organisms can be broken down to form monosaccharides. The various forms of monosaccharides, such as glucose, can be further broken down to form adenosine triphosphate (ATP) in a process called cellular respiration, which will be described in more detail in (2.2.1). The adenosine triphosphate then builds the glucose by forming precursors such as monosaccharides, amino acids, nucleotides, and isoprenoid. The ATP activates these precursors using energy to form complex molecules, such as polysaccharides, lipids, proteins, and nucleic acids.

The other cellular process is cell motility. The cells do actually physical move, which can be seen in healing injuries. The cells are driven by proteins (e.g Myosin). This protein is responsible of mechanical energy in the cells. Myosin is a motor protein worked alongside with other proteins in the cytoskeleton like receptors, crosslinking, bundling, binding, adhesion. [50]. The movement of cells is similar to the movement of worms. In other words, the front of the cells protrudes then it adheres. Then the end of the cells deadheres, which allow the contraction of the cytoskeletal. This allows the cell to move forward. These steps are driven by forces caused by special cytoskeleton forces that include Myosin, the function of which is to hydrolyze the ATP and convert chemical energy to mechanical energy. This energy is then used during various body processes, including the immune reaction, healing injuries, and during cancer progress.

Organisms that contain cells with a nucleus are referred to as eukaryotes, some organisms contain cells that do not contain a nucleus and membrane-bound organelles. Such organisms are called prokaryotes. As mammalian cells are the interest in this study, eukaryotes are discussed more below.

1.7.2 Cell parts

A cell's internal structure is made up of organelles that are responsible for cellular processes [47]. The three major organelles that make up the cell are the cytoplasm, the nucleus, and the cell membrane [51]. The cytoplasm is jelly-like, and it makes up the largest part of the body. The nucleus is the largest organelle, and it is responsible for cell reproduction. The cell membrane protects the cell. Moreover, the cytoskeleton helps cells to move, and the extracellular matrix (ECM) links cells with their surrounding medium. Figure 1.8 shows parts of an animal cell. Each part in the cell has a particular function. The functions of the cell parts that relate to this study are discussed more in each subtitle below.

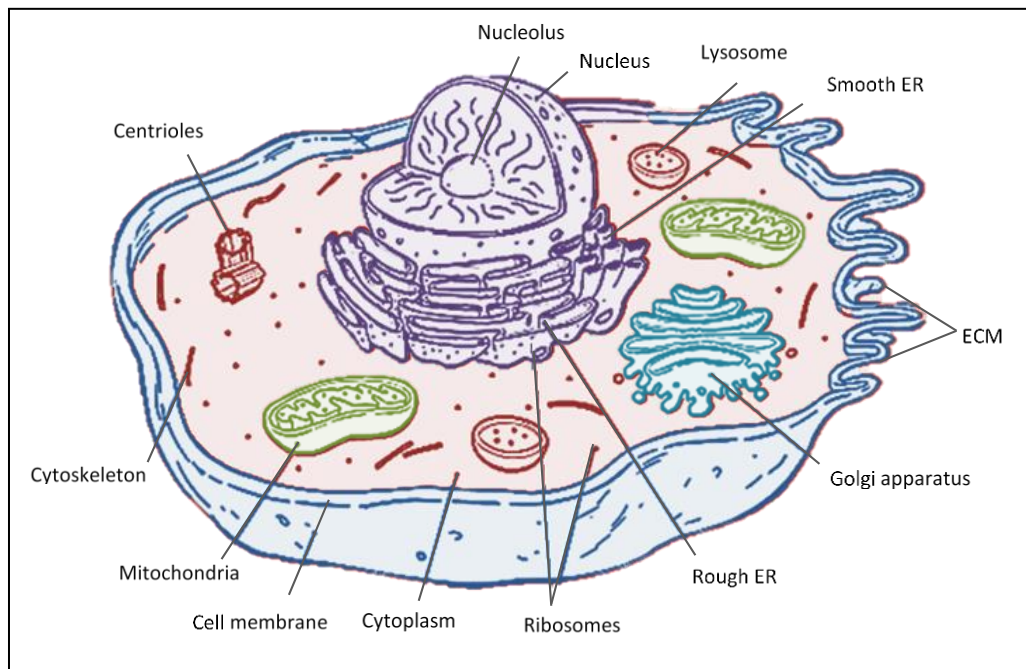


Figure 0.8: organelles of animal cells [51].

1.7.2.1 Organelles

As mentioned above, the main components of a cell are the nucleus, the cell membrane, and the cytoplasm [51]. However, other organelles perform equally important functions, and they include: the endoplasmic reticulum (ER), lysosomes, ribosomes, mitochondria, and Golgi bodies. The endoplasmic reticulum has two regions (one rough, one smooth) that have different functions and structures. The smooth endoplasmic reticulum produces enzymes and hormones, while the rough ER produces protein. The lysosome contains acidic enzymes whose function is to digest macromolecules in the cell.

The mitochondria are round organelles that are surrounded by a double membrane [51]. They play a vital role by releasing the adenosine triphosphate in a process called respiration. The process takes place during the Krebs cycle and in the presence of oxygen [52]. The Krebs cycle begins when the acetyl-CoA combines with oxaloacetate, a carbon acceptor molecule, to form citrate. This process is followed by chemical reactions, with the enzymes as a catalyst. The citrate is made of six carbon molecules, and during

the Krebs cycle, it releases two carbons to form carbon dioxide and NADH molecule. The other remaining carbons react to form an ATP molecule. Then the FAD electron carrier is reduced to FADH₂ and HADH. The reaction regenerates the oxaloacetate, and the cycle is repeated [53]. Generally, one cycle releases two molecules of carbon dioxide, three NADH, one ATP, and one FADH. This process is important in metabolic activities, as well as cell viability. These topics are covered in detail later in this thesis in section (1.9.1).

The three organelles discussed above, (mitochondria, ER and lysosomes) play a role in calcium homeostasis and signaling functions [47]. The ER releases calcium using the receptors that are ligandactivated. The lysosome and the mitochondria serve as a container and keeping the calcium within certain limits so that they can continue with the functions. This process may lead to an increase in the alkalinity level in the cell membrane, resulting in the formation of biomarkers. This may happen when the ligandactivated receptor is bonded to the ATP, and this raises the alkalinity in the areas surrounding the membrane. The calcium ions released from the intercellular stores, and the chloride and hydrogen carbonate ions exchanged through transporters are responsible for the high alkalinity. All ALP attached to the outer layer of the plasma membrane through the glycosylphosphatidylinositol (GPI) anchor. The enzymes that are anchored to the membrane tend to accumulate to form tetrameric clusters.

Additionally, the membrane can generate the ALP, which in turn flows anchorless in a dimeric and plasmasoluble form. This process is more efficient in TNAPs than in IAP or PLAP. The release of TNAP takes place in two ways. The processes are further illustrated in figure 1.9, which shows how the GPI anchor of the ALP is split from the surface of the membrane by phospholipase C (PLC). The ALP and the GPI anchor, which was initially an intact structure linking insoluble membrane vesicles, can break away from the cell [54]. In this case, the anchor is split by the circulation of phospholipase D (PLD) to obtain soluble ALP. However, some ALP may fail to dissolve, leading to inflammatory liver diseases. It has been found that ALP is affected by Ca²⁺ concentration [55]–[57]. Furthermore, the functional and molecular representation of calcium channels that are voltage-operated can be understood better using RT-PCR and patch-clamp methods [58]–[60]. These ion channels allow for significant detection of changes in the concentration of ALP.

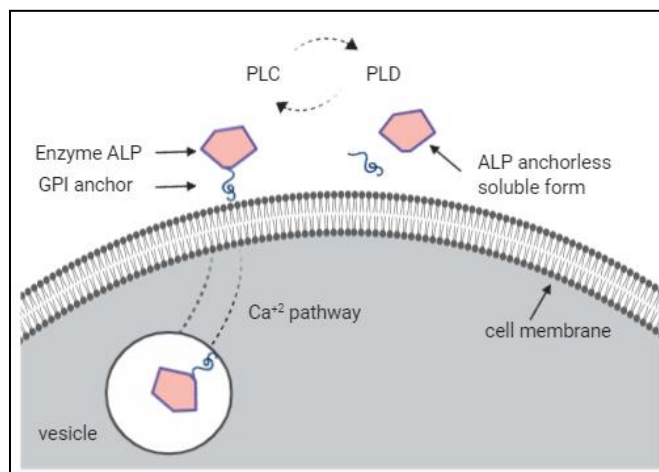


Figure 0.9: mechanism of ALP release

Another organelle that is located far away from the nucleus is the Golgi body or Golgi apparatus [47], [51]. This organelle manufactures, stores and transports products from the endoplasmic reticulum. The Golgi apparatus also takes part in the removal and addition of sugars, which are linked to proteins, such as glycoprotein. The removal and addition of sugar change the glycoprotein into glycosylation, which is more stable and does not fold.

Another vital organelle in the cell is the centriole [47], [51]. This organelle floats in the cytoplasm, and its main function is to separate the chromosomes during cell division. Finally, cytoplasm, a jelly-like substance, is a major organelle in which organelles are suspended. Many processes, such as protein synthesis and respiration, take place on this organelle. The cytoplasm also dissolves some substances, while moving others.

1.7.2.2 Cellular membrane

Cellular membranes are made from long, fatty chain molecules that contain charged phosphates, making one end of the chain soluble in water. The molecules further form two layers when the two ends of a molecule come together. Consequently, the inner layer is fatty, while the outer layer charges electrically when it comes into contact with water [61]. This is illustrated in figure 1.10 below. The layer is about 7.5 nm, and it can fold to form a shell that can contain water. This is how a cellular membrane is basically formed. The two layers and their features enable the cellular membrane to survive in a watery environment, and at the same time maintain an independent intracellular cytoplasm. However, one implication of the double layer is that it does not contain much strength. Nevertheless, the interspersed cholesterol molecules offer some rigidity to the membrane, as shown in figure 1.10. Most of the stability in the cellular membrane, however, comes from the network of proteins surrounding the cell internally and externally. The proteins give the cell its shape and enables it to control its movement, transportation, and adhesion.

The main macromolecules in the cell are essentially the proteins, and they serve various cellular functions. They constitute about 50% of the cellular membrane mass. Proteins can be broadly categorized into integral proteins and peripheral proteins [62]. Integral protein is connected to the cell membrane, while peripheral proteins are found on the inside and outside of the cell. Moreover, integral proteins form channels for the ions. Proteins are responsible for providing structural stability to the cell membrane, transporting ions across the membrane and discarding of other unwanted substances away from the cell. Other forms of protein include: the receptor protein, whose function is to bind the hormone and neurotransmitters; enzymes proteins that catalyze the chemical reactions at the surface of the membrane; and the glycoproteins, which process antibodies and are also responsible for cellular adhesion. More attention will be given to these proteins later in the chapter. The proteins that will be discussed in detail include the one that carries substances across the membrane, those that give the cell membranes structural stability, as well as proteins responsible for adhesion. It is important to understand the functions of these proteins in order to be able to interpret pharmacological manipulation results, as well as the cellular impedance and recorded action potential.

The cellular membrane is made in a special way to assist in its functions. The most remarkable feature of the membrane is its permeability [63]. The permeability properties are further illustrated in figure 1.10. The first property of the cell membrane is that it is permeable to allow small non-polar molecules and uncharged polar molecules to pass through the membrane. Secondly, the membrane is only slightly permeable to water. Thirdly, large polar molecules are impermeable to the cell membrane. For these molecules to pass through the membrane, protein pumps can be used to harness the ATP hydrolysis energy that can be used to move ions against the electrochemical slope. The other method is by using channel proteins to form passages across the membrane, which allow water or some ions to permeate along with the chemical concentration. The large nonpolar molecules can also be made to permeate through transport proteins, which involves binding a single molecule and taking it through a conformational change.

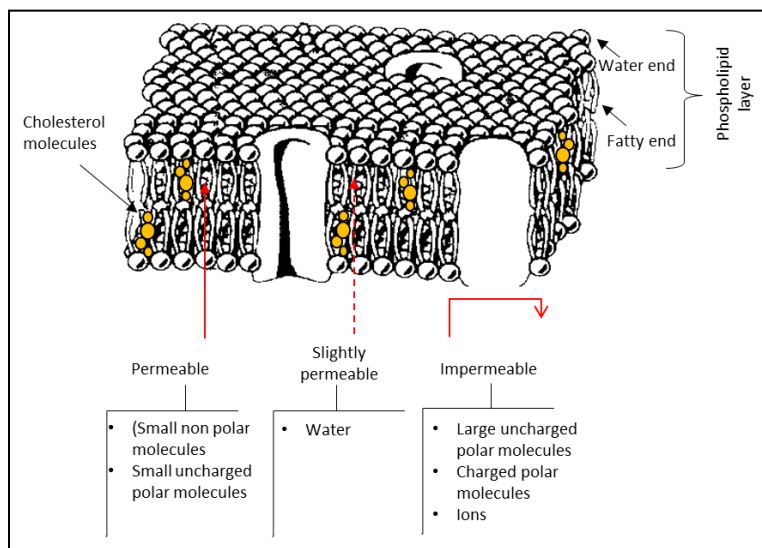


Figure 110: The cell membrane [63].

The cellular membrane separates cells from their surroundings and allows the necessary molecules and ions to permeate through the cell using integral proteins that form channels for the ions and the molecules to pass through. Structural protein also plays a vital role in determining the shape of the cell, adhesions, and movement. These functions are discussed in the next section. Thus, every protein in the cell has its purpose.

1.7.2.3 The cytoskeleton

The cytoskeleton is a type of protein that is responsible for the movement, shaping, and transportation of substances across the membrane [50]. It is cohesive in nature and contains a network of structural filaments that are broadly categorized as actin, microtubules and intermediate filaments. These filaments differ in size and chemical composition [64].

The protein actin is involved in motility [65]. This protein is versatile and available in big numbers on the cellular membrane. The functions of the protein actin are primarily based on polymerization and

depolymerization of the filaments. These two processes are used to control the motility of the cell, as well as enabling the adhesion of the cell. The actin filaments arrange themselves to form bundles and networks that form a structure that makes the cell membrane more stable. The bundles are formed when the actin filaments combine and align themselves in a parallel manner, approximately 8 nm apart. These bundles generally protrude from the surface of the cell. These protrusions form the membrane fingers known as the microvilli and the filopodia. The filopodia help the cell to attach itself to solid surfaces, while the microvilli transport nutrients and other substances in and out of the cell. The two filaments are attached at the edges of a moving cell to make the cell stable on the lower surface. As the cell moves, polymerization changes the shape of the cell to maintain its stability and enable it to move.

The actin filaments also extend to the interior of the cell membrane into the inner layer of the cell membrane [65]. The filaments spread out to form a network of loose filaments that cross one another at right angles. These filaments can be grouped into two: two-dimensional web and three-dimensional structures. The two-dimensional web is linked to the plasma membrane, while the three-dimensional filaments extend to the cytosol. In both networks and acting bundles, the filaments connect to the plasma membrane through a binding protein that secures the lower surfaces of the membrane to the cytoskeleton.

Moreover, microtubules form the largest part of the structure that supports the shape of the cellular membrane [66]. Whereas some structures are reasonably stable, others polymerize and depolymerize to form other stable shapes. Microtubules attach to chromosomes and carry them to the center of the cell poles during cell mitosis. The chromosomes divide in this position. Additionally, various microtubules interact with proteins by sliding over one another to change their shape. This interaction enables the microtubules to carry polysomes, membrane vesicles, and other cytoskeleton components across the cytoplasm. The microtubules are structured in a tubular form with a diameter of about 25 nm. Their lengths range from less than a micrometer to over a hundred micrometers. These structures are long and stand alone in the cytosol. Contrary to the actin filament, they do not form dimensional crisscrossing dimensional networks [65].

Finally, the intermediate filaments lie in the middles of the actin filaments and microtubules, based on the size. Their size is 10nm in diameter, giving them a centrally position relative to the actin filaments that have a diameter of 8nm, and the microtubule, whose diameter is 25nm. Intermediate filament extends to the cytosol and attaches to one end of the membrane. They are responsible for strengthening the plasma membrane as the cell changes shape during migration [64], [65].

1.7.2.4 Extracellular matrix

The extracellular matrix refers to the collection of wide range of proteins such as glycoproteins, and proteoglycans (complexes of polysaccharides and proteins) that surround the cell membrane [67]. (Proteoglycans are complex proteins and polysaccharides, while glycoproteins are connected to carbohydrate chains). Extracellular matrix composition varies with the type of cell and tissue, as well as the cultural condition. However, most of the components are found in the cell culture medium that contains serum.

Moreover, the extracellular matrix links the cells *in vivo* and enables them to be fixed on the *vitro* surfaces. It also exerts some control over the shape of the cell by controlling the cell attachment in the underlying cell culture. Generally, cells are flat when they are attached to a surface and spherical when floating on a liquid [67]. The extracellular matrix alters the shape of the underlying side of the cell culture by changing the pattern of the self-assembled monolayers and connecting the ECM to the surface, thus controlling the cell attachment. Hence, the shape of cells can be controlled by changing the extracellular matrix. For example, they can be made into various shapes, such as oval or squares. Their direct life and death can also be controlled.

Extracellular matrix can build link between cell membrane and the surrounded area of the cell culture. Therefore, it is important to understand the adhesion mechanism of this process, which is usually interpreted and recorded by impedance data acquired with the extracellular electrode. This is further described in section (1.9.2.1).

When a cell rests on a solid surface, adhesion may occur [68]. It is important to note the specific points where the adhesion occurs. These points are referred to as adhesion plaques, or focal contacts. The formation of focal contacts depends on fibronectin and vitronectin proteins that are present in the culture media containing serum. The two proteins form part of the extracellular matrix. Fibronectin and vitronectin proteins attach to the culture surface in a specific sequence recognized by integrin (cell surface receptors).

Understanding cell properties is important in different fields, such as metabolic studies, drug toxicity, mutagenesis, and carcinogenesis. The properties can also be examined and used in screening drugs and developing biological substances in the large-scale manufacture of drugs. The major benefit of using cell culture techniques is that it can give consistent and reproducible results that are reliable. The next section will discuss in detail the cell culture techniques of mammalian cells, as this is the sample used in this thesis.

1.8 Cell culture system

1.8.1 Important

Cell culture is a valuable technique, as a biological platform. It enable scientists to develop novel molecules for the intracellular detection application. In addition, high speeds of resolution, low cost, the mimicking of the human body and ethical issues play a major role [69]. Moreover, cell culture is an essential tool in cell and molecular biology [70]. It provides an exceptional model to study cell physiology and biochemistry. This technique passed through many steps to see the light from the turn of the 20th century to the 1930s. Alexis Carrel in 1912 enlight the idea of transplantations [71]. The efforts done to make this idea applicable always fail. However. In the 1950s, protocols of cell culture were eventually developed and led to the production of the first lines of immortalized cells. Those protocols are still recorded and developed. More details are given below with respect to the mammalian cell culture conditions.

1.8.2 Definition

Cell culture is an *in vitro* routine technique [72]. Cell culturing technique can be defined as the extraction of cells from their original environment (e.g., biological organ) and making them grow in an artificial environment. [73]. The cells could be obtained from living tissues from an organism, or they could be extracted using enzymes in a process known as disaggregation. They could also be extracted from an already developed cell line. A primary culture is the first culture where cells are grown after isolation from an organism [74]. After the cells have filled up the medium in which they grow and are consequently subcultured, they are then referred to as a cell line or sub-clones.

Cell lines from primary cultures have a limited lifespan, making them finite cell lines. The loss of the ability to further proliferate is determined genetically by an event known as senescence. Some cell lines, however, are immortal. This is due to a process known as transformation, which occurs spontaneously, or can be induced chemically or using viruses. A cell line that has the ability to divide indefinitely, or finite cells that have this ability conferred upon them, are known as a continuous cell line. Continuous cell lines are sometime called transformed cells.

1.8.3 Cell division

Cell division is important for the renewal of cells in the body, proliferation, and reproduction. This occurs under the so-called life cell cycle. Figure 1.11 displays the four main phases the cell undergoes in its life cycle [75]. The cell stops in the preliminary phase (G0) for at least 12 hours in order for chemical components and protein to produce for the cell cycle. The cell then goes into the longest phase (interphase) where it goes through three stages: growth phase (G1), growth and duplication phase (S), and growth and preparation of division cell phase (G2). The final phase (cytokinesis phase) comes after the separation phase (Mitotic phase), which has four internal stages (prophase, metaphase, anaphase and telophase) [72]. M phase has two processes: mitosis and cytokinesis. The former responsible for dividing nucleus of the cell, whereas the latter responsible for dividing cytoplasm of the cells, all of which are beyond forming two new cells [76]. When the cell completes a phase it properly enters the following phase. When cells stops dividing that means it is in the quiescence called G0 phase.

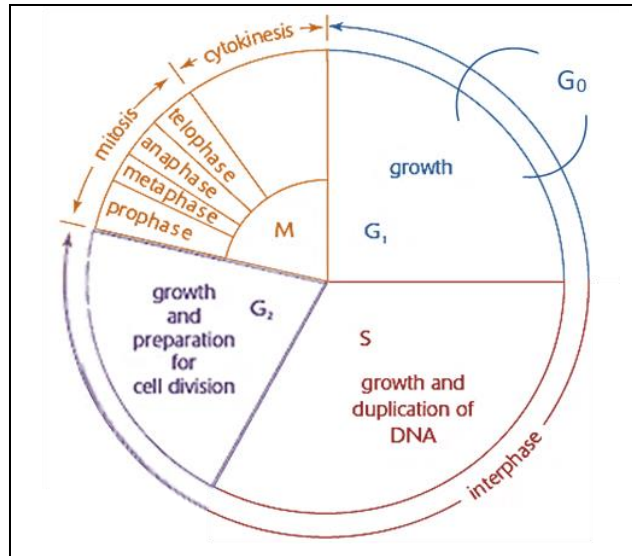


Figure 0.11: The cell life cycle [76].

1.8.4 Culture types

There are two main culture types: adherent cell culture and suspension cell culture [72]. The culture type depends on the cell type, e.g., lymphocytes prefer suspension type, whereas fibroblasts prefer attachment type. The adhesion process depends on the extracellular matrix (ECM) of cells and proteins in serum to adsorb on the artificial substrate (polystyrene). Protein adsorption occurs within seconds through intermolecular attraction forces between the protein and the material of the substrate [77], [78]. The exciting of function groups like carbonyl or amine groups can increase the hydrophilicity, which is preferable for cells adhesion. Notably, the adsorption continues for days, until cell-adhesive ligand removed from the surface degrade or foul due to secreted molecules. Therefore, the polystyrene undergoes many treatments in order to be suitable for long time cell adhesion [79]–[81]

A further advantage of polystyrene is that it is light transparent. This facilitates the easy identification of cells' health morphologies. Morphologies of adhesion cells can be categorized into three groups based on display under a microscope. Fibroblastic cells have a bipolar or multipolar morphology. They have an elongated shape and usually grow attached to a substrate. Epithelial cells have regular dimensions, or a polygonal morphology. Lymphoblast cells have a spherical shape and often grow in suspensions.

1.8.5 Culture condition

Culture condition varies with the specific cell type. However, the *in vitro* environment where cells are invariably cultured often involves an appropriate vessel containing a culture medium that provides vital nutrients needed by the cell type. Growth factors, as well as hormones, are also incorporated in the medium. Specific gases are also provided for microorganisms to grow, including oxygen or carbon (IV) oxide [74]. A regulated physicochemical environment is provided to microorganisms to support their growth. This includes optimum pH, osmotic pressure, and temperature. In the event of surplus cells resulting from sub-culturing, the cells are preserved with an appropriate protecting agent, such as DMSO

or glucerol, and stored at very low temperatures of about -130°C until they are needed for sub-culturing again [82]. This is known as cryopreservation. During cell sub-culturing, a laminar air and flow cabinet is used in order to passage cells in aseptic manner. The Class II safety cabinet can protect the biologist and sample. This simply occurs by withdrawing the surrounded air into the hood through holes made in the surface and then passing sterilized air for the sample. Moreover it has a UV lamp that is used to sterilize the surfaces before and after each passage process. This can also reduce the contamination during experiments. In this section more details on media and buffer system are outlined.

1.8.5.1 Culture media

A cell line of mammalian origin requires amino acids, source of vitamins and metal ions, as well as an energy source, which is normally provided in media [83]. Cells also need another growth factors like proteins, lipids, and carbohydrates, which can be found in serum. Researchers developed simple media like Eagle's basal medium (BME) that included different concentration of amino acid [84]. Later, BME media had their concentrations modified and named as Eagle's minimum essential medium (MEM). MEM underwent another modification by Dulbecco (1959) and therefore named as Dulbecco's minimum essential medium (DMEM). Another media nominated as the name of its inventor "McCoy" has been also developed. McCoy media is the basic of the RPMI 1640 media, which is a reference name of the place where this media was developed "Roswell Park Memorial Institute". RPMI-1640 is used mostly for suspension cells. A more complex medium may be required when there is a need to express a special function. Information about an appropriate medium for a specific cell line can be easily be found in the literature or in cell banks. Investigators can test various media where information is not provided. For example, Eagle's minimum essential medium (EMEM) is modified with sodium pyruvate. This is used mostly to reduce the effect of sodium bicarbonate (NaHCO_3 , 1.5 g/L) normally provided in media.

Serum, on the other hand, has been provided to growth media of concentrations ranging from 5% to 20% [84]. Serum has different types depending on the effective of the growth factors contained. They are fetal bovine serum (FBS) and Newborn calf serum (NBCS). The former is favorable in cancer cells, which are known as fast consuming media. Whereas the latter is used for normal cells.

1.8.5.2 Buffering system

Mammalian cells can grow in neutral pH 7.2-7.4, which is maintained by buffers like sodium bicarbonate [85] 4-(2-hydroxyethyl)-1-piperazineethanesulfonic acid (HEPES). When adding the sodium bicarbonate buffer to the media in the presence of the CO_2 of the incubator and the CO_2 of the cells, this allow balancing the ratio of bicarbonate/ carbonic acid. HEPES can maintain the physiological pH of the cells culture when the culture is in need for long time outside the incubator [83]. At a normal pH, most of the zwitterion ions contain negative anions and positive cations at the same time. Zwitterion ions can provide good buffer solutions, as they resist the change in the pH value of the solution. In the presence of acids, the double ions receive hydrogen ions, but in the case of a base, they give hydrogen ions and thus balance the pH value.

Chapter 1

Phenol red is added to the media as a pH indicator. It has orange-red color in natural pH. The change of color to yellow occur due to the losing of one proton and that indicates low pH. The change of color to fuchsia occur due to the losing of two protons and that indicates high pH [85]. Figure 1.12 shows the change of red phenol over a range of pH. A fall in pH in the growth medium shows a build-up of lactic acid, which is a metabolic by-product. Lactic acid inhibits cell growth since it is toxic to cells. The rate of change in pH is dependent on cell concentrations in the culture. The high cell concentration, the low pH. The desired temperature of mammalian cells is 37 °C, which is maintained by the incubator temperature system.

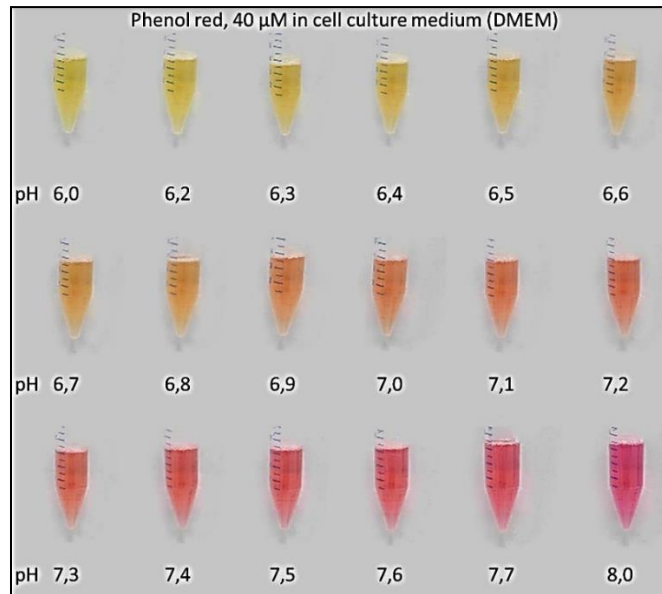


Figure 0.12: The change of red phenol over range of pH [86].

1.8.6 Culture techniques

1.8.6.1 Subculture

Over time cells can proliferate and reach 100% confluence, which makes no space for growing. This exhausts media nutrients, and that cause cells to die. Moreover, the containers (e.g., polystyrene) lose their efficiency and cause cell-adhesive ligand remove from the surface. Therefore, passing cells to another substrate is important. This passing process is called subculture [87]. Figure 1.13 describes the subculture process. Cells are washed twice with Hanks' balanced salts solution (HBSS) and detached by adding trypsin. HBSS is used when cells are exposed to atmospheric conditions and keeps their pH constant. Trypsin is an enzyme, which break down proteins that are responsible for cells adhesion. Trypsin should be incubated with cells for about 5-20 minutes, and then it should be inactivated by adding media to it that has serum. Serum has divalent cations calcium and magnesium that inactive trypsin. The mixture is then transferred into a tube for centrifugation. The supernatant is discarded, and the cells are mixed with fresh media. A portion of this mixture can be taken and added to a new container filled up with the desired volume of fresh media (10% serum). The new container then is incubated to allow cells to attach again.

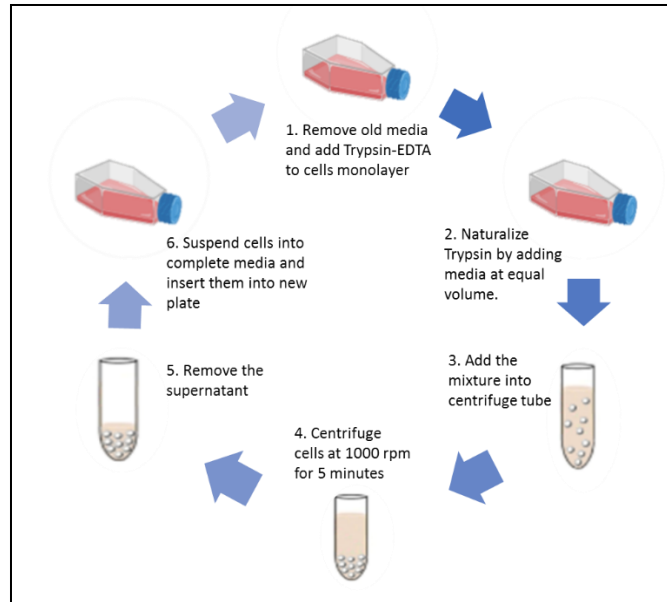


Figure 1.13: sub culturing techniques [87].

1.8.6.2 Seeding

Seeding density is one factor that can affect cell growth, because proliferating ability of cells are different. There are cells need either high or low initial density for proliferate. Therefore, it is important to pay attention to the working area. Multi-well plates have different working areas, so optimizing the desired density of cells is recommended. Moreover, plating techniques are always taken into account in order to reduce errors of cell confluence in multi-well plates. For example, seeding cells in the middle wells of the multi-well plate is a good technique [88]. Media evaporates faster from cells that grow in the edge wells than those in the middle wells. These errors can also be limited by applying autoclaved water to the edge wells, as shown in figure 1.14.

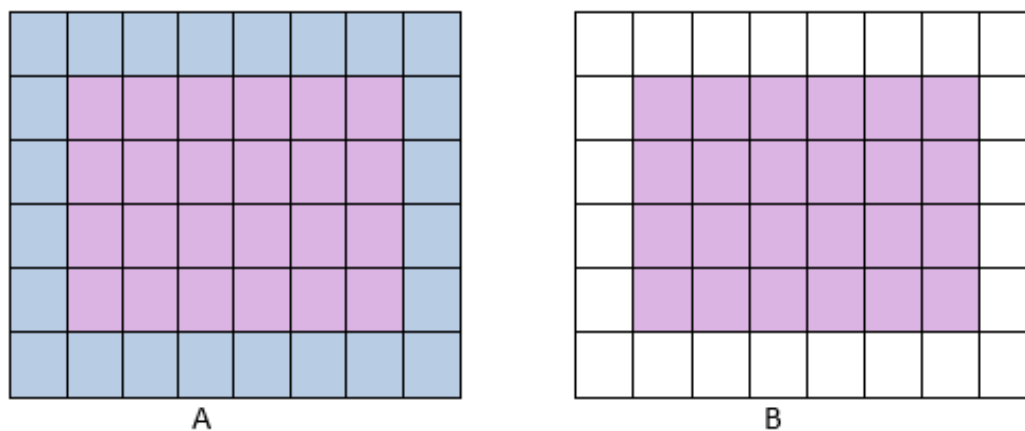


Figure 1.14: Schematic of 48-well plate; A the treatment edge and B non-treatment edge. Blue is autoclaved water and pink is the media [88].

1.8.6.3 Growth phase

Cell growth in a culture follows the various growth stages of the lag phase, where there is little growth, the log phase, where there is an exponential growth, and the stationary phase, where growth rate equals death rate (as shown in figure 1.15) [89]. Cell growth ceases when there is no more room for cells to proliferate. Cells should be subcultured before they reach confluence, specifically during the log phase. In this stage cells highly consume the nutrients in the media. Cells cultured at this stage take longer than normal to recover when they are seeded. Cells in a suspension are also passaged during the log phase. When cells in a suspension reach confluence, they clump together in the suspension, which appears turbid when shaken. Cancer cells are less sensitive to contact inhibitive growth. They can grow even after reaching the confluence stage and forming multilayers.

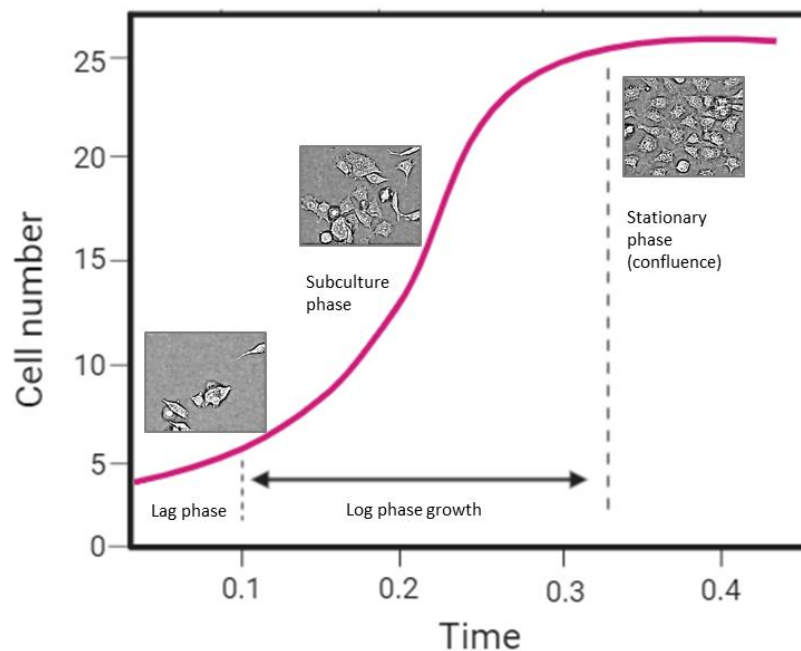


Figure 0.15: Typical curve of cell growth [90].

1.8.7 Cell lines:

Cancer is an urgent global challenge, as it causes one quarter of deaths worldwide. Statistics from 2019, show that lung, breast, and colorectal cancers rank first in terms of incidence [91]. Lung, colorectal cancer occupies first place in mortality, while breast cancer has moved to fifth place, according to the figure 1.16.

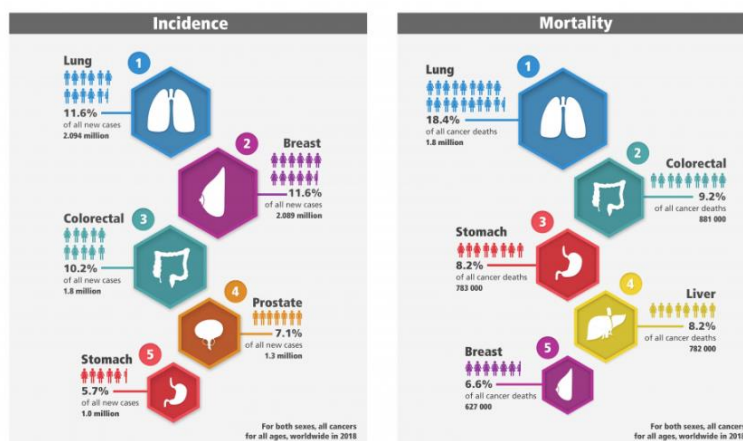


Figure 0.16: Statistics of cancer first ranked due to incidence or mortality [91].

Optimizing media and serum as described earlier, and the addition of hormones and growth factors leads to stable growth cell lines that are able to simulate cancer *in vivo* [73]. This section discusses the embryo cells lines that represent fibroblastic tissue type and cancer cells lines that represent epithelial tissue type, which are of interest in this thesis.

Fibroblastic cells usually display a round morphology at the lag phase and a spindle shape. Fibroblastic cells normally reach the inhibitive contact faster and then fail to continue to grow. Therefore, at confluence phase, they get smaller to maintain their nutrition and stop growing. An example of these cells is embryo cells lines involving Balb 3T3 and NIH 3T3 mouse embryonic fibroblast cells lines and Chinese Hamster Ovary (CHO) cell lines.

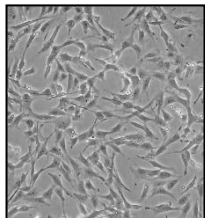
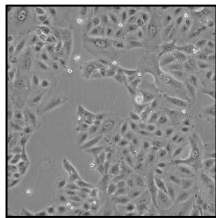
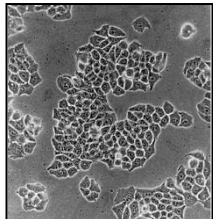
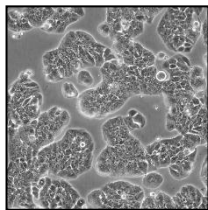
Cancer epithelial cells are extended and distributed over the surface. They have round morphology in the lag phase and are then shaped as polygonal. Epithelial cells are less sensitive to inhibitive growth contact than Fibroblastic cells. Therefore, some of them are more likely to grow in multilayers. Cancer cells are epithelial cells lines. For example, A549, Ht-29 and MCF-7 represent lung cancer, colon cancer and breast cells respectively.

Embryo cells are extensively studied and preferred as they are easy tools for repeated studies [92]. They have adhesion properties similar to those in cancer cells. Also, they have the same mechanism of movements as the cancer cells. These common properties allow them to invade and metastasise. Some enzymes can be secreted from cancer cells, causing collapse of cell-cell or ECM-cell conjugated proteins. Example of these enzyme are the matrix metalloproteinases (MMPs).

Several studies found a connection between alkaline phosphatase and lung [93]–[95] breast [96]–[98] and colon cancer [99], [100]. These studies evaluated the presence of ALP in the serum of patients. In the case of studying and modulating cell lines for those most common cancers, A549 [101], MCF-7 [102] and Ht-29 [103] is the common model. Cell lines usually have many chromosomal, oncogene mutations, as well as gene amplification. The right model of cell line is likely the one that retains its characteristics during many

sub-culture processes. Therefore, it is important to choose the right model when conducting experiments. In this thesis, A549, MCF-7 and Ht-29 were chosen. A549 [94], has a high publication, with approximately 22,000 more than other lung cell lines [104] MCF-7 [105] also has higher publication than other breast cell lines [106], [107] of about 28,000. Publication studies using the Ht-29 of colon cancer cell lines [108], [109] were estimated by 7200. These cells keep their phenotypic properties, which make them optimal models for cancer investigation. Table 1.1 shows typical microscope images, characteristics and population doubling time of attached cells lines.

Table 1.1: Microscope picture of attached cells lines and their characteristics and their tissue type.

Name	Microscope photo	Characteristics	Tissue type	Ref.
Balb/c 3T3		This cell line was isolated from disaggregated 14- to 17-day-old BALB/c mouse embryos. It needs about 24 hour's population doubling time.	Fibroblastic	[110]
A549		This cell line was isolated from a 58-year-old Caucasian male. It needs about 22 hour's population doubling time.	Epithelial	[111]
MCF-7		The cell line was isolated from a 69-year-old Caucasian female. It needs about 29 hour's population doubling time	Epithelial	[112]
Ht-29		The cell line was isolated From 44-year-old Caucasian Female. It needs about 23-30 hours population doubling time	Epithelial	[113]

The live cell assays began to develop in the 1950s when immortalized cell line was established. It was used cytotoxicity assay. This endpoint assay allows for the monitoring of other end points, such as viability assay (live cells). More details are discussed in the following sections in terms of cell viability assays that of interest to this thesis.

1.9 Viability assay

For viability assay, it is useful to look at biological activity of cells (e.g., metabolic activity). The activity of cells can tell more about the cells. This section discusses the main metabolic assays, with particular focus on the resazurin reduction, the assay of this thesis. Metabolic assays can show the viability of cells, but they are limited in terms of analysis of cell physiology. Therefore, the impedance assay was purposed and discussed more in the second section. Impedance detection technique can monitor the tiny change in the cellular membrane by electrical property [114]. This is the technique of interest in this thesis.

1.9.1 Metabolic based assay

Metabolic assay exploits the function of mitochondrial respiratory chain in live cells, as explained in section (1.7.2.1). Reduction of all the oxidized salts provided is believed to be accomplished by reductase or diaphorase-type enzymes. These are assays that rely on cellular metabolism to distinguish viable from nonviable cells. Optical methods, such as colorimetric, fluorescent and bioluminescent, are exploited in determination viable cells based on metabolic activity. Those methods can estimate number of cells when optimizing the assay. The colorimetric assay involves tetrazolium compound (MTT), which converts to a purple color product called formazan. MTT assay has widespread uses in most academic labs, as shown by numerous publications [115]. However, the product is not soluble in water, causing incomplete solubilisation. Therefore, an additional step to solubilize the crystalline precipitate before taking the absorbency rate is developed and forms tetrazolium salts (XTT, MTS, WST-1, WST-8). This step allows for the formation of water- soluble formazan. The pH indicator, which is mostly red-phenol, affects colorimetric assays. Bioluminescence assays involve intercellular ATP changes, which are correlated with viable cells. This assay is more reliable and sensitive than MTT. It can detect as few as 10 cells/well, which makes it useful for low-density populations. However, it requires cell lysis, which ends the assay and limits multiplexing. Fluorescent assay involves Acetoxymethyl ester of calcein (calcein-AM). The esterases inside cells convert calcein AM into green fluorescent dateable agent in case of alive cells and into red fluorescent agent in case of not alive cells. This assay is not affected by the pH indicator of media. However, it is highly toxic to some cells. Resazurin reduction assay allows fluorescent and colorimetric assays and is simpler, because it eliminates the solubilisation steps required in the previous method as well as providing reproducible signals, allowing multiplexing assay. The blue salts called resazurin convert to a pink resorufin and allow fluorescent signal. The next section focuses on resazurin reduction assay, as it is part of this thesis.

1.9.1.1 Resazurin Reduction Assay

This is a cell permeable redox indicator that helps in tracking the number of viable cells [116]. Physiological buffers can absorb resazurin, resulting in a color change to a deep blue solution. The solution is added to cells in a culture. Living and viable cells have an active metabolism and can, therefore, reduce the blue resazurin into a pink fluorescent solution in irreversible reaction. Figure 1.17 shows color changes. For highly active cells, and probably higher density population of cells, the pink fluorescent color starts to shade and converts to the corresponding colorless dihydroresorufin in a reversible reaction. Cakir et al (2010) purposed the mechanism of resazurin reduction [117]. They believed that resazurin has the N-O bond separated and allow resorufin compound to produce. Whereas the resorufin converted to dihydroresorufin due to the electron-coupled proton transfer reaction according to the following diagram (figure 1.17). The fluorescent signal of resorufin is between λ_{ex} of 530 nm and λ_{em} of 590 nm.

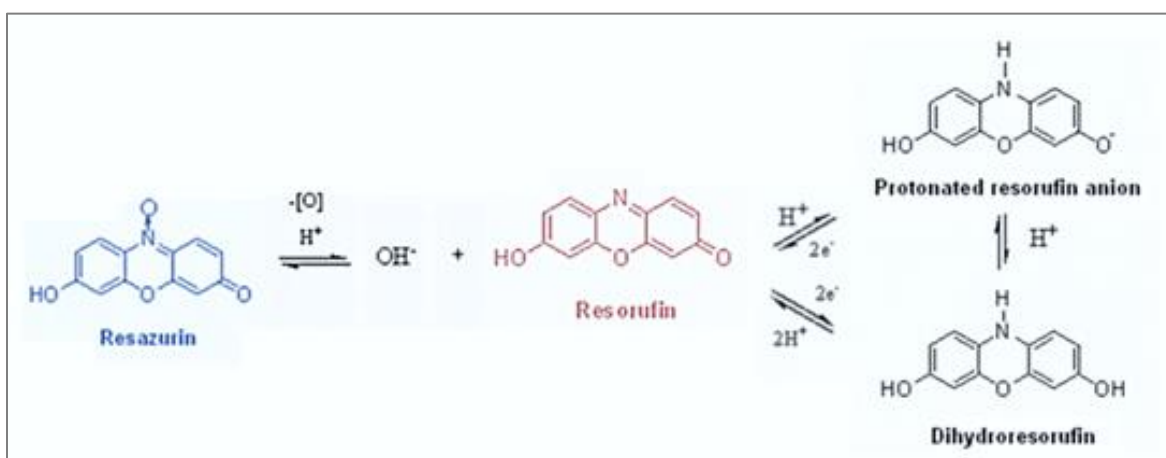


Figure 0.17: The reversible reaction of resazurin and the irreversible reaction of resorufin [117].

Resazurin assay allows for a linear relationship between the degree of color change and the number of viable cells. This proportional relationship only reflects the activity of cells, rather than the number of cells. This correlation permits simplifying resazurin assay to estimate cell number. Three main parameters, involving concentration of the dye used, time of incubation, and the density of cells population, are used for a linearity trend. Figure 1.18 shows a scheme representing an optimization protocol of *in vitro* cytotoxicity assay. Exposure of cells to resazurin reduces ATP, thus bringing about a cytotoxic effect. It is then that the concentration of resazurin should not exceed 800 μM . Incubation time is important to achieve adequate fluorescence. However, this is often dependent on the cell type, the cell density and the culture medium used. The incubation period should be put at a minimum to prevent reagent toxicity; however, it should be long enough to provide adequate sensitivity. Moreover, the method allows for multiplexing [118]. Care must be taken when doing multiplexing to avoid direct chemical interference.

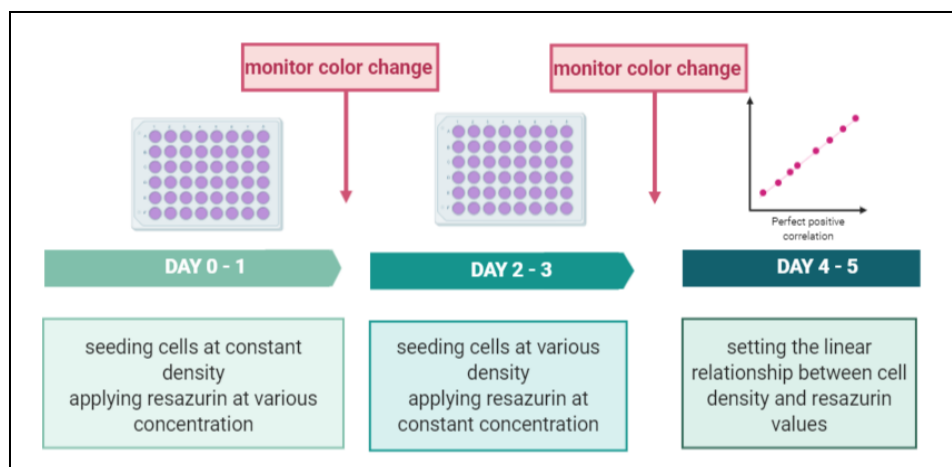


Figure 0.18: Generalized scheme representing an optimization protocol of in vitro cytotoxicity assay.

This assay can promise linearity with a low percent of coefficient variance (CV %). The fourth dimension parameter is the size of working area. This is important for 96-well, 384-well or 1536-well microplates, which can facilitate high throughput screening (HTS) applications [119]. The results of HTS make it easier to understand the initial reaction on a wide scan of samples and provide starting points for drug design. This sort of screening is further expanded to analyse physiological properties of samples (cells) by integrate microtiter with a device consisting of three layers: the substrate, the conducting layer and the insulating passivation layer (which is the cells in this integration). This device is called a microelectrode array (MEA) and is covered solely in section (1.10.2). This combination can define a cellular phenotype resulting from drug treatment. The following section discusses in details impedance-based assays.

1.9.2 Impedance based assay

1.9.2.1 Mechanism of cell adhesion

Three main forces affect initial cell adhesion; electrostatic, electrodynamic and steric stabilization. The first force is getting weak due to the presence of ions in the media. The second force allows the initial interaction. The third force retains a distance between cell membrane and substrate due to the presence the polymer molecules in cell membrane that works as of strict compression and the opposite direction force occurred by the osmotic pressure of water all of which forms steric effects. These forces however are only responsible for the initial adhesion, which called nonspecific forces. The specific forces are the one beyond actual cell adhesion on surfaces [120]. The later force depends on components of the media and serum to allow interaction with proteins presented in the extracellular matrix. Those proteins help in creating focal points with the cytoskeleton proteins like actin and tubulin filaments. The specific forces are responsible of proliferation, shape and attachment of cells [120].

Actin filaments and microtubule proteins contain motor proteins that move along the cytoplasm. They also convert chemical energy to mechanical energy by ATP hydrolysis. The action of mechanical energy depends on the motor protein present. Based on the motor protein type, the mechanical energy can either make the actin filament contract, act as a carrier during movement, or connect the actin filaments

to the cellular membrane. Motor proteins contain a head and tail to allow for linkage. The head and the tail allow them to link to organelles and move along the microtubules. The movement is also made possible by the polymerization and depolymerization processes [121].

When the cells are migrating, they extend the leading edge to create micro-spikes and lamellipodia that enables the cell to attach itself to the underlying solid surface. They also allow the rear side of the cell to contract as a result of the extension. The extension forms focal contacts that act as anchorage points. As the cell attaches to the substrate, the actin filaments change their shape through polymerization, and, in turn, they bind to cell-surface receptors that connect the cell's cytoskeleton to the extracellular matrix. This process exerts hydraulic pressure, which pushes the cytoplasm forward to the foremost part of the cell. As this takes place, the membrane continues to move along with the acting filament. As the process continues, the previous focal contacts for the leading edge continue acting as the anchorage point for the lower side of the cell. With time, the focal points are released [120].

In the case of adhesion, the membrane of an attached cell can tell a lot about its vital information (as seen in sections 1.7.2) whose part components are connected homogeneously and form a complex physiological state. These tiny physiological movements and adhesion can be detected through a technique known as electrochemical impedance spectroscopy (EIS), which senses the adsorption of matters. The next section covers the properties of cells that are exploited and applied in EIS, thus monitoring cell viability parameters.

1.9.2.2 Dielectric properties of cells membrane

First of all, the dielectric properties of a material is the ability of a material to allow current passes through it while the material itself is not electrically conductive. This type of material is called non-conductive materials. They have electrons that are not free to move as they are in the conductive metals, but rather tend to polarize if an electric field is directed on them, and in this case, they are called a capacitor. The electrons are directed to one end of the capacitor (forming a negative pole) while the positive electric charge increases at the opposite end (forming a positive pole) - and this is the meaning of the material's polarization. The cell membrane also acts as capacitor. That can be seen during the ion channel functions. The charged ions go either inside or outside the cells through its membrane, allow accumulation of charges between interfaces with different dielectric properties. Each cell has different dielectric properties due to its components and size [122]. When using cell membrane in electrical cells, its capacitance will dominate on the system. This is because cell membranes have extremely low conductivity, which is considerably less than that of the cytoplasm and the external medium [123], [124].

The dielectric properties of cells and biological tissues are frequency dependent as well. The conductivity of cellular structures increases with frequency, leading to less charge accumulation. This change in cellular permittivity and conductivity takes place through a series of steps known as frequency dispersions [124]–[126]. Table 1.2 show the main dispersion regions: α -, β - and γ -dispersions corresponding to correlating the biological events. The α -dispersion region occurs due to ionic diffusion, the β -dispersion occurs due to the change in interfacial polarization of the cellular plasma membranes, and the γ -dispersion occurs due to the presence of the water [127], [128].

Table 1.2: summarizes the main dispersion regions: α -, β - and γ -dispersions corresponding to correlated biological events.

dispersion regions	Frequency range	Biological event
α -dispersion	centered at about 100 Hz	The counter-ion cloud surrounding the surface of the cellular membrane becomes polarized, resulting in change at this region.
β -dispersion	10 kHz-10 MHz	Cellular membranes become electrically charged (through intra- and extra-cellular pathways) causing change in this region.
γ -dispersion	centered at about 10 GHz	The dispersive behavior of water causes the measured permittivity to change at this region.

1.9.2.3 Electrical Impedance Spectroscopy (EIS)

EIS is an electrochemical technique originally used for corrosion studies and coating evaluations. However, it has been recently widely used in biotechnology, cell culture monitoring and disease modelling [123], [129] Impedance spectroscopy is based on applying an AC excitation signal and measuring the complex impedance, Z , of a system [130]. The measurements are scanned through a range of frequencies to define the impedance spectrum, hence the term spectroscopy [131]. The excitation current or voltage signal is normally very small, allowing for a non-invasive measurement, which is the main reason behind the wide use of impedance spectroscopy in biological applications [132][133].

The EIS can determine both the resistive and capacitive (dielectric) properties of cells, as the membrane works as an insulator (capacitance), and ion channels leak some ions thereby charges increase and then cause conductance. Changes in membrane resistance due to the opening of channels should not significantly alter the capacitance of the measured impedance, since the channel density is relatively low.

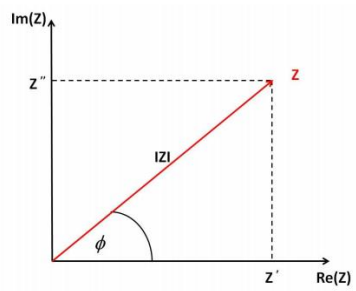
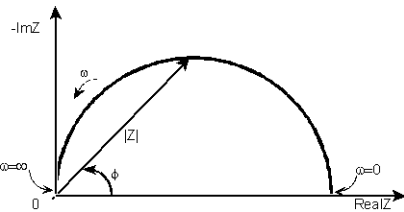
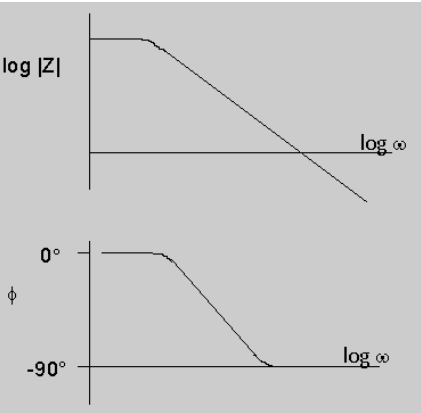
The measured complex impedance represents the ratio between voltage $V(t)$ and current $I(t)$, which are applied as a function of time. The angular frequency ($\omega=2\pi f$) and the phase (ϕ) are shifted between the voltage and the current. This is measured by the unit of impedance or resistance (ohm) and represented in the following equation [131].

$$Z = \frac{V(t)}{I(t)} = \frac{V_o \sin(\omega t)}{I_o \sin(\omega t - \phi)} \quad (\Omega)$$

The voltage and current are only in phase if the system is purely resistive. However, for cellular assays this is usually not the case, as the cell capacitive properties will cause a phase shift between the applied

voltage and measured current. Since cellular dielectric properties depend on frequency, a spectrum of impedances measured at different frequencies would provide more information on cell properties than single frequency measurements [131]. Basic plots to present impedance values are shown in the table 1.3. Complex impedance Z , the simplest, Nyquist plots can represent the impedance of real components. However, the measurement frequencies cannot be extracted from such plots, a drawback that is overcome by Bode plots. In Bode plots, the impedance magnitude, or its phase, is plotted on the y-axis against frequency on the x-axis in logarithmic scale.

Table 0.3: Basic blots of impedance.

Blots	Typical Form	Features
complex impedance plot		The complex impedance Z can be plotted as a vector in a complex plane where the length of the impedance vector indicates the magnitude $ Z $ and the angle between the vector, and the x-axis is the phase shift ϕ .
Nyquist plot		Nyquist plots represents the impedance of real components and can be plotted on the x-axis against the imaginary component on the y-axis.
Bode plot		Bode plots represents the impedance of magnitude or its phase and can be plotted on the y-axis against frequency on the x-axis in logarithmic scale.

1.9.2.4 Electric Cell-Substrate Impedance Sensing

Electric cell-substrate impedance sensing (ECIS) is a system that allows real-time quantifying of cellular function, when cells brought onto the electrodes will work as an insulator during passing current at different time and adherent cells, which impede the flow currents, will yield information about the cells. Giaever and Keese (1984) investigated cellular behaviour by using gold microelectrodes, and they noticed the following factors, all of which make this system more sensitive: size of working area of electrodes and distance between cells and electrodes [134] [135]–[137]. The size of working electrode should be less than 1% of the counter electrode, which will achieve higher impedance for working electrodes. Current passed through an electrical circle is influenced by adherent cell confluence and leads to high impedance. However, the current discriminates three more pieces of information about cells at a particular range of frequency. Figure 1.19 illustrates the current pathways, which bring about data on cell-cell junctions, cellelectrode adhesion and the cell membrane capacitance. When applying low frequency, the current will pass underneath or in-between cells, whereas high frequency current can merge with cell membranes and produce information about their properties [138], [139]. The range of frequency can set the purpose of the study. A frequency range of 60 Hz to 64 kHz was applied to many assays including cytotoxicity, cell growth, and wound healing [140]–[145]. It was found that migration, spreading, and adhesion are being studied mostly at 4 kHz for MCF-7 [146], A549 [147] and Ht-29 [147] while more information is given for cell membranes at higher frequency [146], (taking into account the diameter of the electrodes). Enzyme secretions such as matrix metalloproteinases (MMPs) were studied on ECIS [148], [149].

When applying low frequency, the current will pass underneath or in-between cells, whereas high frequency current can merge with cell membranes and produce information about their properties [138], [139]. The range of frequency can set the purpose of the study. A frequency range of 60 Hz to 64 kHz was applied to many assays including cytotoxicity, cell growth, and wound healing [140]–[145]. It was found that migration, spreading, and adhesion are being studied mostly at 4 kHz for MCF-7 [146], A549 [147] and Ht-29 [147] while more information is given for cell membranes at higher frequency [146], (taking into account the diameter of the electrodes). Enzyme secretions such as matrix metalloproteinases (MMPs) were studied on ECIS [148], [149].

MMPs are extracellular matrix enzymes, which are responsible for cancer invasion, and mycotoxins, which cause inflammation. This investigation was conducted using a sample of fungi and cancer cell lines. ALP enzymes secretions have been investigated. Mintz et al. (2018) undertook an electrochemical impedance study and used an immunoassay approach [134]. The nanowire surface was modified by immobilizing the anti-ALP, and the results indicated that the device was highly efficient at detecting low levels of ALP in the PBS solution ranging from 0.03 to 0.3 U/L, with high selectivity due to antigen-antibody interactions. The study demonstrates the potential of relevant and rapid multiparameter impedimetric ALP assays.

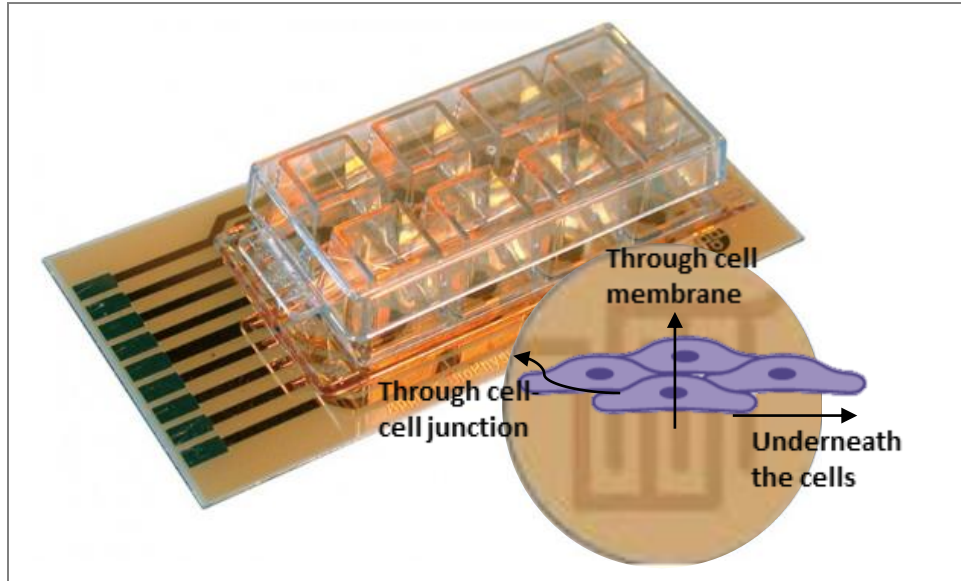


Figure 0.19: Electric cell-substrate impedance sensing (ECIS) cultureware. In the licorice representation, three pathways of the current: through cell-cell junction, underneath the cells, and through cell membrane [136].

1.10 Microarrays technology

1.10.1 History

The electrical activity of cultured cells has characteristically been researched using microwire electrodes or micropipettes. The cells that are being monitored are positioned in a dish located on the stage of a microscope. Micromanipulators are employed to place the recording electrode in the cells [150]. Figure 1.20 shows the development stages of recording electrical activity of cultured cells. Inter-cellular recording is carried out cautiously by implanting a micropipette electrode in the membrane. This method results in a fragile connection, which limits the continuous recordings that are applied for long time. The second way connecting the micropipette with the cell membrane without implantation. This method is called the whole cell patch, which prevents damage to the cells. However, it has an unsteady interface, thereby limiting the experiment duration. Consequently, researchers considered moving a micropipette or microwire and places it near to the cellular membrane. Although the indirect monitoring method may be desirable, it is restricted due to the diminished electrical activity of the cultured cells. Efforts have subsequently been made to bring cells to the sensor. Planar microelectrode collection was utilized as a substrate to the cell's culture. The simple planar microelectrode allows the monitoring of a single cell (as shown in figure 1.20). When the electrode structure is altered, it permits the monitoring of many cells, thereby enhancing the signal strength.

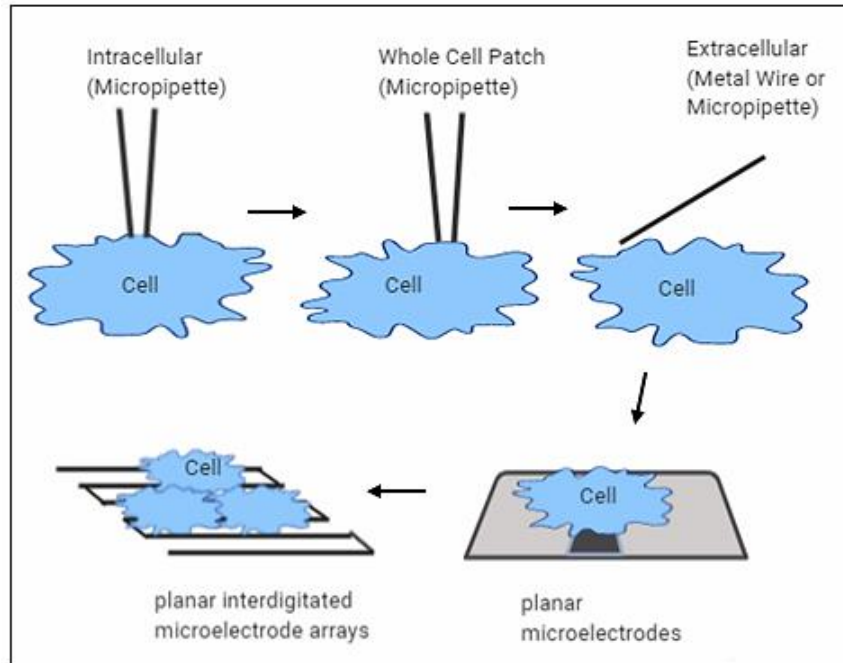


Figure 0.20: The development stages of recording electrical activity of cultured cells [150].

Biocompatibility is a significant feature when developing cells on electrodes. When biocompatible ingredients are not used in the design, the specific sensing cells may not endure the execution of the primarily required signal transduction. There are different degrees of applying biocompatibility. Protracted studies where other constituents contact living tissue require industrious efforts to control biocompatibility.

1.10.2 Microelectrode array

Microelectrode arrays (MEA) are formed from a metallic conducting layer positioned between insulating layers, the passivation, and the substrate layer. Small holes that uncover the metal in certain parts are constructed in the passivation layer to delineate the gauge microelectrodes that are connected to the biological cells. The number, design, arrangement, and size of the microelectrodes rely on the application [151], [152]

The size of the microelectrode depends on the characteristics of the cells being investigated. The sensing microelectrode size has a range of 10-30 μm of the normal cell size for a single study. In ECIS, the working electrode impedance must dominate in order to attain highly sensitive measurements. Consequently, the counter electrode impedance should be expressively smaller. This can be achieved by increasing its surface area. In addition, reducing the size of the working electrode increases the ability of the electrode to control solution resistance. [134] [153]. Keese and Giaever (1994) observed that reducing the area electrode amplifies the sensitivity of ECIS measurements [134], [139], [154]. In a study conducted by Abdur Rahman et al. (2007), an electrode with a diameter of 50 μm was established as a lower limit for microelectrode size. Non-uniform distribution of current and great interfacial capacitance occurred [155].

Capacitance, which is caused by passive electrode interconnections, decreases the sensitivity of the impedance dimensions [156]. When the thickness of the insulating layer is increased it decreases capacitive coupling between the solution and the electrode interconnections. This is because the width of the insulating layer is inversely proportional to the capacitance. Price et al. (2009) found that the ratio of lead trace area to the passivation covering thickness has a significant value of 5.5, through which the impedance influence of the coating is reduced [157]. ECIS normal 8W1E ranges have a passivated capacity of about 14 mm² and a coating width of 2 μ m. The ratio of passivation thickness to the passivation area is higher (~ 700), compared to the significant ratio stated by Price et al. Accordingly, ECIS ranges of a coating capacitive constituent must be maintained at high frequencies.

The electrical action of microelectrodes should be taken into account when making an MEA chip. Electromagnetic interference, noise, and electrode impedance and current density should be considered [151]. Breckenridge et al. (1995) observed that a minimum expanse of 100 μ m must be left between two electrodes in order to minimise signal attenuation and interference [158]. When planning interdigitated microelectrodes, the height, width, number, and spacing amid the interdigitated fingers affect the ratio of noise to signal and sensitivity of measurements. Consequently, they are to be optimized [152], [153], [159], [160]. The heat dissipation, power dissipation, and circuitry used have an impact on the appropriate working of the chip.

Microelectrode arrays may be used as an integrated array or individually addressed depending on the way microelectrodes are linked. Integrated arrays offer an average response for a cell population which is useful for certain cellular assays, e.g., cytotoxicity assays. Individually assessable MEAs are used in neural networks studies, for instance. The manner of addressing electrodes must be considered when making the MEA system.

1.10.2.1. MEA Materials

Microelectrode arrays have three layers- the substrate, insulating passivation, and conducting layers. It is significant to choose the appropriate material to get the right sensitivity and electrode performance [151], [152], [161]. The primary factor is to identify the right substrate when constructing microelectrode arrays. Typical substrates are polymers [162], [163], silicon [156][164] [165], and glass [155], [166], [167]. Silicon is the best substrate for the construction of semiconductors. It is used for MEA construction for biological uses, since it facilitates incorporation of the electronics measurement. Glass is utilized as a MEA substrate, because it is transparent, offers high insulation and temperature resistance, and is biocompatible. Polymers are transparent, biocompatible, and cheaper compared to glass. Consequently, it is used for one-use electrodes. Biocompatibility, durability, cost, availability, and low impedance are to be considered when selecting microelectrode material [151], [152], [168], [169]. Platinum [36], [170]–[172] and gold [37], [155], [178]–[182], [159], [162], [166], [173]–[177] are the most used for making electrodes since MEAs introduced in 1970s [183]. Nowadays, gold nanomaterials are being used for modifying electrode [184][185]. They have low resistance and are inert [169]. Besides, their interfacial impedance may be reduced by enhancing surface roughness. Platinum black has been used for plating gold and platinum, because it leads to diminished impedance [151][186]. Nonetheless, it lacks durability and is thus unstable. Titanium nitride (TiN) may be used to plate platinum and gold, thereby providing lesser

impedance than the naked electrode [187], [188]. In addition to platinum and gold, other electrode materials may be used [167], [189]. For instance, indium-tin-oxide may be used due to its resistance to corrosion, its high transparency, and its biocompatibility. Graphene [190], glassy carbon [191], titanium [165], rhodium [192], and iridium [193] may be used. The major factor when selecting the passivating material is the dielectric constant impacting the electrode capacitance. Similarly, dielectric strength is vital, because, when exceeded, it might cause insulation amid solution and altering the voltage. The width of the passivation layer is also significant. If it is thin it decreases voltage [186]. If it is thick it reduces coating capacitance leading to sensitive measurement. Silicon nitride [181], polyimide [36], [172], silicon dioxide [182], and photoresist [155], [167], [170], [173], [175] are the most utilized electrodes. Silicon nitride has increased impermeability to ions. It is appropriate for unbroken insulative surface coating. While silicon dioxide has effective insulating characteristics, it is not impervious to ions. Some ions may penetrate the layer of the electrode. Polymers could be utilized for passivation, because they have increased biocompatibility and enduring dielectric features.

1.10.2.2. Microelectrode Fabrication and modification

Various approaches may be employed to fabricate MEAs. Fabrication of MEAs mostly uses photolithography [194]. A photolithographic technique makes it likely to fabricate contracted nano-, as well as microelectrodes and multifaceted structures [195]. Screen-printing is cheaper and simpler compared to photolithography. In this procedure, the preferred electrodes are delineated by producing a thixotropic fluid using an accurate mesh screen or template with appropriate electrode designs in the squeegee [196]. Various ink materials are carbon nanotubes, silver, organo-gold, platinum, dielectrics, carbon, gold, and graphite [151]. Laser ablation may be used for micromachining, microelectrode fabrication, and microelectronic device production. A laser beam designs the electrode material through rapid prototyping irradiation, and the cheap manufacture of sophisticated devices and chips. Modification procedures may be utilized to produce sophisticated designs [197]. When fabrication is completed, few superficial changes are completed to increase the chip performance [169]. Electrode coating using materials such as TiN or platinum black may be employed to decrease electrode impedance and upturn the surface area [151][186]. Enhanced cell attachment is facilitated by increasing the surface coating and roughness. Electrode hydrophilicity is important due to the fact that cells do not adhere to a hydrophobic surface [194].

1.11 Summary

1.11.1 The research strategy:

ALP monitoring in clinical analysis is a routine test for diseases that include liver and bone disorders. Recently, ALP has been identified as an early biomarker of many cancers [198], [199]. It has been found that ALP is correlated with cell proliferation, differentiation, and apoptosis [200]-[206]. Real-time monitoring ensures the generation of comprehensive and reliable information about these cellular activities [207]. The common strategies used to date for expressing ALP are as follows: intoxicating cells [208]-[210]; transfection of cells [211]-[215], starvation of cells [216], [217] and inducing differentiation in cells [218]-[220]. These methods are used to trigger specific conditions for *in vitro* studies. For example,

they are used for the purpose of developing anti-cancer drugs [221], simulating diseases [222], studying the function of genes [223] and understanding the basis of cancer progress [224], [225]. The research that has been carried out in these areas helps in the early detection of cancer and, thus, in finding an effective treatment [226]. Differentiation, on the other hand, has a direct impact on point-of-care application. Differentiation has different grades from which the cancer stage can be classified [227]. The grade of differentiation depends on the quantity of biomarker release. Currently, the traditional measurements of differentiation used in clinical analysis (e.g. immunohistochemistry) are unable to keep pace with the development of biosensors and recent innovations in technology. Thus, the demand for cell-based biosensors has focused attention on the development of a methodology for the real-time monitoring of ALP release. Biosensors can sense tiny biological changes and convert these into electrical signals (chapter 1, section 1.5). These simple devices can serve to respond to increasing demands for cancer diagnosis and/or understanding of cancer. Accordingly, microelectrode arrays (MEA) are highly sensitive and can be exploited in electrochemistry. When cells grow on MEA, changes take place in electrochemical properties of MEA, including capacitance, resistance and diffusion current. The electrochemical properties can be detected by impedance-based assay. Confluent tight cells are required for cell-based impedimetric sensing (chapter 6), which depends on analysis of the electrical resistance of cells adhered to electrodes [228]. Changes between cell-cell junctions due to ion expression will reveal minor changes in the conductance. This methodology will enable the monitoring of the physiological changes in living cells and it will record them straight away, thus enabling real-time analysis. Current research has so far relied on immunoassays, including: surface plasmon resonance [229]–[232]; field-effect transistors [233]–[235]; quartz crystal microbalance [236]–[238]; and electrochemical impedance spectroscopy (EIS) [239]–[246]. Correspondingly, this thesis addresses the need to develop a methodology for ALP release without affinity approaches.

1.11.2 The research method

EIS will be exploited in this thesis to reveal the tiny physiological movements and adhesion of cells during ALP release. This will provide convenient methods for real-time analysis of ALP, so far lacking in the scientific literature. To fill this literature gap and meet the aim of this thesis, post-confluence culture was suggested as a manner of differentiation. Post-confluence culture is a way in which cells can stress and thus express biomarkers without additional chemicals [247]. Consequently, the target density of cells is optimized in order to reach the stationary phase. In this phase, cells stop proliferating, because there is no space left. This induces differentiation in cells and causes biomarker release. The experiments were designed to make the cells reach the point of contact-inhibited growth. At this point, cells stopped growing and were, therefore, nominated as a control. Cells were left in the culture for two more days to enable quantifying of ALP activity (chapter 3 and 4). Cell viability assay was used to ensure cell adhesion. To measure the applicability of this experiment, the statistical analysis of z-factor and the p-value was recommended in order to test the excellency of the assay and to test the significant differences between the assay and the control. The cell lines suggested for monitoring ALP release included Balb/c 3T3, MCF-7, A549, and Ht-29. The Balb/c 3T3 cells, which are an embryonic cell line, are important in simulating cancer cells [248], [249]. Cancer cells of A549, MCF-7, and Ht-29 are used as models of the top three cancers diagnosed worldwide. These are: lung (13%), breast (11%), and colon (10%), respectively [250].

1.11.3 The research techniques

1. Cell culture for maintaining samples of cells.
2. Resazurin-based assay for optimising cell density
3. Absorbance assay for optimising ALP release from cells
4. Electrochemical assay for optimizing ALP release from cells
5. Impedance assay for optimising cell adhesion during ALP release on microelectrode array

1.11.5 Future contribution

Two hypotheses relating to the future use of the developed methodology have been formulated. Firstly, the embryonic cells can be used in the investigation of gene regulation in cancer cells using the developed methodology [248]. Secondly, the embryonic cells can be transformed to simulate cancer cells. Thereafter, monitoring the converted state of cells from normal cells to malignant cells in a process called gene mutation could be performed using the developed methodology [249].

1.12 Reference

- [1] McComb, R. B.; Bowers, G. N.; Jr.; Posen, S. Alkaline Phosphatase. New York: Plenum Press. 1979.
- [2] Scriver, C. R., Beaudet, A. L., Sly, W. S., Valle, D., Childs, B., Kinzler, K. W., and Vogelstein, B., eds., The metabolic & molecular bases of inherited disease. 8th ed. New York: McGraw-Hil. 2001.
- [3] Chatterjee, R.; Mitra, A. An overview of effective therapies and recent advances in biomarkers for chronic liver diseases and associated liver cancer. *Int. Immunopharmacol* 2015, 24, 335–345.
- [4] Tartter, P. I.; Slater, G.; Gelernt, I.; Aufses, J. A. H. Screening for liver metastases from colorectal cancer with carcinoembryonic antigen and alkaline phosphatase. *Ann. Surg.* 1981, 193, 357–360.
- [5] Annibali, O.; Petrucci, M. T.; Santini, D.; Mariani, M.; Pisani, F.; Bongarzone, V.; Venditti, O.; Rago, A.; Cerchiara, E.; Fiorini, A.; Franceschini, L.; Vallone, M. L.; Felici, S.; Russano, M.; Pantano, F.; Avvisati, G. Alkaline Phosphatase (ALP) Levels in Multiple Myeloma (MM) And Cancer with Bone Lesions: Is There any Difference? *Clin. Lymphoma Myeloma Leuk.* 2015, 15, 125.
- [6] Abdallah, E. A.; Said, R. N.; Mosallam, D. S.; Moawad, E. M.; Kamal, N. M.; Fathallah, M. G. Serial serum alkaline phosphatase as an early biomarker for osteopenia of prematurity. *Medicine (Baltimore)*. 2016, 95, e483.
- [7] Balzola, F.; Bernstein, C.; Ho, G.-T.; Lees, C. Exogenous alkaline phosphatase for the treatment of patients with moderate to severe ulcerative colitis: Commentary. *Inflamm. Bowel Dis. Monit.* 2010, 11, 83.

- [8] Pickkers, P.; Heemskerk, S.; Schouten, J.; Laterre, P.-F.; Vincent, J.-L.; Beishuizen, A.; Jorens, P.G.; Spapen, H.; Bulitta, M.; Peters, W. H. M.; van der Hoeven, J. G. Alkaline phosphatase for treatment of sepsis-induced acute kidney injury: a prospective randomized double-blind placebo-controlled trial. *Crit. Care* 2012, 16.
- [9] Orsaria, M.; Londero, A. P.; Marzinotto, S.; Loreto, C. D.; Marchesoni, D.; Mariuzzi, L. Placental type alkaline phosphatase tissue expression in ovarian serous carcinoma. *Cancer Biomarkers* 2017, 17, 479–486.
- [10] D’Oronzo, S.; Brown, J.; Coleman, R. The value of biomarkers in bone metastasis. *Eur. J. Cancer Care (Engl)* 2017, 26.
- [11] Maisano, R.; Azzarello, D.; Medico, P. D.; Maisano, M.; Bottari, M.; Egitto, G.; Nardi, M. Alkaline phosphatase levels as a prognostic factor in metastatic colorectal cancer treated with the FOLFOX 4 regimen: a monoinstitutional retrospective study. *Tumori* 2011, 97, 39–42.
- [12] Saif, M. W.; Alexander, D.; Wicox, C. M. Serum alkaline phosphatase level as a prognostic tool in colorectal cancer: A study of 105 patients. *J. Appl. Res.* 2005, 5, 88–95.
- [13] Shiel, W. C.; Stoppler, M. G.; Lee, D.; Marks, J. W.; Mathur, R. Webster’s New World Medical Dictionary. 5th ed. Hoboken. New Jersey: Wiley Publishin. Inc. 2008.
- [14] Fersht, A. Structure and mechanism in protein science. 1999.
- [15] Millan, J. L. Mammalian Alkaline Phosphatases: From Biology to Applications in Medicine and Biotechnology. John Wiley & Sons. 2006.
- [16] Millan, J. L. Alkaline Phosphatases. *Purinergic Signal* 2006, 2, 335.
- [17] Mehrotra, S.; Rishishwar, P.; Sharma, R. K. Malnutrition and hyperphosphatemia in dialysis patient. *Clin. Queries Nephrol* 2015, 4, 25–27.
- [18] Bukowczan, J.; Pattman, S.; Jenkinson, F.; Quinton, R. Regan isoenzyme of alkaline phosphatase as a tumour marker for renal cell carcinoma. *Ann. Clin. Biochem.* 2014, 51, 611–614.
- [19] Rader, B. A. Alkaline Phosphatase, an Unconventional Immune Protein. *Front. Immunol.* 2017, 8, 897.
- [20] Anderson, D. J.; Branum, E. L.; O’Brien J. F. Liver- and bone-derived isoenzymes of alkaline phosphatase in serum as determined by high-performance affinity chromatography. *Clin. Chem.* 1990, 36, 240–6
- [21] Sharp C. A.; Linder, C.; Magnusson, P. Analysis of human bone alkaline phosphatase isoforms: Comparison of isoelectric focusing and ion-exchange high-performance liquid chromatography. *Clin. Chim. Acta.* 2007, 379, 105–112.

- [22] Parviainen, M. T.; Galloway, J. H.; Towers, J. H.; Kanis, J. A. Alkaline phosphatase isoenzymes in serum determined by high-performance anion-exchange liquid chromatography with detection by enzyme reaction. *Clin Chem.* 1988, 34, 2406–9.
- [23] Magnusson, P.; Löfman, O.; Larsson, L. Determination of alkaline phosphatase isoenzymes in serum by high-performance liquid chromatography with post-column reaction detection. *J. Chromatogr. B Biomed. Sci. Appl.* 1992, 576, 79–86.
- [24] Telford, W. G.; Cox, W. G.; Stiner, D.; Singer, V. L.; Doty, S. B. Detection of endogenous alkaline phosphatase activity in intact cells by flow cytometry using the fluorogenic ELF-97 phosphatase substrate. *Cytometry*, 1999, 37, 314–319.
- [25] Shugar, D.; Szenberg, A.; Sierakowska, H. Quantitative histochemistry by means of radioactive indicators - alkaline phosphatase. *Exp. Cell Res.* 1957, 13, 424–426.
- [26] Yi-Wei Tang, C. W. S. *Advanced Techniques in Diagnostic Microbiology*. New York: Springer Science+Business Media 2013.
- [27] Roelofs, H.; Manes, T.; Janszen, T.; Millan, J. L.; Oosterhuis, J. W.; Looijenga, L. H. J. Heterogeneity in alkaline phosphatase isozyme expression in human testicular germ cell tumours: An enzyme/immunohistochemical and molecular analysis. *J. Pathol* 1999, 189, 236–244.
- [28] Mano, H.; Furuhashi, Y.; Morikawa, Y.; Hattori, S. E.; Goto, S.; Tomoda Y., Radioimmunoassay of placental alkaline-phosphatase in ovarian-cancer sera and tissues. *Obstet. Gynecol.* 1986, 68, 759–764.
- [29] Degroote, G.; Dewaele, P.; Vandevoorde, A.; Debroe, M.; Fiers, W. Use of monoclonal-antibodies to detect human placental alkaline-phosphatas., *Clin Chem.* 1983, 29, 115–119.
- [30] Fiskén, J.; Leonard, R. C. F.; Shaw, G.; Bowman, A.; Roulston, J. E. Serum placental-like alkalinephosphatase (PLAP) - a novel combined enzyme linked immunoassay for monitoring ovariancancer. *J. Clin. Pathol.* 1989, 42, 40–45.
- [31] Blake, M. S.; Johnston, K. H.; Russell-Jones, G. J.; Gotschlich, E. C. A rapid, sensitive method for detection of alkaline phosphatase-conjugated anti-antibody on Western blot. *Anal. Biochem.* 1984, 136, 175–179.
- [32] Thiha, A.; Ibrahim, F. A Colorimetric Enzyme-Linked Immunosorbent Assay (ELISA) Detection Platform for a Point-of-Care Dengue Detection System on a Lab-On-Compact-Dis. *Sensors (Basel)* 2015, 15, 11431–11441.
- [33] Terato, K.; Do, C.T.; Cutler, D.; Waritani, T.; Shionoya, H. Preventing intense false positive and negative reactions attributed to the principle of ELISA to re-investigate antibody studies in autoimmune diseases. *Journal of Immunological Methods* 2014.
- [34] Sussman, H. H.; Small, P. J.; Cotlove, E. Human alkaline phosphatase. Immunochemical identification of organ-specific isoenzymes. *J. Biol. Chem.* 1968, 243, 160–166.

Chapter 1

- [35] Singh, I.; Tsang, K. Y. An *in vitro* production of bone specific alkaline phosphatase. Elsevier 1975 95, 347–358.
- [36] Linderholm, P.; Braschler, T.; Vannod, J.; Barrandon, Y.; Brouard, M.; Renaud, P. Two-dimensional impedance imaging of cell migration and epithelial stratification. Lab Chip. 2006.
- [37] Helali, S.; Martelet, C.; Abdelghani, A.; Maaref, M. A.; Jaffrezic-Renault, N. A disposable immunomagnetic electrochemical sensor based on functionalised magnetic beads on gold surface for the detection of atrazine. Electrochim. Act. 2006.
- [38] Zoski, C. G. Handbook of electrochemistry. 2007.
- [39] Horner, G.; Murphy, B.; Tarcy, D.; Bylikin, S. Chemistry. 2014.
- [40] Eliaz, N.; Gileadi, E. Physical electrochemistry: Fundamentals, Techniques, and Applications. 2nd ed. Weinheim: Wiley-VCH. 2019.
- [41] Scholz, F. Electroanalytical methods: Guide to experiments and applications. 2010.
- [42] Thomas, F. G.; Henze, G. Introduction to Voltammetric Analysis: Theory and Practice. Choice Rev. 2002.
- [43] Khan, K. H. Gene Expression in Mammalian Cells and its Applications. Adv. Pharm. Bull. 2013, 3, 257–263.
- [44] Pike, A. F.; Kramer, N. I.; Blaauboer, B. J.; Seinen, W.; Brands, R. A novel hypothesis for an alkaline phosphatase ‘rescue’ mechanism in the hepatic acute phase immune response. BBA - Mol. Basis Dis. 2013, 1832, 2044–2056.
- [45] Haarhaus, M.; Brandenburg, V.; Kalantar-Zadeh, K.; Stenvinkel, P.; Magnusson, P. Alkaline phosphatase: a novel treatment target for cardiovascular disease in CKD. Nat. Rev. Nephrol. 2017, 13, 429–442.
- [46] B. P. Ltd. Exploring Life Science. London: Marshall Cavendish Corporation. 2000.
- [47] Ehrenfeucht, G.; Harju, A.; David, T.; Prescott, P.; Rozenberg, M. Computation in Living Cells: Gene Assembly in Ciliates. Berlin: Springer Berlin Heidelberg. 2004.
- [48] Metzler, D. Biochemistry: The Chemical Reactions of Living Cells. London: Academic Press Inc. 1977.
- [49] Holmes, E. The Metabolism of Living Tissues. Cambridge: Cambridge University Press. 1937.
- [50] Cappuccinelli, P. Motility of Living Cells. London: Chapman and Hall. 1980.
- [51] Kaspar, A.; Yablonski, J. How Plant and Animal Cells Differ. Chicago: Britannica Educational Publishing. 2015.
- [52] Alters, S. Biology: Understanding Life. Jones and Bartlett publisher. 2000.

- [53] Karp, G. Cell and Molecular Biology: Concepts and Experiments. Wiley; 6th Ed. 2009.
- [54] Wedlich, D. Cell Migration in Development and Disease. 2005.
- [55] Takahashi, A.; Lida, T.; Naim, R.; Naykaya, Y.; Honda, T. Chloride secretion induced by thermostable direct haemolysin of *Vibrio parahaemolyticus* depends on colonic cell maturation. *J. Med. Microbiol.* 2001, 50, 870–878.
- [56] Perry, M. D.; Rajendran, V. M.; MacLennan, K. A.; Sandle, G. I. Segmental differences in upregulated apical potassium channels in mammalian colon during potassium adaptation. *Am. J. Physiol. Liver Physiol.* 2016, 311, G785–G793.
- [57] Gerlach, A. C.; Gangopadhyay, N. N.; Devor, D. C. Kinase-dependent Regulation of the Intermediate Conductance, Calcium-dependent Potassium Channel, hIK1. *J. Biol. Chem.* 2000, 275, 585–598.
- [58] Yang, B.; Cao, L.; Liu, B.; McCaig, C. D.; Pu, J. The Transition from Proliferation to Differentiation in Colorectal Cancer Is Regulated by the Calcium Activated Chloride Channel A1. *PLoS One* 2013, 8, e60861.
- [59] Zahanich, I.; Graf, E. M.; Heubach, J. F.; Hempel, U.; Boxberger, S.; Ravens, U. Molecular and Functional Expression of Voltage-Operated Calcium Channels During Osteogenic Differentiation of Human Mesenchymal Stem Cells. *J. Bone Miner. Res.* 2005, 20, 1637–1646.
- [60] Macrae, M. X.; Blake, S.; Jiang, X.; Capone, R.; Estes, D. J.; Mayer, M.; Yang J. A semi-synthetic ion channel platform for detection of phosphatase and protease activity. *ACS Nano* 2009, 3, 3567– 3580.
- [61] Benga, G. Structure and Properties of Cell Membrane Structure and Properties of Cell Membranes. 1st ed. CRC. 1985.
- [62] Starr, C.; Evers, C.; Starr, L. Biology Today and Tomorrow with Physiology. Boston: Cengage Learning. 2016.
- [63] Banfalvi, G. Permeability of biological membranes. Springer; Switzerland. 2016.
- [64] Bray D. Cell Movements: From Molecules to Motility, 2nd Edition. Garland publishing: USA. 2001.
- [65] Dogterom, M.; Koenderink, G. H. Actin–microtubule crosstalk in cell biology. *Nature Reviews Molecular Cell Biology.* 2019.
- [66] Lenz, P. Cell Motility. Marburg. Germany: Springer. 2008.
- [67] Hay, E. D. Cell Biology of Extracellular Matrix. New York: Plenum Press. 1981.
- [68] Pollard, T. D. Guidebook to the extracellular matrix and adhesion proteins. *Trends Biochem. Sci.* 1994.
- [69] Ward, P. A.; Adams, J.; Faustman, D.; Gebhart, G. F.; Geistfeld, J. G.; Imbaratto, J. W.; Peterson, N. C.; Quimby, F.; Marshak-Rothstein, A.; Rowan, A. N.; Scharff, M. D.; Dell, R. B.; Beil, K. A.; Vaupel, S. S.; Williams, M. K.; Grossblatt, N. Monoclonal Antibody Production. National Academies Press (US). 1999.

Chapter 1

[70] Phelan, K.; May K.M. Mammalian Cell Tissue Culture. Current protocols in human genetics. 2017 Jul, 94, A-3G.

[71] Jiang, L. Alexis Carrel's Immortal Chick Heart Tissue Cultures (1912-1946). The Embryo Project Encyclopedia. 2012.

[72] Freshney, I. Culture of Animal Cells: A Manual of Basic Technique and Specialized Applications. New Jersey: John Wiley & Sons. Inc. 2016.

[73] Antoni, D.; Burckel, H.; Josset, E.; Noel, G. Three-dimensional cell culture: a breakthrough *in vivo*. International journal of molecular sciences. 2015 Mar 11, 16, 5517-27.

[74] ThermoFisher Scientific. Introduction to Cell Culture | Thermo Fisher Scientific - KE [Internet]. Thermofisher.com. 2018.

[75] Morgan, D. O. The Cell Cycle: Principles of Control. London: New Science Press Ltd. 2007.

[76] Lodish, H.; Berk, A.; Zipursky, S.L.; Matsudaira, P.; Baltimore, D. Molecular Cell Biology. 4th ed. NEW YORK: W.H. Freeman. 2000.

[77] Mrksich, M. A surface chemistry approach to studying cell adhesion. Chem. Soc. Rev. 2000, 29, 267–273.

[78] Schwarz U. S.; Safran, S. A. Physics of adherent cells, Rev. Mod. Phys. 2013, 85, 1327–1381.

[79] Curtis, A. S. G.; Forrester, J. V.; McInnes, C.; Lawrie, F. Adhesion of Cells to Polystyrene Surfaces. J Cell Biol. 1983, 97, 1500–1506.

[80] Lerman, M. J.; Lembong, J.; Muramoto, S.; Gillen, G.; Fisher, J. P. The Evolution of Polystyrene as a Cell Culture Material. Tissue Eng. Part B Rev. 2018.

[81] Krutty, J. D.; Schmitt, S. K.; Gopalan, P.; Murphy, W. L. Surface functionalization and dynamics of polymeric cell culture substrate. Curr. Opin. Biotechnol. 2016, 40, 164–169.

[82] Phelan, K.; May, K. M. Basic techniques in mammalian cell tissue culture. Current protocols in cell biology. 2015 Mar, 66, 1.

[83] Arora, M. Cell Culture Media: A Review. Mater. Methods. 2013.

[84] Yao, T.; Asayama, Y. Animal-cell culture media: History, characteristics, and current issues. Reproductive Medicine and Biology. 2017.

[85] Berthois, Y.; Katzenellenbogen, J. A.; Katzenellenbogen, B. S. Phenol red in tissue culture media is a weak estrogen: implications concerning the study of estrogen-responsive cells in culture. 1986, 83, 2496-2500.

[86] Wikipedia. Red phenol.

[87] ABM. Cell Culture - Introduction | ABM Inc.

[88] Lundholt, B. K.; Scudder, K. M.; Pagliaro, L. A simple technique for reducing edge effect in cell-based assays. *J. Biomol. Screen.* 2003.

[89] ATCC. ATCC® ANIMAL CELL CULTURE GUIDE tips and techniques for continuous cell lines.

[90] ATCC, ATCC® ANIMAL CELL CULTURE GUIDE tips and techniques for continuous cell lines.

[91] The Union for International Cancer Control's (UICC). New Global Cancer Data: GLOBOCAN 2018 | UICC.

[92] Lonare, M. K.; Vemu, B.; Singh, A. K.; Dumka, V. K.; Singla, S.; Sharma, S. K. Cytotoxicity and Oxidative Stress Alterations Induced by Aldrin in BALB/c 3T3 Fibroblast Cells. *Proc. Natl. Acad. Sci. India Sect. B Biol. Sci.* 2017, 87, 1209–1216.

[93] Li, X.; Li, B.; Zeng, H.; Wang, S.; Sun, X.; Yu, Y.; Wang, L.; Yu, J. Prognostic value of dynamic albumin to alkaline phosphatase ratio in limited stage small-cell lung cancer. *Futur. Oncol.* 2019, 15, 995–1006.

[94] Martínez, V. R.; Aguirre, M. V.; Todaro, J. S.; Piro, O. E.; Echeverría, G. A.; Naso, L. G.; Ferrer, E. G.; Williams, P. A. M. Interaction of Zn with Losartan. Activation of Intrinsic Apoptotic Signaling Pathway in Lung Cancer Cells and Effects on Alkaline and Acid Phosphatases. *Biol Trace Elem Res.* 2018, 186, 413–429.

[95] Zhang, L.; Zhang, H.; Yue, D.; Wei, W.; Chen, Y.; Zhao, X.; Zhu, J.; Zhang, B.; Zhang, Z.; Wang, C. The prognostic value of the preoperative albumin to alkaline phosphatase ratio in patients with nonsmall cell lung cancer after surgery. *Thorac. Cancer* 2019, 10, 1581–1589.

[96] Long, Z.-Q.; Hua, X.; Zhang, W.-W.; Lv, S.-W.; Deng, J.-P.; Guo, L.; He, Z.-Y.; Lin, H.-X. Prognostic impact of the pretreatment albumin to alkaline phosphatase ratio for nonmetastatic breast cancer patients. *Cancer Manag. Res.* 2019, 11, 4809–4814.

[97] Singh, A. K.; Pandey, A.; Tewari, M.; Kumar, R.; Sharma, A.; Singh, K. A.; Pandey, H. P.; Shukla, H. S. Advanced stage of breast cancer hoist alkaline phosphatase activity: risk factor for females in India. *3 Biotech.* 2013, 3, 517–520.

[98] Keshaviah, A.; Dellapasqua, S.; Rotmensz, N.; Lindtner, J.; Crivellari, D.; Collins, J.; Colleoni, M.; Thürlimann, B.; Mendiola, C.; Aebi, S.; Price, K. N.; Pagani, O.; Simoncini, E.; Gertsch, M. C.; Gelber, R. D.; Coates, A. S.; Goldhirsch, A. CA15-3 and alkaline phosphatase as predictors for breast cancer recurrence: a combined analysis of seven International Breast Cancer Study Group trials. *Ann. Oncol.* 2007, 18, 701–708.

[99] Pavkovic, B.; Nenadic, L. K.; Brankovic, M.; Zaric, M.; Brkic, M. P-120 Serum alkaline phosphatase level as an early diagnostic tool in colorectal cancer. *Ann. Oncol.* 2015, 26, iv34.

Chapter 1

- [100] Hung, H.-Y.; Chen, J.-S.; Yeh, C.-Y.; Tang, R.; Hsieh, P.-S.; Tasi, W.-S.; You, Y.-T.; You, J.-F.; Chiang, J.M. Preoperative alkaline phosphatase elevation was associated with poor survival in colorectal cancer patients. *Int. J. Colorectal Dis.* 2017, 32, 1775–1778.
- [101] Wistuba, I. I.; Bryant, D.; Behrens, C.; Milchgrub, S.; Virmani, A. K.; Ashfaq, R.; Minna, J. D.; Gazdar, A. F. Comparison of Features of Human Lung Cancer Cell Lines and Their Corresponding Tumors. *Clin. Cancer Res.* 1999, 5, 991–1000.
- [102] Gazdar, A. F.; Kurvari, V.; Virmani, A.; Gollahon, L.; Sakaguchi, M.; Westerfield, M.; Kodagoda, D.; Stasny, V.; Cunningham, H. T.; Wistuba, I. I.; Tomlinson, G.; Tonk, V.; Ashfaq, R.; Leitch, A. M.; Minna, J. D.; Shay, J. W. Characterization of paired tumor and non-tumor cell lines established from patients with breast cancer. *Int. J. CANCER* 1998, 78, 766–774.
- [103] Forgue-Lafitte, M.-E.; Coudray, A.-M.; Breant, B.; Mester, J. Proliferation of the Human Colon Carcinoma Cell Line HT29: Autocrine Growth and Deregulated Expression of the c-myc Oncogene1. *Cancer Res.* 1989, 49, 6566-6571.
- [104] Yu, S.; Fourman, M. S.; Mahjoub, A.; Mandell, J. B.; Crasto, J. A.; Greco, N. G.; Weiss, K. R. Lung cells support osteosarcoma cell migration and survival. *BMC Cancer* 2017, 17, 78.
- [105] Kato, M.; Brijlall, D.; Adler, S. A.; Kato, S.; Herz, F. EFFECT OF HYPEROSMOLALITY ON ALKALINEPHOSPHATASE AND STRESS-RESPONSE PROTEIN 27 OF MCF-7 BREAST-CANCER CELLS. *Breast Cancer Res. Treat* 1992, 23, 241–249.
- [106] Zheng, A. Inhibitory effects of breast cancer cells on proliferation and differentiation of osteoblasts. 2009.
- [107] Dilenzo, D.; Albertini, A.; Zava, D. Progestin Regulation of Alkaline-Phosphatase In The Human Breast-Cancer Cell-Line T47D. *Cancer Res.* 1991, 51, 4470–4475.
- [108] Chowdhury, M. A.; Peters, A. A.; Roberts-Thomson, S. J.; Monteith, G. R. Effects of differentiation on purinergic and neurotensin-mediated calcium signaling in human HT-29 colon cancer cells. *Biochem Biophys Res Commun.* 2013, 439, 35–39.
- [109] Shin, J.; Carr, A.; Corner, G. A.; Tögel, L.; Dávalos-Salas, M.; Tran, H.; Chueh, A. C.; Al-Obaidi, S.; Chionh, F.; Ahmed, N.; Buchanan, D. D.; Young, J. P.; Malo, M. S.; Hodin, R.A.; Arango, D.; Sieber, O. M.; Augenlicht, L. H.; Dhillon, A. S.; Weber, T. K.; Mariadason, J. M. The Intestinal Epithelial Cell Differentiation Marker Intestinal Alkaline Phosphatase (ALPi) Is Selectively Induced by Histone Deacetylase Inhibitors (HDACi) in Colon Cancer Cells in a Kruppel-like Factor 5 (KLF5)-dependent Manner. *J. Biol. Chem.* 2014, 289, 25306–25316.
- [110] ATCC. BALB/3T3 clone A31 ATCC® CCL-163TM Mus musculus embryo.
- [111] ATCC. A549 ATCC® CCL-185TM.

[112] Samadder, P.; Arthur, G. Decreased Sensitivity to 1-O-Octadecyl-2-O-methyl-glycerophosphocholine in MCF-7 Cells Adapted for Serum-free Growth Correlates with Constitutive Association of Raf-1 with Cellular Membranes. *Cancer Res.* 1999 Oct 1, 59, 4808-15.

[113] ATCC. HT-29 ATCC[®] HTB-38TM Homo sapiens colon colorectal adenocar.

[114] Giaever, I.; Keese, C. R. A morphological biosensor for mammalian cells. *Nature.* 1993.

[115] Riss, T. L.; Moravec, R. A.; Niles, A. L.; Duellman, S.; Benink, H. A.; Worzella, T. J.; Minor, L. Cell Viability Assay.

[116] Ahmed S. A.; Gogal, R. M.; Walsh, J. E. A new rapid and simple nonradioactive assay to monitor and determine the proliferation of lymphocytes: An alternative to [3H] thymidine incorporation assays. *J Immunol Meth.* 1994; 170, 211–224.

[117] Çakir, S.; Arslan, E. Y. Voltammetry of resazurin at a mercury electrode. *Chem. Pap.* 2010.

[118] Farley, J.R.; Stilt-Coffing, B. Apoptosis may determine the release of skeletal alkaline phosphatase activity from human osteoblast-line cells. *Calcified tissue international.* 2001 Jan 1, 68, 43-52.

[119] Shum, D.; Radu, C.; Kim, E.; Cajuste, M.; Shao, Y.; Seshan, V. E.; Djaballah, H. A high density assay format for the detection of novel cytotoxic agents in large chemical libraries. *J. Enzyme Inhib. Med. Chem.* 2008, 23, 931–945.

[120] NHjortso, M. A.; Roos, J. W. *Cell Adhesion in Bioprocessing and Biotechnology.* NEW YORK: CRC. 1994.

[121] Alberts, B.; Johnson, A.; Lewis, J.; Raff, M.; Roberts, K.; Walter, P. *Molecular Biology of the Cell.* 4th edition. New York: Garland Science; Meiosis. New York: Garland Science. 2002.

[122] Ghoshal, K.; Chakraborty, S.; Das, C.; Chattopadhyay, S.; Chowdhury, S.; Bhattacharyya, M. Dielectric properties of plasma membrane: A signature for dyslipidemia in diabetes mellitus. *Arch. Biochem. Biophys.* 2017.

[123] K'Owino, I. O.; Sadik, O. A. Impedance spectroscopy: A powerful tool for rapid biomolecular screening and cell culture monitoring. *Electroanalysis* 2005, 17, 2101–2113.

[124] Heileman, K.; Daoud, J.; Tabrizian, M. Dielectric spectroscopy as a viable biosensing tool for cell and tissue characterization and analysis. *Biosensors and Bioelectronics.* 2013.

[125] Martinsen, O. G.; Grimnes, S.; Schwan, H. P.; Rikshospitalet, O. Interface phenomena and dielectric properties of biological tissue. *Encycl. Surf. Colloid Sci.* 2002.

[126] Grimnes, S.; Martinsen, Ø. G. *Bioimpedance and Bioelectricity Basics.* 2008.

[127] Foster, K. R.; Schwan, H. P. Dielectric properties of tissues and biological materials: a critical review. *Critical Reviews in Biomedical Engineering.* 1989.

- [128] Schwan, H. P. Electrical properties of tissue and cell suspensions. Adv. Biol. Med. Phys. 1957.
- [129] Ciambione, G. J.; Liu, V. F.; Lin, D. C.; McGuinness, R. P.; Leung, G. K.; Pitchford, S. Cellular dielectric spectroscopy: A powerful new approach to label-free cellular analysis. J. Biomol. Screen. 2004.
- [130] Ende, D.; Mangold, K. -M. Impedanzspektroskopie. Chemie unserer Zeit. 1993.
- [131] Pänke, O.; Balkenhohl, T.; Kafka, J.; Schäfer, D.; Lisdat, F. Impedance spectroscopy and biosensing. Adv. Biochem. Eng. Biotechnol. 2007.
- [132] Guan, J. G.; Miao, Y. Q.; Zhang, Q. J. Impedimetric biosensors. Journal of Bioscience and Bioengineering. 2004.
- [133] Borkholder, D. A. Cell Based Biosensors Using Microelectrodes. PhD thesis. 1998.
- [134] Giaever I.; Keese, C. R. Micromotion of mammalian cells measured electrically. Proc. Natl. Acad. Sci. U. S. A. 1991.
- [135] Giaever, I.; Keese, C. R. Monitoring fibroblast behavior in tissue culture with an applied electric field. Proc. Natl. Acad. Sci. U. S. A. 1984.
- [136] Giaever, I.; Keese, C. R. Electric cell-substrate impedance sensing concept to commercialization. Cancer Metastasis - Biol. Treat. 2012.
- [137] Wegener, J.; Seebach, J. Experimental tools to monitor the dynamics of endothelial barrier function: A survey of *in vitro* approaches. Cell and Tissue Research. 2014.
- [138] Wegener, J.; Keese, C. R.; Giaever, I. Electric cell-substrate impedance sensing (ECIS) as a noninvasive means to monitor the kinetics of cell spreading to artificial surfaces. Exp. Cell Res. 2000.
- [139] Keese C. R.; Giaever, I. A Biosensor that Monitors Cell Morphology with Electrical Fields. IEEE Eng. Med. Biol. Mag. 1994.
- [140] Chiu, S. P.; Batsaikhan, B.; Huang, H. M.; Wang, J. Y. Application of Electric Cell-Substrate Impedance Sensing to Investigate the Cytotoxic Effects of Andrographolide on U-87 MG Glioblastoma Cell Migration and Apoptosis. Sensors (Basel) 2019, 19, 2275.
- [141] Chiu, S.-P.; Lee, Y.-W.; Wu, L.-Y.; Tung, T.-H.; Gomez, S.; Lo, C.-M.; Wang, J.-Y. Application of ECIS to Assess FCCP-Induced Changes of MSC Micromotion and Wound Healing Migration. Sensors (Basel) 2019, 19, 3210.
- [142] Jia, j.; Martin, T. A.; Ye, L.; Meng, L.; Xia, N.; Jiang, W. G.; Zhang, X. Fibroblast activation protein- α promotes the growth and migration of lung cancer cells via the PI3K and sonic hedgehog pathways. Int. J. Mol. Med. 2018.

- [143] Yin, H.; Wang, F. L.; Wang, A. L.; Cheng, J.; Zhou, Y. Bioelectrical Impedance Assay to Monitor Changes in Aspirin-Treated Human Colon Cancer HT-29 Cell Shape during Apoptosis. *Anal. Lett.* 2007, 40, 85–94.
- [144] Halaidych, O. V.; Freund, C.; van den Hil, F.; Salvatori, D. C. F.; Riminucci, M.; Mummery, C. L.; Orlova, V. V. Inflammatory Responses and Barrier Function of Endothelial Cells Derived from Human Induced Pluripotent Stem Cells. *Stem Cell Reports* 2018, 10, 1642–1656.
- [145] Stanica, L.; Rosu-Hamzescu, M.; Gheorghiu, M.; Stan, M.; Antonescu, L.; Polonschii, C.; Gheorghiu, E. Electric Cell-Substrate Impedance Sensing of Cellular Effects under Hypoxic Conditions and Carbonic Anhydrase Inhibition. *J. Sensors* 2017, 2017, 1–10.
- [146] Lai, Y.-T.; Chu, Y.-S.; Lo, J.-C.; Hung, Y.-H.; Lo, C.-M. Effects of electrode diameter on the detection sensitivity and frequency characteristics of electric cell-substrate impedance sensing. *Sensors Actuators B. Chem.* 2019, 288, 707–715.
- [147] Mansor, A. F. M.; Ibrahim, I.; Zainuddin, A. A.; Voiculescu, I.; Nordin, A. N. Modeling and development of screen-printed impedance biosensor for cytotoxicity studies of lung carcinoma cells. *Med. Biol. Eng. Comput.* 2018, 56, 173–181.
- [148] Tran, T. B.; Nguyen, P. D.; Baek, C.; Min, J. Electrical dual-sensing method for real-time quantitative monitoring of cell-secreted MMP-9 and cellular morphology during migration process. *Biosens. Bioelectron.* 2016, 77, 631–637.
- [149] Bossou, Y. M.; Serssar, Y.; Allou, A.; Vitry, S.; Momas, I.; Seta, N.; Menotti, J.; Achard, S. Impact of mycotoxins secreted by aspergillus molds on the inflammatory response of human corneal epithelial cells. *Toxins (Basel)* 2017, 9, 197.
- [150] Joshi, R. *Biosensors*. India: Isha book, 2006.
- [151] Huang, X. J.; O'Mahony, A. M.; Compton, R. G. *Microelectrode arrays for electrochemistry: Approaches to fabrication*, Small. 2009.
- [152] Yan, X. F.; Wang, M. H.; An, D. Progress of interdigitated array microelectrodes based impedance immunosensor. *Fenxi Huaxue/ Chinese Journal of Analytical Chemistry*. 2011.
- [153] Wang, H.; Wang, L.; Mitchelson, K.; Yu, Z.; Cheng, J. Analysis of the sensitivity and frequency characteristics of coplanar electrical cell–substrate impedance sensors. *Biosens. Bioelectron.* 2008, 24, 14–21.
- [154] Franks, W.; Schenker, I.; Schmutz, P.; Hierlemann, A. Impedance characterization and modeling of electrodes for biomedical applications. *IEEE Trans. Biomed. Eng.* 2005.
- [155] Abdur Rahman, A. R.; Price, D. T.; Bhansali, S. Effect of electrode geometry on the impedance evaluation of tissue and cell culture. *Sensors Actuators. B Chem.* 2007.

- [156] Narayanan, S.; Nikkhah, M.; Strob, J. S.; Agah, M. Analysis of the passivation layer by testing and modeling a cell impedance micro-sensor. *Sensors Actuators. A Phys.* 2010.
- [157] Price, D. T.; Rahman, A. R. A.; Bhansali, S. Design rule for optimization of microelectrodes used in electric cell-substrate impedance sensing (ECIS). *Biosens. Bioelectron.* 2009
- [158] Breckenridge, L. J.; Wilson, R. J. A.; Connolly, P.; Curtis, A. S. G.; Dow, J. A. T.; Blackshaw, S. E.; Wilkinson, C. D. W. Advantages of using microfabricated extracellular electrodes for *in vitro* neuronal recording. *J. Neurosci. Res.* 1995.
- [159] Min, J.; Baeumner, A. J. Characterization and optimization of interdigitated ultramicroelectrode arrays as electrochemical biosensor transducers. *Electroanalysis.* 2004.
- [160] Varshney, M.; Li, Y. Interdigitated array microelectrodes based impedance biosensors for detection of bacterial cells. *Biosensors and Bioelectronics.* 2009.
- [161] Judy, J. W. *Microelectrode Technologies for Neuroengineered Systems.* 2003.
- [162] Zou, Z.; Kai, J.; Rust, M. J.; Han, J.; Ahn, C.H. Functionalized nano interdigitated electrodes arrays on polymer with integrated microfluidics for direct bio-affinity sensing using impedimetric measurement. *Sensors Actuators. A Phys.* 2007.
- [163] Ohori, T.; Shoji, S.; Miura, K.; Yotsumoto, A. Partly disposable three-way microvalve for a medical micro total analysis system (μ TAS). *Sensors Actuators. A Phys.* 1998.
- [164] Gerwen, P. V.; Laureyn, W.; Laureys, W.; Huyberechts, G.; Beeck, M. O. D.; Baert, K.; Suls, J.; Sansen, W.; Jacobs, P.; Hermans, L.; Merten, R. Nanoscaled interdigitated electrode arrays for biochemical sensors. *Sensors Actuators. B Chem.* 1998.
- [165] Laureyn, W.; Nelis, D.; Van Gerwen, P.; Baert, K.; Hermans, L.; Magnée, R.; Pireaux, J. J.; Maes, G. Nanoscaled interdigitated titanium electrodes for impedimetric biosensing. *Sensors Actuators. B Chem.* 2000.
- [166] Rahman, A. R. A.; Register, J.; Vuppala, G.; Bhansali, S. Cell culture monitoring by impedance mapping using a multielectrode scanning impedance spectroscopy system (CellMap). *Physiol. Meas.* 2008.
- [167] Gross, G. W.; Rhoades, B. K.; Reust, D. L.; Schwalm, F. U. Stimulation of monolayer networks in culture through thin-film indium-tin oxide recording electrodes. *J. Neurosci. Methods.* 1993.
- [168] Neghmouche, N. S. *Analytical Electrochemistry: The Basic Concepts.* Anal. Electrochem. 2007.
- [169] Fejtl, M.; Stett, A.; Nisch, W.; Boven, K. H.; Möller, A. On micro-electrode array revival: Its development, sophistication of recording, and stimulation. in *Advances in Network Electrophysiology: Using Multi-Electrode Arrays.* 2006.
- [170] Colella, L.; Beyer, C.; Fröhlich, J.; Talary, M.; Renaud, P. Microelectrode-based dielectric spectroscopy of glucose effect on erythrocytes. *Bioelectrochemistry.* 2012.

- [171] Ojima, H.; Umedal, M.; Mohamedi, M.; Uchida, I. Electrochemical Detection of Protons Produced in an Electrode Reaction Using Interdigitated Microarray Electrodes. *Electroanalysis*. 2003.
- [172] Green, R. A.; Hassarati, R. T.; Bouchinet, L.; Lee, C. S.; Cheong, G. L. M.; Yu, J. F.; Dodds, C. W.; Suaning, G. J.; Poole-Warren, L. A.; Lovell, N. H. Substrate dependent stability of conducting polymer coatings on medical electrodes. *Biomaterials*. 2012.
- [173] Rahman, A. R. A.; Lo, C. M.; Bhansali, S. A micro-electrode array biosensor for impedance spectroscopy of human umbilical vein endothelial cells. *Sensors Actuators. B Chem*. 2006.
- [174] Valera, E.; Ramón-Azcón, J.; Rodríguez, Á.; Castañer, L. M.; Sánchez, F. J.; Marco, M. P. Impedimetric immunosensor for atrazine detection using interdigitated μ -electrodes (ID μ E's). *Sensors Actuators. B Chem*. 2007.
- [175] Baaken, G.; Sondermann, M.; Schlemmer, C.; Rühle, J.; Behrends, J. C. Planar microelectrode-cavity array for high-resolution and parallel electrical recording of membrane ionic currents. *Lab Chip*. 2008.
- [176] Nagale, M. P.; Fritsch, I. Individually Addressable, Submicrometer Band Electrode Arrays. 1. Fabrication from Multilayered Materials. *Anal. Chem*. 1998.
- [177] Aguiar, F. A.; Gallant, A. J.; Rosamond, M. C.; Rhodes, A.; Wood, D.; Katakly, R. Conical recessed gold microelectrode arrays produced during photolithographic methods: Characterisation and causes. *Electrochem. commun*. 2007.
- [178] Ordeig, O.; Godino, N.; Campo, J. D.; Muñoz, F. X.; Nikolajeff, F.; Nyholm, L. On-chip electric field driven electrochemical detection using a poly(dimethylsiloxane) microchannel with gold microband electrodes. *Anal. Chem*. 2008.
- [179] Saum, A. G. E.; Cumming, R. H.; Rowell, F. J. Use of substrate coated electrodes and AC impedance spectroscopy for the detection of enzyme activity. *Biosens. Bioelectron*. 1998.
- [180] Hou, Y.; Helali, S.; Zhang, A.; Jaffrezic-Renault, N.; Martelet, C.; Minic, J.; Gorojankina, T.; Persuy, M. A.; Pajot-Augy, E.; Salesse, R.; Bessueille, F.; Samitier, J.; Errachid, A.; Akimov, V.; Reggiani, L.; Pennetta, C.; Alfinito, E. Immobilization of rhodopsin on a self-assembled multilayer and its specific detection by electrochemical impedance spectroscopy. *Biosens. Bioelectron*. 2006.
- [181] Mohr, A.; Finger, W.; Foehr, K. J.; Nisch, W.; Goepel, W. Performance of a thin film microelectrode array for monitoring electrogenic cells *in vitro*. 1995.
- [182] Wang, L.; Zhu, J.; Deng, C.; Xing, W. L.; Cheng, J. An automatic and quantitative on-chip cell migration assay using self-assembled monolayers combined with real-time cellular impedance sensing. *Lab Chip*. 2008.
- [183] Pickard, R. S. A review of printed circuit microelectrodes and their production. *Journal of Neuroscience Methods*. 1979.

- [184] MacKay, S.; Abdelrasoul, G. N.; Tamura, M.; Lin, D.; Yan, Z.; Chen, J. Using impedance measurements to characterize surface modified with gold nanoparticles. *Sensors (Switzerland)*. 2017.
- [185] Pringkasemchai, A.; Hoshyargar, F.; Lertanantawong, B.; O'Mullane, A. P. Lightweight ITO Electrodes Decorated with Gold Nanostructures for Electrochemical Applications. *Electroanalysis*. 2019.
- [186] Geddes, L. A.; Roeder, R. Criteria for the selection of materials for implanted electrodes. *Ann. Biomed. Eng.* 2003.
- [187] Hämmerle, H.; Egert, U.; Mohr, A.; Nisch, W. Extracellular recording in neuronal networks with substrate integrated microelectrode arrays. *Biosens. Bioelectron.* 1994.
- [188] Egert, U.; Schlosshauer, B.; Fennrich, S.; Nisch, W.; Fejtl, M.; Knott, T.; Müller, T.; Hämmerle, H. A. A novel organotypic long-term culture of the rat hippocampus on substrate-integrated multielectrode arrays. *Brain Res. Protoc.* 1998.
- [189] Gross, G. W.; Rhoades, B. K.; Azzazy, H. M. E.; Wu, M.-C. The use of neuronal networks on multielectrode arrays as biosensors. *Biosens. Bioelectron.* 1995.
- [190] O'Hare, D.; Macpherson, J. V.; Willows, A. On the microelectrode behaviour of graphite-epoxy composite electrodes. *Electrochem. commun.* 2002.
- [191] Magee, L. J.; Osteryoung, J. Fabrication and Characterization of Glassy Carbon Linear Array Electrodes. *Anal. Chem.* 1989.
- [192] Kuban, P.; Berg, J. M.; Dasgupta, P. K. Durable Microfabricated High-Speed Humidity Sensors. *Anal. Chem.* 2004, 76, 2561–2567.
- [193] Nolan, M. A.; Kounaves, S. P. Microfabricated Array of Iridium Microdisks as a Substrate for Direct Determination of Cu^{2+} or Hg^{2+} Using Square-Wave Anodic Stripping Voltammetry. *Anal. Chem.* 1999, 71, 3567–3573.
- [194] Li, N.; Tourovskaia, A.; Folch, A. Biology on a Chip: Microfabrication for Studying the Behavior of Cultured Cells. *Critical Reviews in Biomedical Engineering*. 2003.
- [195] Zaouk, R.; Park, B. Y.; Madou, M. J. Introduction to microfabrication techniques. *Methods Mol. Biol.* 2006.
- [196] Metters, J. P.; Kadara, R. O.; Banks, C. E. New directions in screen printed electroanalytical sensors: An overview of recent developments. *Analyst*. 2011.
- [197] C. Z. Laser Ablation. In: Li D. (eds) *Encyclopedia of Microfluidics and Nanofluidics*. Boston MA: Springer. 2008.
- [198] Kim, S. H.; Shin, K. H.; Moon, S. H.; Jang, J.; Kim, H. S.; Suh, J. S.; Yang, W. I. Reassessment of alkaline phosphatase as serum tumor marker with high specificity in osteosarcoma. *Cancer medicine* 2017, 6, 1311–1322.

- [199] Heinrich, D.; Bruland, O.; Guise, T. A.; Suzuki, H.; Sartor, O. Alkaline phosphatase in metastatic castration-resistant prostate cancer: Reassessment of an older biomarker. *Future Oncology*. 2018.
- [200] Latner, A. L.; Skillen, A.W. *Isoenzymes in Biology and Medicine*. Academic Press Inc.: London, UK. 1968.
- [201] Sharma, U.; Pal, D.; Prasad, R. Alkaline Phosphatase: An Overview. *Indian J. Clin. Biochem*. 2014, 29, 269–278
- [202] Acton, Q.A. *Transforming Growth Factors—Advances in Research and Application*; Scholarly Editions: 2013.
- [203] Herz, F.; Halwer, A.S.M.; Bogart, L.H. Alkaline phosphatase in HT-29, a human colon cancer cell line: Influence of sodium butyrate and hyperosmolality. *Arch. Biochem. Biophys*. 1981, 210, 581–591.
- [204] Tsai, L.-C.; Hung, M.-W.; Chen, Y.-H.; Su, W.-C.; Chang, G.-G.; Chang, T.-C. Expression and regulation of alkaline phosphatases in human breast cancer MCF-7 cells. *Eur. J. Biochem*. 2000, 267, 1330–1339.
- [205] Hui, M.; Hu, M.; Tenenbaum, H.C. Changes in cell adhesion and cell proliferation are associated with expression of tissue non-specific alkaline phosphatase. *Cell Tissue Res*. 1993, 274, 429–437.
- [206] Guerreiro, S.; Monteiro, R.; Martins, M.J.; Calhau, C.; Azevedo, I.; Soares, R. Distinct modulation of alkaline phosphatase isoenzymes by 17beta-estradiol and xanthohumol in breast cancer MCF-7 cells. *Clin. Biochem*. 2007, 40, 268.
- [207] Alberts, B.; Lewis, J. A. *Molecular Biology of the Cell*. 4th ed. Studying Gene Expression and Function. Garland Science: New York, NY, USA. 2002.
- [208] Yang, T.-T.; Sinai, P.; Kain, S. R. An Acid Phosphatase Assay for Quantifying the Growth of Adherent and Nonadherent Cells. *Anal. Biochem*. 1996, 241, 103–108.
- [209] Friedrich, J.; Eder, W.; Castaneda, J.; Doss, M.; Huber, E.; Ebner, R.; Kunz-Schughart, L. A. A reliable tool to determine cell viability in complex 3-D culture: The acid phosphatase assay. *J. Biomol. Screen*. 2007, 12, 925–937.
- [210] Ivanov, D.P.; Parker, T.L.; Walker, D.A.; Alexander, C.; Ashford, M.B.; Gellert, P.R.; Garnett, M.C. Multiplexing spheroid volume, resazurin and acid phosphatase viability assays for highthroughput screening of tumour spheroids and stem cell neurospheres. *PLoS ONE* 2014, 9, e103817.
- [211] Cullen, B. R.; Malim, M. H. Secreted placental alkaline phosphatase as a eukaryotic reporter gene. *Methods Enzym*. 1992, 216, 362–368.
- [212] Doronin, K. K. Expression of the gene encoding secreted placental alkaline phosphatase (SEAP) by a nondefective adenovirus vector. *Gene*. 1993, 126, 247–250.

- [213] Bronstein, I.; Fortin, J. J.; Voyta, J.C.; Juo, R. R.; Edwards, B.; Olesen, C. E.; Lijam, N.; Kricka, L. J. Chemiluminescent reporter gene assays: sensitive detection of the GUS and SEAP gene products. *Biotechniques* 1994, 17, 172-174, 176-177.
- [214] Chang, T.-C.; Wang, J.-K.; Hung, M.-W.; Chiao, C.-H.; Tsai, L.-C.; Chang, G.-G. Regulation of the expression of alkaline phosphatase in a human breastcancer cell line. *Biochem. J.* 1994, 199-205, 303.
- [215] He, J.; Landau, N. R. Use of a novel human immunodeficiency virus type 1 reporter virus expressing human placental alkaline phosphatase to detect an alternative viral receptor. *J Virol.* 1995, 69, 4587–4592.
- [216] Akcakaya, H.; Aroymak, A.; Gokce, S. A quantitative colorimetric method of measuring alkaline phosphatase activity in eukaryotic cell membranes. *Cell Biol. Int.* 2007, 31, 186–190.
- [217] Sen, M.; Ino, K.; Inoue, K. Y.; Arai, T.; Nishijo, T.; Suda, A.; Kunikata, R.; Shiku, H.; Matsue, T. LSIbased amperometric sensor for real-time monitoring of embryoid bodies. *Biosens. Bioelectron.* 2013, 48, 12–18.
- [218] Chowdhury, M. A.; Peters, A. A.; Roberts-Thomson, S. J.; Monteith, G. R. Effects of differentiation on purinergic and neurotensin-mediated calcium signaling in human HT-29 colon cancer cells. *Biochem Biophys Res Commun.* 2013, 439, 35–39.
- [219] Shin, J.; Carr, A.; Corner, G. A.; Tögel, L.; Dávalos-Salas, M.; Tran, H.; Chueh, A. C.; Al-Obaidi, S.; Chionh, F.; Ahmed, N.; Buchanan, D. D.; Young, J. P.; Malo, M. S.; Hodin, R. A.; Arango, D.; Sieber, O. M.; Augenlicht, L. H.; Dhillon, A. S.; Weber, T. K.; Mariadason, J. M. The Intestinal Epithelial Cell Differentiation Marker Intestinal Alkaline Phosphatase (ALPi) Is Selectively Induced by Histone Deacetylase Inhibitors (HDACi) in Colon Cancer Cells in a Kruppel-like Factor 5 (KLF5)-dependent Manner. *J. Biol. Chem.* 2014, 289, 25306–25316.
- [220] Hodin, R. A.; Meng, S. F.; Archer, S.; Tang, R. Cellular growth state differentially regulates enterocyte gene expression in butyrate-treated HT-29 cells. *CELL GROWTH Differ.* 1996, 7, 647–653.
- [221] Eguchi, T.; Taha, E. A.; Calderwood, S. K.; Ono, K. A. Novel Model of Cancer Drug Resistance: Oncosomal Release of Cytotoxic and Antibody-Based Drugs. *Biology* 2020, 9, 47.
- [222] Zeidler, J. D.; Fernandes-Siqueira, L. O.; Carvalho, A. S.; Cararo-Lopes, E.; Dias, M. H.; Ketzer, L.A.; Galina, A.; Da Poian, A. T. Short-term starvation is a strategy to unravel the cellular capacity of oxidizing specific exogenous/endogenous substrates in mitochondria. *Journal of biological chemistry.* 2017, 292, 14176-14187.
- [223] Kim, T. K.; Eberwine, J. H. Mammalian cell transfection: the present and the future. *Anal Bioanal Chem.* 2010, 397, 3173–3178.
- [224] Terry, S.; Beltran, H. The many faces of neuroendocrine differentiation in prostate cancer progression. *Front. Oncol.* 2014, 4, 60
- [225] Xiao, Z.; Yan, L.; Liang, X.; Wang, H. Progress in deciphering trophoblast cell differentiation during human placentation. *Current Opinion in Cell Biology* 2020, 67, 86-91.

[226] Long, R. M.; Morrissey, C.; Fitzpatrick, J. M.; Watson, R.W.G. Prostate epithelial cell differentiation and its relevance to the understanding of prostate cancer therapies. *Clin Sci (Lond)*. 2005, 108, 1– 11.

[227] Qi, L.; Yanqing, D. Screening of Differentiation-Specific Molecular Biomarkers for Colon Cancer. *Cell Physiol Biochem*. 2018, 46, 2543-2550.

[228] Rahman, A. R. A.; Register, J.; Vuppala, G.; Bhansali, S. Cell culture monitoring by impedance mapping using a multielectrode scanning impedance spectroscopy system (CellMap). *Physiol. Meas*. 2008, 6, S227-39.

[229] Hou, W. B.; Cronin, S. B. A Review of Surface Plasmon Resonance-Enhanced Photocatalysis. *Adv. Funct. Mater*. 2013, 23(, 1612–1619.

[230] Linder, H. C.; Enander, K.; Magnusson, P. Glycation Contributes to Interaction Between Human Bone Alkaline Phosphatase and Collagen Type I. *Calcif Tissue Int*. 2016, 98, 284–293.

[231] Sappia, L.; Piccinini, E.; Santilli, N.; Marmisolé, W.; Madrid, R.; Azzaroni, O. Lectin-modified surfaces for the real-time determination of Bone Alkaline Phosphatase by Surface Plasmon Resonance (SPR) Spectroscopy. 1st Argentine-German Workshop on Nanotechnology and Nanobiosensors. INTI. Buenos Aires, Argentina. 2017.

[232] Wang, K.; Jiang, L.; Zhang, F.; Wei, Y.Q.; Wang, H.S.; Qi, Z.J.; Liu, S. Q. Strategy for in Situ Imaging of Cellular Alkaline Phosphatase Activity Using Gold Nanoflower Probe and Localized Surface Plasmon Resonance Technique. *Anal Chem*. 2018, 90, 14056–14062.

[233] Syu, Y. C.; Hsu, W. E.; Lin, C. T. Review-Field-Effect Transistor Biosensing: Devices and Clinical Applications. *ECS J. SOLID STATE Sci. Technol*. 2018, 7, Q3196–Q3207.

[234] Jang, H. J.; Ahn, J.; Kim, M. G.; Shin, Y. B.; Jeun, M.; Cho, W. J.; Lee, K. H. Electrical signaling of enzyme-linked immunosorbent assays with an ion-sensitive field-effect transistor. *Biosens. Bioelectron*. 2015, 64, 318–323.

[235] Freeman, R.; Gill, R.; Willner, I. Following a protein kinase activity using a field-effect transistor device. *Chem Commun*. 2007, 33, 3450–3452.

[236] Ebersole, R. C.; Ward, M. D. Amplified Mass Immunosorbent Assay with a Quartz Crystal Microbalance. *Am. Chem. Soc*. 1988, 110, 8623–8628.

[237] Kacar, T.; Zin, M.T.; So, C.; Wilson, B.; Ma, H.; Gul-Karaguler, N.; Tamerler, C. Directed Selfimmobilization of Alkaline Phosphatase on Micro-Patterned Substrates Via Genetically Fused Metal-Binding Peptide. *Biotechnol. Bioeng*. 2009, 103, 696–705.

[238] Thammasittirong, A.; Dechklar, M.; Leetachewa, S.; Pootanakit, K.; Angsuthanasombat, C. *Aedes aegypti* Membrane-Bound Alkaline Phosphatase Expressed in *Escherichia coli* Retains HighAffinity Binding for *Bacillus thuringiensis* Cry4Ba Toxin. *Am. Soc. Microbiol. Appl. Environ. Microbiol*. 2011, 77, 6836–6840.

- [239] Gomes, W. P.; Vanmaekelbergh, D. Impedance spectroscopy at semiconductor electrodes: Review and recent developments. *Electrochim. Acta.* 1996, 41, 967–973.
- [240] Cai, Q.; Wei, W.; Wang, R.; Nie, L.; Yao, S. Measurement of Serum Alkaline Phosphatase with a Surface Acoustic Wave Impedance Sensor Device. *Anal. Sci.* 1997, 13, 121–125.
- [241] Lee, J. Y.; Ahn, J. K.; Park, K. S.; Park, H. G. An impedimetric determination of alkaline phosphatase activity based on the oxidation reaction mediated by Cu^{2+} bound to poly-thymine DNA. *RSC Adv.* 2018, 8, 11241–11246.
- [242] Lucarelli, F.; Marrazza, G.; Mascini, M. Enzyme-based impedimetric detection of PCR products using oligonucleotide-modified screen-printed gold electrodes. *Biosens. Bioelectron.* 2009, 20, 2001–2009.
- [243] Ferancova, A.; Hattuniemi, M.; Pääkkönen, S.; Tervo, P.; Ohtonen, E.; Sesay, A.; Rätty, J.; Virtanen, V. Electrochemical Impedance spectroscopy for Monitoring of alkaline Phosphatase reaction with substrate. *Procedia Technol.* 2017, 27, 315–316.
- [244] Shrikrishnan, S.; Sankaran, K.; Lakshminarayanan, V. Electrochemical Impedance Analysis of Adsorption and Enzyme Kinetics of Calf Intestine Alkaline Phosphatase on SAM-Modified Gold Electrode. *J. Phys. Chem. C.* 2012, 116, 16030–16037.
- [245] Hemed, N. M.; Convertino, A.; Shacham-Diamand, Y. Alkaline phosphatase detection using electrochemical impedance of anti-alkaline phosphatase antibody (Ab354) functionalized siliconnanowire-forest in phosphate buffer solution. *Sensors Actuators B. Chem.* 2018, 259, 809–815.
- [246] Kaatz, M.; Schulze, H.; Ciani, I.; Lisdat, F.; Mount, A. R.; Bachmann, T. T. Alkaline phosphatase enzymatic signal amplification for fast, sensitive impedimetric DNA detection. *Analyst* 2012, 137, 59–63.
- [247] Abe, M.; Havre, P. A.; Urasaki, Y.; Ohnuma, K.; Morimoto, C.; Dang, L. H.; Dang, N. H. Mechanisms of confluence-dependent expression of CD26 in colon cancer cell lines. *BMC Cancer* 2011, 11, 51.
- [248] Chetrite, G.; Delalonde, L.; Pasqualini, J. R. Comparative effect of embryonic mouse fibroblasts (Balb/c-3T3) on the proliferation of hormone-dependent (T-47D) and hormone-independent (MDA-MB-231) human breast cancer cell lines. *Breast Cancer Res Tr.* 1993, 25, 29–35.
- [249] Asada, S.; Sasaki, K.; Tanaka, N.; Takeda, K.; Hayashic, M.; Umeda, M. Detection of initiating as well as promoting activity of chemicals by a novel cell transformation assay using v-Ha-rastransfected BALB/c 3T3 cells (Bhas 42 cells) 2005, 588, 7-21.
- [250] Joanne, K.; Itano, J. B.; Conde, F.; Saria, M. Core Curriculum for Oncology Nursing. 5th ed. Elsevier Inc. Amsterdam, The Netherlands. 2016.

Chapter 2

Optimization of Viability Assays for Cell Culture

Note: This chapter has been published in Journal of Applied Science. Please refer to Appendix.

2.1 Aim and objectives

The aim of the work focused on in this chapter was to optimize optimal density of cells for alkaline phosphatase release using a fluorescent detection method. Resazurin was used as an indicator of cell viability. This optimised density would then be used for experiments of real-time monitoring alkaline phosphatase release, as discussed in chapter 3, chapter 4 and chapter 5. The following objectives were designed to achieve the aim of this chapter. The novelty of this aim was that no optimization was done for resazurin concentration with the given cells.

1. To maintain cell confluence at 70% to 85% in 75T flask and make them available in the log phase.
2. To obtain the calibration curve for each cell line by optimizing parameters of the resazurinbased assays involves concentration of resazurin and incubation time.
3. To determine the optimal density of each cell line and verify cell number obtained by the fluorescent signal by using haemocytometer method and microscope images.
4. To investigate the cell viability of the given cells at post-confluence culture using statistical analysis.

2.2 Introduction

2.1.1 Principle

Biological laboratory requires certain devices in order to monitor cells adhesion and cellular responses. Microscope device is normally used to observe the normal morphological shape of cell, thus determination if the cells attach or not attach on substrates. Attachment is a sign of healthy cells. This way allows monitoring of proliferation of cells as well. However, microscope does not quantify of cell number. The common way of accounting cells is by using the haemocytometer device. This way is a standard assay in most of the biological laboratory; however, it is time-consuming, requires cell lysis as well as requires manual account. These limitations cause increment of human errors during conducting experiments. Accordingly, many assays are purposed in this field for measuring cell viability level by using dyes. These dyes can be detected based on different principles. For example, dye-exclusion principle, which uses the microscope to account cells inserted in the haemocytometer. A common dye for this method is Trypan blue, which is used to test the cell membrane integrity. Membrane of living cells will exclude the blue dye whereas the membrane of dead cells will be stained by the blue colour. This way requires cell lysis and allows accounting of the ratio between live/dead cells. Principle of luminescent is used Adenosine triphosphate (ATP) content to measure the living cells. The reaction of converting nonluminescent form "luciferin" into a luminescent form "oxyluciferin" are catalyzed by the enzyme of luciferase, and in the prsence of magnesium ion. This reaction will not occur in living cells unless they produce ATP. Producing ATP means cells alive. This can be detected by luminometric microplate reader. This is the most sensitive method, but it suffers from low reproducibility. It is suitable for very low number of cells. The colorimetric and fluorometric principles take advantages of cells metabolic activity (chapter 1, section 1.9.1).

Metabolic based assays are simple, cheap, and are a one-step assay, thereby avoiding the disadvantages of the above-mentioned assay. Numerous dyes can be used to reflect metabolic activity through redox reactions in live cell membranes. One of these dyes is resazurin, which under constant experimental conditions, can provide a stable rate of fluorescence intensity and quantify cell numbers [1-3]. Resazurin can be defined as a cell permeable redox indicator that helps in tracking the number of viable cells (Figure 2.1). Physiological buffers can absorb resazurin, resulting in a deep blue solution. Viable cells have active metabolisms and can therefore convert resazurin into a pink fluorescent solution [4].

Cell viability that has been used during cancer biomarkers analysis was membrane integrity [5,6], flow cytometry [7], and phase-contrast microscope images [8]. These assays require cell lysis [9] and result in an endpoint assay [10]. Beside that the microscope device is undesirable for applications such as sensors or lab-on-a-chip [11,12]. Accordingly, since these methods showed limitations in applications of cellular adhesion, they made attention drawn towards metabolic-based assay. To the best of our knowledge, this is the first study that discusses cell viability during cancer biomarker release using a resazurin-based assay.

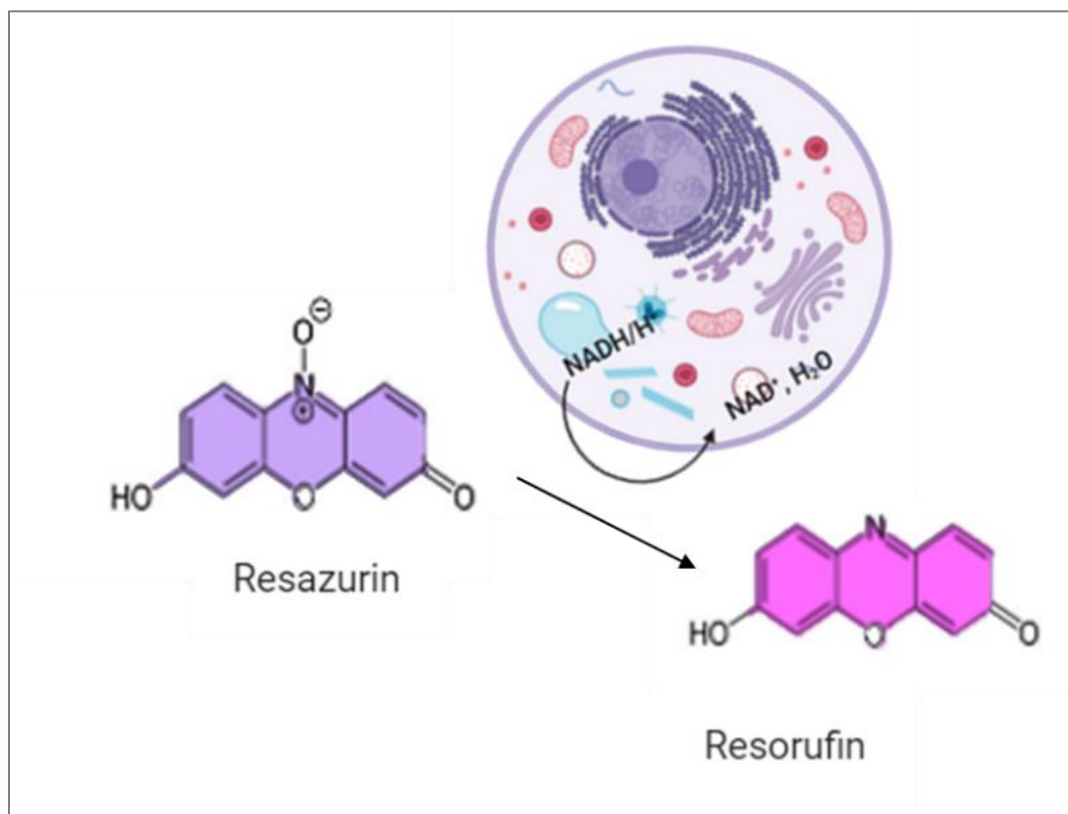


Figure 0.1: reduction of resazurin into resorufin during metabolism activity of cells.

2.1.2 Literature review

The optimization of resazurin-based assay depends on various parameters, including resazurin concentration, incubation time and cell number. This is organised in three steps. (1) Different concentrations of resazurin are added to the culture medium of incubated cells. (2) At various time

intervals, the redox reaction, in which resazurin is reduced by the cells, is measured by fluorescence readings at 544 nm and 590 nm. (3) The optimal concentration of resazurin versus particular cell type is used at different cell numbers to facilitate the relationship between the fluorescent signal and the cell number at constant time. Several reports have shown the optimization of resazurin reduction assays [13] for cytotoxic agents, antifungal agents, antibacterial agents, the identification of parasites, and the drug sensibility of parasites for large-scale screenings, biofilm, and for cell expansion in matrix scaffolds using bacteria [14,15] fungi and yeast [16,17,18], parasites [19,20], and human cells [18,21]. Optimal concentration of resazurin appear to be not well grounded for the suggested cells. For example, the concentration of 44 μM of resazurin has been used for different cells lines (primary rat hepatocytes [22], renal tissue [23], engineered liver and kidney tissues [1] and kidney cell line [21]. Constant concentration of resazurin is inconsistent when measuring different metabolic activity for different cells. This optimization will provide simple and reproducible methods for quantifying cell number during ALP release.

2.1.3 The Problem statement

As describe in the literature review, the concentration of resazurin with cancer cells has not been dealt with in depth. The metabolism activity of cells varies from one to another, which reveal that a neglected area in this field. Therefore, it is important to define the optimal concentration of resazurin for each cell line. It is quite noticeable that Balb/c 3T3 cells, which is an embryonic cell line, is used as it is more sensitive to contact inhibition of cell growth than cancer cell lines. This model of cells will make it easy for indicating the stationary phase of other cells in this chapter.

2.1.4 Summary

In this chapter, calibration curves of resazurin for each cell line was determined. The target density of the cells of Balb/c 3T3, MCF-7, A549 and Ht-29 were determined. All cells were maintained to reach inhibitive growth contact simultaneously in order to allow ALP release. The target density was identified as when cells proliferated for at least four days and then reached contact-inhibited growth. The cell viability was verified by using haemocytometer method and microscope images. The cell viability of the given cells at post-confluence culture was investigated using statistical analysis.

2.3 Methodology

2.3.1 Reagents

Mouse embryo fibroblast cells (Balb/c 3T3 Line), breast carcinoma epithelial cells (MCF-7 line), lung carcinoma epithelial cells (A-549 line), colon carcinoma epithelial cells (Ht-29 line) purchased from (ATCC, the UK). 70% ethanol, and nanopure water provided from (Grade 18 M Ω , Tyndall National Institute, UCC). Newborn calf serum (NBCS), fetal bovine serum (FBS), Dulbecco's modified Eagle's medium (DMEM), minimum essential medium Eagle (MEME), and McCoy's 5A Medium, Hank's balanced salt solution (HBSS), Trypsin/EDTA solution, resazurin, Virkon[®], magnesium chloride (MgCl₂), sodium chloride (NaCl),

diethanolamine (DEA), Triton X-100, and para-nitrophenol phosphate (p-NPP), and calf intestinal phosphatase (ALP) purchased from (Sigma, Ireland).

2.3.2. Instrumentation

Cell culture hood (Esco Airstream® Class II), 5% CO₂ incubator (Incusafe Panasonic), water bath 37 °C (Fisherbarnd), centrifugation (universal 320 Hittch zentrifugen and Eppendorf 5415D Centrifuge) were used. An inverted microscope and camera (Olympus), fluorescent plate readers (Spectra Max Gemini), absorbance plate reader (Diasource ELISA Reader), hemocytometer slide (Reichert Bright-Line), glass cover slips (menzel-gläser) and cell counter, pipettes (Rainin Pipet-X) and micropipettes (Gilson Pipetman®), pipette tips (Greiner Bio-One), pipettors (5 mL, 10 mL, and 25 mL), cell culture vessels (75T flasks, 1.5 mL, 15 mL, 50mL centrifuge tubes, 96- and 48-well plates), and syringes 45 nm filters (Sigma, Ireland) were also used. Figure 2.2 shows the typical equipment of cell culture lab.



Figure 0.2: Typical equipment of cell culture lab.

2.3.3 Cell Culture

The cancer cell lines used during this project were stored in liquid nitrogen prior to being cultured. To begin cell growth, they were removed from storage and quickly defrosted (less than a minute). The entire contents (1 mL) of the cryogenic vial were then pipetted into a 15 mL-tube that contained 9 mL of prewarmed complete media (Table 2.1). The tube was centrifuged to dispose of dimethyl sulfoxide, which was present in the supernatant. The cells were re-suspended in 5 mL complete media and placed in a T75

Chapter 2

flask that already contained 35 mL of completed media in order to reach a volume of 40 mL. The flask was incubated in the incubator at 37 °C and 5% CO₂ to reach 70% confluence.

Table 0.1: The media and serum of each cell line used for cell culture.

	Cell lines	Balb/c 3T3	A549	MCF-7	Ht-29
Complete media	Media	DMEM	DMEM	MEME	McCoy's 5A
	10 % Serum	NBCS	FBS		

Completed media represent the addition of 10% of serum to the media suitable for each cell line, according to the manufacturer's recommendations.

The cells were sub-cultured at least three times before optimization began. Figure 2.3 illustrated a schematic of sub-culturing cells three times before seeding. Briefly, the subculture procedure was achieved by removing old media via a sterile plastic pipette, followed by two washes with pre-warmed HBSS. A total of 4 mL of trypsin was then added, and the flask was incubated for 5–8 min to allow the cells to detach. Then, 6 mL of complete media was added to inactivate the trypsin. The cell suspension was placed in a clean 15 mL centrifuge tube, and the cells were centrifuged for 5 min at 1000 rpm. The supernatant was removed, and the cell pellets were re-suspended in 5 mL of fresh media. The desired cell number was seeded in a 48-well plate, and the final volume of media was added. All experiments were applied in a 48-well plate.

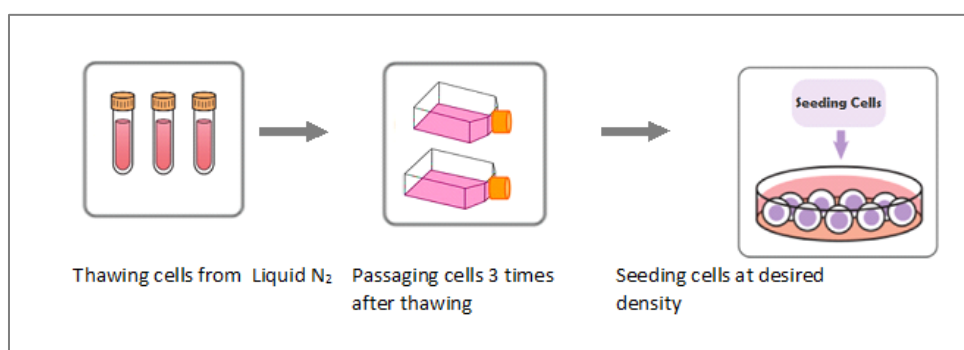


Figure 0.3: Schematic of sub-culturing cells three times before seeding.

2.3.4 Determining the optimal concentration of resazurin

Each cell line required a certain concentration of resazurin to ensure viability. Resazurin was dissolved in HBSS to a final concentration of 2 mM to make a stock solution. The stock solution was filtered using a syringe with 0.45 nm pores. To make an intermediate standard, the stock solution was diluted once more in complete media at 10% giving 200 µM. Two-fold serial dilutions were then made, starting with 200 µM.

This was then added to cells that were previously seeded in triplicate at the same density (250×10^3 cell/mL). The plates were incubated with the various concentrations of resazurin at a final volume of 0.5 mL for 24 h. The fluorescent signal was then recorded at 544 excitation and 590 nm emission wavelengths using the fluorescent plate reader.

2.3.5 Determining the optimal time of incubation with resazurin

Concentrations of 350×10^3 cell/mL were prepared and diluted in 2-fold using the complete media of each cell line. The dilutions were seeded in 48-well plates and incubated at 37 °C for 24 h to allow for attachment. Old media were replaced by the optimal concentration of resazurin in the case of each cell line. The plates were incubated and monitored after two hours and then continuously over a 24-h period. The fluorescent signal was taken at different times at 544 excitation and 590 nm emission wavelengths using the fluorescent plate reader.

2.3.6 Determining the calibration curve of resazurin and cell numbers

Resazurin is a metabolic-based assay that reflects cell viability. In order to make it an assay that measured the cell number, 2-fold serial dilutions of the cell number starting from 250×10^3 cell/mL were seeded in triplicate, and complete media were added for a final volume of 0.5 mL. Cells were incubated for 12 h to allow the cells to attach and avoid duplicating. Old media were replaced by the optimal concentration of resazurin in the case of each cell line. Four hours later, the fluorescent signal was recorded at 544 excitation and 590 nm emission wavelengths using the fluorescent plate reader. The theoretical calibration curves were made from a cell concentration of ($4\text{--}60 \times 10^3$ cell/mL). The resulting linear equation was used to estimate the fluorescent signal for the cell concentration applied in this assay.

2.3.7 Determining the optimal density of cell lines.

The target density for this chapter was identified as when cells proliferated for at least four days and then reached contact-inhibited growth. This was where the target analyte started to express. Five concentrations of cells were prepared ($350, 160, 80, 40, 20 \times 10^3$ cell/mL). The final volume of complete media was 0.5 mL. The cells were incubated at 37 °C and monitored daily for five days. Old media were changed every two days to keep cells healthy and with sufficient nutrients. On day 1, resazurin was added to cells in plate 1, and four hours later, the fluorescence signal was recorded. The process was continued for the other plates until day 5.

2.3.8 Determining cell number based resazurin assay.

The optimal density of each cell line was seeded in triplicate, and cell growth was assessed at 24-h intervals over five days. Old media were changed every two days to keep cells healthy and with sufficient nutrients. To determine the daily fluorescent signal, media were replaced by the optimal concentration of resazurin in the case of each cell line. Four hours after this, the fluorescent signal was recorded. The linear equation of the obtained calibration curve was used to quantify the cell number daily over five days.

2.3.9 Microscope images

Images of cell-confluence were taken at 24-hour intervals over 5 days using the inverted microscope and camera. Due to the presence of phenol red, which interferes with the light of microscopes, cells were washed twice with HBSS. Images were then taken from the centre of the wells.

2.3.10 Hemocytometer assay

Cell viability was also determined using the hemocytometer assay for the optimal density. As previously noted, cells were seeded in triplicate, and cell growth was assessed at 24-h intervals over five days. The old media were changed every two days to keep cells healthy and with sufficient nutrients. After the washing and trypsinization processes, harvested cell pellets were re-suspended in complete media, a coverslip was used to cover the two counting chambers, and then a drop of the solution was inserted, allowing the solution to spread gently. Under the microscope as illustrated in figure 2.4, nine squares were observed to be accounting cells. Accounting cells had to be averaged and multiplied by the three demotions of the hemacytometer, where the width and height equaled 1 mm, and the depth equaled 0.1 mm to get a final concentration of cell per mL using the following equation:

$$C = \frac{n}{10^{-4}}$$

where C is the final concentration of cell numbers per mL and n is the average of cell numbers counted from each square.

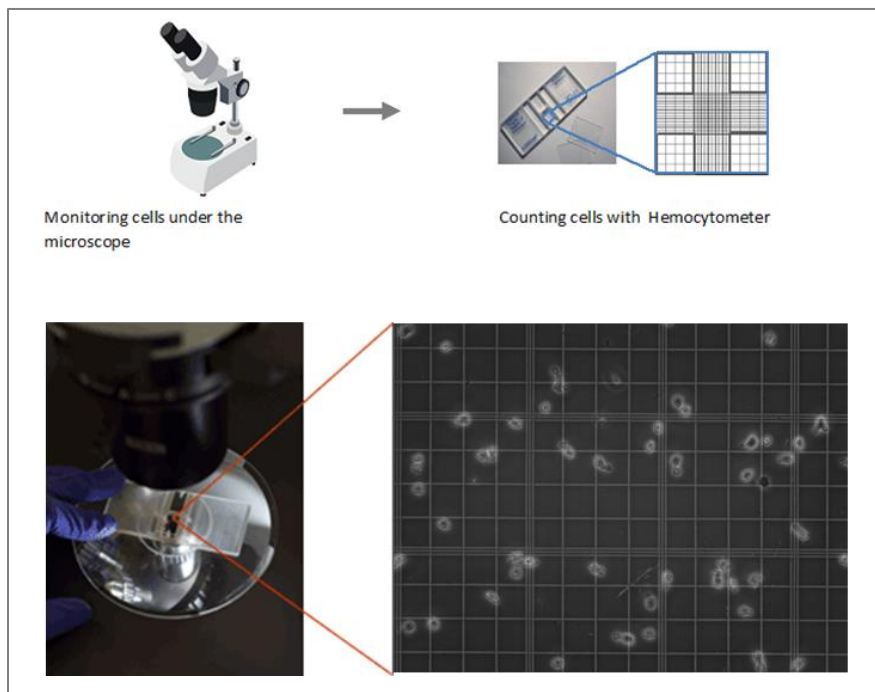


Figure 2.4: Actual accounting of cell number using hemocytometer.

2.3.11 Cell viability at post-confluence culture

Cells can be differentiated using post-confluence culture to ensure ALP release, which makes the determination of the cell viability of cells at post confluence culture important. Cells were seeded in 48well plates at a concentration of 40×10^3 cells/mL for the following cells: Balb/c 3T3, A549, and MCF-7, and at a concentration of 80×10^3 cells/mL for the Ht-29 cells. Cells had the media changed every two day to keep them healthy and with sufficient nutrients. After they achieved their exponential growth and met the 95–100% confluence (Day 4), the cells were maintained in growth media for a further two days. Old media were replaced by the optimal concentration of resazurin in the case of each cell line for the fourth, fifth, and sixth days. Cells were incubated with resazurin for four hours. Vehicle control of each cell was prepared by adding two drops of Virkon® in the complete media for 24 h the night before the assay. A reszurin control was added to media with no cells. The fluorescence signal was recorded for each day.

2.3.12 Data analysis:

Single factor of analysis of variance (ANOVA), MS Excel, and Origin were used in order to analyze the results of the experiments and to ensure the limitation of errors. Results were displayed as mean \pm SD. There were: $n = 3$ was replicated for each condition in each individual experiment and the displayed data represent the mean of at least three independent experiments. The coefficient of variation % and p-values and Z-factor were considered.

2.4 Results and Discussion

2.4.1 Determining the optimal concentration of resazurin

Metabolic activity may differ between cells, which makes optimizing the concentration of resazurin important. Cells were plated in 48-well plates and incubated for 24 h to allow for attachment. Different concentrations of resazurin were added, starting with the highest possible concentration that would not be toxic to cells ($\sim 200 \mu\text{M}$). This was then serially diluted to 1:2 to produce a range of μM /well. All measurements were done with 24-h incubation times. Figure 2.5 A–D shows that the resazurin reduction rate was positively proportional to the resazurin concentration. However, this gradual increase was limited by the highest concentration, where, after the optimal concentration, the rate of resazurin reduction decreased. Figure 2.5 A–C illustrates the highest reduction rate at $50 \mu\text{M}$ and then shows an inverse relationship. Figure 2.5 D shows the highest reduction rate at $100 \mu\text{M}$, while $200 \mu\text{M}$ exhibited a high deviation. This data indicate that the optimal concentration of Balb/c3T3, A549, and MCF-7 was $50 \mu\text{M}$, and that of the Ht-29 cell was $100 \mu\text{M}$. Figure 2.5 E shows the coefficient variance of the analysis data at various resazurin concentrations. At the lowest recorded concentrations of resazurin, the relative variability exceeded 20%. The CV% then fell and reached its lowest level at $100 \mu\text{M}$. However, at higher concentrations, this trend reversed and CV% started to increase. These findings indicate that resazurin at a high concentration may be destructive to cells [24].

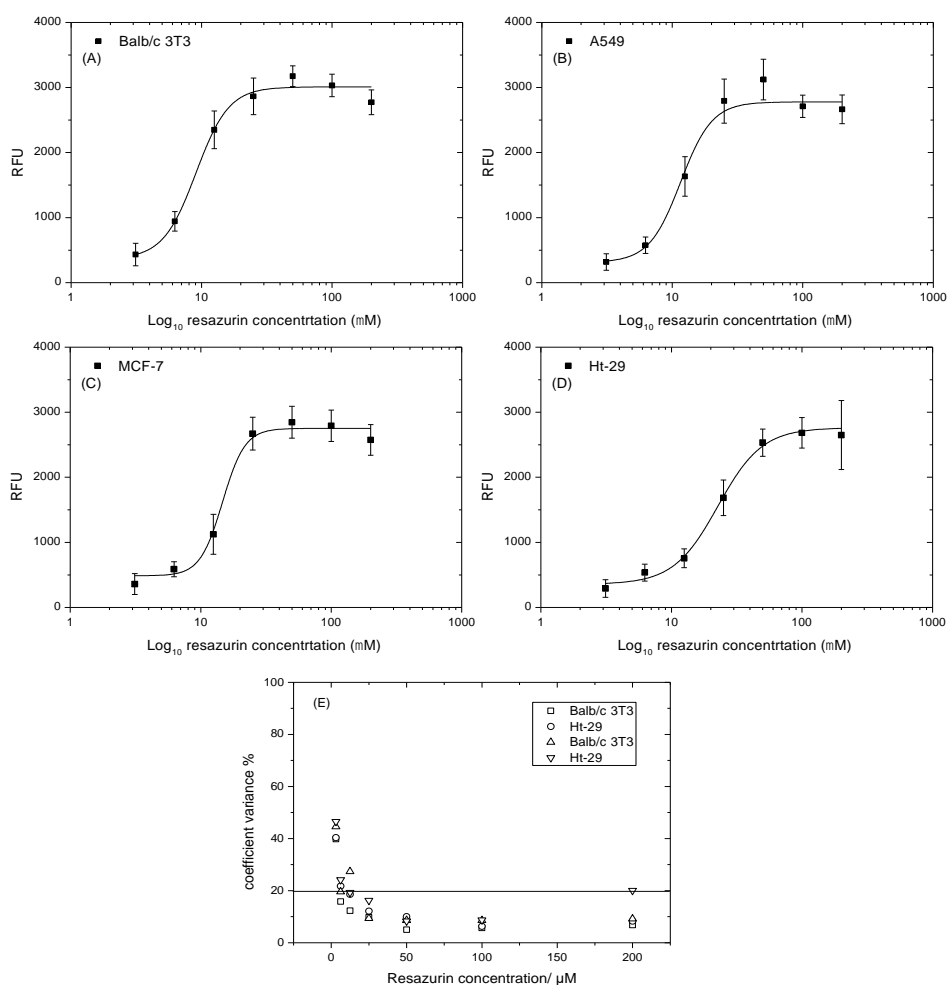


Figure 0.5: Optimization of the concentration of resazurin at various cell lines. (A) Balb/c 3T3 cell lines; (B) A549 cell lines; (C) MCF-7 cell lines; (D) Ht-29 cell lines; (E) coefficient variance % of resazurin concentration of vs cells numbers. Data are expressed as the mean \pm SD of measurements of three independent experiments.

2.4.2 Determining the optimal time of incubation with Resazurin

It is important to determine the resazurin incubation time, because resazurin reduction is affected by time and cell density. Cells were plated at the highest saturation density ($\sim 3 \times 10^5$ cell/mL), then serially diluted in a ratio of 1:2 to produce the range of cell density/well. After 24 h, the attached cells were incubated with a set volume of resazurin working solution for 2, 4, 12, or 24 h in order to cover all the recommended times (1–24 h). Figure 2.6 A–D shows that the number of cells was strongly correlated with the values of resazurin reduction. This correlation was linear from two to four hours, but it started to lose linearity when the incubation time increased from 12 to 24 h. Linearity after two hours was positively proportional to cell densities, but it still demonstrated a low slope, which may underestimate cell numbers. A 4-h incubation time proved to be a preferable incubation time. The slope at the 4-h incubation time was almost two times higher than that of the 2-h incubation time. The occurrence of high density may form

hydroresorufin faster. This high density was avoided in this research study. A 12-h incubation time showed an increase at low density, and then the rate of resazurin reduction started to decline by ($\sim 1 \times 10^5$ cell/mL). This incubation time was avoided to reduce errors for the rest of the investigation where proliferation needed to be detected. After 24 h, the incubation time levelled, since the lowest density had the same rate as the highest, making the 24 h suitable when time parameters were not recommended. Coefficient variance (CV %) was highly reproducible in the non-linearity assays, although it was high at low densities of cells. Figure 2.6 E shows that CV% exceeded a range of 20% at the lowest density of cells in the linear assays. It appears that four hours is the optimal time recommended. This is in agreement with Hamalainen–Laanaya's contributions [25], which state that the cell density should be finely tuned in order to prevent the over-reduction of resazurin and ensure the applicability of the resazurin assay.

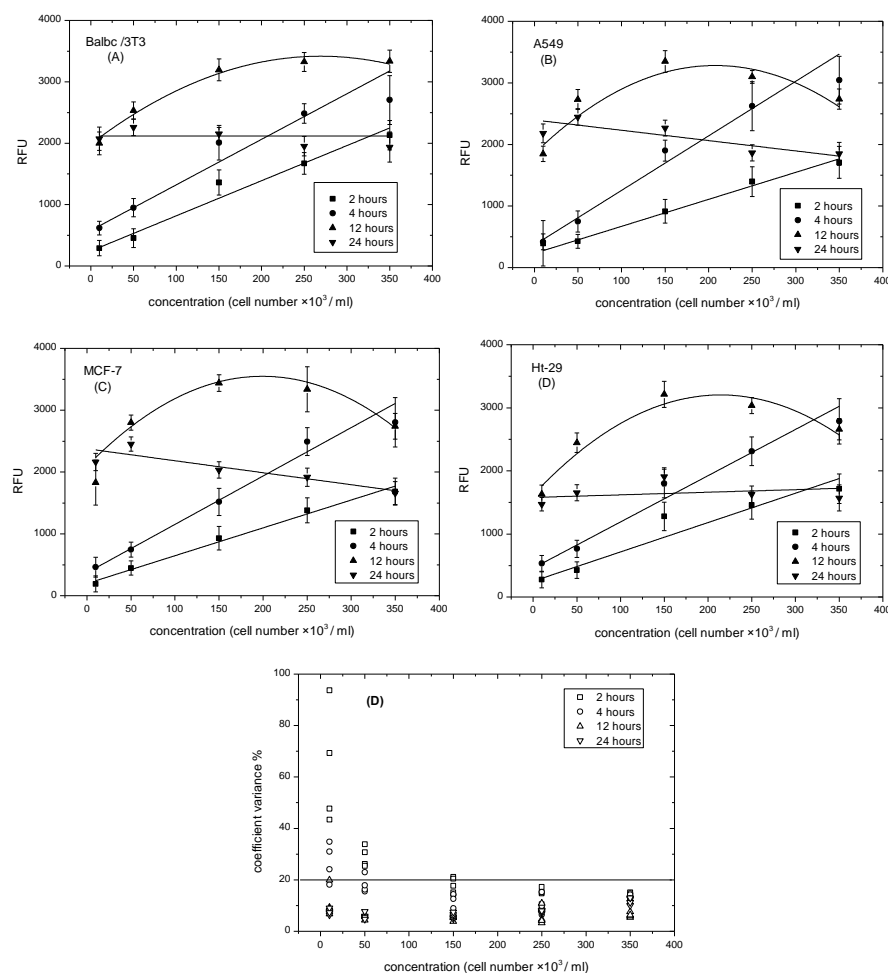


Figure 0.6: Effect of incubation time on fluorescence intensity measured during resazurin reduction using linear function model (2, 4, 12 hours) and rational function model (24 hours). (A) Balbc/3T3 cell lines; (B) A549 cell lines; (C) MCF-7 cell lines; (D) Ht-29 cell lines; (E) Coefficient variance % of incubation time vs. cells numbers. Data are expressed as the mean \pm SD of the measurements of three independent experiments.

2.4.3 Determining the standard curve of Resazurin and cell numbers

Cell numbers can be quantified by the calibration curves of resazurin reduction. The calibration curve of each cell line was generated by plating the cells lines (Balb/c 3T3, A549, MCF-7, and Ht-29) at the same initial density ($\sim 250 \times 10^3$ cell/mL), then serially diluting in a ratio of 1:2 to produce a range of cell density/well. Eight hours later, and before dividing, resazurin solution was added according to the optimal concentration and incubated for four hours. Figure 2.7 A–D shows the experimental and theoretical calibration curves produced by acceptable data over the concentration range of (~ 4 – 250×10^3 cell/mL) of the four cell lines. In comparison with the theoretical calibration curves, which were calculated using the linear equation of cells ranging from (4 – 60×10^3) cell/mL, the experimental curves of the four cell lines displayed an exponential shape at the high concentration with adjusted R-squared of 0.97, 0.97, 0.99, and 0.98 for the cells of Balb/c 3T3, A549, MCF-7 and Ht-29, respectively [26]. The shape was most clear in the Balb/c 3T3 cell lines, where cells reached the inhibitive growth point, and least clear in the MCF-7 cell lines. This saturating trend might result in different cell sizes. For example, the MCF-7 size was 5–7 μm in diameter [27], this then limited the cell attachment to the plate surface. Therefore, the differences between the two curves, theoretical and experimental, were determined for each dilution ratio. Figure 2.7 F illustrates the significant data of cell number (~ 4 – 250×10^3 cell/mL), which were less than 10% for all cell lines. However, at the range of (125 – 250×10^3 cell/mL), the percentage of errors barely exceeded 10% for all cell lines. Notably, the repeatability of results can be interpreted in Figure 2.7 E. The relative variability of the lowest recorded cell numbers barely exceeded 20%, while at high cell numbers, the CV% was the lowest.

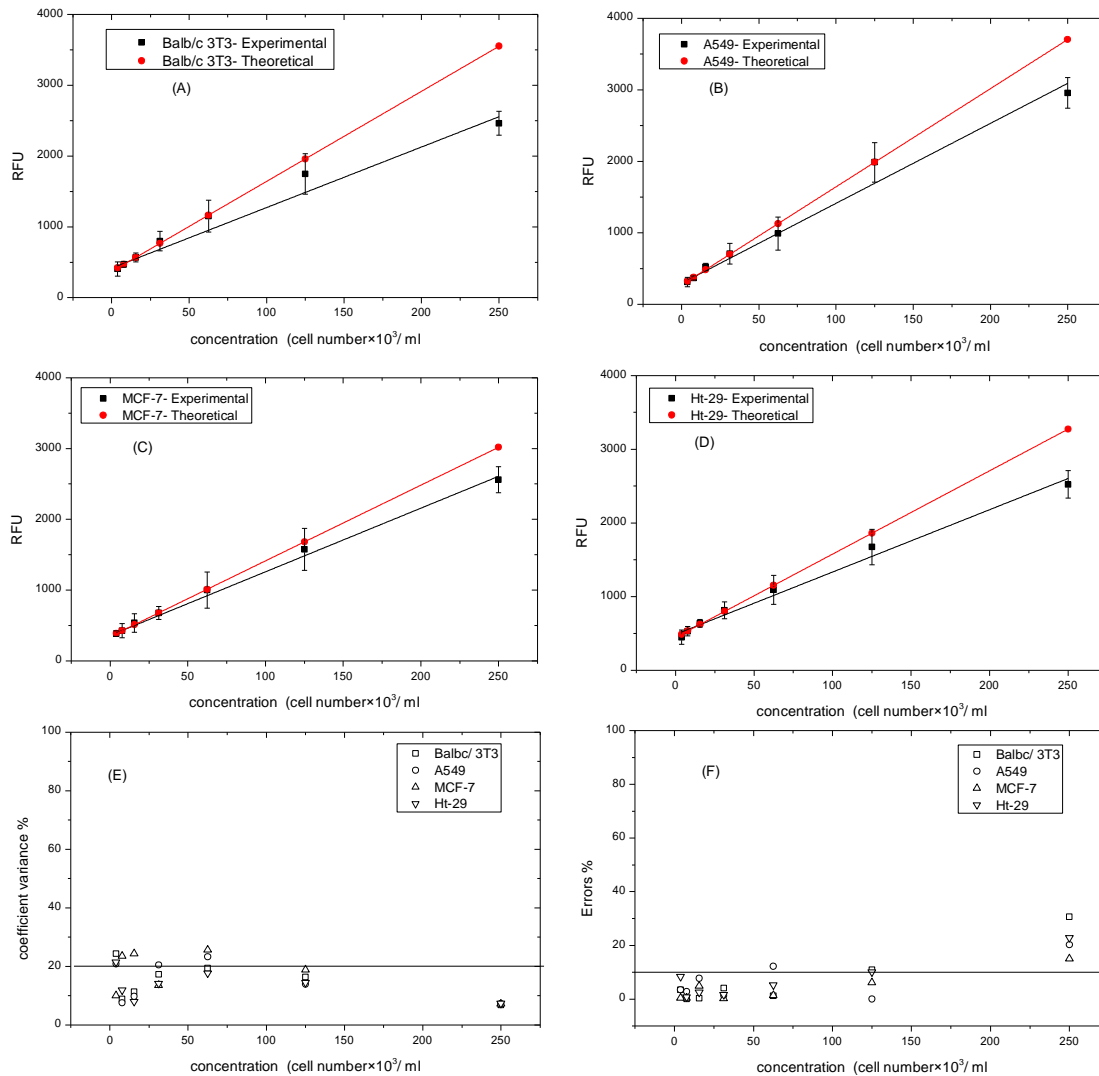


Figure 0.7: Experimental and theoretical standard curves of resazurin at various cell lines. (A) Balbc/3T3 cell lines; (B) A549 cell lines; (C) MCF-7 cell lines; (D) Ht-29 cell lines; (E) Coefficient variance % of experimental curves vs. cells numbers. (F) Errors % of theoretical and experimental curves vs. cell number. Data are expressed as mean \pm SD of measurements of three independent experiments.

2.4.4 Determining the optimal density of cell lines.

There are several stages in the life cycle of mammalian cells. In one of these stages, hormones, protein, enzymes, etc. are produced. To allow the expression of these products, cellular functions such as adhesion, proliferation, migration, or apoptosis are usually investigated [13, 22]. Cells were plated at an initial density of (320×10^3 cell/mL) and then serially diluted in a ratio of 1:2 to produce the range of cell density/well. This was done to make the cells simultaneously reach

contact-inhibited growth. Cell growth was monitored over five days and resazurin reduction was recorded. Figure 2.8A–D shows the growth curves of the four cell lines at the five different densities. Low density with an s-shape expressed logistic growth, whereas high density failed to exhibit an s-shape and levelled out from day 1. Balb/c 3T3 cell lines displayed an s-shape at $20\text{--}40 \times 10^3$ cells/mL, but for the higher densities, $80\text{--}320 \times 10^3$ cell/mL showed approximately level density, although 80×10^3 cell/mL exhibited a little growth at day 1, which means that 40×10^3 cell/mL is the optimal density of the Balb/c 3T3 cell lines (Figure 2.8A). The A549 cell lines behaved the same as the previous cell line, but the s-shape of the lowest density 20×10^3 cell/mL was quite unclear. From Figure 2.8B, it is clear that 40×10^3 cell/mL is the optimal density (Figure 2.8B). Like the Balb/c 3T3 cell lines, the A549 cell lines at the higher densities ranged from $80\text{--}320 \times 10^3$ cell/mL and levelled by day 1. Figure 2.8C shows that the MCF-7 cell lines displayed an s-shape of 20×10^3 cell/mL, but at a very low reduction rate of resazurin (~ 1000 nm). The 40×10^3 cell/mL sample demonstrated a J-shape, which began to level by day 5. The higher densities, ranging from $160\text{--}320 \times 10^3$ cell/mL, did not show any growth behavior. This meant that 40×10^3 cell/mL was the optimal density. Ht-29 behaved quite differently to the other cell lines, where at low densities $20\text{--}40 \times 10^3$ cell/mL, it showed a j-shape (Figure 2.8D), whereas at 80×10^3 cell/mL, it showed an s-shape, which makes it the optimal density. Like the other cells, the Ht29 cell lines at the higher density ranged from $160\text{--}320 \times 10^3$ cell/mL and levelled on day 1 and then started to decrease. The CV% of all five days was less than 20% on day 1, and on day 2, cell numbers barely exceeded 20%. This was probably because of the lag phase and cells adapt themselves in the new environment by responding to the induce of attachment to the substrate. This investigation facilitated the determination of the optimal density of each cell line and makes it applicable for this research study, where the expression of ALP versus cell viability was investigated [28, 29].

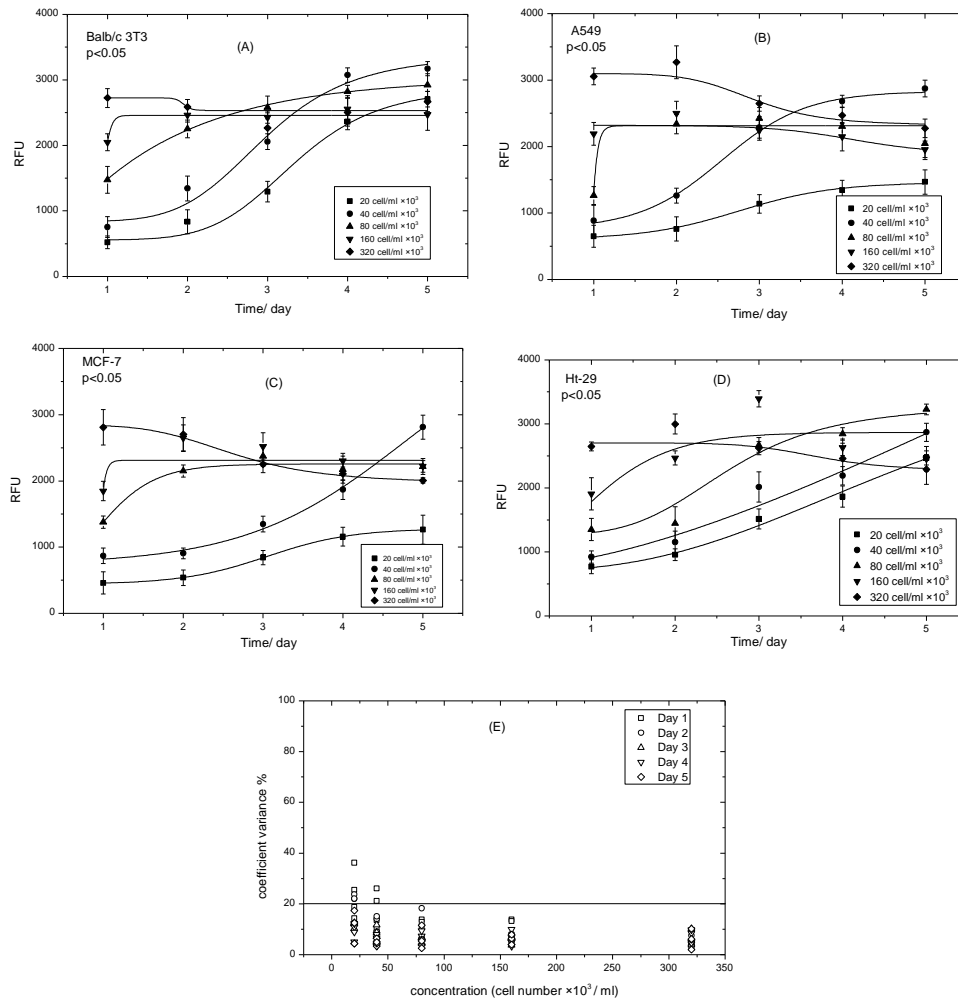


Figure 0.8: Logistic growth curves of the different cell densities at various cell lines over five days. (A) Balb/c 3T3 cell lines; (B) A549 cell lines; (C) MCF-7 cell lines; (D) Ht-29 cell lines; (E) coefficient variance % of growth curves vs. cells numbers. Data are expressed as the mean \pm SD of measurements of three independent experiments.

2.4.5 Microscope images

The determination of cell shape per day is important in order to know the state of the cells when the experiment begins and when sampling starts simultaneously. The optimal density of each cell obtained from the previous experiment was seeded and monitored over five days. It is obvious from Figure 2.9, in the baseline, that the cells behaved differently. The Balb/c 3T3 and MCF-7 cells attached quickly and started to flatten. A549 and Ht-29 cells had a rounder shape, which means that they needed a longer time to attach. Balb/c 3T3 cells showed constant division from day 1 to day 3 and 80–100% confluence by days 4 and 5. This probably means that cells reached the inhibitive growth contact quickly by day 4, and that there was no working area left for more division. This result met the resazurin reduction findings in Figure 2.8 A. A549 cells started to flatten by day 1, had a spindle shape by day 2, and then had sudden doubling,

which explains the results found in Figure 2.7 B. By days 4 and 5, cells seemed to have no space to divide, so they shrank and started to proliferate, as these kinds of cells rarely form multilayers. MCF-7 cells, on the other hand, showed a longer lag phase and slowly divided from day 1 to day 3. Cells barely reached almost 70% confluence by day 4 and had space to confluence in day 5. These findings explain the j-shape displayed in Figure 2.7 C and ensured that no multilayer had formed. Ht-29 cells started to flatten in day 1 and then had confluence from day 2 to day 4. Likewise, for Balb/c 3T3 and A549 cells, Ht-29 cells had no space to double. Ht-29 cells seem to have their extracellular matrix spread out and cover the area in day 3. This extracellular matrix reduced when cells reached confluence in days 4 and 5. Another microscope or dyes might be used to display this division.

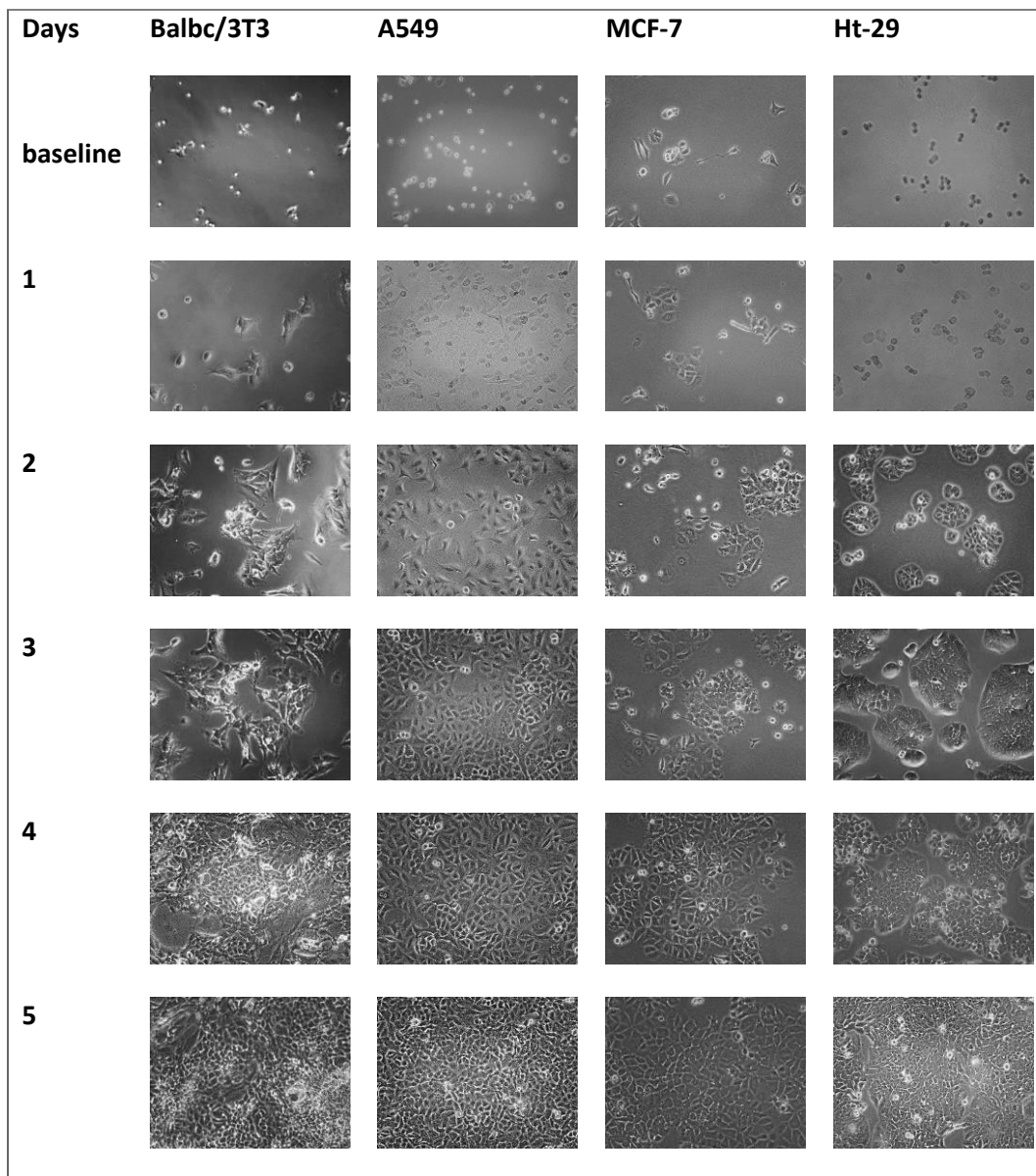


Figure 0.9: Microscope images of the four cells over five days.

2.4.6 Determining cell number and comparing to hemocytometer assay.

The cell culture growth curve represents the number of live cells over a period of time and covering the four phases [30]. In the first two growth phases, cells are more likely to be consistent, while in the stationary phase, cells may be more differentiated. Morphology may become polarized, and has more spreading for the extracellular matrix. Therefore, determination of the viability of cells in using quantitative analysis was required. Resazurin reduction of each cell obtained from the previous experiment was used to estimate viable cells using the linear equation obtained by the calibration curve. For comparison, the number of cells was also compared to manual accounting using the hemocytometer assay. Figure 2.10 shows the comparison of the estimating cell number and accounted cell number. Estimating cell number had the same trend as the resazurin reduction assay previously described in Figure 2.8. The results given by the hemocytometer displayed logistic growth curve. However, there is slight difference between the two assays. Values of the estimated cell numbers in the Balb/c 3T3 and Ht-29 cells were higher than those manually accounted in all phases. A549 cells also had higher estimated values in all phases except for in the stationary phase. On the other hand, MCF-7 demonstrated a different trend, as it showed a J-shape in the estimated cells and an s-shape in the accounted cells. However, the difference between these values on the day of control was high in the Ht-29 cells (84.96×10^3 cells/mL) and MCF-7 cells (70.51×10^3 cells/mL) compared to the difference in Balb/c 3T3 (58.18×10^3 cells/mL) and A549 cells (11.13×10^3 cells/mL). Overall, the growth curves given by the hemocytometer were sharper than the estimated ones. Notably, manual accounting had multiple steps, which increased the chance of losing cells, whereas cell number given by the resazurin assays were estimated theoretically based on a calibration curve, where the possibility of losing cells during assays was low. Moreover, the high standards deviation obtained in the estimated cell number can be minimized by increasing the number of the assay from $n=3$ to $n=9$.

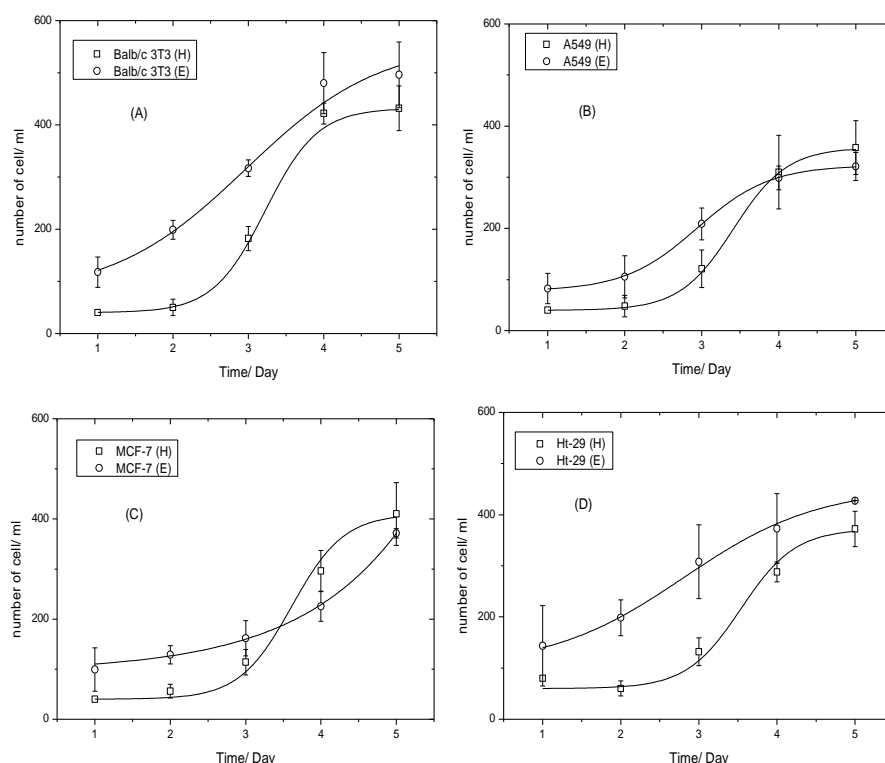


Figure 0.10: Logistic growth curves of (A) Balb/c/3T3 cell lines; (B) A549 cell lines; (C) MCF-7 cell lines; and (D) Ht-29 cell lines, over five days. (○) estimated cell number using linear equation of standard curve and, (□) accounted cell number using hemocytometer; all compared versus incubation time over five days. Data are expressed as the mean \pm SD of measurements of three independent experiments.

2.4.7 Cell viability at post-confluence culture

The cell viability of cells at post-confluence culture was detected. Table 2.2 illustrates the fluorescent signal of resazurin produced during the fourth, fifth, and sixth days for each cell line as well as vehicle control and resazurin control. It is obvious from the data that there was a decrease in cell viability for all of the cells from day 4 to day 6. There was a significant difference between the data of cell viability of day 5 and day 6 compared to that of day 4; but MCF-7 cells in day 5 showed no significant difference ($p > 0.05$) to the control value (day 4). MCF-7 had 70% confluence in day 4, which allow more proliferation (shown in Figure 2.9), which allowed more proliferation. The cells of Balb/c 3T3 and A549 displayed z-factor values between 0.5 and 1 for each culture day compared to the control (day 4). It is quite noticeable that the cells of Balb/c/3T3 and A549 are more unlikely to form multilayers when reaching the contact-inhibited growth point. MCF-7 cells showed a quality assay in day 6, whereas Ht-29 cells illustrated a z-factor less than 0.5 for all the post-confluence culture compared to the control value. That was possible because of the high standard deviation (SD) for all the values in the three days. Notably, the z-factor value mostly depended on the SD. The cell viability of the vehicle controls of the cells of Balb/c 3T3 and MCF-7 was 10.2% and 8.3%, respectively, while those of the cells of A549 and Ht-29 were 18.6% and 18.2%, respectively. Drops of Virkon® may need to be increased for the MCF-7 and HT-29 cells to make dead cells. Optimization of the assay control was then suggested.

Table 2.2: Summary of resazurin data of each cell line versus target days at post-confluence.

	Balb/c 3T3	A549	MCF-7	Ht-29
Day 4	3091.61±28.74	2784.46±43.35	(1887.34±5.36)	(2980.70±44.51)
Day 5	2513.44±7.77 *§	(1952.29±0.82) *§	(1787.48±35.99)	(2655.06±34.07)*
Day 6	1872.74±6.72 *§	(1415.29±44.35) *§	(1407.01±66.13) *§	(2512.21±48.32)*
VC	(412.6±9.9) *§	(597.6±23.3) *§	(237.8±3.1) *§	(623.8±4.5) *§
RC	(97.2±6.3) *§	(78.7±0.9) *§	(80.5±0.3) *§	(82.7±0.7) *§

The data of the cell viability assay-based resazurin was applied for the cells at post-confluence culture. Data are expressed as mean \pm SD of the measurements of three independent experiments. VC (vehicle control,) and RC (resazurin control). Data compared to the control (data of day 4), * (p-value < 0.05 is a significant difference), § (1 > Z-factor > 0.5 is excellent assay).

2.5 Conclusions

ALP determination requires the real-time monitoring of cell behaviour. Various cellular phenotypes are related to gene expression, which helps to understand emerging diseases including cancers. Several previous studies have shown the relationship between ALP and cell viability [38, 39]. However, those studies were conducted under the standard cell culture assay. Function endpoints of those assays are labor-intensive, time-consuming, require detachment of cells, and thus hinder real-time assays and multiplex assays. Quantitative resazurin assays of cell viability have been proposed as a rapid and inexpensive method to evaluate the viability of cells during the release of ALP, which can further be used to verify studies of cell adhesion applications such as cell-based biosensors. The main parameters affecting the results obtained from the resazurin assay include the concentration of resazurin, incubation time, and cell number. The optimal incubation time of resazurin reduction was four hours for all cells. High incubation time is more likely to reduce resorufin and form non-detectable products. The research also focused on different cells, one embryonic fibroblast cell line Balb/c3T3, and three epithelial cancer cell lines, A549, MCF-7, and Ht-29. These cells have different metabolic activities, which were noticed in this study. Ht-29 cells showed the highest activity and had 100 μ M as an optimal concentration of resazurin, whereas the others had 50 μ M.

Optimal density corresponding to the working area is very important in cell adhesion approaches. This enhances the detection of cell viability alongside the release of ALP, which may detect intracellular processes. Cells need to be proliferated for at least four days to release detectable ALP. This time can be further increased if a study is focusing on differentiation where optimizing density is required. Special attention is drawn to the morphology of cells, which was monitored and compared to the resazurin assay.

The cells showed logistic growth curves where the four phases were obvious. Cells that had a longer lag phase had less confluence (about 70–80%, like MCF-7 cells). In comparison, others, which had a smaller lag phase, had a gradual log phase and thus had almost 95–100% confluence by day 4. Cell growth is also influenced by the surrounding environment (e.g., media type, serum). The recommended type of media and serum were used according to the supplier's recommendations. Cell viability of cells at post-confluence culture was determined and data were compared statistically using mean, standard deviation, p-value, and z-factor. The data of embryonic cells, lung cancer cells, and colon cancer cells displayed significant differences in post-confluence culture compared to the control (day 4). Similarly, breast cancer cells showed a p-value < 0.05 in day 6 and $p > 0.05$ in day 5 compared to the control. The cell viability of vehicle controls of the cells Balb/c 3T3, A549, MCF-7, and Ht-29 were 10.2%, 18.6%, 8.3%, and 18.2%, respectively.

The main aim of this chapter was achieved by providing convenient and reliable samples of living cells for sensitively and continuously assaying using resazurin-based measurements, which made it easier for optimizing the methodologies for ALP release in cells-based biosensor.

2.6 Reference

- [1] Uzarski, J.S.; Bijonowski, B.M.; Wang, B.; Ward, H.H.; Wandinger-Ness, A.; Miller, W.M.; Wertheim, J.A. Dual-Purpose Bioreactors to Monitor Noninvasive Physical and Biochemical Markers of Kidney and Liver Scaffold Recellularization. *Tissue Eng. Part C Methods* 2015, 21, 132–1043.
- [2] Ren, X.; Tapias, L.F.; Jank, B.J.; Mathisen, D.J.; Lanuti, M.; Ott, H.C. Ex vivo non-invasive assessment of cell viability and proliferation in bio-engineered whole organ constructs. *Biomaterials* 2015, 52, 103–112.
- [3] Tapias, L.F.; Gilpin, S.E.; Ren, X.; Wei, L.; Fuchs, B.C.; Tanabe, K.K.; Lanuti, M.; Ott, H.C. Assessment of Proliferation and Cytotoxicity in a Biomimetic Three-Dimensional Model of Lung Cancer. *Ann. Thorac. Surg.* 2015, 100, 414–421.
- [4] Ansar Ahmed, S.; Gogal, R.M.; Walsh, J.E. A new rapid and simple non-radioactive assay to monitor and determine the proliferation of lymphocytes: An alternative to [^3H] thymidine incorporation assay. *J. Immunol. Methods* 1994, 170, 211–224.
- [5] Yang, T.-T.; Sinai, P.; Kain, S.R. An Acid Phosphatase Assay for Quantifying the Growth of Adherent and Nonadherent Cells. *Anal. Biochem.* 1996, 241, 103–108.
- [6] Akcakaya, H.; Aroymak, A.; Gokce, S. A quantitative colorimetric method of measuring alkaline phosphatase activity in eukaryotic cell membranes. *Cell Biol. Int.* 2007, 31, 186–190.
- [7] Friedrich, J.; Eder, W.; Castaneda, J.; Doss, M.; Huber, E.; Ebner, R.; Kunz-Schughart, L.A. A reliable tool to determine cell viability in complex 3-D culture: The acid phosphatase assay. *J. Biomol. Screen.* 2007, 12, 925–937.

- [8] Ivanov, D.P.; Parker, T.L.; Walker, D.A.; Alexander, C.; Ashford, M.B.; Gellert, P.R.; Garnett, M.C. Multiplexing spheroid volume, resazurin and acid phosphatase viability assays for high-throughput screening of tumour spheroids and stem cell neurospheres. *PLoS ONE* 2014, 9, e103817.
- [9] Lukić, M.; Šimec, N.; Zatezalo, V.; Jurenec, S.; Radić-Krišto, D. Exclusion of Trypan blue exclusion test for CD34+cell viability determination: P007. *Bone Marrow Transplant*. 2017, 52, S126–S127.
- [10] Menyhárt, O.; Harami-Papp, H.; Sukumar, S.; Schäfer, R.; Magnani, L.; de Barrios, O.; Györfy, B. Guidelines for the selection of functional assays to evaluate the hallmarks of cancer. *BBA Rev. Cancer* 2016, 1866, 300–319.
- [11] Khalili, A.A.; Ahmad, M.R. A Review of Cell Adhesion Studies for Biomedical and Biological Applications. *Int. J. Mol. Sci.* 2015, 16, 18149–18184.
- [12] Koev, S.T.; Dykstra, P.H.; Luo, X.; Rubloff, G.W.; Bentley, W.E.; Payne, G.F.; Ghodssi, R. Chitosan: An integrative biomaterial for lab-on-a-chip devices. *Lab Chip* 2010, 1, 326–342.
- [13] Shum, D.; Radu, C.; Kim, E.; Cajuste, M.; Shao, Y.; Seshan, V.E.; Djaballah, H. A high density assay format for the detection of novel cytotoxic agents in large chemical libraries. *J. Enzym. Inhib. Med. Chem.* 2008, 23, 931–945.
- [14] Kim, H.J.; Jang, S. Optimization of a resazurin-based microplate assay for large-scale compound screenings against *Klebsiella pneumoniae*. *3 Biotech* 2018, 8, 1–6.
- [15] Van den Driessche, F.; Rigole, P.; Brackman, G.; Coenye, T. Optimization of resazurin-based viability staining for quantification of microbial biofilms. *J. Microbiol. Methods* 2014, 98, 31–34.
- [16] Chadha, S.; Kale, S. Simple fluorescence-based high throughput cell viability assay for filamentous fungi. *Lett. Appl. Microbiol.* 2015, 61, 238–244.
- [17] Goughenour, K.D.; Balada-Llasat, J.-M.; Rappleye, C.A. Quantitative microplate-based growth assay for determination of antifungal susceptibility of *histoplasma capsulatum* yeasts. *J. Clin. Microbiol.* 2015, 53, 3286–3295.
- [18] Moreau, K.; Surand, J.; Le Dantec, A.; Mosrin-Huaman, C.; Legrand, A.; Rahmouni, A. Recombinant yeast and human cells as screening tools to search for antibacterial agents targeting the transcription termination factor Rho. *J. Antibiot.* 2018, 71, 447–455.
- [19] Bowling, T.; Mercer, L.; Don, R.; Jacobs, R.; Nare, B. Application of a resazurin-based high-throughput screening assay for the identification and progression of new treatments for human African trypanosomiasis. *Int. J. Parasitol. Drugs Drug Resist.* 2012, 2, 262–270.
- [20] Rolón, M.; Vega, C.; Escario, J.A.; Gómez-Barrio, A. Development of resazurin microtiter assay for drug sensibility testing of *Trypanosoma cruzi* epimastigotes. *Parasitol. Res.* 2006, 99, 103–107.

- [21] Uzarski, J.S.; DiVito, M.D.; Wertheim, J.A.; Miller, W.M. Essential design considerations for the resazurin reduction assay to noninvasively quantify cell expansion within perfused extracellular matrix scaffolds. *Biomaterials* 2017, 129, 163–175.
- [22] O'Brien, J.; Wilson, I.; Orton, T.; Pognan, F. Investigation of the Alamar Blue (resazurin) fluorescent dye for the assessment of mammalian cell cytotoxicity. *Eur. J. Biochem.* 2000, 267, 5421–5426.
- [23] Uzarski, J. S., Su, J., Xie, Y., Zhang, Z. J., Ward, H. H., Wandinger-Ness, A., Miller, W. M., Wertheim, J. A. Tissue Eng Part C Methods. Epithelial Cell Repopulation and Preparation of Rodent Extracellular Matrix Scaffolds for Renal Tissue Development. 2015, 21(10):1032-43. doi: 10.1089/ten.TEC.2014.0665
- [24] Pace, R.T.; Burg, K.J.L. Toxic effects of resazurin on cell cultures. *Cytotechnology* 2015, 67, 13–17.
- [25] Hamalainen-Laanaya, H.K.; Orloff, M.S. Analysis of cell viability using time-dependent increase in fluorescence intensity. *Anal. Biochem.* 2012, 429, 32–38.
- [26] Zheng, F.; Wang, S.; Hou, W.; Xiao, Y.; Liu, P.; Shi, X.; Shen, M. Comparative study of resazurin reduction and MTT assays for cytocompatibility evaluation of nanofibrous materials. *Anal. Methods* 2019, 11, 483–489.
- [27] Adams, D.L.; Zhu, P.; Makarova, O.V.; Martin, S.S.; Charpentier, M.; Chumsri, S.; Li, S.; Amstutz, P.; Tang, C.-M. The systematic study of circulating tumor cell isolation using lithographic microfilters. *Rsc Adv.* 2014, 4, 4334–4342.
- [28] Majeska, R.J.; Rodan, G.A. The Effect of 1,25(OH)₂D₃ on Alkaline-Phosphatase In Osteoblastic Osteo-Sarcoma Cells. *J. Biol. Chem.* 1982, 257, 3362–3365.
- [29] Castrén, E.; Sillat, T.; Oja, S.; Noro, A.; Laitinen, A.; Konttinen, Y.T.; Lehenkari, P.; Hukkanen, M.; Korhonen, M. Osteogenic differentiation of mesenchymal stromal cells in two-dimensional and three-dimensional cultures without animal serum. *Stem Cell Res. Ther.* 2015, 6, 167.
- [30] Xiao, J.; Zhang, Y.; Wang, J.; Yu, W.; Wang, W.; Ma, X. Monitoring of Cell Viability and Proliferation in Hydrogel-Encapsulated System by Resazurin Assay. *Appl. Biochem. Biotechnol.* 2010, 162, 1996–2007.

Chapter 3

Spectrophotometry of Alkaline Phosphatases (ALP) Assays

Note: Some results of this chapter have been published in Journal of Applied Science. Please refer to Appendix.

3.1. Aim and objectives

The aim of this work detailed in this chapter was to optimize real-time monitoring of ALP release from two types of cells: embryo fibroblast cells (Balb/c 3T3); and cancer epithelial cells (A549, MCF-7, Ht-29). Spectrophotometric analysis-absorbance technique was applied. This optimization will be compared with the electrochemical detection of ALP release that is outlined in Chapter 4 and in Chapter 6.

The novelty of this aim was that no colorimetric assay was done for ALP release from the embryonic cell line, Balb/c 3T3. In addition, ALP release has not been detected by colorimetry during differentiation of post-confluence culture for all given cells.

The following objectives detail the aims of this chapter:

1. To establish the activity of ALP at a constant rate by optimizing parameters, including solubilisation methods, trypsin effects, and pH range, as well as enhancer concentrations, such as MgCl_2 and NaCl .
2. To obtain the standard curve of p -nitrophenol (pNP), which will be used to compare the data with capillary electrophoresis experiments in Chapter 6.
3. To optimize incubation time of the substrate p-nitrophenol phosphate (pNPP) with ALP release.
4. To determine the saturation point of the substrate p-nitrophenol phosphate (pNPP) using nonlinear regression analysis of the Michaelis-Menten model.
5. To determine the calibration curve of ALP and to identify the number of Units per Litre (U/L) that can be compared with electrochemical experiments in (Chapter 4).
6. To investigate linearity performance of ALP release with different concentrations of the given cells.
7. To investigate the hydrolysis of different concentrations of the substrate pNPP by ALP release from adhesion cells, and to determine Michaelis constants (V_{max}) and (K_m) for the substrate pNPP for each cell.
8. To facilitate real-time monitoring of ALP release using post-confluence culture for 3 days.

3.2 Introduction

3.2.1 Principle

ALP is a homodimeric protein. It has cofactors, including two zinc atoms and one magnesium atom in each subunit, all of which are important for active sites. These are formed by the link of the two subunits [1], [2]. ALP requires several alkaline pH environments ranging from 8 to 10 for activation. As outlined in the Introduction, ALP is located in almost all living tissue and can be expressed in four isoforms: GCAP, IAP, PALP and TNAP. Abnormal levels of ALP release can be seen in illnesses (such as liver disease, bone disorders, etc.), or during pregnancy and during the rapid growth phases of childhood. Recently, ALP has been studied as a potential cancer biomarker, and its early detection could help in the treatment of the disease.

Real-time monitoring of ALP release offers insights into the basis of the disease, as well as the progression of cancer. ALP, like any enzyme, can catalyze biochemical reactions in the body. Therefore, more intense attention is necessary in order to simulate the enzymatic activity of the human body and to meet the experimental conditions in laboratories. As ALP is an enzyme, and thus a protein in nature, it makes denaturation possible. In experimental conditions, parameters, such as temperature and composition of solvent, need to be taken into account, as well as the potential presence of metal-ion cofactors, which are important for catalytic reactions, such as Mg^{2+} and Zn^{2+} . With respect to the enzyme kinetics, concentration of substrate, temperature, pH, and enzyme concentration all affect the assay. Every enzyme has specific roles, e.g., in the case of ALP, it is to liberate the phosphate (PO_4^{3-}) group. The choice of substrates to be hydrolysed by ALP is also of importance, as it will determine the appropriate detection technique. For example, p-nitrophenyl phosphate (p-NPP) can convert to an absorbance compound (p-nitrophenol (p-NP)). ALP release from cells catalyzes that transphosphorylation reaction in the presence of the transphosphorylating buffer, diethanolamine (DEA). Cofactors like magnesium and zinc ions are used for enhancing the reaction. Optimal wavelength for the formation of p-NP is 405 nm and the change in absorbance can reflect the quantity of ALP release with directly proportional relationship. The following schematic illustrates the colorimetric reaction of ALP release (Figure 3.1) [3].

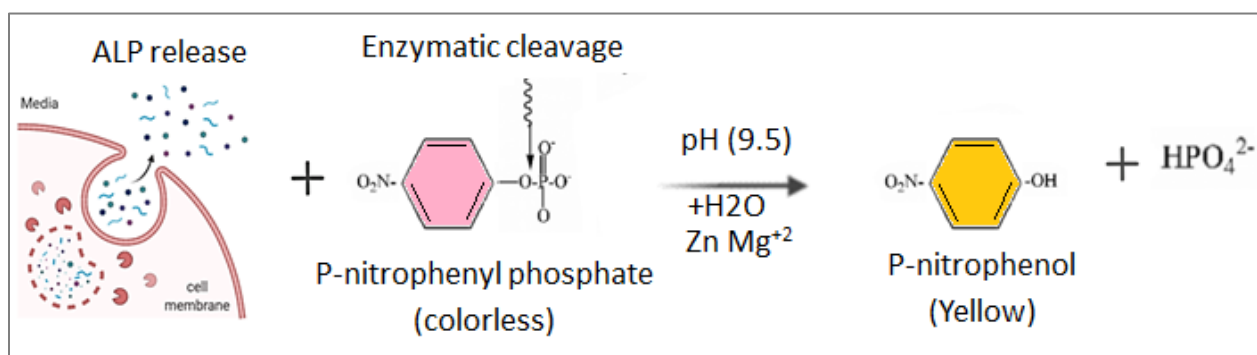


Figure 0.1: schematic of the colorimetric reaction of ALP release.

The development of convenient and reliable assay methods for real-time monitoring of ALP release is extremely important and valuable. This study is focused on quantifying ALP release from living cells in a laboratory setup by optimizing spectrophotometric assay as a less expensive alternative to current methodologies.

3.2.2 Background

Determination methods for ALP assay have undergone continuous developments since its discovery in the 19th century when they were not sensitive enough for a reliable assay. It wasn't until the 1930s that methods began to become more reliable and accurate. However, the limitation of those methods was that they were time consuming due to dependency on the reaction rate. One of the main steps forward that was achieved was optimizing the incubation time, reducing it from 48 hours to 30 minutes [4]. The phosphate esters mainly used were β -glycerophosphate and phenylphosphate. Later, Ohmori in 1937 used the colour of the liberated nitrophenol for qualitative ALP assay and produced a phosphate group

[5]. Bessy, Lowery and Brock (1946) identified that the colour that developed as a result of the reactions was an indication of ALP activity. They later wrote a report where they explained the preparation of a lower-volume sample, which was enough to assay ALP [6]. Furthermore, pNPP was found to be faster and to have a better resolution than previously used substrates. Due to the simplicity of their assay, current clinical analysis depends on their principle for determination of ALP levels in blood serum. The yellow colour of PNP that is generated with the separation of the phosphate group by ALP can be easily detected using spectrophotometric techniques (absorption at 405 nm). The quantity of pNP formed refers to the ALP quantity in the sample. This methodology is standard, and it is frequently carried out in biochemistry laboratories in hospitals. Global companies, including Siemens Healthcare Diagnostics, apply this type of assay by using large instruments to address thousands of samples daily. Commercial kits provide highly specialised reagents, which are quite expensive.

3.2.3 Literature review

The link between ALP and cancers, including lung [7]–[9], breast [10]–[12] and colon cancer [13], [14] has been demonstrated in several studies. The main spectrophotometric analysis methods, including colorimetric [15]–[24], fluorescence [25], [26] and chemiluminescence [27]–[29] analysis, have been used. Real-time detection of ALP levels has been recorded for human serum [30]–[32] and for living cells [33][34][35]. Real-time capability is shown by emission-based assay using chemiluminescence [35] and fluorescence [34] for A549, Ht-29, MCF-7, SM43, NR8383 and mesangial cells.

Nevertheless, emission-based assays are limited by their costs and by the turbidity of solution, which affects the measured readings. Moreover, fluorescent assays measure the change (e.g., on/off) of fluorescence intensity. This is because an increase or decrease in fluorescence intensity could be affected by factors that include fluctuations in light source intensity, pH and media polarity. They are therefore subject to some limitations for practical applications. Absorbance assay, on the other hand, is economically more attractive. It is also simpler and involves no direct sample manipulation, thus preserving its integrity. Researchers have developed methodologies based on absorbance assay for ALP determination expressed from living organisms. ALP release from bacteria [36]–[39], yeast [40]–[43], and fungi [44]–[47] has been recorded. ALP release from cells has slight differences [8], [48]–[54]. Moreover, no colorimetric assay has been done for Balb/c 3T3 cells [55].

It is quite noticeable that colorimetric techniques are more common in the detection of ALP release from the given cells [53], [56]–[59], followed by western blot [60],[61], northern blot [62], real-time RT-PCR [52], and commercial kits [63]. ALP release is reported to be investigated at different cell densities (1-200 ×10⁴) cell/ml and within different working areas (6- 48- 96-well plates) [8], [52], [57], [60], [63]. Methods used for cell differentiation in order to monitor ALP release include the addition of sodium butyrate [52], [53], and post-confluence culture [52], [62]. A wide range of alkaline buffers, including Tris [59]–[61], AMP [56], glycine [8], and DEA [57], were used at pH ranges from 8 to 10.6. In some other rare cases, protease inhibitors [60], [61] and Triton X-100 [58], [59], [64] were used. MgCl₂ was added at different concentrations from 0.5-1 mM [8] [63], while NaCl was added at 150 mM [59], [60], [64]. Before adding buffer assay, cells were washed twice with PBS [57], [64] or thrice with NaCl solution [56], [59] at 4°C. Cells were centrifuged at 1000 rpm at times ranging from 2 minutes to 20 minutes [57], [59], [60], [64]. ALP assay buffer needs the pNPP substrate to be incubated with cells from 15 minutes to 4 hours [57],

[59], [64] The substrate pNPP was either added to the assay buffer and incubated with cells [8], [53], [56], [57], or added later to the cell lysate [58]–[60], [64].

3.2.4 The problem statement

As previously discussed, ALP has been detected from Balb/c 3T3 cells, but no colorimetric assay has been conducted [65]. Therefore, optimization of this cell type formed the basis of the research outlined in this chapter. The other cells used in this thesis, including A549 [66], MCF-7 [56] and Ht-29 [65] have been investigated with colorimetric assay but with different purposes. The afore-mentioned studies depend on buffer components that are effective at high pH, the addition of MgCl_2 and NaCl and the incubation of the sample with the buffer with or without the substrate. These slight differences require minor modifications. The process of measuring ALP release from cells requires the cells to be cleaned first from the old media as this would affect the absorbance detection. Second, the buffer used should also be transparent and water-soluble. Previous studies involving the use of Triz, glycine, AMP and DEA have their own limitations. For example, Triz has poor buffering capacity for mammalian ALP, where a range of up to 10 pH is favourable. Glycine inactivates ALP at certain concentrations. AMP is normally provided as a pure solid with a melting point of up to 28 °C, which means that it is always solid in room temperature and not easy to use. More importantly, AMP is less transphosphorylating than other agents. DEA buffer has pK_a 8.7, which is similar to that of Triz (pK_a 8). However, it has good buffering capacity at 10, which is optimal for mammalian ALP. Therefore, in this thesis DEA buffer was used and compared with other buffers in order to determine the optimum ALP activity for the given cells. The addition of Magnesium chloride (MgCl_2) is important for ALP assays. The reproducibility of ALP measurements is affected by the addition of MgCl_2 . MgCl_2 dissolves poorly in alkaline pH and requires storage under 4 °C [2]. The concentration of MgCl_2 also influences the stability and activity of ALP, with high concentrations inactivating ALP. MgCl_2 works as either a stabilizer for ALP in buffers, such as AMP, or as an activator for ALP in buffers that include DEA. For this thesis, the range of MgCl_2 used was 0–10 mM, because a higher amount would inhibit the mammalian ALP [67] [2]. Moreover, the incubation conditions of MgCl_2 with the assay mixture slightly impacts ALP measurements. Mg^{2+} is either incubated with the sample and substrate together or sample and substrate separately. The addition of MgCl_2 to the sample and substrate was chosen, in line with that suggested by Bowers and McComb [4].

Ionic strength is important for enzymatic assay, and that is the reason for the addition of sodium chloride (NaCl) in ALP assay (1977). NaCl is sometimes added to ALP assays at certain concentrations to avoid inhibition of the enzyme (1960). Concentrations of NaCl higher than 1 M inhibit mammalian ALP [4]. However, concentrations between 0.1–1 M show less resolution. Quantities of approximately 0.05 mM can provide better results [4] [68]. This data is related to ALP detection in serum from previous studies, where the amount used was 0.15 M. [68]. Therefore, the range of NaCl used in this thesis was from 0.20–0.01 M.

3.2.5 Summary

In this chapter, ALP was determined during a period when cells were attached. However, for calibration assays, cells were detached to obtain different cellular concentrations and to measure the optimum ALP

level. Solubilization methods were also considered in addition to trypsinization, pH and concentrations of MgCl_2 and NaCl in order to determine to what extent the given cells could express ALP. Quantity of p -nitrophenol (pNP) was identified in order to compare the data with the capillary electrophoresis experiments that are discussed in Chapter 5. The kinetic enzyme assay including incubation time and optimal concentration of p -nitrophenol phosphate (pNPP) was optimised to obtain the saturation point from detached cells and attached cells. Calibration curve of ALP then was identified in units per litre to allow comparison with the electrochemical experiments discussed in Chapter 4. Stability condition of the assay was investigated by performing linearity analysis. In addition, the hydrolysis of different concentrations of the substrate pNPP by ALP release from adhesion cells was discussed. The differentiation strategies of this thesis was applied in order to prove real-time monitoring of ALP by absorbance.

3.3 Methodology

3.3.1 Reagents

Mouse embryo fibroblast cells (Balb/c 3T3 Line), breast carcinoma epithelial cells (MCF-7 Line), lung carcinoma epithelial cells (A-549 Line), colon carcinoma epithelial cells (Ht-29 Line), 70% ethanol, and nanopure water (Grade 18 M Ω) (Tyndall National Institute, UCC). Newborn calf serum (NBCS), fetal bovine serum (FBS), Dulbecco's modified eagle's medium (DMEM), Minimum Essential Medium Eagle (MEME) and McCoy's 5A Medium, Hank's balanced salt solution (HBSS), Trypsin/EDTA solution, resazurin, HCl, MgCl_2 , KCl, virkon®, Trizma® (TRIS base), 2-Amino-2-Methyl-1-Propanol (AMP), diethanolamine (DEA), Triton X-100, 4-nitrophenol (p -NP), and para-nitrophenol phosphate (p -NPP) (Sigma, Ireland)..

3.3.2 Instrumentation

Cell culture hood (Esco Airstream® Class II); 5% CO_2 incubator (incusafe Panasonic); Water bath 37 °C (fisherbarnd); Centrifugation (universal 320 Hittch zentrifugen) and (Eppendorf 5415D Centrifuge); Inverted microscope and camera (Olympus); Eppendorf® Thermomixer® R; (-80 freezer); Fluorescent platereaders (Spectra Max Gemini), Absorbance platereader (Diasource ELISA Reader); Hemacytometer slide (Reichert Bright-Line); Glass cover slips (menzel-gläser) and cell counter; Pipettes (Rainin Pipet-X) and micropipettes (Gilson Pipetman®); Pipette tips (Greiner Bio-One), Pipettors (5-mL, 10-mL, and 25- mL) cell culture vessels (75T flasks, 1.5-mL, 15-mL, 50mL centrifuge tubes, 96- and 48-well plates); and syringes 45 nm filters (Sigma, Ireland).

3.3.3 ALP release and cell culture

3.3.3.1 Working buffers

Three working buffers were used to determine the assay buffer that could produce stabiles results. It is important to determine the final standard curve of pNP and to compare the results given in this chapter with those obtained in chapter 6. Colorimetric measurements were carried out in triplicate using the wavelength 405 nm. 70 μL of the product pNP range at (15-500 μM) were prepared in 1M DEA buffer, 30

mM TRIS base or 10 mM AMP. Each concentration of pNP were prepared in the presence of 30 μ L of sample mixed with of 5 mM of pNPP. 30 μ L of 1M NaOH was added as it was normally present in the reaction solution. The optical density of each point was read in a platereader against a free-pNP buffer as blank. Graph relating absorbance to concentration of pNP was prepared for regression analysis.

3.3.3.2 Solubilisation methods

ALP normally releases in media but the neutral pH of media and the supplements in media limit the absorbance detection. Therefore, it is important to standardize the assay solution by staining cells in a buffer. Figure 3.2 summarizes the steps of ALP release assay. Plate A) shows ALP release during detachment of cells. Plate B shows ALP release during adhesion of cells.

For preparing sample, the cells were sub-cultured three times before seeding began under aseptic conditions using protocol used in in chapter 2, section (2.3.3). The following steps were performed according to the protocol illustrated in chapter 2 (2.3.8) in order to release ALP from cells. The first step was to enhance ALP releasing at 4-day-old culture by seeding cells as a monolayer at 48-well plates, incubated at 37 °C and 5% CO₂ and changing media every two days. The cell lines used during this study was mouse embryo fibroblast cells (Balb/c 3T3 Line). Media, supplements and washing buffer used for culturing cells were Dulbecco's modified eagle's medium (DMEM), Newborn calf serum (NBCS), and Hank's balanced salt solution (HBSS).

The steps of plate A were followed up; cells were washed twice with HBSS and trypsinized at 37 °C for 2 minutes. Trypsin was naturalized by media and then centrifuged at 1000 rpm for 5 minutes. To get rid of red phenol, cells were washed again with HBSS and centrifuged at 1000 rpm for 5 minutes. To ensure stable condition of cell number, the 4-day-old cells were normalized at concentration of (250 \times 10³ cell/ml). Supernatant was discarded, and cell pellets were resuspended in 70 μ L DEA buffer in the presence of 5 mM MgCl₂, 30 mM NaCl, 0.1% Triton X-100, 5mM pNPP and at pH of 9.5. All the previous steps were done in an ice bath. The vials simultaneously incubated at 37 °C for 30 minutes. 30 μ L of 1M NaOH was added to stop the reaction. The supernatant then centrifuged for 5 minutes to discard of cells and determine the solubilized ALP. Measurements were applied in a 96-well plate in triplicate, and absorbance was taken at 405 nm using spectrophotometer.

Further steps were conducted to ensure that ALP solubilized properly. The first step was sonicating cells at 37 °C for 30 minutes. Then supernatant was collected for the measurement. In the second step, after incubating cells for 30 minutes with the assay buffer, they were frozen at -80 °C for one minute, then thawed at 37 °C for another one minute. The cycle of freeze-thaw was done once, twice or thrice and then supernatant was collected for the measurement in each thawing time.

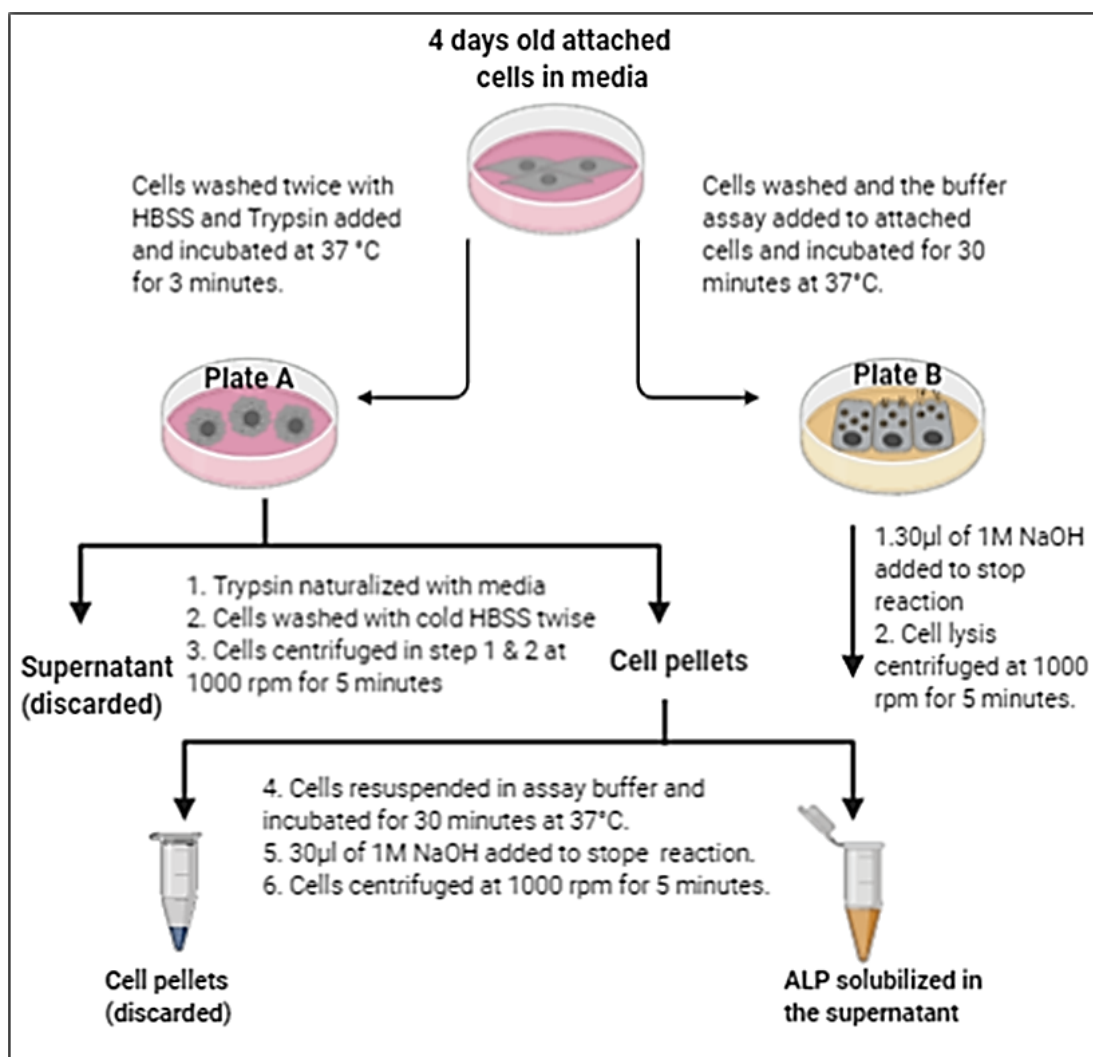


Figure 0.2: A schematic diagram of ALP release. Plate A describes the methods of determination of ALP release from detached cells, where cells were washed with HBSS and then exposed to steps involving trypsinizing, washing and centrifugation and then exposed to the buffer assay. Plate B describes the methods of determination of ALP release from attached cells, where cells were only washed and then directly exposed to the buffer assay. The buffer assay involves 5 mM $MgCl_2$, 30 mM NaCl, and 5 mM pNPP and adjusted to 9.5 pH.

3.3.3.3 Trypsin effects

Trypsin affects ALP release negatively. To ensure that ALP had no trypsin effect, the steps in figure 3.2 (plate A) were followed, where cells were firstly washed twice with HBSS and then incubated with trypsin for 5, 15, 30 or 60 minutes. This was then followed by the naturalizing, washing and centrifugation steps to allow the discard of supernatant. Then cells of (250×10^3 cell/ ml) were incubated in 70 µl of the assay buffer of DEA in the presence of 5 mM, pNPP, 5 mM $MgCl_2$, 30 mM NaCl, at pH 9.5 for 30 minutes. 30µl of 1M NaOH was added to stop the reaction. Microscope images were taken for cells at each target time. Measurements were applied in a 96-well plate in triplicate, and absorbance was taken at 405 nm using a spectrophotometer.

3.3.3.4 MgCl₂ concentration

Magnesium chloride (MgCl₂) is known for activating ALP and the high concentration of ion Mg²⁺ in the buffer reduces the possibility of denaturation of the protein-ALP enzyme, therefore, optimizing the addition the ions Mg²⁺ in ALP assay buffer is important [1], [2]. In triplicate, various concentrations ranging from 2 mM to 10 mM were prepared to make the assay buffer and 0 mM MgCl₂ was used as a blank. After the washing, trypsinizing, naturalizing, and centrifugation steps illustrated in figure 3.2 (plate A), supernatant was discarded and cells of (250×10³ cell/ mL) were incubated in 70 µL of the assay buffer of DEA, which had different concentrations of MgCl₂ and in the presence of 5 mM, pNPP and 30 mM NaCl, at the pH of 9.5 for 30 minutes. 30 µL of 1 M NaOH was added to stop the reaction. Supernatant was added in a 96-well plate in triplicate, and absorbance was taken at 405 nm using a spectrophotometer.

3.3.3.5 NaCl concentration

Sodium chloride (NaCl) is known to enhance the enzymatic reaction and was optimized for ALP release assay. In triplicate, various concentrations ranging from 0.01 M to 0.2 M were prepared to make the assay buffer and 0 M NaCl was used as a blank. After the washing, trypsinizing, naturalizing, and centrifugation steps, which are illustrated in figure 3.2 (plate A), supernatant was discarded and cells of (250×10³ cell/ mL) were incubated in 70 µL of the assay buffer of DEA, which had different concentrations of NaCl and in the presence of 5 mM, pNPP and 8 mM MgCl₂, at a pH of 9.5 for 30 minutes. 30 µL of 1 M NaOH was added to stop the reaction. Supernatant was added in a 96-well plate in triplicate, and absorbance was taken at 405 nm using a spectrophotometer.

3.3.3.6 pH effect

The enzyme ALP works more effectively at high pH, but when pH increases its effectiveness declines. Therefore, it is important to determine the optimal pH of the assay for ALP release. The DEA buffer had its pH varied from 7.5 to 10. After the washing, trypsinizing, naturalizing, and centrifugation steps illustrated in figure 3.2 (plate A), and then the discarding of supernatant, cells of (250×10³ cell/ mL) were incubated in 70 µL of the assay buffer of DEA in the presence of 5 mM, pNPP, 8 mM MgCl₂, 50 mM NaCl, at the specified pH for 30 minutes. (30µL of 1M NaOH was added to stop the reaction) In triplicate, 96well plate measurements were applied, and absorbance was taken at 405 nm using spectrophotometer.

3.3.6 Optimization of absorbance measurement

3.3.6.1 Standard curve of pNP

It is important to determine the final standard curve of pNP and to compare the results given in this chapter with those obtained in chapter 6. Colorimetric measurements were carried out in triplicate using the wavelength 405 nm. 70 µL of the product pNP range at (15-500 µM) were prepared in DEA buffer before or after optimization. Each concentration of pNP were prepared in the presence of 30 µL of sample mixed with of 5 mM of pNPP. 30 µL of 1 M NaOH was added as it was normally present in the reaction solution. The optical density of each point was read in a platereader against a free-pNP buffer as blank. Graph relating absorbance to concentration of pNP was prepared for regression analysis.

3.3.6.2 Time incubation

Incubation period is important in enzyme assays and can be shown by allowing an appositive linear relationship between the time and optical density. This is to reflect the accuracy of the assays and to ensure that the enzyme does not denature during the assay. Cells were incubated for 3 minutes in trypsin, followed by the naturalizing, washing and centrifugation steps to allow discard of supernatant. 70 μ L of a sample with 20 U L⁻¹ of ALP activity mixed with 30 μ L of pNPP 5 mM, 8 mM MgCl₂, and 50 mM NaCl in buffer DEA. 30 μ L of 1M NaOH was added to stop the reaction. The absorbance of the product pNP formed was assessed for interval time of 10 minutes for 60 minutes and measured at 405 nm using a spectrophotometer. A graph relating absorbance to time was prepared for regression analysis.

3.3.6.3 Concentration of the substrate pNPP

The concentration of substrate pNPP is an importance parameter as it's quantity can limit the ALP assay. The incubation time fixed at 30 minutes and 70 μ L of a sample was assessed with different concentration of substrate range at (5, 2.5, 1.25, 0.63, 0.31, 0.16, 0.08, and 0.04 mM pNPP). Each concentration was mixed with 30 μ L of 20 U L⁻¹ of ALP activity and in the present of 8 mM MgCl₂, and 50 mM NaCl in buffer DEA. 30 μ L of 1 M NaOH was added to stop the reaction. Change of absorbance was recorded at 405 nm using spectrophotometer. The non-linear regression analysis of the Michaelis-Menten model was applied between absorbance and concentration to determine constants.

3.3.6.4 Calibration curve of ALP

In order to compare data of optical detection with electrochemical detection, the calibration curve of ALP was applied. 70 μ L of a sample was assessed with 30 μ L of different concentration of ALP activity range at (1-1500 U/L). Each concentration had 6 mM pNPP, 8 mM MgCl₂, and 50 mM NaCl in buffer DEA. After 30 minutes, 30 μ L of 1 M NaOH was added to stop the reaction. Change of absorbance was recorded at 405 nm using spectrophotometer. To quantify the unknowns, Lineweaver-Burk model was plotted between the absorbance and ALP concentrations to obtain the linear equation.

3.3.7 Linearity performance of ALP release vs cell number

To perform the linearity trend of ALP release versus absorbance values, different concentrations of cells were applied. After the washing, trypsinzing, naturalizing, and centrifugation steps that are illustrated in figure 3.2 (plate A), supernatant was discarded. Different concentration of cell numbers was normalized at the range of (250, 125, 63, 31, 16, 8, and 3) $\times 10^3$ cell/ml. The cell concentration was incubated in 70 μ L of the assay buffer in the presence of 6 mM, pNPP, 8 mM MgCl₂, 50 mM NaCl, and pH of 9.5 for 30 minutes. 30 μ L of 1 M NaOH was added to stop the reaction. The optical density of each point was read in a platereader at 405 nm against a free-pNPP buffer as blank. Measurements were applied in a 96-well plate in triplicate, and absorbance was taken for each buffer at 405 nm using a spectrophotometer. A graph relating concentration of cell number to optical density was prepared for regression analysis.

3.3.8 Concentration of the substrate pNPP form adhesion cells

Cells adhesion has a different response from that of liberating cells. Therefore, the concentration of substrate pNPP need to be assessed in order to allow real-time monitoring of ALP from each cell line. Cell lines of 4 days old culture were washed with cold HBSS twice according to the steps illustrated in figure 3.2 (plate B). 2-fold serial dilution of pNPP starting with 5 mM was prepared in the range of (5, 2.5, 1.25, 0.60, 0.30, 0.16, 0.08 and 0.04 mM) in the DEA buffer in the presence of 8 mM MgCl_2 and 50 mM NaCl. Cells were incubated in 70 μL of the specified buffers for 30 minutes. Then, 30 μL of 1M NaOH was added to stop the reaction. Measurements were applied to a 96-well plate in triplicate, and absorbance was taken at 405 nm using a spectrophotometer. The absorbance values were plotted against substrate concentration and fit by linear and non-linear regression analysis, Lineweaver-Burk model and MichaelisMenten model.

3.3.9 Real-time monitoring of ALP release from cells at post-confluence culture

To induce ALP and allow real-time monitoring, cells were differentiated using post-confluence culture. Cells were seeded in 48-well plates at a concentration of 40×10^3 cells/mL for the following cells: Balb/c 3T3, A549, and MCF-7, and at a concentration of 80×10^3 cells/mL for the Ht-29 cells. Cells had the media changed every two days to keep them healthy and with sufficient nutrients. After they reached their exponential growth and met the 95–100% confluence (Day 4), the cells were maintained in growth media for a further two days. Cells were washed twice with HBSS in each target day. ALP assay buffer at pH 9.5 was added in the presence of 8 mM MgCl_2 and 50 mM NaCl, 0.1% Triton X-100, and 6 mM pNPP and 0 mM pNPP as a blank for each cell line. Vehicle control of each cell was prepared by adding two drops of Virkon® in the complete media for 24 h the night before the assay. Cells were then incubated in the 70 μL of the specified buffers for 30 min, and then 30 μL of 1M NaOH was added to stop the reaction. Measurements were applied in 96-well plates in triplicate, and absorbance was taken at 405 nm using a spectrophotometer. Data was collected for statistical analysis.

3.3.10 Statistics analysis

The absorbance data of ALP activity represents the mean of at least three independent experiments and statistically compared to electrochemical and capillary electrophoresis assays using ANOVA analysis and unpaired t-test ($p > 0.05$).

3.4 Results and Discussion

3.4.1 ALP release optimization

3.4.1.1 Working buffers

For optimal absorbance detection of mammalian ALP, the optical active compound p-nitrophenol (pNP) is produced from the enzyme reacting with a p-nitrophenyl phosphate substrate. Hence, buffer materials that display a favourable response towards p-nitrophenol should be promising for this type of absorbance

development. Hence, different buffers, including AMP, Triz and DEA, were used to detect p-nitrophenol optically. The given buffers were prepared in deionized water at pH 9.5, as this pH is an optimal range for mammalian. Figure 3.3 shows the relating absorbance changes when using different buffers. The curves were plotted using linear polynomial fit model due to enzyme reactions. It would appear that the curve of the DEA buffer provides the greatest improvement in analytical signal compared to the Triz and AMP curves.

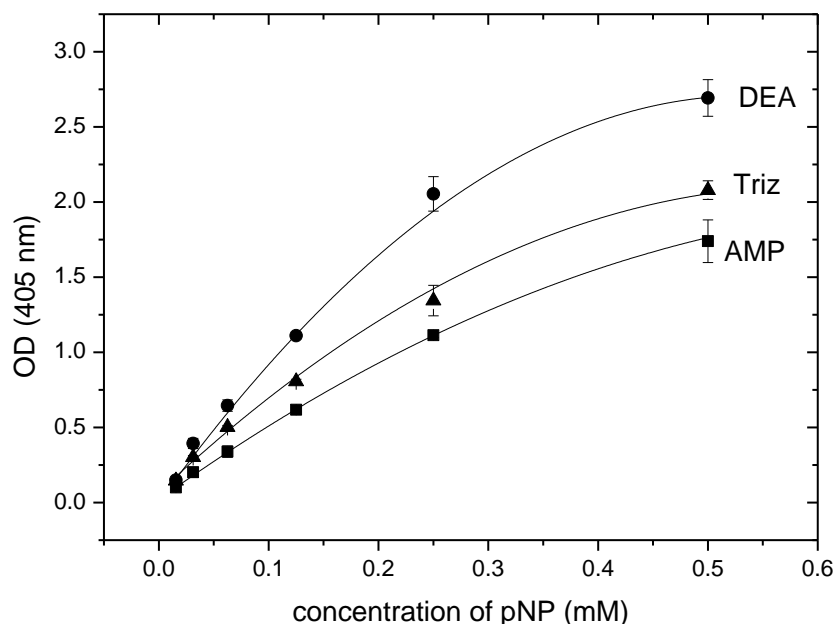


Figure 0.3: Effect of buffer type on pNP concentrations using absorbance detection at 405 nm. All measurements were made at pH 9.5. (Linear polynomial fit model).

This can be further confirmed by viewing the linearity parameters (table 3.1.). The data obtained while plotting linear fit model. However, upon carrying out an ANOVA analysis on the three curves for each buffer opposite to the DEA data, a P-value was higher than 0.05. Therefore, there is no significant difference between the three buffers.

Table 0.1: Linearity parameters for pNP concentrations vs different buffers using absorbance detection at 405 nm.

Buffers	Linear range (mM)	R ²	slope	intercept
DEA	0.02-0.5	0.97	4.38	0.15
Triz	0.02-0.5	0.98	3.24	0.08
AMP	0.02-0.5	0.99	2.79	0.23

The slope increased if the samples were subjected to DEA buffer (pH 9.5). The means of 3 replicates and coefficient regression R² are given (Linear Model).

3.4.1.2 Solubilisation methods

Solubilisation methods were applied to attain the maximum enzyme expression ability of treated cells [69], which was then compared to the quantity of ALP released through the suggested methodology. In Table 3.2, the solubilisation method of ALP release was summarized from Balb c/3T3, and analysis parameter was added: means, 95% C.L. and p-values. The methods were: (a) trypsin only, (b) trypsin and sonication, (c) trypsin and freeze-thaw once, (d) trypsin and freeze-thaw twice, and (e) trypsin and freezethaw thrice. The quantity of ALP release from 250×10^3 cell/ml in the presence of 5 mM $MgCl_2$, 30 mM NaCl, and at pH 9.5 was analysed using absorbance at 405 nm. It is obvious that the highest results of ALP release were obtained from sample freeze-thawed twice whereas the lowest were obtained from the sonicate method. Moreover, the mean values of each method were compared to the trypsin only method by using Student's t-test. There was a significant difference ($p < 0.05$) between the absorbance values of the ALP release of trypsin only method and those which were sonicated, freeze-thawed once or freezethawed twice. There was no difference with that freeze-thawed three times due to high standard deviation. Despite the fact that the overestimated values of freeze-thaw cycles were expected, it differs from the method of trypsin only by (± 0.11). Accordingly, this method was used in all steps of this thesis to meet the aim of determining ALP release when cells are at the attachment state.

Table 0.2: effect of solubilisation methods of ALP release.

Solubilisation methods	Meann(SD) absorbance at 405 nm	95% C.L.	Statistical comparisons vs. trypsinized only
Blank	0.093 (0.005)	0.0057	-
Trypsinized only	0.475 (0.012)	0.0137	-
Trypsinized /sonicate	0.432 (0.013)	0.0142	$P < 0.05^*$
Trypsinized /freeze-thaw (1X)	0.550 (0.010)	0.0111	$P < 0.05^*$
Trypsinized /freeze-thaw (2X)	0.580 (0.011)	0.0119	$P < 0.05^*$
Trypsinized /freeze-thaw (3X)	0.533 (0.025)	0.0283	NS

After the detachment step using trypsin, the sensitivity is significantly increased if the samples are subjected to sonication or freeze-thaw cycle once or twice (37 °C and -80 °C). The means of 3 replicates and 95% confidence limits (95% C.L.) are given. * $P < 0.05$ using student's t-test. NS, not significantly different.

3.4.1.3 Optimization of factors affected ALP release

Some factors were considered for assaying ALP release involving trypsin, ionic strength, pH and a proper concentration of essential ions that were responsible for catalyzing the reaction. Trypsin negatively affects ALP [70]. Therefore, it was incubated with samples several times from 5 minutes to 60 minutes. After the washing steps, cells were incubated with the assay buffer and absorbance was taken. ALP release

remained unchanged up to 15 minutes. And by increasing the incubation time of trypsin with cells to 30 minutes and 60 minutes, the values of ALP release decreased by 12-15%. This met the findings investigated by Catherine et al. (1985) [70]. Microscopic images of cells showed slight differences in the morphology of cells during incubation with Trypsin at different time. In 5 minutes, some cells did not detached from the plate, while those in 15 minutes had just left the plate. This is shown by the spindle shape illustrated in the images inserted in figure 3.4 (A). The morphology of cells in 30 minutes and 60 minutes had absolute circle shape and they already resuspended in the media. It is important to determine the optimal concentration of MgCl_2 for ALP release as Mg^{2+} ions are responsible for enhancing the enzymatic reaction [71]. ALP release was obtained in the presence of varying MgCl_2 ion concentrations range from (2, 4, 6, 8 and 10 mM), and 0 mM was used as blank (Fig. 3.4 B). The analysis curve showed that a slight increase in ALP release occurred as MgCl_2 concentration raised from 2 mM to 8 mM. The activation of alkaline phosphatase by MgCl_2 also levelled off at 10 mM [72], which was corresponding to concentration used in ALP kit of Siemens company. ALP release is accelerated by the presence of cations like Na^+ and K^+ [73]. Addition of NaCl was reported for ALP release [68]. The experiment was carried out by applying the 2-fold serial dilution of NaCl starting from 0.2 M, and the 0 M was used as the control (Fig. 3.4 C). In experiments to determine optimal concentration of NaCl, release ALP was monitored by measuring the absorbance change in the presence of varying NaCl concentrations. The analysis curve showed that a progressive increase in ALP release occurred as NaCl concentration was raised from 0 M to 0.05 M. The values levelled off up to 0.2 M. The highest concentration shows high variance (about 9 % CV), because of the high viscosity of the solution and the hard separation of cell pellets from the supernatant. 0.05 mM obtained was suggested for further experiments. The influence of the pH value of the buffer on the performance of enzyme assay was investigated. Fig. 3.4 (D) shows a typical pH curve of enzyme reaction. At lower pH, the ALP values were lower, because this enzyme works properly in higher pH. The increment of the values of ALP continued from 7.5 to 9.5, followed by a decrement at 10 pH. It is obvious that ALP release is pH dependent and that 9.5 pH is the optimal. When there is about $(0.5\pm)$ of the optimal pH occurs, the values of absorbance change to lower. This might indicate sensitivity of the enzyme where its amino acid charge changed and caused enzyme denaturation. Therefore, the mammalian ALP has the optimal pH of 9.5 and at this pH the ALP is more stabilized and more active. All the experiments were carried out in pH 9.5 of DEA.

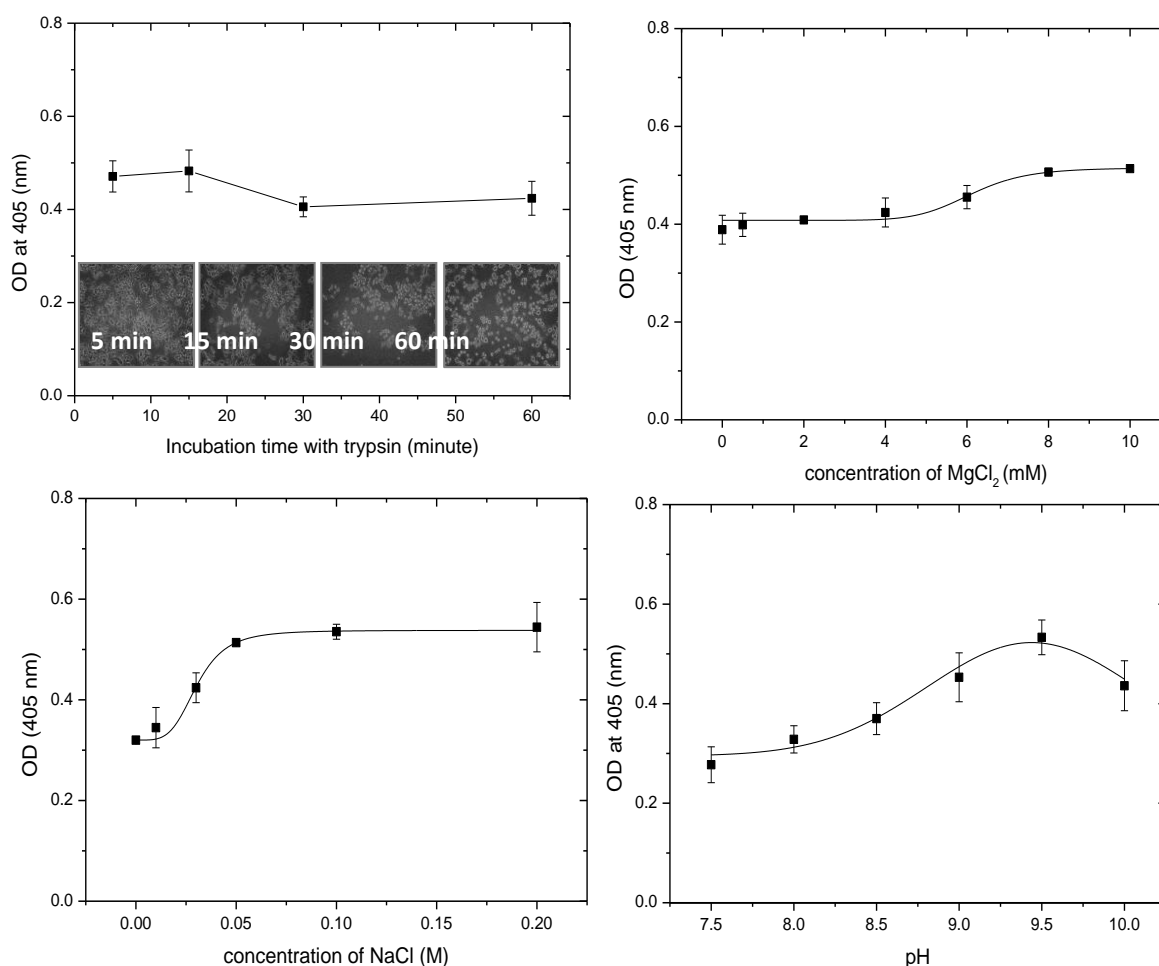


Figure 0.4: Optimization of factors affected ALP release from Balb/c 3T3 cells (250×10^3 cells/mL) using absorbance detection (405 nm) and DEA buffer. (A) Effect of Trypsin on ALP release at different incubation times. ALP release remains constant if trypsin is incubated with sample for up to 15 minutes. In the inset, the microscope images of cells exposed to trypsin. (B) The influence of concentration of MgCl₂ on the ALP release. (C) The influence of increasing concentration of NaCl on the ALP release. (D) The influence of pH of DEA buffer on the ALP release. ALP release has the highest value if the buffer pH is 9.5

3.4.2 Optimization of absorbance measurement

DEA buffer displayed better results (Fig. 3.3), and therefore was chosen as the optimal buffer for application in the rest of the experiments. The buffer assay had, in addition, optimized like MgCl₂ and NaCl, which affect the performance of the standard values of pNP concentration. In order to obtain the linear equation of the standard curve of pNP and use it for comparison with the data found in chapter 6, different concentrations of pNP was made in the optimised DEA buffer and linear relationship was applied. Figure 3.5 (A) showed good linear performance, with coefficient

regression R^2 of 0.98, the slope was 5.3 and the intercept was 0.34. This would appear to indicate that the curve provides sensitivity greater than that not optimized (Table 3.1). However, an ANOVA analysis of the data for not optimised DEA buffer and the data of optimized DEA buffer revealed a p-value that was higher than 0.05. Hence, there is no significant difference between the two buffers in sensitivity.

The absorbance determination of ALP release versus time was performed and showed a linear dependence manner. When time of incubation increases, the ALP release increase. Figure 3.5 (B) shows that values raised slowly up to 40 minutes and then levelled off slowly. However, the linearity relationship has very good coefficient regression R^2 of 0.98. In accordance with these results, an incubation time of 30 minutes was then selected for further absorbance experiments. Longer incubation time shows less variance, which also improve the response.

In order to determine the optimal amount of substrate, it is obviously essential to ensure that the concentration of substrate is not the limiting factor. The absorbance values were plotted against substrate concentration and fitted by non-linear regression analysis to the Michaelis-Menten model, with coefficient regression R^2 of 0.98. The corresponding V_{max} of 1.34 and K_m of 0.33 mM and the corresponding concentration of pNPP at 95 % of V_{max} was 6 mM, which all were estimated from the analysis are shown in (Fig. 3.5 C). This amount is almost 20 times higher than the K_m which is saturated for the enzyme assay reaction [74]. These results are compatible with the study done by Sancenon et al. (2015) where pNPP hydrolysed by ALP reach the K_m in the range of 0.385 ± 0.250 mM in room temperature and at pH of 9.5 [75]. The calibration curve of ALP was applied in order to convert absorbance values to an enzyme unit (e.g., U/L). Figure 3.5 (D) shows that the absorbance values of ALP concentration (1-1500 U/L) were plotted using Lineweaver-Burk model with good linear regression of R^2 of 0.99. The linear equation obtained was used later for normalising data to the enzyme unit of U/L.

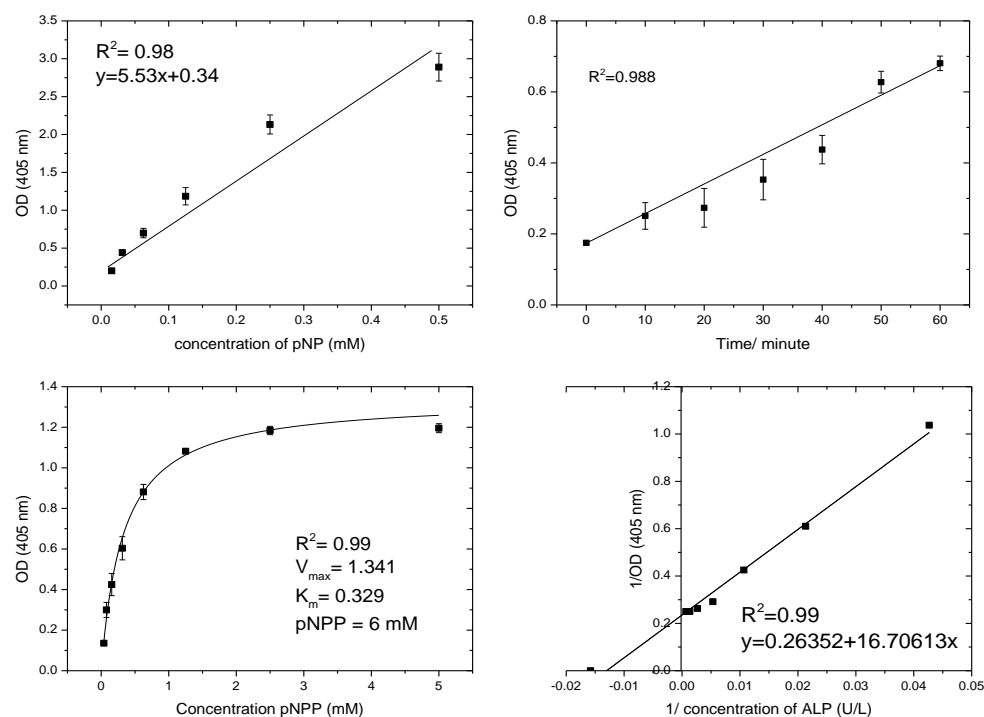


Figure 3.5: Absorbance optimization of ALP release applied at 405 nm and pH 9.5. (A) standard curve of concentration of pNP (0.16-5 mM) relating to absorbance response ($R^2 = 0.98$). (B) Optimization of reaction time for the enzymatic assay of ALP release. (C) Optimization of pNPP concentrations (0.2-5 mM pAPP) at 30 minutes incubation time. (D) The calibration curve of ALP activity ranging from 1.5-1500 U/L fitted by Lineweaver-Burk model ($R^2 = 0.99$).

3.4.3 Linearity performance of ALP release vs cell number

The linear relationship between ALP release and cell number was analysed. It is usual to use a concentration of substrate about 10-20-fold higher than the K_m in order to determine the level of an enzyme in a sample. Cells were exposed to the assay buffer in the presence of 6 mM pNPP following the steps in plate A in figure (3.2). The absorbance was linear for ALP released from the four cells (Fig. 3.6). This indicated a steady state conditions throughout the assay for all given cells. In Balbc/3 T3 cells, the highest value of ALP released was 0.96 while that of MCF-7 cells was 0.72, which was also the lowest value of ALP released among other cells. At the lowest concentration of (4×10^3 cell/ ml), the MCF-7 cells showed absorbance of 0.37, which is better than that observed from Balb/c 3T3 cells of 0.25. Both showed a linear response ($R^2 = 0.84$ for Balb/c 3T3 cells and 0.88 for MCF-7 cells). ALP release from A549 cells and Ht-29 cells showed higher values 2.34 and 2.89, respectively, and better resolution than previous cells with a highly linear response ($R^2 = 0.98$) for both cells. Moreover, the latter value expressed from Ht-29 cells had levelled off from the concentration of (60×10^3 cell/ ml), which indicates one of the limitations of optical detection techniques. The short linearity interval displayed by Ht-29 cells also indicated that ALP release is at high concentration. It is suggested to reduce the cell number for future experiments when applying linear trend.

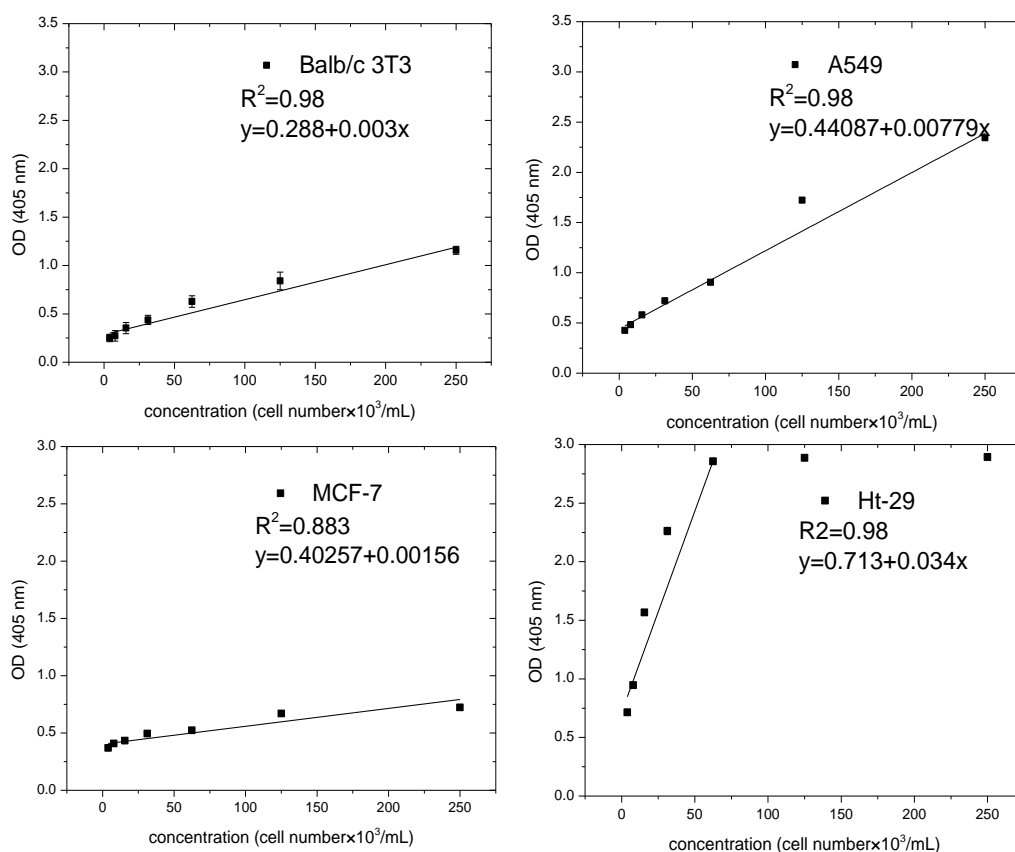


Figure 0.6: The linearity of the ALP release from the given cells was determined by linear regression analysis of the A405 absorbance values opposite different number of cells.

3.4.4 Concentration of the substrate pNPP from adhesion cells

When cells undergo many steps, the possibility of errors increases. In addition, cells are lost. For example, the trypsin steps means that cells are exposed to the washing and centrifugation twice. This analysis follows the steps in figure 3.2 (plate B). 4 days-old cells were washed twice with cold HBSS and were incubated with the assay buffer at a concentration range of 0.1 to 5 mM pNPP. The absorbance values were plotted against substrate concentration and fitted by non-linear regression analysis to the MichaelisMenten model. Figure 3.7 illustrates the enzymatic reaction of release ALP from Balb/c 3T3, A549, MCF7, and Ht-29 cells versus different concentrations of the substrate pNPP. Due to the non-regression (R^2 was less than 0.9), the Lineweaver-Burk model was applied to determine the constants of V_{max} and K_m (as is illustrated in the insert). Each cell line shows linear regression with $R^2=0.97$. The corresponding constants and the corresponding concentration of pNPP at 95 % of V_{max} was calculated for each cell line. Table 3.3 summaries the performance analysis. The K_m values of pAPP from each cell line were as follows: Balb/c 3T3 = 0.18 mM, A549 = 0.24 mM, MCF-7 = 0.25 mM and Ht-29 = 0.93 mM. The V_{max} values were as follows: Balb/c 3T3 = 0.604, A549 = 1.017, MCF-7 = 0.902 and Ht-29 = 1.986. The

corresponding concentration of pNPP at 95 % of V_{max} was as follow: 3.4 mM for Balb/c 3T3 cells; 4.4 mM for A549; 4.75 mM for MCF-7; and, 17.67 mM for Ht-29. The differentiation of the parameters indicates the different activity of ALP in each cell line. The obtained kinetic data from Lung cancer cells and breast cancer cells were compatible with the study done by Sancenon et al. (2015) where the pNPP concentration at half maximal velocity in pH 9.5 was in the range of 0.385 ± 0.250 mM [75]. On the other hand, colon cancer cell lines exhibited the highest activity and the embryonic cell line has the lowest activity according to their substrate concentration consumed at half maximal velocity. It is suggested to increase the initial concentration of the substrate when applying kinetic enzyme assay for ALP release from Ht-29 cells in the future work. This can be seen by the curvature. The line curved at (1.6) and the plateau level estimated by the model was at (1.9).

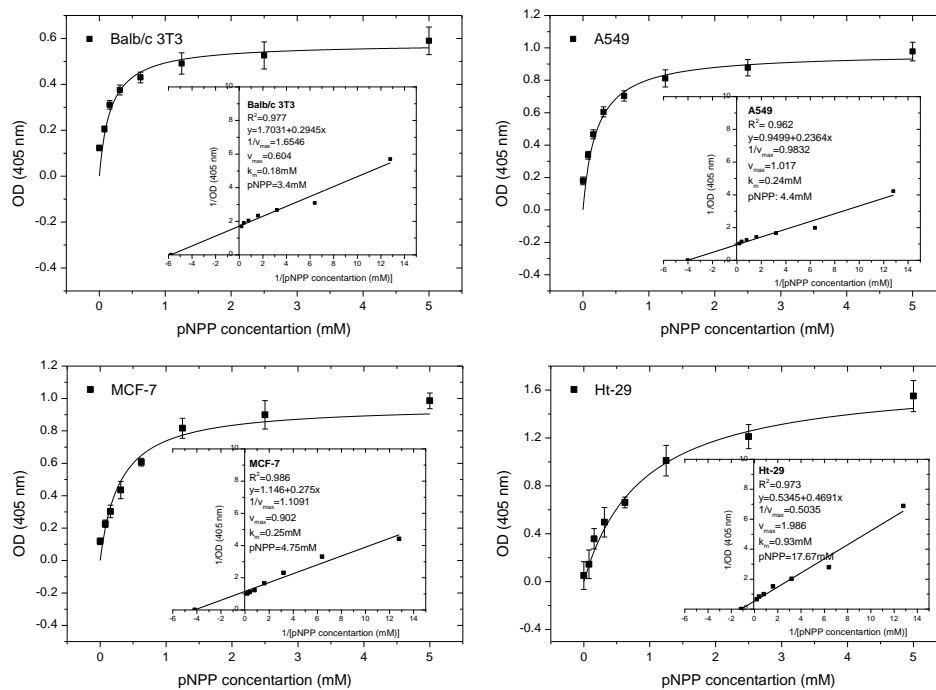


Figure 0.7: Optimization of pNPP substrate for adhesion cells fitted to the Michaelis-Menten model with R^2 less than 0.9 for all cells. In the inset, the Lineweaver-Burk model of enzyme release and pNPP concentration with linear regression R^2 higher than 0.9 for all cells.

Table 0.3: A summary of the performance analysis of pNPP from different cells.

Cells	Vmax	Km (mM)	intercept	slope	R2	pNPP (mM)
Balb/c 3T3	0.60	0.18	1.70	0.29	0.98	3.4
A549	1.02	0.24	0.95	0.24	0.97	4.4
MCF-7	0.90	0.25	1.46	0.28	0.99	4.8
Ht-29	1.99	0.93	0.53	0.47	0.97	17.7

After applying various concentrations of pNPP on adhesion cells and incubating for 30 minutes, absorbance was taken and the plots of M-M and L-B were fitted the data ($n=3$) with good regression analysis. Constants V_{max} , K_m and linear equation were determined. Optimal pNPP for ALP release from each cell line was calculated.

3.4.5 Real-time monitoring of ALP release from cells at post-confluence culture

Real-time monitoring of ALP release from Balb/c 3T3 cells, A549 cells, MCF-7 cells, and HT-29 cells was conducted. ALP was induced by differentiation using post-confluence culture. Cells were cultured for two more days after reaching 95-100 % confluence on day 4. Table 3.4 summarizes the results of ALP release in the target days for each cell with the vehicle control (VC), and the blank. It is obvious that the ALP release increases gradually from day 4 to day 6. This rise was shown from all cells. Furthermore, the data in day 5 and day 6 was compared to the control (data of day 4) using an unpaired t-test.

There was a significant difference between the data of ALP release from day 5 and day 6 compared to that released from day 4. Balb/c 3T3 cells had an average level of ALP of 0.489 on day 4 and the value increased on day 5 and day 6 (0.601 and 0.856, respectively). The value of lung cancer cells exhibited a sharp increment from day 4 to day 6, which was 0.721, 0.905 and 1.72. The breast cancer cells showed slight incensement from the fourth day to the sixth day, and that was 0.547, 0.670 and 0.724, respectively. The colon cancer had the highest release value of ALP (1.701) at confluence day compared to others and also for the post-confluence day 5 and day 6 of 2.262 and 2.856, respectively. Vehicle control of all cells showed less values. The cells of Balbc/ 3T3 and A549 cells had 0.172 and 0.178, respectively, whereas the MCF-7 and Ht-29 cells had 0.218 and 0.274, respectively, all of which represented significant differences when compared to the control. The buffer blank of all data was very low as no substrate was added to the assay. Confluent cells are used in the releasing enzyme [52], [62]. This monolayer can provide the most physiologically relevant conditions of impedance assays [76].

Table 0.4: Summary of ALP release from each cell line versus target days at post-confluence culture.

	Day 4	Day 5	Day 6	VC	Blank
Balb/c 3T3	(0.489 ± 0.010)	(0.601 ± 0.026) *	(0.856 ± 0.020) *	(0.172 ± 0.006) *	(0.045 ± 0.01) *
A549	(0.721 ± 0.021)	(0.905 ± 0.006) *	(1.723 ± 0.017) *	(0.178 ± 0.015) *	(0.053 ± 0.02) *
MCF-7	(0.547 ± 0.019)	(0.670 ± 0.018) *	(0.724 ± 0.015) *	(0.218 ± 0.016) *	(0.064 ± 0.01) *
Ht-29	(1.701 ± 0.036)	(2.262 ± 0.031) *	(2.856 ± 0.004) *	(0.274 ± 0.072) *	(0.055 ± 0.2) *

After exposing cells to the corresponding optimal substrate concentration of pNPP, absorbance 405 detection was used and obtained data were expressed as mean ± SD of measurements of three independent experiments with VC (vehicle control) that had dead cells, and the blank with no cells and no substrate. P-value of post-confluence culture compared to control (data of day 4), * p<0.05 significant is difference.

3.5 Conclusion

Alkaline phosphatase is a cancer biomarker, and real-time monitoring allows an understanding of the basis of diseases and progression of cancer. The aim of this research was to develop a methodology for realtime monitoring of ALP release from two types of cells: embryo fibroblast cells (Balb/c 3T3) and cancer epithelial cells (A549, MCF-7, Ht-29) using spectrophotometric analysis.

At alkaline pH, the enzyme ALP hydrolyzes the colourless p-nitrophenol phosphate to the yellow, p-nitrophenol, with absorbance of 405 nm. Many buffering materials exhibit good buffering at high pH like DEA, AMP and Triz. These materials are preferable and recommended in alkaline enzymatic assays and therefore were investigated in this study. The absorbance values obtained from different concentrations of pNP as the final product of the enzyme assay in the presence of 1 M DEA buffer brought about the highest shift of absorbance compared to AMP and Triz, although no significant difference was shown (Fig. 3.3). Hence, it was used throughout the experiments.

The DEA buffer was decided to be the alkaline environment of enzymatic reaction of ALP release. To release ALP, cells membranes need to be broken and therefore 0.1% of Triton X-100 was added to the assay buffer. Accordingly, the results of ALP release from cells were determined and compared to solubilization methods, including sonication and freeze-thawing cycles. Such methods can attain the maximum enzyme expression from treated cells. It was found that freeze-thawing the samples twice brought about the highest enzyme level (0.580). As there was (± 0.11) difference between the control methods (Trypsinized only) and the (freeze-thawing twice) of ALP release, it is recommended the method of (Trypsinized only) can express a proper ALP and facilitate the elimination of multiple steps (Table 3.2).

In this study, liberating of cells from plate was required by using trypsin. The effect of trypsin addition was investigated. After incubation cells at different time with trypsin, ALP release was determined. It was found that ALP release remains constant if trypsin is incubated with a sample for up to 15 minutes (Fig. 3.4 A). DEA is a biological buffer, in which its pKa depends on the buffer concentration and temperature. Cofactors were important in enzymatic assays, which were investigated in this study. Findings revealed that magnesium chloride and sodium chloride brought about better resolution of ALP release if the concentrations of them added were not less than 8 mM and 50mM respectively (Fig. 3.4 B) and (Fig. 3.4 C). ALP release was determined at pH range and at 37 °C. It was found that 9.5 pH displayed the best buffering (Fig. 3.4 D).

The parameters considered for this assay were optimized and displayed well-standardized curve of pNP. (Figure 3.5 A). Slope and intercept were obtained for comparison in chapter 6. The positive linear dependence manner of enzymatic assay with time can show stability of the enzyme over the time. ALP release over time was investigated, and it was found that the assay is time-dependent and 30 minutes was recommended (Fig. 3.5 B). pNPP substrate was optimized using detached cells and had Michaelis constants (K_M) of 0.32 mM, (V_{max}) of 1.34. As such, an optimal p-NPP concentration of (10-20 x K_M), 6 mM was found (Fig. 3.5 C). In order to facilitate a comparison of the obtained data from spectrophotometric analysis with those obtained from electrochemical analysis, calibration curve of alkaline phosphatase was investigated (Fig. 3.5 D). Units were converted using the obtained linear equation for comparison in chapter 6.

ALP release was determined from various cell number linearity analysis. All cells exhibited linear trend with good regression analysis (Fig. 3.6). Ht-29 exceeded the reference range of the spectrophotometer at the concentration of ($\sim 60 \times 10^3$ cell/ml) (Fig. 3.9 D). pNPP substrate was investigated during cellular adhesion, and it was found that there was a difference in (k_m) and (V_{max}) values (Fig. 3.7). The embryonic cells and lung and breast cancer cells displayed quite similar enzyme activity whereas colon cancer cells

has very high enzyme activity. Cells were differentiated using post-confluence culture for two days (day 5 and day 6) and compared to control (day 4), where confluence reached 95-100%. ALP release was increased gradually from day 4 to day 6. An incensement of ALP release was shown from all cells during the three days (Table 3.4).

The main aim of this study was achieved by providing convenient and reliable samples of ALP release for sensitively and continuously assaying using absorbance measurements, which made it easier for optimizing the methodologies for ALP release using electrochemical measurements in next chapter.

3.6 Reference

- [1] Kim, E. E.; Wyckoff, H. W. Reaction mechanism of alkaline phosphatase based on crystal structures. Two-metal ion catalysis. *J. Mol. Biol.* 1991.
- [2] Dirnbach, E.; Steel, D. G.; Gafni, A. Mg^{2+} binding to alkaline phosphatase correlates with slow changes in protein lability. *Biochemistry.* 2001.
- [3] Dean, R. L. Kinetic studies with alkaline phosphatase in the presence and absence of inhibitors and divalent cations, *biochemistry and molecular biology education.* 2006.
- [4] McComb, R. B.; Bowers, G. N.; Jr; Posen, S. *Alkaline Phosphatase.* New York: Plenum Press.1979.
- [5] Kind, P. R. N.; King, E. J. Estimation of Plasma Phosphatase by Determination of Hydrolysed Phenol with Amino-antipyrine. *J. Clin. Pathol.* 1954, 7, 322–326.
- [6] Bessey, O. A.; Lowry, O. H.; Brock, M. J. A method for the rapid determination of alkaline phosphates with five cubic millimeters of serum. *J Biol Chem.* 1946, 164, 321.
- [7] Li, X.; Li, B.; Zeng, H.; Wang, S.; Sun, X.; Yu, Y.; Wang, L.; Yu, J. Prognostic value of dynamic albumin-toalkaline phosphatase ratio in limited stage small-cell lung cancer. *Futur. Oncol.* 2019, 15, 995– 1006.
- [8] Martínez; Valeria, R.; Aguirre; María, V.; Todaro; Juan, S.; Piro; Oscar, E.; Echeverría; Gustavo, A.; Naso; Luciana, G.; Ferrer; Evelina, G.; Williams; Patricia, A. M. Interaction of Zn with Losartan. Activation of Intrinsic Apoptotic Signaling Pathway in Lung Cancer Cells and Effects on Alkaline and Acid Phosphatases. *Biol Trace Elem Res.* 2018, 186, 413–429.
- [9] Zhang, L.; Zhang, H.; Yue, D.; Wei, W.; Chen, Y.; Zhao, X.; Zhu, J.; Zhang, B.; Zhang, Z.; Wang, C. The prognostic value of the preoperative albumin to alkaline phosphatase ratio in patients with nonsmall cell lung cancer after surgery. *Thorac. Cancer* 2019, 10, 1581–1589.
- [10] Long, Z.-Q.; Hua, X.; Zhang, W.-W.; Lv, S.-W.; Deng, J.-P.; Guo, L.; He, Z.-Y.; Lin, H.-X. Prognostic impact of the pretreatment albumin to alkaline phosphatase ratio for nonmetastatic breast cancer patients. *Cancer Manag. Res.* 2019, 11, 4809–4814.

- [11] Singh, A. K.; Pandey, A.; Tewari, M.; Kumar, R.; Sharma, A.; Singh, K. A.; Pandey, H. P.; Shukla, H. S. Advanced stage of breast cancer hoist alkaline phosphatase activity: risk factor for females in India. 3 Biotech. 2013, 3, 517–520.
- [12] Keshaviah, A.; Dellapasqua, S.; Rotmensz, N.; Lindtner, J.; Crivellari, D.; Collins, J.; Colleoni, M.; Thürlimann, B.; Mendiola, C.; Aebi, S.; Price, K. N.; Pagani, O.; Simoncini, E.; Gertsch, M. C.; Gelber, R. D.; Coates, A. S.; Goldhirsch, A. CA15-3 and alkaline phosphatase as predictors for breast cancer recurrence: a combined analysis of seven International Breast Cancer Study Group trials. Ann. Oncol. 2007, 18, 701–708.
- [13] Hung, H.-Y.; Chen, J.-S.; Yeh, C.-Y.; Tang, R.; Hsieh, P.-S.; Tasi, W.-S.; You, Y.-T.; You, J.-F.; Chiang, J.M. Preoperative alkaline phosphatase elevation was associated with poor survival in colorectal cancer patient. Int. J. Colorectal Dis. 2017, 32, 1775–1778.
- [14] Pavkovic, B.; Nenadic, L. K.; Brankovic, M.; Zaric, M.; Brkic, M. P-120 Serum alkaline phosphatase level as an early diagnostic tool in colorectal cancer. Ann. Oncol. 2015, 26, iv34.
- [15] Li, C. M.; Li, Y. F.; Zhen, S. J.; Wang, J.; Huang, C. Z. A gold nanoparticles-based colorimetric assay for alkaline phosphatase detection with tunable dynamic range. Biosens. Bioelectron. 2013, 43, 366– 371.
- [16] Hayat, A.; Bulbul, G.; Andreescu, S. Probing phosphatase activity using redox active nanoparticles: A novel colorimetric approach for the detection of enzyme activity. Biosens. Bioelectron. 2014, 56, 334–339.
- [17] Hu, Q.; Zhou, B.; Li, F.; Kong, J.; Zhang, X. Turn-On Colorimetric Platform for Dual Activity Detection of Acid and Alkaline Phosphatase in Human Whole Blood. Chem. – An Asian J. 2016, 11, 3040– 3045.
- [18] Hu, Q.; Zhou, B.; Dang, P.; Li, L.; Kong, J.; Zhang, X. Facile colorimetric assay of alkaline phosphatase activity using Fe(II)-phenanthroline reporter. Anal Chim Acta. 2017, 950, 170–177.
- [19] Song, H.; Wang, H.; Li, X.; Peng, Y.; Pan, J.; Niu, X. Sensitive and selective colorimetric detection of alkaline phosphatase activity based on phosphate anion-quenched oxidase-mimicking activity of Ce(IV) ions. Anal Chim Acta. 2018, 1044, 154–161.
- [20] Cao, X.; Kong, F.; Zhang, Q.; Liu, W.; Liu, X.; Li, G.; Zhong, R.; Fan, L.; Xiao, H.; Cao, C. iPhone-imaged and cell-powered electrophoresis titration chip for the alkaline phosphatase assay in serum by the moving reaction boundary. Lab Chip 2018, 18, 1758–1766.
- [21] Qiong, H.; Minhui, H.; Yaqi, M.; Wenjie, F.; Su, J.; Jinming, K.; Xueji, Z. Sensitive and selective colorimetric assay of alkaline phosphatase activity with Cu(II)-phenanthroline complex. Talanta 2017, 163, 146–152.
- [22] Huang, Q.; He, C.; Zhang, J.; Li, W.; Fu, Y. Unlocking the hidden talent of DNA: Unexpected catalytic activity for colorimetric assay of alkaline phosphatase. Anal Chim Acta. 2019, 1055, 98–105.

- [23] Wu, T.; Hou, W.; Ma, Z.; Liu, M.; Liu, X.; Zhang, Y.; Yao, S. Colorimetric determination of ascorbic acid and the activity of alkaline phosphatase based on the inhibition of the peroxidase-like activity of citric acid-capped Prussian Blue nanocubes. *Microchim. Acta*. 2019, 186, 123–127.
- [24] Chen, X.; Chen, J.; Zhang, H.-Y.; Wang, F.-B.; Wang, F.-F.; Ji, X.-H.; HE, Z.-K. Colorimetric Detection of Alkaline Phosphatase on Microfluidic Paper-based Analysis Devices. *Chinese J. Anal. Chem.* 2016, 44, 591–596.
- [25] Liu, X.-G.; Xing, X.-J.; Li, B.; Guo, Y.-M.; Zhang, Y.-Z.; Yang, Y.; Zhang, L.-F. Fluorescent assay for alkaline phosphatase activity based on graphene oxide integrating with λ exonuclease. *Biosens. Bioelectron.* 2016, 81, 460–464.
- [26] Qu, F.; Pei, H.; Kong, R.; Zhu, S.; Xia, L. Novel turn-on fluorescent detection of alkaline phosphatase based on green synthesized carbon dots and MnO₂ nanosheets. *Talanta* 2017, 165, 136–142.
- [27] Sasamoto, H.; Maeda, M.; Tsuji, A. Chemiluminescent assay of alkaline phosphatase using phenacyl phosphate. *Anal Chim Acta*. 1995, 306, 161–166.
- [28] Ximenes, V. F.; Campa, A.; Baader, W. J.; Catalani, L. H. Facile chemiluminescent method for alkaline phosphatase determination. *Anal Chim Acta*. 1999, 402, 99–104.
- [29] Kokado, A.; Arakawa, H.; Maeda, M. Chemiluminescent assay of alkaline phosphatase using dihydroxyacetone phosphate as substrate detected with lucigenin. *Luminescence* 2002, 17, 5–10.
- [30] Deng, J.; Yu, P.; Wang, Y.; Mao, L. Real-time Ratiometric Fluorescent Assay for Alkaline Phosphatase Activity with Stimulus Responsive Infinite Coordination Polymer Nanoparticles. *Anal Chem.* 2015, 87, 3080–3086.
- [31] Qian, Z.; Chai, L.; Tang, C.; Huang, Y.; Chen, J.; Feng, H. Carbon Quantum Dots-Based Recyclable RealTime Fluorescence Assay for Alkaline Phosphatase with Adenosine Triphosphate as Substrate. *Anal Chem.* 2015, 87, 2966–2973.
- [32] Wang, X.; Wang, Z.; Zhang, Z.; Ma, X.; Wen, J.; Geng, Z. Real-time fluorescence assays of alkaline phosphatase and ATP sulfurylase activities based on a novel PPi fluorescent probe. *Talanta* 2015, 137, 156–160.
- [33] Chen, J.; Jiao, H.; Li, W.; Liao, D.; Zhou, H.; Yu, C. Real-Time Fluorescence Turn-On Detection of Alkaline Phosphatase Activity with a Novel Perylene Probe. *Chem. – An Asian J.* 2013, 8, 276–281.
- [34] Chen, L.; Yang, G.; Wu, P.; Cai, C. Real-time fluorescence assay of alkaline phosphatase in living cells using boron-doped graphene quantum dots as fluorophores. *Biosens. Bioelectron.* 2017, 96, 294–299.
- [35] Meng, Y.; Kasai, A.; Hiramatsu, N.; Hayakawa, K.; Takeda, M.; Shimizu, F.; Kawachi, H.; Yao, J.; Kitamura, M. Real-time monitoring of mesangial cell-macrophage cross-talk using SEAP *in vitro* and *ex vivo*. *Kidney Int.* 2005, 68, 886–893.

- [36] Yamashita, Y.; Toyoshima, K.; Yamazaki, M.; Hanada, N.; Takeharal, T. Purification and characterization of alkaline phosphatase from lactic acid bacteria. *RSC Adv.* 2019, 9, 336–354.
- [37] Noskova, Y.; Likhatskaya, G.; Terentieva, N.; Son, O.; Tekutyeva, L.; Balabanova, L. A Novel Alkaline Phosphatase/Phosphodiesterase, CamPhoD, from Marine Bacterium *Cobetia amphilecti* KMM 296. *Mar. Drugs* 2019, 17, 657.
- [38] Amoozadeh, M.; Behbahani, M.; Mohabatkar, H.; Keyhanfar, M. Analysis and comparison of alkaline and acid phosphatases of Gram-negative bacteria by bioinformatic and colorimetric methods. *J Biotechnol.* 2020, 308, 56–62.
- [39] Singh, S.; Hinkley, T.; Nugen, S. R.; Talbert, J. N. Colorimetric detection of *Escherichia coli* using engineered bacteriophage and an affinity reporter system. *Anal Bioanal Chem.* 2019, 411, 7273–7279.
- [40] Fernandes, J.; Amorim, R.; Azevedo, I.; Martins, M. J. *In vitro* modulation of alkaline phosphatase activity of *Saccharomyces cerevisiae* grown in low or high phosphate medium. *BRAZILIAN J. Med. Biol. Res.* 2008, 41, 41–46.
- [41] Hu, Y.-M.; Boehm, D. M.; Chung, H.; Wilson, S.; Bird, A. J. Zinc-dependent activation of the Pho8 alkaline phosphatase in *Schizosaccharomyces pombe*. *J Biol Chem.* 2019, 294, 12392–12404.
- [42] Onishi, H. R.; Tkacz, J. S.; Lampen, J. O. Glycoprotein nature of yeast alkaline phosphatase. Formation of active enzyme in the presence of tunicamycin. *J. Biol. Chem.* 1979, 254, 11943.
- [43] Fernandez, M.P.; Gascon, S.; Schwencke, J. Some enzymatic properties of vacuolar alkaline phosphatase from yeast. *Curr. Microbiol.* 1981, 6, 121–126.
- [44] Ming, T.; Hui, C. Effects of arbuscular mycorrhizal fungi alkaline phosphatase activities on *Hippophae rhamnoides* drought-resistance under water stress conditions. *Trees* 1999, 14, 113–115.
- [45] Gomez-Guinan, Y. Activity of acid and alkaline phosphatases (intracellular and extracellular) in rhizosphere fungi from *Arachis hypogaea* (Papilionaceae). *Rev. Biol. Trop.* 2004, 52, 287–295.
- [46] Bae, K.; Barton, L.; Alkaline Phosphatase and Other Hydrolyases Produced by *Cenococcum graniforme*, an Ectomycorrhizal Fungus. *Appl. Environ. Microbiol.* 1989, 55, 2511–2516.
- [47] Ho, I. Acid phosphatase, alkaline phosphatase, and nitrate reductase activity of selected ectomycorrhizal fungi. *Can. J. Bot.* 1989, 67, 750–753.
- [48] Yu, S.; Fourman, M. S.; Mahjoub, A.; Mandell, J. B.; Crasto, J. A.; Greco, N. G.; Weiss, K. R. Lung cells support osteosarcoma cell migration and survival. *BMC Cancer* 2017 Jan 25, 17, 78.
- [49] Kato, M.; Brijlall, D.; Adler, S. A.; Kato, S.; Herz, F. EFFECT OF HYPEROSMOLALITY ON ALKALINEPHOSPHATASE AND STRESS-RESPONSE PROTEIN 27 OF MCF-7 BREAST-CANCER CELLS. *Breast Cancer Res. Treat.* 1992, 23, 241–249.

- [50] Zheng, A. Inhibitory effects of breast cancer cells on proliferation and differentiation of osteoblasts. 2009.
- [51] Diloranzo, D.; Albertini, A.; Zava, D. Progesterone Regulation of Alkaline-Phosphatase in The Human Breast-Cancer Cell-LINE T47D. *Cancer Res.* 1991, 51, 4470–4475.
- [52] Chowdhury, M. A.; Peters, A. A.; Roberts-Thomson, S. J.; Monteith, G. R. Effects of differentiation on purinergic and neurotensin-mediated calcium signaling in human HT-29 colon cancer cells. *Biochem Biophys Res Commun.* 2013, 439, 35–39.
- [53] Shin, J.; Carr, A.; Corner, G. A.; Tögel, L.; Dávalos-Salas, M.; Tran, H.; Chueh, A. C.; Al-Obaidi, S.; Chionh, F.; Ahmed, N.; Buchanan, D. D.; Young, J. P.; Malo, M. S.; Hodin, R. A.; Arango, D.; Sieber, O. M.; Augenlicht, L. H.; Dhillon, A. S.; Weber, T.K.; Mariadason, J. M. The Intestinal Epithelial Cell Differentiation Marker Intestinal Alkaline Phosphatase (ALPi) Is Selectively Induced by Histone Deacetylase Inhibitors (HDACi) in Colon Cancer Cells in a Kruppel-like Factor 5 (KLF5)-dependent Manner. *J. Biol. Chem.* 2014, 289, 25306–25316.
- [54] Stoddart, M. *Mammalian Cell Viability: Methods and Protocols*. Totowa, NJ: Springer Science+Business Media, LLC. 2011.
- [55] Lonare, M. K.; Vemu, B.; Singh, A. K.; Dumka, V. K.; Singla, S.; Sharma, S. K. Cytotoxicity and Oxidative Stress Alterations Induced by Aldrin in BALB/c 3T3 Fibroblast Cell. *Proc. Natl. Acad. Sci. India Sect. B Biol. Sci.* 2017, 87, 1209–1216.
- [56] Gazdar, A. F.; Kurvari, V.; Virmani, A.; Gollahon, L.; Sakaguchi, M.; Westerfield, M.; Kodagoda, D.; Stasny, V.; Cunningham, H. T.; Wistuba, I. I.; Tomlinson, G.; Tonk, V.; Ashfaq, R.; Leitch, A. M.; Minna, J. D.; Shay, J. W. Characterization of paired tumor and non-tumor cell lines established from patients with breast cancer. *Int. J. CANCER* 1998, 78, 766–774.
- [57] Min, J.; Yuan, L.; Hai-Liang, X.; Ting-Ting, H.; Nai-Dai, Z.; Hong-Tao, X.; Qiao-Yan, Z.; Lu-Ping, Q. Estrogenic activity of osthole and imperatorin in MCF-7 cells and their osteoblastic effects in Saos2 cells. *Chin. J. Nat. Med.* 2016, 14, 413–420.
- [58] Guerreiro, S.; Monteiro, R.; Martins, M. J.; Calhau, C.; Azevedo, I.; Soares, R. Distinct modulation of alkaline phosphatase isoenzymes by 17 β -estradiol and xanthohumol in breast cancer MCF-7 cells. *Clin. Biochem.* 2007, 40, 268.
- [59] Tsai, L.-C.; Hung, M.-W.; Chen, Y.-H.; Su, W.-C.; Chang, G.-G.; Chang, T.-C. Expression and regulation of alkaline phosphatases in human breast cancer MCF-7 cells. *Eur. J. Biochem.* 2000, 267, 1330–1339.
- [60] Sánchez-Pérez, Y.; Chirino, Y. I.; Osornio-Vargas, Á. R.; Morales-Bárcenas, R.; Gutiérrez-Ruiz, C.; Vázquez-López, I.; García-Cuellar, C. M. DNA damage response of A549 cells treated with particulate matter (PM₁₀) of urban air pollutants. *Cancer Lett.* 2009, 278, 192–200.

- [61] Singh, N.; Zaidi, D.; Shyam, H.; Sharma, R.; Balapure, A. K. Polyphenols Sensitization Potentiates Susceptibility of MCF-7 and MDA MB-231 Cells to Centchroman. *PLoS One* 2012, 7, e37736.
- [62] Hodin, R. A.; Meng, S. F.; Archer, S.; Tang, R. Cellular growth state differentially regulates enterocyte gene expression in butyrate-treated HT-29 cells. *CELL GROWTH Differ.* 1996, 7, 647–653.
- [63] Singh R. P.; Sharma, G.; Sonali, S. S.; Kumar, M.; Pandey, B. L.; Koch, B.; Muthu, M. S. Vitamin E TPGS conjugated carbon nanotubes improved efficacy of docetaxel with safety for lung cancer treatment. *Colloids Surfaces B Biointerfaces* 2016, 141, 429–442.
- [64] Chang, T.-C.; Wang, J.-K.; Hung, M.-W.; Chiao, C.-H.; Tsai, L.-C.; Chang, G.-G. Regulation of the expression of alkaline phosphatase in a human breastcancer cell line. *Biochem. J.* 1994, 99-205, 303.
- [65] Forgeue-Lafitte, M.-E.; Coudray, A.-M.; Breant, B.; Mester, J. Proliferation of the Human Colon Carcinoma Cell Line HT29: Autocrine Growth and Deregulated Expression of the c-myc Oncogene¹. *Cancer Res.* 1989, 49, 6566-6571.
- [66] Wistuba, I. I.; Bryant, D.; Behrens, C.; Milchgrub, S.; Virmani, A. K.; Ashfaq, R.; Minna, J. D.; Gazdar, A. F. Comparison of Features of Human Lung Cancer Cell Lines and Their Corresponding Tumors. *Clin. Cancer Res.* 1999, 5, 991–1000.
- [67] Rej, R.; Bretauiere, J. P. Effects of metal ions on the measurement of alkaline phosphatase activity. *Clin. Chem.* 1980.
- [68] UTIDA, S. Effect o f Sodium Chloride on Alkaline Phosphatase Activity in Intestinal Mucosa o f the Rainbow Trout. *Proc. Japan Acad.* 1967, 43.
- [69] Sabokbar, A.; Millett, P. J.; Myer, B.; Rushton, N. A rapid, quantitative assay for measuring alkaline phosphatase activity in osteoblastic cells *in vitro*. *Bone Miner.* 1994.
- [70] Catherine, J. F. C.; Roberts, H. Trypsin-modified Alkaline Phosphatase. *J. Biol. Chem.* 1985, 260, 7557–7561.
- [71] Olorunniji, F.; Igunnu, A.; Adebayo, J.; Arise, R.; Malomo, S. Cofactor interactions in the activation of tissue non-specific alkaline phosphatase: Synergistic effects of Zn²⁺ and Mg²⁺ ions. *Biokemistri.* 2010.
- [72] Casey, H.; Zanobini, A.; Firenzuoli, A. M.; Treves, C.; Bianchi, A. Influence of Zn⁺⁺ and of Mg⁺⁺ on alkaline phosphatase activity of different origins. *Boll. Soc. Ital. Biol. Sper.* 1980.
- [73] Poe, R. W.; Sangadala, V. S.; Brewer, J. M. Effects of various salts on the steady-state enzymatic activity of E. coli alkaline phosphatase. *J. Inorg. Biochem.* 1993.
- [74] Reymond, J. L.; Fluxa, V. S.; Maillard, N. Enzyme assays. *Chem Commun.* 2009, 1, 34–46.
- [75] Sancenon, V.; Goh, W. H.; Sundaram, A.; Er, K. S.; Johal, N.; Mukhina, S.; Carr, G.; Dhakshinamoorthy, S. Development, validation and quantitative assessment of an enzymatic assay suitable for small molecule screening and profiling: A case-study. *Biomol. Detect. Quantif.* 2015.

[76] De Blasio, B. F.; Laane, M.; Walmann, T.; Giaever, I. Combining optical and electrical impedance techniques for quantitative measurement of confluence in MDCK-I cell cultures. *Biotechniques*. 2004.

Chapter 4

Electrochemical Assay of Alkaline Phosphatases (ALP)

Note: This chapter has been published in Journal of Biosensor. Please refer to Appendix.

4.1. Aim and Objectives

The aim of the research outlined in this chapter was to optimize real-time monitoring of ALP release from two types of cells: embryo fibroblast cells (Balb/c 3T3) and cancer epithelial cells (A549, MCF-7, Ht-29), with electrochemical analysis-linear sweep voltammetry technique being applied. This optimization would then be compared with optical detection of ALP in chapter 3. The novelty of this aim was that no electrochemistry assay was done for ALP release from the given cells. In addition, ALP release have not been detected by electrochemistry assay during differentiation of post-confluence culture for all gievn cells.

These aims were achieved through the following objectives:

1. To characterize graphite screen-printed electrodes and use potassium Ferri/Ferrocyanide solution before and after the cleaning process.
2. To obtain the standard curve of p-aminophenol (pAP) and thus observe the parameters of linear sweep voltammetry of pAP oxidation peaks.
3. To optimize incubation time of the substrate p-aminophenol phosphate (pAPP) with ALP release.
4. To determine the saturation point of the substrate pAPP using non-linear regression analysis (e.g. Michaelis-Menten model).
8. To determine the calibration curve of ALP and identify the amount in Units per Litre (U/L) that can be compared with absorbance experiments in chapter 3.
5. To investigate linearity performance of ALP release with different concentrations of the given cells.
6. To investigate the hydrolysis of different concentrations of the substrate pAPP by ALP release from adhesion cells and determine Michaelis constants (I_{max}) and (K_m) for the substrate pAPP for each cell.
7. To allow real-time monitoring of ALP release using post-confluence culture for 3 days.

4.2. Introduction

4.2.1. Principle

The determination of ALP release from cells is conducted by the absorbance principle, which is performed in the presence of p-nitrophenyl phosphate and DEA as the alkaline buffer and at absorbance of 405 nm. As described in chapter 3, this method is simpler and cheaper than other spectrophotometric methods, such as fluorescence [1]–[3] and chemiluminescence [4]–[6]. Therefore, it is still recommended by European Society for clinical chemistry and mostly applied by international companies like the (Siemens). Electrochemical principle is important, because the point-of-care testing increases dramatically and the absorbance techniques hardly meet the medical revolution. The detection of ALP using electrochemical detection contributes to the integration systems field, hence enhancing the detection of biological targets

based on the electrochemical change of electrode interfaces. This enhancement supports the pharmaceutical research and design system for drug analysis, and therefore, it is important to develop a methodology based on the electrochemical method for real-time ALP release.

Electrochemistry allows integration in small devices that is required for point-of-care testing. Electrochemical detection techniques are relatively easy to use and offer relatively fast detection. This is reflected in Clark's work (1954) [7]. Electrochemical biosensors for ALP have rapidly developed since 1991, when Thomson and his team published their work comparing ALP resolution of electrochemical to results of optical detection [8]. The principle was based on hydrolyzing o-phosphate by ALP in the presence of the p-aminophenyl phosphate (pAPP), where the non-electroactive substrate under the alkaline environment served to generate an electroactive (pAP). The research of the group has contributed to developing ALP electrochemical detection, which has allowed researchers to take advantage of Thompson's contributions and apply different approaches (Table 4.1).

Table 0.1: The research contributed to the development of ALP biosensors.

Year	Contribution	Substrate	Biological sample	Pros /cons	Ref.
2000	Reduce the over-potential by using Tyrosinase	Phenol phosphatse	serum	Good stability but has two reactions steps.	[9]
2009	minimized the reaction in one single step	Phenol phosphatse	-	No biological sample was used	[10]
2012	amplify the electrochemical signals	p-nitrophenol phosphate	-	ionic liquid was used for more conductivity	[11]
2013	self-assembled monolayers to modify gold electrodes for redox cycling	p-aminophenol phosphate	-	Enhancing detection by cysteamine, tris(2-carboxyethyl) phosphine (TCEP), or nicotinamide adenine dinucleotide (NADH).	[12]
2015	signal amplification using a single molecular exonuclease-assisted signal	-	serum	It is more sensitive than the immobilization-based electrochemical methods	[13]

So far, investigations of ALP release from MCF-7 of breast cancer, A549 of lung cancer, and HT-29 of colon cancer have only been carried out using fluorescence and chemiluminescence. The optimization achieved

as a result of spectroscopy would be negatively affected by the limitations (e.g., the cost, and the size of instruments). Accordingly, this chapter will explore the parameters of enzyme assay and apply electrochemical assay for ALP release from living cells. Figure 4.1 illustrated the schematic reaction for this study.

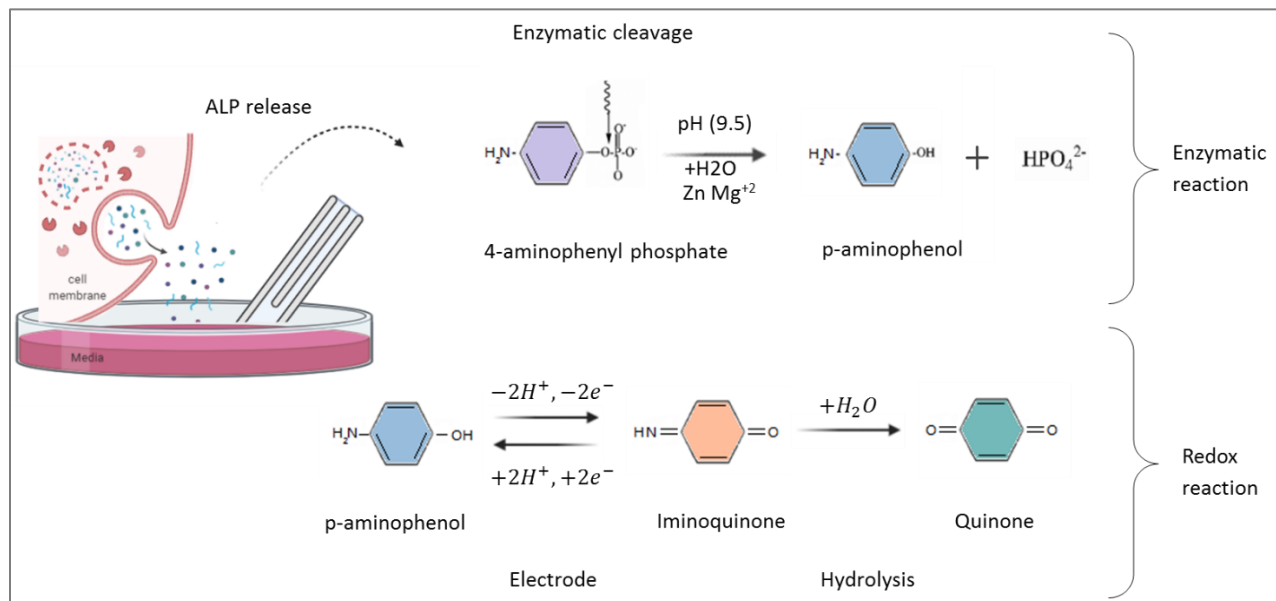


Figure 0.1: Schematic of the electrochemical reaction of ALP release [8].

4.2.2. Background

Investigation of ALP release as a quantitative indicator of gene reporting in mammalian cells began in 1988 [14]. However, it was not until the development of the electrochemical immunoassay [15] that the electrochemistry of ALP release as a secretion enzyme from cells began to grow in popularity [16]–[18]. Almost ten years later, a proper protocol of ALP release was investigated using methods of molecular biology, biochemistry, enzymology, and chemiluminescence. These methods were conducted using genetic methodologies for manipulating ALP release from cells using different transfection and transformation tactics [19]–[23]. These findings enhance the detection of ALP using electrochemistry [24]–[27]. Kelso et al. (2000) exploited electrochemical immunoassay, and were likely the first to detect secreted ALP in media using screen-printed electrodes and 2-naphthyl phosphate [28]. Kelso's group took advantages of the developed progress from electrochemical immunoassay contributions. They infected CHO cell lines to release ALP, which showed sufficient results that could be further optimized to increase sensitivity.

4.2.3. Literature review

Electrochemical analysis can increase the effective detection of ALP release from cells. The initial protocols of developed methods of ALP release *in vitro* used the same strategies used for β -galactosidase, like JM109, chromosomal gene fusion, yeast-two hybrid system, and viral vectors of CRE- (CMV)-SPAP [45]. With gene-modified strategies in place, vector of (CRE-SRE- (CMV)-SPAP) were originally called

Cytomegalovirus —they were, after all, used for cell infection to allow ALP release [19]–[23], [28] They soon became known as gene modifiers when scientists realized that controlling ALP release of inflammation means modifying them in order to make them work more efficiently. Three of these modified vectors are pNF α B-SEAP, pSEAP2-control and pSEAP2-basic [29].

Compared to the infection method, the use of modified vectors is a very delicate experiment, only appearing around the addition of plasmids. The addition of plasmids to cells occurred in the presence of Opti-MEM I media and lipofectamine and incubated for 5 hours and then replaced by the routine media. ALP release was carried out in the HEBES buffer and 5 mM pAPP 150 mM NaCl, 4.2 mM KCl and 11.2 mM glucose and by using platinum electrodes. The developed methodology, however, allowed a detectable ALP release of 7 nA at 5×10^5 cell/ml compared to the control which was 3 nA using the amperometric technique. However, low ALP expression from MCF-7 cancer cells was because breast cancer cells is poor expressing genes compared to the benign breast tumour [30]. Moreover, the designed plasmid DNA required standards addition of lipofectamine for safe delivery of exogenous DNA into cells [31]. They used large working area about 8.8 cm^2 .

The following development was add another step to the transfection method which was the infection method. It was believed that receptors expressed from genetically engineered cells will recognize the addition of endotoxin and then will activate NF- κ B (nuclear factor kappa B) that is control expression of ALP release. Different concentration of Escherichia coli bacteria was used as source of endotoxin and incubated with 1.5 mM pAPP with cells for 24 hours [32], [33]. This method used embryonic kidney cell lines, which was commercially transfected has ALP released up to 60 nA from 1×10^5 cell/ml for 24 hours. Nevertheless, this data were shown at the optimal pH of endotoxin which was 6.5 and at alkaline pH the data started to shrink and saturated at about 25 nA. Moreover this method affect cell viability as the incubation with bacteria took 24 hours.

In this method, more attention was paid to the electrolyte. After transfection, cells were washed with 10 mM HEBES buffer and incubated for 10 minutes with the same buffer containing 150 mM NaCl, 4.2 mM KCl, 11.2 mM glucose, 1mM Na 2 HPO 4 and at pH of 7. This solution was then transferred to the assay buffer, which was also HEBES, but at 9.5 pH in the presence of 4.7 mM pAPP. ALP release from treated cells was about 70 pA and that from non treated cells was 30 pA. Although a proper ALP release was achieved and a significant difference appeared compared to the control, the experimental set up caused inappropriate cell viability. Cells stay alive for 1 hour after exposure to the indicator pAPP. The cell density in this assay was hard to control, which means that the number of cells shown does not reflect the actual ALP release. The assay also suffered from the rate reaction of pAPP, which caused high standard deviation. Thus, an attempt was made to develop the determination of the number of cells that undergo the assay and minimise the concentration of pAPP at about 1 mM [34]. This assay showed 95 % of viable cells at the first hour of incubation with assay buffer and viability reduced by 55% points to stay 40% alive after 2 hours of incubation. The average of ALP release from treated cells was up or 10 pA, at the first minute. By 10 minutes, it was 20 pA, and by 20 minutes it was 30 pA. When pAP could move into grooves made between microwells the oxidation current to 70 pA. Although the mobility (diffusion) that the assay could achieve (for pAP), the oxidation current stayed constant when time increase. Also untreated cells showed

better regular increase with traditional design of microwell compared to that integrated with grooves, hence, more experiments were required for controlling the assay and reducing the background current.

The overlap and the low current resulted in the enzymatic reaction of ALP release requires experiment optimization. There were a number of matters need to be considered, for example, interfering with endoALP, which believed it is the reason behind the noise. These matters were investigated by comparing ALP release in supernatant and in media for treated and untreated cells [35]. Studies have shown that, there is no ALP release in the supernatant of untreated cells and the data was the same as the background. ALP release was shown in the media of untreated cells with high standard deviation. On the other hand, ALP release in media from treated cells was as twice as that released in supernatant. This assay used 5×10^4 cell/ml and incubated with the substrate for 4 hours to indicate the results. As the endoALP became further related to ALP release, its level can be further optimised to allow reporter gene analysis.

At the same time, the development methodology carried out for ALP release returned back to the immunoassay detection techniques and used ALP antibody-antigen immobilised on a substrate in the presence of 4.7 mM pAPP and HEBES buffer in order to test the accuracy of the assay. The findings observed relationship between cell number and ALP release, the lower cell number the higher standard deviation. The findings observed was high at lower cell number and indicated a positive relationship between cell number and ALP release. Prior research suggested that better electrochemical signal results in high ALP concentration, which can be achieved by increasing cell number. It is worth noting that transfection methodology is more suitable for less cell number. Another method to monitor ALP release from 1000-2000 embryonic stem cells were applied in the presence of β -mercaptoethanol to avoid differentiation of cells [36]. Cells inserted into the working area and Triz buffer was added instead of the usual HEBES buffer and that involved 4.7 mM pAPP and pH of 9.5. The replacement buffers was because of the pH stability as the HEBES provide alkaline environment of up to 8.2, whereas ALP reaction needs higher pH around 9.5 to bring about a reliable electrochemical signal. Their findings were qualitative and compared the size of the cells' aggregation to the resulting current and verified it by glucose addition as a positive control. However, the experiment conditions of 3 hours might influence the results. For example, the absence of glucose for 3 hours affected the viability of cells, hence deactivating ALP release. The long-time monitoring of ALP release caused accumulation of pAP in the buffer, thus illustrating high quantity of ALP release.

The approach of addition or absence of supplements was avoided in the work done by Yildirim-Semerici et al. in 2015 [37]. They used an osteoblastic cell line, as it's known for its self-differentiation and, accordingly, releasing ALP. Their methodology relied on associating ALP release to cell number, which was verified by Trypan blue assay. The measuring solution was 50mM of Triz buffer containing 5 mM pAPP, 0.1 mM ZnCl_2 , 1 mM MgCl_2 and had a final pH of 8.0. This method paid more attention to the component of assay solution. The obtained findings based on electrochemical activity assay were in line with incubation time, as there was an increase of ALP release when the incubation time of sample was increased. ALP increased in bone cells during the first stage. When the minimization step started, the ALP decreased, which was optioned in the previous method. However, cells number could increase as well and cause ALP increase. Also, electrode surface was isolated by cells confluence and hindered pAP diffusion which might cause ALP levelling at day 6..

Accordingly, the trend towards recording ALP from different cells lines is perhaps more favoured towards differentiation ALP. Ragones et al. in 2015 presented an electrochemical sensor that avoided attaching the electrode to cells and allowed for the direct measurement detection on close proximity or in contact with three different colon cancer cells involving Ht-29, HCT116 and Colo320 cells [38]. The sensor had a stable signature and good detection response to ALP enzyme even in repeated tests. The number of cells was 2×10^6 and 1×10^6 cells/ml, allowing pAPP oxidation peaks around 120 nA and 60 nA for Colo320 cell lines. Total electrolyte volume might influence the assay time as the volume was very shallow and parley covered the cells.

4.2.4. The problem statement

Exploiting advantages of the afore-mentioned studies and designing a methodology for ALP release using electrochemical analysis is of significance. There are multiple reasons why electrochemical methods of real-time monitoring are still being developed. Firstly, ALP release differentiated strategies fluctuate depending on cell type. The infection method was initially popular, then transfection methods took their place. This was followed by a combination of both methods for studying cells like CHO cell, Hela, and kidney cells. These methodologies are limited, as ALP shows less concentration. Other methods were developed, such as using some reducing agent (e.g., β -mercaptoethanol) that had to be used to stabilize cells under one condition and prevent differentiation and then allow ALP release based on the size of cells. The addition of that agent may result in the inactivity of intracellular ALP and that may be the reason why cells display low ALP [39]–[41] (besides the absence of glucose).

ALP release could be carried from self-differentiation cells without addition like bone cell lines. This plan couldn't differentiate between the quantities of ALP if it was of the cell number growth or was of first stage of growth bone where ALP is believed to be increased. It is so handy and merely by continuing monitoring ALP from different cells, which was done by choosing different cells lines of the same cancer. The sample carried out so far by way of electrochemical analysis were as a single-cell analysis [30], [31], [34], biopsies [42], tissues [43] and cells lines [33], [35], [37], [38]. The Cells lines used were commercially engineered including MCF-7 and Hela, or infecting by bacteria including kidney cells lines. On the other hand, MBA-15 that derived from osteogenic cell line; and Ht-29, HCT116 and Colo320 that derived from colon cancer cells lines. The only embryonic cells have been used was stem cells [36]. This thesis is interested in releasing ALP from lung cancer cells, breast cancer cells and colon cancer cells. Moreover, Balb/c 3T3 embryonic mouse cells lines was used because it is a suitable transfection host [44].

Secondly, previous literatures identified some limitations in electrochemical measurement, such as working area and volume size of the electrolytes corresponding to sample size. For example, the working area was about 3.5-8.8 cm². This limited high throughput screening. Also, electrochemistry parameters are required during the assay, including the type of electrode, positioning of sample into the working area, as well as components of the electrolyte. For instance, above-noted studies for real-time ALP monitoring utilized fixed potential principle like amperometry. The potential is always seen at 0.3 V, as it is believed that this is the optimal where pAP can be detected. This potential, however, is suitable only with electrochemical immunoassay where antibodies are immobilized on the working area of electrodes [45], but when using bare electrodes, the potential shift will decrease [46], [47]. This notification was

mentioned during monitoring ALP from cancer and healthy tissues of biopsies. In that assay the potential reduced to 0.22 V, which is still higher.

Also, sample positions within the working areas were an obstacle for electrical flow current to pass. This was solved by closing the electrode to the cell layers instead of growing cells on the top of the electrode. However, this way also illustrated low diffusion of the analyte through the assay, which was the reason beyond the solution volume that was shallow over the cells. Thirdly, the challenge of companion pH suitable for cell viability near 7.4 and suitable for ALP catalyse near 9.5 made the electrolyte components affect the ALP assay. Numerous attempts can be seen when using HEBES buffer or Triz buffer materials, the presence or absence of salts in the electrolyte and the variety of concentrations used of pAPP from 0.1 -5 mM. Moreover, the incubation time of the substrate with the sample does not show a kinetic reaction where incubation time increases at 3, 3.5 and to 24 hours.

4.2.5. Summary

In this chapter, electrochemical assay was applied and the parameters of enzyme assay was determined for ALP release from living cells. Linear sweep voltammetry has been used, because it has a wide potential window, as it is a droplet-based assay and requires no stirring solution. These are important factors for point-of care application. Characterization of graphite screen-printed electrodes (graphite-SPE) was performed before and after cleaning process; standard curve of p-aminophenol (pAP) was obtained. Optimization of incubation time for the substrate p-aminophenol phosphate (pAPP hydrolysed by ALP release was investigated and the saturation point of the substrate pAPP was obtained. Linearity behaviour of the assay was analysed between cell number and current response. Two methods were used for realtime ALP release; non-adherent cells and adherent cells. The findings allowed comparison with optical data obtained in chapter 3.

4.3. Methodology

4.3.1. Chemicals and Instruments

Alkaline phosphatase (ALP, calf intestinal phosphatase) or 4-aminophenol (p-AP) was purchased from Sigma (Ireland) and used to make stock solution at a final concentration of 1500 U/L or 5 mM. The alkaline buffer assay at pH 9.5 was made by adding sterile deionized water at grade 18 MΩ provided from Tyndall National Institute (UCC), which contained diethanolamine (DEA) 1 M, magnesium chloride (MgCl_2) 8 mM, sodium chloride (NaCl) 50 mM, potassium chloride (KCl) 100 mM, para-aminophenol phosphate (p-APP) and HCl purchased from Sigma (Wicklow, Ireland). The electrochemical measurements were performed on screen printed carbon electrodes with each individual sensor consisting of a graphite working and counter electrode and Ag/AgCl reference electrode (graphite-SPE) (Kanichi Research Limited, England, the UK) with a working volume of 70 μL performed on palmSens portable potentiostat (Palm Instruments BV, Houten, the Netherlands). The graphite-SPE was cleaned before using for 20 min by Plasma Surface Treatment (Harrick plasma, Ithaca, NY, the US).

4.3.2. ALP Release and Cell Culture

In order to release ALP from cells, the following steps were performed according to the protocols developed in chapter 2 (section 2.3.12). The first step was to enhance ALP release in 4-day-old culture by seeding cells as a monolayer on 48-well plates (Sigma, Ireland), incubating at 37 °C and 5% CO₂ (incusafe Panasonic incubator) and changing media every two days. Figure 4.2 shows the two ways of optimization quantity of ALP from non- adherent cells (plate A) and adherent cell (plate B).

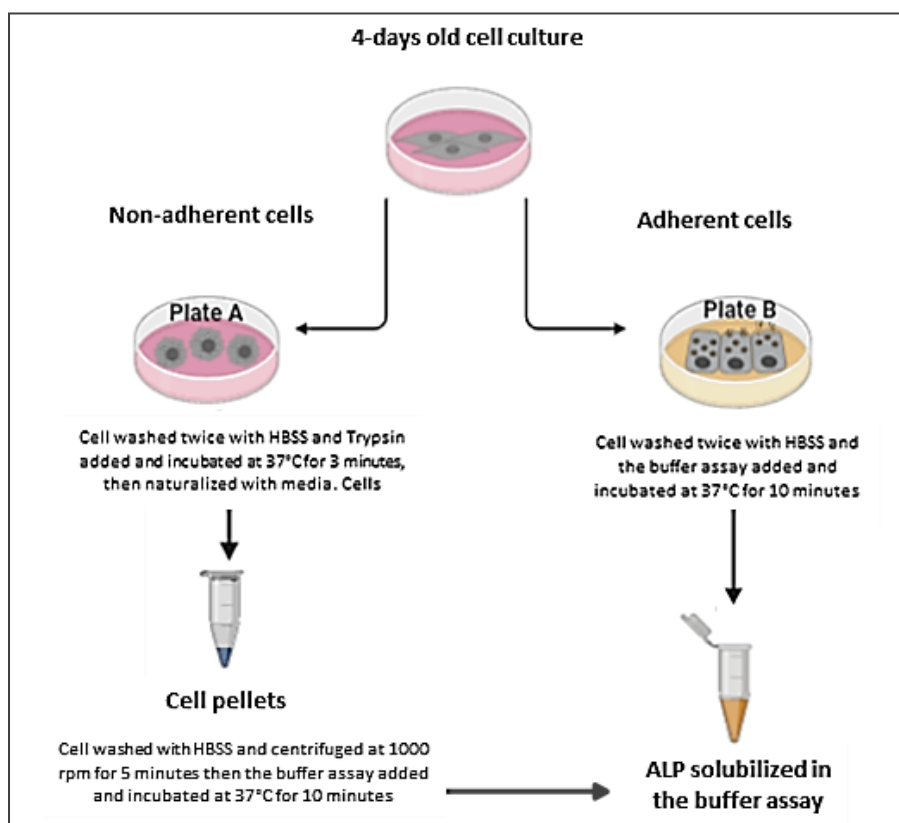


Figure 0.2: A schematic diagram of ALP release. Plate A describes the methods of determination of ALP release from detached cells, where cells are washed with Hank's balanced salt solution (HBSS) and undergo trypsinization, washing and centrifugation before being exposed to the buffer assay. Plate B describes the methods of determination of ALP release from attached cells, where cells are only washed before being directly exposed to the buffer assay.

The cell lines used during this study were purchased from ATCC (UK), including mouse embryo fibroblast cells (Balb/c 3T3 Line), breast carcinoma epithelial cells (MCF-7 Line), lung carcinoma epithelial cells (A549 Line), and colon carcinoma epithelial cells (Ht-29 Line). The media, supplements, and washing buffer used for culturing cells were Dulbecco's modified Eagle's medium (DMEM), minimum essential medium Eagle (MEME) and McCoy's 5A medium, newborn calf serum (NBCS), fetal bovine serum (FBS), and Hank's balanced salt solution (HBSS), which were purchased from Sigma (Ireland). Table 4.2 summarises the cell numbers used and the composition of media. The cells were sub-cultured three times before seeding began under aseptic conditions using a cell culture hood (Esco Airstream® Class II).

Table 0.2: A summary of the cell number and the composition of media used in this study.

Cell Line	Concentration ($\times 10^3$ Cells/mL)	Media	Supplements
Balb/c 3t3	40	DMEM	10% NBCS
A549	40	DMEM	10% FBS
MCF-7	40	MEME	10% FBS
Ht-29	80	McCoy's 5A	10% FBS

4.3.3. Stabilization of Graphite Screen-Printed Electrodes

Graphite screen-printed electrodes (graphite-SPE) were first cleaned using iso-propanol and a plasmon cleaner device for 10 min or for 20 min and compared to non-cleaned electrodes. Potassium $[\text{Fe}(\text{CN})_6]^{3-/4-}$ (1 mM) was dissolved in 1.0 M of KCl. $[\text{Fe}(\text{CN})_6]^{3-/4-}$ solution (5 mL) was used to immerse the graphite-SPE. A Palmsens potentiostat device was used to carry out the cyclic voltammetry assay and to compare the data before and after the cleaning process. The cyclic voltammetry detection techniques were applied at scan rates from 5 mV/s to 200 mV/s and at initial potential of -0.2 V and final potential of 0.6 V versus the Ag/AgCl reference electrode. The potential range of each scan rate of cyclic voltammograms was plotted against the response current. The reduction peaks' current (ipc) and oxidation peaks' current (ipa) were plotted versus the square root of the scan rate $((\text{mV/S})^{1/2})$.

4.3.4. Optimization of Electrochemical Measurement

Samples of cells were freshly prepared at a concentration of 250×10^3 cells/mL. The cells were washed twice with HBSS, centrifuged for 5 min at 1000 rpm and resuspended in the assay buffer. Graphite screenprinted electrodes were first cleaned using plasma cleaner for 20 min and linear sweep voltammetry measurements were carried out at potentials ranging from -1.2 V to 1.5 V vs. Ag/AgCl. The measurements were completed in triplicate at a volume of $70 \mu\text{L}$ and a scan rate of 100 mV/S . To determine a probable working range for the product pAP, serial dilutions of pAP, starting with 5 mM were prepared in the presence of $30 \mu\text{L}$ of sample mixed with $100 \mu\text{M}$ of pAPP. The linear sweep voltammetry was measured for each concentration at three separate electrodes. A free-pAP buffer was used as blank. A graph charting current response to concentration of pAP was prepared for regression analysis. The incubation time evaluation for ALP release was performed using $70 \mu\text{L}$ of a sample with 20 U/L of ALP activity mixed with $30 \mu\text{L}$ of pAPP 5 mM in buffer DEA and assessed at 5-min intervals over 60 min. NaOH ($30 \mu\text{L}$ of 1 M) was added in order to stop the reaction. The reaction time was fixed to 10 min, and the activity of the sample was assessed with different concentrations of substrate range (5, 2.5, 1.25, 0.63, 0.31, 0.16, 0.08, and 0.04 mM pAPP). The optimal concentration of substrate obtained was used in a calibration plot of ALP release. The sample was spiked with various concentrations of ALP (calf intestinal phosphatase) at a range of 1.51500 U/L .

4.3.5. Linearity Performance of ALP Release vs. Cell Number

In order to complete a linearity trend of ALP release versus current density, different concentrations of cells were used ($250, 125, 63, 31, 16, 8$, and 3×10^3 cells/mL). The cells were incubated in the assay buffer

for 10 min before measurement. Linear sweep voltammetry was applied in triplicate in three separate graphite-SPEs at a final volume of 70 μL , against a free-pAPP buffer that was used as a blank. We measured it at 100 mV/s and a potential range from -1.2 V to 1.5 V versus the reference of Ag/Ag/Cl. exhibited good anodic peaks at 100 mV/s. The wide range was chosen in order to identify if there was any other oxidation peaks for interferences during the assay. A graph relating the concentration of cells to the current density was prepared for regression analysis.

4.3.6. Concentration of the Substrate pAPP from Adhesion Cells

Adherent cells have different responses from non-adherent cells in terms of releasing ALP. Therefore, the concentration of substrate pAPP needed to be assessed in order to allow for real-time monitoring of ALP. The serial dilution of pAPP, starting with 5 mM, was carried out in the range of 5, 2.5, 1.25, 0.60, 0.30, 0.16, 0.08 and 0.04 mM in the assay buffer. The range of diluted pAPP was incubated with cells for 10 min. The electrochemical assay was applied with a final volume of 70 μL against a free-pAPP buffer as blank. A graph relating the concentration of pAPP to current density fit by non-linear regression analysis to the Michaelis-Menten model for each cell line was completed.

4.3.7 Real-time monitoring of ALP release from cells at post-confluence culture

To meet the aim of this chapter and allowing ALP release, post-confluence culture strategy was used. As described in chapter 3 section 3.3.9, cells were seeded in 48-well plates at concentration of 40×10^3 cells/ml for the following cells: Balb/c 3T3, A549, and MCF-7, and at concentration of 80×10^3 cells/ml for Ht-29 cells. Cells had the media changed every two day for keeping them healthy and nutrientized and after they reach their exponential growth and meet the 95-100% (Day 4) the cells were maintained in growth media for a further two days. Cells were washed twice with HBSS in each target day. ALP assay buffer at pH 9.5 was added in the presence of 8 mM MgCl_2 and 50 mM NaCl and 100 mM KCl involving 9.67 mM of pAPP and 0 mM pAPP as a blank for each cell line. Vehicle control of each cell was prepared by adding two drops of Virkon[®] in the complete media for 24 h the night before the assay. Cells were then incubated in the 70 μL of the specified buffers for 10 minutes and then 30 μL of 1M NaOH was added to stop the reaction. Linear sweep voltammetry were applied in triplicate in three separate graphite-SPE against a free-pAPP buffer as blank. The detection was applied at 100 mV/s and potential range from -1.2 V to 1.5 V versus Ag/AgCl reference electrode. Data was collected for statistical analysis.

4.3.8 Statistics analysis

The electrochemical data of ALP activity represents the mean of at least three independent experiments and statistically compared to colorimetric and capillary electrophoresis assays using unpaired t-test ($p > 0.05$).

4.4. Results and Discussion

4.4.1. Stabilization of Graphite Screen-Printed Electrodes

Cyclic voltammetry was applied where 1 M KCl was used as the electrolyte for the standard reaction redox of ferri/ferrocyanide. Non-cleaned electrodes and cleaned electrodes for 10 min and cleaned electrodes for 20 min were compared. Figure 4.3 shows the cyclic voltammogram background of electrodes before and after cleaning using Plasmon cleaner. It is evident that the potential window of the cleaned electrodes (Figure 4.3 B,C) is narrow compared to that of non-cleaned electrodes (Figure 4.3 A). In the insert in Figure 2, the linear relationship observed between the peak current and the square root of the scan rate with a high linear regression R^2 of 0.98 is outlined. The anodic (ipa) and cathodic (ipc) current peaks display a sensitive performance in electrodes cleaned for 20 min compared to the other electrodes. The electrochemical performance of cleaned electrodes for 20 min in plasmon cleaner was more stable than others. The other electrodes displayed shifts in the potential as the scan rate increased. It appears that the faradic current was affected by any background current. Table 4.3 summarizes the influence of the scan rate on the half peak potential (E_{mid} vs. Ag/AgCl) and peak-to-peak separation (ΔE_p) of anodic and cathodic peaks. The anodic and cathodic peak ratio was 0.98–1.03 as the scan rate increased performance in electrodes cleaned for 20 min. This showed the reversible reaction of $[\text{Fe}(\text{CN})_6]^{3-/4-}$.

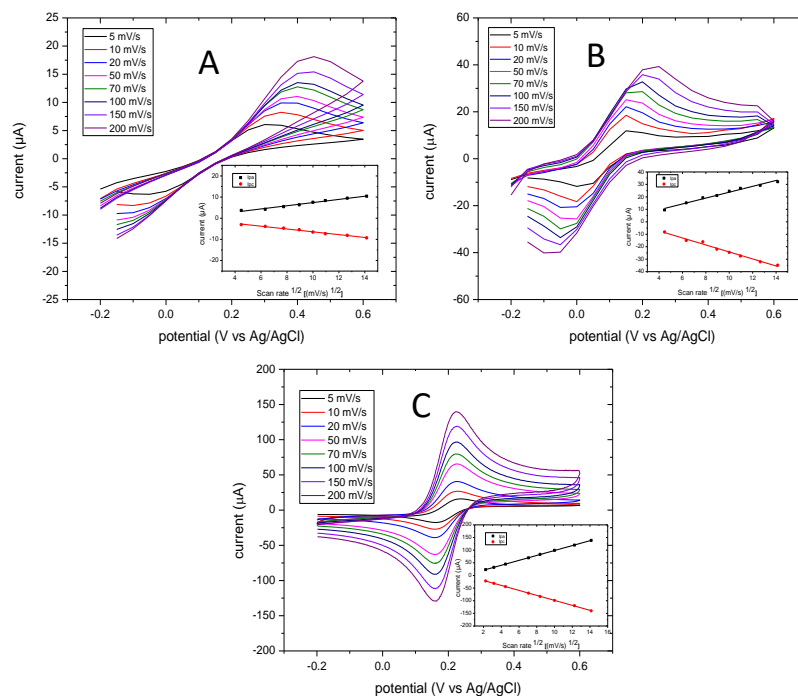


Figure 4.3: Cyclic voltammograms of 1 mM $[\text{Fe}(\text{CN})_6]^{3-/4-}$ on non-cleaned electrodes (A), cleaned electrodes (10 min) (B), and cleaned electrodes (20 min) (C). The inset demonstrates the curves of reduction peaks' current (ipc) and oxidation peaks' current (ipa) versus the square root of the scan rate ($(\text{mV/S})^{1/2}$). The cyclic voltammograms were carried out at an initial potential of -0.2 V and final potential of 0.6 V vs. the Ag/AgCl reference electrode.

Table 4.3: A summary of the influence of the scan rate on the half peak potential (E_{mid} vs. Ag/AgCl) and peak-to-peak separation (ΔE_p) of anodic and cathodic peaks.

Scan Rate	^a E_{mid} vs. Ag/AgCl			^b ΔE_p (mV)		
	0 min	10 min	20 min	0 min	10 min	20 min
5	0.2285	0.0768	0.198	175	146.4	76
10	0.2465	0.08145	0.194	207	143.1	68
20	0.261	0.09155	0.192	230	144.9	68
50	0.2715	0.1163	0.192	247	137.4	64
70	0.277	0.1225	0.191	260	151	62
100	0.282	0.1305	0.191	270	153	62
150	0.294	0.135	0.194	288	162	64
200	0.298	0.1585	0.193	300	163	58

^a Measured from the value of $1/2(E_{pc} + E_{pa})$ versus Ag/AgCl reference electrode. ^b $\Delta E_p = E_{pa} - E_{pc}$.

The potential of the oxidation peak as the scan rate increased for electrodes cleaned for 20 min was 0.19–0.19 V, and that of electrodes cleaned for 10 min was 0.2–0.3 V. Electrodes that had not been cleaned had a potential oxidation peak of 0.3–0.45 V as the scan rate increased. This indicates that the cleaning process can positively enhance electron transfer, and that a 20-min cleaning time is sufficient to overcome the limitations of diffusion processes. Moreover, the value of ΔE_p at 200 mV/s presented by non-cleaned electrodes was too high (300 mV), which indicates that some sort of contamination occurred on the electrode surface. Cleaning the surface electrodes was important as, after 10 min and 20 min, decrements of the value ΔE_p were observed, which were 163 mV and 58 mV, respectively. Considering the theoretical value of ΔE_p is 59 mV for single electron transfer of $[\text{Fe}(\text{CN})_6]^{3-/4-}$, the closest experimental value achieved was 58 mV. Therefore, treatment with oxygen plasma for 20 min was constantly used for further electrochemical investigations.

4.4.2. Optimization of Electrochemical Measurement

For the electrochemical detection of mammalian ALP release, the electroactive compound p-aminophenol (pAP) is produced from the enzyme reacting with a p-aminophenyl phosphate substrate. The linear sweep voltammetry detection technique was applied to read the current generated at different concentrations of the product pAP. Figure 4.4 (A) shows the linear sweep voltammograms of different concentrations of pAP (0.16–5 mM). The measurements were carried out at a scan rate of 100 mV/s and at a range of potentials between –1.2 and 1.5 V. The current response of the pAP increased in potentials at points between 0 and 0.3 V. The insert curve shows the standard curve of the mass-transfer limited current of pAP. Furthermore, the values of intercept and slope of regression lines from these six concentrations were calculated as 5.931 and 11.866. The current response for the oxidation of pAP indicated a good linear relationship, where R^2 was 0.996. pAP (5 mM) generated 180 μA , and the lowest concentration of 0.16 mM generated 20 μA . These results indicate that the voltammetric detection of pAP did not affect the electrode surface during the assay.

The electrochemical determination of ALP release versus time was performed and showed a linear dependence. When time of incubation increased, the ALP release increased. Figure 4.4 (B) shows the linear sweep voltammograms of current increased as incubation time increased, reaching a steady state at 40 min. The linear sweep voltammograms were applied at 100 mV/S and at potentials ranging from -1.2 to 1.5 V vs. Ag/AgCl. In the insert of Figure 4.4 (B), the values of current increased rapidly up to 10 min and then continued slowly up to 40 min. They levelled off at between 40 and 50 min. The oxidation peak started to increase with increasing time after 10 min, so 10 min was taken as the optimum incubation time for subsequent measurements. This corresponds to data already published by Sappia et al. [43]. The linearity relationship had a very good coefficient regression R^2 of 0.998.

The optimal concentration of substrate for the evaluation of enzyme activity using this method was investigated. The current responses of pAPP substrate at different concentrations ranging from 0.1 to 5 mM are shown in Figure 4.4 (C). ALP release was determined from the constant cell number of 250×10^3 cells/mL. The cells were incubated with the substrate concentration for 10 min at 37°C . The current responses reached a plateau at 1.25 mM of pAPP. The current values were fitted using the MichaelisMenten model with a coefficient regression R^2 of 0.88. The corresponding I_{max} and k_m were $136.59 \mu\text{A}$ and 0.548 mM . The corresponding concentration of pAPP at 95% of I_{max} was 9.69 mM . The optimal concentration of pAPP was almost 20 times higher than the k_m [44].

Linear sweep voltammetry was applied for different concentrations of ALP (1.5–1500 U/L) to allow for conversion of the unit and to compare it to the absorbance values. Figure 4.4 (D) shows the Lineweaver–Burk plots of the current responses ($1/\text{current}$) versus ALP concentration ($1/\text{concentration}$) as obtained by linear sweep voltammetry with good linear regression of R^2 of 0.99. The intercept (I_{max}) and the slope (k_m/I_{max}) were 0.0058 and 0.767, and the LOD was 0.043 U/L. LOD was calculated using three times of a standard deviation divided by the slope.

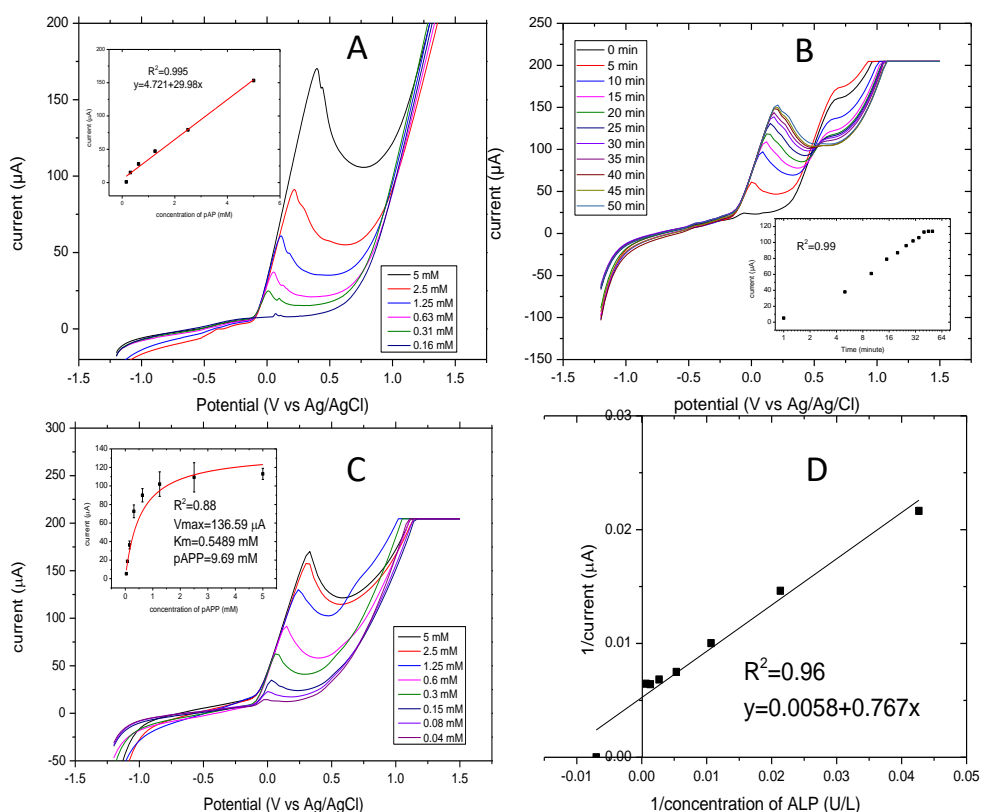


Figure 0.4: Linear sweep voltammograms of electrochemical optimization of ALP release applied at a potential of -1.2 V to -1.5 V, and a scan rate of 100 mV/S. (A) The linear sweep voltammograms of a concentration of pAP of 0.16 – 5 mM and in the insert is the standard curve of the current response. (B) Optimization of the reaction time for the enzymatic assay of ALP release and in the inset is current response versus time. (C) Optimization of pAPP concentrations 0.2 – 5 mM pAPP and in the insert is the current response versus concentrations of pAPP. (D) The calibration curve of ALP activity ranging from 1.5 – 1500 U/L fitted by the Lineweaver-Burk model.

4.4.3. Linearity Performance of ALP Release vs. Cell Number

The linear relationship between ALP release and cell number was analysed. The final concentration of substrate pAPP was about 10–20-fold higher than the K_m . The linear voltammograms of ALP release from different concentrations of cells (4 , 8 , 16 , 31 , 63 , 125 , and 250×10^3 cells/mL) were determined for each cell line. Figure 4.5 illustrates the linear sweep voltammetry that was performed at a scan rate of 100 mV/S and at potentials that ranged from -1.2 V to 1.5 V. The potential of the anodic response shifted as the cell number increased. The results are as follows: ALP release from Balb/c 3T3 cells shows oxidation of pAP beginning at -100 mV and ending at 150 mV. ALP release from A549 cells and MCF-7 cells shows oxidation of pAP beginning at -100 mV and ending at 200 mV. Ht-29 cells had slightly wider potential. We found oxidation of pAP beginning at -100 mV and ending at 300 mV. The oxidation peaks displayed by ALP release of the three cells, Balb/c 3T3, A549 and MCF-7, were narrower than those of Ht-29 cells. This indicated that Ht-29 cells release more enzyme amount than other cells.

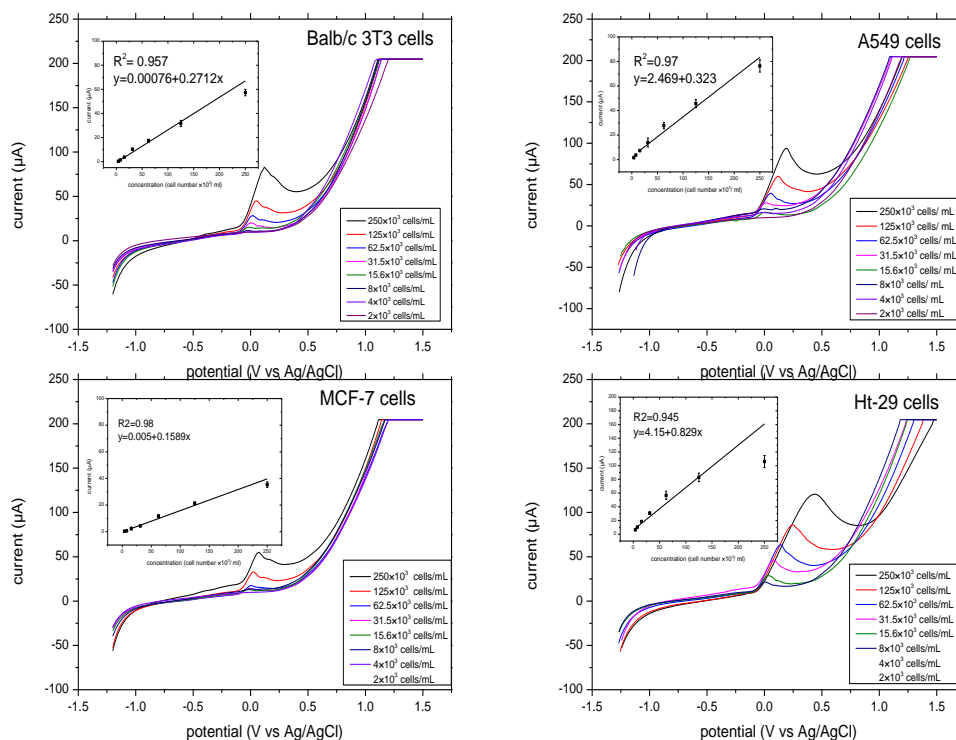


Figure 0.5: Linear sweep voltammograms of ALP release for each cell range from 2–250 $\times 10^3$ cells/mL at a scan rate of 100 mV/S, incubation time of 10 min and potential range from –1.2–1.5 V. In the insert, the linearity performance of the ALP release from the given cells versus the current responses with linear regression analysis is outlined. All the measurements were applied in triplicate in separate graphite-SPE in the presence of 9.7 mM pAPP and at final volume of 70 μ L.

There was good linear correlation between the current response and ALP released from the four cells. The cells of Balb/c 3T3 showed the highest value of ALP released at 75 μ A, while MCF-7 cells had 50 μ A, which was also the lowest value of ALP released among other cells at a concentration of 250 $\times 10^3$ cells/mL. At the lowest concentration of 4 $\times 10^3$ cells/mL, the MCF-7 cells showed a current response of 10 μ A, while that of Balb/c 3T3 cells was 9 μ A. Both showed a good linear response R^2 of 0.95 and 0.98 for Balb/c 3T3 cells and MCF-7 cells. ALP release from A549 cells and Ht-29 cells showed higher values of currents at 80 μ A and at 100 μ A, respectively, and also a good linear response ($R^2 = 0.94$ for A549 cells and 0.94 for Ht29 cells). Moreover, the current response in Ht-29 cells had levelled off from the concentration of 1.25 $\times 10^3$ cells/mL, which indicates that the substrate concentration was running out. Ht-29 cells can release higher amounts of ALP compared to other cells. Therefore, this showed the importance of optimizing substrate concentration for each cell type.

4.4.4. Concentration of the Substrate pAPP from Adhesion Cells

The optimal concentration of pAPP for the evaluation of ALP release from adhesion cells was investigated. The linear sweep voltammograms of the pAP formed by ALP release from Balb/c 3T3 cells, A549 cells, MCF-7 cells, and Ht-29 cells with different concentrations of substrate ranging from 0.2 to 5 mM pAPP are

illustrated in Figure 4.6. The measurements were taken at a scan rate of 100 mV/s, initial potential of -1.2 V and final potential of 1.5 V. pAP formed by enzymatic reaction at 37°C after 10 min was measured. The oxidation peaks of pAP began at 0.0 mV and ended at 150 mV for all cells. The current values were plotted against substrate concentration and fitted by the Michaelis–Menten model (Figure 4.6, insert). The enzymatic reaction of ALP release from Balb/c 3T3, A549, MCF-7, and Ht-29 cells versus different concentrations of the substrate pAPP displayed good non-linear regression, with $R^2 = 0.97$. The K_m values of pAPP from each cell line were as follows: Balb/c 3T3 = 4.75 mM, A549 = 5.03 mM, MCF-7 = 10.19 mM and Ht-29 = 1.85 mM. The I_{max} values were as follows: Balb/c 3T3 = 96.5 μA , A549 = 69.24 μA , MCF-7 = 82.68 μA and Ht-29 = 61.67 μA . The corresponding concentrations of pAPP at 95% of I_{max} were as follows: 47.5 mM for Balb/c 3T3 cells; 50.3 mM for A549; 101.9 mM for MCF-7; and 18.5 mM for Ht-29. The differentiation of the parameters indicates the different activity of ALP in each cell line, where the colon cancer cell lines exhibited the highest activity and the breast cancer cell lines had the lowest activity according to their substrate concentration consumed at half maximal velocity. Quite notably, Balb/c 3T3 cells and MCF-7 cells displayed high standard deviations which effected the related results of I_{max} and K_m . Increasing the number of experiments from $n=3$ to $n=9$ was suggested. In addition, shoulders appeared in the oxidation peaks at potential of 0.5 V indicated that the substrate pNPP had not been fully consumed. Therefore, increasing incubation time from 10 min to 30 min was suggested.

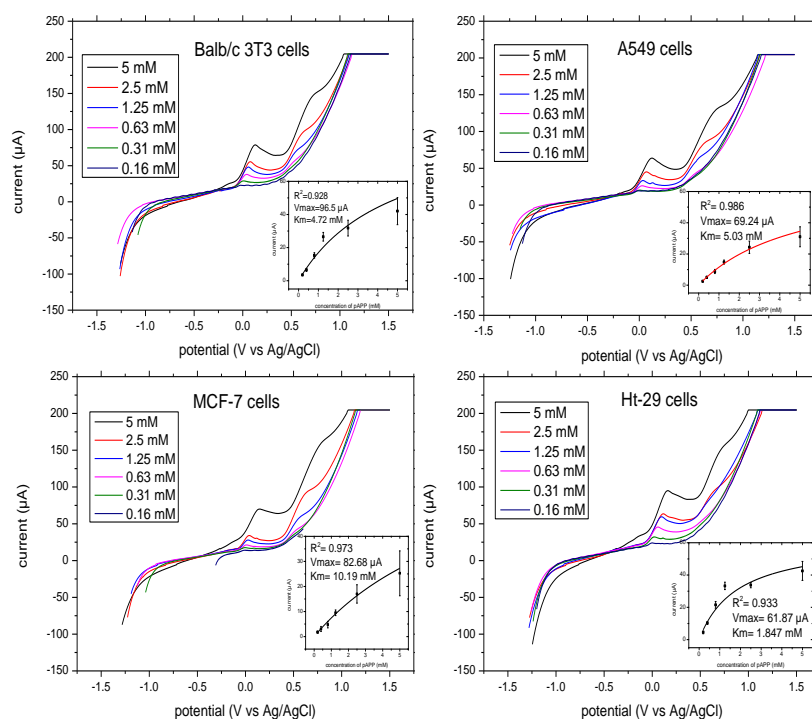


Figure 4.6. Linear sweep voltammograms of ALP release for adhesion cells in the presence of different concentrations of substrate pAPP (2–5 mM) at a scan rate of 100 mV/S, potential range of -1.2 – 1.5 V and incubation time of 10 min. In the insert, the concentration of pAPP substrate versus the current responses with non-linear regression analysis is outlined. All the measurements were applied in triplicate in separate graphite-SPE and at final volume of 70 μL .

4.4.5 Real-time monitoring of ALP release from cells at post-confluence culture

Real-time monitoring of ALP release from Balb/c 3T3 cells, A549 cells, MCF-7 cells, and HT-29 cells was performed. ALP was induced by differentiation using post-confluence culture. Cells were cultured two more days after reaching 95-100 % confluence on day 4, which the cell proliferation decreases. Table 4.4 summarized the results of ALP release in the target days for each cell with the vehicle control (VC), and the blank. It is obvious that the ALP release increases gradually from day 4 to day 6. This raise was shown from all cells. Furthermore, the data of post-confluence culture (day 5 and day 6) was compared to the control (data of day 4) using unpaired t-test. There were a significant difference between the data of ALP release from day 5 and day 6 compared to that released from day 4. Balb/c 3T3 cells had average level of ALP of 14.46 on day 4 and the value increased on day 5 and day 6, which was 21.39 and 28.34. The value of lung cancer A549 exhibited a sharp increment from day 4 to day 6 and that was 27.85, 36.22 and 68.54. The breast cancer cells showed slight incensement from the fourth day to the sixth day, and that was 22.43, 26.88 and 31.36, respectively. The colon cancer; Ht-29 had the highest release value of ALP (45.30) at confluence day compared to others and also for the post-confluence day 5 and day 6; (58.23) and (74.11). Vehicle control of all cells showed less values. Balb/c 3T3 and A549 cells had (5.12) and (6.52) whereas MCF-7 and Ht-29 cells had (3.47) and (8.25), all of which had significant difference compared to control. The buffer blank of all data was very low as no substrate added to the assay.

Table 0.4: Summary of ALP release from each cell line versus target days at post-confluence culture.

	Day 4	Day 5	Day 6	VC	Blank
Balb/c 3T3	(14.46 ± 0.012)	(21.39 ± 0.015) *	(28.34 ± 0.045) *	(5.12 ± 0.009) *	(0.0002) *
A549	(27.85 ± 0.011)	(36.22 ± 0.041) *	(68.54 ± 0.030) *	(6.52 ± 0.003) *	(0.0001) *
MCF-7	(22.43 ± 0.024)	(26.88 ± 0.036) *	(31.36 ± 0.023) *	(3.47 ± 0.001) *	(0.0002) *
Ht-29	(45.30 ± 0.037)	(58.23 ± 0.061) *	(74.11 ± 0.037) *	(8.25 ± 0.015) *	(0.0003) *

After exposing cells to the corresponding optimal substrate concentration of pAPP, LSV detection at 100 mV/s was used and obtained data were expressed as mean ± SD of measurements of three independent experiments with VC (vehicle control) that had dead cells, and the blank with no cells and no substrate. Pvalue of post-confluence culture compared to control (data of day 4), unpaired t-test (* p<0.05 significant is difference).

4.5 Conclusions

Alkaline phosphatase is a cancer biomarker, and the monitoring of ALP release from cells contributes to an understanding of the basis of diseases and the progression of cancer. The aim of this chapter was to develop a methodology for monitoring ALP release from two types of cells: embryo fibroblast cells (Balb/c 3T3) and cancer epithelial cells (A549, MCF-7, Ht-29), using electrochemical analysis. At alkaline pH, the

enzyme ALP hydrolyzes the non-electroactive p-aminophenol phosphate to generate the electroactive, paminophenol. The electrochemical behaviour of the sensors used was investigated using cyclic voltammetry and using the solution $[\text{Fe}(\text{CN})_6]^{3-/4-}$ as the model for single transfer electrons (Fig.4.3).

A cleaning duration of 20 min for the sensors in the Plasmon cleaner gives good electrochemical behaviour (Table 4.3). The anodic and cathodic peak ratio was almost 1 ($i_a/i_c = 1$), and the half peak potential (E_{mid} vs. Ag/AgCl) showed a reversibility reaction. The peak-to-peak separation (ΔE_p) of anodic and cathodic peaks was 62 mV. Electrochemical optimization was conducted by linear sweep voltammetry detection with graphite-SPE at a scan rate of 100 mV/S and at a potential ranging from -1.2 V to 1.5 V vs. a reference electrode of Ag/AgCl (Fig 4.4). This demonstrated the standard curve of pAP, and allowed for observation of the potential where oxidation peaks occur. This was at 0–0.15 V of the current response (0–150 μA) displayed when the concentration of pAP (0.16–5 mM) was increasing. The oxidation peaks of pAP began at -100 mV and ended at 300 mV as the concentration increased. The samples were incubated with substrate for different amounts of time. They displayed a positive linear dependence and 10 min was selected as the time to do the rest of the experiments. The substrate pAPP was optimized using detached cells and had a Michaelis constant (K_m) of 0.55 mM, (I_{max}) of 136.59 and an optimal p-APP concentration of 9.69 mM. A calibration plot was obtained based on the optimization measurements from a range of 1.5–1500 U/L. ALP release was determined from various cell numbers for linearity analysis (Fig 4.5). All cells exhibited linear trends with good regression analysis. The pAPP substrate was investigated during cellular adhesion, and K_m and I_{max} were calculated for each cell line and displayed different kinetic enzyme assay (Fig 4.6). ALP level was determined at post-confluence culture and all cells illustrated an increase of ALP level from day 4 to day 6 (Table 4.4).

The aim of this chapter was achieved by determining the quantity of ALP released from each cells line at (95-100%) confluence and at differentiation (post-confluence culture). These findings were proofed in next chapter using impedance assay.

4.6 References

- [1] Liu, X.-G.; Xing, X.-J.; Li, B.; Guo, Y.-M.; Zhang, Y.-Z.; Yang, Y.; Zhang, L.-F. Fluorescent assay for alkaline phosphatase activity based on graphene oxide integrating with λ exonuclease. *Biosens. Bioelectron.* 2016, 81, 460–464.
- [2] Qu, F.; Pei, H.; Kong, R.; Zhu, S.; Xia, L. Novel turn-on fluorescent detection of alkaline phosphatase based on green synthesized carbon dots and MnO_2 nanosheets. *Talanta* 2017, 165, 136–142.
- [3] Liu, H.; Li, M.; Xia, Y.; Ren, X. A Turn-On Fluorescent Sensor for Selective and Sensitive Detection of Alkaline Phosphatase Activity with Gold Nanoclusters Based on Inner Filter Effect. *ACS Appl Mater Interfaces* 2017, 9, 120–126.
- [4] Sasamoto, H.; Maeda, M.; Tsuji, A. Chemiluminescent assay of alkaline phosphatase using phenacyl phosphate. *Anal Chim Acta.* 1995, 306, 161–166.

- [5] Ximenes, V. F.; Campa, A.; Baader, W. J.; Catalani, L. H. Facile chemiluminescent method for alkaline phosphatase determination. *Anal Chim Acta*. 1999, 402, 99–104.
- [6] Kokado, A.; Arakawa, H.; Maeda, M. Chemiluminescent assay of alkaline phosphatase using dihydroxyacetone phosphate as substrate detected with lucigenin. *Luminescence* 2002, 17, 5–10.
- [7] Zhu, C.; Yang, G.; Li, H.; Du, D.; Lin, Y.; R. W. A. Pacific Northwest National Lab, Electrochemical Sensors and Biosensors Based on Nanomaterials and Nanostructures. *Anal Chem*. 2015, 87, 230–249.
- [8] Thompson, R. Q.; Barone, G. C.; Halsall, H. B.; Heineman, W. R. Comparison of methods for following alkaline-phosphatase catalysis - spectrophotometric versus amperometric detection. *Anal Biochem*. 1991, 192, 90–95.
- [9] Ito, S.; Yamazaki, S.; Kano, K.; Ikeda, T. Highly sensitive electrochemical detection of alkaline phosphatase. *Anal Chim Acta*. 2000, 424, 57–63.
- [10] Wang, J. H.; Wang, K.; Bartling, B.; Liu, C. C. The Detection of Alkaline Phosphatase Using an Electrochemical Biosensor in a Single-Step Approach. *Sensors (Basel)* 2009, 9, 8709–8721.
- [11] RU, S.-P.; WU, J.; YING, Y.-B.; JI, F. Electrochemical Detection of Alkaline Phosphatase Using Ionic Liquid Modified Carbon Nanotubes Electrode. *Chinese J. Anal. Chem*. 2012, 40, 835–840.
- [12] Xia, N.; Ma, F.; Zhao, F.; He, Q.; Du, J.; Li, S.; Chen, J.; Liu, L. Comparing the performances of electrochemical sensors using p-aminophenol redox cycling by different reductants on gold electrodes modified with self-assembled monolayers. *Electrochim. Acta*. 2013, 109, 348–354.
- [13] Zhang, L. F.; Hou, T.; Li, H. Y.; Li, F. A highly sensitive homogeneous electrochemical assay for alkaline phosphatase activity based on single molecular beacon-initiated T7 exonuclease-mediated signal amplification. *Analyst* 2015, 140, 4030–4036.
- [14] Berger, J.; Hauber, J.; Hauber, R.; Geiger, R.; Cullen, B. R. Secreted placental alkaline phosphatase: a powerful new quantitative indicator of gene expression in eukaryotic cells. *Gene*. 1988, 66, 1–10.
- [15] Ho, W. O.; Athey, D.; McNeil, C. J. Amperometric detection of alkaline phosphatase activity at a horseradish peroxidase enzyme electrode based on activated carbon: potential application to electrochemical immunoassay. *Biosens. Bioelectron*. 1995, 10, 683–691.
- [16] Rupicault, S.; Linioges, B.; Dcpwncl, C. Alkaline Phosphatase Assay Using a Redox Procationic Labeled Substrate and a Renewable Nafion-Loaded Carbon Paste Electrode. *Electroanalysis*, 1996, 8.
- [17] Limoges, B.; Degrand, C. Ferrocenylethyl Phosphate: An Improved Substrate for the Detection of Alkaline Phosphatase by Cathodic Stripping Ion-Exchange Voltammetry. Application to the Electrochemical Enzyme Affinity Assay of Avidin. *Anal Chem*. 1996, 68, 4141–4148.

- [18] Bauer, C. G.; Eremenko, A. V.; Ehrentreich-Förster, E.; Bier, F. F.; Makower, A.; Halsall, H. B.; Heineman, W. R.; Scheller, F. W. Zeptomole-Detecting Biosensor for Alkaline Phosphatase in an Electrochemical Immunoassay for 2,4-Dichlorophenoxyacetic acid. *Anal Chem.* 1996, 68, 2453–2458.
- [19] Cullen, B. R.; Malim, M. H. Secreted placental alkaline phosphatase as a eukaryotic reporter gene. *Methods Enzym.* 1992, 216, 362–368.
- [20] Doronin, K. K. Expression of the gene encoding secreted placental alkaline phosphatase (SEAP) by a nondefective adenovirus vector. *Gene* 1993, 126, 247–250.
- [21] Bronstein, I.; Fortin, J. J.; Voyta, J. C.; Juo, R. R.; Edwards, B.; Olesen, C. E.; Lijam, N.; Kricka, L. J. Chemiluminescent reporter gene assays: sensitive detection of the GUS and SEAP gene products. *Biotechniques* 1994, 17, 172-174, 176-177.
- [22] Chang, T.-C.; Wang, J.-K.; Hung, M.-W.; Chiao, C.-H.; Tsai, L.-C.; Chang, G.-G. Regulation of the expression of alkaline phosphatase in a human breastcancer cell line. *Biochem. J.* 1994, 199-205, 303.
- [23] He, J.; Landau, N. R. Use of a novel human immunodeficiency virus type 1 reporter virus expressing human placental alkaline phosphatase to detect an alternative viral receptor. *J Virol.* 1995, 69, 4587–4592.
- [24] Kain, R. S. Use of Secreted Alkaline Phosphatase as a Reporter of Gene Expression in Mammalian Cells. *Methods Mol Biol.* 1997, 63, 49–60.
- [25] Yang, T.-T.; Sinai, P.; Kitts, P. A.; Kain, S. R. Quantification of Gene Expression with a Secreted Alkaline Phosphatase Reporter System. *Biotechniques* 1997, 23, 1110–1114.
- [26] Bettan, M.; Darteil, R.; Scherman, D. Secreted Human Placental Alkaline Phosphatase as a Reporter Gene for *in Vivo* Gene Transfer. *Anal Biochem.* 1999, 271, 187–189.
- [27] Cullen, B. R. Utility of the secreted placental alkaline phosphatase reporter enzyme. *Methods Enzymol.* 2000, 326, 159–164.
- [28] Kelso, E.; McLean, J.; Cardosi, M. F. Electrochemical detection of secreted alkaline phosphatase: Implications to cell based assays. *Electroanalysis* 2000, 12, 490–494.
- [29] Torisawa, Y.-S.; Ohara, N.; Nagamine, K.; Kasai, S.; Yasukawa, T.; Shiku, H.; Matsue, T. Electrochemical monitoring of cellular signal transduction with a secreted alkaline phosphatase reporter system *Anal Chem* 2006, 78, 7625–7631.
- [30] Nashimoto, Y.; Takahashi, Y.; Yamakawa, T.; Torisawa, Y.-S.; Yakusawa, T.; Ito-Sasaki, T.; Yokoo, M.; Abe, H.; Shiku, H.; Kambara, H.; Matsue, T. Measurement of Gene Expression from Single Adherent Cells and Spheroids Collected Using Fast Electrical Lysis. *Anal Chem* 2007, 79, 6823–6830.
- [31] Murata, T.; Yasukawa, T.; Shiku, T.; Matsue, T. Electrochemical single-cell gene-expression assay combining dielectrophoretic manipulation with secreted alkaline phosphatase reporter system. *Biosens. Bioelectron.* 2009, 25, 913–919.

- [32] Inoue, K. Y.; Yasukawa, T.; Shiku, H.; Matsue, T. Cell-Based Electrochemical Assay for Endotoxin Using a Secreted Alkaline Phosphatase Reporter System. *Electrochem. J-Stage* 2008, 76, 525–528.
- [33] Inoue, K. Y.; Yasukawa, T.; Shiku, H.; Matsue, T. Cell-Based Electrochemical Assay for Endotoxin Using a Secreted Alkaline Phosphatase Reporter System. *Electrochem. J-Stage* 2008, 76, 525–528.
- [34] Shiku, H.; Suzuki, J.; Murata, T.; Ino, K.; Matsue, T. Chronoamperometric characterization of secreted alkaline phosphatase from single-cell entrapped in a poly(dimethylsiloxane) microwell. *Electrochim. Acta* 2010, 55, 8263–8267.
- [35] Şen, M.; Ino, K.; Shiku, H.; Matsue, T. A new electrochemical assay method for gene expression using hela cells with a secreted alkaline phosphatase (SEAP) reporter system. *Biotechnol. Bioeng.* 2012, 109, 2163–2167.
- [36] Sen, M.; Ino, K.; Inoue, K. Y.; Arai, T.; Nishijo, T.; Suda, A.; Kunikata, R.; Shiku, H.; Matsue, T. LSI-based amperometric sensor for real-time monitoring of embryoid bodie., *Biosens. Bioelectron.* 2013, 48, 12–18.
- [37] Yildirim-Semerçi, C.; Benayahu, D.; Adamovski, M.; Wollenberger, U. An Electrochemical Assay for Monitoring Differentiation of the Osteoblastic Cell Line (MBA-15) on the Sensor Chip. *Electroanalysis* 2015, 27, 1350–1358.
- [38] Ragones, H.; Schreiber, D.; Inberg, A.; Berkh, O.; Kósa, G; Freeman, A.; Shacham-Diamand, Y. Disposable electrochemical sensor prepared using 3D printing for cell and tissue diagnostics. *Sensors Actuators. B Chem.* 2015, 216, 434–442.
- [39] Ikehara, Y.; Mansho, K.; Takahashi, K.; Kato, K. Purification and characterization of alkaline phosphatase from plasma membranes of rat ascites hepatoma. *J. Biochem.* 1978, 83, 1471–1483.
- [40] Sone, M.; Kishigami, S.; Yoshihisa, T.; Ito, K. Roles of Disulfide Bonds in Bacterial Alkaline Phosphatase. *J. Biol. Chem.* 1997, 272, 6174–6178.
- [41] Satou, Y.; Al-Shawafi, H. A.; Sultana, S.; Makita, S.; Sohda, M.; Oda, K. Disulfide bonds are critical for tissue-nonspecific alkaline phosphatase function revealed by analysis of mutant proteins bearing a C201-Y or C489-S substitution associated with severe hypophosphatasia. *BBA - Mol. Basis Dis.* 2012, 1822, 581–588.
- [42] Vernick, S.; Freeman, A.; Rishpon, J.; Niv, Y.; Vilkin, A.; Shacham-Diamand, Y. Electrochemical Biosensing for Direct Biopsy Slices Screening for Colorectal Cancer Detection. *J. Electrochem. Soc.* 2011, 158, P1–P4.
- [43] Porat-Ophir, C.; Dergachev, V.; Belkin, A.; Vernick, S.; Freynd, G.; Katsnelson, M.; Chetvernykh, V.; Rishpon, J.; Shacham-Diamand, Y. Chip level agitation effects on the electrochemical sensing of alkaline-phosphatase expressed from integrated liver tissue. *Sensors Actuators B. Chem.* 2015, 213, 465–473.
- [44] Benham, F. J.; Fogh, J.; Harris, H. Alkaline phosphatase expression in human cell lines derived from various malignancies. *Int J Cancer* 1981, 27, 637–644.

[45] Moore, E. J.; Pravda, M.; Kreuzer, M. P.; Guilbault, G. G. Comparative Study of 4-Aminophenyl Phosphate and Ascorbic Acid 2-Phosphate, as Substrates for Alkaline Phosphatase Based Amperometric Immunosensor. *Anal. Lett.* 2003, 36, 303–315.

[46] Rosen, I.; Rishpon, J. Alkaline phosphatase as a label for a heterogeneous immunoelectrochemical sensor: An electrochemical study. *J. Electroanal. Chem.* 1989, 258, 21–39.

[47] Pemberton, R. M.; Hart, J. P.; Stoddard, P.; Foulkes, J. A. A comparison of 1-naphthyl phosphate and 4 aminophenyl phosphate as enzyme substrates for use with a screen-printed amperometric immunosensor for progesterone in cows' milk. *Biosens. Bioelectron.* 1999, 14, 495–503.

Chapter 5

Capillary Electrophoresis: Comparative Studies for Alkaline Phosphatase (ALP)

Note: This chapter has been published in Journal of Biosensor. Please refer to Appendix.

5.1 Aim and objectives

The aim of the work detailed in this chapter was to introduce a comparative study of alkaline phosphatase release from living cells using p-nitrophenyl phosphate (pNPP) as substrate. Capillary electrophoresis analysis was carried out on samples of two types of cells: embryo fibroblast cells (Balb/c 3T3); and cancer epithelial cells (A549, MCF-7, Ht-29). The findings from this study will be compared with the absorbance data outlined in Chapter 3. ALP activity for spectrophotometric analysis (Chapter 3) and for electrochemical analysis (Chapter 4) will be examined in order to compare sensitivity.

The novelty of this aim was that the ALP release from the optimal density (inhibitive growth point) of the given cells were determined by capillary electrophoresis

The following objectives detail the aims of this chapter:

1. To obtain the standard curve of p -nitrophenol (pNP) and unknown concentrations of ALP release from given cells using capillary electrophoresis experiments. This will be used to compare the data with absorbance analysis.
2. To illustrate a comparative analysis of ALP activity obtained from spectrophotometric analysis (Chapter 3) and from electrochemical analysis (Chapter 4).

5.2 Introduction

5.2.1 Principle

Alkaline phosphatase is responsible for the dephosphorylating process in the cells. As described earlier in Chapter 1 (section 1.3), ALP has four main isoenzymes: germ cell alkaline phosphatase (GCAP); intestinal alkaline phosphatase (IAP); placental alkaline phosphatase (PLAP); and tissue-nonspecific alkaline phosphatase (TNAP), all of which have their own physiological role. For example, TNAP is expressed mostly in the liver, the kidney, and bones. The functional role of bone isoenzyme is seen in bone mineralization, while the function of liver and kidney isoenzymes remains unknown[1], [2]. The functional roles of the other isoenzymes- GCAP, IAP, and PLAP, are still not known (this is described in Chapter 1 in figure 1.2) [3]. Therefore, it is important to facilitate isoenzyme analysis. As described in Chapter 1 (section 1.3), the conventional methods used for the separation and analysis of ALP isoenzymes are electrophoresis techniques, including affinity electrophoresis with wheatgerm lectin [4], [5] and isoelectric focusing in immobilized pH gradients [6], [7]. These methods require large samples and tedious sample manipulations. Enzyme-linked immunosorbent assay (ELISA) has also been used for isoenzyme analysis [8]. It is well-known that ELISA has limitations – it is a labor-intensive and expensive tool, and many sophisticated steps have to be carried out in order to obtain a specific antibody.

Capillary electrophoresis (CE), on the other hand, has advantages over traditional assays. CE is faster and more capable when used with small samples. Moreover, it allow quantitative and qualitative analysis of isoenzymes. CE can be miniaturized [9] and integrated in different systems [10] [11]. CE can be defined as

a capillary positioned between two reservoirs, allowing electrophoretic mobility to occur during applying of an electric field.

The capillary is usually made with glass. The glass is limited by high temperature and relatively low flexibility and robustness, all of which are improved by using fused silica. The silica's outer surface is sometimes coated by polymer. The thinner fused silica capillary allows small volumes of samples. This enhances the ratio of surface-to-volume. The small size of the capillary tube also reduces the heat and voltage, which reduces the denaturing of protein during separation. Figure 5.1 illustrates a schematic of the principle of detection pNP in CE. (pNP) is the product of the enzyme reaction of alkaline phosphatase and the substrate (pNPP). (pNP) has chromophores that make it sensitive for spectrometric detection. pNP has two functional groups; one is the OH and the other is NO₂. These occupy opposite ends of the benzene ring. The absorption spectra occur in 405 nm for this compound. Fused silica is negatively charged [12] and the alkaline buffer in the two reservoirs has negative charge. This means that, combined, they are electrostatic repulsive forces. [13]. The enzyme ALP is considered a protein, and the electrostatic repulsive forces that occur between the buffer and the wall prevent the attachment of protein in the wall. In this chapter the detection of ALP will be through the product formed as a result of the hydrolysis of pNPP to pNP. Inside the capillary, the product pNP is detected by absorbance when the separation occurs at a particular rate of migration. The linear equation that results from the peaks area and the different concentration of pNP, is used to determine ALP release from living cells. The objectives of this chapter is to illustrate the findings of the separation and compare it with the spectrophotometric analysis outlined in Chapter 3.

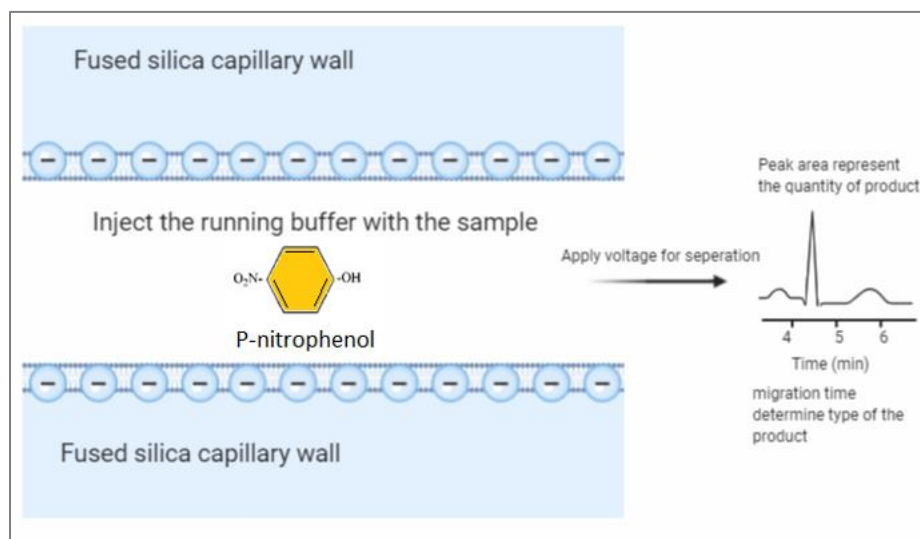


Figure 0.1: Schematic of Capillary Electrophoresis Principle [15].

5.2.2 Background

The basic concept of electrophoresis dates back to approximately 1931. Electrophoresis principle was defined as a separation of solutes based on different rates of migration when applying an electric field and in the presence of an electrolyte (running buffer). Arne Tiselius (1937) developed the technique and

used filter papers and gels as supporting media [16]. His work allowed for the establishment of gel electrophoresis methodologies. It was not until 1960 that electrophoresis became a known technique to separate biological molecules with respect to their physical and chemical differences. Alkaline phosphatase was also one of those biological molecules separated by electrophoresis methods. In 1965, Beckman, Nilson and Baker performed starch gel electrophoresis on the enzyme ALP [17]. They determined different bands, indicating three different isoenzymes in the samples. Two years later, Yong investigated different inhibitors in order to define the isoenzymes using agar gel electrophoresis. In 1971, Savage et al. used polyacrylamide gel electrophoresis to study the migration rate of ALP, revealing 5 different isoenzymes [18]. Previous experiments were applied with different type of gels with the purpose of identifying the sample that had the most ALP isoenzymes. Electrophoresis was improved to allow an efficient separation.

One of the methods developed was capillary electrophoresis. Capillary electrophoresis has come a long way in its relatively short history [19], [20]. Lukacs and his professor, Professor Jorgenson, published a paper in 1983 that illustrated the possibility of using capillaries to overcome the limitations of gel electrophoresis. They noticed that the complex system of capillary zone electrophoresis made by Hjerten and Catsimpoolas could be improved to reduce the interferences between bands [21], [22]. Their experiments paved the way of other researcher since then. Capillary electrophoresis is a complementary method to modern separation instruments that can be improved to allow microdevices of separation. The technique generates band-broadening in peaks better than modern separating methods, but it is less efficient than modern separation methods in terms of limit of detection and reproducibility. Therefore, more investigations are being undertaken in order to improve the efficient analytical separation of capillary electrophoresis.

5.2.3 Literature review

There is increasing interest in research that focuses on enzymatic reactions in fused capillary electrophoresis. Many detectors can be integrated to capillary electrophoresis including UV-Vis, fluorescence and electrochemical detector. The substrate for ALP analysis is related to the used detector. Researchers have long assumed that UV-Vis absorbance detector is the most suitable for detecting ALP activity. For instance, Xu et al (1998) evaluated the enzymatic reaction of ALP with pNPP [23]. Their assays illustrated Michaelis constant of 4.8 mM for the substrate pNPP, and LOD of 4.4×10^{-5} IU for the commercial ALP. Enzyme detection needs complex conditions inside the capillary. Many of them might simply be optimized, including concentration, temperature, pH and component of buffer. Within the framework of these criteria, Iqbal (2011) characterized ALP activities by using a running buffer of sodium phosphate at pH 8.5 in the presence of the substrate pNPP, which was detected at 322 nm [25]. Iqbal modified the capillary with polycationic polybrene in order to control protein adsorption [26]. The modification with polycationic polybrene demanded optimization of pH [27]. Grodner et al. (2017) evaluated the inhibitory effect of a propylamine group for ALP activities [28]. The running buffer was sodium dihydrogen phosphate with a pH of 2.5, and the substrate pNPP was detected at 200 nm. This optimization resulted in a Michaelis' constant of 1.5 mM, which is far better than Xu et al's findings. However, the shortcoming of the work of Grodner et al. was the use of very low pH - many experts contend

that the use of high pH is better for ALP separation. Gattu et al. (2018) identified a sequence enzyme assay of ALP using capillary electrophoresis coupled to mass spectrometry [29]. ALP was immobilized in the capillary to provide efficient separation for peptides. What this new research does, then, is comprehensively studies enzyme assay parameters neglected by many earlier researchers, that concentration of substrate, pH puffer, and incubation time of sample inside the capillary was considered. Although the optimization done by Gattu et al optimization allowed Michael constant of 1.100 mM , their findings were limited to peptide determination. Recent studies like these shed light on another parameter, migration time, which previous studies had not addressed. Takayanagi et al. (2020) discussed ALP activities with pNPP [30] and argued that there was a relationship between migration time and rate of reaction. They also considered the inhibition analysis of ALP, which was determined by the low signal.

Another way to detect ALP is to apply a laser-induced fluorescence detector [31]. Most of the literature used laser-induced fluorescence detector, reported the approach of affinity binding [32]–[37]. ALP enzyme reaction using a fluorogenic substrate was monitored using fluorescence detector. Many troubleshoots were argued, for example, adhesion of ALP in the capillary, activation of ALP, using different metal chelators for inhibition and applying a range of labels (e.g. glycosphingolipids) at different buffers. Integrating the detector of laser-induced fluorescence with capillary electrophoresis provides great sensitivity for enzyme and protein analysis. The major limitation of laser-induced fluorescence detection is that most fluorogenic dyes are limited to functional groups presented compound and are not highly efficient with others. For example, Fluorescein isothiocyanate is less reactive at low concentrations of amines group, whereas rhodamine dye is more efficient with the succinidyl ester group. One more limitation of fluorescence detector is the lack of standardizing assay. This make researchers use nanomaterials, such as nanoparticles. Quantum dots [38] and magnetic nanoparticles [39] have been reported for ALP enzyme assay. The size of nanoparticles can provide unique physical properties, which enhance the immunoaffinity inside the capillary.

Fluorescent-based assays are always expensive, which has led to a focus on electrochemical detectors, for example, conductivity detectors could be integrated to capillary electrophoresis. These two systems can be minimized to develop microdevices [40], [41]. The substrate used to investigate ALP by is disodium phenol phosphate, which converts to phenol [42], [43]. Sun et al (2004), argued that the use of a substrate of disodium phenyl phosphate that converted to phenol would achieve a lower LOD of $3.5 \times 10^{-21} \text{ mol/L}$ [24]. Ultimately, when it came to the nature of enzyme reaction, their aim was to study ALP from cell lysis. They separated ALP isoenzymes in mouse bone marrow cell lines using bicarbonate buffer for lysis solution. There has been some disagreement concerning the use of disodium phenyl phosphate due to indirect detection of the quantity of phenol formed. This require integration of amperometry to quantify the amount of phenol formed in each zone. Another chemistry group, Sun et al. (2006) used the technique to measure ion-transfer currents. This protocol was an extension of work carried out by Bard et al. (1995), who investigated the current generated by redox reaction [44], [45]. Studies that rely on contactless conductivity cannot be considered as conclusive, because the process involving the integration of the two systems is still being developed [46], [47]. Conductivity detector integration is very suitable for molecules that has no redox group or display weak redox reaction, but remains briefly addressed in the literature in

terms of effects of pH [48] and conductivity [49]. Therefore, many sophistication and modification strategies are required to improve the interfaces of electrolyte and electrode surfaces.

5.2.4 The Problem statement

As identified in the literature, integration system of detectors with capillary electrophoresis is preferable for the identification of ALP isoenzyme assay. UV-vis is the simplest detector for the purposes of optimization measurement, and has been gaining importance in recent years. The substrate of pNPP was chiefly reported and therefore was used in this chapter. The optical substrate pNPP was used, as it is selfindicating and facilitates linear performance.

Previous research has documented the chief conditions for optimizing enzyme reactions in capillary electrophoresis methodology. The most important variables in studies included: the running buffer and its pH; ionic strength; temperature of the capillary; and the relationship between incubation time and quantity of the product. The methodology of using two different buffer pHs (7.4 and 2.5) was reviewed for discontinuous enzyme assay. This is very important for real-time monitoring of enzyme release in cell culture [50], [51]. The findings conducted by Ying et al. (2012) and Řemínek et al. (2015) of using two pH gradients were not related to ALP enzyme assay. In the case of ALP determination, the two pH gradients would be (7.4 and 9.5) – this has not been addressed in the literature. Another variable, which was the performing dynamic assay performed by Takayanagi et al (2020) for ALP analysis. The dynamic assay and its relationship with time was investigated for optimization of the continuous enzyme assay. These studies have helped to improve the set-up conditions of ALP assay. However, each assay has its own calibration issues. These include: limitations of the device, running buffer, applied voltage, component, and the type of the assay (continuous or discontinuous). The investigation of ALP revealed the relationship between the quantity of product formed and incubation time in serum and commercial sample. None of previous literatures used ALP release from living cells for UV-vis detector.

A very rare study has studied ALP release from cells. Sun et al. (2004) investigated ALP isoenzyme release from a Balb/c 3T3 cell line [24]. They inserted a cell inside the capillary followed by cell lysis dissolved in bicarbonate buffer, and they used cell lysis without cells as a blank. Nevertheless, use of a bicarbonate buffer that has pKa of 6.1 might limit the assay, because its pka is very different from the optimal pH of ALP. DEA is purposed in this study as it enhances the symmetric peaks. They also used the substrate of disodium phenyl phosphate, which has a wavelength of 288 nm. This substrate displayed very low sensitivity in absorbance detection of about 10%, compared to pNPP, which has 100% sensitivity [52]. Therefore, Sun's group used another detection method, ampeopmetry, to determine the amount of phenol formed. This increased the steps in the experiment.

Capillary electrophoresis is a separation method, and many sequences have to be done in experiments in order to allow validation assay for isoenzyme of ALP release from cancer cells. Cell lysis mixture or media is a complex environment for enzyme release from cells. Optimization of these components is very important for isoenzyme identification and selective inhibition assays. The samples in CE can be also diluted to approximately 100X due its sensitivity. In the assay carried out for this chapter, the NaCl and MgCl₂ were diluted (10X), because the ionic strength of the buffer could have reduced the electrostatic

effects [14]. The standards and samples were injected, and a voltage of 15 kV was applied for the separation.

5.2.5 Summary

In this chapter the capillary electrophoresis technique was used to analyse ALP release from living cells. UV-vis absorbance detector mode was used. The enzymatic reactions that occurred in the tubes were stopped before capillary electrophoresis analysis was performed. A standard curve of p -nitrophenol (pNP) and of unknown concentrations of ALP release from cells was carried out in CE. A linearity equation of the standard curve was determined between peak areas and concentration of pNP. This simplified comparison with the absorbance analysis detailed in Chapter 3. In addition, data obtained from Chapter 3 and Chapter 4 were compared to illustrate the sensitivity improvement in the developed method.

5.3 Methodology

5.3.1 Reagents and instruments

4-nitrophenol (p-NP) was purchased from (Sigma, Ireland) and used to make a stock solution at a final concentration of 500 μ M. The alkaline buffer assay of pH 9.5 was made by adding sterile deionized water at grade 18 M Ω provided from (Tyndall National Institute, UCC) and containing diethanolamine (DEA) 1 M, magnesium chloride (MgCl₂) 8 mM, sodium chloride (NaCl) 50 mM, para-nitrophenol phosphate (pNPP) and HCL purchased from (Sigma, Ireland). The capillary electrophoresis measurements were performed using 50 μ m i.d. and 375 μ m o.d. fused-silica capillary (CM Scientific Ltd., Silsden, UK). Agilent 7100 Capillary Electrophoresis System (Waldbronn, Germany) the software Agilent Chemstation (Version B.02.01) were also used.

5.3.2 ALP release and cell culture

The target density for this thesis was identified as being when cells proliferated for at least four days and then reached contact-inhibited growth. This was where the target analyte started to express. This was investigated to make the cells simultaneously reach contact-inhibited growth (Chapter 2 section 2.3.7). Accordingly, the findings of the experiments (Chapter 2 section 2.4.4) were used for all experiments in this chapter. The cells used during this study were Balb/c 3T3 cells, A549 cells, MCF-7 cells and Ht-29 cells. The initial concentration of each cell line and the corresponding media and supplements are shown in Table 5.1.

Table 0.1: A summary of the cell number and the composition of media used in this study.

Cell line	Concentration ($\times 10^3$ cells/mL)	Media	Supplements
Balb/c 3t3	40	DMEM	10% NBCS
A549	40	DMEM	10% FBS
MCF-7	40	MEME	10% FBS
Ht-29	80	McCoy's 5A	10% FBS

In order to standardise the assay, the steps outlined in Figure 5.2 were followed - cells were washed twice with HBSS and trypsinized at 37 °C for 2 minutes. Trypsin was naturalized by media and then centrifuged at 1000 rpm for 5 minutes. To get rid of red phenol, cells were washed again with HBSS and centrifuged at 1000 rpm for 5 minutes. To ensure the stable condition of cell numbers, the 4-day-old cells were normalized at a concentration of (250×10^3 cell/ ml). Supernatant was discarded, and cell pellets were resuspended in the assay buffer. All the previous steps were done in an ice bath. The vials simultaneously incubated at 37 °C for 30 minutes, or 10 minutes for absorbance or electrochemical analysis. 30 μ l of 1M NaOH was added to stop the reaction. The supernatant then centrifuged for 5 minutes to discard cells and determine the solubilized ALP.

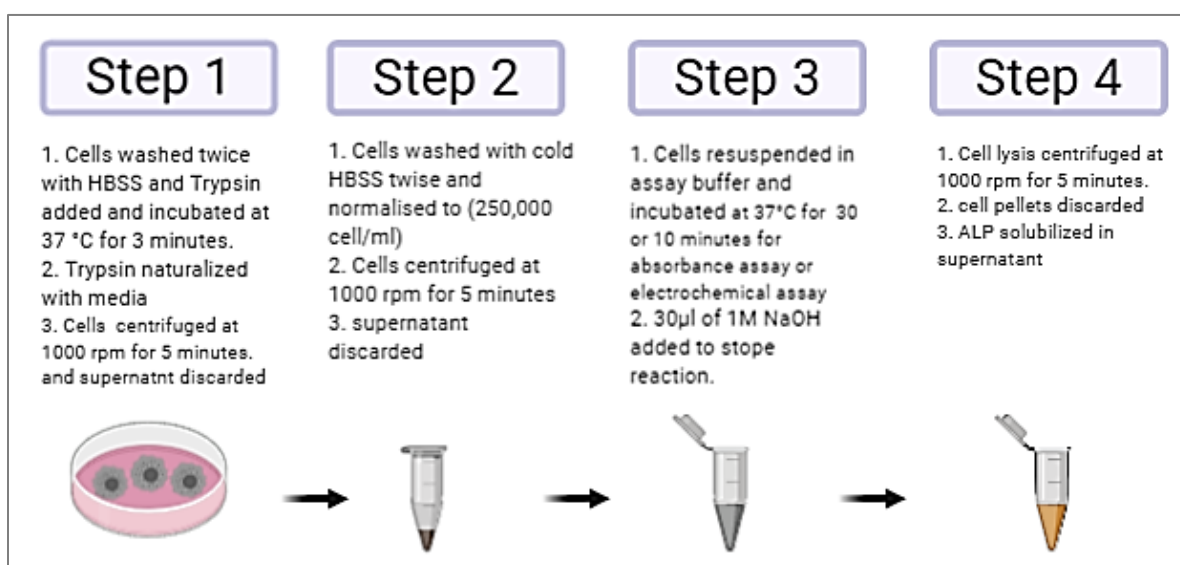


Figure 0.2: A schematic diagram of ALP release from non-adhesion cells.

For preparing unknown samples, the steps in Figure 5.3 were used. The cells were sub-cultured three times before seeding began under aseptic conditions using the same protocol as that in Chapter 2, Section (2.3.3). The following steps were performed according to the protocol illustrated in chapter 2 (2.3.8) in order to release ALP from cells. The first step was to enhance ALP release of 4-day-old cultures by seeding cells as a monolayer at 48-well plates, incubating at 37 °C and 5% CO₂ and changing media every two days. Before the addition of the assay buffer, cells were washed twice with cold HBSS. Cells were then incubated for 10 minutes or 30 minutes with the assay buffer for electrochemical or absorbance analysis.

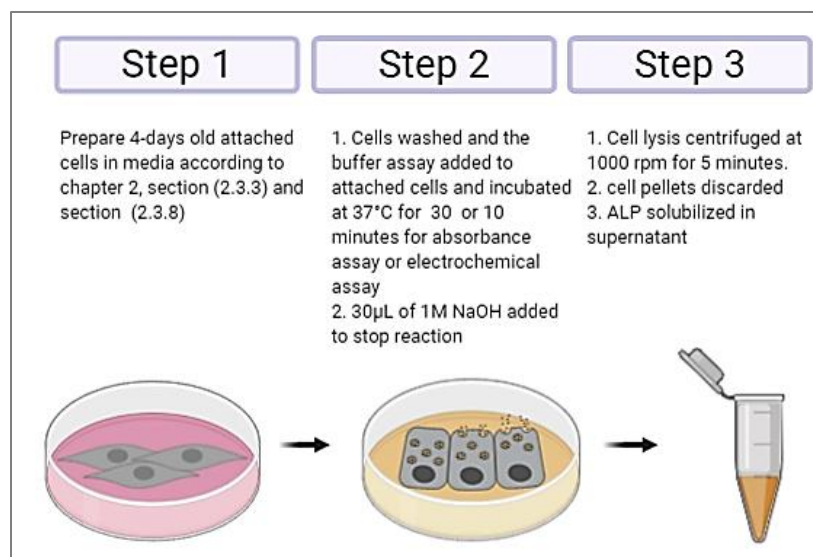


Figure 0.3: A schematic diagram of ALP release from attached cells. Cells were washed with Hank's balanced salt solution (HBSS) before being exposed to the buffer assay.

5.3.3 Capillary electrophoresis experiment (standard curve)

Capillary electrophoresis was applied due to its selective monitoring of p-nitrophenol, and because it eliminates any interference with endogenous ALP in the sample [29]. 70 μ L of the product pNP range at (15-500 μ M) was prepared in DEA buffer. Each concentration of pNP was prepared in the presence of 30 μ L of sample mixed with of 6 mM of pNPP. 30 μ L of 1M NaOH was added as it was normally present in the reaction solution. For the unknown samples, 100 μ L of sample mixed with 6 mM of pNPP were incubated for 30 minutes (Figure 5.2). 30 μ L of 1M NaOH was added to stop the reaction. Capillary electrophoresis was carried out. The separation of standards and samples was performed in a 50 μ m inner diameter fusedsilica capillary with a length of 15 cm. The running conditions included: a voltage of 15 kV; a capillary temperature of 20 °C; and a wavelength of 405 nm. Injection of the sample was for 5 seconds and 15 mbar. The data were collected and processed using the capillary electrophoresis system and Agilent ChemStation software. A graph relating peak area of absorbance to concentration of pNP was prepared for regression analysis. The slope and intercept of the reaction were used for normalizing the data of samples in molarity.

5.3.4 Absorbance experiment (standard curve)

Data recorded in Chapter 3 (Figure 3.5 A) were compared to the data found in this chapter using the standard curve of pNP according to procedures shown in (Chapter 3, Section 3.3.6.1). Briefly, 70 μ L of the product pNP range at (15-500 μ M) were prepared in DEA buffer. Each concentration of pNP was prepared in the presence of 30 μ L of sample mixed with of 6 mM of pNPP. 30 μ L of 1 M NaOH was added as it was normally present in the reaction solution. For the unknown samples, 100 μ L of sample mixed with 6 mM of pNPP were incubated for 30 minutes (Figure 5.2). 30 μ L of 1 M NaOH was added to stop the reaction. The optical density of each point was read in a platereader against a free-pNP buffer as blank at 405 nm. A graph relating absorbance to concentration of pNP was prepared for regression analysis.

5.3.5 Absorbance experiment (calibration curve)

A calibration plot of absorbance assay of ALP activity was obtained, as seen in Figure (3.5 D). Lineweaver-Burk model was plotted between the absorbance and ALP concentrations to obtain the linear equation and normalise the data. Briefly, ALP release was performed using 70 μL of a sample spiked with various concentrations of ALP (calf intestinal phosphatase) at a range of 1500-1 U/L dissolved in 30 μL of pNPP 6 mM in buffer DEA and incubated for 30 minutes. 30 μL of 1M NaOH was added to stop the reaction. For the unknown samples, 100 μL of sample mixed with 6 mM of pNPP were incubated for 30 minutes (Figure 5.2). 30 μL of 1M NaOH was added to stop the reaction. The optical density of each point was read in a platereader against a free-pNPP buffer as blank at 405 nm. A graph relating absorbance to concentration of ALP was prepared for regression analysis.

5.3.6 Electrochemical experiment (calibration curve)

A calibration plot of electrochemical assay of ALP activity was obtained and is outlined in Figure 4.4 (D). Lineweaver-Burk model was plotted between the current density and ALP concentrations to obtain the linear equation and normalise the data. Briefly, ALP release was performed using 70 μL of a sample spiked with various concentrations of ALP (calf intestinal phosphatase) at a range of 1500-1 U/L dissolved in 30 μL of pAPP 9.69 mM in buffer DEA and incubated for 10 minutes. 30 μL of 1M NaOH was added to stop the reaction. For the unknown samples, 100 μL of sample mixed with 9.7 mM of pAPP were incubated for 30 minutes (Figure 5.2). 30 μL of 1 M NaOH were added to stop the reaction. The optical density of each point was read in a platereader against a free-pNPP buffer as blank at 405 nm. A graph relating absorbance to concentration of ALP was prepared for regression analysis. Linear sweep voltammetry was applied on graphite screen-printed electrodes, which were cleaned for 20 minutes by plasma cleaner. The linear sweep voltammetry measurements were carried out at potentials ranging from -1.2 V to 1.5 V vs Ag/AgCl and at a scan rate of 100 mV/s.

5.4 Results and discussion

5.4.1 Comparison between capillary electrophoresis and colorimetric analysis for ALP release from living cells

Capillary electrophoresis and absorbance analyses were conducted. The analyses were carried out in the presence of 70 μL of the product pNP in the range of (15-500 μM) and 30 μL of sample mixed with 6 mM of pNPP. Figure 5.4 (A) shows electropherograms of different concentrations of p-nitrophenol in the presence of 1 mM DEA adjusted to pH = 9.5, temperature 20 °C, voltage of 15 kV and wavelength of 405 nm. pNP measurements were taken in a fused-silica capillary with an effective length of 15 cm and a diameter of 50 μm . The peaks of pNP displayed at migration time of 5 minutes. This also was confirmed by other studies [28], [30], [34]. The separation peaks were affected by the length of incubation time and by other studies [28], [30], [34]. The separation peaks were affected by the length of incubation time and by applied voltage [34]. CE is an ideal assay for further investigation of ALP isoenzymes, as it performs sensitive detection in alkaline buffer. This is an appropriate environment for ALP. The insert (Figure 5.4 A) details the calibration plot of pNP concentrations versus the peak areas, which displayed very good linear

regression of $R^2 = 0.99$, slope of $70.13 \text{ mAU}/\mu\text{M}$ and intercept of 9.68 mAU . This was used for normalizing the peaks' areas of ALP release from living cells (Figure 6 B) with values obtained by colorimetric analysis. Figure 5.4 (B) displays the peak areas of pNP formed due to releasing ALP from cells. Ht-29 cells had the highest peak area of 23.75 mAU , whereas Balb/c 3T3 had the lowest peak area of 2.3 mAU . It was quite noticeable that ALP released from A549 cells was slightly higher than ALP released from MCF-7 cells, which was seen in the peak areas 6.05 mAU and 5.2 mAU , respectively. Figure 5.4 (C) shows the linearity studies of colorimetric assay carried out in the presence of different concentrations of pNP ($15\text{--}500 \mu\text{M}$). The regression analysis was 0.99 , and the slope and intercept of the curves were found to be 5.53 and 0.34 . These were used for normalizing data (Chapter 3) and comparing them with the capillary electrophoresis assay (data from Chapter 5). Figure 5.4 (D) shows the normalizing data of ALP release from cells represented by formation of the product pNP. Capillary electrophoresis and colorimetric assay displayed a good correlation. No significant difference ($p > 0.05$) resulted from the two methods. It is obvious that the lowest ALP level was determined by Balb/c 3T3 cells, which was ($0.16\text{--}0.17 \text{ mM}$), whereas the highest level of ALP was of colon cancer cells and was in the range of ($0.48\text{--}0.50 \text{ mM}$). Lung and breast cancer cells had almost the same levels of ALP, ($0.21\text{--}0.22 \text{ mM}$) and ($0.20\text{--}0.21 \text{ mM}$). Moreover, the ALP of lung cancer was slightly higher than breast cancer, and results showed very small standard deviation.

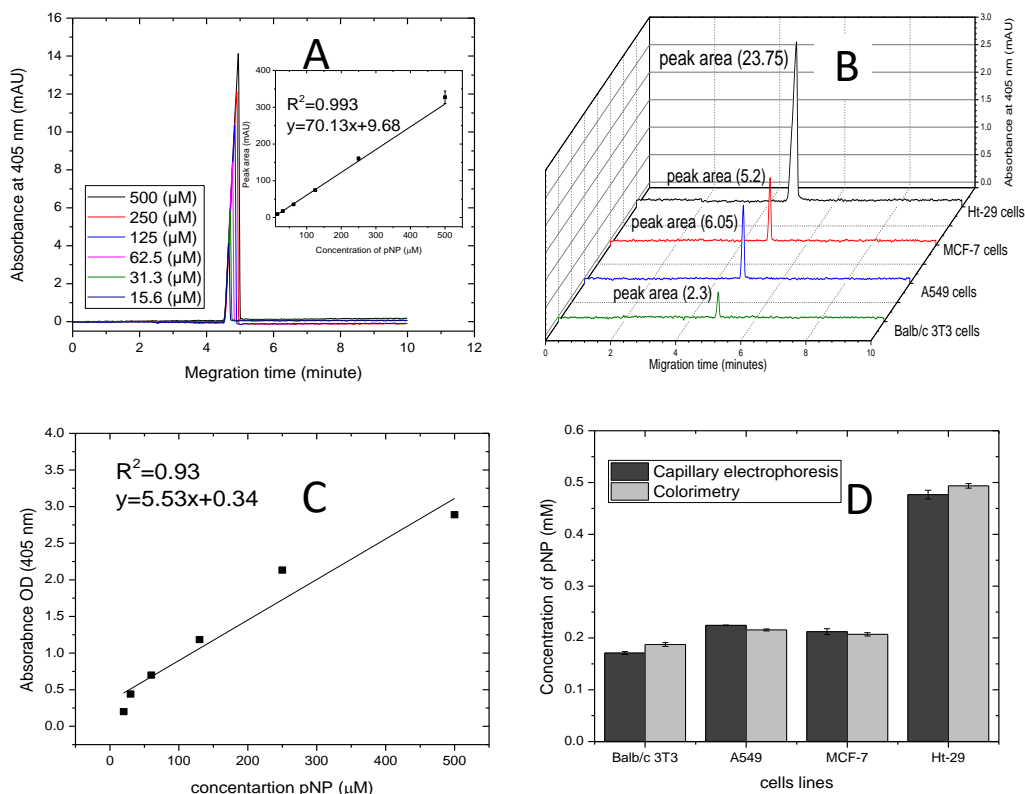


Figure 5.4: Comparative studies of capillary electrophoresis and colorimetry toward ALP release from living cells. (A) Electropherograms of pNP concentration formed by ALP release from living cells. (B) Electropherograms of standard pNP concentration ($15\text{--}500 \mu\text{M}$) and in the insert is the linear trend of peak areas. (C) The linear trend of absorbance to pNP concentration ($15\text{--}500 \mu\text{M}$). (D) Histograms of ALP release from living cells measured by capillary electrophoresis and colorimetry.

5.4.2 Comparison between absorbance and electrochemical analysis for ALP release from living cells

ALP release from living cells was compared using absorbance and electrochemistry analysis. Figure 5.5 (A) shows the calibration curve of absorbance versus various concentrations of ALP ranging from 1.5-1500 U/L and fitted by the logistic model. The standards had 30 μ L of sample dissolved with pNPP 6 mM in buffer DEA and were incubated for 30 minutes. Data in triplicate were plotted using Origin software. The correlation coefficient was found to be 0.99. In the insert (Figure 5.5 A) is the linear trend of Michaelis-menten equation. The correlation slope (km/V_{max}) and intercept ($1/V_{max}$) were calculated from the constants and were used for comparing data with electrochemical assay. Figure 5.5 (B) shows the calibration curve of current versus various concentrations of ALP ranging from 1.5-1500 U/L and fitted by the logistic model. The standards had 30 μ L of sample dissolved with pNPP 9.69 mM in buffer DEA and were incubated for 10 minutes. Data in triplicate were plotted using Origin software. The correlation coefficient was found to be 0.96. In the insert (Figure 5.5 B) is the linear trend of Michaelis-menten equation. The correlation slope (km/V_{max}) and intercept ($1/V_{max}$) were calculated from the constants and were used for comparing data with absorbance assay. The logistic model shows the dynamic linear range of both assays, which were (11.7-750 U/L) and (5.85-750 U/L) for absorbance and electrochemistry. LOD were calculated for absorbance and electrochemistry, which were (0.94 U/L) and (0.043 U/L). It is obvious from these data that electrochemical analysis is more sensitive. It has wider linear range and lower LOD.

Details of the comparative analysis performed on the absorbance and optimized electrochemical assay of ALP release from living cells are outlined in Figure 5.5 (C). The electrochemical or optical data of ALP release from cells were normalized using the Lineweaver-Burke equations shown in Figure 5.5 (A &B). There was a significant difference ($p>0.05$) in the activity of ALP release from cells between electrochemical and optical assays. The electrochemical results of ALP activity from Balb/c 3T3, A549, MCF-7 and Ht-29 were higher than ALP activity obtained by absorbance analysis. This optimization demonstrated that evaluation of ALP release by electrochemical assay was more sensitive than by optical assay. Moreover, it showed faster detection as optical active substrate needed 30 minutes for evaluating ALP release in samples while that of electro active substrate only needed 10 minutes.

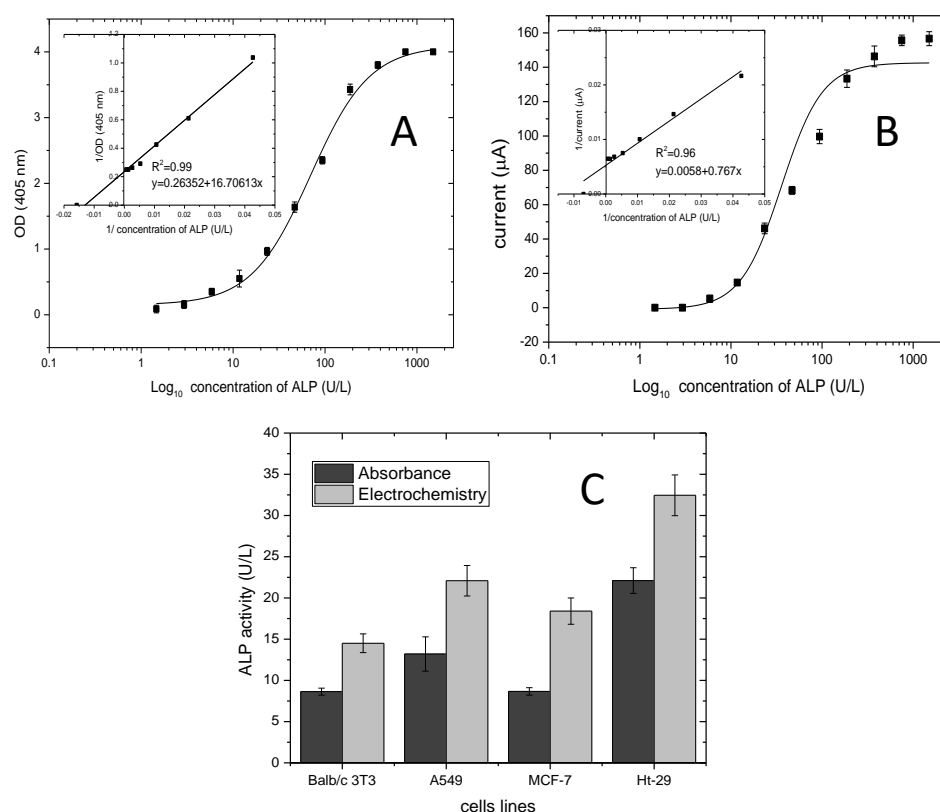


Figure 0.5: Comparative studies of absorbance and electrochemical analysis toward ALP release from living cells. (A) Calibration curve of current to concentration of ALP and in the insert is the Lineweaver-Burke plot. (B) Calibration curve of absorbance to concentration of ALP and in the insert is the Lineweaver-Burke plot. (C) Histograms of ALP release from living cells measured by absorbance and electrochemistry.

5.5 Conclusion

Capillary electrophoresis and colorimetric methods were applied for comparative analysis. The samples were introduced onto the capillary automatically. The average detection time for p-nitrophenol was 5 minutes. Colorimetry, which is the standard assay of ALP in clinical analysis, showed compatible values with CE (Figure 5.4). A calibration curve of ALP was created to allow for comparison of the data obtained by optical and electrochemical analysis. This revealed a significant difference between the two, indicating that the electrochemical investigation resulted in a more sensitive and rapid assay than the optical analysis (Figure 5.5). CE allows for the detection of ALP release with substrates at the same time, which can be used for distinguishing ALP iso-enzymes for future work.

5.6 Reference

[1] Mohamadnia, A. R.; Shahbazkia, H. R.; Sharifi, S.; Shafaei, I. Bone-specific alkaline phosphatase as a good indicator of bone formation in sheepdogs. *Comp. Clin. Path.* 2007.

- [2] Golub, E. E.; Boesze-Battaglia, K. The role of alkaline phosphatase in mineralization. *Current Opinion in Orthopaedics*. 2007.
- [3] Sharma, U.; Pal, D.; Prasad, R. Alkaline Phosphatase: An Overview. *Indian J. Clin. Biochem.* 2014, 29, 269–278.
- [4] Somani, B. L.; Ambade, V. N.; Arora, M. M. Polyacrylamide Gel Affinity Electrophoresis for Separation of Enzyme Isoforms. *Medical journal. Armed Forces India* 2003, 59, 125–127.
- [5] Dziedziejko, V.; Safranow, K.; Słowik-Zyłka, D.; Machoy-Mokrzyńska, A.; Millo, B.; Machoy, Z.; Chlubek, D. Comparison of rat and human alkaline phosphatase isoenzymes and isoforms using HPLC and electrophoresis. *Biochim. Biophys. Acta - Proteins Proteomics* 2005, 1752, 26–33.
- [6] Schumacher, U.; Trudrung, P. Direct tissue isoelectric focusing on mini ultrathin polyacrylamide gels followed by subsequent western blotting, enzyme detection, and lectin labeling as a tool for enzyme characterization in histochemistry. *Anal. Biochem.* 1991, 194, 256–258.
- [7] Righetti, P. G.; Gianazza, E.; Bianchi-Bosisio, A.; Sinha, P.; Köttgen, E. Isoelectric focusing in immobilized pH gradients: applications in clinical chemistry and forensic analysis. *Journal of Chromatography B: Biomedical Sciences and Applications*. 1991.
- [8] Hocchi, K.; Ohashi, T.; Miura, T.; Sasagawa, K.; Sato, Y.; Nomura, F.; Tomonaga, T.; Sunaga, M.; Kojima, R.; Katayama, K.; Kato, T.; Sato, T.; Komoda, T.; Oda, K. Development of an ELISA method for detecting immune complexes between tissue-nonspecific alkaline phosphatase and immunoglobulin G. *J. Clin. Lab. Anal.* 2007.
- [9] Manz, A.; Graber, N.; Widmer, H. M. Miniaturized total chemical analysis systems: A novel concept for chemical sensing. *Sensors Actuators B. Chem.* 1990.
- [10] Harrison, D. J.; Manz, A.; Lüdi, H.; Widmer, H. M.; Fan, Z. Capillary Electrophoresis and Sample Injection Systems Integrated on a Planar Glass Chip. *Anal. Chem.* 1992.
- [11] Manz, A.; Lüdi, H.; Widmer, H. M. Planar chips technology for miniaturization and integration of separation techniques into monitoring systems. Capillary electrophoresis on a chip. *J. Chromatogr. A* 1992.
- [12] Lee, K.-J.; Heo, G. S. Free solution capillary electrophoresis of proteins using untreated fused-silica capillaries. *J. Chromatogr. A* 1991, 559, 1–2.
- [13] Bullock, J. A.; Yuan, L. -C. Free solution capillary electrophoresis of basic proteins in uncoated fused silica capillary tubing. *J. Microcolumn. Sep* 1991.
- [14] Green, J. S.; Jorgenson, J. W. Minimizing adsorption of proteins on fused silica in capillary zone electrophoresis by the addition of alkali metal salts to the buffers. *J. Chromatogr. A* 1989, 478, 63–70.
- [15] DeLaney, K.; Sauer, C. S.; Vu, N. Q.; Li, I. Recent Advances and New Perspectives in Capillary Electrophoresis-Mass Spectrometry for Single Cell ‘Omics’. *Molecules* 2018, 24, 42.

- [16] Tiselius, A. A new apparatus for electrophoretic analysis of colloidal mixtures. *Trans. Faraday Soc.* 1937.
- [17] BECKMAN, L.; NILSON, L. R. VARIATIONS OF SERUM ENZYMES IN BIRD SPECIES AND HYBRIDS. *Hereditas*. 1965.
- [18] Savage, T. F.; Collins, W. M.; Smith, E. C. Detection of isoenzymes of chicken serum alkaline phosphatase using polyacrylamide disc electrophoresis. *Poult. Sci.* 1971.
- [19] Jorgenson, J. W.; Lukacs, K. D. Zone Electrophoresis in Open-Tubular Glass Capillaries. *Anal. Chem.* 1981.
- [20] Jorgenson, J. W.; Lukacs, K. D. Zone electrophoresis in open-tubular glass capillaries: Preliminary data on performance. *J. High Resolut. Chromatogr.* 1981.
- [21] Jorgenson, J. W.; Lukacs, K. D. Capillary zone electrophoresis. *Science*. 1983.
- [22] Jorgenson, J. W. Zone electrophoresis in open-tubular capillaries. *Trends in Analytical Chemistry*. 1984.
- [23] Xu, Y.; Liu, X.; Ip, M. P. C. Michaelis-Menten analysis of alkaline phosphatase by capillary electrophoresis using plug-plug reaction. *J. Liq. Chromatogr. Relat. Technol.* 1998.
- [24] Sun, X.; Jin, W.; Li, D.; Bai, Z. Measurement of alkaline phosphatase isoenzymes in individual mouse bone marrow fibroblast cells based on capillary electrophoresis with on-capillary enzymecatalyzed reaction and electrochemical detection. *Electrophoresis* 2004, 25, 1860–1866.
- [25] Iqbal, J. An enzyme immobilized microassay in capillary electrophoresis for characterization and inhibition studies of alkaline phosphatases. *Anal. Biochem.* 2011.
- [26] Wang Y.; Dubin, P. L. Capillary modification by noncovalent polycation adsorption: Effects of polymer molecular weight and adsorption ionic strength. *Anal. Chem.* 1999.
- [27] Aptisa, G.; Benavente, F.; Sanz-Nebot, V.; Chirila, E.; Barbosa, J. Evaluation of migration behaviour of therapeutic peptide hormones in capillary electrophoresis using polybrene-coated capillaries. *Anal. Bioanal. Chem.* 2010.
- [28] Grodner, B.; Napiórkowska, M. Characterization and inhibition studies of tissue nonspecific alkaline phosphatase by aminoalkanol derivatives of 1,7-dimethyl-8,9-diphenyl-4-azatricyclo [5.2.1.0^{2,6}] dec-8-ene-3,5,10-trione, new competitive and non-competitive inhibitors, by capillary elec. *J. Pharm. Biomed. Anal.* 2017.
- [29] Gattu, S.; Criehtfield, C. L.; Lu, G.; Bwanali, L.; Veltri, L. M.; Holland, L. A. Advances in enzyme substrate analysis with capillary electrophoresis. *Methods*. 2018.
- [30] TAKAYANAGI, T.; MINE, M.; MIZUGUCHI, H. Capillary Electrophoresis/Dynamic Frontal Analysis for the Enzyme Assay of 4-Nitrophenyl Phosphate with Alkaline Phosphatase. *Anal. Sci.* 2020.

- [31] Nguyen, B. T.; Kang, M. J. Application of capillary electrophoresis with laser-induced fluorescence to immunoassays and enzyme assays. *Molecules*. 2019.
- [32] Craig, D. B.; Wong, J. C. Y.; Dovichi, N. J. Detection of attomolar concentrations of alkaline phosphatase by capillary electrophoresis using laser-induced fluorescence detection. *Anal. Chem.* 1996.
- [33] Whisnant, A. R.; Johnston, S. E.; Gilman, S. D. Capillary electrophoretic analysis of alkaline phosphatase inhibition by theophylline. 2000.
- [34] Murakami, Y.; Morita, T.; Kanekiyo, T.; Tamiya, E. On-chip capillary electrophoresis for alkaline phosphatase testing. 2001.
- [35] Whisnant, A. R.; Gilman, S. D. Studies of reversible inhibition, irreversible inhibition, and activation of alkaline phosphatase by capillary electrophoresis. *Anal. Biochem.* 2002.
- [36] Neel, C. A. Studies of Alkaline Phosphatase Inhibition by Metal Chelators using Capillary Electrophoresis. MSc thesis, University of Tennessee. 2005.
- [37] Sarver, S. A.; Keithley, R. B.; Essaka, D. C.; Tanaka, H.; Yoshimura, Y.; Palcic, M. M.; Hindsgaul, O.; Dovichi, N. J. Preparation and electrophoretic separation of Bodipy-Fl-labeled glycosphingolipids. *J Chromatogr A*. 2012.
- [38] Li, C.; Wang, H. Selective enzymatic cleavage and labeling for sensitive capillary electrophoresis laserinduced fluorescence analysis of oxidized DNA bases. *J Chromatogr A*. 2015.
- [39] Ramana, P.; Adams, E.; Augustijns, P.; Schepdael, A. V. Trapping magnetic nanoparticles for in-line capillary electrophoresis in a liquid based capillary coolant system. *Talanta*. 2017.
- [40] Zemann, A. J.; Schnell, E.; Volgger, D.; Bonn, G. K. Contactless Conductivity Detection for Capillary Electrophoresis. *Anal. Chem.* 1998.
- [41] Kubáň, P.; Hauser, P. C. Contactless conductivity detection for analytical techniques: Developments from 2016 to 2018. *Electrophoresis*. 2019.
- [42] Sun, X.; Gao, N.; Jin, W. Monitoring yoctomole alkaline phosphatase by capillary electrophoresis with on-capillary catalysis-electrochemical detection. *Anal. Chim. Acta*. 2006.
- [43] Schuchert-Shi, A.; and Hauser, P. C. Study of acetylcholinesterase inhibitors using CE with contactless conductivity detection. *Electrophoresis*. 2009.
- [44] Fan, F. R. F.; Bard, A. J. Electrochemical detection of single molecules. *Science* (80-.). 1995.
- [45] Fan, F. R. F.; Kwak, J.; Bard, A. J. Single molecule electrochemistry. *J. Am. Chem. Soc.* 1996.
- [46] Fracassi da Silva, J. A.; Guzman, N.; do Lago, C. L. Contactless conductivity detection for capillary electrophoresis: Hardware improvements and optimization of the input-signal amplitude and frequency. *J Chromatogr A*. 2002.

- [47] Brito-Neto, J. G. A.; Fracassi da Silva, J. A.; Blanes, L.; do Lago, C. L. Understanding capacitively coupled contactless conductivity detection in capillary and microchip electrophoresis. Part 1. Fundamentals. *Electroanalysis*. 2005.
- [48] Sha, B. B.; Yin, X. B.; Zhang, X. H.; He, X. W.; Yang, W. L. Capillary electrophoresis coupled with electrochemical detection using porous etched joint for determination of antioxidants. *J Chromatogr A*. 2007.
- [49] Sisk, G. D.; Herzog, G.; Glennon, J. D.; Arrigan, D. W. M. Assessment of ion transfer amperometry at liquid-liquid interfaces for detection in CE. *Electrophoresis*. 2009.
- [50] Kwan, Y. H.; Thormann, W. Electrophoretically mediated microanalysis for characterization of the enantioselective CYP3A4 catalyzed N-demethylation of ketamine. *Electrophoresis*. 2012.
- [51] Řemínek, R.; Glatz, Z.; Thormann, W. Optimized on-line enantioselective capillary electrophoretic method for kinetic and inhibition studies of drug metabolism mediated by cytochrome P450 enzymes. *Electrophoresis*. 2015.
- [52] McComb, R. B.; Bowers, G. N.; Jr; Posen, S. *Alkaline Phosphatase*. New York: Plenum Press. 1979.

Chapter 6

Impedance Analysis for Real-time Alkaline Phosphatases (ALP) Release

Note: This chapter is peer-reviewed in Journal of Analytical Letters. Please refer to Appendix.

6.1. Aims and objectives of the novelty of the thesis

The aim of the work focused on in this chapter was to prove the concept of real-time monitoring of ALP release simultaneously with cell viability of Balb/c 3T3 embryo fibroblast cell lines, A549 lung cancer cell lines, MCF-7 breast cancer cell lines, and Ht-29 colon cancer cell lines using impedance analysis. Microelectrode arrays was used as a sensing surface of cell viability following objectives were designed to achieve the aim of this chapter.

1. To obtain the optimal frequency of each cell line mentioned above.
2. To allow linearity performance using different cell number
3. To investigate real-time monitoring of cell viability for the optimal density
4. To proof real-time monitoring of ALP release using differentiation including post-confluence culture and sodium butyrate (NaBt).

6.2. Introduction

6.2.1 Principle

Alkaline phosphatase (ALP), an enzyme [1], [2] was recently evaluated to be an early cancer biomarker [3], [4]. During cancer forming, a multistep process occurs and makes an improper life cycle. Consequently, normal cellular reaction of an individual cell will differ from that of a cancer cell, thereby cellular electrical activity is going to change. For example, the function of cell signaling (e.g. concentration of calcium ions) affected by the metabolic activity, which makes the producing rate of ATP increase [5]–[7] [8]–[10]. This process may raise the alkalinity of cellular membrane, causing the formation of early biomarkers (e.g., ALP release) [11] [12]. This mean that receptors in the cells may be deficient or disordered and that might promote cancer. The deficiency or disordering of the receptor can be study through the changes in the genes regulating the receptor proteins (e.g mRNA) [13]. Therefore, it is important to study the mechanisms underlying regulation of gene expression to solve problems in cells and find the medicine. This can be studied by a useful reporter enzyme that tell what happens inside the cell. This enzyme should allow quantitative assay and not affected by endogenous activity. Enzymes used so far as a reporter are (a) chloramphenicol acetyltransferase (CAT), (b) β -galactosidase, and (c) luciferase, which all are not produced by mammalian cells. Those enzymes require cell lysis for assaying gene expression, thereby increasing the steps of the experiment and errors [14]. On the other hand, ALP release can be secreted from mammalian cells and allow qualitatively and quantitatively reporter assay of mRNA. Unlike the non-mammalian reporter enzymes, ALP does not need any cell lysis and can be directly released into the media. ALP release, therefore, was nominated as a gene reporter in quantification of the intracellular ALP mRNA [15]. Thus, the demand of real-time ALP-related study has raised the attention to develop biosensor-based strategies.

For example surface plasmon resonance [16]–[19]; field-effect transistor [20]–[22]; quartz crystal microbalance [23]–[25]; and electrochemical impedance spectroscopy (EIS) [26]–[33] can provide realtime detection for ALP analysis. However, these techniques so far relied on affinity approaches. Among them EIS was exploited in this chapter to reveal the tiny physiological movements and adhesion of cells during ALP release. Unlike previous reports, this approach can provide a direct measurement. Impedance technique depended on measuring resistivity and capacitivity (dielectric) properties of cells as the membrane works as an insulator (capacitance). So, to allow real-time quantifying of cellular function during ALP release, the commercial electric cell-substrate impedance sensing (ECIS) system was suggested. The cultureware (ECIS-8W10E+) consisted of 40 microelectrodes per well (8 wells). The total surface area of the 40 microelectrodes per well is 1.96 cm². The cells can grow on the 40 microelectrodes and grow on the insulating layer that mounted on the polycarbonate substrate. The latter and the thin film of microelectrodes are transparent and thus permit microscopic monitoring of cells. The walls of wells are made of polystyrene and they have a capacity of 600 μ L for culture media. During applying the alternating current (AC), the change of the impedance due to the change of the capacitance of the monolayer of cells are recorded.

Figure 6.1 shows a schematic of the impedance characteristics of adhesion cells. As described in chapter 1 (section 1.9.2) the impedance will increase when cell proliferation increase. Cells will impede the pathway of current. Any change in impedance through proliferation can show motility of cells. A decrement in impedance identifies death of cells. Not alive cells are going to lose the ability of attachment with surface and allow current to pass through working electrode. Electrochemical impedance spectroscopy requires confluence of cells for ALP release monitoring. The interface changes between cells attached and releasing ALP directly influence of impedance and allow real-time monitoring. High ALP release means the permeability of cell membrane increases, which cause a decrement in the impedance magnitude and an increment of the capacitance.

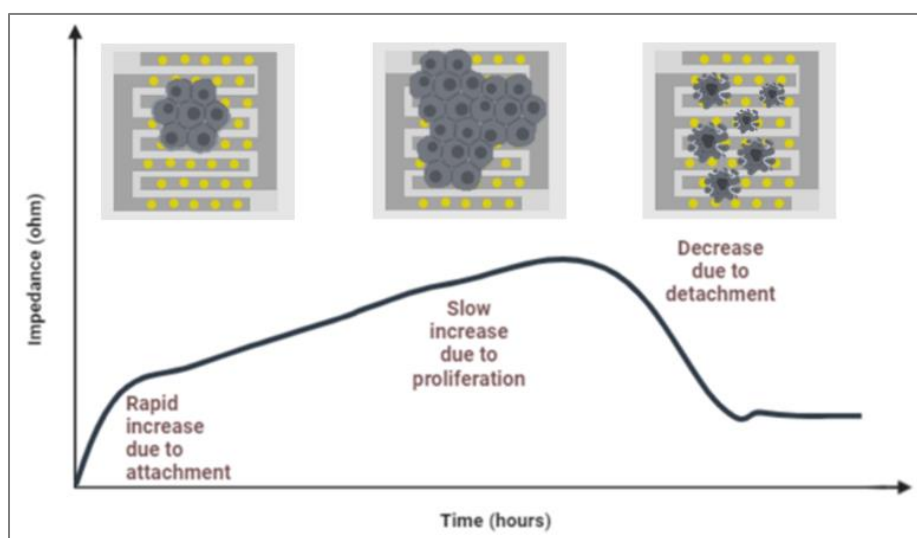


Figure 6.1: shows a schematic of the impedance characteristics of adhesion cells.

6.2.2 Background and literature review

Literature review here is twofold. First, contributions have been performed for determination activity of ALP with lack information about cellular responses. Second, contributions have been designed for determination activity of ALP simultaneously with monitoring cell morphology. Researchers believed that neglected of monitoring cells causes less effective resolution of cancer diagnosis and therefore more attention paid for monitoring cells viability during ALP release. Meng et al. (2005) monitored the response of a sensor when cells release ALP during exposing to activated macrophages [34]. The response was of the accumulating of macrophages. This made research turn toward investigation of cell viability simultaneously when ALP release. This attitude raised the potential of taking advantages of microelectrode arrays technology. It was Matsue's group then who kept developing this attitude and helped trigger its revival with the onset of microarrays sensors. They considered some different methods for assaying cell viability during ALP release. For example, they tested the attachment of cell after exposing them to high pH [35] tested the respiratory activity of cells [36] used optical micrograph microscope [37] and finally exploited the technology of scanning electrochemical microscopy (SECM) [38]–[47]. Matsue's group (2015) found that SECM for bioimaging ALP release is the best for the redox cyclic principle they used to use [48]. However, some factors affects this principle for example, the high distance between the electrodes cause low electrochemical signal, therefore considering small distance are significant. Moreover, their methodology does not reveal any physiological behavior of treated cells. One more strategy was suggested by We et al (2016), used enzyme-induced metallization [49]. Their findings of digital analysis solves the existing problems associated with fluctuations in electrochemical signal detection and heterogeneity of single enzyme activities. However, a number of questions regarding living cells morphology remain to be addressed. Sun et al (2019) purposed detection of ALP activity inside cells using an integration technique of microfluidic droplet-based SERS- surface-enhanced Raman scattering [50]. Although the sensitivity of the assay, no cellular response identified. Previous research can only be considered a first step towards a more profound understanding of the combination of SERS and microdroplet technique. For example, research has provided evidence for avoiding limitations of the SERS technique. It was claimed that the poorly quantitative analysis of SERS was overcome. However, lack of control of SERS factors is the main limitation of this technique. The method introduced by Sun et al. had remains limited by one factor, which is aggregation time. Furthermore, the using of metal nanoparticles for the probing solution (colloids) harm biological sample. Another method such as phase contrast microscope have been employed by Yildirim-Semerici et al. (2015) [51]. Although this technique appear consistent with prior research, it appears inconsistent with integration in microdevices. Also, phase contrast microscope can measure structure of cells during ALP release. However, the thickness of cells during differentiation is more likely to scatter the light and cause low resolution and cause false positive phase-contrast. The literature pertaining to cell viability monitoring strongly suggests that digital signals are preferred.

6.2.3 The Problem statement

A closer look to the literature on analysis of cells using bioimaging of ALP activity and optical microscope, however, reveal a number of gaps and shortcomings when designing microarrays. The other method that

depended on optical microscope has limitation of integration with other system, thus hindered with developed clinical devices [52]. Moreover, although research has illuminated overcoming of some limitation of SERS (e.g. control of aggregation time), the study has not examined particle size for instant and did not illustrated performance of the distribution of analytes on the surface (e.g. cells morphology). To fill this literature gap, it is suggested to identify the cells morphology (cellular response) during ALP release. Therefore, additional studies to understand more completely the key tenets of cellular response during ALP release are required. This chapter intended to develop the methodology for real-time ALP release from living cells based microelectrode arrays.

6.2.4 Summary

The aim of the work focused in this chapter was to proof the concept of real-time monitoring of ALP release simultaneously with viability assay of Balb/c 3T3 embryo fibroblast cell lines, A549 lung cancer cell lines, MCF-7 breast cancer cell lines, and Ht-29 colon cancer cell lines using impedance analysis. Cell were brought onto the microelectrode arrays would work as an insulator during passing current at different time and adherent cells impede the flow currents would bring about information of cells. The following objectives were designed to achieve the aim of this chapter. By obtaining the optimal frequency of each cell line mentioned above, we would be able to unify that frequency on the rest of the assay related to that cell. In addition, linearity performance of the assay allow stable conditions therefore different cell number were going to be used for each cell line. To attain real-time monitoring of cell viability during ALP release, the optimal density was obtained from chapter 2 were applied. Finally, to meet the aim of this thesis real-time monitoring of ALP release, cells were differentiated by two ways; post-confluence culture (Balb/ c3T3, A549, MCF-7, and Ht-29) and sodium butyrate (Ht-29) for the purpose of inducing ALP. The viability of cells was verified by resazurin assay and microscopy. ALP activity was assessed by amperometry in the presence of the electroactive substrate of substrate p-aminophenyl phosphate (pAPP).

6.3. Methodology:

6.3.1. Reagent

Mouse embryo fibroblast cells (Balb/c 3T3 Line), breast carcinoma epithelial cells (MCF-7 Line), lung carcinoma epithelial cells (A-549 Line), colon carcinoma epithelial cells (Ht-29 Line), 70% ethanol, and nanopure water (Grade 18 M Ω) (Tyndall National Institute, UCC). Newborn calf serum (NBCS), fetal bovine serum (FBS), Dulbecco's modified eagle's medium (DMEM), Minimum Essential Medium Eagle (MEME) and McCoy's 5A Medium, Hank's balanced salt solution (HBSS), Trypsin/EDTA solution, resazurin, Virkon®, magnesium chloride (MgCl₂), sodium chloride (NaCl), potassium chloride (KCl), diethanolamine (DEA), para-aminophenol phosphate (p-APP), calf intestinal phosphatase (ALP), L-cysteine, sodium butyrate (NaBt), (Sigma, Ireland).

6.3.2. Instruments

Cell culture hood (Esco Airstream® Class II), 5% CO₂ incubator (incusafe Panasonic), water bath 37 °C (fisherbarnd), Centrifugation (universal 320 Hittch zentrifugen) and (Eppendorf 5415D Centrifuge).

Inverted microscope and camera (Olympus), fluorescent platereaders (Spectra Max Gemini), absorbance platereader (Diasource ELISA Reader), hemocytometer slide (Reichert Bright-Line), glass cover slips (menzel-gläser) and cell counter, pipettes (Rainin Pipet-X) and micropipettes (Gilson Pipetman®), pipette tips (Greiner Bio-One), pipettors (5-mL, 10-mL, and 25- mL), cell culture vessels (75T flasks, 1.5-mL, 15-mL, 50mL centrifuge tubes, 96- and 48-well plates), and syringes 45 nm filters (Sigma, Ireland). Electric cellsubstrate impedance sensing (ECIS-8W10E+) (ibid, Germany), Metrohm Autolab analyser (Metrohm, Netherland) palmSens portable potentiostat (Palm Instruments BV, the Netherlands), graphite screen printed electrodes (Kanichi Research Limited).

6.3.3. Cell culture

The cancer cell lines used during this project were stored in liquid nitrogen prior to being cultured. To begin cell growth, they were removed from storage and quickly defrosted (less than a minute). The entire contents (1 mL) of the cryogenic vial were then pipetted into a 15 mL- tube, which contained 9 ml of prewarmed complete media (Table 6.1). The tube was centrifuged to dispose of dimethyl sulfoxide, which was present in the supernatant. The cells were re-suspended in 5 ml complete media and placed in T75 flask that already contained 35 ml of completed media in order to reach a volume of 40 ml. The flask was incubated in the incubator at 37 °C and 5% CO₂ to reach 70% confluence.

Table 0.1: The media and serum of each cell line used for cell culture.

	Cell lines	Balb/c 3T3	A549	MCF-7	Ht-29
Complete media	Media	DMEM	DMEM	MEME	McCoy's 5A
	10 % Serum	NBCS	FBS		

Completed media represent the addition of 10% of serum to the media suitable for each cell lines according to the manufacture's recommendations.

The cells were sub-cultured at least three times before optimization began. Briefly, the subculture procedure was achieved by removing old media via a sterile plastic pipette, followed by two washes with pre-warmed HBSS. 4 ml of trypsin were then added, and the flask was incubated for 5-8 minutes to allow the cells to detach. 6 ml of complete media were then added to inactivate the trypsin. The cell suspension was placed in a clean 15-ml centrifuge tube, and the cells were centrifuged for 5 min at 1,000 rpm. The supernatant was removed, and the cell pellets were re-suspended in 5 ml of fresh media. The desired cell number were seeded in a 48-well plate, and the final volume of media was added. All the experiments were applied in the same working area: 95 cm²; 48-well plate.

6.3.4. Pretreatment and characterization of microelectrodes

Microelectrode surfaces were treated with 10 mM L-cysteine diluted in deionized water. Then 200 µL Lcysteine solution was added to wells and left at room temperature for 10 minutes. Wells were cleaned twice with 200 µl of deionized water and kept under UV light for 30 minutes before seeding cells. The

commercial electric cell-substrate impedance sensing (ECIS-8W10E+) cultureware is illustrated in Figure 6.2.

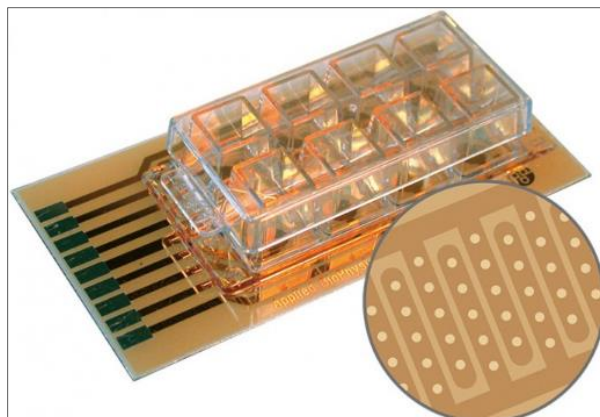


Figure 0.2: The commercial ECIS 8W10E+ cultureware. In the licorice representation, microelectrode arrays.

6.3.5. Real-time impedance measurement of cell viability

6.3.5.1. Frequency Range

Electrical impedance spectroscopy measurements were calculated using a Metrohm Autolab analyser. During the measurements the cultureware (ECIS 8W10E+) was placed in a cell culture hood (figure 6.3). The instrument was connected to electrodes with crocodile clips and controlled with Nova software. The Nova software was used to analyse the acquired data and to model the measured spectra. For impedance measurements, the equipment delivered an alternating voltage with 0.5 mV amplitude in a frequency range of between 1 K Hz and 1000 K Hz. Cell number (20×10^3 cells/ml) was seeded in each well. The resistance change was monitored for four days.

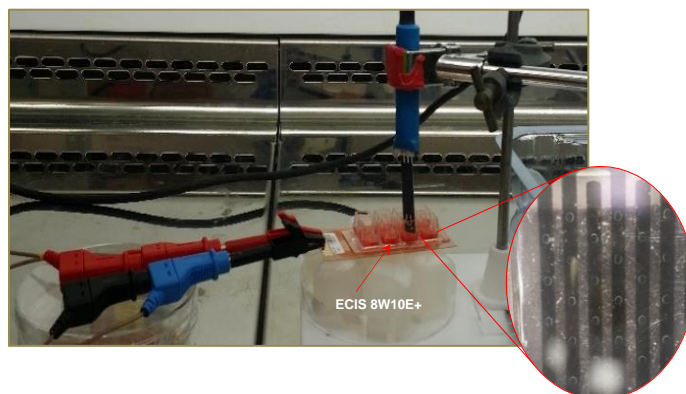


Figure 0.3: The work station during ALP release monitoring.

6.3.5.2. Linearity performance

Linearity performance was measured by changing the concentration of the cell number at the optimal frequency in the case of each cell line. A range for the cell numbers (10, 20, 30, 40 $\times 10^3$ cell/ml) was used for Balb/c 3T3, A549 and MCf-7 cells. Ht-29 cells had a range of (20, 40, 60, 80 $\times 10^3$ cell/ml). Electrical impedance spectroscopy measurements were performed at one-hour intervals over 10 hours to avoid the duplication of cell numbers. The equation of cell index (CI) was used to normalize the measured electrical resistance and to plot the calibration curve of CI value and cell density.

$$CI = \frac{R_i}{R_{\text{cell-free}}} - 1$$

Where R_i is the resistance of the cell-covered electrodes, and $R_{\text{cell-free}}$ is the resistance of blank electrodes (free-serum media).

6.3.5.3. Impedance monitoring of cell monolayer growth

To obtain the growth curve of each cell line and reach the inhibitive contact growth, an initial concentration of cell number (40 $\times 10^3$ cell/ml) was used for Balb/c 3T3, A549 and MCf-7 cells, while (80 $\times 10^3$ cell/ml) was used for Ht-29 cells. Cell growth was assessed at 24-hour intervals over 6 days by applying electrical impedance spectroscopy measurements using the optimal frequency in the case of each cell line. Figure 6.4 shows the schematic of the cell growth on microelectrodes (A) and the typical curve (B). The data of impedance were normalized using CI index and fitted by logistic growth model using Origin software.

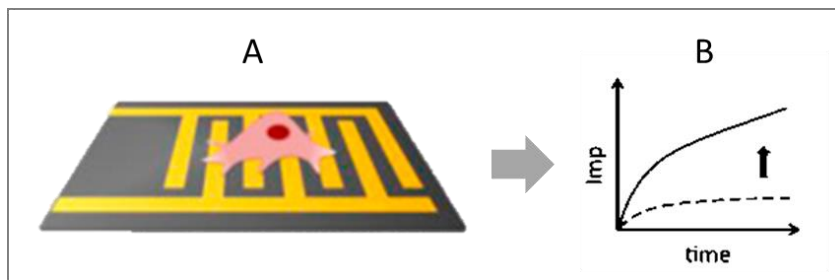


Figure 0.4: The schematic of the cell growth on microelectrodes (A) and the typical curve (B).

6.3.5.5 Impedance monitoring of cell monolayer during ALP release when exposing to ALP buffer

Cells were seeded in the ECIS at a concentration of 40 $\times 10^3$ cells/ml for Balb/c 3T3, A549, and MCF-7 cells, and at a concentration of 80 $\times 10^3$ cells/ml for Ht-29 cells. The media was changed every two days to keep the cells healthy and nutrientized. After they achieved their exponential growth and met the 95-100% confluence (Day 4), the cells were washed with HBSS twice and exposed to ALP assay buffer. VC was also assessed. Control cells, treated cells and VC cells were assessed using electrical impedance spectroscopy measurements. Cell viability was verified by taking resazurin measurements.

6.3.6 Real-time monitoring of ALP release using impedance spectroscopy

6.3.6.1 Differentiation in HT-29 cells

Impedance spectroscopy was carried out during the differentiation experiment in order to monitor cell monolayer behaviour during ALP release. It was proven that in post-confluence culture ALP increases (chapter 3 and 4). The Ht-29 cell line was monitored during post-confluence culture under routine conditions. The cells were seeded in ECIS cultureware and in a 48-well plate at a density of 80×10^3 cell/mL medium containing 10% FBS. Cells were cultivated in ECIS and in a 48-well plate for three day to reach 7090% confluence. The cells were maintained in growth media for a further 3–6 days with media changes every two days. This monitoring was used as differentiation control. In order to further enhance differentiation in HT-29 cells, Sodium butyrate (NaBt) was applied to the culture medium. NaBt is a natural inducer for colon differentiation [53], [54]. Ht-29 cell line ECIS cultureware and 48-well plate was treated with 0.5mM or 1mM NaBt after 72 hours of cultivation.

Cells were incubated with NaBt for 14 hours. The medium was changed to a routine medium, and the cells were incubated at 37 °C for two more days. Untreated cells were used as a control. The vehicle control had dead cells. Real-time monitoring of the cell monolayer was performed using an impedance signal. Microscope images of cells adhered to ECIS or 48-well plate were taken in order to investigate the morphology of cells during ALP release.

6.3.6.3 Amperometry detection

Differentiation in HT-29 cells led to ALP release in the routine media. Amperometry of ALP release in media of NaBt-non-treated cells, NaBt-treated cells and the media of vehicle control was assessed. The graphite screen-printed electrodes were immersed in 400 μ L of the routine media of the cells with 400 μ L of the ALP assay buffer (5 U/L ALP, 8 mM MgCl_2 , 50 mM NaCl, and 10 mM pAPP and pH 9.5). The amount of p-aminophenol (pAP) was measured at positive potential 0.15 V for 10 seconds using palmSens potentiostat (Figure 6.5). When the current reached the stable baseline, it was measured at the fourth second.

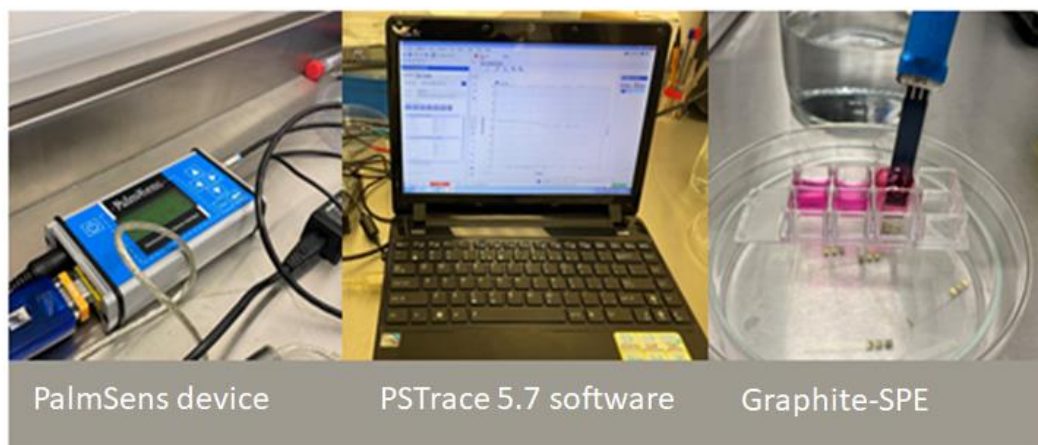


Figure 0.5: The workstation of detection amperometry measurement.

6.3.7. Microscope images

Images of cell-confluence were taken at 24-hour intervals over 5 days using the inverted microscope and camera. Due to the presence of phenol red, which interferes with the light of microscopes, cells were washed twice with HBSS. As the microelectrodes were not transparent to the light, images of cells were taken from the area between the interdigitated microelectrodes.

6.3.8 Cell viability

The viability of the cells was evaluated using resazurin-based assay according to methodology of (Chapter 2, Section 2.3.8). Resazurin was prepared in HBSS and diluted to the optimal concentration in the case of each cell line. Cells were seeded at the optimal initial density in the case of each cell line in the ECIS cultureware. Culturewares incubated with cells for 4 hours. Negative control or vehicle control was performed by addition of two drops of Virkon® to the routine media and incubated with cell for 24 hours. Fluorescent measurement was measured at at 544 excitation and 590 nm emission as an optimal wavelength range of resazurin.

6.4 Results and discussion

6.4.1. Electrochemical impedance spectroscopy

Three ranges were used to monitor bioimpedance events, with the β -dispersion being the most sensitive to changes in cell membrane. Frequencies ranging between 1-1000 KHz were applied and used to monitor the growth of the four given cells. The bode plot in figure 6.6 shows the spectra of impedance of the monolayer of cells. Cells were plated at an initial density of (20×10^3 cells/ ml) and incubated at 37°C and 5% CO₂. Impedance change was scanned over four days. A regular increase of impedance was shown for each cell line over the four days. The impedance spectra of Balb/c 3T3 cells and MCF-7 cells exhibited similar behaviours at low frequency. The double layer capacitance of the electrodes dominated the magnitude impedance signal at frequencies of less than 5000 Hz. The impedance spectra of A549 cells and Ht-29 cells was affected by the electric double layer formed at the electrode/electrolyte interface, but at a frequency (less than 10000 Hz). When the range of frequency increased, the bulk electrolyte resistance dominated the magnitude of impedance, hence revealing the conductivity of the ions in the medium and emphasizing the linearity performance of the monolayer of cells over four days. The bulk resistance influenced the impedance spectra of Balb/c 3T3 cells at a frequency of (5-150 KHz), which was the highest range among the cells. MCF-7 cells showed bulk resistance at a range of (5-50 KHz), which was the shortest range of frequency among the cells. A549 cells and Ht-29 cells were slightly different, as they demonstrated bulk resistance at frequencies of (10-100 KHz) and (10-150 KHz). This corresponded to many *in vitro* studies, where cell viability and cell growth was monitored [55]–[60]. The different range of frequency presented by each type of cell was due to the different size and type of each cell line. The permittivity of the interior of the cell (e.g., cytoplasm) characterizes each cell line. When the permittivity of cytoplasm is less than the permittivity of the suspension medium, it causes less dielectric capacitance, thus resulting in higher impedance.

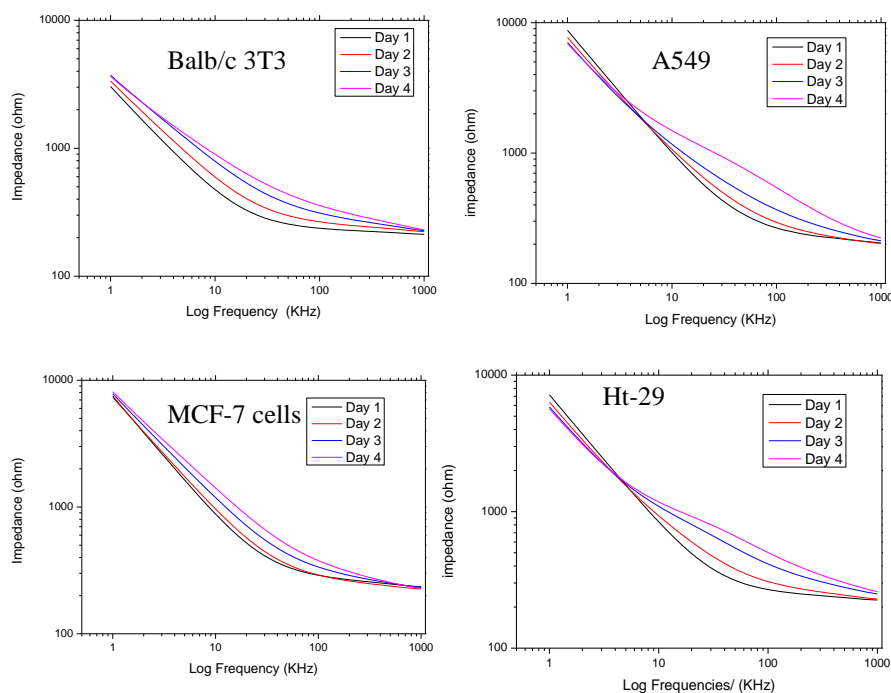


Figure 0.6: Bode plots of the impedance spectra of experimental data in frequency range of between 1 KHz and 1000 KHz. The spectrum was obtained for 20×10^3 cells/ mL of the cells of (Balb/c 3T3, A549, MCF-7 and Ht-29) proliferated for over 4 days in the presence of routine media.

6.4.3. Impedance responses to various concentrations of cells

The microelectrode arrays were validated via monocultures of the Balb/c 3T3 fibroblast embryonic cells and the A549, MCF-7 and Ht-29 epithelial cancer cells in normal proliferative conditions. The optimal frequencies outlined in Figure 2 were used for each cell line. These were 40 KHz, 60 KHz, 30 KHz, and 60 KHz for the Balb/c 3T3, A549, MCF-7 and Ht-29 cells, respectively. Figure 6.7 shows the resistance responses when single electrodes were challenged using various concentrations of cells from 10×10^3 cells/ mL to 40×10^3 cells/ mL, and from 20×10^3 cells/ mL to 80×10^3 cells/ mL. The routine media of each cell line was used as 0 cell concentration, and the resistance of free-serum media was used as a blank. The data obtained during 10 hours was fitted by the linear polynomial model that displayed very good regression analysis. During adhesion on the microelectrodes cells moved, causing increases and decreases in the impedance. From 0 hour to 3 hours, the resistance curves corresponded to the adsorption of cells membrane indicating an electrostatic attraction. From 4 hours to 7 hours, the resistance increased because cells were rearranging themselves to find the proper binding site. From 8 hours to 10 hours resistance increased marginally and then remained constant, indicating the attachment of the cell membrane to the surface of the microelectrode. Cells at this stage required another 10 hours to duplicate. Therefore, cell number throughout this stage were estimated by using the cell index (CI). After 10 hours, a calibration curve was plotted, which represented the correlation between CI value and cell seeding density (Figure 3). The rises and falls shown in the curves during the movements and attachment of cells on 40 microelectrodes were better than the results when applying a single microelectrode [61].

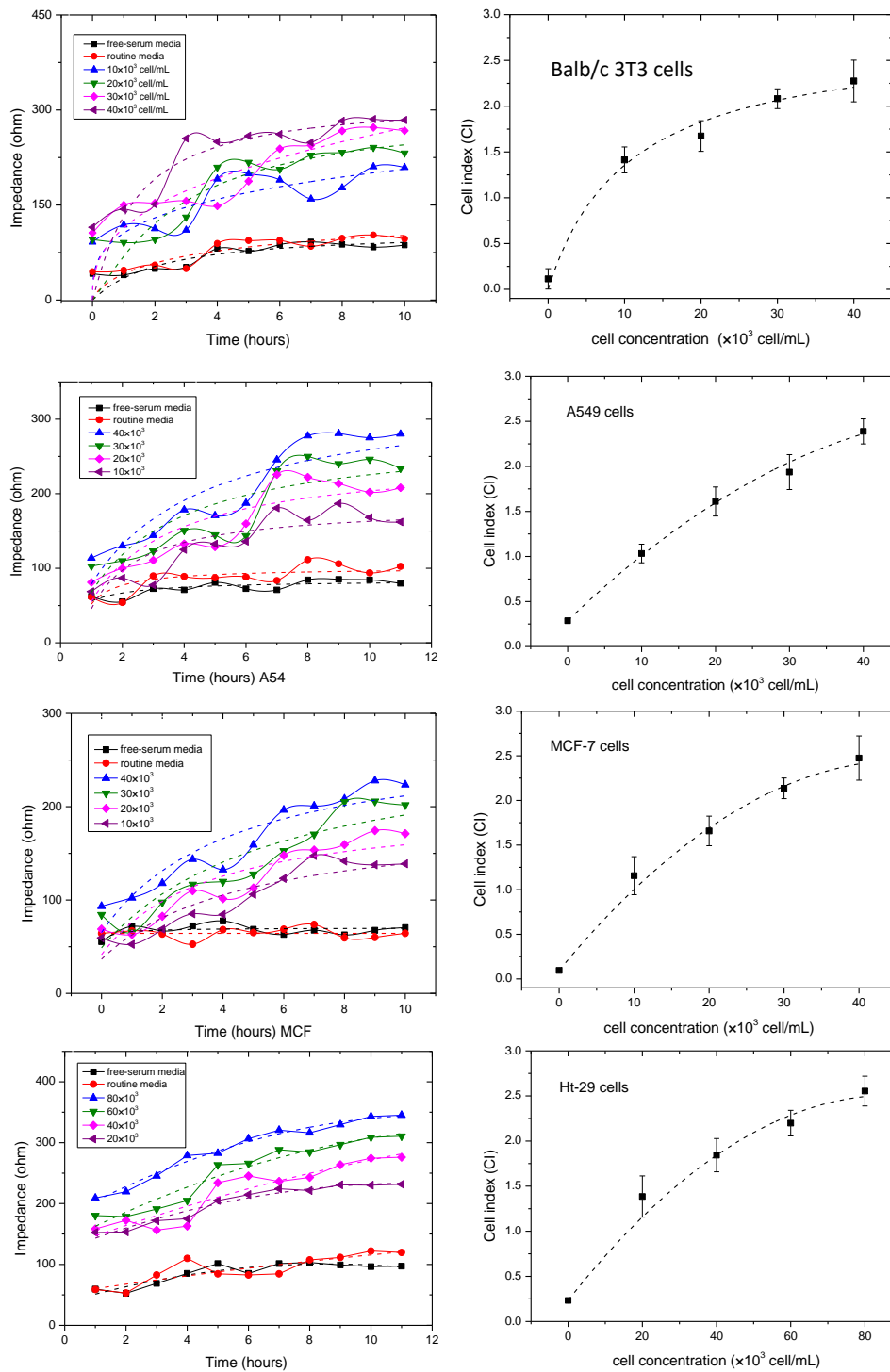


Figure 0.7: (Left curves) Resistance responses of microelectrode array to various concentrations of the Balb/c 3T3, A549, MCF-7 and Ht-29 cells in monoculture for 10 hours. (Right curves) Calibration curve represents the correlation between cell density and cell index value.

6.4.4. Cell monolayer monitoring by impedance

The growth of adherent cells was evaluated using impedance signals. The resulting data were normalized using the CI values recorded in Figure 6.7. The data were fitted by growth model to illustrate the phases of cells growth. Figure 6.8 shows the normalised data, illustrating an s-shape growth curve for all cells. This data is slightly different from the data recorded in Chapter 2 (Figure 2.10), where all cells showed an s-shape growth curve, and MCF-7 cells displayed a j-shape curve. However, cells required different times to reach the stationary phase. The growth of the cells of Balb/c 3T3 and A549 levelled by day 4. MCF-7 cells levelled by day 6 and presented long lag phase [62]. Ht-29 cells showed continued growth, which correlates with the findings by Witzel et al. (2015) [63]. Overall, the impedimetric measurements of cell growth over long periods of time were stable, and the routine media of all cells represented very low resistance [64].

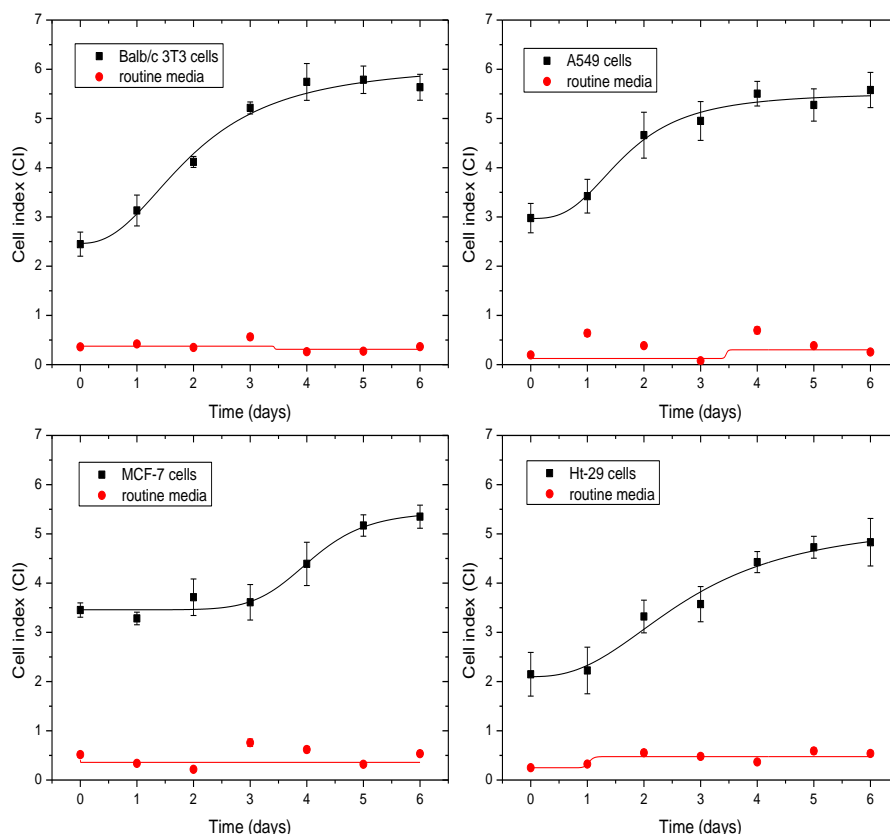


Figure 6.8: Logistic growth curves of Balb/c 3T3 cells; A549 cells; MCF-7 cells; and Ht-29 cells, over six days. The normalised CI values of resistance changes at optimal frequency in the case of each cell line.

6.4.5. Cellular morphology on MEAs

Microscope images were taken to evaluate the growth of cells' monolayers over 5 days. Figure 6.9 demonstrates that the four cell types displayed a healthy fitted monolayer from day 1 to day 5.

Microscope images corresponded to bioimpedance responses (Figure 6.8), and showed that Balb/c 3T3 and A549 cells had a 24- hour doubling time. MCF-7 cells had the longest lag phase among other cells, as it was seen in Figure 6.8. MCF-7 cells needed 48 hours for attachment and then they doubled themselves every 24 hours [62]. On the other hand, Ht-29 cells showed doubling time every 36 hours, which was seen in the microscope images. The resistance changes recorded in Figure 6.8 displayed the extracellular matrix of Ht-29 cells. Colon cancer cells expressed more extracellular matrix before doubling themselves, a fact that was shown clearly in the microscope images [65]. The embryonic cells of Balb/c 3T3 illustrated sensitivity to the inhibitive growth contact, which was seen in both figure 6.8 and also in microscope images. Cancer cells were less sensitive to inhibitive growth contact phenomena. A549 cells displayed a monolayer (90-100% confluence) from day 3 to day 5. A549 cells were less likely to show a multilayer [66]. A549 cells became stationary by day 3 and stayed constant until day 5. In contrast, the cells of MCF7 and Ht-29 reached the stationary phase by day 5 [62], [65], [67]–[70]. The cellular growth corresponded to the findings in Chapter 2 (Figure 2.9), which indicated the biocompatibility of MEAs surface for cell culture. The microscope images of cells during growth correlated to the results of resistance changes.

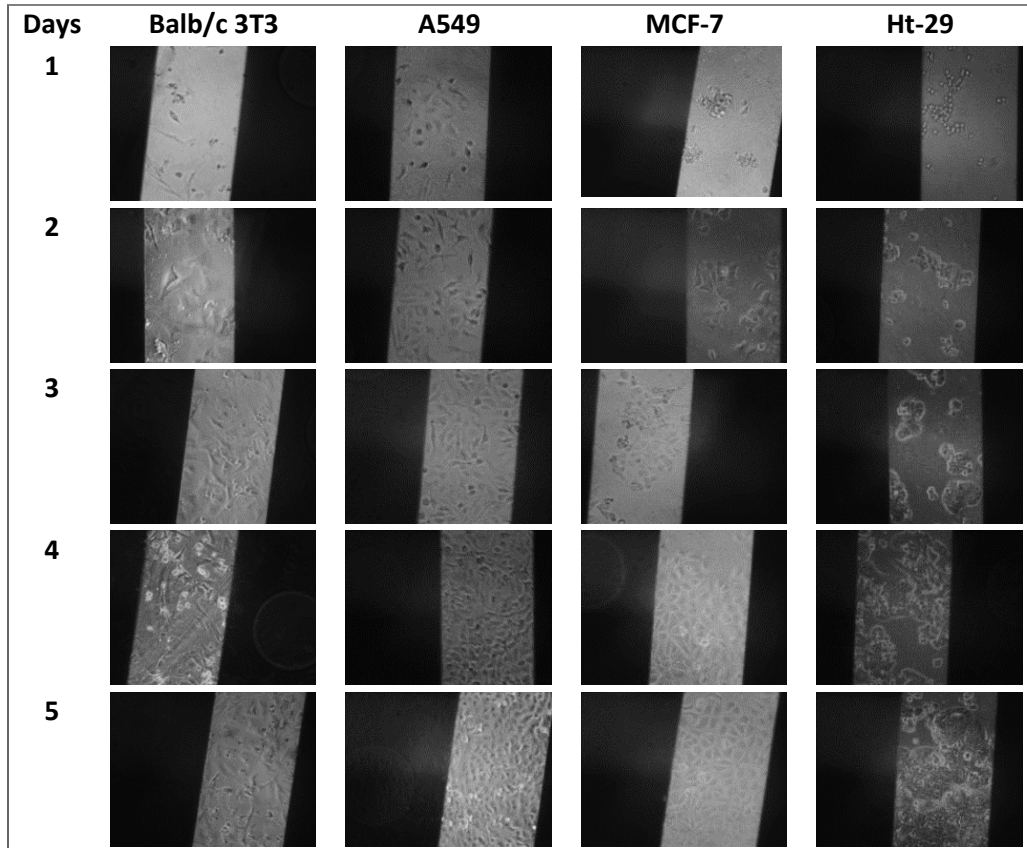


Figure 0.9: Microscope images of the four cell types over a 5-day incubation on microelectrode array.

6.4.6. Impedance responses during alkalinity buffer

Electrochemistry impedance spectroscopy measurements were performed to analyse cell viability during the exposure of cells to the ALP buffer. Bode and Nyquist plots for the four cells were presented in Figure 6.10. It was important to have a full understanding of the effect of the alkalinity buffer on cells grown on the ECIS system. Figure 6.10 illustrates the average responses of impedance of Balb/c 3T3, A549, MCF-7 and Ht-29 cells before (positive control) and after exposure to the DEA buffer (pH 9.5). Impedance of dead cells was monitored as a negative control (vehicle control). Impedance in the positive control was higher as the cells' membranes impeded the flow of the current. When cells were exposed to the alkaline environment, they started to lose their viability. The cells' membranes slightly detached from the surfaces of electrodes and caused a decrease in impedances. The magnitude of impedances of cells in pH 9.5 was significantly different from vehicle control data (dead cells), which meant that cells still alive. This opens the opportunity for multiplex assay. Cell viability was verified by resazurin assay (Figure 6.10). Balb/c 3T3, A549, MCF-7, and Ht-29 cells that were exposed to the DEA buffer for 10 minutes had (78 %), (64 %), (60 %), and (83 %) of their viability, respectively. These data were significantly different from the negative control. They all displayed p-values less than (0.05), which were (0.002), (0.006), (0.006), and (0.002) for the cells of Balb/c 3T3, A549, MCF-7, and Ht-29 cells, respectively using unpaired t-test.

Nyquist plots presented in Figure 6.10 showed different charge transfer resistances of each cell line before and after exposure to the DEA buffer. The charge transfer resistances for the Balb/c 3T3, A549, MCF-7, and Ht-29 cells before the addition of the ALP buffer were 76 Ω , 23 Ω , 35 Ω , and 33 Ω , respectively. When cells were exposed to the alkalinity buffer for 10 minutes, the charge transfer resistances of each cell line declined as expected to 59 Ω , 11 Ω , 17 Ω , and 20 Ω , for the Balb/c 3T3, A549, MCF-7, and Ht-29 cells, respectively. These data were expected, as the ion diffusion increased and caused an increase in the conductivity of the electrolyte. These data were slightly higher than the vehicle controls, where cells were not completely attached onto the surface. In the vehicle controls, the charge transfer resistances for the Balb/c 3T3, A549, MCF-7, and Ht-29 cells were 4 Ω , 9 Ω , 7 Ω , and 15 Ω , respectively. The slope values of the non-vertical line were at their lowest before the addition of the ALP buffer and increased after the addition of the ALP buffer. The slope recorded the highest values when cells were completely dead at vehicle controls. This indicates that the slope was affected by the electrolyte concentration [32], [71].

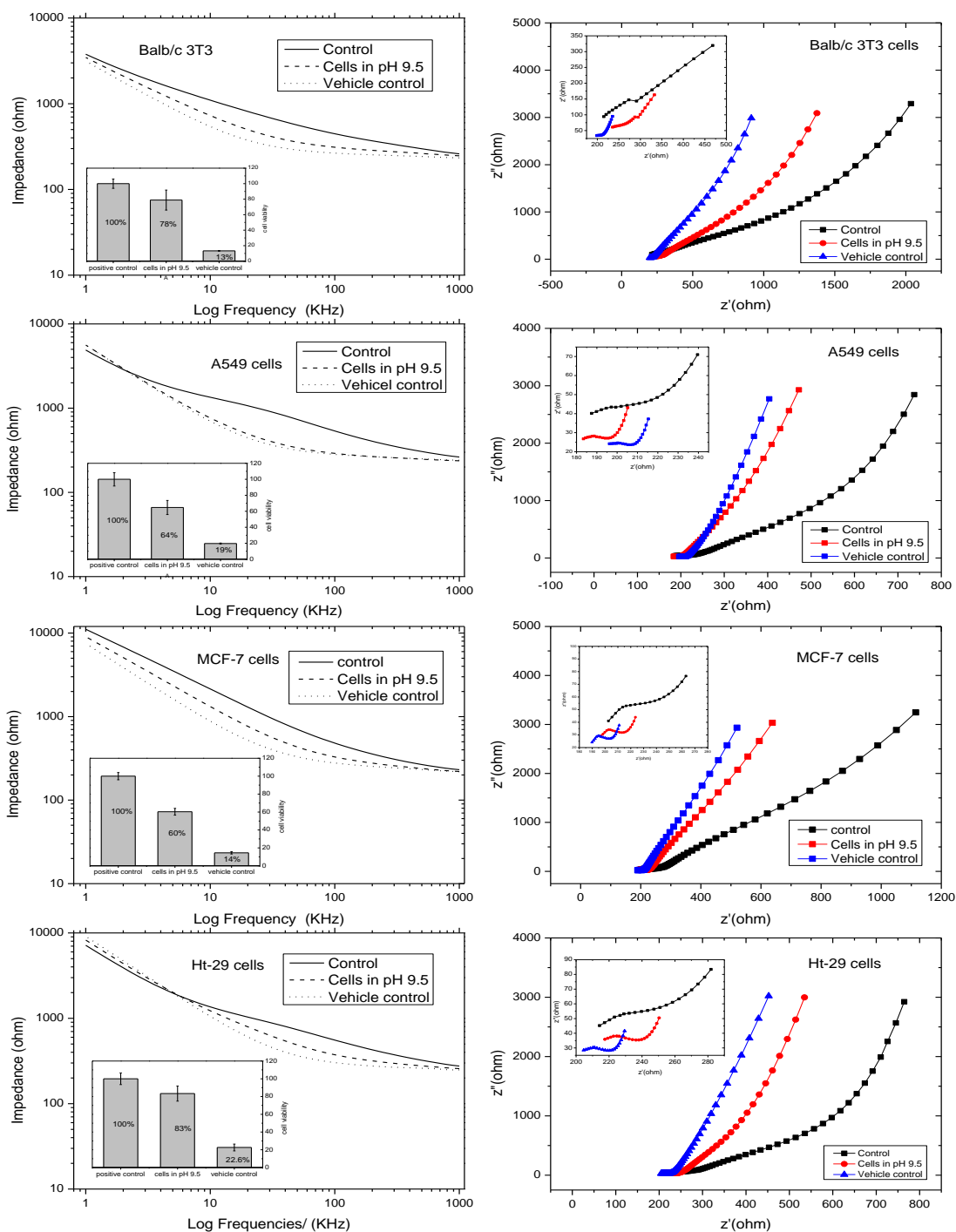


Figure 6.10: EIS results of the four cell types grew on the working electrode before and after exposure to DEA buffer. (Left) Bode plots, and (Right) Nyquist plots.

6.4.7. Real-time monitoring of ALP release

The impedance response of the cell line Ht-29 during differentiation was recorded via ECIS. ALP release in Balb/c 3T3, A549, MCF-7 and Ht-29 cells was monitored during post-confluence culture (Chapter 3, Table 3.4) and (Chapter 4, Table 4.4). As discussed earlier, post-confluence culture can induce the differentiation of many cancer cells. The Ht-29 cell line indicated the highest quantity of ALP release, and, therefore, was used for further impedance detection. Sodium butyrate (NaBt), on the other hand, mediates differentiation in many kinds of colon cancer cells [53], [54], [72]. Therefore, it was used specifically to induce the biomarker of ALP release in the culture media of Ht-29 cells [73]–[75] while attaching on ECIS. NaBt was mixed with routine media at two concentrations (0.5 mM) and (1mM) and incubated with cells for 14 hours. Figure 6.11 (A) shows the impedimetric responses of Ht-29 cell line in three cases: NaBt-non-treated cells, NaBt-treated cells at concentration of (0.5 mM) and (1mM)' and dead cells (vehicle control). The routine media with no cells was used as blank. The measurement was applied at the optimal frequency obtained in Figure (6.6) of 60 kHz. Real-time monitoring of the cells' monolayer was applied as cells were seeding, attaching and reaching the 70-90% confluence. The real-time monitoring was continued during differentiation with post-confluence and NaBt treatment. Normal exponential curve was observed from 1-72 hours. Cells were treated on day 3 and monitored for 14 hours. The media was changed, cells were incubated for another 72 hours and impedimetric signals were recorded. The impedance values illustrated slight decreases when low amounts of NaBt were applied compared to the positive control. A significant decline was shown when applying high amount of NaBt. This indicated a relationship between the amount of NaBt and cellular response.

NaBt concentration needs a range of concentrations in order to determine the limit of detection of relationship between NaBt and cellular response. The significant differences between the values of differentiated cells and vehicle control indicated that the cells released ALP while alive. NaBt might inhibit the growth factor of Histone deacetylase (HDAC), which led to decrease the cell growth rapidly as seen in Figure 6.11 (A). Microscope images (Figure 6.11, B) illustrated morphological changes in cells membrane. NaBt-non-treated cells appeared strongly attached to each other while NaBt-treated cells looked more likely to separate from each other. These results corresponding to the findings of Joseph et al (2004) [76]. NaBt affected cell–cell adhesion, which was seen in the changes in the monolayer shape [77].

The viability of cells was measured as shown in figure 6.11 (C). Untreated cells (positive control) had the highest viability (100 %) as cells maintained in their routine condition. The viability of NaBt-treated cells with (0.5 mM) and (1 mM) was (87.5%) and (82.3%). The viability of cells decreased as the concentration of NaBt increased. This might be the reason of for HDAC inhibition. There was no significant different for the viability values of NaBt-treated cells compared to the viability value of NaBt-non-treated cells (positive control). Vehicle control had the lowest level of viability (20.4%), because cells were already dead

Real-time monitoring of ALP release from colon cancer cells lines (Ht-29) was performed using Amperometry (Figure 6.11 D). The current responses were applied in the media of NaBt-non-treated cells (positive control), the media of dead cells (vehicle control), and the media of NaBt- treated cells. It is noticeable that the current generated by the oxidation of pAP when using 1 mM of NaBt was 24.5 μ A, while 0.5 mM of NaBt allowed a generated current of 12 μ A. There was a small rise in NaBt-non-treated cells (control), which was approximately 7.5 μ A. The increase of the current density indicated that differentiation of Ht-29 cells with NaBt was enhanced. The vehicle control generated almost the lowest

level of current at 0.9 μA . Amperometric readings of the electroactive product pAP for all the four sample cells was calculated at 10 seconds and generated almost 800 μL .

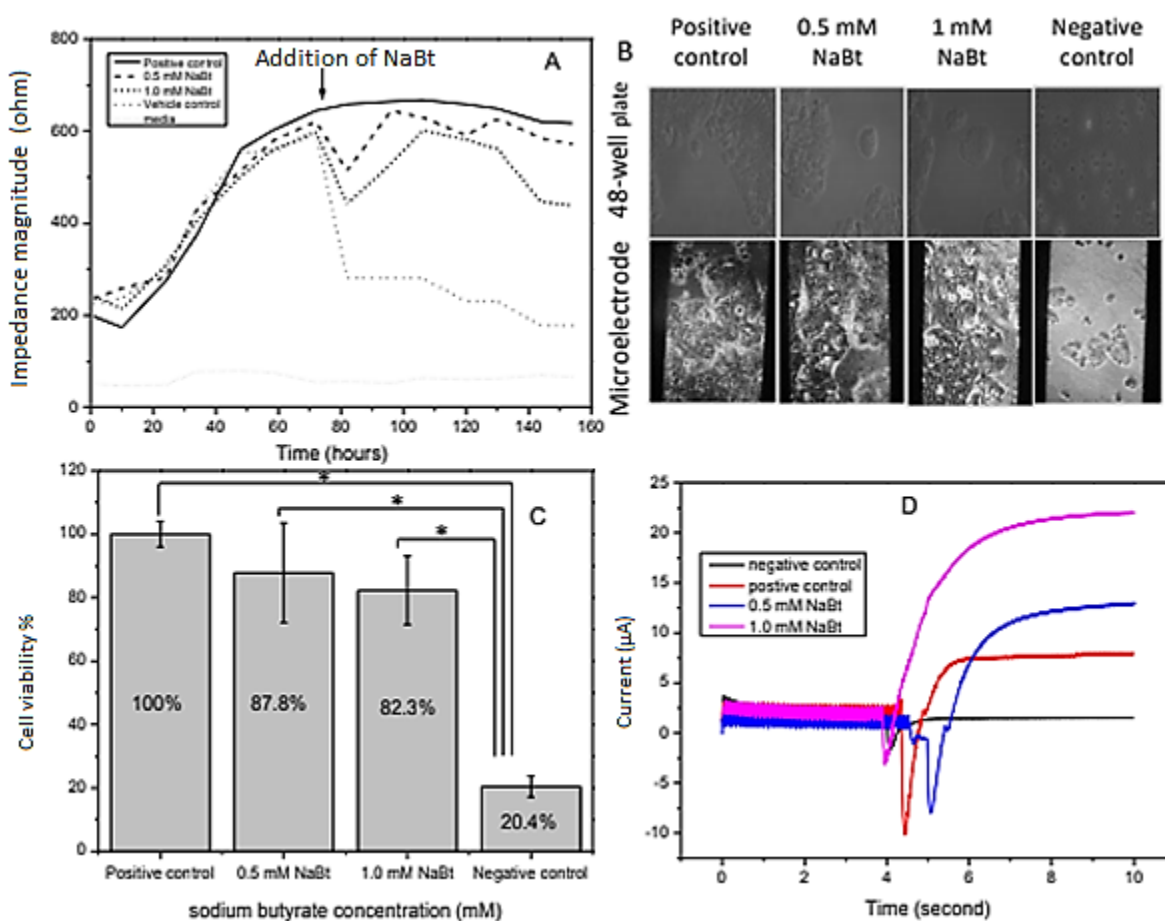


Figure 6.11: (A) Relative impedance changes of Ht-29 cells during ALP release. (B) Microscope images of cells adhesion on 48-well plate and microelectrode array after exposure to NaBt. (C) Resazurin-based assay for cells attached on microelectrode array after differentiation. unpaired t -test (* $p < 0.05$ significant is different). (D) Amperometric current-time response curve of ALP release. Measurement was applied at a potential of 0.15 V and at assay buffer of DEA (9.5) in the presence of 10 mM pAPP.

6.5. Future tests

The methodology for monitoring ALP release in real-time was proven in Figure (6.11). However, it is required to apply different concentration of NaBt to determine with purpose of determination of limit of the detection. It is also required to apply NaBt on the other cells presented in this thesis. This could give a comprehensive investigation of ALP release and cell viability during using ECIS system.

6.6. Conclusion

Impedance-based sensing technology has gained a great deal of attention relating to the study of cellular activities. The aim of this research was to report a real-time monitoring of ALP release and cell viability utilizing microelectrode arrays.

The impedance will increase when cell proliferation increases and vice versa. The impedance will change if there is any change in the interface between the attached cells and microelectrodes' surface during ALP release. Each cell line has membrane properties that differ from the other, which results in different capacities the dielectric properties of the cell membrane). This made the frequency improvement important for each cell line. Impedance spectra of each cell line at a range of frequency from 1 KHz to 1000 KHz was presented in Bode plots (Figure 6.6). The cells of Balb/c 3T3, A549, MCF-7 and Ht-29 displayed different frequency ranges, which were (5-150) KHz, (10-100) KHz, (5-50) KHz and (10-150) KHz, respectively. The highest impedance of the cells' membrane for Balb/c 3T3, A549, MCF-7 and Ht-29 cells were 40 KHz, 60 KHz, 30 KHz, and 60 KHz, respectively

In order to verify of the constancy of the assay, calibration curve was obtained cells concentration and resistance responses over 10 hours and the polynomial model fitted the data with very good regression analysis (Figure 6.7). The data was normalized using cell index equation to facilitate tracking cell number. The microelectrode arrays biocompatible as cells showed logistic growth curves and clearly displayed the four phases (figure 6.8). Special attention was drawn to the morphology of cells, which was monitored and compared to the resistance changes (figure 6.9). It was important to monitor the cell viability during exposing to ALP buffer (pH 9.5). EIS measurements were performed and presented in Bode and Nyquist plots in order to analyze the magnitude of impedance of cell monolayer in the day 4 and compared it to the vehicle control (Figure 6.10). Cell viability was verified by resazurin assay and a verity in charge transfer resistance of each cell line before and after exposing to DEA buffer was also investigated. The ion diffusion (the permittivity) increased and caused an increase in the conductivity of the electrolyte, thus decrease in the impedance.

Relative impedance changes of Ht-29 cells during ALP release were observed during differentiation by using post-confluence culture and using NaBt (Figure 6.11). Microscope images of cells adhesion on 48well plate and microelectrode array after exposure to NaBt were recorded and compared. Resazurin-based assay for cells attached on microelectrode array after differentiation was verified. The amperometric response of ALP release in media was reported using a graphite screen-printed electrode at a potential of 0.15 V and at assay buffer of DEA (9.5) in the presence of 10 mM pAPP. The data clearly indicated a correlation between ALP activity and cell differentiation. Shifts in current (μA) obtained from concentration of NaBt indicated an increase of ALP activity. This may suggest optimizing the relationship between the amount of NaBt and the cellular response.

The main aim of this chapter was achieved. It was provided a developed methodology for real-time ALP release in cells. Future tests are required for the rest of the other cells studied in this thesis. Furthermore, transfection methods (e.g., using plasmid) are required to assay ALP release at different states of the cells.

6.6. References

- [1] Kim, E. E.; Wyckoff, H. W. Reaction mechanism of alkaline phosphatase based on crystal structures. Two-metal ion catalysis. *J. Mol. Biol.* 1991.
- [2] Dirnbach, E.; Steel, D. G.; Gafni, A. Mg^{2+} binding to alkaline phosphatase correlates with slow changes in protein lability. *Biochemistry.* 2001.
- [3] Kim, S. H.; Shin, K.H.; Moon, S.H.; Jang, J.; Kim, H.S.; Suh, J.S.; Yang, W. I. Reassessment of alkaline phosphatase as serum tumor marker with high specificity in osteosarcoma. *Cancer Med.* 2017, 6, 1311–1322.
- [4] Heinrich, D.; Bruland, O.; Guise, T. A.; Suzuki, H.; Sartor, O. Alkaline phosphatase in metastatic castration-resistant prostate cancer: Reassessment of an older biomarker. *Future Oncology.* 2018.
- [5] Takahashi, A.; Lida, T.; Naim, R.; Naykaya, Y.; Honda, T. Chloride secretion induced by thermostable direct haemolysin of *Vibrio parahaemolyticus* depends on colonic cell maturation. *J. Med. Microbiol.* 2001, 50, 870–878.
- [6] Perry, M. D.; Rajendran, V. M.; MacLennan, K. A.; Sandle, G. I. Segmental differences in upregulated apical potassium channels in mammalian colon during potassium adaptation. *Am. J. Physiol. Liver Physiol.* 2016, 311, G785–G793.
- [7] Gerlach, A. C.; Gangopadhyay, N. N.; Devor, D. C. Kinase-dependent Regulation of the Intermediate Conductance. Calcium-dependent Potassium Channel. hK1. *J. Biol. Chem.* 2000, 275, 585–598.
- [8] Yang, B.; Cao, L.; Liu, B.; McCaig, C. D.; Pu, J. The Transition from Proliferation to Differentiation in Colorectal Cancer Is Regulated by the Calcium Activated Chloride. Channel A1. *PLoS One* 2013, 8, e60861.
- [9] Zahanich, I.; Graf, E. M.; Heubach, J. F.; Hempel, U.; Boxberger, S.; Ravens, U. Molecular and Functional Expression of Voltage-Operated Calcium Channels During Osteogenic Differentiation of Human Mesenchymal Stem Cells. *J. Bone Miner. Res.* 2005, 20, 1637–1646.
- [10] Macrae, M. X.; Blake, S.; Jiang, X.; Capone, R.; Estes, D. J.; Mayer, M.; Yang, J. A semi-synthetic ion channel platform for detection of phosphatase and protease activity. *ACS Nano* 2009, 3, 3567– 3580.
- [11] Petre, I.; Harju, T.; Ehrenfeucht, A.; Prescott, D. M.; Rozenberg, G. Computation in Living Cells: Gene Assembly in Ciliates. Berlin: Springer Berlin Heidelberg. 2004.

- [12] Wedlich, D. Cell Migration in Development and Disease. Wiley VCH Verlag GmbH & Co. KGaA: Weinheim. 2005.
- [13] Müller-Pillasch, F.; Wallrapp, C.; Lacher, U.; Adler, G.; Gress, T. M.; Friess, H.; Büchler, M. Identification of a new tumour-associated antigen TM4SF5 and its expression in human cancer. *Gene*. 1998.
- [14] Cullen, B. R. Utility of the secreted placental alkaline phosphatase reporter enzyme. *Methods Enzymol.* 2000, 326, 159–164.
- [15] Berger, J.; Hauber, J.; Hauber, R.; Geiger, R.; Cullen, B. R. Secreted placental alkaline phosphatase: a powerful new quantitative indicator of gene expression in eukaryotic cells. *Gene* 1988, 66, 1–10.
- [16] Hou, W. B.; Cronin, S. B. A Review of Surface Plasmon Resonance-Enhanced Photocatalysis. *Adv. Funct. Mater.* 2013, 23, 1612–1619.
- [17] Linder, H. C.; Enander, K.; Magnusson, P. Glycation Contributes to Interaction Between Human Bone Alkaline Phosphatase and Collagen Type I. *Calcif Tissue Int.* 2016, 98, 284–293.
- [18] Sappia, L.; Piccinini, E.; Santilli, N.; Marmisolé, W.; Madrid, R.; Azzaroni, O. Lectin-modified surfaces for the real-time determination of Bone Alkaline Phosphatase by Surface Plasmon Resonance (SPR) Spectroscopy. 1st Argentine-German Workshop on Nanotechnology and Nanobiosensors. INTI. Buenos Aires, Argentina. 2017.
- [19] Wang, K.; Jiang, L.; Zhang, F.; Wei, Y. Q.; Wang, H. S.; Qi, Z. J.; Liu, S. Q. Strategy for in Situ Imaging of Cellular Alkaline Phosphatase Activity Using Gold Nanoflower Probe and Localized Surface Plasmon Resonance Technique. *Anal Chem.* 2018 90, 14056–14062.
- [20] Syu, Y. C.; Hsu, W. E.; Lin, C. T. Review-Field-Effect Transistor Biosensing: Devices and Clinical Applications. *ECS J. SOLID STATE Sci. Technol.* 2018, 7, Q3196–Q3207.
- [21] Jang, H. J.; Ahn, J.; Kim, M. G.; Shin, Y. B.; Jeun, M.; Cho, W. J.; Lee, K. H. Electrical signaling of enzymelinked immunosorbent assays with an ion-sensitive field-effect transistor. *Biosens. Bioelectron.* 2015, 64, 318–323.
- [22] Freeman, R.; Gill, R.; Willner, I. Following a protein kinase activity using a field-effect transistor device. *Chem Commun.* 2007, 33, 3450–3452.
- [23] Ebersole, R. C.; Ward, M. D. Amplified Mass Immunosorbent Assay with a Quartz Crystal Microbalance. *Am. Chem. Soc.* 1988, 110, 8623–8628.
- [24] Kacar, T.; Zin, M. T.; So, C.; Wilson, B.; Ma, H.; Gul-Karaguler, N.; Tamerler, C. Directed Selfimmobilization of Alkaline Phosphatase on Micro-Patterned Substrates Via Genetically Fused Metal-Binding Peptide. *Biotechnol. Bioeng.* 2009, 103, 696–705.
- [25] Thammasittirong, A.; Dechklar, M.; Leetachewa, S.; Pootanakit, K.; Angsuthanasombat, C. *Aedes aegypti* Membrane-Bound Alkaline Phosphatase Expressed in *Escherichia coli* Retains High-Affinity

Binding for *Bacillus thuringiensis* Cry4Ba Toxin. *Am. Soc. Microbiol. Appl. Environ. Microbiol.* 2011, 77, 6836–6840.

[26] Gomes, W. P.; Vanmaekelbergh, D. Impedance spectroscopy at semiconductor electrodes: Review and recent developments. *Electrochim. Acta.* 1996, 41, 967–973.

[27] Cai, Q.; Wei, W.; Wang, R.; Nie, L.; Yao, S. Measurement of Serum Alkaline Phosphatase with a Surface Acoustic Wave Impedance Sensor Device. *Anal. Sci.* 1997, 13, 121–125.

[28] Lee, J. Y.; Ahn, J. K.; Park, K. S.; Park, H. G. An impedimetric determination of alkaline phosphatase activity based on the oxidation reaction mediated by Cu^{2+} bound to poly-thymine DNA. *RSC Adv.* 2018, 8, 11241–11246.

[29] Lucarelli, F.; Marrazza, G.; Mascini, M. Enzyme-based impedimetric detection of PCR products using oligonucleotide-modified screen-printed gold electrodes. *Biosens. Bioelectron.* 2005, 20, 2001–2009.

[30] Ferancova, A.; Hattuniemi, M.; Pääkkönen, S.; Tervo, P.; Ohtonen, E.; Sesay, A.; Rätty, J.; Virtanen, V. Electrochemical Impedance Spectroscopy for Monitoring of Alkaline Phosphatase Reaction with Substrate. *Procedia Technol.* 2017, 27, 315–316.

[31] Shrikrishnan, S.; Sankaran, K.; Lakshminarayanan, V. Electrochemical Impedance Analysis of Adsorption and Enzyme Kinetics of Calf Intestine Alkaline Phosphatase on SAM-Modified Gold Electrode. *J. Phys. Chem. C.* 2012, 116, 16030–16037.

[32] Hemed, M. N.; Convertino, A.; Shacham-Diamand, Y. Alkaline phosphatase detection using electrochemical impedance of anti-alkaline phosphatase antibody (Ab354) functionalized siliconnanowire-forest in phosphate buffer solution. *Sensors Actuators B. Chem.* 2018, 259, 809–815.

[33] Kaatz, M.; Schulze, H.; Ciani, I.; Lisdat, F.; Mount, A. R.; Bachmann, T. T. Alkaline phosphatase enzymatic signal amplification for fast, sensitive impedimetric DNA detection. *Analyst* 2012, 137, 59–63.

[34] Meng, Y.; Kasai, A.; Hiramatsu, N.; Hayakawa, K.; Takeda, M.; Shimizu, F.; Kawachi, H.; Yao, J.; Kitamura, M. Real-time monitoring of mesangial cell-macrophage cross-talk using SEAP *in vitro* and *ex vivo*. *Kidney Int.* 2005, 68, 886–893.

[35] Sen, M.; Ino, K.; Inoue, K. Y.; Arai, T.; Nishijo, T.; Suda, A.; Kunikata, R.; Shiku, H.; Matsue, T. LSI-based amperometric sensor for real-time monitoring of embryoid bodies. *Biosens. Bioelectron.* 2013, 48, 12–18.

[36] Torisawa, Y.-S.; Ohara, N.; Nagamine, K.; Kasai, S.; Yasukawa, T.; Shiku, H.; Matsue, T. Electrochemical monitoring of cellular signal transduction with a secreted alkaline phosphatase reporter system. *Anal. Chem.* 2006, 78, 7625–7631.

[37] Inoue, K. Y.; Yasukawa, T.; Shiku, H.; Matsue, T. Cell-Based Electrochemical Assay for Endotoxin Using a Secreted Alkaline Phosphatase Reporter System. *Electrochem. J-Stage* 2008, 76, 525–528.

- [38] Murata, T.; Yasukawa, T.; Shiku, H.; Matsue, T. Electrochemical single-cell gene-expression assay combining dielectrophoretic manipulation with secreted alkaline phosphatase reporter system. *Biosens. Bioelectron.* 2009, 25, 913–919.
- [39] Lin, Z.; Takahashi, Y.; Kitagawa, Y.; Umemura, T.; Shiku, H.; Matsue, T. An addressable microelectrode array for electrochemical detection. *Anal Chem.* 2008, 80, 6830–6833.
- [40] Lin, Z. Y.; Takahashi, Y.; Murata, T.; Takeda, M.; Ino, K.; Shiku, H.; Matsue, T. Electrochemical GeneFunction Analysis for Single Cells with Addressable Microelectrode/Microwell Arrays. *Angew. CHEMIE-INTERNATIONAL Ed.* 2009, 48, 2044–2046.
- [41] Takeda, M.; Shiku, H.; Ino, K.; Matsue, T. Electrochemical chip integrating scalable ring-ring electrode array to detect secreted alkaline phosphatase, *Analyst* 2011, 136, 4991–4996.
- [42] Şen, M.; Ino, K.; Shiku, H.; Matsue, T. A new electrochemical assay method for gene expression using hela cells with a secreted alkaline phosphatase (SEAP) reporter system. *Biotechnol. Bioeng.* 2012, 109, 2163–2167.
- [43] Ino, K.; Nishijo, T.; Arai, T.; Kanno, Y.; Takahashi, Y.; Shiku, H.; Matsue, T. Local Redox-Cycling-Based Electrochemical Chip Device with Deep Microwells for Evaluation of Embryoid Bodies. *Angew Chem Int Ed Engl.* 2012, 124, 6752–6756.
- [44] Sen, M.; Ino, K.; Shiku, H.; Matsue, T. Accumulation and detection of secreted proteins from single cells for reporter gene assays using a local redox cycling-based electrochemical (LRC-EC) chip device. *Lab Chip* 2012, 12, 4328–4335.
- [45] Ino, K.; Nishijo, T.; Kanno, Y.; Ozawa, F.; Arai, T.; Takahashi, Y.; Shiku, H.; Matsue, T. Electrochemical device with interdigitated ring array electrodes for investigating the relationship between cardiomyocyte differentiation from embryonic stem cells and alkaline phosphatase activity. *Electrochemistry.* 2013.
- [46] Ino, K.; Kanno, Y.; Nishijo, T.; Komaki, H.; Yamada, Y.; Yoshida, S.; Takahashi, Y.; Shiku, H.; Matsue, T. Densified Electrochemical Sensors Based on Local Redox Cycling between Vertically Separated Electrodes in Substrate Generation/Chip Collection and Extended Feedback Modes. *Anal Chem.* 2014, 86, 4016–4023.
- [47] Ino, K.; Goto, T.; Kanno, Y.; Inoue, K. Y.; Takahashi, Y.; Shiku, H.; Matsue, T. Droplet array on local redox cycling-based electrochemical (LRC-EC) chip device. *Lab Chip* 2014, 14, 787–794.
- [48] Kanno, Y.; Ino, K.; Shiku, H.; Matsue, T. A local redox cycling-based electrochemical chip device with nanocavities for multi-electrochemical evaluation of embryoid bodies. *Lab Chip* 2015, 15, 4404–4414.
- [49] Wu, Z.; Zhou, C.-H.; Pan, L.-J.; Zeng, T.; Zhu, L.; Pang, D. W.; Zhang, Z.-L. Reliable Digital Single Molecule Electrochemistry for Ultrasensitive Alkaline Phosphatase Detection. *Anal Chem.* 2016, 88, 9166–9172.

- [50] Sun, D.; Cao, F.; Cong, L.; Xu, W.; Chen, Q.; Shic, W.; Xu, S. Cellular heterogeneity identified by singlecell alkaline phosphatase (ALP) via a SERRS-microfluidic droplet platform. *Lab Chip* 2019, 19, 335–342.
- [51] Yildirim-Semerici, C.; Benayahu, D.; Adamovski, M.; Wollenberger, U. An Electrochemical Assay for Monitoring Differentiation of the Osteoblastic Cell Line (MBA-15) on the Sensor Chip. *Electroanalysis* 2015, 27, 1350–1358.
- [52] Ino, K.; Shiku, H.; Matsue, T. Bioelectrochemical applications of microelectrode arrays in cell analysis and engineering. 2017, 5, 146–151.
- [53] Harig, J. M.; Soergel, K. H.; Komorowski, R. A.; Wood, C. M. Treatment of Diversion Colitis with ShortChain-Fatty Acid Irrigation. *N. Engl. J. Med.* 1989.
- [54] Velcich, A.; Augenlicht, L. H. Regulated expression of an intestinal mucin gene in HT29 colonic carcinoma cells. *J. Biol. Chem.* 1993.
- [55] Chiu, S. P.; Batsaikhan, B.; Huang, H. M.; Wang, J. Y. Application of Electric Cell-Substrate Impedance Sensing to Investigate the Cytotoxic Effects of Andrographolide on U-87 MG Glioblastoma Cell Migration and Apoptosis. *Sensors (Basel)* 2019, 19, 2275.
- [56] Chiu, S.-P.; Lee, Y.-W.; Wu, L.-Y.; Tung, T.-H.; Gomez, S.; Lo, C.-M.; Wang, J.-Y. Application of ECIS to Assess FCCP-Induced Changes of MSC Micromotion and Wound Healing Migration. *Sensors (Basel)* 2019, 19, 3210.
- [57] Jia, J.; Martin, T. A.; Ye, L.; Meng, L.; Xia, N.; Jiang, W. G.; Zhang, X. Fibroblast activation protein- α promotes the growth and migration of lung cancer cells via the PI3K and sonic hedgehog pathways. *Int. J. Mol. Med.* 2018.
- [58] Yin, H.; Wang, F. L.; Wang, A. L.; Cheng, J.; Zhou, Y. Bioelectrical Impedance Assay to Monitor Changes in Aspirin-Treated Human Colon Cancer HT-29 Cell Shape during Apoptosis. *Anal. Lett.* 2007, 40, 85–94.
- [59] Halaidych, O. V.; Freund, C.; van den Hil, F.; Salvatori, D. C. F.; Riminucci, M.; Mummery, C. L.; Orlova, V. V. Inflammatory Responses and Barrier Function of Endothelial Cells Derived from Human Induced Pluripotent Stem Cells. *Stem Cell Reports* 2018, 10, 1642–1656.
- [60] Stanica, L.; Rosu-Hamzescu, M.; Gheorghiu, M.; Stan, M.; Antonescu, L.; Polonschii, C.; Gheorghiu, E. Electric Cell-Substrate Impedance Sensing of Cellular Effects under Hypoxic Conditions and Carbonic Anhydrase Inhibition. *J. Sensors*, 2017, 2017, 1–10.
- [61] Tran, T. B.; Baek, C.; Min, J. Electric cell-substrate impedance sensing (ecis) with microelectrode arrays for investigation of cancer Cell - Fibroblasts interaction. *PLoS One*. 2016.
- [62] Sutherland, R. L.; Hall, R. E.; Taylor, I. W. Cell Proliferation Kinetics of MCF-7 Human Mammary Carcinoma Cells in Culture and Effects of Tamoxifen on Exponentially Growing and Plateau-Phase Cells. *Cancer Res.* 1983.

- [63] Witzel, F.; Fritsche-Guenther, R.; Lehmann, N.; Sieber, A.; Blüthgen, N. Analysis of impedance-based cellular growth assays. *Bioinformatics*. 2015.
- [64] Moore, E.; Rawley, O.; Wood, T.; Galvin, P. Monitoring of cell growth *in vitro* using biochips packaged with indium tin oxide sensors. *Sensors Actuators B Chem.* 2009, 139, 187–193.
- [65] Li, Z. L.; Wang, Z. J.; Wei, G. H.; Yang, Y.; Wang, X. W. Changes in extracellular matrix in different stages of colorectal cancer and their effects on proliferation of cancer cells. *World J. Gastrointest. Oncol.* 2020.
- [66] Croce, M. V.; Colussi, A. G.; Segal-Eiras, A.; Price, M. R. Identification and Characterization of Different Subpopulations in a Human Lung Adenocarcinoma Cell Line (A549). *Pathology and Oncology Research* 1999, 5, 197-204.
- [67] Hekmati, M.; Ben-Shaul, Y.; Polak-Charcon, S. A morphological study of a human adenocarcinoma cell line (HT29) differentiating in culture. Similarities to intestinal embryonic development. *Cell Differ. Dev.* 1990.
- [68] Biazik, J. M.; Jahn, K. A.; Su, Y.; Wu, Y. N.; Braet, F. Unlocking the ultrastructure of colorectal cancer cells *in vitro* using selective staining. *World J. Gastroenterol.* 2010.
- [69] Krause, S.; Maffini, M. V.; Soto, A. M.; Sonnenschein, C. The microenvironment determines the breast cancer cells' phenotype: Organization of MCF7 cells in 3D cultures. *MC Cancer*. 2010.
- [70] Hekmati, M.; Ben-Shaul, Y.; Polak-Charcon, S. A morphological study of a human adenocarcinoma cell line (HT29) differentiating in culture. Similarities to intestinal embryonic development. *Cell Differentiation and Development* 1990, 31, 207-218.
- [71] Mei, B. A.; Munteshari, O.; Lau, J.; Dunn, B.; Pilon, L. Physical Interpretations of Nyquist Plots for EDLC Electrodes and Devices. *J. Phys. Chem. C*. 2018.
- [72] Hossain, Z.; Kurihara, H.; Hosokawa, M.; Takahashi, K. Growth inhibition and induction of differentiation and apoptosis mediated by sodium butyrate in Caco-2 cells with algal glycolipids. *Vitr. Cell. Dev. Biol. – Anim.* 2005.
- [73] Hodin, R. A.; Meng, S. F.; Archer, S.; Tang, R. Cellular growth state differentially regulates enterocyte gene expression in butyrate-treated HT-29 cells. *CELL GROWTH Differ.* 1996, 7, 647–653.
- [74] Herz, A. S. F.; Halwer, M.; Bogart, L. H. Alkaline phosphatase in HT-29, a human colon cancer cell line: influence of sodium butyrate and hyperosmolality. *Arch Biochem Biophys.* 1981, 581–591.
- [75] Orchel, A.; Dzierzewicz, Z.; Parfiniewicz, B.; Węglarz, L.; Wilczok, T. Butyrate-induced differentiation of colon cancer cells is PKC and JNK dependent. *Dig. Dis. Sci.* 2005.
- [76] Joseph, J.; Mudduluru, G.; Antony, S.; Vashistha, S.; Ajitkumar, P.; Somasundaram, K. Expression profiling of sodium butyrate (NaB)-treated cells: Identification of regulation of genes related to cytokine signaling and cancer metastasis by NaB. *Oncogene*. 2004.

[77] Fiorino, A. S.; Zvibel, I. Disruption of cell-cell adhesion in the presence of sodium butyrate activates expression of the 92 kDa type IV collagenase in MDCK cells. *Cell Biol. Int.* 1996.

Chapter 7

Conclusions and Future Work

7.1. Conclusion

In this thesis, we have developed a methodology for measuring real-time ALP release from cells using electrochemical and impedance techniques. One of the main contributions of our work is to express these methods as cell-based strategies, and to propose methods to track cells viability based on optical assays. Different types of methods have been presented. Our contribution here is twofold. First, an experimental optimization of sample size and reagent concentrations has been performed. Second, electrochemical methods based on redox and impedance have been designed.

The main focus of this thesis was on the optimization itself. An approach based on an estimation of cell viability was introduced for quantifying cell numbers and to overcome the limitations of the endpoint assay. Its foundations rely on the reduction of salts (e.g. resazurin) during the metabolic activity of cells, which is an important part of cell adhesion-based applications. Our contribution here was to adapt concentrations of resazurin to the cell type and the size of sample. This, to our knowledge, has never been addressed before for the purposes of cancer biomarker release. In particular, we proposed a postconfluence culture for the differentiation of cells in order to induce the biomarker ALP. This contribution can certainly be exploited in other differentiation strategies, thereby enlarging the potential application field of resazurin-based assays in gene expression investigations.

Another contribution relates to the optical detection of ALP from embryonic and cancer cells using an absorbance technique. Our research resulted in an enzymatic assay suitable for ALP monitoring from mammalian cells and enabled comparison with other methods, including electrochemistry and capillary electrophoresis. From an experimental point of view, our contribution lies in the comparison of the performance of redox in both absorbance and electrochemistry. Our experiments were performed for the different types of cells. The use of the optimized conditions in absorbance allowed for better resolution of electrochemical findings. The kinetic enzyme assay has been detailed. A parallel investigation of this method was proposed using capillary electrophoresis. This contribution means that it is now possible to discriminate the isoenzyme of ALP by using selective inhibitors.

Finally, another contribution pertains to real-time ALP monitoring. For the purposes of our research, up-to-date fluorescence techniques were applied to ALP release from the MCF-7 of breast cancer, A549 of lung cancer, and HT-29 of colon cancer. Fluorescence-based assays are known for their limitation in integration in microdevices. The use of microelectrode arrays with electrochemical detection techniques contributes to the development of miniaturized devices. ALP release were analysed during differentiation of cells using a real-time impedance-based method. Specifically, electric cell-substrate impedance sensing was used to monitor and investigate cellular responses and cell morphology during enzyme release. These experiments were performed in order to examine the differentiation of the colon cancer cells by postconfluence culture and by using NaBt, and applying different detection techniques, including impedance, resazurin, microscopic images and amperometric detection techniques. Results showed that our approach indicated a correlation between ALP activity and cell differentiation, which was clearly indicated when using different concentrations of NaBt. The amperometric current (μA) obtained from concentrations of NaBt indicated increases in ALP activity. The resulting data from amperometry and

impedance can be used for optimizing the relationship between the amount of NaBt and the cellular response in order to determine the limits of detection.

7.2 Future work

7.2.1 Experiments of interests

Many different tests and experiments could not be performed due to time limitations (i.e., the experiments with cell cultures required days to finish a single test).

Future work could involve deeper analysis of the bioimpedance of cell tissue during ALP release using methods such as transfection. Transfection cells with a plasmid of dual promoter alkaline phosphatase (pSF-CMV-PGK-SEAP) can enhance ALP release. pSF-CMV-PGK-SEAP is a promoter of CMV that drives the gene of interest and promotes the terminating transcription at the same poly-adenylation signal, thereby allowing the expression of ALP (Figure 7.1). Briefly, this method involves seeding cells in the ECIS at a density of 40×10^3 cell/mL with routine media and allowing them to cultivate for three days to reach 70-90% confluence. On day 3, cells are transfected by the addition of 500 μ L of Opti-MEM I medium containing 5 μ g of plasmid CMV at different concentrations of the transfection reagent (e.g. Lipofectamine Reagents). This is followed by incubation for several hours. The transfection medium is then changed to a routine medium, and the cells are incubated at 37 °C for one or two more days. Untreated cells are used as a control, and dead cells are used as a vehicle control.

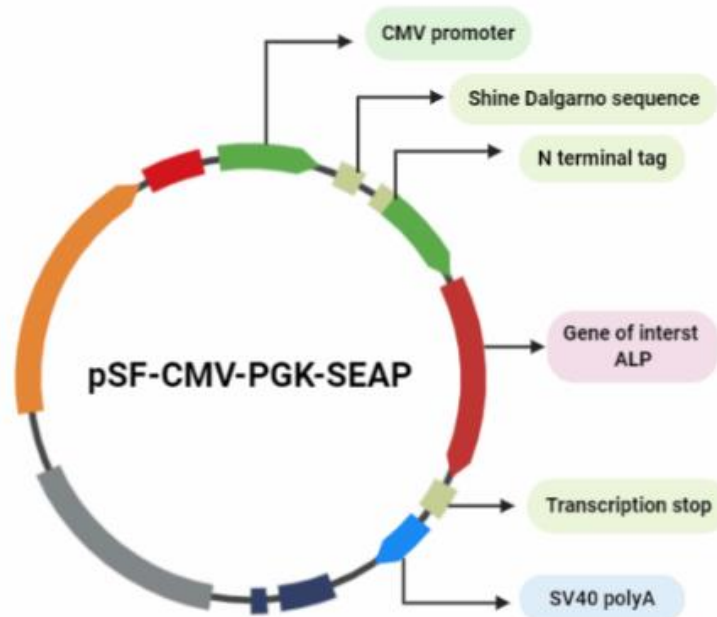


Figure 0.1: Expression vector of alkaline phosphatase (pSF-CMV-PGK-SEAP) predicting the location of the promoter CMV and the gene of interest ALP.

There are a number of ideas that I would like to have tried during the description of ALP release in capillary electrophoresis. These include using an incubated buffer assay, monitoring the enzyme reaction inside capillaries and applying selective inhibitors. Other ideas, such as using cytotoxicity assay inside the capillary, would be a great challenge. It is hypothesised that the aloe vera plant can inhibit ALP release.

We obtained preliminary data that shows aloe vera can inhibit ALP enzyme in the MCF-7 cell line. This data was part of one of the 4th year project. The aloe vera plant was extracted in methanol at cold for 2 days using rotary evaporation (Figure 7.2). The extraction was dissolved in DMSO at a final stock solution of (100 mg/mL). The stock solution was further filtered using a syringe of 0.45 nm pores before using stock solution in the cell culture. Two concentrations were used as an optimal (0.001 μ L) and (0.0001 μ L) for cytotoxicity measurements. The higher concentration affected cell viability. The cells were seeded in a 48well plate at a density of 40×10^3 cell/mL of EMEM medium containing 10% FBS. Cells were cultivated in a 48-well plate for three days to reach 70-90% confluence. On day 3 cells were cytotoxic due to the addition of (0.001 μ L) and (0.0001 μ L) of extraction to routine media. This was followed by incubation for 24 hours. The cytotoxicity medium was changed to a routine medium, and the cells were incubated at 37 °C with resazurin for cell viability assay. The others were in a parallel plate and had their cells tested for ALP enzyme activity. Untreated cells were used as control. The vehicle control had dead cells. Microscope images of cells adhering to the 48-well plate were taken in order to investigate the morphology of cells during ALP release. The cells displayed different shape, which described in the same project of the 4th year student. It is thought that more investigation is needed to verify the effect of aloe vera extractions on ALP enzyme.

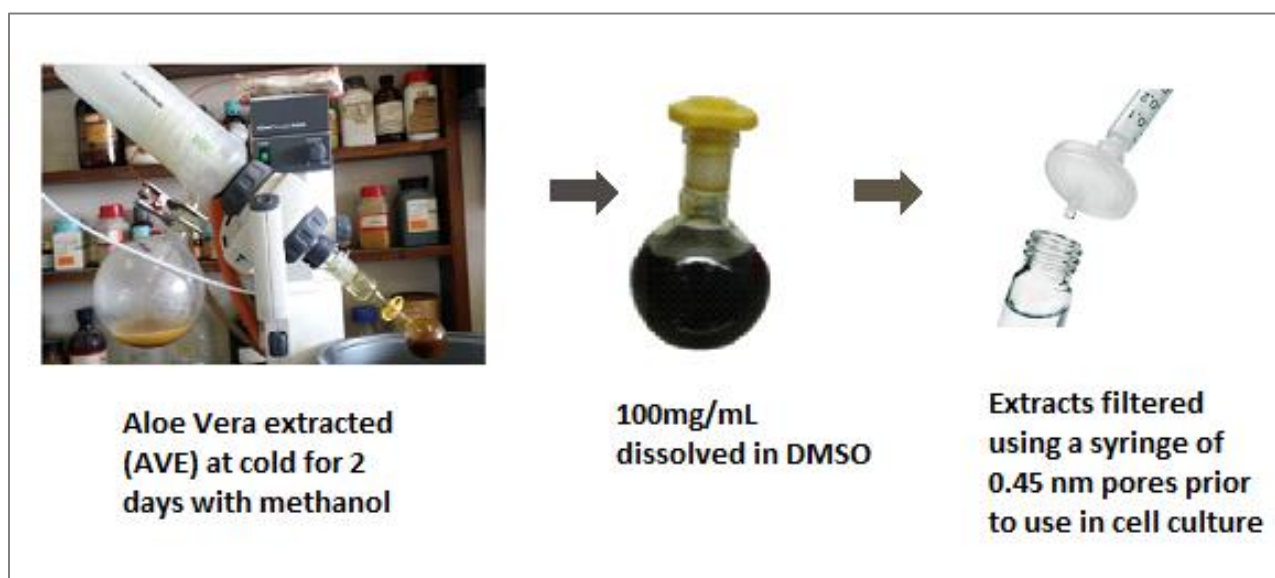


Figure 0.2: steps of Aloe vera extraction (AVE).

7.2.2 Cells models and three-dimension cell culture:

This thesis has mainly focused on differentiation in embryonic and cancer cells lines for releasing the ALP biomarker. Most of the differentiation discussed in the literature focuses on investigating the mineralization of one cell line (e.g., osteoblasts cells). It would be interesting to consider differentiation in osteoblasts cells and to collect data and images relating to cell size or function with respect to stage of differentiation.

These types of cells are the perfect model for investigations relating to differentiation [1]. Moreover, the three dimensions (3D) of cell culture attract much research today. Resazurin assays are now being optimized for applications used 3D cell culture model [2] [3] [4].

7.2.3 Nanomaterials

For the determination of ALP using amperometry, there are also many ideas that could be exploited to obtain an effective convergence towards the best solution. An example of this is the use of enzyme-linked immunosorbent assay, which is the standard method. Using specific anti-ALP immobilized on electrodes' surfaces can selectively detect ALP release in media and allow free-label techniques. Mintz et al. (2018) created an electrochemical impedance device to detect ALP in a phosphate buffer saline (PBS) solution by using anti-ALP functionalized silver nanowires (SiNWs). A three-electrode cell was used to measure electrochemical impedance where the electrode functioned as a highly disordered and very dense array of SiNWs. The device was highly efficient, selective, and sensitive in detecting very low ALP concentrations in PBS solution ranging 0.03–0.3 U/L. In addition, it was highly sensitive to antigen and antibody interactions. The high selectivity and sensitivity means that the device provides an effective approach for quantitative sensing and real-time detection of ALP [5]. Simão et al. (2018) integrated CNTs within osteointegration implants and found increased ALP mineralization activity detection using these implants. The device can rapidly detect ALP within blood serum, by immobilizing the covalent anti-ALP antibody towards ALP. The biosensor showed excellent performance, with two linear ranges from 0.5 to 50 IU/L and from 100 to 600 IU/L and limits of detection which ranged from 0.25 to 84.6 IU/L, respectively [6]. Nanomaterials can also be exploited in paper based analytical devices (PADs) for ALP release. Pandey et al. (2018) presented a platform for detecting ALP levels using -MoO₃-x nano-flakes and zinc oxide. Once ALP is introduced to the complex, there is a rapid transformation of blue -MoO₃-x to colourless -MoO₃ using zinc as a cofactor. The sensitivity level was found to be 0.1 M of enzyme concentration and allowed detection by the naked eye [7].

7.2.4 Microelectrode arrays

In vitro microelectrode array technology has evolved into a widely used and effective technique in studying cultured cells. Ino et al. have previously reviewed the bioelectrochemical applications of these technologies [8]. The way the ECIS is constructed in this thesis could also be changed - Instead of using eight wells with 1.96 mm² working area of electrode surface/ well, a smaller size well with the same working area of electrodes could be used (Figure 7.3). Such a study could reveal whether cell adhesion, growth and proliferation are affected by size [9] [10]. The limitations of commercial ECIS mean that exploiting three-dimensional (3D) printing technology is of significance. This technology provides low-cost platforms and a novel approach to biological material for *in vitro* applications [11]. Moreover, it is important to use a microscope with a high resolution light in order to monitor the very tiny changes inside cells.

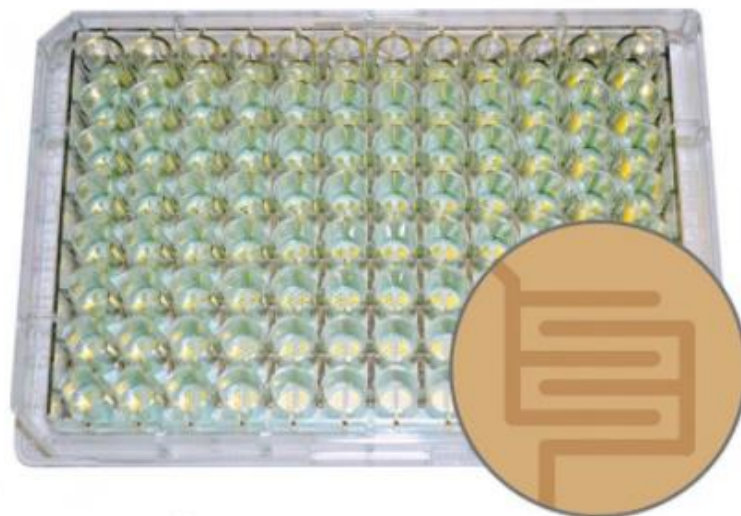


Figure 0.3: Electric cell-substrate impedance sensing cultureware (1.96 mm^2 electrode surface/well).

7.2.5 Lab on chip

The development of lab-on-chip sensors has been undertaken to enhance ALP detection in cell cultures. Lab-on-chip approaches can provide good selectivity and portable detection. Besides, the chip limits the interferences and can therefore be used in ALP detection assay in complex samples. These devices are digital, and examples include using a smartphone camera to sense ALP enzymes in one single cell. Cao et al. (2018) created a simple electrophoresis titration (ET) device for ALP detection by using a reaction boundary (MRB). In this model, ALP accelerated the dephosphorylation of the 4-methylumbelliferyl phosphate disodium salt substrate in the cathode and 4-methylumbelliferone (4-MU) with blue fluorescence and negative charge under UV excitation. The 4-MU moved under the electric field into the channel. This process resulted in the neutralization of the acidic Tris-HCl buffer, thereby creating MRB and quenching 4-MU. The sensitivity of the device was high at 0.1 U/L, and the results were better than the ones obtained from chemiluminescence, electrochemical, and colorimetric methods for ALP assays. The sensitivity of the ET technology was good (0.1 U/L), linearity ($V = 0.033A + 3.87$, $R^2 = 0.9980$), with relative standard deviation of about (2.4% to 6.8%) and recoveries (101% to 105%). The technology was successfully used to detect ALP in serum samples [12]. Sun et al. (2019) explored a new technique for investigating a low abundance of ALP created through individual cells through the use of a microfluidic droplet-based SERS method. The researchers first created a co-flow drop-maker model in which they suspended cells in a solution using BCIP as an enzymatic substrate and AuNPs as a signal agent to encapsulate individual cells in the drops. The difference between normal liver cell lines (BNL.CL2) and hepatocellular carcinoma cell lines (HepG2) was compared in terms of their ALP expression. It was observed that normal liver cells had 40% lower ALP expression than hepatocellular carcinoma (HepG2). The results also revealed that the ALP activity of droplet-isolated cells fluctuate in a large range compared to cluster cells, even if the overall ALP expression of the two cases was similar. An ultrasensitive high output analytical process was realized for ALP detection using a single cell SERS-based microfluidic droplet method [13].

7.3 References

- [1] Hu, C.; Ashok, D.; Nisbet, D. R.; Gautam, V. Bioinspired surface modification of orthopedic implants for bone tissue engineering. *Biomaterials*. 2019.
- [2] Tapias, L. F.; Gilpin, S. E.; Ren, X.; Wei, L.; Fuchs, B. C.; Tanabe, K. K.; Lanuti, M.; Ott, H. C. Assessment of Proliferation and Cytotoxicity in a Biomimetic Three-Dimensional Model of Lung Cancer. *Ann. Thorac. Surg.* 2015, 100, 414–421.
- [3] Uzarski, J. S.; DiVito, M. D.; Wertheim, J. A.; Miller, W. M. Essential design considerations for the resazurin reduction assay to noninvasively quantify cell expansion within perfused extracellular matrix scaffolds. *Biomaterials* 2017, 129, 163–175.
- [4] Uzarski J. S.; Bijonowski, B. M.; Wang, B.; Ward, H. H.; Wandinger-Ness, A.; Miller, W. M.; Wertheim, J. A. DualPurpose Bioreactors to Monitor Noninvasive Physical and Biochemical Markers of Kidney and Liver Scaffold Recellularization. *Tissue Eng. Part C Methods* 2015, 21, 132–1043.
- [5] Mintz Hemed, N.; Convertino, A.; Shacham-Diamand, Y. Alkaline phosphatase detection using electrochemical impedance of anti-alkaline phosphatase antibody (Ab354) functionalized silicon-nanowire-forest in phosphate buffer solution. *Sensors Actuators B. Chem.* 2018, 259, 809–815.
- [6] Simão, E. P.; Frías, I. A. M.; Andrade, C. A. S.; Oliveira, M. D. L. Nanostructured electrochemical immunosensor for detection of serological alkaline phosphatase. *Colloids Surfaces B Biointerfaces* 2018, 171, 413–418.
- [7] Pandey, S.; Sharma, A. K.; Sharma, K. H.; Nerthigan, Y.; Khan, M.S.; Hang, D. R.; Wu, H. F. Rapid naked eye detection of alkaline phosphatase using [alpha]-MoO₃-x nano-flakes *Sensors Actuators B. Chem.* 2018, 254, 514.
- [8] Ino, K.; Shiku, H.; Matsue, T. Bioelectrochemical applications of microelectrode arrays in cell analysis and engineering. 2017, 5, 146–151.
- [9] Subramani, K.; Lavenus, S.; Rozé, J.; Louarn, G.; Layrolle, P. Impact of nanotechnology on dental implants. *Emerging Nanotechnologies in Dentistry: Second Edition*. 2018.
- [10] Surmenev, R. A.; Surmeneva, M. A. A critical review of decades of research on calcium phosphate-based coatings: How far are we from their widespread clinical application? *Current Opinion in Biomedical Engineering*. 2019.
- [11] Foo, C. Y.; Lim, H. N.; Mahdi, M. A.; Wahid, M. H.; Huang, N. M. Three-Dimensional Printed Electrode and Its Novel Applications in Electronic Devices. *Sci. Rep.* 2018.
- [12] Cao, X. Y.; Kong, F. Z.; Zhang, Q.; Liu, W.W.; Liu, X. P.; Li, G. Q.; Cao, C. X. iPhone-imaged and cell-powered electrophoresis titration chip for the alkaline phosphatase assay in serum by the moving reaction boundary. *Lab Chip* 2018, 18, 1758–1766.
- [13] Sun, D.; Cao, F.; Cong, L.; Xu, W.; Chen, Q.; Shic, W.; Xu, S. Cellular heterogeneity identified by single-cell alkaline phosphatase (ALP) via a SERRS-microfluidic droplet platform. *Lab Chip* 2019, 19, 335–342.

Appendix

A.1 Modules

PG6001 - STEPS Scientific Trng for Enhanced PG Studies (2016)

PG6009 - Graduate Information Literacy Skills (2016)

PG7003 - The PhD II: From Development to Completion (2016)

ST6013 - Statistics and Data Analysis for Postgraduate (2017)

PG6026 - Teaching & Demonstrating, SEFS (2017)

A.2 Publication and conference attendance

1. Peer reviewing paper

Balbaied, T. and Moore, E. (2020). Real-time Impedance Analysis of Alkaline Phosphatase (ALP) Release by Microelectrode Arrays. *Aanalytical letters*.

2. Publication:

Balbaied, T. and Moore, E. (2020). Electrochemical detection and capillary electrophoresis; comparative studies for alkaline phosphatase (ALP) release from living cells. *Biosensor*, 10(8), 95. DOI.org/10.3390/bios10080095

Balbaied, T. and Moore, E. (2020). Resazurin-Based Assay for Quantifying Living Cells during Alkaline Phosphatase (ALP) Release. *Applied Sciences*, 10(11), 3840. DOI: 10.3390/app10113840

Balbaied, T. and Moore, E. (2019). Overview of Optical and Electrochemical Alkaline Phosphatase (ALP) Biosensors: Recent Approaches in Cells Culture Techniques. *Biosensors*, 9(3), 102. DOI: 10.3390/bios9030102

3. Conference paper

Balbaied, T., Messina, W. and Moore, E. (2018) Development of real-time monitoring of alkaline phosphatase (ALP) biomarker released from cells based on microelectrode arrays for clinical analysis. IMCS 2018-17th International Meeting on Chemical Sensors, Vienna, Austria, 15-19 July. DOI: 10.5162/IMCS2018/EC1.2

4. Oral presentation

Balbaied, T and Moore, E., (2019) Quantitative resazurin assay of cell viability for release alkaline phosphatase (ALP). 71 st Irish Universities Chemistry Research Colloquium, Dublin, Ireland 20-21 June

Balbaied, T., Messina, W. and Moore, E. (2018) Development of real-time monitoring of alkaline phosphatase (ALP) biomarker released from cells based on microelectrode arrays for clinical analysis. IMCS 2018-17th International Meeting on Chemical Sensors, Vienna, Austria, 15-19 July.

Appendix

5. Posters

Balbaied, T and Moore, E., (2018) Real-time monitoring of alkaline phosphatase (ALP) released from cells based on microelectrode arrays (μ EAs) for clinical analysis. The 9th conference in analytical sciences (CASI) Maynooth, Ireland ,16-17 May

Balbaied, T (2017) Comprehensive learning outcomes based on pedagogical framework. Postgraduate Students Symposium, Teaching and Demonstrating Skills for College of Science, Engineering and Food Science (SEFS) at University College Cork. 24 April

Balbaied, T and Moore, E., (2016) Development of sensor arrays to monitor alkaline phosphatase released from cells. 8th Conference on Analytical Sciences, Dublin, Ireland, 14-15 April.

A.3 Workshops

1. How to Plan Your PhD, 23rd Feb 2016, Brookfield Health Science building, UCC, Cork, Ireland. This workshop helped me a lot in planning my PhD project. It gave me idea how to set daily, monthly and mid-term objectives to meet the annual aims.

2. PhD Workshop: Turbocharge your writing, 22rd Feb 2016, Brookfield Health Science building, UCC, Cork, Ireland. This workshop let me recognise the small details in writing PhD thesis.

3. The Seven Secrets of Highly Successful Research Students, 23 Jan 2017, Brookfield Health Science building, UCC, Cork, Ireland. This workshop clarified the steps of presenting the lab report to a publishing paper.

4. NOVA Metrohm software. 21 st Jun 2017, Metrohm Ireland Ltd, Carlow. I needed this course as I had to use NOVA Metrohm software during my PhD project.

5. Getting the best data from your cells: From tissue culture to final analysis, 3 rd May 2017, WEBINAR, online.

6. Entrepreneurship Opportunities for PhD's & Post-Docs, 17 Jan 2020, Lapp's Quay, Centre for Executive Education, Lapps Quay, Cork, Ireland. This course gave me more knowledge to come up with business ideas and develop my own venture.

Overview of optical and electrochemical alkaline phosphatase (ALP) biosensors: Recent approaches in cells culture techniques

Thanih Balbaied ¹ and Eric Moore ^{1,*}

¹University College Cork, Sensing & Separation Group, School of Chemistry and life Science Interface, Tyndall National Institute, Ireland.

*Correspondence: e.moore@ucc.ie

Received: date; Accepted: date; Published: date

Abstract: Alkaline phosphatase (ALP), which catalyzes the dephosphorylation process of proteins, nucleic acids, and small molecules, can be found in a variety of tissues (intestine, liver, bone, kidney, and placenta) of almost all living organisms. This enzyme has been extensively used as a biomarker in enzyme immunoassays and molecular biology. ALP is also one of the most commonly assayed enzymes in routine clinical practice. Due to its close relation to a variety of pathological processes, ALP's abnormal level is an important diagnostic biomarker of many human diseases, such as liver dysfunction, bone diseases, kidney acute injury, and cancer. Therefore, the development of convenient and reliable assay methods for monitoring ALP activity/level is extremely important and valuable, not only for clinical diagnoses but also in the area of biomedical research. This paper comprehensively reviews the strategies of optical and electrochemical detection of ALP and discusses the electrochemical techniques that have been addressed to make them suitable for ALP analysis in cell culture.

Keywords: Alkaline phosphatase (ALP); optical biosensors; electrochemical biosensors; nanomaterials; microarrays technology; Lab-on-chip technology

1. Introduction

The detection of alkaline phosphatase (ALP) was commenced in the late 19th century, and was recognized as an enzyme family after Robison's contributions in 1932 [1]. McComb et al. (1979) summarized several attempts by scientists for the detection of ALP and displayed several topics that are of significance for multidisciplinary researchers [1]. The primary importance of detecting ALP is to identify the possibility of diseases and carry out immediate preventive or treatment operations [2]. In point of care applications, ALP is known to be measured in routine blood tests with high levels of serum considered as indications of bone disease, liver disease, or bile duct obstruction and recently appears to be a significant independent prognostic biomarker for indicating cancers [3,4,5,6,7,8,9,10,11,12]. ALP levels have various reference ranges depending on age, gender and patient history. ALP can be defined as an enzyme that liberates phosphate under alkaline conditions and is made in the liver, bone, and other tissues [13].

The X-ray crystallography technique characterizes ALP by obtaining a three-dimensional structure of the enzyme under study through diffracting its crystallized form [14]. Fersht et al. discusses how the three-dimensional structure is crucial in determining the functionality of the molecules. On the other hand, nuclear magnetic resonance technique uses energy transitions through a range of wavelengths. This technique characterizes enzymes by making a difference in the spectrum which appears in the strength of the electromagnetic field around the nucleus [14]. The approach thus provides an extended shift of efficiency allowing the determination of which type of atom or particles about their specific environment, thus, respective characteristics can be derived. Figure 1 illustrates that ALP is a homodimeric enzyme shaped in two monomers (A and B) where the central core of ALP (active sites) is formed by the link of the

two monomers. The author elaborates that this property allows it to reach a stable heating capacity with a maximum capacity at very high pH [14]. Similarly, an active site found on the enzyme where one magnesium and two zinc ions located has the function of acting as a catalyst site. This occurs when Mg^{2+} and Zn^{2+} activate and inhibit, respectively, protein tyrosine phosphatase 1B (PTP1B). Millan describes the occurrence as molecular dynamics simulations, metadynamics, and quantum chemical calculations in combination with experimental investigations demonstrate that Mg^{2+} and Zn^{2+} compete for the same binding site in the active site only in the closed conformation of the enzyme in its phosphorylated state [15]. At this point, the cations have different effects on hydrolysis resulting in a difference in the establishment of the structural enzymology PTP1B.

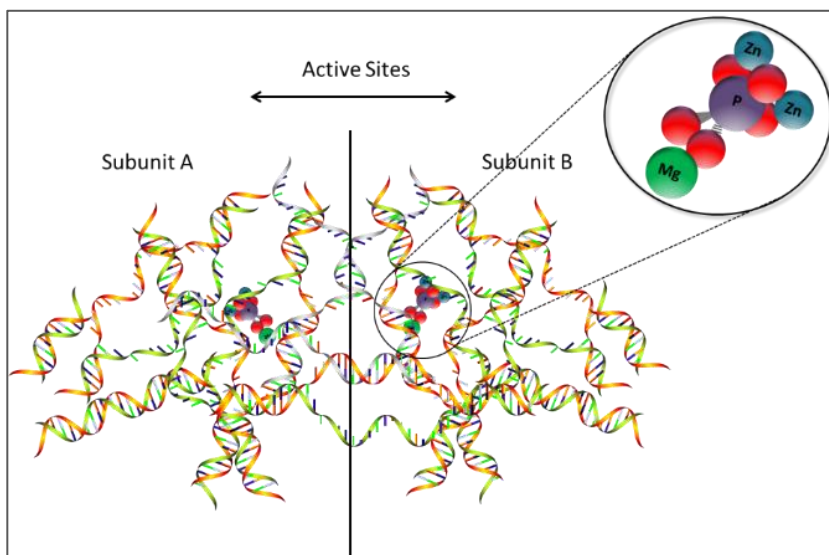


Figure 1. Illustrates the 3D structure of ALP shaped in two monomers (A and B). The central core of ALP (active sites) is formed by the link of the two monomers. The metals position in the edge of both monomers (red). In the licorice representation, the inorganic phosphate and metal ions are presented [16].

Details of ALP isoenzymes and their test regarding their physical and chemical properties are discussed below. Furthermore, we have discussed some point taken into account the methods of discriminating between those isoenzymes.

2. ALP isoenzyme and tests

Mammalian ALPs are present as different isoenzymes. Figure 2 shows the main four isoenzymes of ALP, which are germ cell alkaline phosphatase (GCAP), intestinal alkaline phosphatase (IAP), placental alkaline phosphatase (PLAP) and tissue-nonspecific alkaline phosphatase (TNAP). GCAP, IAP and PALP, are located in chromosome 2, whereas TNAP is located in chromosome 1—all of which their precise physiological and neoplastic functions are unknown. However, TNAP was found to be responsible for calcification in bone and concern regarding regulating the secretory activities in liver, but as mentioned earlier their main function still unidentified. ALP isoenzyme can be referred to as a biomarker for cancer before a tumor is formed. Fishman (1980) contends that PLAP is sometimes found in individuals with ulcerative colitis or polyposis of the colon, and it is through this that they enhance the capability of acquiring cancer [17]. Bukowczan et al. also examined that PLAP has a relationship with different tumors such as renal cell carcinoma (RCC) [18].

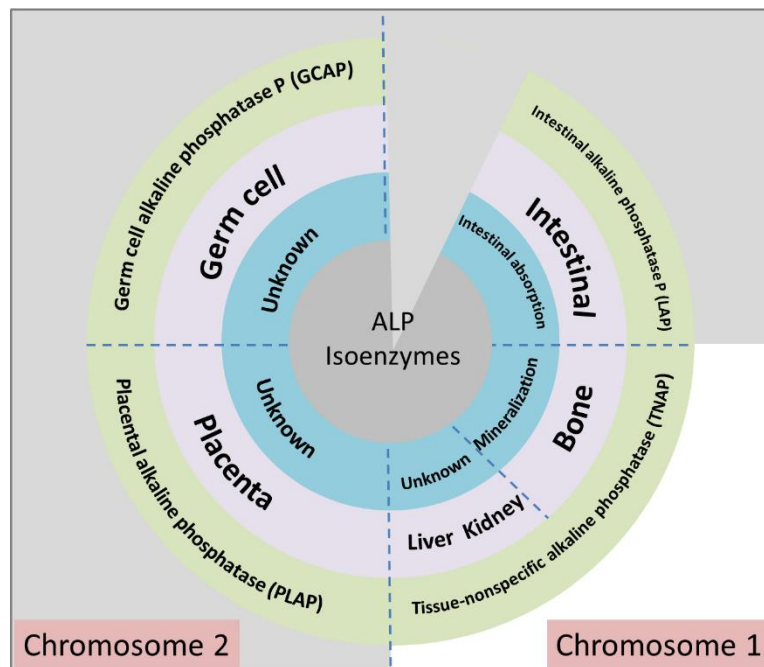


Figure 2. ALP isoenzyme with common names, place function limitation [19].

Some physical and chemical properties are considered when discriminating between isoenzymes. Webster points out that the concentration of cysteine and histidine which inhibits alkaline phosphatase activity and the phosphotransferase activity of different isoenzyme preparations are similar [13]. Other physical and chemical properties include heat stability at 56°, electrophoretic mobility, and the concentrations of Zn ions, l-phenylalanine, and l-tryptophan required to inhibit enzyme activity by 50% are different. This variety was exploited to discriminate ALP isoenzyme. Some traditional methods depend on deactivating ALP, such as using selective inhibitors (e.g., l-phenylalanine, l-homoarginine, levamisole) or heat treatment. The classic approach is to heat the serum of ALP up to 56 °C for 10 min to distinguish between liver and bone ALP, for example. Whereas the other methods such as electrophoretic, isoelectric focusing and lectin-based rely on sieving media or non-sieving media. These methods use polyacrylamide, agarose gel, or the wheat-germ lectin for limiting the mobility of ALP isoenzymes in buffers. Moreover, separation-based methods are conducted to distinguish ALP isoenzymes, and are occasionally coupled with other techniques to give quantity of ALP. For example, chromatography methods such as affinity chromatography [20] have been applied to distinguish ALP isoenzymes and are occasionally associated with solid-phase immunoassay to give data of ALP levels. This method is still insufficient, although optimized by using wheat germ agglutinin (WGA) conjugate to the silica particle [21]. Liquid chromatography is applied instead with different anion exchange [22]. Per et al. used weak anion exchange to determine and separate ALP isoenzyme [23]. This assay improves sensitivity and selectivity over electrophoresis methods. However, the temperature for the analytical column must be strictly controlled, otherwise retention times and peak heights will be affected. These separation methods however, although useful as a research tool, have limited applications in the routine clinical laboratory.

Due to the complicated nature of ALP in terms of its physical and chemical properties and the fact that it has various levels between people and isoenzymes that indicate related diseases, particular expression systems are required to express ALP and makes it detectable *in vitro* assays, which will be expanded upon in the next section.

3. 3. ALP secretion system

There are many expression systems for proteins including mammalian cell, bacteria and yeast. Among them, mammalian cells help in the folding of proteins, post-translational modifications and product assembly, which all are important in harnessing mammalian cells for protein production [24]. In addition, mammalian cells have proved to be well suited with an efficient expression system that leads to good productivity due to containing glycosylation, which is required for secretion and stability. However, a mammalian cell is more complex and costlier than other expression systems such as bacteria and yeast. ALP is located in the membrane of mammalian cells and is found to be in periplasmic space of *E. coli* bacteria [2]. Figure 3 shows that ALP is made in the nucleus. Then formed to protein in endoplasmic reticulum (ER) and in Golgi body formed as an isoenzymes. These processes are all under natural pH. ALP is then bonded to a cell membrane where the pH is 7.5. This pH does not allow ALP to induce unless the environment surrounding it rises to an alkaline pH. For example, during cell metabolism or necrosis inflammation where HCO_3^- raises causes an increment of alkalinity in the cell membrane, thus activating ALP [25].

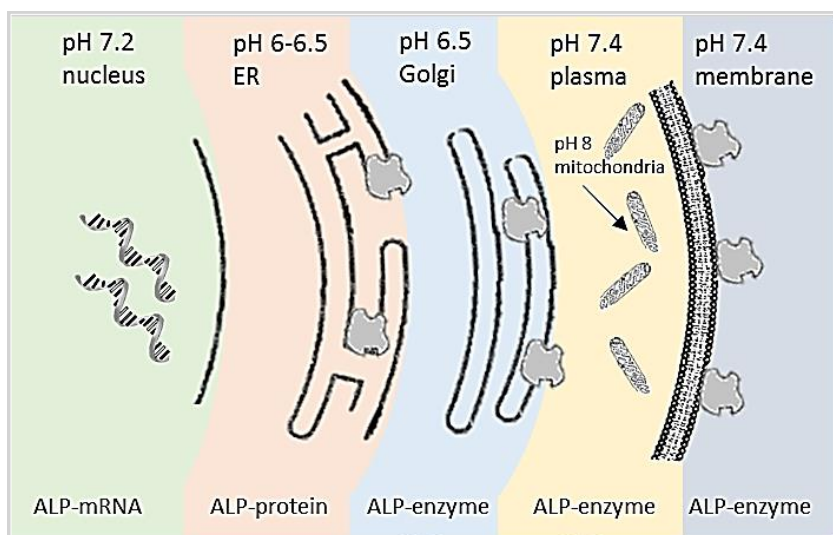


Figure 2. ALP produced in each stage in cells [26].

The technique of cell culture is efficient to study the physiological effect of ALP *in vitro* assays and develop cancer research. Cell culture is the technique of extracting cells from a living organism and growing them in an artificial environment producing cells lines simulating cancer *in vivo* [27]. The number of cell lines are ever increasing and this has attracted the need for finding the right model for cancer. For example, A549 cell lines investigated many biomarkers in lung cancer includes C4b-binding protein [28], microRNAs [29], volatile biomarkers for apoptosis and necrosis [30] and ALP biomarker—which was significant in modulating A549 cell phenotype [31]. MCF-7 cell line was developed about 48 years ago with about 25,000 published reports, making it the most published cell line after the HeLa cell line, which has about 80,000 publications. MCF-7 studied many biomarkers such as P glycoprotein [32], doxorubicin-resistant [33] and 52 K glycoprotein [34] ALP [35]. HT-29 cell lines can express brush border linked to hydrolases which are common in the small intestines, though they have a lower enzymatic activity than that of *in vivo* cells. Ht-29 received a lot of interested in food digestion and bioavailability [36,37,38], the transport of drugs and food, immune response, adhesion and invasion of microorganisms [39] and diagnosing ALP as biomarkers in each stage of colon cancer [12] as well as studying the regulation of ALP [40].

There are various ions across lipid membranes in cells where ALP was found to be conducted due to the membrane permeability for K⁺ [41]. Along similar lines, Gerlach et al. argued that the membrane conductance of ALP is a calcium-dependent potassium channel (hIK1) [42]. Another study by Bo Yang et al. suggested that the calcium activated chloride channel A1 (CLCA1) may regulate the transition from proliferation to differentiation in colon cell lines; Caco-2 cells [43]. Another study found that ALP affected the concentration of calcium ion [44]. Patch-clamp and RT-PCR approaches help understand the functional and molecular expression of voltage-operated calcium channels [45]. As such, the researchers investigated whether voltage-operated calcium channels play a role in osteogenic differentiation of human bone marrows. Results revealed that mRNA for pore-forming 1C and 1G subunits of T-type and L-type Ca²⁺ channels were found to be present in comparable amounts in cells cultured in maintenance medium. The techniques were also found to be effective in detecting progressive bone mineralization of increased activity of ALP. Macrae et al. explored techniques for using synthetic derivative gramicidin A for the ion-channel forming peptide [46]. The device was developed to report variations in the local environment to external stimuli. The results revealed that gramicidin A ion channels give substantial detection for changes in ALP concentrations and environmental alterations.

A number of approaches have been extensively developed to understand the gene expression of ALP *in vitro* diagnostic tests where the reason for causing diseases as well as tracking the effectiveness of pharmaceuticals was unveiled. Therefore, accurate quantification of ALP level provides a signature of ALP function and gives a better understanding about the prognostic level of ALP in different cancers.

4. Traditional ALP methods

There are three main traditional methods that have been adopted to achieve better quantification of ALP level. Firstly, the fluorescence-based methods include flow cytometry, histochemical and immunohistochemical. The sample precipitate with substrates such as enzyme-labeled fluorescence-97 (ELF-97) phosphatase, naphthol phosphate, and menadiol diphosphate coupled with some of salts and dyes such as azo dye, diazonium salts and tetrazolium salts so as to produce insoluble colored products detected by fluorescence. These methods allow high sensitivity and fast detection. However, their expensive instrumentations hinder their convenient use alongside the need for highly skilled personnel [15,47,48].

Secondly, mRNA-based methods; northern blot [49] and a reverse transcriptase-polymerase chain reaction (RT-PCR) [50] can detect real-time ALP level. The former method is an old and classic method used to detect a specific isoform of ALP based on the level of its mRNA [49]. The RT-PCR approach is also based on RNA expression, but it combines with a single nucleotide primer extension assay to discriminate ALP isoenzymes [49].

Thirdly, immunoreaction-based method including western blot, radioimmunoassay (RIA), and enzyme-linked immune-sorbent assay (ELISA) have been conducted to gain more selectivity and sensitivity [51]. Western blot involves an electrophoretic sieving, which allows ALP separated by size and then the results transferred to a membrane producing bands. The membrane is incubated with labels of specific antibodies. This method, although sensitive, is time-consuming and has a high demand in terms of experience of the experimenter. Additionally, it requires multiple optimizations of the experimental conditions. In RIA, polyclonal are optimized to monoclonal antibodies to eliminate the cross reactivity. Thus, RIA is considered a method valid to detect ALP. RIA requires radioactive isotopes of iodine as an indicator. In such assay, a certain bead such as polystyrene coated with polyclonal rabbit anti-ALP are incubated with test samples and iodinated by chloramine—a radioactive compound—then, the radioactivity is counted by a gamma counter [52]. Although RIA is a sensitive method, it requires frequent preparation of radioactive antibodies as well as exposure to radiation hazards. Additionally, it require multiple steps for handle, storage, and disposal of radioactive materials.

One solution that succeeded to provide a similar sensitivity based solid phase and with no radiohazard is ELISA. In this technique, an enzyme conjugate and monoclonal antibodies are used. Colorimetric assay is then used in the presence of an appropriate chromophore (e.g., p-nitrophenyl phosphate) [53]. Although simple, this technique is a lab-based application [54]. In care-of-point application, ELISA based antibodies may cause false results [55]. For example, the human body can continue producing antibodies even though the person may have had the disease earlier and has recovered. In addition, some people are poor producers of an antibody or have some interfering substance in their blood, thus the amount of antibody may be too low to measure accurately or may go undetected. Cross reactivity may occur as a result of unrelated antibody reacts with the antigen non-specifically, thus bringing about positive signals for false reaction [56]. Another limitation with monoclonal antibodies is that immunoassays cannot identify the isoenzyme ALP [57,58].

Traditional methods mentioned earlier have some advantages, however; they are affected by requirements of multiple external controls for quantitative analysis as well as sequencing experiments to allow reliability. Additionally, a large sample volume, expensive instruments, and costly reagents are mostly needed. In addition, clinical ramifications need a simpler and more sensitive technique for testing of ALP expression.

Enabling high throughput technologies such as biosensors in point of care applications require some features such as portability, simplicity, and cost effective—all of which can be achieved through electrochemical methods. Literatures so far have developed methodologies for ALP detection in biological samples. For instance, Millan reviewed the use of conventional approaches in ALP analysis [15]. This paper is an updated version to solely cover for the available optical and electrochemical techniques for ALP detection. A brief outline of the recent advancements in optical detection strategies for ALP followed by electrochemical detection strategies are highlighted. More importantly, it was highlighted that recent technologies have been addressed to make each of the techniques suitable for ALP analysis in cell culture.

5. Optical detection techniques

The development of revolutionary technologies for imaging real-time events in living cells has been on the rise in the past decades. Today, enzymes have been put at work and optically acquired images have been significant in helping researchers to understand biological processes compared to abstract measurements [59]. Specifically, live-cell imaging with optical microscopy methods is powerful because they enable real-time detection of cellular processes [60]. Optical events are detected using bioluminescent and fluorescent probes that emit radiation at near-infrared or visible wavelengths, which are detected using optical cameras [60]. Optical methods have been used in detecting analytes because of their simple application. Cagnin et al. pointed out different optical techniques based on target labelling use radioisotopes, fluorophores, and UV-absorbing molecules. Fluorescence is used to elaborate molecular events results to light absorption when compounds such as polyaromatic hydrocarbons or heterocycles are used [61]. Upon being excited by light, these compounds can change their energy levels and decay from the excited state and in the process emit fluorescent light [61]. In comparison, some optical methods such as non-linear optical sensing techniques and optical tomography and spectroscopy are based on label free detection where detection is achieved through nonpolar reactions, polar reactions, ionic reaction, hydrogen bonding, and covalent binding [62].

The common optical assays of ALP determination are most likely fluorescence, chemiluminescence, Raman spectroscopy, infrared spectra and colorimetric as well as surface plasmon resonance—all of which are expanded upon in the next section.

5.1. Fluorescence methods

Fluorescence methods involve the use of fluorophore which is excited by energy light. Ejected electrons are transitioned within a molecule from ground state to an excited state. When the electrons relax,

they fall to the lowest energy level emitting their energy into an emitted photon [61]. Fluorescence methods offer advantages such as being simple, specific and fairly sensitive and can detect low quantities in samples as well. Unfortunately, the fluorescence technique is limited to samples that are able to emit light [59,61]. Many strategies in fluorescence methods have been widely used in ALP detection involve real-time, label-free, affinity principle, and developing probes.

Deng et al. (2015) demonstrated a simple and effective radiometric fluorescent technique used in real-time detection of ALP based on stimulus-responsive coumarin@Terbium-guanine monophosphate nanoparticles [63]. The technique is real-time, sensitive, and robust as it has double signal response read-out with linear detection limits for ALP ranging from 0.025–0.2 U/mL. Qian et al. (2015) developed a label-free real-time fluorometric assay for highly sensitive ALP detection based on aggregation and disaggregation of CQDs using Cu²⁺ [64]. The presence of carboxyl groups on the CQDs enables aggregation due to fluorescence quenching by copper ions, with subsequent interaction among PPI, copper ions, and carboxyl initiating disaggregation inducing fluorescence emission. The new techniques can quantitatively detect ALP to high sensitivity levels of up to 1.1 U/L in human serum. Liu et al. (2016) designed a new fluorescence turn-on sensing technique for ALP activities based on the variations of graphene oxide (GO) affinity with double stranded DNA (dsDNA) and single-stranded DNA (ssDNA) coupled with λ exonuclease cleavage [65]. The new method exhibits high sensitivity to ALP with detection limits of 0.19 U/L – which is high enough in the practical determination of ALP in human serum. Qu et al. (2017) developed a single-step hydrothermal treatment of the *Sterculia lychnophora* seed with strong blue luminescence and water solubility [66]. The synthetic technique was found to be facile without post-treatment or complex techniques. The CDs-MnO₂ nanocomposite as used as a new sensing probe for label-free and sensitive detection of ALP with its detection limit being as low as 0.4 U/L. The findings from these studies suggest that fluorescence assays can have an effect on *vivo* assays for real-time ALP detection. Chen et al. (2017) described a novel assay strategy for real-time detection of ALP *in vivo* based on the fluorescence quench-recovery technique at physiological pH using boron-doped GQDs as a fluorophore and ATP as a substrate [67]. The assay is able to discriminate ALP expression in cells up to very low concentrations of 10 ± 5 cells mL⁻¹.

5.2. Chemiluminescence methods

Chemiluminescence methods are based on the emission of light (luminescence) from a sample being investigated as a result of a chemical reaction. The luminescence reagent is continuously added to the sample and mixed with the column eluate in the mixer. The resulting luminescence from the chemical reaction is then measured using a photomultiplier tube when the luminescence raises to its highest intensity [68]. The advantages of chemiluminescence methods are limited to high sensitivity, broad dynamic range, and applicability over a broad spectral range, although during detection impurities can cause nonspecific background signals that degrade its sensitivity. The effectiveness of this assay may be seen in the strength of chemiluminescent. Sasamoto et al. (1995) studied the application of lucigenin as a chemiluminescent reagent in enzymatic activity assay for ALP detection [69]. The reagent reacted with hydrogen peroxide and phenacyl phosphate as a substrate for ALP detection. The phenacyl alcohol created an enzyme-catalyzed reaction with lucigenin giving luminescence with a detection limit of 3.4×10^{-1} mol and can be applied in enzyme immunoassays. Ximenes et al. (1999) developed hydrolytic action upon disodium (2-methyl-1-propenyl)phosphate (Na₂MPP) to detect ALP activity [70]. The Na₂MPP releases enol from isobutyraldehyde and is oxidized to HRP/H₂O₂ system producing chemiluminescence. The limit of detection (LOD) was 1.5 femtomole of ALP per assay, which is at the same range as other chemiluminescent methodologies. Kokado et al. (2002) developed a simple and sensitive chemiluminescent assay (CL) for ALP detection using dihydroxyacetone phosphate [71]. ALP hydrolyzation transformed new substrates to dihydroxyacetone, which reacted with lucigenin producing strong chemiluminescence. Under optimal conditions, the limits of detection were 3.8×10^{19} and 1.5×10^{-18} moles of ALP. When applied to enzyme

immunoassay of 17β -oestradiol, the proposed CL method had a measurable range of 15–4000 pg/mL with four times more sensitivity compared to colorimetric assay for ALP when 4-nitrophenyl phosphate was used as the substrate. Overall, these strategies support the view that chemiluminescence methods can detect ALP in real-time. Meng et al. (2005) developed a new system for continuous and real-time monitoring of cross-talk between mesangial and macrophage cells in *ex vivo* and *in vitro* [72]. The technique provides simple and reliable tools for monitoring mesangial cells and macrophages which can be applied in the therapeutic management of infiltrating leukocytes and resident glomerular cells.

5.3. Raman spectroscopy

Raman spectroscopy is based on the light scattering technique known as the Raman Effect. The Raman Effect relies on a fraction of small scattered radiation, which is different from the frequency of monochromatic incident radiation when incident radiation interacts with vibrating molecules. The scattered radiation gives information about the molecular structure of the sample. The laser line is used as the reference point with the peak measured as a shift from the laser line using vibrational energies associated with bonds in the molecules [73]. The advantage of Raman spectroscopy relates to its capacity to require very small samples and can be used with gases, liquids, or solids. Samples can also be analyzed directly in blisters, bags, or bottles with no vacuum requirements. However, the disadvantages include the inability to detect alloys or metals and that the Raman Effect is weak, resulting in low sensitivity. Other disadvantages include equipment cost depending on their applications. A recent study reported by Cottat et al. (2017) supported the hypothesis that Raman spectroscopy can detect ALP [74]. They examined variations between phosphorylated and unphosphorylated protein forms (e.g., Spleen Tyrosine Kinase (Syk)). Spectral similarities between dephosphorylated-Syk and unphosphorylated-Syk indicated that phosphorylated Syk was able to reverse its conformation after unphosphorylated due to phosphatase treatment. This study would seem to suggest that using advanced materials and the affinity approach can be used for avoiding low sensitivity. Yang et al. (2017) develop a new surface-enhance Raman spectroscopy (SERS) immunoassay to high selectivity and sensitivity of cancer markers such as AFP using enzyme-assisted Agdeposition on 4-mercaptobenzoic acid labeled gold nanoparticles (AuNPs) seeds [75]. The formed Au@Ag nanostructure had strong SERS signal detection for AFP ranging from 0.5 to 100 pg/mL with LOD of 0.081 pg/mL (3σ). Bozkurt et al. (2018) developed alternative methods using ALP activity for *E. coli* detection [76]. Three steps were using including modification of spherical magnetic gold coated core-shell nanoparticles and application of immunomagnetic separation to capture *E. coli* from solution. The ALP was immobilized on Au-NRs, and indirect detection of *E. coli* base on SERS done. Satisfactory limit of quantification (LOQ) (30 cfu/mL) and LOD (10 cfu/mL) were detected using sandwich immunoassay in less than 3 h.

5.4. Infrared spectra techniques

Infrared spectra techniques use the principle that molecules appear to absorb specific light frequencies characteristic with their molecular structure. The energies rely on the shape of molecular surfaces, mass corresponding to atoms, and associated vibronic coupling. Molecules, for example, are able to absorb energy present in the incident light and this results in either pronounced vibration or faster rotation [73]. The advantage of the infrared spectra method is that it does not destroy the sample and can thereby give qualitative and quantitative chemical data about the sample. The sample preparation process is simple with no specific requirements, and the spectra are very sensitive—even in small samples—in addition to being versatile in gas, liquid, solid, and semisolid detections. The disadvantage of the technique includes difficult handling procedures and sample maintenance, with the use of properly tuned and highly sensitive devices. Ren et al. (2015) demonstrated that inferred spectroscopy can detect phosphatase activities *in situ*; in osteoblast cells with the use of natural substrates without labeling [77]. The researchers recorded overall phosphatase activity in cells through a single step via substrate and protein concentration measurements.

Specific activity in osteoblasts was 116 ± 13 nmol/min/mg for PPI to 56 ± 11 nmol/min/mg for AMP, to 79 ± 23 nmol/min/mg for beta-glycerophosphate and to 73 ± 15 nmol/min/mg for 1-alpha-D glucose phosphate. Furthermore, the absorption bands were recorded 1107 cm⁻¹ for PPI, 977 cm⁻¹ for AMP, 990 cm⁻¹ for beta-glycerophosphate, and 990 cm⁻¹ for 1-alpha-D glucose phosphate. It appears likely that the high standard deviation is due to protein concentration. Although the overlap was recorded in this assay, a definite need for a novel probe appears to be required. Li et al. (2017) reported a novel near infrared fluorescent probe based on hemicyanine dye in detecting endogenous ALP activity [78]. The new probe exhibited high sensitivity to ALP with 10-fold improvement when 2.0 U/mL ALP is added. Gao et al. (2018) designed and synthesized a near-infrared fluorescence probe to image and assess endogenous ALP changes in different tumor line cells [79]. The probe contained two parts: heptamethine cyanine as fluorescence modulator and phosphate monester as a response moiety for ALP enzymatic reaction. The technique showed high sensitivity to ALP detection in cancer cells. Wu et al. (2018) designed an ALP-activatable near-infrared photoacoustic probe [80]. Once the ALP is dephosphorylated, it self-assembles into nanostructures with enhanced photoacoustic signal for tumor imaging. The new device had 2.3-fold in detection limit at 4 h after 1P injection. Xu et al. (2019) made a successful synthesis of hemicyanine dye-mimic near-infrared fluorescent probe (NIR MTR) where they used 2-methylbenzo[d]-thiazole to replace 2,3,3-trimethyl-3H-indole [81]. The developed probe exhibited good ALP sensing performance showing detection limit of 0.042 U/L and linear range of 0–8 U/L.

5.5. Colorimetry methods

Colorimetry methods are based on the Beer-Lambert's law where light absorption transmitted through a medium is considered to be directly proportional to the concentration in the medium. In sample detection, a beam of light of a specific wavelength passes through a solution through several lenses that navigate the colored light to a measuring device. The device analyzes the color and compares it to the known standards and the microprocessor is used to calculate the percentage of transmittance or absorbance [82]. The advantages of the colorimetry technique include being fast, inexpensive, lightweight and portable, requiring a small sample size, minimal instrumentation and power, and the ability to customize array for specific analytes. However, some of the shortcomings include reproducibility of printing, reproducibility of imaging, difficulty of determining individual components of a mixture, and stability/shelf life. Chen et al. (2016) developed a low-cost, rapid, simple, and highly sensitive colorimetric technique using microfluidic paper-based analytical devices (μ PADs) for monitoring serum ALP levels [83]. The coloration was recorded using Gel documentation systems. The LOD was noted to have a low detection limit of up to 0.78 U/L serum ALPs. Hu et al. (2017) developed a versatile technique for a selective and sensitive colorimetric assay for ALP activity based on absorption properties of Fe(II)-phenanthroline [84]. The technique exhibited good quantitative detection of ALP activity over a range of 0–220 mU mL⁻¹ with a detection limit of 0.94 mU mL⁻¹. It is likely that novel probes will improve colorimetric assays. Hu et al. (2017) proposed a practical and simple method for the selective and sensitive colorimetric assay of ALP activity [85]. The researchers used a water soluble and biologically conducive Cu(II)-phenanthroline complex as a probe. A two-step chromogenic reaction was used and was responsible for the turn-on spectral absorption in the visible region in addition to a distinct color change in the solution absorbed at the 424 nm band. Without the need for complex instruments and protocols, the new technique allowed for a sensitive readout of ALP activity where its linear range was wide at 0–200mU/mL, while the detection limit was down to 1.25mU/mL. Huang et al. (2018) developed a metal co-factor free deoxyribonucleic acid (DNA) and found that it displays H₂O₂ activity under mild conditions when acetic acid is used as an activator [86]. The new device demonstrated that in situ generations of peracetic acid results from guanine-rich oligonucleotides facilitation and subsequent tetramethylbenzidine (TMB) oxidation. The device had a detection limit of ALP in the linear range from 0.05 to 15 mU/mL, giving the LOD of 0.01 mU/mL. The new device can be used for colorimetric tests in analyzing real samples from human serum. Both Hu and Hu

share LOD higher than Chen' findings. These results would therefore appear to point out a definite need of improving more sensitive probes. Wu et al. (2019) have demonstrated that prussian blue nanocubes (PB NCs) can be used to make colorimetric probes for sensitive and selective monitoring of ascorbic acid and ALP activities [87]. The method is based on peroxidase activity of PB NCs which can be inhibited by ascorbic acid due to PB NCs being reduced to Prussian White. The method showed it can be used to detect ALP activity with a detection limit of as low as 0.23 U·L⁻¹. Generally, optical methods show several advantages including being non-intrusive, presenting high accuracy, real-time detection, and being robust in ALP detection. However, they remain expensive, fragile, influenced by the environment, and are not readily portable.

5.6. Surface Plasmon Resonance

Surface plasmon resonance is a resonant oscillator based on electron conduction at the interface between positive and negative permittivity materials that are triggered by an incident light. The generated incident photons are absorbed at the metal layer surface by free electrons before being converted to surface plasmon waves when some conditions such as incidence angle, polarization, and wavelength have been achieved [88]. Researchers have further explored the properties of ALP from the surface plasmon resonance (SPR) perspective. For instance, Linder et al. (2016) explored the binding properties of human collagen and ALP of human bone through SPR analysis, and validated their research using blotting and electrophoresis [89]. Results revealed that bone ALP binds strongly to collagen in contrast to ALP detected in non-mineralizing tissue samples, and that binding affinity increased as the response rose. Sappia et al. (2017) researched SPR for the real time detection of ALP by using WGA-modified surfaces, where ALP absorbs and the signal increases [90]. Wang et al. (2018) created a probe using gold nanoflower in detecting cellular ALP and found that the ALP activity could be detected up to limits of about 0.03 $\mu\text{U L}^{-1}$ [91]. In addition, the ALP activity of the mammalian cells was able to be attracted using the develop probe.

Nonetheless, despite clever and manipulating tactics of optical methods in ALP detection, the use of fluorophore can be affected by the biological events and cause low fluorescence intensity [29]. The fluorophore may lose its fluorescence during tissue fixation or subsequent processing. In addition, reagents should be fresh enough, placing samples in appropriate positions, and recording should be immediate—otherwise false values will be recorded as well as the simplicity of the colormetric may give insufficient resolutions. Moreover, experiments *in vitro* assays usually require multiple steps to prepare sample. Therefore, enabling electrochemical detection *in vitro* assays will minimize the steps of washing samples, centrifuge etc., thus limiting disturbing samples and obtaining appropriate results with less errors

6. Electrochemistry detection techniques

Electrochemical methods give good grounds for expecting efficiency and sensitivity over optical methods. It was noted that optical devices are commonly used in laboratory settings due to their simplicity in microfluidic-detector interface. However, electrochemical detection offers better detection limits than optical devices for different biological analytes [92,93]. Also, it is easier to integrate electrochemical devices to microfluidic components within different chips in assay detection [94]. As a result, electrochemical methods offer real-time monitoring of biological occurrence and convert it into electronic signal. This type of signal can be easily integrated and observed in microdevices [95].

Electrochemical methods accomplish the measurement of ALP levels *in vitro* assays. The ALP level is determined according to different electrochemical signals including current, potential, conductivity and impedance. A certain reaction occurs in the presence of a particular substrate and produces electroactive properties such electron transfer, potential change, ionic species or current resistance. Thompson et al. (1991) compared the resolution of ALP resulting in amperometric detection over optical detection and found that amperometric had results 20 times better than that of optical [96]. The research of Thompson et al. has contributed to developing ALP electrochemical detection, which makes researchers to take

advantage of Thompson's contributions and apply different approaches such as using various substrates, self-assembled monolayers, immunoconjugates, and label free. In light of these considerations, it will be shown that several studies could detect secreted ALP in biological samples such as serum, cells, tissues and biopsy as well as by using different tactics for amplifying electrochemical signals. Electrochemical assays such as amperometric, potentiometric, and conductometric are common in detection ALP; therefore, they are further explained in the next paragraphs.

6.1. Amperometric

Amperometric techniques work by monitoring the change in a current once a constant potential has been applied. Potential changes are closely connected to enzymatic reduction and oxidation reactions inside the electrolyte solution within the working electrode [97]. In the process, the current can be compared to the electro-active specie concentration inside the sample. For instance, the presence of ALP works to hydrolyze o-phosphate at the p-aminophenyl phosphate (pAPP), where the non-electroactive substrate under the alkaline environment serves to generate an electroactive enzyme which contains redox cycling characteristics. Taking advantages of this principle allow for many studies to develop the detection of ALP in biological samples. Kelso et al. (2000) were most likely the first to detect secreted ALP in media using screen printed electrodes and 2-naphthyl phosphate [98]. They infected CHO cell lines to release ALP, which showed sufficient results that could be further optimized to increase sensitivity. On their print, a foot number of studies showing up developed amplifications. For example, the electrochemical signal of p-aminophenol can be amplified by bioelectrocatalysis using diaphorase and NADH, for instance. Ito et al. (2000) have used Tyrosinase with phenol phosphate to reduce the over-potential and obtained detectable results in the bovine serum. Although phenol phosphate has good stability, it needs two reactions to be detected [99]. Wang et al. (2009) have minimized the reaction in one single step, but they did not use any biological samples [100]. Shi-Ping et al. (2012) have used p-nitrophenol phosphate; the common optical substrate; and used ionic liquid to amplify the electrochemical signals [101]. They detected ALP in range of 1–100 U/L with good linearity. They did not use secreted ALP in their measurements. Xia et al. (2013) developed more sensitive electrochemical sensors for ALP detection using p-Aminophenol redox cycling [102]. The researchers compared the performance of various reductants in p-Aminophenol redox cycling using self-assembled monolayers that were on modified gold electrodes. For redox cycling, three reagents were found to be suitable in enhancing detection including cysteamine, tris(2-carboxyethyl) phosphine (TCEP), and nicotinamide adenine dinucleotide (NADH). The reaction rate in electrochemical detection of ALP decreases in the rate of cysteamine < TCEP < NADH. Some other methods used self-assembled monolayer (SAM) but without substrates. For example, Zhang et al. used a self-assembled monolayer technique where in the absence of ALP, they immobilized phosphorylated peptides (CPPY) onto gold electrodes forming the negatively charged self-assembled monolayers (SAMs), and in the process it enabled access to positively charged $[\text{Ru}(\text{NH}_3)_6]^{3+}$ probes onto the surface of the electrode. Once the electrode was incubated with ALP and CPPY, the ALP removed the phosphate group in CPPY. Although this trend uses cheap reagents, it allows for the indirect detection of ALP. Zhang et al. (2015) further developed a highly sensitive and facile homogenous electrochemical biosensor technique for ALP detection based on a single molecular exonuclease-assisted signal amplification [103]. The model was able to directly detect ALP levels up to 0.1 U/L, which is better than fluorescence methods and up to three times more sensitive than the immobilization-based electrochemical methods. These contributions aided to enable direct monitoring of ALP activity in living cells. Yildirim-Semerici et al. (2015) used an electrochemical assay for indicating the activities of cell-bound ALP using voltammetry on in-vitro cell culture [104]. The assay was based on p-aminophenol oxidation indication using square wave voltammetry, cell cultivation on gold microelectrodes on microplate wells, and catalytic hydrolysis of p-aminophenyl phosphate by ALP attached to cells. Detection of ALP activity was achieved through a signal increase associated with the number of cells and the rate of p-aminophenol formation rate. The obtained findings based on

electrochemical activity assay were in line with calorimetric results obtained from p-nitrophenol formation rate. Porat-Ophir et al. (2015) have also reported the high effectiveness of the electrochemical technique in ALP detection using an integrated 'tissue on a chip' model [105]. The model is based on detecting ALP activity using 1-naphthyl phosphate substrate from tissue samples placed on micro-electrochemical cells. Vernick et al. (2011) have compared healthy and unhealthy tissue using biopsies samples. Their investigation supported the fact that states that health tissues of intestinal exhibit higher activity of ALP than cancerous ones. Their direct electrochemical measurement assay of multiple samples uses a high capacity biosensing chamber which enables for the analysis of cell differentiation [106]. Ragonis et al. (2015) presented a new electrochemical sensor based on an exceptional 3D architecture that allows for the direct measurement detection on close proximity or in contact with biological samples [107]. The chip was made of biocompatible substrates of electrochemical cells with a silver/silver chloride electrode and two gold electrodes (working and counter electrodes). The sensor had a stable signature and high detection response to ALP enzyme even in repeated tests. All the studies reviewed so far, however, try to avoid the disadvantages of amperometry assays.

6.2. Potentiometric

The potentiometric method works on a similar principle alike the amperometric measurement, but the difference is that there is no potential applied. Instead, the circuit remains open and the potential difference observed between the two electrodes is recorded [108]. During redox reactions, potentiometry is able to measure changes in cell potential in addition to monitoring the concentration of ion gradients via the ion-selective membranes. Moreover, potential changes on the working and reference electrodes are measured (commonly the Ag/AgCl electrodes are used) and this can be modified to improve the selectivity in sample detection through membranes. Keyes allow potentiometric detection of ALP in aqueous fluids. Katsu et al. (1996) constructed a hordenine sensitive membrane electrode and is used to detect ALP in blood serum [109]. Keyes allow for potentiometric detection of ALP in aqueous fluids. Katsu et al. (1996) constructed a hordenine sensitive membrane electrode and used it to detect ALP in blood serum [110]. The hordenine electrode was constructed using 2-fluoro-2'-nitrodiphenyl ether as a solvent mediator and sodium tetrakis [3,5-bis(2-methoxyhexafluoro-2-propyl)phenyl] borate was used as an ion-exchanger. The results confirmed that the device had high sensitivity to ALP compared to detection done using colorimetry and phenyl phosphate substrate. Many studies utilized the ability of ALP to catalyze monofluorophosphate hydrolysis alongside using fluoride ion-selective electrode to sense fluoride release to detect ALP. The amount of fluoride ion generated from the substrate in the course of the reaction is proportional to ALP activity. Koncki et al. (2005) developed a simple potentiometric assay in evaluating alkaline and acidic phosphatase activities [111]. Enzymatic catalyzation of monofluorophosphate was investigated as the primary focus of the assay. In the course of the hydrolysis, fluoride ions formed were detected using conventional fluoride ion-selective electrode based on a membrane made from lanthanum fluoride. Maximal sensitivity of acid phosphatase was observed at 10^{-3} M at pH 6.0; a pH of 4.8 was recommended to eliminate the effect of alkaline phosphatase. Koncki et al. (2006) developed a simple flow injection system for potentiometric detection of ALP activity. The researchers used monofluorophosphate as an ALP specific substrate [112]. The use of the substrate helped in improving the application of fluoride ion selective electrode in detecting enzyme-catalyzed reactions. Moreover, the low cost and chemical stability of monofluorophosphate makes it possible to use it as a substrate for the component carrier. Results show that the device allows for an inhibitive detection of vanadate and beryllium ions at ppb levels that have high selectivity, high throughput on the system, and a short time of analysis at nearly 8 samples per hour. Ogończyk et al. (2007) developed a flow injection system to detect ALP activity in human serum samples [113]. The researchers used an inexpensive and specific monofluorophosphate as an ALP substrate for their kinetic assay. The study also applied LaF₃-crystalline membrane for biocatalytic hydrolysis of monofluorophosphate to enhance detection of fluorine ions on the ion-selective electrode. The optimized

system showed high relativity and sensitivity to the short-time analysis of ALP of 5–6 samples per hour. The volume of the required serum was 0.05 mL and the system can detect ALP levels in human serum samples at pathological and physiological levels, and also in detecting the iso-enzymatic forms of ALP. Hassan et al. (2009) developed a new poly (vinyl chloride) matrix membrane detector responsive to 4-nitrophenylphosphate in assaying ALP and potentiometric assay [114]. The sensor was based on using an ion-association complex of 4-nitrophenylphosphate with a nickel (II)-bathophenanthroline cation as electrode active material, while the solvent mediator was nitrophenyloctyl ether. Results indicated that the sensor displays good stability and selectivity in detecting ALP and potentiometric assay of acid enzymes in patients suffering from prostate cancer, acute myelocytic leukemia, and alcoholic cirrhosis. For real-time ALP potentiometric methods, Kanno et al. (2016) described potentiometric bioimaging for enzyme activities based on a large scale integration-based electrochemical device of up to 400 sensors [115]. The potentiometric mode was used in the detection of ALP and glucose oxidase enzyme activities. The findings revealed that the enzyme activities were quantitatively detected in concentration ranges of 25–250 µg/mL for glucose oxidase and 0.10–5.0 ng/mL for ALP.

6.3. Conductometric

Conductometric methods work by measuring conductivity as a function of ionic species in a sample solution. The device contains two electrodes that are positioned to measure the conductivity of an electrolyte material that is adjacent to the surface of the electrode [97]. For instance, in the presence of electrolytes, ALP dissolves and in the process it induces catalytic reactions that are able to generate ionic species. This method does not involve a reference electrode, which makes it simpler than amperometric and potentiometric methods [116]. Guedri and Durrieu (2008) designed a conductometric biosensor to detect ALP activity in water using the microalgae *Chlorella vulgaris* [117]. The biosensor consisted of a microalgae bioreceptor and a transducer formed by platinum electrodes. The device had good repeatability measurements. Upadhyay and Verma (2015) developed a new and simple conductometric biosensor for indirectly determining phosphate ions in solution [118]. The biosensor was based on the inhibition of immobilized ALP in the presence of phosphate ions. Results indicated that the biosensor had a broad linear response (when compared to biosensors reported in past studies) for phosphate ion detection ranging from 0.5 to 5.0 mM with a correlation coefficient of R^2 995. The researchers also used different optimized parameters as a buffer at concentrations of 30 mM, pH 9.0, and substrate concentration of 1.0 mM for the device. Chouteau et al. (2004) developed a biosensor based on immobilized *Chlorella vulgaris* and tested it the using ALP analysis [119]. The sensor was used in detecting toxic compounds such as cadmium ions in the marine environment. The algae were immobilized in bovine serum albumin membranes and cross-connected with glutaraldehyde vapors. When compared to bioassays, Chouteau et al. noted that the results of conductometric biosensors using algae appeared more sensitive in detecting low-level cadmium ions. Besides, the ALP based biosensor is highly sensitive due to its specificity to toxic compounds. Compared to the use of biological systems, Berezhetskyab et al. (2008) created an ALP based conductometric biosensor that contained enzyme membranes and interdigitated gold electrodes were used in assessing heavy-metal ions in water [120]. The analytes acted as enzyme inhibitors and the findings show that toxicity of different metals that were tested ranged in the order of $\text{Cd}^{2+} > \text{Co}^{2+} > \text{Zn}^{2+} > \text{Ni}^{2+} > \text{Pb}^{2+}$. The limits of detection were about 40 ppm for Pb^{2+} , 5 ppm for Ni^{2+} , 2 ppm for both Zn^{2+} and Co^{2+} , and 0.5 ppm for Cd^{2+} .

7. Other detection techniques

The subsequent techniques utilised their exclusive characteristics in detecting ALP either directly, investigating some of its properties, or applying it as a label. The utilized techniques are electrochemical impedance spectroscopy, quartz crystal microbalance, and field-effect transistor—all of which enable real-time detection.

7.1. Electrochemical impedance spectroscopy

Electrochemical impedance spectroscopy denotes the frequency-dependent resistance in terms of its relation with current flow in circuit elements (inductor, capacitor, resistor etc.) [121]. In this measurement type, it can either detect the capacitance at the electrolyte/electrode interface or it can detect stray capacitance between two opposite electrodes by responding to minute amplitude AC voltage. The impedance spectroscopy methods make it possible to monitor changes of mobile or linked charges on the volume around the interface regions. In 1996, Cai et al. purposed an impedance device based on a surface acoustic wave [122]. Their device allows conductivity of ALP measured in human serum samples where the higher ALP, the higher variations occur in the oscillation circuit. Lee et al. (2018) described a new impedimetric method of detecting ALP based on Cu²⁺ mediated oxidation of ascorbic acid on specific DNA probe-modified electrodes [123]. Researchers used PPI able to complex with Cu²⁺ as the ALP substrate enzyme. Free copper ions were bound to poly-thymine DNA probe attached to the surface and reduced forming copper nanoparticles through concomitant oxidation of ascorbic acid. The electrode surface accumulates the oxidation products and this increases electron transfer resistance as it interrupts the flow of electrons on the electrode. In contrast, the absence of ALP means that the PPI remains constant to suitably capture Cu²⁺, preventing the oxidation of ascorbic acid and continued the increase of electron transfer resistance. The detection rate was higher than results from electrochemical impedance spectroscopy with ALP detection of 6.5 pM (7.2 U/L) and also displays excellent selectivity.

The affinity approach was used in this technique. For example, Lucarelli et al. (2005) used an enzyme-linked electrochemical genosensor for ALP detection [124]. They describe the process of optimizing the performance of an enzyme-linked electrochemical genosensor created using a disposable oligonucleotide screen printed on gold electrodes. Researchers performed a qualitative analysis on the thiol-tethered probe using faradic impedance spectroscopy. Obtained impedance spectra revealed that thiol moiety contributed to unambiguous immobilization of oligonucleotide probe. Moreover, both hybridization efficiencies and probe surface densities were quantified via chronocoulometric measurements. Moreover, the researchers performed electrochemical transduction of the hybridization process via faradic impedance spectroscopy. The detection limits from the device were 1.2 pmol/L, demonstrating the usefulness of impedimetric genosensor in detecting ALP in samples. Ferancova et al. (2017) investigated the immunoassay events using three different electroactive substrates 1-naphthyl phosphate, 2-phospho-1-ascorbic acid, and hydroquinone diphosphate (HQ) as an opposite of chromogenic substrates in immunoassays [125]. Their result show that the substrates are significantly affected by blocking agents, but HQ is not affected. Another one was the adsorption approach, which is similar to immobilization. Shrikrishnan et al. (2012) detected ALP on a self-assembled monolayer modified gold electrode [126]. Their results show a decrease in impedance resolution when the protein of ALP adsorbed on to the monolayer due to the increment of ionic charges resulting in their reactions. Their study allows for a simple kinetic investigation of ALP comparable to ELISA. Advanced materials were used due to their affinity properties. Mintz et al. (2018) undertook an electrochemical impedance study to detect ALP in a phosphate buffer saline (PBS) solution using anti-ALP functionalized silicon nanowires [127]. The nanowire surface was modified by immobilizing the anti-ALP. The results indicated that the device was highly efficient in detecting low levels of ALP in the PBS solution ranging from 0.03 to 0.3 U/L with high selectivity due to antigen-antibody interactions. Kaatz et al. (2012) developed a device based on the impedimetric detection of enzymatic signals on the electrode surface [128]. The study demonstrated a technique which gives the needed detection levels at significantly reduced levels of enzyme reaction times and also shows the needed detection can discriminate samples. The study opens up to the potential of relevant and rapid multiparameter impedimetric ALP assays in the future.

7.2. Quartz crystal microbalance

Quartz crystal microbalance can detect change in a tiny mass as it monitors the frequency of oscillating shifts in crystals as a result of changes in pressure on the crystal surface resulting from mass loading. As the mass loading increases on the sensitive surface, there is a reduction in oscillation frequency [129]. ALP

activities were analysed using quartz crystal microbalance. The approach is meant to increase the existing biotechnological application of microchips, protein arrays, and biosensors that are focused on kinetic immobilization of enzymes. The unique features of ease of genetic manipulation, self-assembly, and recognition make binding affinity a reliable molecular tool for site-specific enzyme immobilization Ebersole and Ward (1988) described amplified mass immunosorbent assay using crystal microbalance in detecting ALP and human chorionic gonadotropin [130]. The results indicated a high detection rate of the ALP and hormones on the quartz-crystal microbalance surface. The technique contributed to enzymatic amplification detection with significant enhancement of the detected limits. Kacar et al. (2009) demonstrated the use of the gold-binding peptide as a molecular linker immobilized on a gold substrate and genetically linked to alkaline phosphatase [131]. The enzymes were expressed in *E. coli* cells and gold bindings peptides focused on the N-terminus of alkaline phosphatase. The device demonstrated self-immobilization of the bi-functional enzyme on a micro-pattern substrate, while genetically linked end showed high enzymatic activity per area. The findings show a promising use of inorganic binding peptides as sites for specific molecular linkage for enzyme immobilization with retained activities. Thammasittirong et al. (2011) determined quantitative binding analysis of ALP immobilized on a gold electrode using a quartz crystal microbalance, which showed decrement in frequency at binding of *Bacillus thuringiensis* toxin (Cry4Ba) as a result of the mass raise [132].

7.3. Field-effect transistor

Field-effect transistor methods are designed around semiconductor material that consist of metal-oxide semiconductor structures. Any changes in the metal potential results in the induction of the electric field triggering the band bending of the semiconductor channel appropriately [133]. The process then results in changes to the channel carrier concentration including inversion, depletion, or accumulation. Most studies used field-effect transistor in terms of ALP applications where applying ALP as a label is fundamental of other methods. For example, Jang et al. (2015) demonstrated a new immunoassay ELISA based on an electrochemical method for optical and electrical signaling. The process was achieved by combining an ion-sensitive field effect with Enzyme-Linked immunoassay [134]. The device was then set to harness a catalytic reaction of alkaline phosphatase which precipitated silver particles. Small signals that ranged from 1 pg/mL to 10 ng/mL were greatly amplified with ALP labeled despite the buffer conditions. Results revealed that the developed sensor platform outperformed the sensing capacity of conventional ELISA, which is considered to have a LOD of about 1 ng/mL. Obtained findings were also compared with the results of horseradish peroxidase, which is commonly applied in the optical analysis of ELISA. The findings showed that the immunoassay device based on the ion-sensitive field-effect transistor (ISFET) based on portable sensors and can be used as a point of care tool for various diseases in workplaces limited by the use of expensive equipment such as spectrophotometers. Freeman et al. (2007) have demonstrated the label-less specific analysis kinase activity using a field-effect transistor device [135]. They treat sensors with ALP where sensing interface ALP can dephosphorylate enzyme kinase and then change the potential to lower level.

Advanced technologies including nanomaterials, microarrays, and lab-on-a-chip are massively exploited for ALP detection, which encourages researchers to develop better methodologies as well as design small devices for point of care applications. The following section displays recent progresses in this field.

8. Recent technology

8.1. Optical Nanomaterials

Biological samples often have an extremely low concentration of cancer biomarkers. As a result, there is a high demand for highly ultrasensitive and selective detector probes to make it possible to detect the

low levels of cancer biomarkers in biological samples. In the optical biosensors, the low levels of biomarkers are detected by using nanomaterials that help amplify the low signals by taking advantages of the nanomaterial characteristics. Table 1 illustrates number of nanomaterials that have been used so far in amplifying ALP signal in biological samples. Following the introduction of nanotechnology in the biosensor field, selectivity and sensitivity and other analytical properties of biosensors have been largely improved. Among the widely applied nanomaterials, gold nanoparticles, carbon nanotubes, photonic crystals, and graphene have stood out because of their unique ultrasensitive and selective properties [124]. For example, some of the advantages of nanomaterial properties include strong amplification effect on signals, high surface energy, superior biocompatibility, and high stability that make them excellent choices when looking for biosensor probes. Gold nanomaterials have become widely applied in the field of biosensors considering their unique advantages such as increased signal response or detection—especially for biological samples with low biomarker concentration [124]. Xia et al. (2013) also noted that gold nanoparticles improve ALP detection through signal amplification resulting in high selectivity and sensitivity [102,125,136]. Graphene nanoparticles have also been widely used in biosensors considering their unique electrical conductivity, high surface area, thermal conductivity, and electron mobility [137].

Table 1. Number of nanomaterials for enhancing optical assays.

Detection Technique	Nanomaterials	Linear Range	Limit of Detection	Ref.
Colorimetric	gold nanoparticles	100–600 U/L	1000 U/L	[138]
Raman spectroscopy	gold nanoparticles	4×10^{-11} M to 4×10^{-15} M	4×10^{-15} M	[139]
Raman spectroscopy	gold nanoparticles	0.72 to 3 U/L	0.01 U/L	[140]
Fluorescence	gold nanoclusters	0.02–2.0 U/L.	0.005 U/L	[141]
Fluorescence	silver nanoclusters	1–100 U/L	0.63 U/L	[142]
Fluorescence	copper nanoclusters	0.5 to 150 mU/mL	0.1 mU/mL	[143]
Fluorescence	nitrogen-doped carbon dots	2.5 to 45 U/L	0.4 U/L	[144]
Naked eye	α -moo3- × nano-flakes	0.06 to 1 IU		[145]

Several studies have been published using various nanostructure including nanoparticles, nanocluster, nanoflakes and carbon quantum dots alongside various optical assays to enhance ALP detection. In terms of colorimetry assays, Choi et al. (2007) used gold nanoparticles (AuNP) to increase ALP detection sensitivity [146]. The researchers used the presence of dephosphorylated Tyrosine-Arginine (Tyr-Arg) to aggregate AuNP. A model substrate for this platform was based on a phosphorylated dipeptide phospho (pTyr-Arg) with an amidated C-termini and a free N-termini for the target ALP enzyme. As such, the dephosphorylation only generated cationic Tyr-Arg. In contrast, Serizawa et al. (2010) reported the detection of ALP based on product- or substrate-dependent synthesis of AuNPs in HEPES buffer [147]. The researchers used phosphorylated dipeptide pTyr-Arg with free amidated C-termini and N-termini for the target ALP enzyme, generating cationic Tyr-Arg. The effects of enzyme and substrate concentrations on detection were explored in detail and found to be applicable to inhibitor assays. The method does not

require specific storing, synthesis, or purification of AuNPs, making it a simple and facile detection technique. Li et al. (2013) developed a label-free and simple calorimetric assay to detect ALP [138]. Their sensor was based on conjugated AuNPs and adenosine triphosphate (ATP), creating a highly selective and sensitive assay. In the system, ATP induced the aggregation of cetyltrimethylammonium bromide (CTAB)-capped AuNPs while ALP stimulated disaggregation of AuNPs, thereby converting ATP into adenosine via enzymatic dephosphorylation. The presence of ALP can be visually observed (change in grey to red color) and monitored as a result of surface plasmon resonance shift and AuNP absorption band. On the other hand Song et al. (2018) proposed a facile colourimetric assay based on phosphate anion-quenched oxidase-mimicking activity of Ce(IV) ions to enhance the selective and sensitive detection of ALP activity [148]. Free Ce(IV) ions showed strong oxidase-like activity with 40 times more catalytic turnover when compared with CeO₂ when catalyzing the oxidation colourless TMB into its blue product. The detection for ALP was in two linear scopes of 0–50 U/L and 50–250 U/L, and a limit down to 2.3 U/L.

In terms of SERS, Ruan et al. (2006) detected ALP activity at ultralow concentration, where AuNP was used as SERS material in 5-bromo-4-chloro-3-indolyl phosphate (BCIP) presence [139]. Enzymatic hydrolysis of BCIP contributed to the formation of indigo dyes that were noted to be highly active in detecting ALP activity at ultralow concentrations using the SERS technique. Jiang et al. further used AuNP as scattering in the presence of ALP substrate where ALP was catalysed, the ascorbic 2-phosphate (AAP) was hydrolyzed and formed ascorbic acid. The activity of the enzymatic reaction was stopped using H₃PO₄ and HAuCl₄ was used in reacting ascorbic acid create AuNP that displayed resonance scattering (RS) with ALP product. These properties of AuNP make it possible to have a rapid electron transfer in detecting biomolecules when used as biosensors. Moreover, gold-based nanotubes also allow for rapid electron transfer and help reduce the inconsistent signal amplification of metallic nanoparticles often encountered in traditional biosensors such as low selectivity and sensitivity. Zeng et al. (2017) designed a SERS kit for ALP detection based on 'hot spots' amplification approach [140]. The kit consisted of enzyme substrate, Ag⁺, and alkyne-tagged AuNPs for clinical assay detection of ALP in human samples. Due to electrostatic interaction, silver ions are adsorbed to the Au surface and the enzymatic catalysis of ALP trigger reduction of silver ions forming hot spots on Au core and Ag shell resulting in high SERS signal amplification. The ALP detection limit for the assay is 0.01 U/L (2.3 pg/mL) and the kit can be used at point-of-care for efficacious, reliable, and highly sensitive ALP detection potentially reducing the need for time-consuming clinical tests.

Other techniques such as naked eyes and ultraviolet–visible spectroscopy (UV-vis) have been used with different materials in detection ALP. For example, AL-Rubaei et al. (2015) used UV-vis spectroscopy in a developed platform for ALP detection in saliva-based on titanium dioxide NPs (TiO₂ NPs) [149]. Findings from the study showed that the technique could be applied in sensitive and selective detection of ALPs in patients with gingivitis. Zhang et al. (2017) developed an inexpensive ALP detection device that uses low-cost μ PADs [150]. Under an optimal environment, the new technique promotes quantitative detection of ALP in buffer samples that range from 0.075 to 5 U/mL and have a visual detection limit of 0.075 U/mL. Pandey et al. (2018) presented a platform for detecting ALP levels using -MoO_{3-x} nano-flakes and zinc oxide [145]. Once ALP is introduced to the complex, there is a rapid transformation of blue -MoO_{3-x} to colourless -MoO₃ using zinc as a cofactor. The sensitivity level was found to be 0.1 M of enzyme concentration.

Fluorescence assays allow many manipulating tactics to make novel probes that take advantage of nanomaterials properties. For example, Cao et al. (2016) synthesized a fluorescence nanoprobe by combining isomers of phosphorylated fluoresceinamine on the surface of mesoporous silica-coated superparamagnetic iron oxide (Fe₃O₄@mSiO₂) nanoparticle [151]. The phosphorylated fluoresceinamine was hydrolysed in the presence of ALP, leading to fluorescence recovery of ALP. Increased fluorescence intensity during high-level ALP expression provides a rapid and non-toxic method for cellular detection of ALP activity. Hu et al. (2017) proposed a new fluorescent sensing platform that uses nitrogen-doped

carbon dots (N-CDs) as a probe for fluorescence signal transmission for ALP and PPI [144]. Cu^{2+} quench high fluorescent N-CDs and can be recovered when PPI is added since PPI binds to Cu^{2+} . The strategy shows that N-CDs can be used in selective and sensitive detection of ALP and PPI at low detection levels of 0.16 μM and 0.4 U/L for PPI and ALP, respectively. The assay is simple, rapid, sensitive, low-cost, and convenient. More recently, nanomaterials have been used in enhancing sensitivity; for example, He and Jiao (2017) described a fluorometric technique in detecting ALP activity [142]. When ALP is added, AAP is hydrolysed, forming ascorbic acid (AA) which reduces Ag^+ ions forming metallic silver that hinders the formation of fluorescent silver nanoclusters causing low fluorescence. There is a linear correlation in fluorescence intensity in the 1–100 U/L ALP concentration range and a detection limit of 0.63 UL. Wang et al. (2018) developed a sensitive fluorometric assay for determining ALP activity using a composite generated from copper nanoclusters (CuNCs) and flower-like cobalt oxyhydroxide (CoOOH) [143]. Upon the formation of CuNC- CoOOH aggregates, the fluorescence of CuNCs is reduced due to CoOOH sheets. If AA is added, the CoOOH sheets are reduced to Co(II) ions, recovering the fluorescence, and ALP is hydrolysed and detected at an excitation wavelength of 335 to 410 nm. The assay can result in high ALP detection to a range of 0.5 to 150 mU/mL and a detection limit of up to 0.1 mU/mL. Liu et al. (2019) used the common on-off approach to enhance sensitivity of ALP detection [141]. They functionalized gold nanoclusters by 3-aminophenylboronic acid (APBA-Au NCs). ALP can catalyze hydrolysis of phenyl phosphate to phenol, which can be subsequently hydroxylated to generate catechol in the presence of tyrosinase (TYR). Due to the special covalent combination between the catechol and boric acid group, the five-membered cyclic esters can be formed on the ligands of APBA-Au NCs—leading to the fluorescence quenching of the Au NCs.

8.2. Electrical Nanomaterials

Nanomaterials have also been widely applied in electrochemical biosensors as sensing probes to achieve high conductivity, catalytic activity, and biocompatibility, where they accelerate signal transduction and amplify biorecognition of biomarkers. Table 2 shows some nanomaterials used for signal amplification. Applying carbon and metal nanomaterials to modify the surface of electrodes can improve signal labelling and sensitivity, thereby enhancing the biomarker detection in complex environments. Several studies have been published where they have used nanomaterials to improve the detection of ALP. For example, Ru et al. (2013) confirmed that ionic liquid modified carbon nanotubes electrode can be applied in dynamic detection of ALP and the technique was found to be time efficient, have good precision, high sensitivity, and a wide linear range [152]. Peng et al. (2015) synthesized copper sulphide nanoparticle graphene sheets (CuS/GR) and used it in signal amplification for electrochemical detection of ALP [102,153]. The platform increased the detection of ALP in human serum linearly with the concentration of 0.1 to 100 U/L with a detection limit of 0.02 U/L. Zhou et al. (2016) created a selective and sensitive electrochemical biosensor assay for protein kinase activity [154]. Multiple signal amplification approaches using streptavidin (SiO_2), SiO_2 biocomposite, and carbon nanospheres (Au@C). The peptides were modified on the electrode surface after phosphorylation using protein kinase A in the presence of ATP. The ALP detection limit was 0.014 u/mL and the method showed high detection selectivity and sensitivity. Panday et al. (2017) reported a new self-aligned process for AuNP decorated polypyrrole (Ppy) biosensing microelectrode, where AuNP electro-grows out of Ppy in a selective manner [155]. The self-aligned approach promoted on-chip AuNP deposition and preparation in a single step approach saving cost and time. Zhao et al. (2018) developed a sensitive electrochemical ALP biosensor AAP as the substrate on an AuNPs decorated single-walled carbon nanotube (GNP/SWNT) and a modified glassy carbon electrode (GCE) [156]. The activity of ALP was determined indirectly according to the concentration AA, generated from AAP hydrolysis. The biosensor showed high selectivity and sensitivity at a concentration ranging 3 to 50 U/L with a detection limit of 0.2 U L-1. Simão et al. (2018) integrated CNTs within osteointegration implants and found increased ALP mineralization activity detection using the implants [157]. The device

can rapidly detect ALP within blood serum, by immobilizing the covalent anti-ALP antibody towards ALP. The biosensor showed excellent performance with two linear ranges from 0.5 to 50 IU/L and from 100 to 600 IU/L and limits of detection ranged 0.25 and 84.6 IU/L, respectively. Mintz et al. (2018) created an electrochemical impedance device to detect ALP in phosphate buffer saline (PBS) solution by using anti-ALP functionalized silver nanowires (SiNWs) [127]. A three-electrode cell was used to measure electrochemical impedance where the electrode functioning as a highly disordered and very dense array of SiNWs. The device was highly efficient, selective, and sensitive in detecting very low ALP concentrations in PBS solution ranging 0.03–0.3 U/L, in addition to being highly selective to antigen and antibody interaction. The high selectivity and sensitivity make the device an effective approach for quantitative sensing and real-time detection of ALP.

Table 2. Number of nanomaterials for enhancing electrochemical assays.

Detection Technique	Nanomaterials	Linear Range	Limit of Detection	Ref
Impedance	silicon-nanowire	0.03–0.3 U/L	0.3 U/L	[127]
Electrochemical	copper sulfide nanoparticle	0.1 to 100 U/L	0.02 U/L	[153]
Electrochemical	gold nanoparticle	3 to 50 U/L	0.2 U/L	[156]
Electrochemical	gold nanoparticle-carbon nanotubes	0.5 to 600 IU/L	0.25 IU/L	[157]
Photo-Electrochemical	graphitic carbon nitride (g-C ₃ N ₄)/TiO ₂ nanotubes	0.3 mU/L–1 U/L	0.1 mU/L.	[158]

8.3. Microarray techniques

The microarray detection involves an advance in technology to enhance ALP detection *in vitro* or cell culture. Over the years, *in vitro* microelectrode array technology has evolved into a widely used and effective technique in studying cultured cells. Lin et al. (2008) orthogonally arranged row and column electrodes on two different glass substrates, achieving an addressable microelectrode device for the comprehensive electrochemical detection of ALP [159]. The addressable microelectrode was simple and its advantage includes ease in assembling, but it consists of only 10 × 10 addressable detection points on a single chip. The detected electrochemical response at 100 single points was achieved within 22 s. The device was used to successfully image the spots of ALP on array substrate with high-throughput imaging and detection of biochemical species. Lin et al. (2009) created a microwell array and incorporated it to the addressable device in ensuring high-throughput screening of bioparticles and genetically engineered cells [160]. The researchers demonstrated the importance of the device in rapid electrochemical detection of secreted ALP from a single genetically engineered HeLa cell using microwell/microelectrode array device. The results showed that the average decline in currency for 100 microwells is proportional to PAP concentration ranging from 0.5 to 50 µM. Murata et al. (2009) monitored the electronic expression of ALP at the single-cell level using a scanning electrochemical microscopy (SECM) [161]. The SECM measurement showed that tumor necrosis factor (TNF)-α stimulate a considerable rise in the response of transfected cells array on poly(dimethylsiloxane) (PDMS) micro-stencil without exposing them to positive-dielectrophoresis (pDEP). The overall response of untreated cells rose during the 5-h culture promoting cell adhesion and indicating that pDEP-induced stress triggers intracellular signalling, resulting in the

production of ALP. Shiku et al. (2010) noted that single-cell analysis has been used as a powerful technique in constructing new types of whole cell sensors in addition to integrating individual cellular responses [162]. Nonetheless, the current sensitivity levels are insufficient when analysing a large number of data-sets since individual single-cell responses show high fluctuations. Takeda et al. (2011) microfabricated an electrochemical platform for the parallel monitoring of secreted ALP using a mammalian-cell array chip [163]. A 4 ring-ring electrode array was developed at the rim at round cellular patterns with a diameter of 270 nm. The researchers then carried out electrochemical characterization and found a collection efficiency of 50% in the dual mode when outer and inner ring electrodes were selected as the generator and collector electrodes, respectively. The present amplification mode for dual mode normal to single mode was 2.84. Ino et al. (2012) also developed a deep microwell and included them into local redox cycling-based electrochemical (LRC-EC) devices to trap single 3D culture cells and evaluate the activity of the cells [164]. Corresponding experiments and simulations were undertaken to identify the impact of deep microwells on LRC-EC system. The demonstrations that were anchored on microwell models showed that deep microwell arrays and fine interdigitated array (IDA) electrodes resulted in low cross-talk influence but high sensitivity compared to conventional techniques that use electrode arrays in comprehensive detection. The estimated time to attain a steady-state was short and this shows that the electrochemical image with 256 pixels was achieved in 10.3 s using the LRC-device. A study by Wu et al. (2016) developed a new digital single molecule electrochemical detection method (dSMED) strategy to address the problem of single molecule electrochemistry (SME) reliability based on the integration with the digital analysis in enzyme-induced metallization (EIM), which improves the application of SME in a biological system [165]. The created EIM can enhance electrochemical signals up to 100 times when compared to conventional techniques of direct oxidation of enzyme materials that offer better signal detection for single molecule detection. The incorporation of digital analysis solves the existing problems associated with fluctuations in signal detection and heterogeneity of single enzyme activities, further reducing the detection limit of ALP to 1 aM compared to the original levels of 50 aM. The use of microarrays greatly improves the reliability and accuracy of SME through the integration of a digital system that enables dSMED to ensure successful application in ALP detection in complex liver cells.

8.4. Lab-on-chip technique

Development of lab-on-chip sensors has been undertaken in advance technology to enhance ALP detection in cell culture. Lab-on-chip approaches can provide good selectivity and portable detection. Besides, the chip limits the affectance of interferences and can therefore be used in ALP detection assay in complex samples. Şen et al. (2012) examined electrochemical detection of secrete ALP secreted from single transformed HeLa cells using a chip comprising 256 microwells of single addressable sensor points, which had been modified using anti-secreted ALP [166]. The secreted ALP was successfully separated and analysed using the developed LRC-EC chip, which was found to have broad potential for single cell analysis applications. Şen et al. (2012) also proposed a new electrochemical assay for the detection of secreted ALP from transfectant HeLa cells using SECM and a microarray device [167]. The assay was reported to increase intactness and accuracy in ALP detection by eliminating undesired influence. Chen et al. (2013) developed a new and simple microfabricated device for feeder-isolated co-culture of stem cells that allows for the use of normal mouse embryonic fibroblasts (mEF) as feeder layers in addition to pure mouse embryonic stem (mES) cells without additional purification [168]. The device has significant advantages of simplicity and efficiency where the mES cells and feeder layers are spatially attached to the PDMS porous membrane and forms 3D cell colonies that have high viability. The pluripotency and self-renewal mES cells were confirmed through ALP expression. The device supported a robust and simple ALP detection *in vitro* stem cell co-cultures with a significant advantage in simplicity and efficiency from mEFs co-cultures without additional separation or purification. Ino et al. (2014) have recently fabricated a new type of LRC-EC chip device for the detection of a droplet array [169]. Pt pseudo-reference/counter

electrodes were used to improve the electrochemical detection of redox compounds in droplets, by incorporating the individual sensors of the LRC-EC chip device. The cyclic voltammetry for LRC-EC chip with internal Pt pseudo-reference electrodes showed well-elaborate voltammograms based on redox cycling for single sensor points. The device was used in the detection of ALP activity of HeLa cells in single droplets on sensor points. The results reveal that the technology was simple, low-cost, rapid, and has the potential for clinical analysis of ALP assays. Ino et al. (2014) [170] fabricated a new LRC-EC chip device with a densely packed electrode array that has a vertical separation. The electrochemical performance of this device was assessed using amperometry and voltammetry [170]. The LRC-EC device indicated significant enhancement of electrochemical image resolution and largely applied to imaging of HRP and ALP in SG/CC and extended feedback modes. When compared to SECM imaging, electrochemical imaging, using LRC-EC systems is appropriate for continuous imaging of biomaterials since LRC-EC makes it possible to achieve rapid image acquisition. Cao et al. (2018) created a simple electrophoresis titration (ET) device for ALP detection through moving reaction boundary (MRB) [171]. In this model, ALP sped up the dephosphorylation of the 4-methylumbelliferyl phosphate disodium salt substrate in the cathode and 4-methylumbelliferone (4-MU) with blue fluorescence and negative charge under UV excitation. The 4-MU moved under the electric field into the channel and in the process resulted in the neutralization of the acidic Tris-HCl buffer, thereby creating MRB and quenching 4-MU. The sensitivity of the device was high at 0.1 U/L, and the results were better than the ones obtained from chemiluminescence, electrochemical, and colorimetric methods for ALP assays. The sensitivity of the ET technology was good (0.1 U/L), linearity ($V = 0.033A + 3.87$, $R^2 = 0.9980$), stability with relative standard deviation about (2.4% to 6.8%) and recoveries (101% to 105%). The technology was successfully used to detect ALP in serum samples. Sun et al. (2019) explored a new technique for investigating a low abundance of ALP created through individual cells by the use of microfluidic droplet-based SERS method [172].

The researchers first created a co-flow drop-maker model in which they suspended cells in a solution using BCIP as an enzymatic substrate and AuNPs as a signal agent to encapsulate individual cells in the drops. The difference of normal liver cell lines (BNL.CL2) and hepatocellular carcinoma cell lines (HepG2) were contrasted in their ALP expression and it was observed that normal liver cells indicate that 40% lower ALP expression compared to hepatocellular carcinoma (HepG2). The results also revealed that the ALP activity of droplet-isolated cells fluctuate in a large range compared to cluster cells, even if the overall ALP expression of the two cases was similar. An ultrasensitive high output analytical process was realized for ALP detection using single cell SERS-based microfluidic droplet method.

9. Conclusion and perspectives

This paper has thoroughly reviewed recent strategies concerning optical and electrochemical detection of ALP and has discussed the electrochemical techniques that have been addressed to make each of the techniques suitable for ALP analysis in cell culture. It has been shown that using advanced materials can enhance the signal of ALP detection, although the linear range was slightly low. Moreover, real-time detection of ALP with cells viability are monitored using microscopic images, fluorescent images and scanning electrochemical microscopy. Other effective methods includes dyes to indicate metabolic activities and the use of cell adhesion with impedance measurement. Quartz crystal microbalance, field-effect transistor and surface plasmon resonance are also advantageous methods. Real-time detection of ALP is also visible by naked eyes using advanced mobile phone cameras. Many optical and electrochemical approaches have been applied with advanced materials and recent technologies such as microarrays and lab-on-a-chip. Ino et al. have previously reviewed the bioelectrochemical applications of these technologies but focused on where analyzing and monitoring cell functions is possible [173]

In electrochemical detection strategies, the development of electrodes, electrolytes and the analysis of other parameters regarding these techniques can contribute to the development of more suitable ALP biosensors. Whereas it is obvious that a considerable amount of work needs to be performed to meet the

remaining challenges, as well as limiting the influence of parameters set on electrochemical signals, these literature reviews contained in this paper suggest a strong foundation for the development of methodologies for ALP analysis. Further enhancement of the ALP detection in order to achieve the desired level of accuracy and sensitivity is required.

Funding: This research was funded by Ministry of Higher Education of Saudi Arabia.

Acknowledgments: The authors would like to acknowledge the financial support of Ministry of Higher Education of Saudi Arabia.

Conflicts of Interest: The authors declare no conflict of interest.

References

- [1] McComb, R.B.; Bowers, G.N., Jr.; Posen, S. Alkaline Phosphatase; Plenum Press: New York, NY, USA, 1979. [Google Scholar]
- [2] Scriver, C.R. The Metabolic & Molecular Bases of Inherited Disease, 8th ed.; McGraw-Hill: New York, NY, USA, 2001. [Google Scholar]
- [3] Chatterjee, R.; Mitra, A. An overview of effective therapies and recent advances in biomarkers for chronic liver diseases and associated liver cancer. *Int. Immunopharmacol.* 2015, 24, 335–345. [Google Scholar] [CrossRef] [PubMed]
- [4] Tartter, P.I.; Slater, G.; Gelernt, I.; Aufses, A.H., Jr. Screening for liver metastases from colorectal cancer with carcinoembryonic antigen and alkaline phosphatase. *Ann. Surg.* 1981, 193, 357–360. [Google Scholar] [CrossRef] [PubMed]
- [5] Annibali, O.; Petrucci, M.T.; Santini, D.; Mariani, M.; Pisani, F.; Bongarzone, V.; Avvisati, G. Alkaline Phosphatase (ALP) Levels in Multiple Myeloma (MM) and Cancer with Bone Lesions: Is There any Difference? *Clin. Lymphoma Myeloma Leuk.* 2015, 15 (Suppl. 3), e125. [Google Scholar] [CrossRef]
- [6] Abdallah, E.A.; Said, R.N.; Mosallam, D.S.; Moawad, E.M.; Kamal, N.M.; Fathallah, M.G. Serial serum alkaline phosphatase as an early biomarker for osteopenia of prematurity. *Medicine* 2016, 95, e4837. [Google Scholar] [CrossRef] [PubMed]
- [7] Balzola, F.; Bernstein, C.; Ho, G.T.; Lees, C. Exogenous alkaline phosphatase for the treatment of patients with moderate to severe ulcerative colitis: Commentary. *Inflamm. Bowel Dis. Monit.* 2010, 11, 83. [Google Scholar]
- [8] Pickkers, P.; Heemskerk, S.; Schouten, J.; Laterre, P.F.; Vincent, J.L.; Beishuizen, A.; van der Hoeven, J.G. Alkaline phosphatase for treatment of sepsis-induced acute kidney injury: A prospective randomized double-blind placebo-controlled trial. *Crit. Care* 2012, 16. [Google Scholar] [CrossRef] [PubMed]
- [9] Orsaria, M.; Londero, A.P.; Marzinotto, S.; Di Loreto, C.; Marchesoni, D.; Mariuzzi, L. Placental type alkaline phosphatase tissue expression in ovarian serous carcinoma. *Cancer Biomark.* 2017, 17, 479–486. [Google Scholar] [CrossRef]

- [10] D'Oronzo, S.; Brown, J.; Coleman, R. The value of biomarkers in bone metastasis. *Eur. J. Cancer Care* 2017, 26. [Google Scholar] [CrossRef]
- [11] Maisano, R.; Azzarello, D.; Del Medico, P.; Maisano, M.; Bottari, M.; Egitto, G.; Nardi, M. Alkaline phosphatase levels as a prognostic factor in metastatic colorectal cancer treated with the FOLFOX 4 regimen: A monoinstitutional retrospective study. *Tumori* 2011, 97, 39–42. [Google Scholar] [CrossRef]
- [12] Saif, M.W.; Alexander, D.; Wicox, C.M. Serum alkaline phosphatase level as a prognostic tool in colorectal cancer: A study of 105 patients. *J. Appl. Res.* 2005, 5, 88–95. [Google Scholar]
- [13] William, C.S.; Melissa, G.S.; Lee, D.; Jay, W.M.; Mathur, R. Webster's New World Medical Dictionary, 5th ed.; Wiley Publishing, Inc.: Hoboken, NJ, USA, 2008. [Google Scholar]
- [14] Fersht, A. Structure and Mechanism in Protein Science: A Guide to Enzyme Catalysis and Protein Folding; World Scientific: Hackensack, NJ, USA, 2017. [Google Scholar]
- [15] Millán, J.L. Mammalian Alkaline Phosphatases: From Biology to Applications in Medicine and Biotechnology; John Wiley and Sons: Hoboken, NJ, USA, 2010. [Google Scholar]
- [16] Millán, J.L. Alkaline Phosphatases. *Purinergic Signal.* 2006, 2, 335. [Google Scholar] [CrossRef] [PubMed]
- [17] Mehrotra, S.; Rishishwar, P.; Sharma, R.K. Malnutrition and hyperphosphatemia in dialysis patients. *Clin. Queries Nephrol.* 2015, 4, 25–27. [Google Scholar] [CrossRef]
- [18] Bukowczan, J.; Pattman, S.; Jenkinson, F.; Quinton, R. Regan isoenzyme of alkaline phosphatase as a tumour marker for renal cell carcinoma. *Ann. Clin. Biochem.* 2014, 51, 611–614. [Google Scholar] [CrossRef] [PubMed]
- [19] Rader, B.A. Alkaline Phosphatase, an Unconventional Immune Protein. *Front. Immunol.* 2017, 8, 897. [Google Scholar] [CrossRef] [PubMed]
- [20] Anderson, D.J.; Branum, E.L.; O'Brien, J.F. Liver- and bone-derived isoenzymes of alkaline phosphatase in serum as determined by high-performance affinity chromatography. *Clin. Chem.* 1990, 36, 240–246. [Google Scholar]
- [21] Sharp, C.A.; Linder, C.; Magnusson, P. Analysis of human bone alkaline phosphatase isoforms: Comparison of isoelectric focusing and ion-exchange high-performance liquid chromatography. *Clin. Chim. Acta* 2007, 379, 105–112. [Google Scholar] [CrossRef]
- [22] Parviainen, M.T.; Galloway, J.H.; Towers, J.H.; Kanis, J.A. Alkaline phosphatase isoenzymes in serum determined by high-performance anion-exchange liquid chromatography with detection by enzyme reaction. *Clin. Chem.* 1988, 34, 2406–2409. [Google Scholar]
- [23] Magnusson, P.; Löfman, O.; Larsson, L. Determination of alkaline phosphatase isoenzymes in serum by high-performance liquid chromatography with post-column reaction detection. *J. Chromatogr. B Biomed. Sci. Appl.* 1992, 576, 79–86. [Google Scholar] [CrossRef]
- [24] Khan, K.H. Gene Expression in Mammalian Cells and its Applications. *Adv. Pharm. Bull.* 2013, 3, 257–263. [Google Scholar] [CrossRef]

- [25] Pike, A.F.; Kramer, N.I.; Blaauboer, B.J.; Seinen, W.; Brands, R. A novel hypothesis for an alkaline phosphatase 'rescue' mechanism in the hepatic acute phase immune response. *BBA Mol. Basis Dis.* 2013, 1832, 2044–2056. [Google Scholar] [CrossRef]
- [26] Haarhaus, M.; Brandenburg, V.; Kalantar-Zadeh, K.; Stenvinkel, P.; Magnusson, P. Alkaline phosphatase: A novel treatment target for cardiovascular disease in CKD. *Nat. Rev. Nephrol.* 2017, 13, 429–442. [Google Scholar] [CrossRef] [PubMed]
- [27] Antoni, D.; Burckel, H.; Josset, E.; Noel, G. Three-dimensional cell culture: A breakthrough *in vivo*. *Int. J. Mol. Sci.* 2015, 16, 5517–5527. [Google Scholar] [CrossRef] [PubMed]
- [28] Luo, X.; Liu, Y.; Wang, R.; Hu, H.; Zeng, R.; Chen, H. A high-quality secretome of A549 cells aided the discovery of C4b-binding protein as a novel serum biomarker for non-small cell lung cancer. *J. Proteom.* 2011, 74, 528–538. [Google Scholar] [CrossRef] [PubMed]
- [29] Chen, X.; Ba, Y.; Ma, L.; Cai, X.; Yin, Y.; Wang, K.; Guo, J.; Zhang, Y.; Chen, J.; Guo, X.; et al. Characterization of microRNAs in serum: A novel class of biomarkers for diagnosis of cancer and other diseases. *Cell Res.* 2008, 18, 997–1006. [Google Scholar] [CrossRef] [PubMed]
- [30] Pyo, J.S.; Ju, H.K.; Park, J.H.; Kwon, S.W. Determination of volatile biomarkers for apoptosis and necrosis by solid-phase microextraction–gas chromatography/mass spectrometry: A pharmacometabolomic approach to cisplatin's cytotoxicity to human lung cancer cell lines. *J. Chromatogr. B* 2008, 876, 170–174. [Google Scholar] [CrossRef] [PubMed]
- [31] Daniela Viačková, J.P.; Kubala, L.; Pacherník, J. Modulation of cell proliferation and differentiation of human lung carcinoma cells by the interferon-alpha. *Gen. Physiol. Biophys.* 2009, 28, 294–301. [Google Scholar]
- [32] Doyle, L.A.; Yang, W.; Abruzzo, L.V.; Krogmann, T.; Gao, Y.; Rishi, A.K.; Ross, D.D. A Multidrug Resistance Transporter from Human MCF-7 Breast Cancer Cells. *Proc. Natl. Acad. Sci. USA* 1998, 95, 15665–15670. [Google Scholar] [CrossRef]
- [33] Kovalchuk, O.; Filkowski, J.; Meservy, J.; Ilnytsky, Y.; Tryndyak, V.P.; Chekhun, V.F.; Pogribny, I.P. Involvement of microRNA-451 in resistance of the MCF-7 breast cancer cells to chemotherapeutic drug doxorubicin. *Mol. Cancer Ther.* 2008, 7, 2152–2159. [Google Scholar] [CrossRef]
- [34] Vignon, F.; Capony, F.; Chambon, M.; Freiss, G.; Garcia, M.; Rochefort, H. Autocrine growth stimulation of the MCF 7 breast cancer cells by the estrogen-regulated 52 K protein. *Endocrinology* 1986, 118, 1537–1545. [Google Scholar] [CrossRef]
- [35] Singh, A.K.; Pandey, A.; Tewari, M.; Kumar, R.; Sharma, A.; Singh, K.A.; Shukla, H.S. Advanced stage of breast cancer hoist alkaline phosphatase activity: Risk factor for females in India. *3 Biotech* 2013, 3, 517–520. [Google Scholar] [CrossRef]
- [36] Bellion, P.; Olk, M.; Will, F.; Dietrich, H.; Baum, M.; Eisenbrand, G.; Janzowski, C. Formation of hydrogen peroxide in cell culture media by apple polyphenols and its effect on antioxidant biomarkers in the colon cell line HT-29. *Mol. Nutr. Food Res.* 2009, 53, 1226–1236. [Google Scholar] [CrossRef]

- [37] Hong, J.; Lu, H.; Meng, X.; Ryu, J.H.; Hara, Y.; Yang, C.S. Stability, cellular uptake, biotransformation, and efflux of tea polyphenol (-)-epigallocatechin-3-gallate in HT-29 human colon adenocarcinoma cells. *Cancer Res.* 2002, 62, 7241–7246. [Google Scholar] [PubMed]
- [38] Chen, C.; Shen, G.X.; Hebbar, V.; Hu, R.; Owuor, E.D.; Kong, A.N.T. Epigallocatechin-3-gallate-induced stress signals in HT-29 human colon adenocarcinoma cells. *Carcinogenesis* 2003, 24, 1369–1378. [Google Scholar] [CrossRef] [PubMed]
- [39] Matsumoto, H.; Erickson, R.H.; Gum, J.R.; Yoshioka, M.; Gum, E.; Kim, Y.S. Biosynthesis of alkaline-phosphatase during differentiation of the human colon cancer cell-line caco-2. *Gastroenterology* 1990, 98, 1199–1207. [Google Scholar] [CrossRef]
- [40] Kovaříková, M.; Pacherník, J.; Hofmanová, J.; Zadák, Z.; Kozubík, A. TNF- α modulates the differentiation induced by butyrate in the HT-29 human colon adenocarcinoma cell line. *Eur. J. Cancer* 2000, 36, 1844–1852. [Google Scholar] [CrossRef]
- [41] Perry, M.D.; Rajendran, V.M.; MacLennan, K.A.; Sandle, G.I. Segmental differences in upregulated apical potassium channels in mammalian colon during potassium adaptation. *Am. J. Physiol. Gastrointest. Liver Physiol.* 2016, 311, G785–G793. [Google Scholar] [CrossRef]
- [42] Gerlach, A.C.; Gangopadhyay, N.N.; Devor, D.C. Kinase-dependent Regulation of the Intermediate Conductance, Calcium-dependent Potassium Channel, hIK1. *J. Biol. Chem.* 2000, 275, 585–598. [Google Scholar] [CrossRef]
- [43] Yang, B.; Cao, L.; Liu, B.; McCaig, C.D.; Pu, J. The Transition from Proliferation to Differentiation in Colorectal Cancer Is Regulated by the Calcium Activated Chloride Channel A1. *PLoS ONE* 2013, 8, e60861. [Google Scholar] [CrossRef]
- [44] Takahashi, A.; Iida, T.; Naim, R.; Naykaya, Y.; Honda, T. Chloride secretion induced by thermostable direct haemolysin of *Vibrio parahaemolyticus* depends on colonic cell maturation. *J. Med. Microbiol.* 2001, 50, 870–878. [Google Scholar] [CrossRef]
- [45] Zahanich, I.; Graf, E.M.; Heubach, J.F.; Hempel, U.; Boxberger, S.; Ravens, U. Molecular and Functional Expression of Voltage-Operated Calcium Channels During Osteogenic Differentiation of Human Mesenchymal Stem Cells. *J. Bone Miner. Res.* 2005, 20, 1637–1646. [Google Scholar] [CrossRef]
- [46] Macrae, M.X.; Blake, S.; Jiang, X.; Capone, R.; Estes, D.J.; Mayer, M.; Yang, J. A semi-synthetic ion channel platform for detection of phosphatase and protease activity. *ACS Nano* 2009, 3, 3567–3580. [Google Scholar] [CrossRef] [PubMed]
- [47] Telford, W.G.; Cox, W.G.; Stiner, D.; Singer, V.L.; Doty, S.B. Detection of endogenous alkaline phosphatase activity in intact cells by flow cytometry using the fluorogenic ELF-97 phosphatase substrate. *Cytometry* 1999, 37, 314–319. [Google Scholar] [CrossRef]
- [48] Shugar, D.; Szenberg, A.; Sierakowska, H. Quantitative histochemistry by means of radioactive indicators - alkaline phosphatase. *Exp. Cell Res.* 1957, 13, 424–426. [Google Scholar] [CrossRef]

- [49] Yi-Wei, T.; Charles, W.S. *Advanced Techniques in Diagnostic Microbiology*, 2nd ed.; Springer: New York, NY, USA, 2013. [Google Scholar]
- [50] Roelofs, H.; Manes, T.; Janszen, T.; Millan, J.L.; Oosterhuis, J.W.; Looijenga, L.H.J. Heterogeneity in alkaline phosphatase isozyme expression in human testicular germ cell tumours: An enzyme-/immunohistochemical and molecular analysis. *J. Pathol.* 1999, 189, 236–244. [Google Scholar] [CrossRef]
- [51] Mano, H.; Furuhashi, Y.; Morikawa, Y.; Hattori, S.E.; Goto, S.; Tomoda, Y. Radioimmunoassay of placental alkaline-phosphatase in ovarian-cancer sera and tissues. *Obstet. Gynecol.* 1986, 68, 759–764. [Google Scholar] [PubMed]
- [52] Degroote, G.; Dewaele, P.; Vandevoorde, A.; Debroe, M.; Fiers, W. Use of monoclonal-antibodies to detect human placental alkaline-phosphatase. *Clin. Chem.* 1983, 29, 115–119. [Google Scholar]
- [53] Fiskens, J.; Leonard, R.C.F.; Shaw, G.; Bowman, A.; Roulston, J.E. Serum placental-like alkaline-phosphatase (PLAP)-a novel combined enzyme linked immunoassay for monitoring ovarian-cancer. *J. Clin. Pathol.* 1989, 42, 40–45. [Google Scholar] [CrossRef] [PubMed]
- [54] Ake, M.S.; Johnston, K.H.; Russell-Jones, G.J.; Gotschlich, E.C. A rapid, sensitive method for detection of alkaline phosphatase-conjugated anti-antibody on Western blots. *Anal. Biochem.* 1984, 136, 175–179. [Google Scholar] [CrossRef]
- [55] Thiha, A.; Ibrahim, F. A Colorimetric Enzyme-Linked Immunosorbent Assay (ELISA) Detection Platform for a Point-of-Care Dengue Detection System on a Lab-on-Compact-Disc. *Sensors (Basel)* 2015, 15, 11431–11441. [Google Scholar] [CrossRef]
- [56] Hammar, F. Chemgapedia. 2018. Available online: <http://www.chemgapedia.de/vsengine/en/index.html> (accessed on 12 April 2018).
- [57] Sussman, H.H.; Small, P.J.; Cotlove, E. Human alkaline phosphatase. Immunochemical identification of organ-specific isoenzymes. *J. Biol. Chem.* 1968, 243, 160–166. [Google Scholar]
- [58] Singh, I.; Tsang, K.Y. An *in vitro* production of bone specific alkaline phosphatase. *Exp. Cell Res.* 1975, 95, 347–358. [Google Scholar] [CrossRef]
- [59] Rosivatz, E. Imaging the boundaries—innovative tools for microscopy of living cells and real-time imaging. *J. Chem. Biol.* 2008, 1, 3–15. [Google Scholar] [CrossRef] [PubMed]
- [60] Tseng, J.C.; Kung, A.L. *In vivo* imaging of endogenous enzyme activities using luminescent 1,2-dioxetane compounds. *J. Biomed. Sci.* 2015, 22. [Google Scholar] [CrossRef] [PubMed]
- [61] Cagnin, S.; Caraballo, M.; Guiducci, C.; Martini, P.; Ross, M.; Santaana, M.; Lanfranchi, G. Overview of Electrochemical DNA Biosensors: New Approaches to Detect the Expression of Life. *Sensors (Basel)* 2009, 9, 3122–3148. [Google Scholar] [CrossRef] [PubMed]
- [62] Peltomaa, R.; Glahn-Martínez, B.; Benito-Peña, E.; Moreno-Bondi, M. Optical Biosensors for Label-Free Detection of Small Molecules. *Sensors* 2018, 18, 4126. [Google Scholar] [CrossRef]

- [63] Deng, J.J.; Yu, P.; Wang, Y.; Mao, L. Real-time Ratiometric Fluorescent Assay for Alkaline Phosphatase Activity with Stimulus Responsive Infinite Coordination Polymer Nanoparticles. *Anal. Chem.* 2015, 87, 3080–3086. [Google Scholar] [CrossRef] [PubMed]
- [64] Zhao, S.Q.; Lu, J.C.; Huang, Y.Y.; Tang, C.; Shen, J.J.; Chen, J.R.; Feng, H. A real-time fluorescent assay for the detection of alkaline phosphatase activity based on carbon quantum dots. *Biosens. Bioelectron.* 2015, 68, 675–680. [Google Scholar]
- [65] Liu, X.G.; Xing, X.J.; Li, B.; Guo, Y.M.; Zhang, Y.Z.; Yang, Y.; Zhang, L.F. Fluorescent assay for alkaline phosphatase activity based on graphene oxide integrating with λ exonuclease. *Biosens. Bioelectron.* 2016, 81, 460–464. [Google Scholar] [CrossRef]
- [66] Qu, F.L.; Pei, H.; Kong, R.; Zhu, S.; Xia, L. Novel turn-on fluorescent detection of alkaline phosphatase based on green synthesized carbon dots and MnO₂ nanosheets. *Talanta* 2017, 165, 136–142. [Google Scholar] [CrossRef]
- [67] Chen, L.; Yang, G.; Wu, P.; Cai, C. Real-time fluorescence assay of alkaline phosphatase in living cells using boron-doped graphene quantum dots as fluorophores. *Biosens. Bioelectron.* 2017, 96, 294–299. [Google Scholar] [CrossRef]
- [68] Siraj, N.; El-Zahab, B.; Hamdan, S.; Karam, T.E.; Haber, L.H.; Li, M.; Warner, I.M. Fluorescence, Phosphorescence, and Chemiluminescence. *Anal. Chem.* 2016, 88, 170–202. [Google Scholar] [CrossRef] [PubMed]
- [69] Sasamoto, H.; Maeda, M.; Tsuji, A. Chemiluminescent assay of alkaline phosphatase using phenacyl phosphate. *Anal. Chim. Acta* 1995, 306, 161–166. [Google Scholar] [CrossRef]
- [70] Ximenes, V.F.; Campa, A.; Baader, W.J.; Catalani, L.H. Facile chemiluminescent method for alkaline phosphatase determination. *Anal. Chim. Acta* 1999, 402, 99–104. [Google Scholar] [CrossRef]
- [71] Kokado, A.; Arakawa, H.; Maeda, M. Chemiluminescent assay of alkaline phosphatase using dihydroxyacetone phosphate as substrate detected with lucigenin. *Luminescence* 2002, 17, 5–10. [Google Scholar] [CrossRef] [PubMed]
- [72] Meng, Y.; Kasai, A.; Hiramatsu, N.; Hayakawa, K.; Takeda, M.; Shimizu, F.; Kitamura, M. Real-time monitoring of mesangial cell-macrophage cross-talk using SEAP *in vitro* and *ex vivo*. *Kidney Int.* 2005, 68, 886–893. [Google Scholar] [CrossRef] [PubMed]
- [73] Larkin, P.; ProQuest. *Infrared and Raman Spectroscopy: Principles and Spectral Interpretation*, 2nd ed.; Elsevier: Amsterdam, The Netherlands, 2018. [Google Scholar]
- [74] Cottat, M.; Yasukuni, R.; Homma, Y.; Lidgi-Guigui, N.; Varin-Blank, N.; de la Chapelle, M.L.; Le Roy, C. Phosphorylation impact on Spleen Tyrosine kinase conformation by Surface Enhanced Raman Spectroscopy. *Sci. Rep.* 2017, 7, 39766. [Google Scholar] [CrossRef]
- [75] Yang, L.; Gao, M.X.; Zhan, L.; Gong, M.; Zhen, S.J.; Huang, C.Z. An enzyme-induced Au@Ag core-shell nanoStructure used for an ultrasensitive surface-enhanced Raman scattering immunoassay of cancer biomarkers. *Nanoscale* 2017, 9, 2640–2645. [Google Scholar] [CrossRef]

- [76] Bozkurt, A.G.; Buyukgoz, G.G.; Soforoglu, M.; Tamer, U.; Suludere, Z.; Boyaci, I.H. Alkaline phosphatase labeled SERS active sandwich immunoassay for detection of Escherichia coli. *Spectrochim. Acta Part A Mol. Biomol. Spectrosc.* 2018, 194, 8–13. [Google Scholar] [CrossRef]
- [77] Ren, Z.Y.; Do, L.D.; Bechkoff, G.; Mebarek, S.; Keloglu, N.; Ahamada, S.; Buchet, R. Direct Determination of Phosphatase Activity from Physiological Substrates in Cells. *PLoS ONE* 2015, 10, e0120087. [Google Scholar] [CrossRef]
- [78] Li, S.J.; Li, C.Y.; Li, Y.F.; Fei, J.J.; Wu, P.; Yang, B.; Nie, S.X. Facile and Sensitive Near-Infrared Fluorescence Probe for the Detection of Endogenous Alkaline Phosphatase Activity *in Vivo*. *Anal. Chem.* 2017, 89, 6854–6860. [Google Scholar] [CrossRef]
- [79] Gao, Z.; Gao, M.; Sun, J.; Yu, F.; Chen, L.; Chen, Q. A unique off-on near-infrared cyanine-based probe for imaging of endogenous alkaline phosphatase activity in cells and *in vivo*. *Sens. Actuators B Chem.* 2018, 265, 565–574. [Google Scholar] [CrossRef]
- [80] Wu, C.F.; Zhang, R.; Du, W.; Cheng, L.; Liang, G.L. Alkaline Phosphatase-Triggered Self-Assembly of Near-Infrared Nanoparticles for the Enhanced Photoacoustic Imaging of Tumors. *Nano Lett.* 2018, 18, 7749–7754. [Google Scholar] [CrossRef] [PubMed]
- [81] Xu, L.B.; He, X.; Huang, Y.B.; Ma, P.Y.; Jiang, Y.X.; Liu, X.; Wang, X.H. A novel near-infrared fluorescent probe for detecting intracellular alkaline phosphatase and imaging of living cells. *J. Mater. Chem. B* 2019, 7, 1284–1291. [Google Scholar] [CrossRef]
- [82] Im, H.; Hong, S.; Lee, Y.; Lee, H.; Kim, S. Colorimetric Sensing Systems: A Colorimetric Multifunctional Sensing Method for Structural-Durability-Health Monitoring Systems (*Adv. Mater.* 23/2019). *Adv. Mater.* 2019, 31, 1970163. [Google Scholar] [CrossRef]
- [83] Chen, X.; Chen, J.; Zhang, H.Y.; Wang, F.B.; Wang, F.F.; Ji, X.H.; He, Z.K. Colorimetric Detection of Alkaline Phosphatase on Microfluidic Paper-based Analysis Devices. *Chin. J. Anal. Chem.* 2016, 44, 591–596. [Google Scholar] [CrossRef]
- [84] Hu, Q.; Zhou, B.; Dang, P.; Li, L.; Kong, J.; Zhang, X. Facile colorimetric assay of alkaline phosphatase activity using Fe(II)-phenanthroline reporter. *Anal. Chim. Acta* 2017, 950, 170–177. [Google Scholar] [CrossRef]
- [85] Hu, Q.; He, M.; Mei, Y.; Feng, W.; Jing, S.; Kong, J.; Zhang, X. Sensitive and selective colorimetric assay of alkaline phosphatase activity with Cu(II)-phenanthroline complex. *Talanta* 2017, 163, 146–152. [Google Scholar] [CrossRef] [PubMed]
- [86] Huang, Q.; He, C.; Zhang, J.; Li, W.; Fu, Y. Unlocking the hidden talent of DNA: Unexpected catalytic activity for colorimetric assay of alkaline phosphatase. *Anal. Chim. Acta* 2019, 1055, 98–105. [Google Scholar] [CrossRef] [PubMed]
- [87] Wu, T.T.; Hou, W.L.; Ma, Z.Y.; Liu, M.L.; Liu, X.Y.; Zhang, Y.Y.; Yao, S.Z. Colorimetric determination of ascorbic acid and the activity of alkaline phosphatase based on the inhibition of the peroxidase-like activity of citric acid-capped Prussian Blue nanocubes. *Microchim. Acta* 2019, 186, 123–127. [Google Scholar] [CrossRef] [PubMed]

- [88] Hou, W.B.; Cronin, S.B. A Review of Surface Plasmon Resonance-Enhanced Photocatalysis. *Adv. Funct. Mater.* 2013, 23, 1612–1619. [Google Scholar] [CrossRef]
- [89] Halling Linder, C.; Enander, K.; Magnusson, P. Glycation Contributes to Interaction Between Human Bone Alkaline Phosphatase and Collagen Type, I. *Calcif. Tissue Int.* 2016, 98, 284–293. [Google Scholar] [CrossRef] [PubMed]
- [90] Sappia, L.; Piccinini, E.; Santilli, N.; Marmisolé, W.; Madrid, R.; Azzaroni, O. Lectin-modified surfaces for the real-time determination of Bone Alkaline Phosphatase by Surface Plasmon Resonance (SPR) Spectroscopy. In *Proceedings of the 1st Argentine-German Workshop on Nanotechnology and Nanobiosensors, Buenos Aires, Argentina, 4–7 July 2017*. [Google Scholar]
- [91] Wang, K.; Jiang, L.; Zhang, F.; Wei, Y.Q.; Wang, H.S.; Qi, Z.J.; Liu, S.Q. Strategy for in Situ Imaging of Cellular Alkaline Phosphatase Activity Using Gold Nanoflower Probe and Localized Surface Plasmon Resonance Technique. *Anal. Chem.* 2018, 90, 14056–14062. [Google Scholar] [CrossRef] [PubMed]
- [92] Yi, C.; Zhang, Q.; Li, C.W.; Yang, J.; Zhao, J.; Yang, M. *Optical and Electrochemical Detection Techniques for Cell-Based Microfluidic Systems*; Springer: Berlin/Heidelberg, Germany, 2006; Volume 384, pp. 1259–1268. [Google Scholar]
- [93] Stradiotto, N.R.; Yamanaka, H.; Zanoni, M.V.B. Electrochemical sensors: A powerful tool in analytical chemistry. *J. Braz. Chem. Soc.* 2003, 14, 159–173. [Google Scholar] [CrossRef]
- [94] Sołoducho, J.; Cabaj, J. *Electrochemical and Optical Biosensors in Medical Applications*; Intech Open, Science Open Mind: London, UK, 2015. [Google Scholar]
- [95] Lee, T.M.H.; Hsing, I.M. DNA-based bioanalytical microsystems for handheld device applications. *Anal. Chim. Acta* 2006, 556, 26–37. [Google Scholar] [CrossRef] [PubMed]
- [96] Thompson, R.Q.; Barone, G.C.; Halsall, H.B.; Heineman, W.R. Comparison of methods for following alkaline-phosphatase catalysis—spectrophotometric versus amperometric detection. *Anal. Biochem.* 1991, 192, 90–95. [Google Scholar] [CrossRef]
- [97] Matysik, F.M. Advances in amperometric and conductometric detection in capillary and chip-based electrophoresis. *Microchim. Acta* 2008, 160, 1–14. [Google Scholar] [CrossRef]
- [98] Kelso, E.; McLean, J.; Cardosi, M.F. Electrochemical detection of secreted alkaline phosphatase: Implications to cell based assays. *Electroanalysis* 2000, 12, 490–494. [Google Scholar] [CrossRef]
- [99] Ito, S.; Yamazaki, S.I.; Kano, K.; Ikeda, T. Highly sensitive electrochemical detection of alkaline phosphatase. *Anal. Chim. Acta* 2000, 424, 57–63. [Google Scholar] [CrossRef]
- [100] Wang, J.H.; Wang, K.; Bartling, B.; Liu, C.C. The Detection of Alkaline Phosphatase Using an Electrochemical Biosensor in a Single-Step Approach. *Sensors (Basel)* 2009, 9, 8709–8721. [Google Scholar] [CrossRef]

- [101] Ru, S.P.; Wu, J.; Ying, Y.B.; Ji, F. Electrochemical Detection of Alkaline Phosphatase Using Ionic Liquid Modified Carbon Nanotubes Electrode. *Chin. J. Anal. Chem.* 2012, 40, 835–839. [Google Scholar] [CrossRef]
- [102] Xia, N.; Ma, F.; Zhao, F.; He, Q.; Du, J.; Li, S.; Liu, L. Comparing the performances of electrochemical sensors using p-aminophenol redox cycling by different reductants on gold electrodes modified with self-assembled monolayers. *Electrochim. Acta* 2013, 109, 348–354. [Google Scholar] [CrossRef]
- [103] Zhang, L.; Hou, T.; Li, H.; Li, F. A highly sensitive homogeneous electrochemical assay for alkaline phosphatase activity based on single molecular beacon-initiated T7 exonuclease-mediated signal amplification. *Analyst* 2015, 14, 43–436. [Google Scholar] [CrossRef] [PubMed]
- [104] Yildirim-Semerici, C.; Benayahu, D.; Adamovski, M.; Wollenberger, U. An Electrochemical Assay for Monitoring Differentiation of the Osteoblastic Cell Line (MBA-15) on the Sensor Chip. *Electroanalysis* 2015, 27, 1350–1358. [Google Scholar] [CrossRef]
- [105] Porat-Ophir, C.; Dergachev, V.; Belkin, A.; Vernick, S.; Freynd, G.; Katsnelson, M.; Shacham-Diamand, Y. Chip level agitation effects on the electrochemical sensing of alkaline-phosphatase expressed from integrated liver tissue. *Sens. Actuators B Chem.* 2015, 213, 465–473. [Google Scholar] [CrossRef]
- [106] Vernick, S.; Freeman, A.; Rishpon, J.; Niv, Y.; Vilkin, A.; Shacham-Diamand, Y. Electrochemical Biosensing for Direct Biopsy Slices Screening for Colorectal Cancer Detection. *J. Electrochem. Soc.* 2011, 158, P1–P4. [Google Scholar] [CrossRef]
- [107] Ragonis, H.; Schreiber, D.; Inberg, A.; Berkh, O.; Kósa, G.; Freeman, A.; Shacham-Diamand, Y. Disposable electrochemical sensor prepared using 3D printing for cell and tissue diagnostics. *Sens. Actuators B Chem.* 2015, 216, 434–442. [Google Scholar] [CrossRef]
- [108] Zdrachek, E.; Bakker, E. Potentiometric Sensing. *Anal. Chem.* 2019, 91, 2–26. [Google Scholar] [CrossRef] [PubMed]
- [109] Keyes, M.H. Electrochemical Potentiometric Method for Selectively Determining Alkaline Phosphatase Content in Aqueous Fluids. U.S. Patent 3896008A, 22 July 1975. [Google Scholar]
- [110] Katsu, T.; Yamanaka, K.; Hiramaki, S.; Tanaka, T.; Nagamatsu, T. Potentiometric Determination of Alkaline Phosphatase in Blood Serum Using a Hordenine-Sensitive Membrane Electrode. *Electroanalysis* 1996, 1101–1104. [Google Scholar] [CrossRef]
- [111] Koncki, R.; Ogończyk, D.; Głab, S. Potentiometric assay for acid and alkaline phosphatase. *Anal. Chim. Acta* 2005, 538, 257–261. [Google Scholar] [CrossRef]
- [112] Koncki, R.; Rudnicka, K.; Tymecki, Ł. Flow injection system for potentiometric determination of alkaline phosphatase inhibitors. *Anal. Chim. Acta* 2006, 577, 134–139. [Google Scholar] [CrossRef]

- [113] Ogończyk, D.; Koncki, R. Potentiometric flow-injection system for determination of alkaline phosphatase in human serum. *Anal. Chim. Acta* 2007, 600, 194–198. [Google Scholar] [CrossRef] [PubMed]
- [114] Hassan, S.S.M.; Sayour, H.E.M.; Kamel, A.H. A simple-potentiometric method for determination of acid and alkaline phosphatase enzymes in biological fluids and dairy products using a nitrophenylphosphate plastic membrane sensor. *Anal. Chim. Acta* 2009, 640, 75–81. [Google Scholar] [CrossRef] [PubMed]
- [115] Kanno, Y.; Ino, K.; Sakamoto, C.; Inoue, K.Y.; Matsudaira, M.; Suda, A.; Matsue, T. Potentiometric bioimaging with a large-scale integration (LSI)-based electrochemical device for detection of enzyme activity. *Biosens. Bioelectron.* 2016, 77, 709–714. [Google Scholar] [CrossRef] [PubMed]
- [116] Kucherenko, I.S.; Kucherenko, D.Y.; Soldatkin, A.P.; Soldatkin, O.O.; Lagarde, F.; Dzyadevych, S.V. A novel conductometric biosensor based on hexokinase for determination of adenosine triphosphate. *Talanta* 2016, 150, 469–475. [Google Scholar] [CrossRef] [PubMed]
- [117] Guedri, H.; Durrieu, C. A self-assembled monolayers based conductometric algal whole cell biosensor for water monitoring. *Microchim. Acta* 2008, 163, 179–184. [Google Scholar] [CrossRef]
- [118] Upadhyay, L.S.B.; Verma, N. Alkaline phosphatase inhibition based conductometric biosensor for phosphate estimation in biological fluids. *Biosens. Bioelectron.* 2015, 68, 611–616. [Google Scholar] [CrossRef] [PubMed]
- [119] Chouteau, C.; Dzyadevych, S.; Chovelon, J.M.; Durrieu, C. Development of novel conductometric biosensors based on immobilised whole cell *Chlorella vulgaris* microalgae. *Biosens. Bioelectron.* 2004, 19, 1089–1096. [Google Scholar] [CrossRef] [PubMed]
- [120] Berezhetsky, A.L.; Sosovska, O.F.; Durrieu, C.; Chovelon, J.M.; Dzyadevych, S.V.; Tran-Minh, C. Alkaline phosphatase conductometric biosensor for heavy-metal ions determination. *IRBM* 2008, 29, 136–140. [Google Scholar] [CrossRef]
- [121] Gomes, W.P.; Vanmaekelbergh, D. Impedance spectroscopy at semiconductor electrodes: Review and recent developments. *Electrochim. Acta* 1996, 41, 967–973. [Google Scholar] [CrossRef]
- [122] Cai, Q.; Wei, W.; Wang, R.; Nie, L.; Yao, S. Measurement of Serum Alkaline Phosphatase with a Surface Acoustic Wave Impedance Sensor Device. *Anal. Sci.* 1997, 13, 121–125. [Google Scholar] [CrossRef]
- [123] Lee, J.Y.; Ahn, J.K.; Park, K.S.; Park, H.G. An impedimetric determination of alkaline phosphatase activity based on the oxidation reaction mediated by Cu²⁺ bound to poly-thymine DNA. *RSC Adv.* 2018, 8, 11241–11246. [Google Scholar] [CrossRef]
- [124] Lucarelli, F.; Marrazza, G.; Mascini, M. Enzyme-based impedimetric detection of PCR products using oligonucleotide-modified screen-printed gold electrodes. *Biosens. Bioelectron.* 2005, 20, 2001–2009. [Google Scholar] [CrossRef] [PubMed]

- [125] Ferancova, A.; Hattuniemi, M.; Pääkkönen, S.; Tervo, P.; Ohtonen, E.; Sesay, A.; Virtanen, V. Electrochemical Impedance Spectroscopy for Monitoring of Alkaline Phosphatase Reaction with Substrate. *Procedia Technol.* 2017, 27, 315–316. [Google Scholar] [CrossRef]
- [126] Shrikrishnan, S.; Sankaran, K.; Lakshminarayanan, V. Electrochemical Impedance Analysis of Adsorption and Enzyme Kinetics of Calf Intestine Alkaline Phosphatase on SAM-Modified Gold Electrode. *J. Phys. Chem. C* 2012, 116, 16030–16037. [Google Scholar] [CrossRef]
- [127] Mintz Hemed, N.; Convertino, A.; Shacham-Diamand, Y. Alkaline phosphatase detection using electrochemical impedance of anti-alkaline phosphatase antibody (Ab354) functionalized silicon-nanowire-forest in phosphate buffer solution. *Sens. Actuators B Chem.* 2018, 259, 809–815. [Google Scholar] [CrossRef]
- [128] Kaatz, M.; Schulze, H.; Ciani, I.; Lisdat, F.; Mount, A.R.; Bachmann, T.T. Alkaline phosphatase enzymatic signal amplification for fast, sensitive impedimetric DNA detection. *Analyst* 2012, 137, 59–63. [Google Scholar] [CrossRef] [PubMed]
- [129] Sekar, S.; Giermanska, J.; Chapel, J.P. Reusable and recyclable quartz crystal microbalance sensors. *Sens. Actuators B Chem.* 2015, 212, 196–199. [Google Scholar] [CrossRef]
- [130] Ebersole, R.C.; Ward, M.D. Amplified Mass Immunosorbent Assay with a Quartz Crystal Microbalance. *Am. Chem. Soc.* 1988, 110, 8623–8628. [Google Scholar] [CrossRef]
- [131] Kacar, T.; Zin, M.T.; So, C.; Wilson, B.; Ma, H.; Gul-Karaguler, N.; Tamerler, C. Directed Self-Immobilization of Alkaline Phosphatase on Micro-Patterned Substrates Via Genetically Fused Metal-Binding Peptide. *Biotechnol. Bioeng.* 2009, 103, 696–705. [Google Scholar] [CrossRef]
- [132] Thammasittirong, A.; Dechklar, M.; Leetachewa, S.; Pootanakit, K.; Angsuthanasombat, C. *Aedes aegypti* Membrane-Bound Alkaline Phosphatase Expressed in *Escherichia coli* Retains High-Affinity Binding for *Bacillus thuringiensis* Cry4Ba Toxin. *Appl. Environ. Microbiol.* 2011, 77, 6836–6840. [Google Scholar] [CrossRef]
- [133] Syu, Y.C.; Hsu, W.E.; Lin, C.T. Review-Field-Effect Transistor Biosensing: Devices and Clinical Applications. *ECS J. Solid State Sci. Technol.* 2018, 7, Q3196–Q3207. [Google Scholar] [CrossRef]
- [134] Jang, H.J.; Ahn, J.; Kim, M.G.; Shin, Y.B.; Jeun, M.; Cho, W.J.; Lee, K.H. Electrical signaling of enzyme-linked immunosorbent assays with an ion-sensitive field-effect transistor. *Biosens. Bioelectron.* 2015, 64, 318–323. [Google Scholar] [CrossRef] [PubMed]
- [135] Freeman, R.; Gill, R.; Willner, I. Following a protein kinase activity using a field-effect transistor device. *Chem. Commun.* 2007, 3450–3452. [Google Scholar] [CrossRef] [PubMed]
- [136] Favero, G.; Fusco, G.; Mazzei, F.; Tasca, F.; Antiochia, R. Electrochemical Characterization of Graphene and MWCNT Screen-Printed Electrodes Modified with AuNPs for Laccase Biosensor Development. *Nanomaterials* 2015, 5, 1995–2006. [Google Scholar] [CrossRef] [PubMed]

- [137] Adams, N.M.; Jackson, S.R.; Haselton, F.R.; Wright, D.W. Design, Synthesis, and Characterization of Nucleic-Acid-Functionalized Gold Surfaces for Biomarker Detection. *Langmuir* 2012, 28, 1068–1082. [Google Scholar] [CrossRef] [PubMed]
- [138] Li, C.M.; Li, Y.F.; Zhen, S.J.; Wang, J.; Huang, C.Z. A gold nanoparticles-based colorimetric assay for alkaline phosphatase detection with tunable dynamic range. *Biosens. Bioelectron.* 2013, 43, 366–371. [Google Scholar] [CrossRef]
- [139] Ruan, C.M.; Wang, W.; Gu, B.H. Detection of alkaline phosphatase using surface-enhanced Raman spectroscopy. *Anal. Chem.* 2006, 78, 3379–3384. [Google Scholar] [CrossRef]
- [140] Zeng, Y.; Ren, J.Q.; Wang, S.K.; Mai, J.M.; Qu, B.; Zhang, Y.; Hu, J.M. Rapid and Reliable Detection of Alkaline Phosphatase by a Hot Spots Amplification Strategy Based on Well-Controlled Assembly on Single Nanoparticle. *ACS Appl. Mater. Interfaces* 2017, 9, 29547–29553. [Google Scholar] [CrossRef]
- [141] Liu, Q.; Li, H.; Li, N.; Jin, R.; Yan, X.; Su, X. Ultrasensitive detection alkaline phosphatase activity using 3-aminophenylboronic acid functionalized gold nanoclusters. *Sens. Actuators B Chem.* 2019, 281, 175–181. [Google Scholar] [CrossRef]
- [142] He, Y.; Jiao, B. Determination of the activity of alkaline phosphatase based on the use of ssDNA-templated fluorescent silver nanoclusters and on enzyme-triggered silver reduction. *Microchim. Acta* 2017, 184, 4167–4173. [Google Scholar] [CrossRef]
- [143] Wang, H.B.; Li, Y.; Chen, Y.; Zhang, Z.P.; Gan, T.; Liu, Y.M. Determination of the activity of alkaline phosphatase by using nanoclusters composed of flower-like cobalt oxyhydroxide and copper nanoclusters as fluorescent probes. *Microchim. Acta* 2018, 185, 1–8. [Google Scholar] [CrossRef] [PubMed]
- [144] Hu, Y.L.; Geng, X.; Zhang, L.; Huang, Z.M.; Ge, J.; Li, Z.H. Nitrogen-doped Carbon Dots Mediated Fluorescent on-off Assay for Rapid and Highly Sensitive Pyrophosphate and Alkaline Phosphatase Detection. *Sci. Rep.* 2017, 7, 5849. [Google Scholar] [CrossRef] [PubMed]
- [145] Pandey, S.; Sharma, A.K.; Sharma, K.H.; Nerthigan, Y.; Khan, M.S.; Hang, D.R.; Wu, H.F. Rapid naked eye detection of alkaline phosphatase using $[\alpha]$ -MoO₃ nano-flakes. *Sens. Actuators B Chem.* 2018, 254, 514. [Google Scholar] [CrossRef]
- [146] Choi, Y.; Ho, N.H.; Tung, C.H. Sensing phosphatase activity by using gold nanoparticles. *Angew. Chem. Int. Ed.* 2007, 46, 707–709. [Google Scholar] [CrossRef]
- [147] Serizawa, T.; Hirai, Y.; Aizawa, M. Detection of enzyme activities based on the synthesis of gold nanoparticles in HEPES buffer. *Mol. Biosyst.* 2010, 6, 1561–1564. [Google Scholar] [CrossRef]
- [148] Song, H.; Wang, H.; Li, X.; Peng, Y.; Pan, J.; Niu, X. Sensitive and selective colorimetric detection of alkaline phosphatase activity based on phosphate anion-quenched oxidase-mimicking activity of Ce (IV) ions. *Anal. Chim. Acta* 2018, 1044, 154–161. [Google Scholar] [CrossRef] [PubMed]

- [149] AL-Rubaei, E.A.S.; Abd, S.T.; Kadim, N.M. The Effect of Titanium Dioxide Nanoparticles on Salivary Alkaline Phosphatase Activity. *Eur. J. Mol. Biotechnol.* 2015, 10, 188–196. [Google Scholar] [CrossRef]
- [150] Zhang, L.; Nie, J.F.; Wang, H.L.; Yang, J.H.; Wang, B.Y.; Zhang, Y.; Li, J.P. Instrument-free quantitative detection of alkaline phosphatase using paper-based devices. *Anal. Methods* 2017, 9, 3375–3379. [Google Scholar] [CrossRef]
- [151] Cao, F.Y.; Fan, J.X.; Long, Y.; Zeng, X.; Zhang, X.Z. A Smart Fluorescence Nanoprobe for the Detection of Cellular Alkaline Phosphatase Activity and Early Osteogenic Differentiation. *Nanomed. Nanotechnol. Biol. Med.* 2015, 12, 1313–1322. [Google Scholar] [CrossRef]
- [152] Ru, S.-P.; Wu, J.; Ying, Y.-B.; Ji, F. Electrochemical Detection of Alkaline Phosphatase Using Ionic Liquid Modified Carbon Nanotubes Electrode: Electrochemical Detection of Alkaline Phosphatase Using Ionic Liquid Modified Carbon Nanotubes Electrode. *Chin. J. Anal. Chem. (Chin. Version)* 2013, 40, 835–840. [Google Scholar] [CrossRef]
- [153] Peng, J.; Han, X.X.; Zhang, Q.C.; Yao, H.Q.; Gao, Z.N. Copper sulfide nanoparticle-decorated graphene as a catalytic amplification platform for electrochemical detection of alkaline phosphatase activity. *Anal. Chim. Acta* 2015, 878, 87–94. [Google Scholar] [CrossRef] [PubMed]
- [154] Zhou, Y.; Yin, H.; Li, Z.; Li, X.; Ai, S.; Lin, H. Electrochemical biosensor for protein kinase A activity assay based on gold nanoparticles-carbon nanospheres, phos-tag-biotin and β -galactosidase. *Biosens. Bioelectron.* 2016, 86, 508–515. [Google Scholar] [CrossRef] [PubMed]
- [155] Pandey, R.; Almog, R.O.; Sverdllov, Y.; Shacham-Diamand, Y. Self-Aligned Electrochemical Fabrication of Gold Nanoparticle Decorated Polypyrrole Electrode for Alkaline Phosphatase Enzyme Biosensing. *J. Electrochem. Soc.* 2017, 164, B168–B175. [Google Scholar] [CrossRef]
- [156] Zhao, L.; Zhao, L.; Miao, Y.; Zhang, C. Gold Nanoparticle-Decorated Single-Walled Carbon Nanotubes as a Catalytic Amplification Platform for the Electrochemical Detection of Alkaline Phosphatase Activity. *Int. J. Electrochem. Sci.* 2018, 13, 1293–1307. [Google Scholar] [CrossRef]
- [157] Simão, E.P.; Frías, I.A.M.; Andrade, C.A.S.; Oliveira, M.D.L. Nanostructured electrochemical immunosensor for detection of serological alkaline phosphatase. *Colloids Surf. B Biointerfaces* 2018, 171, 413–418. [Google Scholar] [CrossRef] [PubMed]
- [158] Kang, Q.; Wang, X.; Ma, X.; Kong, L.; Zhang, P.; Shen, D. Sensitive detection of ascorbic acid and alkaline phosphatase activity by double-channel photoelectrochemical detection design based on g-C₃N₄/TiO₂ nanotubes hybrid film. *Sens. Actuators B Chem.* 2016, 230, 231–241. [Google Scholar] [CrossRef]
- [159] Lin, Z.; Takahashi, Y.; Kitagawa, Y.; Umemura, T.; Shiku, H.; Matsue, T. An addressable microelectrode array for electrochemical detection. *Anal. Chem.* 2008, 80, 6830–6833. [Google Scholar] [CrossRef]

- [160] Lin, Z.Y.; Takahashi, Y.; Murata, T.; Takeda, M.; Ino, K.; Shiku, H.; Matsue, T. Electrochemical Gene-Function Analysis for Single Cells with Addressable Microelectrode/Microwell Arrays. *Angew. Chem. Int. Ed.* 2009, 48, 2044–2046. [Google Scholar] [CrossRef]
- [161] Murata, T.; Yasukawa, T.; Shiku, H.; Matsue, T. Electrochemical single-cell gene-expression assay combining dielectrophoretic manipulation with secreted alkaline phosphatase reporter system. *Biosens. Bioelectron.* 2009, 25, 913–919. [Google Scholar] [CrossRef]
- [162] Shiku, H.; Suzuki, J.; Murata, T.; Ino, K.; Matsue, T. Chronoamperometric characterization of secreted alkaline phosphatase from single-cell entrapped in a poly(dimethylsiloxane) microwell. *Electrochim. Acta* 2010, 55, 8263–8267. [Google Scholar] [CrossRef]
- [163] Takeda, M.; Shiku, H.; Ino, K.; Matsue, T. Electrochemical chip integrating scalable ring-ring electrode array to detect secreted alkaline phosphatase. *Analyst* 2011, 136, 4991–4996. [Google Scholar] [CrossRef] [PubMed]
- [164] Ino, K.; Nishijo, T.; Arai, T.; Kanno, Y.; Takahashi, Y.; Shiku, H.; Matsue, T. Local Redox-Cycling-Based Electrochemical Chip Device with Deep Microwells for Evaluation of Embryoid Bodies. *Angew. Chem. Int. Ed. Engl.* 2012, 124, 6752–6756. [Google Scholar] [CrossRef]
- [165] Wu, Z.; Zhou, C.H.; Pan, L.J.; Zeng, T.; Zhu, L.; Pang, D.W.; Zhang, Z.L. Reliable Digital Single Molecule Electrochemistry for Ultrasensitive Alkaline Phosphatase Detection. *Anal. Chem.* 2016, 88, 9166–9172. [Google Scholar] [CrossRef] [PubMed]
- [166] Sen, M.; Ino, K.; Shiku, H.; Matsue, T. Accumulation and detection of secreted proteins from single cells for reporter gene assays using a local redox cycling-based electrochemical (LRC-EC) chip device. *Lab Chip* 2012, 12, 4328–4335. [Google Scholar] [CrossRef] [PubMed]
- [167] Şen, M.; Ino, K.; Shiku, H.; Matsue, T. A new electrochemical assay method for gene expression using hela cells with a secreted alkaline phosphatase (SEAP) reporter system. *Biotechnol. Bioeng.* 2012, 109, 2163–2167. [Google Scholar] [CrossRef]
- [168] Chen, Q.S.; Wu, J.; Zhuang, Q.C.; Lin, X.X.; Zhang, J.; Lin, J.M. Microfluidic isolation of highly pure embryonic stem cells using feeder-separated co-culture system. *Sci. Rep.* 2013, 3, 2433. [Google Scholar] [CrossRef] [PubMed]
- [169] Ino, K.; Kanno, Y.; Nishijo, T.; Komaki, H.; Yamada, Y.; Yoshida, S.; Matsue, T. Densified Electrochemical Sensors Based on Local Redox Cycling between Vertically Separated Electrodes in Substrate Generation/Chip Collection and Extended Feedback Modes. *Anal. Chem.* 2014, 86, 4016–4023. [Google Scholar] [CrossRef]
- [170] Ino, K.; Goto, T.; Kanno, Y.; Inoue, K.Y.; Takahashi, Y.; Shiku, H.; Matsue, T. Droplet array on local redox cycling-based electrochemical (LRC-EC) chip device. *Lab Chip* 2014, 14, 787–794. [Google Scholar] [CrossRef]

- [171] Cao, X.Y.; Kong, F.Z.; Zhang, Q.; Liu, W.W.; Liu, X.P.; Li, G.Q.; Cao, C.X. iPhone-imaged and cell-powered electrophoresis titration chip for the alkaline phosphatase assay in serum by the moving reaction boundary. *Lab Chip* 2018, 18, 1758–1766. [Google Scholar] [CrossRef]
- [172] Sun, D.; Cao, F.H.; Cong, L.L.; Xu, W.Q.; Chen, Q.D.; Shi, W.; Xu, S.P. Cellular heterogeneity identified by single-cell alkaline phosphatase (ALP) via a SERRS-microfluidic droplet platform. *Lab Chip* 2019, 19, 335–342. [Google Scholar] [CrossRef]
- [173] Ino, K.; Shiku, H.; Matsue, T. Bioelectrochemical applications of microelectrode arrays in cell analysis and engineering. *Curr. Opin. Electrochem.* 2017, 5, 146–151. [Google Scholar] [CrossRef]



© 2019 by the authors. Submitted for possible open access publication under the terms and conditions of the Creative Commons Attribution (CC BY) license (<http://creativecommons.org/licenses/by/4.0/>).

Resazurin-Based Assay for Quantifying Living Cells during Alkaline Phosphatase (ALP) Release

Thanih Balbaied and Eric Moore*

University College Cork, Sensing & Separation Group, School of Chemistry and life Science Interface, Tyndall National Institute, T12R5CP Cork, Ireland

* Correspondence: e.moore@ucc.ie

Received: 31 March 2020; Accepted: 29 May 2020; Published: date

Abstract: Alkaline phosphatase (ALP) is an important reporter gene in the gene expression system, therefore monitoring cellular behavior including cell viability during ALP release is of significance. This assay produced a quantitative resazurin-based assay for cell viability in embryonic and cancer cells during alkaline phosphatase (ALP) release. A post-confluence culture method was applied to induce ALP in the cells of Balb/c 3T3, A549, MCF-7, and Ht-29. The density of each cell type was optimized using the standard cell culture assay. The main parameters affecting the results of resazurin involve the concentration of resazurin, incubation time, and cell number. The redox reaction, in which resazurin is reduced by the cells, was measured by fluorescence at 544 nm and 590 nm. The obtained data were compared with the hemocytometer assay. ALP release was determined using the optical active substrate p-nitrophenyl phosphate and colorimetric assay.

Keywords: resazurin-based assays; cell viability; alkaline phosphatase; Balb/c 3T3 cells; A549 cells; MCF-7 cells.

1. Introduction

Biomedical studies use cell adhesion approaches in their applications (e.g., on sensors or on lab-on-a-chip [1,2]). Simplifying the determination of cell viability on these applications is important. The common membrane integrity assay [3] that is used widely requires cell lysis and results in an endpoint assay [4]. Metabolic based assays are simple, cheap, and are a one-step assay, thereby avoiding the limitations of the above-mentioned assay. Numerous dyes can be used to reflect metabolic activity through redox reactions in live cell membranes. One of these dyes is resazurin, which under constant experimental conditions, can provide a stable rate of fluorescence intensity and quantify cell numbers [5,6,7]. Resazurin can be defined as a cell permeable redox indicator that helps in tracking the number of viable cells. Physiological buffers can absorb resazurin, resulting in a deep blue solution. Viable cells have active metabolisms and can therefore convert resazurin into a pink fluorescent solution [8]. Figure 1 shows a schematic of an optimization protocol for quantifying cell number by the resazurin assay. Different concentrations of resazurin are added to the culture medium of incubated cells. At various time intervals, the redox reaction, in which resazurin is reduced by the cells, is measured by fluorescence readings at 544 nm and 590 nm. The optimal concentration of resazurin versus particular cell type is used at different cell numbers to facilitate the relationship between the fluorescent signal and the cell number at constant time. Resazurin is more sensitive and allows multiple assays compared to other dyes [9].

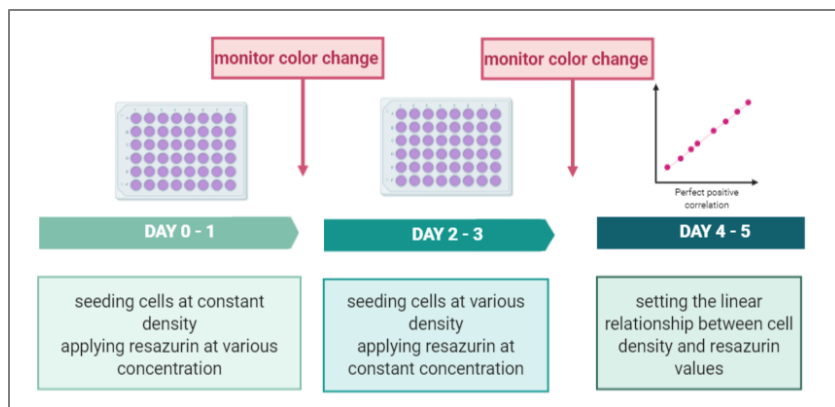


Figure 1. Generalized scheme representing an optimization protocol of a resazurin-based assay for the determination of cancer cell numbers.

Several reports have shown the optimization of resazurin reduction assays [10] for cytotoxic agents, antifungal agents, antibacterial agents, the identification of parasites, and the drug sensibility of parasites for large-scale screenings, biofilm, and for cell expansion in matrix scaffolds using bacteria [11,12] fungi and yeast [13,14,15], parasites [16,17], and human cells [15,18]. To the best of our knowledge, this is the first paper that discusses cell viability during cancer biomarker release using a resazurin-based assay. Alkaline phosphatase, which is the early biomarker of many cancers, is correlated with cell proliferation, differentiation, and apoptosis [19-25], and, therefore, is important in cell-based biosensors [26]. Cell viability was determined for cancer biomarkers using membrane integrity [27], flow cytometry [28], and phase-contrast microscope images [29]. The aim of this paper was to provide simple and reproducible methods for quantifying cell number during ALP release from different cell types. The cancer cell lines including MCF-7, A549, and Ht-29 are used as models of the top three cancers diagnosed worldwide: lung (13%), breast (11%), and colon (10%), respectively [30]. In addition, Balb/c 3T3, which is an embryonic cell line, is used as it is more sensitive to contact inhibition of cell division than cancer cell lines. The ALP level is investigated using optical methods, and the cell number is verified using the hemocytometer assay.

2. Methodology

2.1. Reagents

Mouse embryo fibroblast cells (Balb/c 3T3 Line), breast carcinoma epithelial cells (MCF-7 line), lung carcinoma epithelial cells (A-549 line), colon carcinoma epithelial cells (Ht-29 line) purchased from (ATCC, the UK). 70% ethanol, and nanopure water provided from (Grade 18 M Ω , Tyndall National Institute, UCC). Newborn calf serum (NBCS), fetal bovine serum (FBS), Dulbecco's modified Eagle's medium (DMEM), minimum essential medium Eagle (MEME), and McCoy's 5A Medium, Hank's balanced salt solution (HBSS), Trypsin/EDTA solution, resazurin, Virkon[®], magnesium chloride (MgCl₂), sodium chloride (NaCl), diethanolamine (DEA), Triton X-100, and para-nitrophenol phosphate (p-NPP), and calf intestinal phosphatase (ALP) purchased from (Sigma, Ireland).

2.2. Instrumentation

Cell culture hood (Esco Airstream[®] Class II), 5% CO₂ incubator (Incusafe Panasonic), water bath 37 °C (Fisherbarnd), centrifugation (universal 320 Hittch zentrifugen and Eppendorf 5415D Centrifuge) were used. An inverted microscope and camera (Olympus), fluorescent plate readers (Spectra Max Gemini), absorbance plate reader (Diasource ELISA Reader), hemocytometer slide (Reichert Bright-Line), glass cover slips (menzel-gläser) and cell counter, pipettes (Rainin Pipet-X) and micropipettes (Gilson Pipetman[®]),

pipette tips (Greiner Bio-One), pipettors (5 mL, 10 mL, and 25 mL), cell culture vessels (75T flasks, 1.5 mL, 15 mL, 50mL centrifuge tubes, 96- and 48-well plates), and syringes 45 nm filters (Sigma, Ireland) were also used.

2.3. Cell Culture

The cancer cell lines used during this project were stored in liquid nitrogen prior to being cultured. To begin cell growth, they were removed from storage and quickly defrosted (less than a minute). The entire contents (1 mL) of the cryogenic vial were then pipetted into a 15mL-tube that contained 9 mL of pre-warmed complete media (Table 1). The tube was centrifuged to dispose of dimethyl sulfoxide, which was present in the supernatant. The cells were re-suspended in 5 mL complete media and placed in a T75 flask that already contained 35 mL of completed media in order to reach a volume of 40 mL. The flask was incubated in the incubator at 37 °C and 5% CO₂ to reach 70% confluence.

Table 1. The media and serum of each cell line used for cell culture.

	Cell lines	Balb/c 3T3	A549	MCF-7	Ht-29
Complete media	Media	DMEM	DMEM	MEME	McCoy's 5A
	10 % Serum	NBCS		FBS	

Completed media represent the addition of 10% of serum to the media suitable for each cell line, according to the manufacturer's recommendations.

The cells were sub-cultured at least three times before optimization began. Briefly, the subculture procedure was achieved by removing old media via a sterile plastic pipette, followed by two washes with pre-warmed HBSS. A total of 4 mL of trypsin was then added, and the flask was incubated for 5–8 min to allow the cells to detach. Then, 6 mL of complete media was added to inactivate the trypsin. The cell suspension was placed in a clean 15 mL centrifuge tube, and the cells were centrifuged for 5 min at 1000 rpm. The supernatant was removed, and the cell pellets were re-suspended in 5 mL of fresh media. The desired cell number was seeded in a 48-well plate, and the final volume of media was added. All experiments were applied in a 48-well plate.

2.4. Determining the Optimal Concentration of Resazurin

Each cell line required a certain concentration of resazurin to ensure viability. Resazurin was dissolved in HBSS to a final concentration of 2 mM to make a stock solution. The stock solution was filtered using a syringe with 0.45 nm pores. To make an intermediate standard, the stock solution was diluted once more in complete media at 10% giving 200 µM. Two-fold serial dilutions were then made, starting with 200 µM. This was then added to cells that were previously seeded in triplicate at the same density (250×10^3 cell/mL). The plates were incubated with the various concentrations of resazurin at a final volume of 0.5 mL for 24 h. The fluorescent signal was then recorded at 544 excitation and 590 nm emission wavelengths using the fluorescent plate reader.

2.5. Determining the Optimal Time of Incubation with Resazurin

Concentrations of 350×10^3 cell/mL were prepared and diluted in 2-fold using the complete media of each cell line. The dilutions were seeded in 48-well plates and incubated at 37 °C for 24 h to allow for attachment. Old media were replaced by the optimal concentration of resazurin in the case of each cell line. The plates were incubated and monitored after two hours and then continuously over a 24-h period. The

fluorescent signal was taken at different times at 544 excitation and 590 nm emission wavelengths using the fluorescent plate reader.

2.6. Determining the Calibration Curve of Resazurin and Cell Numbers

Resazurin is a metabolic-based assay that reflects cell viability. In order to make it an assay that measured the cell number, 2-fold serial dilutions of the cell number starting from 250×10^3 cell/mL were seeded in triplicate, and complete media were added for a final volume of 0.5 mL. Cells were incubated for 12 h to allow the cells to attach and avoid duplicating. Old media were replaced by the optimal concentration of resazurin in the case of each cell line. Four hours later, the fluorescent signal was recorded at 544 excitation and 590 nm emission wavelengths using the fluorescent plate reader. The theoretical calibration curves were made from a cell concentration of $(4\text{--}60 \times 10^3$ cell/mL). The resulting linear equation was used to estimate the fluorescent signal for the cell concentration applied in this assay.

2.7. Determining the Optimal Density of Cell Lines

The target density for this paper was identified as when cells proliferated for at least four days and then reached contact-inhibited growth. This was where the target analyte started to express. Five concentrations of cells were prepared ($350, 160, 80, 40, 20 \times 10^3$ cell/mL). The final volume of complete media was 0.5 mL. The cells were incubated at 37°C and monitored daily for five days. Old media were changed every two days to keep cells healthy and with sufficient nutrients. On day 1, resazurin was added to cells in plate 1, and four hours later, the fluorescence signal was recorded. The process was continued for the other plates until day 5.

2.8. Determining Cell Number Based Resazurin Assay

The optimal density of each cell line was seeded in triplicate, and cell growth was assessed at 24-h intervals over five days. Old media were changed every two days to keep cells healthy and with sufficient nutrients. To determine the daily fluorescent signal, media were replaced by the optimal concentration of resazurin in the case of each cell line. Four hours after this, the fluorescent signal was recorded. The linear equation of the obtained calibration curve was used to quantify the cell number daily over five days.

2.9. Microscope Images

Images of cell-confluence were taken at 24-h intervals over five days using the inverted microscope and camera. Due to the presence of phenol red, which interferes with the light of microscopes, cells were washed twice with HBSS. Images were then taken from the center of the wells.

2.10. Hemocytometer Assay

Cell viability was also determined using the hemocytometer assay for the optimal density. As previously noted, cells were seeded in triplicate, and cell growth was assessed at 24-h intervals over five days. The old media were changed every two days to keep cells healthy and with sufficient nutrients. After the washing and trypsinization processes, harvested cell pellets were re-suspended in complete media, a coverslip was used to cover the two counting chambers, and then a drop of the solution was inserted, allowing the solution to spread gently. Under the microscope, nine squares were observed to be accounting cells. Accounting cells had to be averaged and multiplied by the three demotions of the hemacytometer, where the width and height equaled 1 mm, and the depth equaled 0.1 mm to get a final concentration of cell per mL using the following equation:

$$C = \frac{n}{10^{-4}} \quad (1)$$

where C is the final concentration of cell numbers per mL and n is the average of cell numbers counted from each square.

2.11. Cell Viability at Post-Confluence Culture

Cells can be differentiated using post-confluence culture to ensure ALP release, which makes the determination of the cell viability of cells at post confluence culture important. Cells were seeded in 48-well plates at a concentration of 40×10^3 cells/mL for the following cells: Balb/c 3T3, A549, and MCF-7, and at a concentration of 80×10^3 cells/mL for the Ht-29 cells. Cells had the media changed every two day to keep them healthy and with sufficient nutrients. After they achieved their exponential growth and met the 95–100% confluence (Day 4), the cells were maintained in growth media for a further two days. Old media were replaced by the optimal concentration of resazurin in the case of each cell line for the fourth, fifth, and sixth days. Cells were incubated with resazurin for four hours. Vehicle control of each cell was prepared by adding two drops of Virkon® in the complete media for 24 h the night before the assay. A reszurin control was added to media with no cells. The fluorescence signal was recorded for each day.

2.12. Alkaline Phosphatase Release from Cells at Post-Confluence Culture

To induce ALP and allow real-time monitoring, cells were differentiated using post-confluence culture. Cells were seeded in 48-well plates at a concentration of 40×10^3 cells/mL for the following cells: Balb/c 3T3, A549, and MCF-7, and at a concentration of 80×10^3 cells/mL for the Ht-29 cells. Cells had the media changed every two days to keep them healthy and with sufficient nutrients. After they reached their exponential growth and met the 95–100% confluence (Day 4), the cells were maintained in growth media for a further two days. Cells were washed twice with HBSS in each target day. The ALP assay buffer at pH 9.5 was added in the presence of 0.8 mM MgCl_2 and 50 mM NaCl, 0.1% Triton X-100, and 8 mM pNPP and 0 mM pNPP as a blank for each cell line. Vehicle control of each cell was prepared by adding two drops of Virkon® in the complete media for 24 h the night before the assay. Cells were then incubated in the specified buffers for 30 min. For the standard curve, a commercial ALP had its concentration varied from 1.5 U/L to 1500 U/L. A Lineweaver–Burk model was plotted between the absorbance values and ALP concentrations to obtain the linear equation. Measurements were applied to the 96-well plate in triplicate, and absorbance was taken at 405 nm using the spectrophotometer at a final volume of 150 μL .

2.13. Data Analysis

Single factor of analysis of variance (ANOVA), MS Excel, and Origin were used in order to analyze the results of the experiments and to ensure the limitation of errors. Results were displayed as mean \pm SD. There were: $n = 3$ was replicated for each condition in each individual experiment and the displayed data represent the mean of at least three independent experiments. The coefficient of variation % and p-values and Z-factor were considered.

3. Results and Discussion

3.1. Determining the Optimal Concentration of Resazurin

Metabolic activity may differ between cells, which makes optimizing the concentration of resazurin important. Cells were plated in 48-well plates and incubated for 24 h to allow for attachment. Different concentrations of resazurin were added, starting with the highest possible concentration that would not be toxic to cells ($\sim 200 \mu\text{M}$). This was then serially diluted to 1:2 to produce a range of μM /well. All measurements were done with 24-h incubation times. Figure 2A–D shows that the resazurin reduction rate was positively proportional to the resazurin concentration. However, this gradual increase was limited by the highest concentration, where, after the optimal concentration, the rate of resazurin reduction decreased. Figure 2A–C illustrates the highest reduction rate at 50 μM and then shows an inverse relationship. Figure 2D shows the highest reduction rate at 100 μM , while 200 μM exhibited a high deviation. This data indicate that the optimal concentration of Balb/c3T3, A549, and MCF-7 was 50 μM , and

that of the Ht-29 cell was 100 μM . Figure 2E shows the coefficient variance of the analysis data at various resazurin concentrations. At the lowest recorded concentrations of resazurin, the relative variability exceeded 20%. The CV% then fell and reached its lowest level at 100 μM . However, at higher concentrations, this trend reversed and CV% started to increase. These findings indicate that resazurin at a high concentration may be destructive to cells [31].

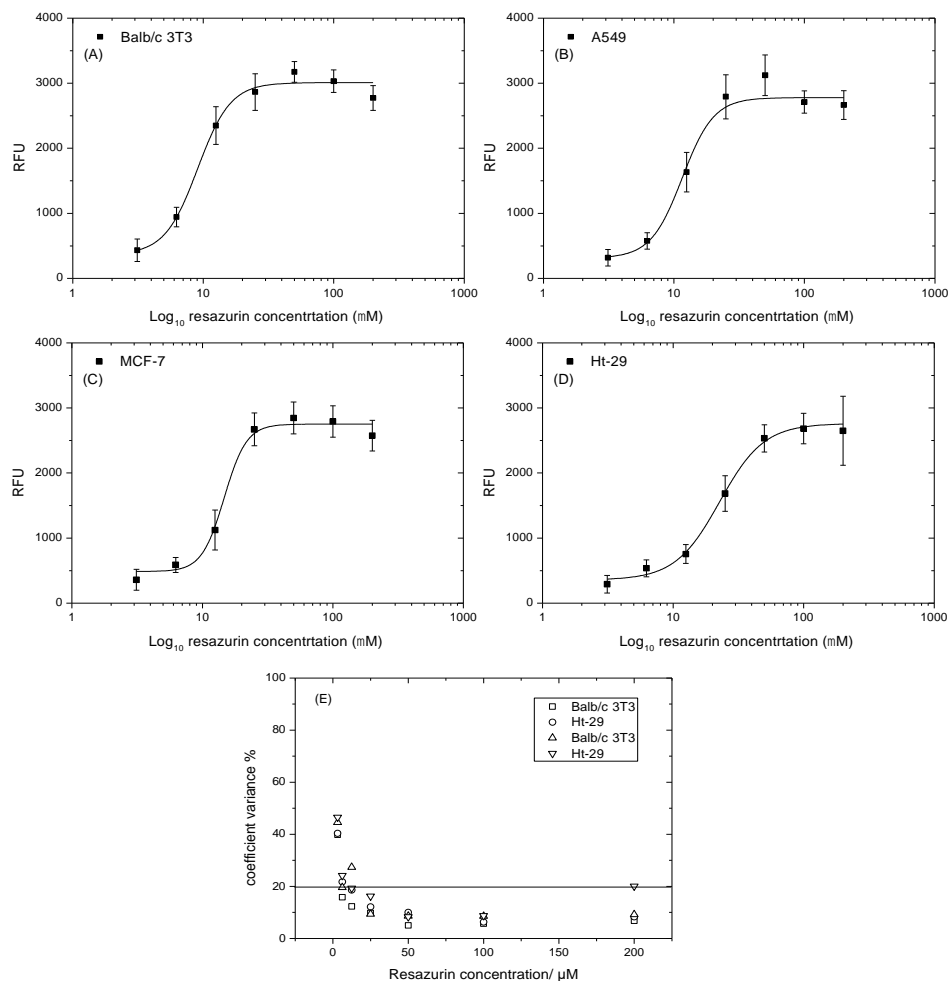


Figure 2. Optimization of the concentration of resazurin at various cell lines. (A) Balb/c/3T3 cell lines; (B) A549 cell lines; (C) MCF-7 cell lines; (D) Ht-29 cell lines; (E) coefficient variance % of resazurin concentration of vs cells numbers. Data are expressed as the mean \pm SD of measurements of three independent experiments.

3.2. Determining the Optimal Time of Incubation with Resazurin

It is important to determine the resazurin incubation time, because resazurin reduction is affected by time and cell density. Cells were plated at the highest saturation density ($\sim 3 \times 10^5$ cell/mL), then serially diluted in a ratio of 1:2 to produce the range of cell density/well. After 24 h, the attached cells were incubated with a set volume of resazurin working solution for 2, 4, 12, or 24 h in order to cover all the recommended times (1–24 h). Figure 3A–D shows that the number of cells was strongly correlated with the values of resazurin reduction. This correlation was linear from two to four hours, but it started to lose

linearity when the incubation time increased from 12 to 24 h. Linearity after two hours was positively proportional to cell densities, but it still demonstrated a low slope, which may underestimate cell numbers. A 4-h incubation time proved to be a preferable incubation time. The slope at the 4-h incubation time was almost two times higher than that of the 2-h incubation time. The occurrence of high density may form hydroresorufin faster. This high density was avoided in this research study. A 12-h incubation time showed an increase at low density, and then the rate of resazurin reduction started to decline by ($\sim 1 \times 10^5$ cell/mL). This incubation time was avoided to reduce errors for the rest of the investigation where proliferation needed to be detected. After 24 h, the incubation time levelled, since the lowest density had the same rate as the highest, making the 24 h suitable when time parameters were not recommended. Coefficient variance (CV%) was highly reproducible in the non-linearity assays, although it was high at low densities of cells. Figure 3E shows that CV% exceeded a range of 20% at the lowest density of cells in the linear assays. It appears that four hours is the optimal time recommended. This is in agreement with Hamalainen-Laanya's contributions [32], which state that the cell density should be finely tuned in order to prevent the over-reduction of resazurin and ensure the applicability of the resazurin assay.

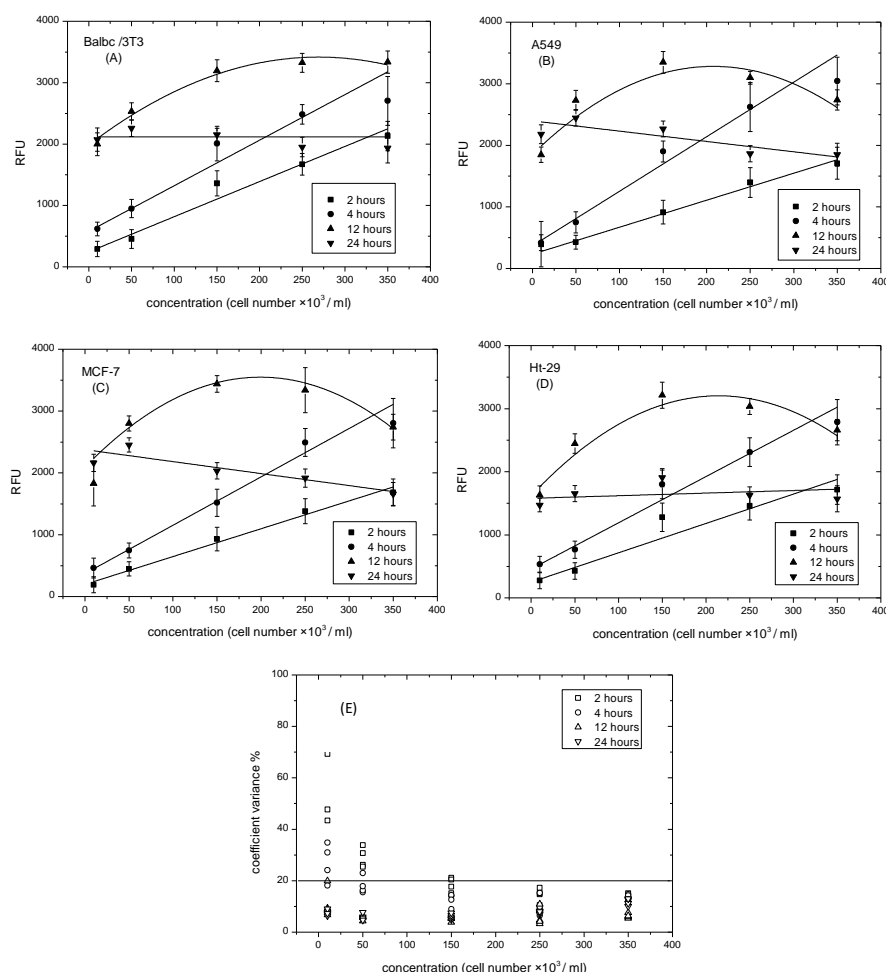


Figure 3. Effect of incubation time on fluorescence intensity measured during resazurin reduction. (A) Balbc/3T3 cell lines; (B) A549 cell lines; (C) MCF-7 cell lines; (D) Ht-29 cell lines; (E) Coefficient variance % of incubation time vs. cells numbers. Data are expressed as the mean \pm SD of the measurements of three independent experiments.

3.3. Determining the Standard Curve of Resazurin and Cell Numbers

Cell numbers can be quantified by the calibration curves of resazurin reduction. The calibration curve of each cell line was generated by plating the cells lines (Balb/c 3T3, A549, MCF-7, and Ht-29) at the same initial density ($\sim 250 \times 10^3$ cell/mL), then serially diluting in a ratio of 1:2 to produce a range of cell density/well. Eight hours later, and before dividing, resazurin solution was added according to the optimal concentration and incubated for four hours. Figure 4A–D shows the experimental and theoretical calibration curves produced by acceptable data over the concentration range of (~ 4 – 250×10^3 cell/mL) of the four cell lines. In comparison with the theoretical calibration curves, which were calculated using the linear equation of cells ranging from (4 – 60×10^3)cell/mL, the experimental curves of the four cell lines displayed an exponential shape at the high concentration with adjusted R-squared of 0.97, 0.97, 0.99, and 0.98 for the cells of Balb/c 3T3, A549, MCF-7 and Ht-29, respectively [33]. The shape was most clear in the Balb/c 3T3 cell lines, where cells reached the inhibitive growth point, and least clear in the MCF-7 cell lines. This saturating trend might result in different cell sizes. For example, the MCF-7 size was 5–7 μm in diameter [34], this then limited the cell attachment to the plate surface. Therefore, the differences between the two curves, theoretical and experimental, were determined for each dilution ratio. Figure 4F illustrates the significant data of cell number (~ 4 – 250×10^3 cell/mL), which were less than 10% for all cell lines. However, at the range of (125 – 250×10^3 cell/mL), the percentage of errors barely exceeded 10% for all cell lines. Notably, the repeatability of results can be interpreted in Figure 4E. The relative variability of the lowest recorded cell numbers barely exceeded 20%, while at high cell numbers, the CV% was the lowest.

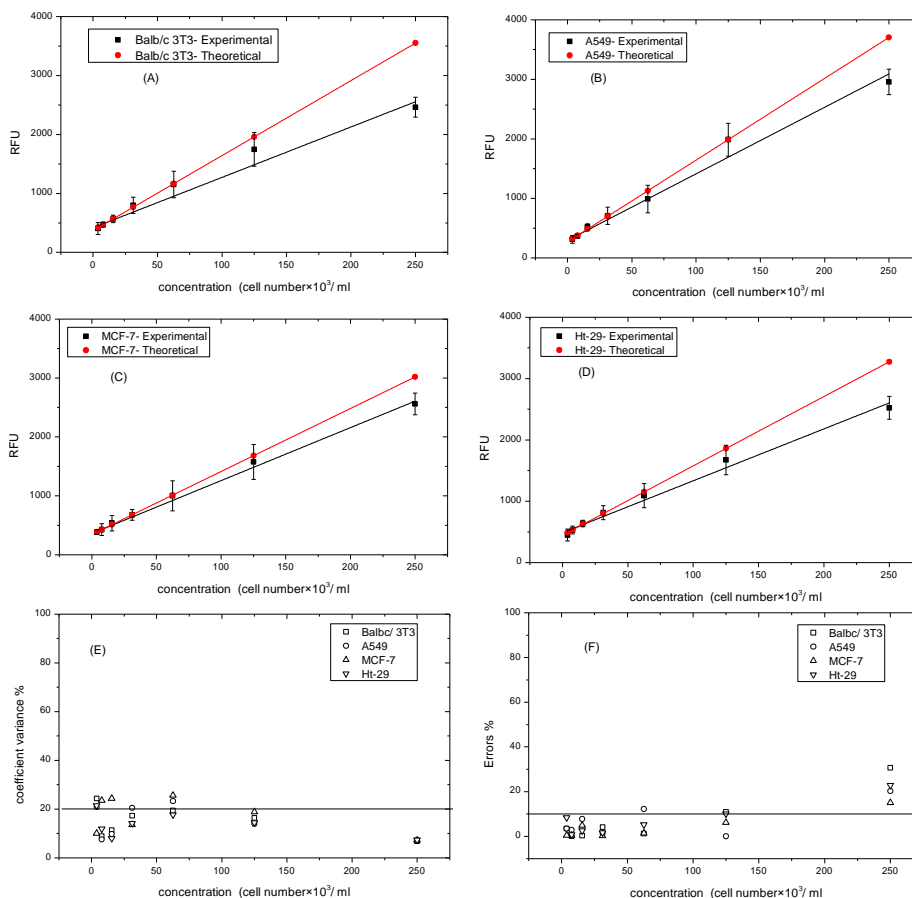


Figure 4. Experimental and theoretical standard curves of resazurin at various cell lines. (A) Balbc/3T3 cell lines; (B) A549 cell lines; (C) MCF-7 cell lines; (D) Ht-29 cell lines; (E) Coefficient variance % of experimental curves vs. cells numbers. (F) Errors % of theoretical and experimental curves vs. cell number. Data are expressed as mean \pm SD of measurements of three independent experiments.

3.4. Determining the Optimal Density of Cell Lines.

There are several stages in the life cycle of mammalian cells. In one of these stages, hormones, protein, enzymes, etc. are produced. To allow the expression of these products, cellular functions such as adhesion, proliferation, migration, or apoptosis are usually investigated [9,10]. Cells were plated at an initial density of (320×10^3 cell/mL) and then serially diluted in a ratio of 1:2 to produce the range of cell density/well. This was done to make the cells simultaneously reach contact-inhibited growth. Cell growth was monitored over five days and resazurin reduction was recorded. Figure 5A–D shows the growth curves of the four cell lines at the five different densities. Low density with an s-shape expressed logistic growth, whereas high density failed to exhibit an s-shape and levelled out from day 1. Balb/c 3T3 cell lines displayed an s-shape at $20\text{--}40 \times 10^3$ cells/mL, but for the higher densities, $80\text{--}320 \times 10^3$ cell/mL showed approximately level density, although 80×10^3 cell/mL exhibited a little growth at day 1, which means that 40×10^3 cell/mL is the optimal density of the Balb/c 3T3 cell lines (Figure 5A). The A549 cell lines behaved the same as the previous cell line, but the s-shape of the lowest density 20×10^3 cell/mL was quite unclear. From Figure 5B, it is clear that 40×10^3 cell/mL is the optimal density (Figure 5B). Like the Balb/c 3T3 cell lines, the A549 cell lines at the higher densities ranged from $80\text{--}320 \times 10^3$ cell/mL and levelled by day 1. Figure 5C shows that the MCF-7 cell lines displayed an s-shape of 20×10^3 cell/mL, but at a very low reduction rate of resazurin (~ 1000 nm). The 40×10^3 cell/mL sample demonstrated a J-shape, which began to level by day 5. The higher densities, ranging from $160\text{--}320 \times 10^3$ cell/mL, did not show any growth behavior. This meant that 40×10^3 cell/mL was the optimal density. Ht-29 behaved quite differently to the other cell lines, where at low densities $20\text{--}40 \times 10^3$ cell/mL, it showed a j-shape (Figure 5D), whereas at 80×10^3 cell/mL, it showed an s-shape, which makes it the optimal density. Like the other cells, the Ht-29 cell lines at the higher density ranged from $160\text{--}320 \times 10^3$ cell/mL and levelled on day 1 and then started to decrease. The CV% of all five days was less than 20% on day 1, and on day 2, cell numbers barely exceeded 20%. This was probably because of the lag phase and the ability of cells to divide and adjust themselves in the new environment. This investigation facilitated the determination of the optimal density of each cell line and makes it applicable for this research study, where the expression of ALP versus cell viability was investigated [35,36].

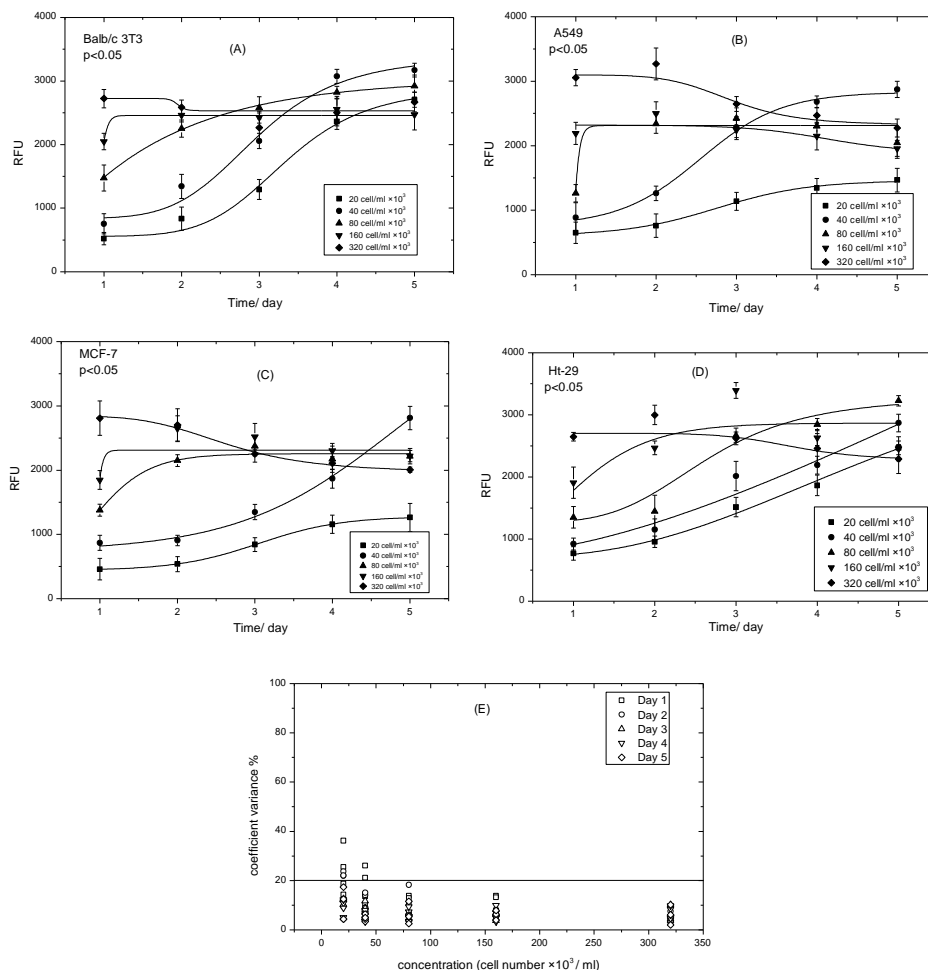


Figure 5. Logistic growth curves of the different cell densities at various cell lines over five days. **(A)** Balb/c 3T3 cell lines; **(B)** A549 cell lines; **(C)** MCF-7 cell lines; **(D)** Ht-29 cell lines; **(E)** coefficient variance % of growth curves vs. cells numbers. Data are expressed as the mean \pm SD of measurements of three independent experiments.

3.5. Microscope Images

The determination of cell shape per day is important in order to know the state of the cells when the experiment begins and when sampling starts simultaneously. The optimal density of each cell obtained from the previous experiment was seeded and monitored over five days. It is obvious from Figure 6, in the baseline, that the cells behaved differently. The Balb/c 3T3 and MCF-7 cells attached quickly and started to flatten. A549 and Ht-29 cells had a rounder shape, which means that they needed a longer time to attach. Balb/c 3T3 cells showed constant division from day 1 to day 3 and 80–100% confluence by days 4 and 5. This probably means that cells reached the inhibitive growth contact quickly by day 4, and that there was no working area left for more division. This result met the resazurin reduction findings in Figure 5A. A549 cells started to flatten by day 1, had a spindle shape by day 2, and then had sudden doubling, which explains the results found in Figure 4B. By days 4 and 5, cells seemed to have no space to divide, so they shrank and started to proliferate, as these kinds of cells rarely form multilayers. MCF-7 cells, on the other hand, showed a longer lag phase and slowly divided from day 1 to day 3. Cells barely reached almost 70%

confluence by day 4 and had space to confluence in day 5. These findings explain the j-shape displayed in Figure 4C and ensured that no multilayer had formed. Ht-29 cells started to flatten in day 1 and then had confluence from day 2 to day 4. Likewise, for Balb/c 3T3 and A549 cells, Ht-29 cells had no space to double. Ht-29 cells seem to have their extracellular matrix spread out and cover the area in day 3. This extracellular matrix reduced when cells reached confluence in days 4 and 5. Another microscope or dyes might be used to display this division.

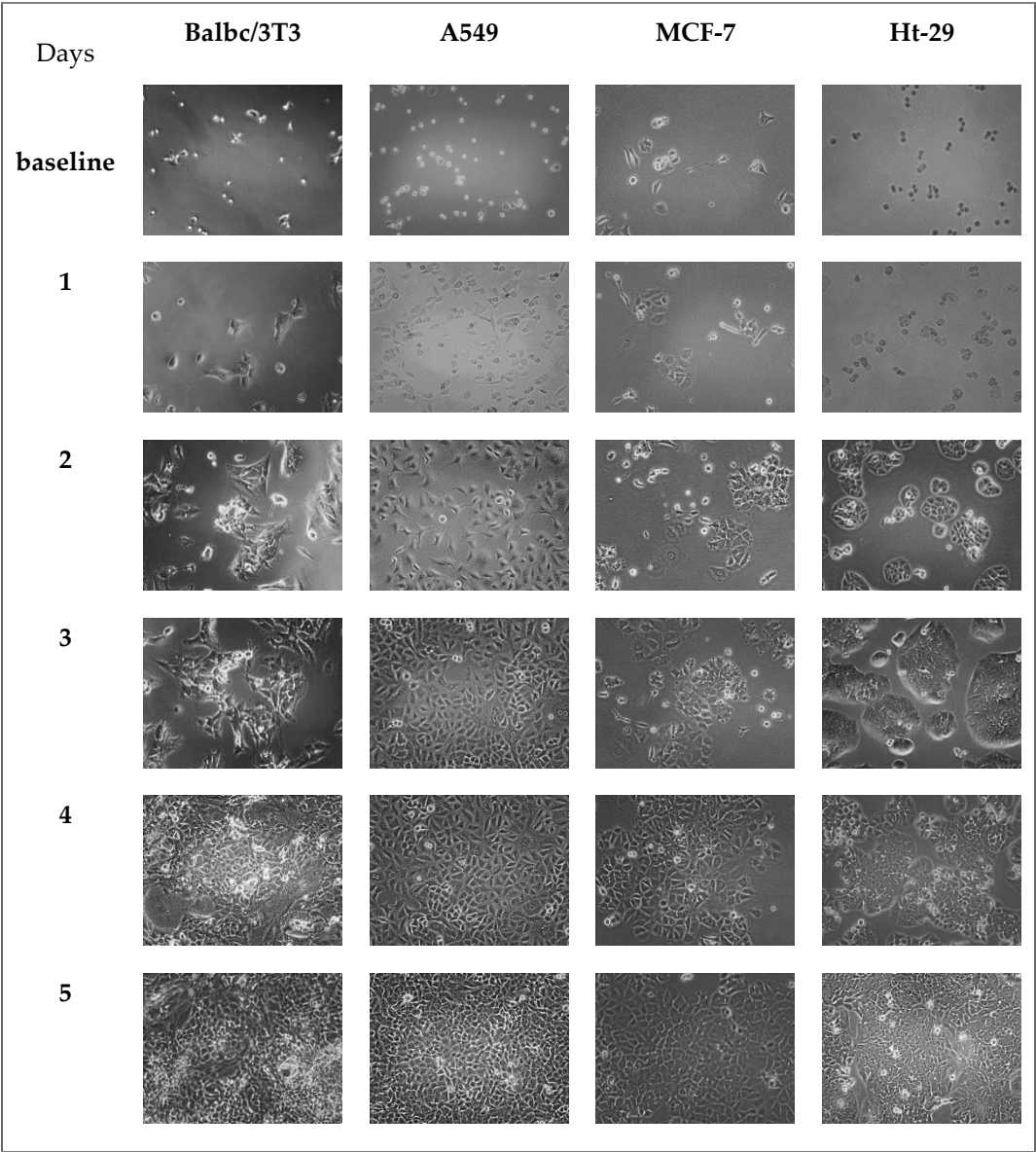


Figure 6. Microscope images of the four cells over five days..

3.6. Determining Cell Number and Comparison to Hemocytometer Assay

The cell culture growth curve represents the number of live cells over a period of time and covering the four phases [37]. In the first two growth phases, cells are more likely to be consistent, while in the stationary phase, cells may be more differentiated. Morphology may become polarized, and has more spreading for the extracellular matrix. Therefore, determination of the viability of cells in using quantitative

analysis was required. Resazurin reduction of each cell obtained from the previous experiment was used to estimate viable cells using the linear equation obtained by the calibration curve. For comparison, the number of cells was also compared to manual accounting using the hemocytometer assay. Figure 7 shows the comparison of the estimating cell number and accounted cell number. Estimating cell number had the same trend as the resazurin reduction assay previously described in Figure 5. In contrast, the results given by the hemocytometer displayed slight differences. However, both assays displayed the growth curve. Values of the estimated cell numbers in the Balb/c 3T3 and Ht-29 cells were higher than those manually accounted in all phases. A549 cells also had higher estimated values in all phases except for in the stationary phase. On the other hand, MCF-7 demonstrated a different trend, as it showed a J-shape in the estimated cells and an s-shape in the accounted cells. However, the difference between these values on the day of control was high in the Ht-29 cells (84.96×10^3 cells/mL) and MCF-7 cells (70.51×10^3 cells/mL) compared to the difference in Balb/c 3T3 (58.18×10^3 cells/mL) and A549 cells (11.13×10^3 cells/mL). Overall, the growth curves given by the hemocytometer were sharper than the estimated ones. Notably, manual accounting had multiple steps, which increased the chance of losing cells, whereas cell number given by the resazurin assays were estimated theoretically based on a calibration curve, where the possibility of losing cells during assays was low.

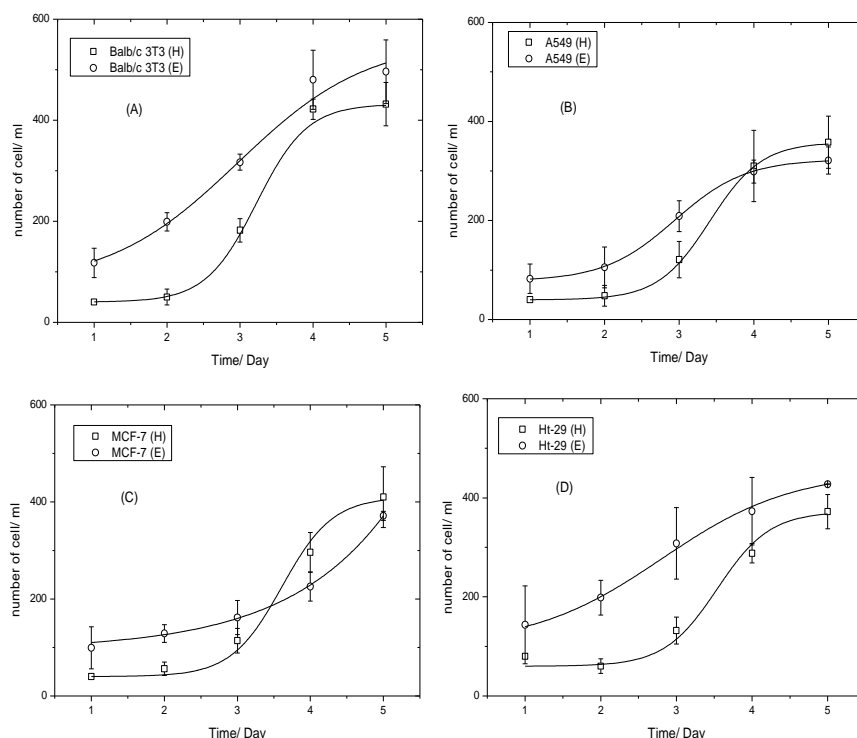


Figure 7. Logistic growth curves of (A) Balb/c 3T3 cell lines; (B) A549 cell lines; (C) MCF-7 cell lines; and (D) Ht-29 cell lines, over five days. (□) estimated cell number using linear equation of standard curve and, (○) accounted cell number using hemocytometer; all compared versus incubation time over five days. Data are expressed as the mean \pm SD of measurements of three independent experiments.

3.7. Cell Viability at Post-Confluence Culture

The cell viability of cells at post-confluence culture was detected. Table 2 illustrates the fluorescent signal of resazurin produced during the fourth, fifth, and sixth days for each cell line as well as vehicle

control and resazurin control. It is obvious from the data that there was a decrease in cell viability for all of the cells from day 4 to day 6. There was a significant difference between the data of cell viability of day 5 and day 6 compared to that of day 4; but MCF-7 cells in day 5 showed no significant difference ($p > 0.05$) to the control value (day 4). This was probably because there was 70% confluence in day 4 (shown in Figure 6), which allowed more proliferation. The cells of Balb/c 3T3 and A549 displayed z-factor values between 0.5 and 1 for each culture day compared to the control (day 4). It is quite noticeable that the cells of Balb/c 3T3 and A549 are more unlikely to form multilayers when reaching the contact-inhibited growth point. MCF-7 cells showed a quality assay in day 6, whereas Ht-29 cells illustrated a z-factor less than 0.5 for all the post-confluence culture compared to the control value. That was possible because of the high standard deviation (SD) for all the values in the three days. Notably, the z-factor value mostly depended on the SD. The cell viability of the vehicle controls of the cells of Balb/c 3T3 and MCF-7 was 10.2% and 8.3%, respectively, while those of the cells of A549 and Ht-29 were 18.6% and 18.2%, respectively. Drops of Virkon® may need to be increased for the MCF-7 and HT-29 cells to make dead cells.

Table 2. Summary of the resazurin data of each cell line versus the target days at post-confluence.

	Balb/c 3T3	A549	MCF-7	Ht-29
Day 4	3091.61 ± 28.74	2784.46 ± 43.35	(1887.34 ± 5.36)	(2980.70 ± 44.51)
Day 5	2513.44 ± 7.77 *§	(1952.29 ± 0.82) *§	(1787.48 ± 35.99)	(2655.06 ± 34.07)*
Day 6	1872.74 ± 6.72 *§	(1415.29 ± 44.35) *§	(1407.01 ± 66.13) *§	(2512.21 ± 48.32)*
VC	(412.6 ± 9.9) *§	(597.6 ± 23.3) *§	(237.8 ± 3.1) *§	(623.8 ± 4.5) *§
RC	(97.2 ± 6.3) *§	(78.7 ± 0.9) *§	(80.5 ± 0.3) *§	(82.7 ± 0.7) *§

The data of the cell viability assay-based resazurin was applied for the cells at post-confluence culture. Data are expressed as mean ± SD of the measurements of three independent experiments. VC (vehicle control,) and RC (resazurin control). Data compared to the control (data of day 4), * (p -value < 0.05 is a significant difference), § ($1 > Z$ -factor > 0.5 is excellent assay).

3.8. Alkaline Phosphatase Release from Cells at Post-Confluence Culture

The standard curve of ALP was applied in order to convert absorbance values to an enzyme unit (e.g., U/L). Figure 8 shows that the absorbance values of ALP concentration ranged from (1.5–1500 U/L). This was plotted using the Lineweaver–Burk model with good linear regression of R^2 of 0.99 and linear equation obtained using Origin software. Monitoring of ALP release from Balb/c 3T3 cells, A549 cells, MCF-7 cells, and HT-29 cells was conducted. ALP was induced by differentiation using post-confluence culture. Cells were cultured for two more days after reaching 95–100% confluence on day 4. Table 3 summarizes the results of ALP release in the target days for each cell with the vehicle control (VC) and the blank. It is obvious that the ALP release increased gradually from day 4 to day 6. This rise was shown from all cells. Furthermore, the data of post-confluence culture (day 5 and day 6) were compared to the control (data of day 4) using an unpaired t-test. There was a significant difference between the data of ALP release from day 5 and day 6 compared to that released from day 4. Balb/c 3T3 cells had an average level of ALP of 7.24 U/L on day 4 and the value increased on day 5 and day 6 (8.67 U/L and 11.67 U/L, respectively). The value of lung cancer cells exhibited a sharp increment from day 4 to day 6, which was 10.12 U/L, 12.21 U/L, and 19.60 U/L. The breast cancer cells showed slight incensement from the fourth day to the sixth day, and that was 7.97 U/L, 9.51 U/L, and 10.19 U/L, respectively. The colon cancer cell had the highest release value of

ALP (19.62 U/L) at confluence day compared to the others and also for the post-confluence day 5 and day 6 of 23.68 U/L and 27.22 U/L, respectively. Vehicle control of all cells showed less values. The cells of Balbc/3T3 and A549 had 2.75 U/L and 2.84 U/L, respectively, whereas the MCF-7 and Ht-29 cells had 3.44 U/L and 4.27 U/L, respectively, all of which represented significant differences when compared to the control. The buffer blank of all data was very low as no substrate was added to the assay.

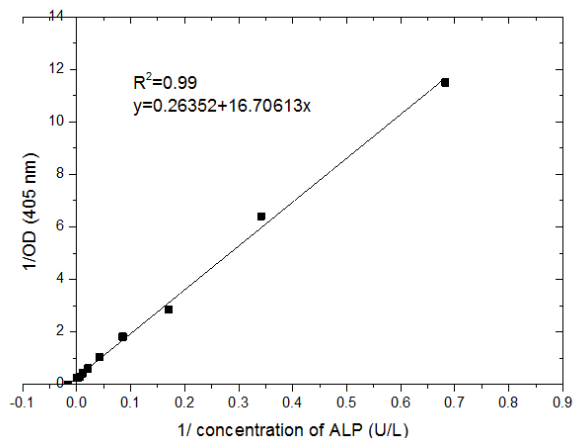


Figure 8. The standard curve of the absorbance values vs. alkaline phosphatase (ALP) concentration ranging from 1.5–1500 U/L was fitted by the Lineweaver–Burk model with $R^2 = 0.99$.

Table 3. Summary of ALP release from each cell line versus target days at post-confluence culture.

Quantity of ALP Release (U/L) in Each Day					
	Day 4	Day 5	Day 6	VC	Blank
Balb/c 3T3	(7.24 ± 0.17)	(8.67 ± 0.43)*	(11.67 ± 0.33)*	(2.75 ± 0.10)*	(0.74 ± 0.17)*
A549	(10.12 ± 0.35)	(12.21 ± 0.10)*	(19.60 ± 0.28)*	(2.84 ± 0.25)*	(0.87 ± 0.33)*
MCF-7	(7.97 ± 0.32)	(9.51 ± 0.30)*	(10.19 ± 0.25)*	(3.44 ± 0.27)*	(1.05 ± 0.26)*
Ht-29	(19.62 ± 0.60)	(23.68 ± 0.51)*	(27.22 ± 0.10)*	(4.27 ± 1.18)*	(0.91 ± 0.32)*

After exposing cells to the corresponding optimal substrate concentration of pNPP, absorbance 405 detection was converted to unit per liter using the equation in Figure 8. The obtained data were expressed as the mean ± SD of measurements of three independent experiments with VC (vehicle control) that had dead cells, and the blank with no cells and no substrate. *p*-value of post-confluence culture compared to the control (data of day 4), * $p < 0.05$ is significantly different..

4. Conclusions

ALP determination requires the real-time monitoring of cell behavior. Various cellular phenotypes are related to gene expression, which helps to understand emerging diseases including cancers. Several previous studies have shown the relationship between ALP and cell viability [38,39]. However, those studies were conducted under the standard cell culture assay. Function endpoints of those assays are labor-intensive, time-consuming, require detachment of cells, and thus hinder real-time assays and multiplex assays. Quantitative resazurin assays of cell viability have been proposed as a rapid and inexpensive

method to evaluate the viability of cells during the release of ALP, which can further be used to verify studies of cell adhesion applications such as cell-based biosensors.

The main parameters affecting the results obtained from the resazurin assay include the concentration of resazurin, incubation time, and cell number. The optimal incubation time of resazurin reduction was four hours for all cells. High incubation time is more likely to reduce resorufin and form non-detectable products. The research also focused on different cells, one embryonic fibroblast cell line Balb/c3T3, and three epithelial cancer cell lines, A549, MCF-7, and Ht-29. These cells have different metabolic activities, which were noticed in this study. Ht-29 cells showed the highest activity and had 100 μM as an optimal concentration of resazurin, whereas the others had 50 μM .

Optimal density corresponding to the working area is very important in cell adhesion approaches. This enhances the detection of cell viability alongside the release of ALP, which may detect intracellular processes. Cells need to be proliferated for at least four days to release detectable ALP. This time can be further increased if a study is focusing on differentiation where optimizing density is required. Special attention is drawn to the morphology of cells, which was monitored and compared to the resazurin assay. The cells showed logistic growth curves where the four phases were obvious. Cells that had a longer lag phase had less confluence (about 70–80%, like MCF-7 cells). In comparison, others, which had a smaller lag phase, had a gradual log phase and thus had almost 95–100% confluence by day 4. Cell growth is also influenced by the surrounding environment (e.g., media type, serum). The recommended type of media and serum were used according to the supplier's recommendations.

Cell viability of cells at post-confluence culture was determined and data were compared statistically using mean, standard deviation, *p*-value, and *z*-factor. The data of embryonic cells, lung cancer cells, and colon cancer cells displayed significant differences in post-confluence culture compared to the control (day 4). Similarly, breast cancer cells showed a *p*-value < 0.05 in day 6 and *p* > 0.05 in day 5 compared to the control. The cell viability of vehicle controls of the cells Balb/c 3T3, A549, MCF-7, and Ht-29 were 10.2%, 18.6%, 8.3%, and 18.2%, respectively. ALP release was increased gradually from day 4 to day 6. An increase of ALP release was shown from all cells during the three days. The levels of ALP during day 4, day 5, and day 6 from the Balb/c 3T3 cells were 7.24 U/L, 8.67 U/L, and 11.67 U/L, respectively; those from the A549 cells were 10.12 U/L, 12.21 U/L, and 19.60 U/L, respectively; those from the MCF-7 cells were 7.97 U/L, 9.51 U/L, and 10.19 U/L, respectively; and those from Ht-29 were 19.62 U/L, 23.68 U/L, and 27.22 U/L, respectively. Moreover, there was a significant difference between the data of ALP release from day 5 and day 6 compared to that released from day 4.

The main aim of this study was achieved by providing convenient and reliable samples of living cells for sensitively and continuously assaying using resazurin-based measurements, which made it easier for optimizing the methodologies for ALP release.

Author Contributions: Contributions: supervision, E.M.; writing—original draft preparation, T.B. All authors have read and agreed to the published version of the manuscript.

Funding: This research was funded by the Ministry of Higher Education of Saudi Arabia.

Acknowledgments: The authors would like to acknowledge the financial support of the Ministry of Higher Education of Saudi Arabia.

Conflicts of Interest: The authors declare that there are no conflicts of interest.

Reference

- [1] Khalili, A.A.; Ahmad, M.R. A Review of Cell Adhesion Studies for Biomedical and Biological Applications. *Int. J. Mol. Sci.* 2015, 16, 18149–18184. [Google Scholar] [CrossRef]
- [2] Koev, S.T.; Dykstra, P.H.; Luo, X.; Rubloff, G.W.; Bentley, W.E.; Payne, G.F.; Ghodssi, R. Chitosan: An integrative biomaterial for lab-on-a-chip devices. *Lab Chip* 2010, 1, 326–342. [Google Scholar] [CrossRef] [PubMed]

- [3] Lukić, M.; Šimec, N.; Zatezalo, V.; Jurenec, S.; Radić-Krišto, D. Exclusion of Trypan blue exclusion test for CD34+cell viability determination: P007. *Bone Marrow Transplant.* 2017, 52, S126–S127. [Google Scholar]
- [4] Menyhárt, O.; Harami-Papp, H.; Sukumar, S.; Schäfer, R.; Magnani, L.; de Barrios, O.; Györfy, B. Guidelines for the selection of functional assays to evaluate the hallmarks of cancer. *BBA Rev. Cancer* 2016, 1866, 300–319. [Google Scholar] [CrossRef] [PubMed]
- [5] Uzarski, J.S.; Bijonowski, B.M.; Wang, B.; Ward, H.H.; Wandinger-Ness, A.; Miller, W.M.; Wertheim, J.A. Dual-Purpose Bioreactors to Monitor Noninvasive Physical and Biochemical Markers of Kidney and Liver Scaffold Recellularization. *Tissue Eng. Part C Methods* 2015, 21, 132–1043. [Google Scholar] [CrossRef]
- [6] Ren, X.; Tapias, L.F.; Jank, B.J.; Mathisen, D.J.; Lanuti, M.; Ott, H.C. Ex vivo non-invasive assessment of cell viability and proliferation in bio-engineered whole organ constructs. *Biomaterials* 2015, 52, 103–112. [Google Scholar] [CrossRef]
- [7] Tapias, L.F.; Gilpin, S.E.; Ren, X.; Wei, L.; Fuchs, B.C.; Tanabe, K.K.; Lanuti, M.; Ott, H.C. Assessment of Proliferation and Cytotoxicity in a Biomimetic Three-Dimensional Model of Lung Cancer. *Ann. Thorac. Surg.* 2015, 100, 414–421. [Google Scholar] [CrossRef]
- [8] Ansar Ahmed, S.; Gogal, R.M.; Walsh, J.E. A new rapid and simple non-radioactive assay to monitor and determine the proliferation of lymphocytes: An alternative to [³H] thymidine incorporation assay. *J. Immunol. Methods* 1994, 170, 211–224. [Google Scholar] [CrossRef]
- [9] O'Brien, J.; Wilson, I.; Orton, T.; Pognan, F. Investigation of the Alamar Blue (resazurin) fluorescent dye for the assessment of mammalian cell cytotoxicity. *Eur. J. Biochem.* 2000, 267, 5421–5426. [Google Scholar] [CrossRef]
- [10] Shum, D.; Radu, C.; Kim, E.; Cajuste, M.; Shao, Y.; Seshan, V.E.; Djaballah, H. A high density assay format for the detection of novel cytotoxic agents in large chemical libraries. *J. Enzym. Inhib. Med. Chem.* 2008, 23, 931–945. [Google Scholar] [CrossRef]
- [11] Kim, H.J.; Jang, S. Optimization of a resazurin-based microplate assay for large-scale compound screenings against *Klebsiella pneumoniae*. *3 Biotech* 2018, 8, 1–6. [Google Scholar] [CrossRef] [PubMed]
- [12] Van den Driessche, F.; Rigole, P.; Brackman, G.; Coenye, T. Optimization of resazurin-based viability staining for quantification of microbial biofilms. *J. Microbiol. Methods* 2014, 98, 31–34. [Google Scholar] [CrossRef] [PubMed]
- [13] Chadha, S.; Kale, S. Simple fluorescence-based high throughput cell viability assay for filamentous fungi. *Lett. Appl. Microbiol.* 2015, 61, 238–244. [Google Scholar] [CrossRef] [PubMed]
- [14] Goughenour, K.D.; Balada-Llasat, J.-M.; Rappleye, C.A. Quantitative microplate-based growth assay for determination of antifungal susceptibility of *histoplasma capsulatum* yeasts. *J. Clin. Microbiol.* 2015, 53, 3286–3295. [Google Scholar] [CrossRef] [PubMed]
- [15] Moreau, K.; Surand, J.; Le Dantec, A.; Mosrin-Huaman, C.; Legrand, A.; Rahmouni, A. Recombinant yeast and human cells as screening tools to search for antibacterial agents targeting the transcription termination factor Rho. *J. Antibiot.* 2018, 71, 447–455. [Google Scholar] [CrossRef] [PubMed]
- [16] Bowling, T.; Mercer, L.; Don, R.; Jacobs, R.; Nare, B. Application of a resazurin-based high-throughput screening assay for the identification and progression of new treatments for human African trypanosomiasis. *Int. J. Parasitol. Drugs Drug Resist.* 2012, 2, 262–270. [Google Scholar] [CrossRef]
- [17] Rolón, M.; Vega, C.; Escario, J.A.; Gómez-Barrio, A. Development of resazurin microtiter assay for drug sensibility testing of *Trypanosoma cruzi* epimastigotes. *Parasitol. Res.* 2006, 99, 103–107. [Google Scholar] [CrossRef]
- [18] Uzarski, J.S.; DiVito, M.D.; Wertheim, J.A.; Miller, W.M. Essential design considerations for the resazurin reduction assay to noninvasively quantify cell expansion within perfused extracellular matrix scaffolds. *Biomaterials* 2017, 129, 163–175. [Google Scholar] [CrossRef]
- [19] Latner, A.L.; Skillen, A.W. *Isoenzymes in Biology and Medicine*; Academic Press Inc.: London, UK, 1968. [Google Scholar]
- [20] Sharma, U.; Pal, D.; Prasad, R. Alkaline Phosphatase: An Overview. *Indian J. Clin. Biochem.* 2014, 29, 269–278. [Google Scholar] [CrossRef]
- [21] Acton, Q.A. *Transforming Growth Factors—Advances in Research and Application*; Scholarly Editions: 2013. Available online: <https://books.google.td/books?id=dARP4d1Io3wC> (accessed on 12 April 2019).

- [22] Herz, F.; Halwer, A.S.M.; Bogart, L.H. Alkaline phosphatase in HT-29, a human colon cancer cell line: Influence of sodium butyrate and hyperosmolality. *Arch. Biochem. Biophys.* 1981, 210, 581–591. [Google Scholar] [CrossRef]
- [23] Tsai, L.-C.; Hung, M.-W.; Chen, Y.-H.; Su, W.-C.; Chang, G.-G.; Chang, T.-C. Expression and regulation of alkaline phosphatases in human breast cancer MCF-7 cells. *Eur. J. Biochem.* 2000, 267, 1330–1339. [Google Scholar] [CrossRef] [PubMed]
- [24] Hui, M.; Hu, M.; Tenenbaum, H.C. Changes in cell adhesion and cell proliferation are associated with expression of tissue non-specific alkaline phosphatase. *Cell Tissue Res.* 1993, 274, 429–437. [Google Scholar] [CrossRef] [PubMed]
- [25] Guerreiro, S.; Monteiro, R.; Martins, M.J.; Calhau, C.; Azevedo, I.; Soares, R. Distinct modulation of alkaline phosphatase isoenzymes by 17beta-estradiol and xanthohumol in breast cancer MCF-7 cells. *Clin. Biochem.* 2007, 40, 268. [Google Scholar] [CrossRef] [PubMed]
- [26] Alberts, B.; Lewis, J.A. *Molecular Biology of the Cell*, 4th ed.; Studying Gene Expression and Function; Garland Science: New York, NY, USA, 2002. [Google Scholar]
- [27] Yang, T.-T.; Sinai, P.; Kain, S.R. An Acid Phosphatase Assay for Quantifying the Growth of Adherent and Nonadherent Cells. *Anal. Biochem.* 1996, 241, 103–108. [Google Scholar] [CrossRef] [PubMed]
- [28] Friedrich, J.; Eder, W.; Castaneda, J.; Doss, M.; Huber, E.; Ebner, R.; Kunz-Schughart, L.A. A reliable tool to determine cell viability in complex 3-D culture: The acid phosphatase assay. *J. Biomol. Screen.* 2007, 12, 925–937. [Google Scholar] [CrossRef] [PubMed]
- [29] Ivanov, D.P.; Parker, T.L.; Walker, D.A.; Alexander, C.; Ashford, M.B.; Gellert, P.R.; Garnett, M.C. Multiplexing spheroid volume, resazurin and acid phosphatase viability assays for high-throughput screening of tumour spheroids and stem cell neurospheres. *PLoS ONE* 2014, 9, e103817. [Google Scholar] [CrossRef]
- [30] Joanne, K.; Itano, J.B.; Conde, F.; Saria, M. *Core Curriculum for Oncology Nursing*, 5th ed.; Elsevier Inc.: Amsterdam, The Netherlands, 2016. [Google Scholar]
- [31] Pace, R.T.; Burg, K.J.L. Toxic effects of resazurin on cell cultures. *Cytotechnology* 2015, 67, 13–17. [Google Scholar] [CrossRef]
- [32] Hamalainen-Laanaya, H.K.; Orloff, M.S. Analysis of cell viability using time-dependent increase in fluorescence intensity. *Anal. Biochem.* 2012, 429, 32–38. [Google Scholar] [CrossRef]
- [33] Zheng, F.; Wang, S.; Hou, W.; Xiao, Y.; Liu, P.; Shi, X.; Shen, M. Comparative study of resazurin reduction and MTT assays for cytocompatibility evaluation of nanofibrous materials. *Anal. Methods* 2019, 11, 483–489. [Google Scholar] [CrossRef]
- [34] Adams, D.L.; Zhu, P.; Makarova, O.V.; Martin, S.S.; Charpentier, M.; Chumsri, S.; Li, S.; Amstutz, P.; Tang, C.-M. The systematic study of circulating tumor cell isolation using lithographic microfilters. *Rsc Adv.* 2014, 4, 4334–4342. [Google Scholar] [CrossRef]
- [35] Majeska, R.J.; Rodan, G.A. The Effect of 1,25(OH)₂D₃ on Alkaline-Phosphatase In Osteoblastic Osteo-Sarcoma Cells. *J. Biol. Chem.* 1982, 257, 3362–3365. [Google Scholar] [PubMed]
- [36] Castrén, E.; Sillat, T.; Oja, S.; Noro, A.; Laitinen, A.; Konttinen, Y.T.; Lehenkari, P.; Hukkanen, M.; Korhonen, M. Osteogenic differentiation of mesenchymal stromal cells in two-dimensional and three-dimensional cultures without animal serum. *Stem Cell Res. Ther.* 2015, 6, 167. [Google Scholar] [CrossRef] [PubMed]
- [37] Xiao, J.; Zhang, Y.; Wang, J.; Yu, W.; Wang, W.; Ma, X. Monitoring of Cell Viability and Proliferation in Hydrogel-Encapsulated System by Resazurin Assay. *Appl. Biochem. Biotechnol.* 2010, 162, 1996–2007. [Google Scholar] [CrossRef] [PubMed]
- [38] Kang, J.; Martins, A.M. The strong correlation between alkaline phosphatase activity and cell viability. *Cell Biol. Int.* 2008, 32, 163–164. [Google Scholar] [CrossRef] [PubMed]
- [39] Akcakaya, H.; Aroymak, A.; Gokce, S. A quantitative colorimetric method of measuring alkaline phosphatase activity in eukaryotic cell membranes. *Cell Biol. Int.* 2007, 31, 186–190. [Google Scholar] [CrossRef] [PubMed]



© 2020 by the authors. Submitted for possible open access publication under the terms and conditions of the Creative Commons Attribution (CC BY) license (<http://creativecommons.org/licenses/by/4.0/>).

Electrochemical Detection and Capillary Electrophoresis: Comparative Studies for Alkaline Phosphatase (ALP) Release from Living Cells

Thanih Balbaied, Anna Hogan and Eric Moore *

Sensing & Separation Group, School of Chemistry and Life Science Interface, University College Cork, Tyndall National Institute, T12R5CP Cork, Ireland

* Correspondence: e.moore@ucc.ie

Received: 30 June 2020; Accepted: 4 August 2020; Published: date

Abstract: Alkaline phosphatase (ALP) is one of the main biomarkers that is clinically detected in bone and liver disorders using optical assays. The electrochemical principle is important because point-of-care testing is increasing dramatically and absorbance techniques hardly compete with the medical revolution that is occurring. The detection of ALP using electrochemical detection is contributing to the integration systems field, and hence enhancing the detection of biological targets for pharmaceutical research and design systems. Moreover, *in vitro* electrochemical measurements use cost effective materials and simple techniques. Graphite screen-printed electrodes and linear sweep voltammetry were used to optimize the electrochemistry of the enzymatic product p-aminophenol using the enzyme kinetic assay. ALP release from embryonic and cancer cells was determined from adhesion cell culture. Additionally, capillary electrophoresis and colorimetric methods were applied for comparison assays. The resulting assays showed a dynamic range of ALP ranging from 1.5 to 1500 U/L, and limit of detection of 0.043 U/L. This was achieved by using 70 μ L of the sample and an incubation time of 10 min at an optimal substrate concentration of 9.6 mM of p-aminophenol phosphate. A significant difference ($p < 0.05$) was measured between the absorbance assays. This paper demonstrates the advantages of the electrochemical assay for ALP release from cells, which is in line with recent trends in gene expression systems using microelectrode array technologies and devices for monitoring electrophysiological activity.

Keywords: electrochemistry; linear sweep voltammetry; alkaline phosphatase; capillary electrophoresis; colorimetry; cancer cells; embryonic cells

1. Introduction

ALP is a homodimeric enzyme. It has cofactors that include two zinc atoms and one magnesium atom in each subunit, which are important for the active sites [1]. ALP is found in almost all living tissue and can be expressed in four isoforms. Abnormal levels of ALP release can be seen in illnesses (such as liver disease, bone disorders, etc.), or during pregnancy or the rapid growth phases of childhood [2,3]. Recently, ALP has been identified as a potential cancer biomarker, and its early detection could potentially help in the treatment of the disease [4].

Electrochemistry allows integration in small devices, which is required for point-of-care testing. Electrochemical detection techniques are relatively easy to use and offer relatively fast detection. This is reflected in Clark's work (1954) [5]. Electrochemical biosensors for ALP have rapidly developed since 1991, when Thomson and his team published their work comparing ALP resolution using an electrochemical

assay to results from optical detection [6]. The principle was based on hydrolyzing o-phosphate by ALP in the presence of the p-aminophenyl phosphate (pAPP), where the non-electroactive substrate under the alkaline environment served to generate an electroactive substrate (pAP). This research has contributed to the development of ALP electrochemical detection [7,8,9,10,11].

Investigation of ALP release as a quantitative indicator of gene reporting in mammalian cells began in 1988 [12]. However, it was not until the development of the electrochemical immunoassay [13] that the electrochemistry of ALP release as a secretion enzyme from cells began to grow in popularity [14,15,16]. Almost ten years later, a proper protocol of ALP release was investigated using methods of molecular biology, biochemistry, enzymology, and chemiluminescence. These findings enhanced the detection of ALP using electrochemistry [17,18,19,20]. Kelso et al., 2000 exploited the electrochemical immunoassay, and were likely the first to detect secreted ALP in media using screen-printed electrodes and 2-naphthyl phosphate [21]. The initial protocols of ALP release *in vitro* used the same strategies used for β -galactosidase [22,23,24,25,26]. This was carried out by way of electrochemical analysis and using different samples, including single-cell analysis [27,28,29], biopsies [30], tissues [31] and accumulation of cells [32,33]. These strategies have their own disadvantages. For example, using a reducing agent (e.g., β -mercaptoethanol) caused inactivation of intracellular ALP [34,35,36]. Moreover, issues relating to electrochemical analysis, including buffer components, volume of the electrolyte, and the parameters required during the assay, were not optimised [37,38,39]. This caused less concentration of ALP release.

So far, investigations of ALP release from MCF-7 breast cancer cells, A549 lung cancer cells, and HT-29 colon cancer cells have only been carried out using fluorescence [40]. The optimization achieved as a result of spectroscopy would be negatively affected by the limitations (e.g., the cost, and the size of instruments). Accordingly, this paper will explore the parameters of the enzyme assay and apply the electrochemical assay for ALP release from living cells. Therefore, linear sweep voltammetry was used because it has a wide potential window, as it is a droplet-based assay and requires no stirring solution. These are important factors for point-of care application. The incubation time of the sample, the kinetic enzyme assay of the substrate, and calibration plots were studied in order to carry out regression analysis using the two methods illustrated in plate A and plate B (Figure 1). Separation techniques that included capillary electrophoresis were also used. Capillary electrophoresis was used because it distinguishes isoenzymes alongside the standard methods of colorimetry [41]. Finally, the assays were compared in order to assess the sensitivity of electrochemistry analysis.

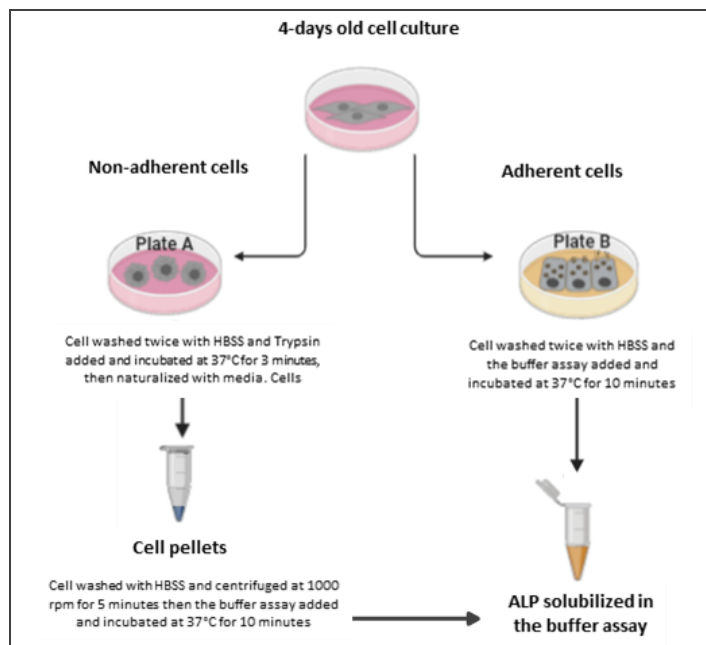


Figure 1. A schematic diagram of ALP release. Plate A describes the methods of determination of ALP release from detached cells, where cells are washed with Hank's balanced salt solution (HBSS) and undergo trypsinization, washing and centrifugation before being exposed to the buffer assay. Plate B describes the methods of determination of ALP release from attached cells, where cells are only washed before being directly exposed to the buffer assay.

2. Methodology

2.1. Chemicals and Instruments

Alkaline phosphatase (ALP, calf intestinal phosphatase) or 4-aminophenol (p-AP) was purchased from Sigma (Ireland) and used to make stock solution at a final concentration of 1500 U/L or 5 mM. The alkaline buffer assay at pH 9.5 was made by adding sterile deionized water at grade 18 MΩ provided from Tyndall National Institute (UCC), which contained diethanolamine (DEA) 1 M, magnesium chloride (MgCl₂) 8 mM, sodium chloride (NaCl) 50 mM, potassium chloride (KCl) 100 mM, para-aminophenol phosphate (p-APP) and HCl purchased from Sigma (Wicklow, Ireland). The electrochemical measurements were performed on screen printed carbon electrodes with each individual sensor consisting of a graphite working and counter electrode and Ag/AgCl reference electrode (graphite-SPE) (Kanichi Research Limited, England, UK) with a working volume of 70 µL performed on palmSens portable potentiostat (Palm Instruments BV, Houten, The Netherlands). The graphite-SPE was cleaned before using for 20 min by Plasma Surface Treatment (Harrick plasma, Ithaca, NY, USA). Separations were performed using 50 µm i.d. and 375 µm o.d. fused-silica capillary (CM Scientific Ltd., Silsden, UK). Agilent 7100 Capillary Electrophoresis System (Waldbronn, Germany) the software Agilent Chemstation (Version B.02.01) were also used.

2.2. ALP Release and Cell Culture

In order to release ALP from cells, the following steps were performed according to the protocols developed by Thanih et al. [42]. The first step was to enhance ALP release in 4-day-old culture by seeding cells as a monolayer on 48-well plates (Sigma, Ireland), incubating at 37 °C and 5% CO₂ (incusafe Panasonic incubator) and changing media every two days. The cell lines used during this study were purchased from

ATCC (UK), including mouse embryo fibroblast cells (Balb/c 3T3 Line), breast carcinoma epithelial cells (MCF-7 Line), lung carcinoma epithelial cells (A-549 Line), and colon carcinoma epithelial cells (Ht-29 Line). The media, supplements, and washing buffer used for culturing cells were Dulbecco's modified Eagle's medium (DMEM), minimum essential medium Eagle (MEME) and McCoy's 5A medium, newborn calf serum (NBCS), fetal bovine serum (FBS), and Hank's balanced salt solution (HBSS), which were purchased from Sigma (Ireland). Table 1 summarises the cell numbers used and the composition of media. The cells were sub-cultured three times before seeding began under aseptic conditions using a cell culture hood (Esco Airstream® Class II).

Table 1. A summary of the cell number and the composition of media used in this study.

Cell Line	Concentration ($\times 10^3$ Cells/mL)	Media	Supplements
Balb/c 3T3	40	DMEM	10% NBCS
A549	40	DMEM	10% FBS
MCF-7	40	MEME	10% FBS
Ht-29	80	McCoy's 5A	10% FBS

2.3. Stabilization of Graphite Screen-Printed Electrodes

Graphite screen-printed electrodes (graphite-SPE) were first cleaned using iso-propanol and a plasmon cleaner device for 10 min or for 20 min and compared to non-cleaned electrodes. Potassium $[\text{Fe}(\text{CN})_6]^{3-/4-}$ (1 mM) was dissolved in 1.0 M of KCl. $[\text{Fe}(\text{CN})_6]^{3-/4-}$ solution (5 mL) was used to immerse the graphite-SPE. A Palmsens potentiostat device was used to carry out the cyclic voltammetry assay and to compare the data before and after the cleaning process. The cyclic voltammetry detection techniques were applied at scan rates from 5 mV/S to 200 mV/S and at initial potential of -0.2 V and final potential of 0.6 V vs. the Ag/AgCl reference electrode. The potential range of each scan rate of cyclic voltammograms was plotted against the response current. The reduction peaks' current (ipc) and oxidation peaks' current (ipa) were plotted versus the square root of the scan rate $((\text{mV/S})^{1/2})$.

2.4. Optimization of Electrochemical Measurement

Samples of cells were freshly prepared at a concentration of 250×10^3 cells/mL. The cells were washed twice with HBSS, centrifuged for 5 min at 1000 rpm and resuspended in the assay buffer. Graphite screen-printed electrodes were first cleaned using plasma cleaner for 20 min and linear sweep voltammetry measurements were carried out at potentials ranging from -1.2 V to 1.5 V vs. Ag/AgCl. The measurements were completed in triplicate at a volume of $70 \mu\text{L}$ and a scan rate of 100 mV/S . To determine a probable working range for the product pAP, serial dilutions of pAP, starting with 5 mM were prepared in the presence of $30 \mu\text{L}$ of sample mixed with $100 \mu\text{M}$ of pAPP. The linear sweep voltammetry was measured for each concentration at three separate electrodes. A free-pAP buffer was used as blank. A graph charting current response to concentration of pAP was prepared for regression analysis. The incubation time evaluation for ALP release was performed using $70 \mu\text{L}$ of a sample with 20 U/L of ALP activity mixed with $30 \mu\text{L}$ of pAPP 5 mM in buffer DEA and assessed at 5-min intervals over 60 min. NaOH ($30 \mu\text{L}$ of 1 M) was added in order to stop the reaction. The reaction time was fixed to 10 min, and the activity of the sample was assessed with different concentrations of substrate range ($5, 2.5, 1.25, 0.63, 0.31, 0.16, 0.08$, and 0.04 mM pAPP). The optimal concentration of substrate obtained was used in a calibration plot of ALP release. The sample was spiked with various concentrations of ALP (calf intestinal phosphatase) at a range of $1\text{--}1500 \text{ U/L}$.

2.5. Linearity Performance of ALP Release vs. Cell Number

In order to complete a linearity trend of ALP release versus current density, different concentrations of cells were used (250, 125, 63, 31, 16, 8, and 3×10^3 cells/mL). The cells were incubated in the assay buffer for 10 min before measurement. Linear sweep voltammetry was applied in triplicate in three separate graphite-SPEs at a final volume of 70 μ L, against a free-pAPP buffer that was used as a blank. We measured it at 100 mV/S and a potential range from -1.2 V to 1.5 V versus the reference of Ag/Ag/Cl. A graph relating the concentration of cells to the current density was prepared for regression analysis.

2.6. Concentration of the Substrate pAPP from Adhesion Cells

Adherent cells have different responses from non-adherent cells in terms of releasing ALP. Therefore, the concentration of substrate pAPP needed to be assessed in order to allow for real-time monitoring of ALP. The serial dilution of pAPP, starting with 5 mM, was carried out in the range of 5, 2.5, 1.25, 0.60, 0.30, 0.16, 0.08 and 0.04 mM in the assay buffer. The range of diluted pAPP was incubated with cells for 10 min. The electrochemical assay was applied with a final volume of 70 μ L against a free-pAPP buffer as blank. A graph relating the concentration of pAPP to current density fit by non-linear regression analysis to the Michaelis-Menten model for each cell line was completed.

2.7. Comparative Study of ALP Activity

The conditions of samples in the comparative methods are the same as those in the electrochemical method. Capillary electrophoresis or colorimetric measurements were carried out in triplicate at a volume of 70 μ L at a range of the product pNP (15–500 μ M) using the wavelength 405 nm. The serial dilutions of pNP were prepared in the presence of 30 μ L of sample mixed with 6 mM of pNPP. A graph relating peak area of absorbance to concentration of pNP was prepared for regression analysis. The slopes and intercepts of the reaction were used for normalizing the data in molarity. The separation of samples was performed in a 50 μ m inner diameter fused-silica capillary with a length of 15 cm. The data were collected and processed using the capillary electrophoresis system and Agilent ChemStation software. The running conditions included a voltage of 15 kV, a capillary temperature of 20 °C and a wavelength of 405 nm, and injection of the sample was for 5 s and 15 mbar. A calibration plot of absorbance assay of ALP activity was obtained using the same sample preparation in electrochemical measurement. ALP release was performed using 70 μ L of a sample spiked with various concentrations of ALP (calf intestinal phosphatase) at a range of 1–1500 U/L dissolved in 30 μ L of pNPP 6 mM in buffer DEA and incubated for 30 min. NaOH (30 μ L of 1 M) was added to stop the reaction. The Michaelis-Menten model was used to fit the data. The resulting slope and intercept were determined using V_{max} and k_m constants to normalize the data.

3. Results and Discussion

3.1. Stabilization of Graphite Screen-Printed Electrodes

Cyclic voltammetry was applied where 1 M KCl was used as the electrolyte for the standard reaction redox of ferri/ferrocyanide. Non-cleaned electrodes and cleaned electrodes for 10 min and cleaned electrodes for 20 min were compared. Figure 2 shows the cyclic voltammogram background of electrodes before and after cleaning using Plasmon cleaner. It is evident that the potential window of the cleaned electrodes (Figure 2B,C) is narrow compared to that of non-cleaned electrodes (Figure 2A). In the insert in Figure 2, the linear relationship observed between the peak current and the square root of the scan rate with a high linear regression R^2 of 0.98 is outlined. The anodic (ipa) and cathodic (ipc) current peaks display a sensitive performance in electrodes cleaned for 20 min compared to the other electrodes. The electrochemical performance of cleaned electrodes for 20 min in plasmon cleaner was more stable than others. The other electrodes displayed shifts in the potential as the scan rate increased. It appears that the faradic current was affected by any background current. Table 2 summarizes the influence of the scan rate on the half peak potential (E_{mid} vs. Ag/AgCl) and peak-to-peak separation (ΔE_p) of anodic and cathodic

peaks. The anodic and cathodic peak ratio was 0.98–1.03 as the scan rate increased performance in electrodes cleaned for 20 min. This showed the reversible reaction of $[\text{Fe}(\text{CN})_6]^{3-/4-}$.

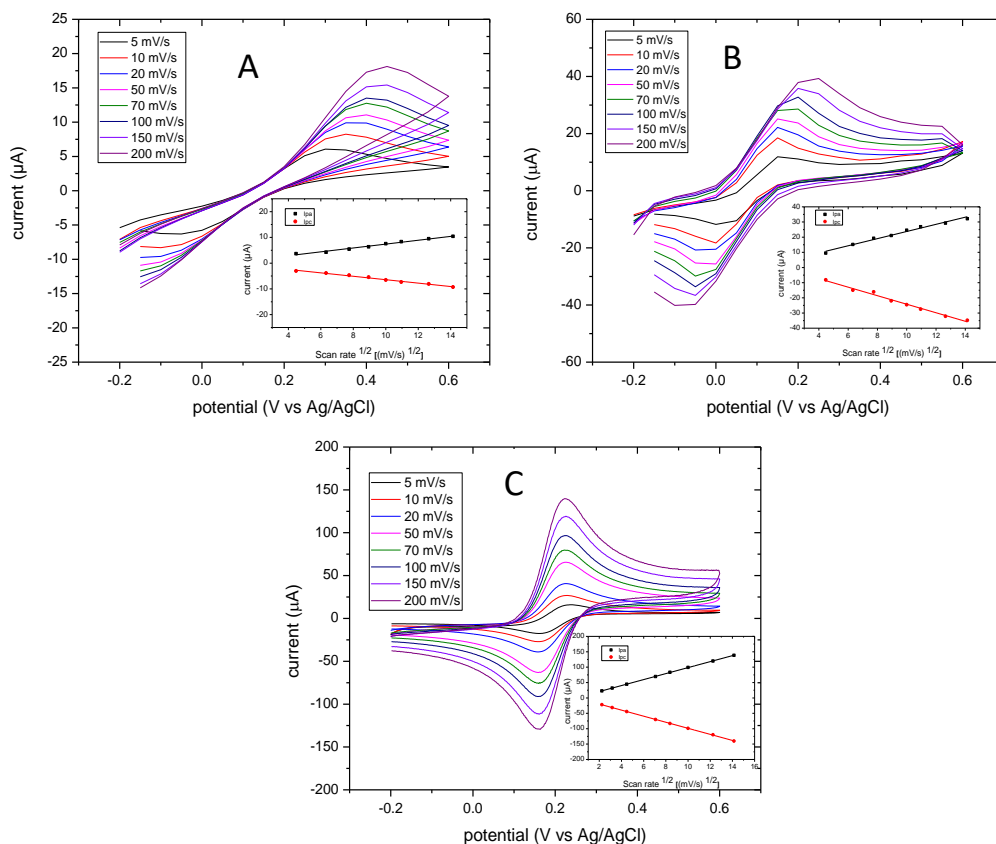


Figure 2. Cyclic voltammograms of 1 mM $[\text{Fe}(\text{CN})_6]^{3-/4-}$ on non-cleaned electrodes (A), cleaned electrodes (10 min) (B), and cleaned electrodes (20 min) (C). The inset demonstrates the curves of reduction peaks' current (ipr) and oxidation peaks' current (ipa) versus the square root of the scan rate ($(\text{mV/s})^{1/2}$). The cyclic voltammograms were carried out at an initial potential of -0.2 V and final potential of 0.6 V vs. the Ag/AgCl reference electrode.

Table 2. A summary of the influence of the scan rate on the half peak potential (E_{mid} vs. Ag/AgCl) and peak-to-peak separation (ΔE_p) of anodic and cathodic peaks.

Scan Rate	^a E_{mid} vs. Ag/AgCl			^b ΔE_p (mV)		
	0 min	10 min	20 min	0 min	10 min	20 min
5	0.2285	0.0768	0.198	175	146.4	76
10	0.2465	0.08145	0.194	207	143.1	68
20	0.261	0.09155	0.192	230	144.9	68
50	0.2715	0.1163	0.192	247	137.4	64
70	0.277	0.1225	0.191	260	151	62
100	0.282	0.1305	0.191	270	153	62
150	0.294	0.135	0.194	288	162	64
200	0.298	0.1585	0.193	300	163	58

^a Measured from the value of $1/2(E_{\text{pc}} + E_{\text{pa}})$ versus Ag/AgCl reference electrode. ^b $\Delta E_p = E_{\text{pa}} - E_{\text{pc}}$.

The potential of the oxidation peak as the scan rate increased for electrodes cleaned for 20 min was 0.19–0.19 V, and that of electrodes cleaned for 10 min was 0.2–0.3 V. Electrodes that had not been cleaned had a potential oxidation peak of 0.3–0.45 V as the scan rate increased. This indicates that the cleaning process can positively enhance electron transfer, and that a 20-min cleaning time is sufficient to overcome the limitations of diffusion processes. Moreover, the value of ΔE_p at 200 mV/S presented by non-cleaned electrodes was too high (300 mV), which indicates that some sort of contamination occurred on the electrode surface. Cleaning the surface electrodes was important as, after 10 min and 20 min, decrements of the value ΔE_p were observed, which were 163 mV and 58 mV, respectively. Considering the theoretical value of ΔE_p is 59 mV for single electron transfer of $[\text{Fe}(\text{CN})_6]^{3-/4-}$, the closest experimental value achieved was 58 mV. Therefore, treatment with oxygen plasma for 20 min was constantly used for further electrochemical investigations.

3.2. Optimization of Electrochemical Measurement

For the electrochemical detection of mammalian ALP release, the electroactive compound p-aminophenol (pAP) is produced from the enzyme reacting with a p-aminophenyl phosphate substrate. The linear sweep voltammetry detection technique was applied to read the current generated at different concentrations of the product pAP. Figure 3A shows the linear sweep voltammograms of different concentrations of pAP (0.16–5 mM). The measurements were carried out at a scan rate of 100 mV/S and at a range of potentials between –1.2 and 1.5 V. The current response of the pAP increased in potentials at points between 0 and 0.3 V. The insert curve shows the standard curve of the mass-transfer limited current of pAP. Furthermore, the values of intercept and slope of regression lines from these six concentrations were calculated as 5.931 and 11.866. The current response for the oxidation of pAP indicated a good linear relationship, where R^2 was 0.996. pAP (5 mM) generated 180 μA , and the lowest concentration of 0.16 mM generated 20 μA . These results indicate that the voltammetric detection of pAP did not affect the electrode surface during the assay.

The electrochemical determination of ALP release versus time was performed and showed a linear dependence. When time of incubation increased, the ALP release increased. Figure 3B shows the linear sweep voltammograms of current increased as incubation time increased, reaching a steady state at 40 min. The linear sweep voltammograms were applied at 100 mV/S and at potentials ranging from –1.2 to 1.5 V vs. Ag/AgCl. In the insert of Figure 3B, the values of current increased rapidly up to 10 min and then continued slowly up to 40 min. They levelled off at between 40 and 50 min. The oxidation peak started to increase with increasing time after 10 min, so 10 min was taken as the optimum incubation time for subsequent measurements. This corresponds to data already published by Sappia et al. [43]. The linearity relationship had a very good coefficient regression R^2 of 0.998.

The optimal concentration of substrate for the evaluation of enzyme activity using this method was investigated. The current responses of pAPP substrate at different concentrations ranging from 0.1 to 5 mM are shown in Figure 3C. ALP release was determined from the constant cell number of 250×10^3 cells/mL. The cells were incubated with the substrate concentration for 10 min at 37 °C. The current responses reached a plateau at 1.25 mM of pAPP. The current values were fitted using the Michaelis-Menten model with a coefficient regression R^2 of 0.88. The corresponding I_{max} and k_m were 136.59 μA and 0.548 mM. The corresponding concentration of pAPP at 95% of I_{max} was 9.69 mM. The optimal concentration of pAPP was almost 20 times higher than the k_m [44].

Linear sweep voltammetry was applied for different concentrations of ALP (1.5–1500 U/L) to allow for conversion of the unit and to compare it to the absorbance values. Figure 3D shows the Lineweaver–Burk plots of the current responses (1/current) versus ALP concentration (1/concentration) as obtained by linear sweep voltammetry with good linear regression of R^2 of 0.99. The intercept (I_{max}) and the slope (k_m/I_{max}) were 0.0058 and 0.767, and the LOD was 0.043 U/L.

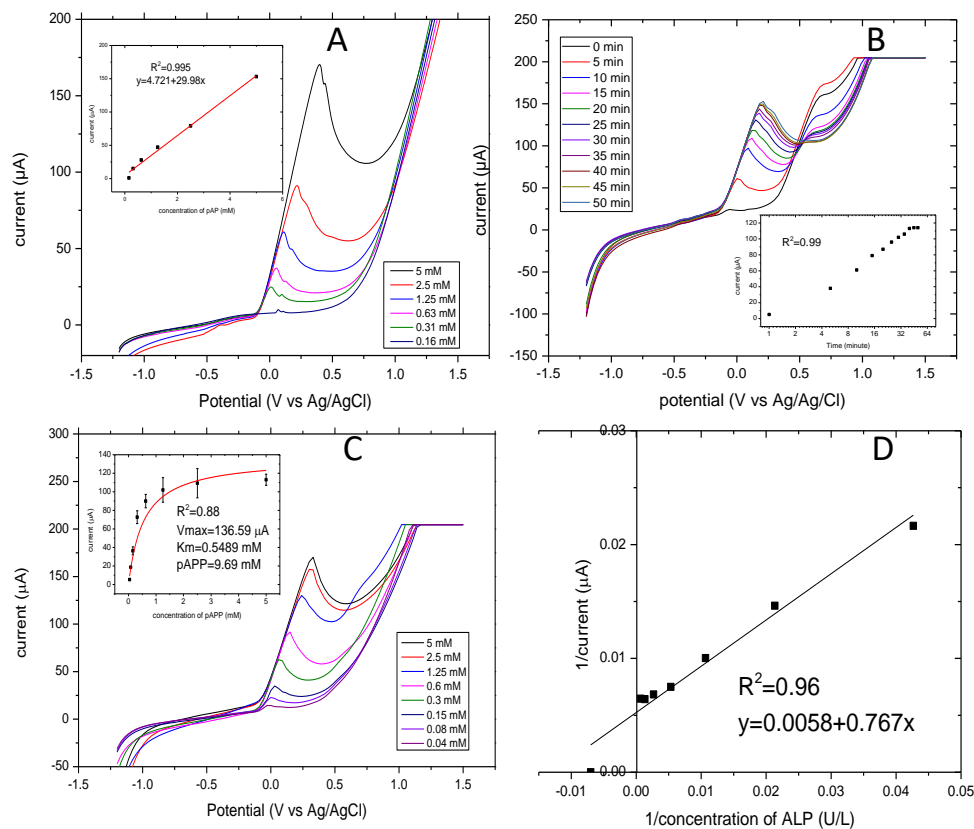


Figure 3. Linear sweep voltammograms of electrochemical optimization of ALP release applied at a potential of -1.2 V to -1.5 V , and a scan rate of 100 mV/S . **(A)** The linear sweep voltammograms of a concentration of pAP of $0.16\text{--}5 \text{ mM}$ and in the insert is the standard curve of the current response. **(B)** Optimization of the reaction time for the enzymatic assay of ALP release and in the inset is current response versus time. **(C)** Optimization of pAPP concentrations $0.2\text{--}5 \text{ mM}$ pAPP and in the insert is the current response versus concentrations of pAPP. **(D)** The calibration curve of ALP activity ranging from $1.5\text{--}1500 \text{ U/L}$ fitted by the Lineweaver-Burk model.

3.3. Linearity Performance of ALP Release vs. Cell Number

The linear relationship between ALP release and cell number was analysed. The final concentration of substrate pAPP was about 10–20-fold higher than the K_m . The linear voltammograms of ALP release from different concentrations of cells ($4, 8, 16, 31, 63, 125$, and $250 \times 10^3 \text{ cells/mL}$) were determined for each cell line. Figure 4 illustrates the linear sweep voltammetry that was performed at a scan rate of 100 mV/S and at potentials that ranged from -1.2 V to 1.5 V . The potential of the anodic response shifted as the cell number increased. The results are as follows: ALP release from Balb/c 3T3 cells shows oxidation of pAP beginning at -100 mV and ending at 150 mV . ALP release from A549 cells and MCF-7 cells shows oxidation of pAP beginning at -100 mV and ending at 200 mV . Ht-29 cells had slightly wider potential. We found oxidation of pAP beginning at -100 mV and ending at 300 mV . The oxidation peaks displayed by ALP release of the three cells, Balb/c 3T3, A549 and MCF-7, were narrower than those of Ht-29 cells.

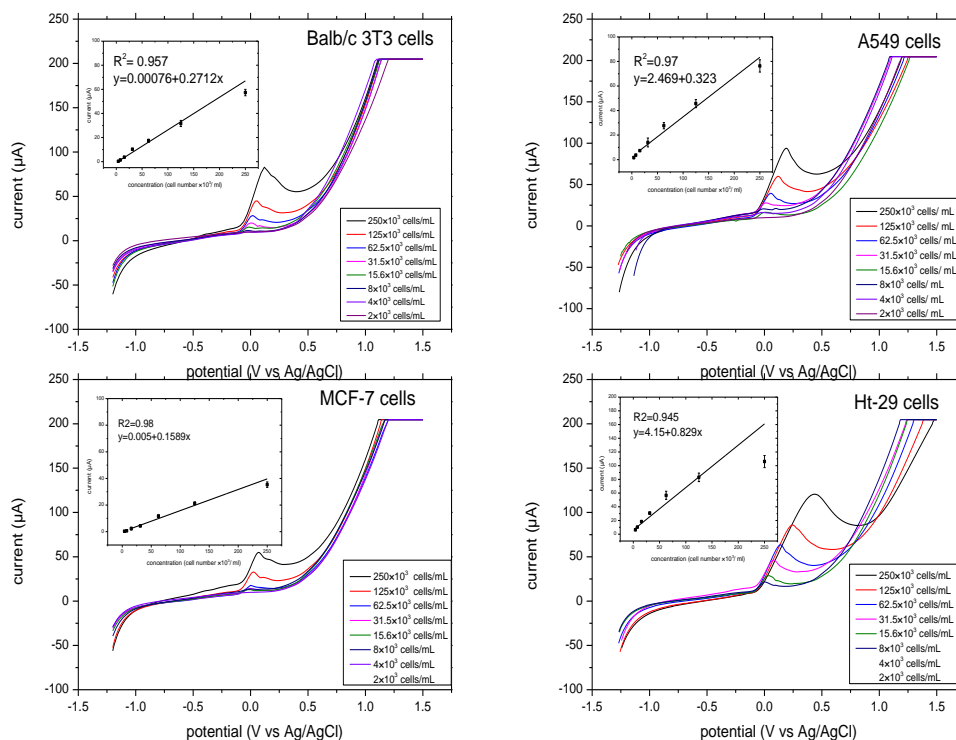


Figure 4. Linear sweep voltammograms of ALP release for each cell range from $2\text{--}250 \times 10^3$ cells/mL at a scan rate of 100 mV/S, incubation time of 10 min and potential range from $-1.2\text{--}1.5$ V. In the insert, the linearity performance of the ALP release from the given cells versus the current responses with linear regression analysis is outlined. All the measurements were applied in triplicate in separate graphite-SPE in the presence of 9.7 mM pAPP and at final volume of 70 μL .

There was good linear correlation between the current response and ALP released from the four cells. The cells of Balb/c 3T3 showed the highest value of ALP released at 75 μA , while MCF-7 cells had 50 μA , which was also the lowest value of ALP released among other cells at a concentration of 250×10^3 cells/mL. At the lowest concentration of 4×10^3 cells/mL, the MCF-7 cells showed a current response of 10 μA , while that of Balb/c 3T3 cells was 9 μA . Both showed a good linear response R^2 of 0.95 and 0.98 for Balb/c 3T3 cells and MCF-7 cells. ALP release from A549 cells and Ht-29 cells showed higher values of currents at 80 μA and at 100 μA , respectively, and also a good linear response ($R^2 = 0.94$ for A549 cells and 0.94 for Ht-29 cells). Moreover, the current response in Ht-29 cells had levelled off from the concentration of 1.25×10^3 cells/mL, which indicates that the substrate concentration was running out. Ht-29 cells can release higher amounts of ALP compared to other cells. Therefore, this showed the importance of optimizing substrate concentration for each cell type.

3.4. Concentration of the Substrate pAPP from Adhesion Cells

The optimal concentration of pAPP for the evaluation of ALP release from adhesion cells was investigated. The linear sweep voltammograms of the pAP formed by ALP release from Balb/c 3T3 cells, A549 cells, MCF-7 cells, and Ht-29 cells with different concentrations of substrate ranging from 0.2 to 5 mM pAPP are illustrated in Figure 5. The measurements were taken at a scan rate of 100 mV/S, initial potential of -1.2 V and final potential of 1.5 V. pAP formed by enzymatic reaction at 37 $^\circ\text{C}$ after 10 min was measured. The oxidation peaks of pAP began at 0.0 mV and ended at 150 mV for all cells. The current values were

plotted against substrate concentration and fitted by the Michaelis–Menten model (Figure 5, insert). The enzymatic reaction of ALP release from Balb/c 3T3, A549, MCF-7, and Ht-29 cells versus different concentrations of the substrate pAPP displayed good non-linear regression, with $R^2 = 0.97$. The K_m values of pAPP from each cell line were as follows: Balb/c 3T3 = 4.75 mM, A549 = 5.03 mM, MCF-7 = 10.19 mM and Ht-29 = 1.85 mM. The I_{max} values were as follows: Balb/c 3T3 = 96.5 μ A, A549 = 69.24 μ A, MCF-7 = 82.68 μ A and Ht-29 = 61.67 μ A. The corresponding concentrations of pAPP at 95% of I_{max} were as follows: 47.5 mM for Balb/c 3T3 cells; 50.3 mM for A549; 101.9 mM for MCF-7; and 18.5 mM for Ht-29. The differentiation of the parameters indicates the different activity of ALP in each cell line, where the colon cancer cell lines exhibited the highest activity and the breast cancer cell lines had the lowest activity according to their substrate concentration consumed at half maximal velocity.

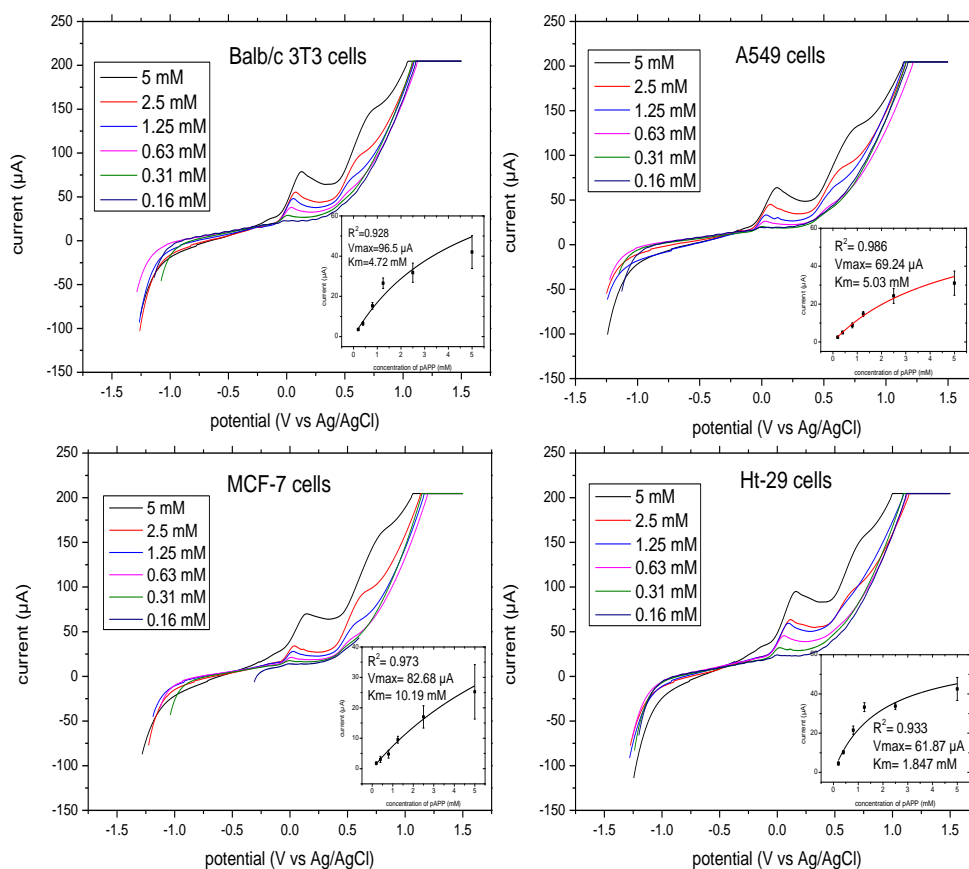


Figure 5. Linear sweep voltammograms of ALP release for adhesion cells in the presence of different concentrations of substrate pAPP (2–5 mM) at a scan rate of 100 mV/S, potential range of –1.2–1.5 V and incubation time of 10 min. In the insert, the concentration of pAPP substrate versus the current responses with non-linear regression analysis is outlined. All the measurements were applied in triplicate in separate graphite-SPE and at final volume of 70 μ L.

3.5. Comparative Study of ALP Activity

An electrochemical optimized assay was compared to absorbance outputs using the optical active substrate pNPP and two different methods: capillary electrophoresis and colorimetry. The former was applied due to its selective monitoring of p-nitrophenol and because it eliminates any interference with

endogenous ALP in the sample. The latter is a standard method for ALP analysis. The analysis was carried out in the presence of 70 μL of the product pNP in the range of 15–500 μM and 30 μL of sample mixed with 6 mM of pNPP. Figure 6A shows electropherograms of different concentrations of p-nitrophenol in the presence of 1 mM DEA adjusted to pH = 9.5, temperature 20 $^{\circ}\text{C}$, voltage of 15 kV and wavelength of 405 nm. The measurements of pNP taken in a fused-silica capillary with an effective length of 15 cm and a diameter of 50 μm displayed peaks at migration time of 5 min. This also was confirmed by other studies [45,46,47]. The separation peaks were affected by the length of incubation time and by applied voltage [45]. CE is an ideal assay for further investigation of ALP isoenzymes, as it performs sensitive detection in alkaline buffer. This is an appropriate environment for ALP. The insert details the calibration plot of pNP concentrations versus the peak areas, which displayed very good linear regression of $R^2 = 0.99$, slope of 70.13 mAU/ μM and intercept of 9.68 mAU. This was used for normalizing the peaks' areas of ALP release from living cells with values obtained by colorimetric analysis. Figure 6B shows the calibration curve of absorbance versus various concentrations of ALP ranging from 1.5–1500 U/L and fitted by the Michaelis–Menten model. The standards had 30 μL of sample dissolved with pNPP 6 mM in buffer DEA and were incubated for 30 min. Data in triplicate were plotted using origin software. The correlation coefficient was found to be 0.99, and the V_{max} and K_m of the curve were found to be 4.25 and 67.81 U/L. The correlation slope (K_m/V_{max}) and intercept ($1/V_{\text{max}}$) were calculated from the constants and were used for comparing data with the electrochemical assay. The insert outlines the linearity studies of colorimetric assay carried out in the presence of different concentrations of pNP (14–500 μM). The regression analysis was 0.99, and the slope and intercept of the curves were found to be 5.53 and 0.34. These were used for normalizing data and comparing them with the capillary electrophoresis assay. Figure 6C shows the normalizing data of ALP release from cells represented by formation of the product pNP. Capillary electrophoresis and colorimetric assay displayed good correlation. No significant difference ($p > 0.05$) resulted from the two methods. It is obvious that the lowest ALP level was determined by Balb/c 3T3 cells, which was 0.16–0.17 mM, whereas the highest level of ALP was of colon cancer cells and was in the range of 0.48–0.50 mM. Lung and breast cancer cells had almost the same levels of ALP (0.21–0.22 mM and 0.20–0.21 mM, respectively). Moreover, the ALP of lung cancer was slightly higher than breast cancer, and results showed very small standard deviation. Figure 6D outlines details of the comparative analysis performed on the absorbance and optimized electrochemical assay of ALP release from living cells. The electrochemical or optical data of ALP release from cells were normalized using the Lineweaver–Burke equation shown in Figure 3C and the Michaelis–Menten model shown in Figure 6B. There was a significant difference ($p > 0.05$) in the activity of ALP release from cells between electrochemical and optical assays. The electrochemical results of ALP activity from Balb/c 3T3, A549, MCF-7 and Ht-29 were higher than ALP activity obtained by absorbance analysis. This optimization demonstrated that evaluation of ALP release by electrochemical assay was more sensitive than by optical assay. Moreover, it showed faster detection as the optical active substrate needed 30 min for evaluating ALP release in samples, while that of the electro active substrate only needed 10 min.

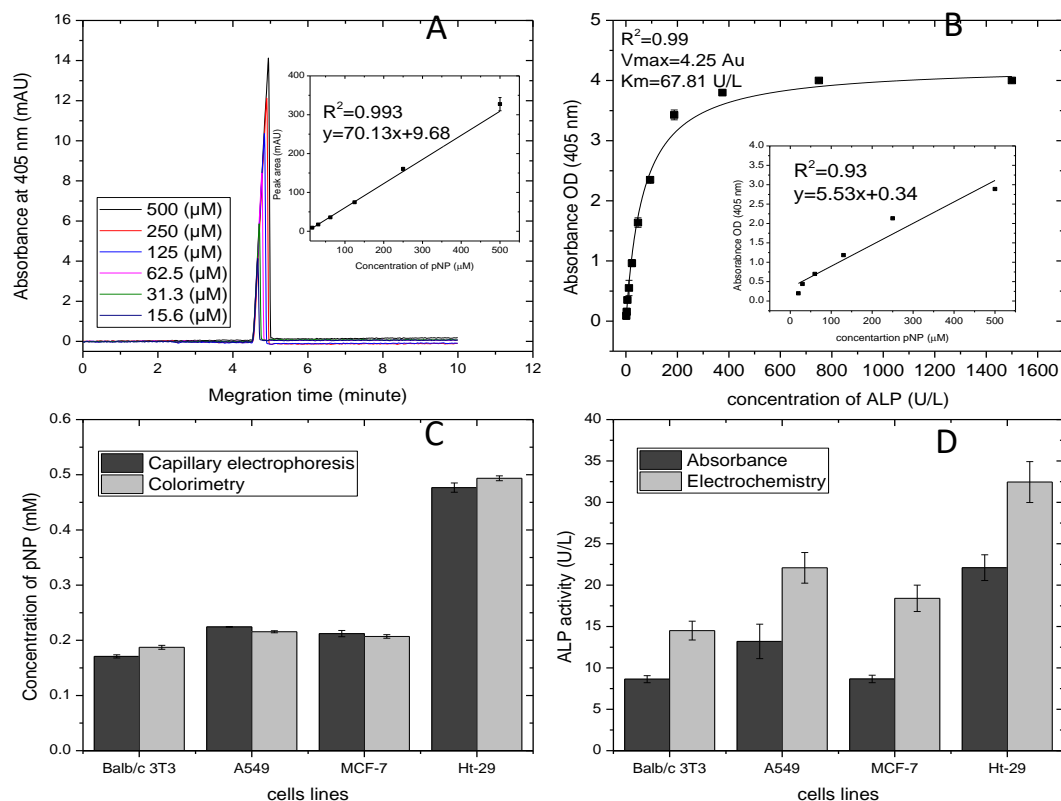


Figure 6. Comparative studies of absorbance and electrochemistry toward ALP release from living cells. (A) Electropherograms of pNP concentration and in the insert is the linear trend of peak areas. (B) Calibration curve of absorbance values relating to ALP concentration ranging from 1.5–1500 U/L, fitted by the Michaelis-Menten model, and in the insert is the linear trend of absorbance to pNP concentration (15–500 μM). (C) Histograms of ALP release measured by capillary electrophoresis and colorimetry. (D) Histograms of ALP release measured by absorbance and electrochemistry.

4. Conclusions

Alkaline phosphatase is a cancer biomarker, and the monitoring of ALP release from cells contributes to an understanding of the basis of diseases and the progression of cancer. The aim of this paper was to develop a methodology for monitoring ALP release from two types of cells: embryo fibroblast cells (Balb/c 3T3) and cancer epithelial cells (A549, MCF-7, Ht-29), using electrochemical analysis. At alkaline pH, the enzyme ALP hydrolyzes the non-electroactive p-aminophenol phosphate to generate the electroactive, p-aminophenol. The electrochemical behaviour of the sensors used was investigated using cyclic voltammetry and using the solution $[\text{Fe}(\text{CN})_6]^{3-/4-}$ as the model for single transfer electrons. A cleaning duration of 20 min for the sensors in the Plasmon cleaner gives good electrochemical behaviour. The anodic and cathodic peak ratio was almost 1 ($i_a/i_c = 1$), and the half peak potential (E_{mid} vs. Ag/AgCl) showed a reversibility reaction. The peak-to-peak separation (ΔE_p) of anodic and cathodic peaks was 62 mV. Linear sweep voltammetry detection techniques that have a wide window of potential were applied using graphite-SPE at a scan rate of 100 mV/S and at a potential ranging from -1.2 V to 1.5 V vs. a reference electrode of Ag/AgCl. This demonstrated the standard curve of pAP, and allowed for observation of the potential where oxidation peaks occur. This was at 0 – 0.15 V of the current response (0 – 150 μA) displayed when the concentration of pAP (0.16 – 5 mM) was increasing. The oxidation peaks of pAP began at -100 mV

and ended at 300 mV as the concentration increased. The samples were incubated with substrate for different amounts of time. They displayed a positive linear dependence and 10 min was selected as the time to do the rest of the experiments. The substrate pAPP was optimized using detached cells and had a Michaelis constant (K_m) of 0.548 mM, (I_{max}) of 136.59 and an optimal p-APP concentration of 9.69 mM. A calibration plot was obtained based on the optimization measurements from a range of 1–1500 U/L. ALP release was determined from various cell numbers for linearity analysis. All cells exhibited linear trends with good regression analysis. The pAPP substrate was investigated during cellular adhesion, and K_m and I_{max} were calculated for each cell line. Capillary electrophoresis and colorimetric methods were applied for comparative analysis. CE allows for the detection of ALP release with substrates at the same time, which can be used for distinguishing ALP iso-enzymes. The samples were introduced onto the capillary automatically. The average detection time for p-nitrophenol was 5 min. Colorimetry, which is the standard assay of ALP in clinical analysis, showed compatible values with CE. A calibration curve of ALP was created to allow for comparison of the data obtained by optical and electrochemical analysis. This revealed a significant difference between the two, indicating that the electrochemical investigation resulted in a more sensitive and rapid assay than the optical analysis.

Author Contributions: Supervision, A.H. and E.M.; Writing – original draft, T.B. All authors have read and agreed to the published version of the manuscript.

Funding: This research was funded by the Ministry of Higher Education of Saudi Arabia.

Acknowledgments: The authors would like to acknowledge the financial support of the Ministry of Higher Education of Saudi Arabia.

Conflicts of Interest: The authors declare that there are no conflicts of interests from any parts.

References

- [1] Millán, J.L. *Mammalian Alkaline Phosphatases: From Biology to Applications in Medicine and Biotechnology*; Wiley-Blackwell: Hoboken, NJ, USA, 2006. [Google Scholar]
- [2] Tartter, P.I.; Slater, G.; Gelernt, I.; Aufses, A.H. Screening for Liver Metastases from Colorectal Cancer with Carcinoembryonic Antigen and Alkaline Phosphatase. *Ann. Surg.* 1981, 193, 357–360. [Google Scholar] [CrossRef]
- [3] Annibali, O.; Petrucci, M.; Santini, D.; Mariani, M.; Pisani, F.; Bongarzone, V.; Venditti, O.; Rago, A.; Cerchiara, E.; Fiorini, A.; et al. Alkaline Phosphatase (ALP) Levels in Multiple Myeloma (MM) And Cancer With Bone Lesions: Is There any Difference? *Clin. Lymphoma Myeloma Leuk.* 2015, 15, e125. [Google Scholar] [CrossRef]
- [4] Abdallah, E.A.; Said, R.N.; Mosallam, D.S.; Moawad, E.M.; Kamal, N.; Fathallah, M.G.-D. Serial serum alkaline phosphatase as an early biomarker for osteopenia of prematurity. *Medicine* 2016, 95, e4837. [Google Scholar] [CrossRef] [PubMed]
- [5] Zhu, C.; Yang, G.; Li, H.; Du, D.; Lin, Y. Electrochemical Sensors and Biosensors Based on Nanomaterials and Nanostructures. *Anal. Chem.* 2014, 87, 230–249. [Google Scholar] [CrossRef] [PubMed]
- [6] Thompson, R.Q.; Barone, G.C.; Halsall, H.; Heineman, W.R. Comparison of methods for following alkaline phosphatase catalysis: Spectrophotometric versus amperometric detection. *Anal. Biochem.* 1991, 192, 90–95. [Google Scholar] [CrossRef]
- [7] Ito, S.; Yamazaki, S.-I.; Kano, K.; Ikeda, T. Highly sensitive electrochemical detection of alkaline phosphatase. *Anal. Chim. Acta* 2000, 424, 57–63. [Google Scholar] [CrossRef]
- [8] Wang, J.H.; Wang, K.; Bartling, B.; Liu, C.-C. The Detection of Alkaline Phosphatase Using an Electrochemical Biosensor in a Single-Step Approach. *Sensors* 2009, 9, 8709–8721. [Google Scholar] [CrossRef] [PubMed]
- [9] Ru, S.-P.; Wu, J.; Yi-Bin, Y.; Ji, F. Electrochemical Detection of Alkaline Phosphatase Using Ionic Liquid Modified Carbon Nanotubes Electrode. *Chin. J. Anal. Chem.* 2012, 40, 835–840. [Google Scholar] [CrossRef]

- [10] Xia, N.; Ma, F.; Zhao, F.; He, Q.; Du, J.; Li, S.; Chen, J.; Liu, L. Comparing the performances of electrochemical sensors using p-aminophenol redox cycling by different reductants on gold electrodes modified with self-assembled monolayers. *Electrochim. Acta* 2013, 109, 348–354. [Google Scholar] [CrossRef]
- [11] Zhang, L.; Hou, T.; Li, H.; Li, F. A highly sensitive homogeneous electrochemical assay for alkaline phosphatase activity based on single molecular beacon-initiated T7 exonuclease-mediated signal amplification. *Analyst* 2015, 140, 4030–4036. [Google Scholar] [CrossRef]
- [12] Berger, J.; Hauber, J.; Hauber, R.; Geiger, R.; Cullen, B.R. Secreted placental alkaline phosphatase: A powerful new quantitative indicator of gene expression in eukaryotic cells. *Gene* 1988, 66, 1–10. [Google Scholar] [CrossRef]
- [13] Ho, W.; Athey, D.; McNeil, C. Amperometric detection of alkaline phosphatase activity at a horseradish peroxidase enzyme electrode based on activated carbon: Potential application to electrochemical immunoassay. *Biosens. Bioelectron.* 1995, 10, 683–691. [Google Scholar] [CrossRef]
- [14] Rupicault, S.; Linioges, B.; Dcpwncl, C. Alkaline Phosphatase Assay Using a Redox Procationic Labeled Substrate and a Renewable Nafion-Loaded Carbon Paste Electrode. *Electroanalysis* 1996, 8. [Google Scholar] [CrossRef]
- [15] Limoges, B.; DeGrand, C. Ferrocenylethyl Phosphate: An Improved Substrate for the Detection of Alkaline Phosphatase by Cathodic Stripping Ion-Exchange Voltammetry. Application to the Electrochemical Enzyme Affinity Assay of Avidin. *Anal. Chem.* 1996, 68, 4141–4148. [Google Scholar] [CrossRef]
- [16] Bauer, C.G.; Eremenko, A.V.; Ehrentreich-Förster, E.; Bier, F.F.; Makower, A.; Halsall, H.B.; Heineman, W.R.; Scheller, F.W. Zeptomole-Detecting Biosensor for Alkaline Phosphatase in an Electrochemical Immunoassay for 2,4-Dichlorophenoxyacetic acid. *Anal. Chem.* 1996, 68, 2453–2458. [Google Scholar] [CrossRef] [PubMed]
- [17] Kain, S.R. Use of Secreted Alkaline Phosphatase as a Reporter of Gene Expression in Mammalian Cells. *Recomb. Protein Protoc.* 2003, 63, 49–60. [Google Scholar] [CrossRef]
- [18] Yang, T.-T.; Sinai, P.; Kitts, P.A.; Kain, S.R. Quantification of Gene Expression with a Secreted Alkaline Phosphatase Reporter System. *Biotechniques* 1997, 23, 1110–1114. [Google Scholar] [CrossRef]
- [19] Bettan, M.; Darteil, R.; Scherman, D. Secreted Human Placental Alkaline Phosphatase as a Reporter Gene for *in Vivo* Gene Transfer. *Anal. Biochem.* 1999, 271, 187–189. [Google Scholar] [CrossRef]
- [20] Cullen, B.R. Utility of the secreted placental alkaline phosphatase reporter enzyme. *Methods Enzymol.* 2000, 326, 159–164. [Google Scholar] [CrossRef]
- [21] Kelso, E.; McLean, J.; Cardosi, M.F. Electrochemical Detection of Secreted Alkaline Phosphatase: Implications to Cell Based Assays. *Electroanalysis* 2000, 12, 490–494. [Google Scholar] [CrossRef]
- [22] Cullen, B.R.; Malim, M. Secreted placental alkaline phosphatase as a eukaryotic reporter gene. *Methods Enzymol.* 1992, 216, 362–368. [Google Scholar] [CrossRef] [PubMed]
- [23] Doronin, K.; Zakharchuk, A.; Grinenko, N.; Yurov, G.; Krougliak, V.; Naroditsky, B. Expression of the gene encoding secreted placental alkaline phosphatase (SEAP) by a nondefective adenovirus vector. *Gene* 1993, 126, 247–250. [Google Scholar] [CrossRef]
- [24] Bronstein, I.; Fortin, J.J.; Voyta, J.C.; Juo, R.R.; Edwards, B.; E Olesen, C.; Lijam, N.; Kricka, L.J. Chemiluminescent reporter gene assays: Sensitive detection of the GUS and SEAP gene products. *Biotechniques* 1994, 17, 176–177. [Google Scholar]
- [25] Chang, T.C.; Wang, J.K.; Hung, M.W.; Chiao, C.H.; Tsai, L.C.; Chang, G.G. Regulation of the expression of alkaline phosphatase in a human breast-cancer cell line. *Biochem. J.* 1994, 303, 199–205. [Google Scholar] [CrossRef]
- [26] He, J.; Landau, N.R. Use of a novel human immunodeficiency virus type 1 reporter virus expressing human placental alkaline phosphatase to detect an alternative viral receptor. *J. Virol.* 1995, 69, 4587–4592. [Google Scholar] [CrossRef]
- [27] Murata, T.; Yasukawa, T.; Shiku, H.; Matsue, T. Electrochemical single-cell gene-expression assay combining dielectrophoretic manipulation with secreted alkaline phosphatase reporter system. *Biosens. Bioelectron.* 2009, 25, 913–919. [Google Scholar] [CrossRef]
- [28] Inoue, K.Y.; Yasukawa, T.; Shiku, H.; Matsue, T. Cell-Based Electrochemical Assay for Endotoxin Using a Secreted Alkaline Phosphatase Reporter System. *Electrochemistry* 2008, 76, 525–528. [Google Scholar] [CrossRef]
- [29] Şen, M.; Ino, K.; Inoue, K.Y.; Arai, T.; Nishijo, T.; Suda, A.; Kunikata, R.; Shiku, H.; Matsue, T. LSI-based amperometric sensor for real-time monitoring of embryoid bodies. *Biosens. Bioelectron.* 2013, 48, 12–18. [Google

- Scholar] [CrossRef]
- [30] Vernick, S.; Freeman, A.; Rishpon, J.; Niv, Y.; Vilkin, A.; Shacham-Diamand, Y. Electrochemical Biosensing for Direct Biopsy Slices Screening for Colorectal Cancer Detection. *J. Electrochem. Soc.* 2011, 158, P1–P4. [Google Scholar] [CrossRef]
 - [31] Porat-Ophir, C.; Dergachev, V.; Belkin, A.; Vernick, S.; Freynd, G.; Katsnelson, M.; Chetvertnykh, V.; Rishpon, J.; Shacham-Diamand, Y. Chip level agitation effects on the electrochemical sensing of alkaline-phosphatase expressed from integrated liver tissue. *Sens. Actuators B Chem.* 2015, 213, 465–473. [Google Scholar] [CrossRef]
 - [32] Yildirim-Semerici, C.; Benayahu, D.; Adamovski, M.; Wollenberger, U. An Electrochemical Assay for Monitoring Differentiation of the Osteoblastic Cell Line (MBA-15) on the Sensor Chip. *Electroanalysis* 2015, 27, 1350–1358. [Google Scholar] [CrossRef]
 - [33] Shacham-Diamand, Y.; Schreiber, D.; Inberg, A.; Berkh, O.; Kósa, G.; Freeman, A.; Shacham-Diamand, Y. Disposable electrochemical sensor prepared using 3D printing for cell and tissue diagnostics. *Sens. Actuators B Chem.* 2015, 216, 434–442. [Google Scholar] [CrossRef]
 - [34] Ikehara, Y.; Mansho, K.; Takahashi, K.; Kato, K. Purification and Characterization of Alkaline Phosphatase from Plasma Membranes of Rat Ascites Hepatoma1. *J. Biochem.* 1978, 83, 1471–1483. [Google Scholar] [CrossRef] [PubMed]
 - [35] Sone, M.; Kishigami, S.; Yoshihisa, T.; Ito, K. Roles of Disulfide Bonds in Bacterial Alkaline Phosphatase. *J. Boil. Chem.* 1997, 272, 6174–6178. [Google Scholar] [CrossRef]
 - [36] Satou, Y.; Al-Shawafi, H.A.; Sultana, S.; Makita, S.; Sohda, M.; Oda, K. Disulfide bonds are critical for tissue-nonspecific alkaline phosphatase function revealed by analysis of mutant proteins bearing a C201-Y or C489-S substitution associated with severe hypophosphatasia. *Biochim. et Biophys. Acta (BBA). Mol. Basis Dis.* 2012, 1822, 581–588. [Google Scholar] [CrossRef]
 - [37] Moore, E.J.; Pravda, M.; Kreuzer, M.P.; Guilbault, G.G. Comparative Study of 4-Aminophenyl Phosphate and Ascorbic Acid 2-Phosphate, as Substrates for Alkaline Phosphatase Based Amperometric Immunosensor. *Anal. Lett.* 2003, 36, 303–315. [Google Scholar] [CrossRef]
 - [38] Rosén, I.; Rishpon, J. Alkaline phosphatase as a label for a heterogeneous immunoelectrochemical sensor. *J. Electroanal. Chem. Interfacial Electrochem.* 1989, 258, 27–39. [Google Scholar] [CrossRef]
 - [39] Pemberton, R.M.; Hart, J.; Stoddard, P.; A Foulkes, J. A comparison of 1-naphthyl phosphate and 4 aminophenyl phosphate as enzyme substrates for use with a screen-printed amperometric immunosensor for progesterone in cows' milk. *Biosens. Bioelectron.* 1999, 14, 495–503. [Google Scholar] [CrossRef]
 - [40] Chen, L.; Yang, G.; Wu, P.; Cai, C. Real-time fluorescence assay of alkaline phosphatase in living cells using boron-doped graphene quantum dots as fluorophores. *Biosens. Bioelectron.* 2017, 96, 294–299. [Google Scholar] [CrossRef]
 - [41] Gattu, S.; Criehtfield, C.; Lu, G.; Bwanali, L.; Veltri, L.M.; Holland, L.A. Advances in enzyme substrate analysis with capillary electrophoresis. *Methods* 2018, 146, 93–106. [Google Scholar] [CrossRef]
 - [42] Balbaied, T.; Moore, E. Resazurin-Based Assay for Quantifying Living Cells during Alkaline Phosphatase (ALP) Release. *Appl. Sci.* 2020, 10, 3840. [Google Scholar] [CrossRef]
 - [43] Sappia, L.; Felice, B.; Sanchez, M.; Marti, M.; Madrid, R.; Pividori, M.; Pividori, I. Electrochemical sensor for alkaline phosphatase as biomarker for clinical and *in vitro* applications. *Sens. Actuators B Chem.* 2019, 281, 221–228. [Google Scholar] [CrossRef]
 - [44] Reymond, J.-L.; Fluxa, V.S.; Maillard, N. Enzyme assays. *Chem. Commun.* 2008, 34–46. [Google Scholar] [CrossRef] [PubMed]
 - [45] Murakami, Y.; Morita, T.; Kanekiyo, T.; Tamiya, E. On-chip capillary electrophoresis for alkaline phosphatase testing. *Biosens. Bioelectron.* 2001, 16, 1009–1014. [Google Scholar] [CrossRef]
 - [46] Grodner, B.; Napiórkowska, M. Characterization and inhibition studies of tissue nonspecific alkaline phosphatase by aminoalkanol derivatives of 1,7-dimethyl-8,9-diphenyl-4-azatricyclo[5.2.1.0 2,6]dec-8-ene-3,5,10-trione, new competitive and non-competitive inhibitors, by capillary electrophoresis. *J. Pharm. Biomed. Anal.* 2017, 143, 285–290. [Google Scholar] [CrossRef]
 - [47] Takayanagi, T.; Mine, M.; Mizuguchi, H. Capillary Electrophoresis/Dynamic Frontal Analysis for the Enzyme

Appendix

Assay of 4-Nitrophenyl Phosphate with Alkaline Phosphatase. Anal. Sci. 2020. [Google Scholar] [CrossRef]



© 2020 by the authors. Submitted for possible open access publication under the terms and conditions of the Creative Commons Attribution (CC BY) license (<http://creativecommons.org/licenses/by/4.0/>).

Real-time Impedance Monitoring of Alkaline Phosphatase (ALP) Release by Microelectrode Arrays

Thanih Balbaied and Eric Moore *

Sensing & Separation Group, School of Chemistry and Life Science Interface, University College Cork, Tyndall National Institute, T12R5CP Cork, Ireland

* Correspondence: e.moore@ucc.ie

Abstract: Alkaline phosphatase (ALP) is a reporter enzyme widely used in point-of-care applications. Real-time monitoring of ALP accelerates understanding of the emergence diseases and cancer progress, which can be achieved through biosensor-based strategies. This paper demonstrates a developed approach for real-time monitoring of ALP release of the differentiation of cultured human colon cancer cells (Ht-29). Electric cell-substrate impedance sensing was used to generate changes of Ht-29 cells during ALP release and the data was compared with amperometry. The findings indicated a correlation between the cell response and shift in impedance magnitude and current. Relevant results had similar attitude during monitoring of cell morphology and cell viability. Our analysis is a clear advance on the current methods such as enzyme-linked immunosorbent assay. The developed method can contribute to the development of microfluidic testing that would facilitate work on small scale techniques.

Keywords: Alkaline phosphatase; cell viability; microelectrode array; amperometry; impedance; colon cancer

1 Introduction

Alkaline phosphatase (ALP) is an enzyme [1], [2] routinely determined in clinical analysis for diseases related to liver and bone disorders. Recently it was evaluated to be an early cancer biomarker [3], [4] due to the fact that many reports of colon cancer presented always correlate ALP rise and emerging diseases that causing cancer including ulcerative colitis or polyposis of the colon [5] [6], [7].

Ht-29 cells lines are frequently used as model to represent colon cancer for in vitro studies [8], [9]. These cells keep their phenotypic properties, which make them optimal models for colon cancer investigation [10]. During cancer forming, a multistep process occurs and makes an improper life cycle of cells. Consequently, normal cellular reaction of an individual cell will differ from that of a cancer cell, thereby cellular electrical activity is going to change and cause releasing of biomarkers. ALP release, was nominated as a gene reporter in quantification of the intracellular ALP mRNA [11]. Therefore, it is important to study the mechanisms underlying ALP release to monitor problems in cells and resolve them.

A number of techniques have been used in this regard including staining methods [12], mRNA-based methods [13], and ELISA [14], [15]. Although the sensitivity of immunoassay, it is still lab-based applications [16] [17]. Another limitation with monoclonal antibodies is that immunoassays cannot identify the isoenzyme ALP [18] [19]. Therefore, scientific attentions were drawn towards label-free methods. Development of the bio-devices based on microelectrode arrays contribute in characterizing cell activity parameters, such as respiratory activity, release, enzyme activity, and action potential and allow regular clinical diagnostics and fasten drug discovery [20]. Biosensor-based strategies include surface plasmon resonance [21; field-effect transistor [22]; quartz crystal microbalance [23]; and electrochemical impedance

spectroscopy (EIS) [24]–[26]. However, these reports so far relied on indirect methods using immunoassay approaches. This paper intended to avoid affinity approaches and reveal the direct tiny physiological movements of adhesion of cells during ALP release using electrochemical impedance spectroscopy (EIS).

Impedance technique depended on measuring resistivity and capacitively (dielectric) properties of cells as the membrane works as an insulator (capacitance). So, to allow real-time quantifying of cellular function during ALP release, the electric cell-substrate impedance sensing (ECIS) system was suggested. ECIS model designed by Giaever and Keese (1984), integrates microelectrode array with biological targets in order to measure the cellular responses [27–29].

In this method, the cultureware (ECIS-8W10E+) consisted of 40 microelectrodes per well (8 wells) have been used as a solid surface for attaching cell. Cells were differentiated by two ways; post-confluence culture and sodium butyrate for the purpose of inducing ALP. High ALP release means the permeability of cell membrane increases, which cause a decrement in the impedance magnitude and an increment of the capacitance. The viability of cells was verified by resazurin assay and microscopy. ALP activity was assessed by amperometry in the presence of the electroactive substrate of p-aminophenyl phosphate (pAPP).

2 Methodology:

2.1 Reagent and instruments

Colon carcinoma epithelial cells (Ht-29 Cell Line) (ATCC, Ireland) was cultivated in McCoy's 5A medium (Sigma, Ireland) in the presence of 10% fetal bovine serum (FBS) (Sigma, Ireland) at 37 °C and 5% CO₂. The standard condition of subculture was performed by using Hank's balanced salt solution (HBSS) (Sigma, Ireland) for washing cells and using trypsin/EDTA solution (Sigma, Ireland) for detachments of cells. Cells was seeded at density of 80,000 cell/mL in 48-well plate (Corning®, Sigma, Ireland) or electric cell-substrate impedance sensing cultureware (ECIS-8W10E+, ibid, Germany). Hemocytometer slide (Reichert Bright-Line) was used for accounting of cells. The culture ware was treated with L-cysteine (Sigma, Ireland). For viability assay resazurin and virkon® were used (Sigma, Ireland) and the fluorescent measurement was recorded by the fluorescent platereaders (Spectra Max Gemini). Cells morphology was monitored by an inverted microscope and camera (Olympus). Cells was differentiation by sodium butyrate (NaBt), (Sigma, Ireland). Metrohm autolab analyser (Metrohm, Netherland) was used for impedance detection. For alkaline phosphatase (ALP) determination, the following buffer was used. It consist of magnesium chloride (MgCl₂), sodium chloride (NaCl), potassium chloride (KCl), diethanolamine (DEA), para-aminophenol phosphate (pAPP), and alkaline phosphatase (ALP) all of which were purchased from (Sigma, Ireland). PalmSens portable potentiostat (Palm Instruments BV, the Netherlands) and graphite screen printed electrodes (Kanichi Research Limited) was used for the amperometric detection.

2.2 Pretreatment of microelectrodes

Microelectrode surfaces were treated with 10 mM L-cysteine diluted in deionized water. Then 200 µL L-cysteine solution was added to wells and left at room temperature for 10 minutes. Wells were cleaned twice with 200 µl of deionized water and kept under UV light for 30 minutes before seeding cells.

2.3 Cell culture

According to the manufacture, Ht-29 cells preferred McCoy's 5A (modified) medium with 10 % FBS serum for cell culturing. Cells was sub-cultured three time before seeding application. For sub-culturing, old media was removed and cells was washed with HBSS and then the monolayer of cells was de-adhered from substrate by trypsin method as reported by Thanih *et al.* [30]. Cells was seeded in the 48-well plate or in cultureware at the desired density using the hemocytometer for cell accounting and incubated at 37 °C and 5% CO₂.

2.4 Optimization of impedance measurement

Electrochemical impedance spectroscopy measurements were calculated using a Metrohm Autolab analyser. During the measurements, the cultureware (ECIS 8W10E+) was placed in a cell culture hood (figure 1). The cultureware consisted of 40 microelectrodes per well (8 wells) and the total surface area of

the 40 microelectrodes per well is 1.96 cm². The cells grew on the 40 microelectrodes and grew on the insulating layer that mounted on the polycarbonate substrate. The latter and the thin film of microelectrodes are transparent and thus permit microscopic monitoring of cells. The walls of wells are made of polystyrene and they have a capacity of 600 µL for culture media. During applying the alternating current (AC), the change of the impedance due to the change of the capacitance of the monolayer of cells are recorded. The instrument was connected to electrodes with crocodile clips and controlled with Nova software. The Nova software was used to analyse the acquired data and to model the measured spectra. For impedance measurements, the equipment delivered an alternating current with 10 mV amplitude in a frequency range of between 1 k Hz and 1000 k Hz. The run of frequency of 50 points generated was from the high to the low. For determination of optimal frequency, the given cell line seeded at cell number of (20×10³ cells/ ml) and the resistance change was monitored for four days. The stability of the assay was confirmed by linearity analysis. The optimal frequency was fixed and the concentration of the cell number at range of (20, 40, 60, 80 ×10³ cell/ml) was changed and measured at one-hour intervals over 10 hours. The equation of cell index (CI) was used to normalize the measured electrical resistance and to plot the calibration curve of CI value and cell density. The long-term assay was confirmed by obtaining the normal growth curve of Ht-29 cells. This was performed by seeding the cells at an initial concentration of 80 ×10³ cell/ml. Cell growth was assessed at 24-hour intervals over 6 days. The data of impedance were normalized using CI index and fitted by logistic growth model using Origin software.

$$CI = (R_i/R_{cell-free}) - 1$$

Where R_i is the resistance of the cell-covered electrodes, and $R_{cell-free}$ is the resistance of blank electrodes (free-serum media).

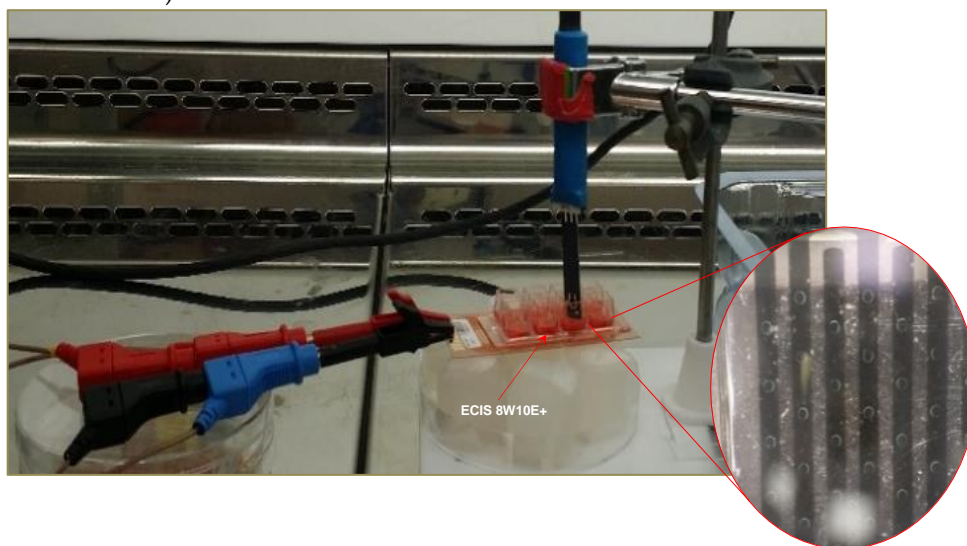


Figure.1 The workstation during ALP release monitoring, displaying the commercial (ECIS 8W10E+) cultureware. In the licorice representation, microelectrode arrays.

2.5 Impedance response during alkalinity buffer

Cells were seeded in the ECIS at a concentration of 80 × 10³ cells/ml for Ht-29 cells. The media was changed every two days to keep the cells healthy and nutrientized. After they achieved their exponential growth and met the 95-100% confluence (Day 4), the cells were washed with HBSS twice and exposed to ALP assay buffer. Control cells, treated cells and VC cells were assessed using electrochemical impedance spectroscopy measurements. Cell viability was verified by applying resazurin measurements.

2.6 Differentiation by sodium butyrate

Electrochemical impedance spectroscopy was carried out during the differentiation experiment in order to monitor cell monolayer behaviour during ALP release. The Ht-29 cell line was monitored during

post-confluence culture under routine conditions. The cells were seeded in ECIS cultureware and in a 48-well plate at a density of 80×10^3 cell/mL medium containing 10% FBS. Cells were cultivated in ECIS and in a 48-well plate for three day to reach 70-90% confluence. The cells were maintained in growth media for a further 3–6 days with media changes every two days. This monitoring was used as differentiation control. In order to further enhance differentiation in HT-29 cells, Sodium butyrate (NaBt) was applied to the culture medium. NaBt is a natural inducer for colon differentiation [31], [32]. Ht-29 cell line ECIS cultureware and 48-well plate was treated with 0.5mM or 1mM NaBt after 72 hours of cultivation. Cells were incubated with NaBt for 14 hours. The medium was changed to a routine medium, and the cells were incubated at 37 °C for two more days. Untreated cells were used as a control. The vehicle control had dead cells. Real-time monitoring of the cell monolayer was performed using an impedance signal. Microscope images of cells adhered to ECIS or 48-well plate were taken in order to investigate the morphology of cells during ALP release. The viability of the cells was also evaluated using resazurin-based assay.

2.7 Amperometric detection

Differentiation in HT-29 cells led to ALP release in the routine media. Amperometry of ALP release in media of NaBt-non-treated cells, NaBt-treated cells and the media of vehicle control was assessed. The graphite screen-printed electrodes (graphite-SPE) were immersed in 400 μ L of the routine media of the cells with 400 μ L of the ALP assay buffer (5 U/L ALP, 8 mM $MgCl_2$, 50 mM NaCl, and 10 mM pAPP and pH 9.5). The amount of p-aminophenol (pAP) was measured at positive potential 0.15 V for 10 seconds using palmSens portable potentiostat (Figure 2). When the current reached the stable baseline, it was measured at the fourth second.



Figure 2 The work station of detection amperometry measurement

2.8 Microscope images

Images of cell-confluence were taken at 24-hour intervals over 5 days using the inverted microscope and camera. Due to the presence of phenol red, which interferes with the light of microscopes, cells were washed twice with HBSS. As the microelectrodes were not transparent to the light, images of cells were taken from the area between the interdigitated microelectrodes.

2.9 Cell viability

Resazurin was prepared in HBSS and diluted to 100 μ M in McCoy A5 media. Cells were seeded at 80×10^3 cell/ mL in the ECIS cultureware. It incubated with cells for 4 hours. Negative control or vehicle control was performed by addition of two drops of Virkon® to the routine media and incubated with cell for 24 hours. Fluorescent measurement was measured at at 544 excitation and 590 nm emission as an optimal wavelength range of resazurin.

3 Results and discussion

3.1 Electrochemical impedance spectroscopy

Three frequency ranges are usually used to monitor bioimpedance events; α -, β - and γ -dispersions. In this study, frequency range of (1-1000 kHz) within the β -dispersion was applied, because this study meant to monitor changes in interfacial polarization of the cellular plasma membranes. The bode plot in figure 3 shows the spectra of impedance of the monolayer of cells. Cells were plated at an initial density of (20×10^3 cells/ ml) and incubated at 37°C and 5% CO_2 . Impedance change was scanned over four days. A regular increase of impedance was shown for each cell line over the four days. The impedance spectra of Ht-29 cells was affected by the electric double layer formed at the electrode/electrolyte interface at a frequency (less than 10000 Hz). When the range of frequency increased, the bulk electrolyte resistance dominated the magnitude of impedance, hence revealing the conductivity of the ions in the medium and emphasizing the linearity performance of the monolayer of cells over four days. The bulk resistance influenced the impedance spectra of Ht-29 cells at a frequency of (10-150 kHz). This corresponded to many *in vitro* studies, where cell viability and cell growth was monitored [33], [34]. The permittivity of the interior of the cell (e.g. cytoplasm) characterizes the cell line. When the permittivity of cytoplasm is less than the permittivity of the suspension medium, it causes less dielectric capacitance, thus resulting in higher impedance.

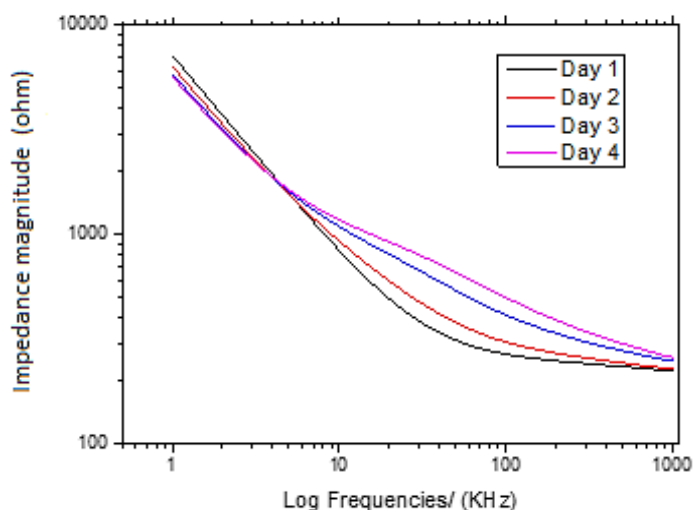


Figure 3. Bode plots of the impedance spectra of experimental data in frequency range between 1 kHz and 1000 kHz. The spectrum was obtained for 20×10^3 cells/ mL of the cells of (Ht-29) proliferated for over 4 days in the presence of routine media.

3.2 Cellular morphology on MEAs

The microelectrode arrays were validated via monocultures of the epithelial cancer cells of Ht-29 in normal proliferative conditions. The frequency outlined in Figure 3 were used for this results, which was 60 kHz. Figure 4 (A) shows the impedance responses when single electrodes were challenged using various concentrations of cells from 20×10^3 cells/ mL to 80×10^3 cells/ mL. The routine media of each cell line was used as 0 cell concentration, and the resistance of free-serum media was used as a blank. The data obtained during 10 hours was fitted by the polynomial model that displayed very good regression analysis. During adhesion on the microelectrodes cells moved, causing increases and decreases in the impedance. From 0 hour to 3 hours, the resistance curves corresponded to the adsorption of cells membrane indicating an electrostatic attraction. From 4 hours to 7 hours, the resistance increased because cells were rearranging themselves to find the proper binding site. From 8 hours to 10 hours resistance increased marginally and

then remained constant, indicating the attachment of the cell membrane to the surface of the microelectrode. Cells at this stage required another 10 hours to duplicate. Therefore, cell number throughout this stage were estimated by using the cell index (CI). After 10 hours, a calibration curve was plotted, which represented the correlation between CI value and cell seeding density (Figure 4 B). The rises and falls shown in the curves during the movements and attachment of cells on 40 microelectrodes were better than the results when applying a single microelectrode [35].

The growth of adherent cells was evaluated using impedance signals. The resulting data were normalized using the CI values calculated from Figure 4 (C) The data were fitted by growth model to illustrate the phases of cells growth. Figure 6.8 shows the normalised data, illustrating an s-shape growth curve for Ht-29 cells. Ht-29 cells showed continued growth, which correlates with the findings by Witzel et al. (2015) [36]. Overall, the impedimetric measurements of cell growth over long periods of time were stable, and the routine media of no cells represented very low resistance [37].

Microscope images were taken to evaluate the growth of cells' monolayers over 5 days. Figure 6.9 demonstrates that the cells displayed a healthy fitted monolayer from day 1 to day 5. The microscope images of cells during growth correlated to the results of resistance changes (Figure 6.8), and showed that Ht-29 cells had a 36- hour doubling time. The resistance changes recorded in Figure 6.8 displayed the extracellular matrix of Ht-29 cells. Colon cancer cells expressed more extracellular matrix before doubling themselves, a fact that was shown clearly in the microscope images [38]. The cells of Ht-29 reached the stationary phase by day 5 [38-40].

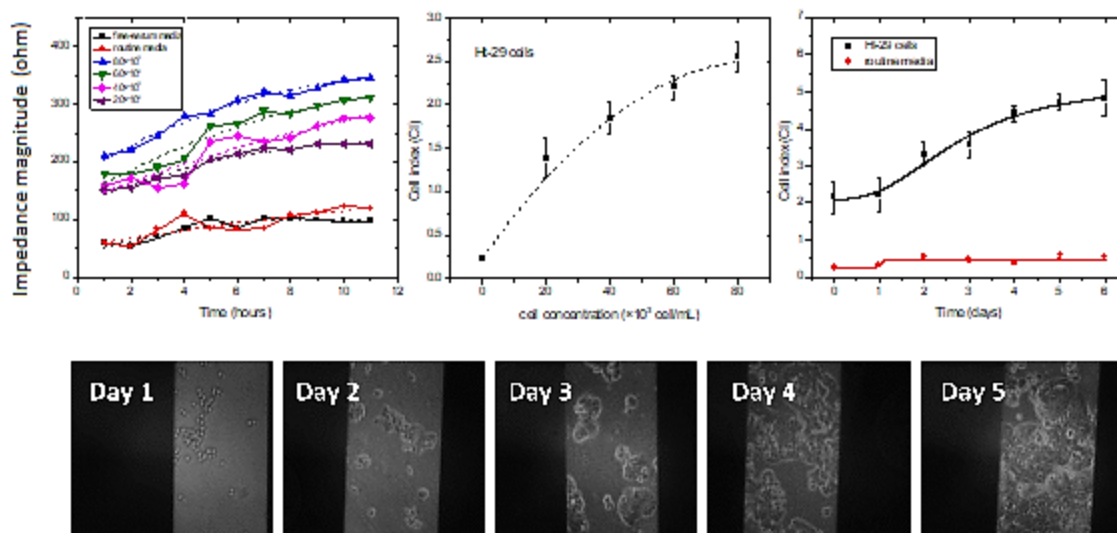


Figure 4. (A) Impedance responses of microelectrode array to various concentrations of the Balb/c 3T3, A549, MCF-7 and Ht-29 cells in monoculture for 10 hours. (B) Calibration curve represents the correlation between cell density and cell index value. (C) Logistic growth curves of Balb/c 3T3 cells; A549 cells; MCF-7 cells; and Ht-29 cells, over six days. The normalised CI values of resistance changes at optimal frequency in the case of each cell line. Microscope images of the cells over a 5-day incubation on microelectrode array.

3.3 Impedance responses during alkalinity buffer

It was important to have a full understanding of the effect of the alkalinity buffer on cells grown on the ECIS system. Therefore, EIS measurements were performed to analyse cell viability during the exposure

of cells to the ALP buffer. Bode plot in Figure 5 (A) illustrates the average responses of impedance of Ht-29 cells before (positive control) and after exposure to the DEA buffer (pH 9.5). Impedance of dead cells was monitored and nominated as a negative control (vehicle control).

Impedance in the positive control was higher as the cells' membranes impeded the flow of the current. When cells were exposed to the alkaline environment, they started to lose their viability. The cells' membranes slightly detached from the surfaces of electrodes and caused a decrease in impedances. The magnitude of impedances of cells in pH 9.5 was significantly different from vehicle control data (dead cells), which meant that cells still alive. In the insert of Figure 5 (A), cell viability was verified by resazurin assay. Ht-29 cells that were exposed to the DEA buffer for 10 minutes had (83 %) of their viability. These data were significantly different from the negative control, which was (22.6%).

Nyquist plots presented in Figure 5 (B) showed different charge transfer resistances of the cell line before and after exposure to the DEA buffer. The charge transfer resistances for Ht-29 cells before the addition of the ALP buffer were $33 \Omega \text{ m}^2$. When cells were exposed to the alkalinity buffer for 10 minutes, the charge transfer resistances of the cell line declined as expected to $20 \Omega \text{ m}^2$. These data were expected, as the ion diffusion increased and caused an increase in the conductivity of the electrolyte. These data were slightly higher than the vehicle controls, where cells were not completely attached onto the surface. In the vehicle controls, the charge transfer resistances was $15 \Omega \text{ m}^2$. The slope values of the non-vertical line were at their lowest before the addition of the ALP buffer and increased after the addition of the ALP buffer. The slope recorded the highest values when cells were completely dead at vehicle controls. This indicates that the slope was affected by the electrolyte concentration [41], [42].

Quite notably, in Nyquist plot, the diameters of semicircles refers to the charge-transfer resistance [43] and they forms a proportional relationship with impedance magnitude to the flow of electrons at the interface. Figure 5B (insert) shows that when ALP released at pH 9.5 the permeability of cell membrane increases, which cause a decrement in the impedance magnitude compared to the positive control. These assays were applied at constant voltage (10 mV). therefore, the negative control shows the lowest impedance. In the negative control, the colon cancer cell line (Ht-29) were supposed to separate from electrodes surfaces and the current flowing in the equivalent electrical circuit increaseing. In this assay, the charge transfer resistances of negative control was $15 \Omega \text{ m}^2$. This could be solved by using sufficient chemical instead of virkon®.

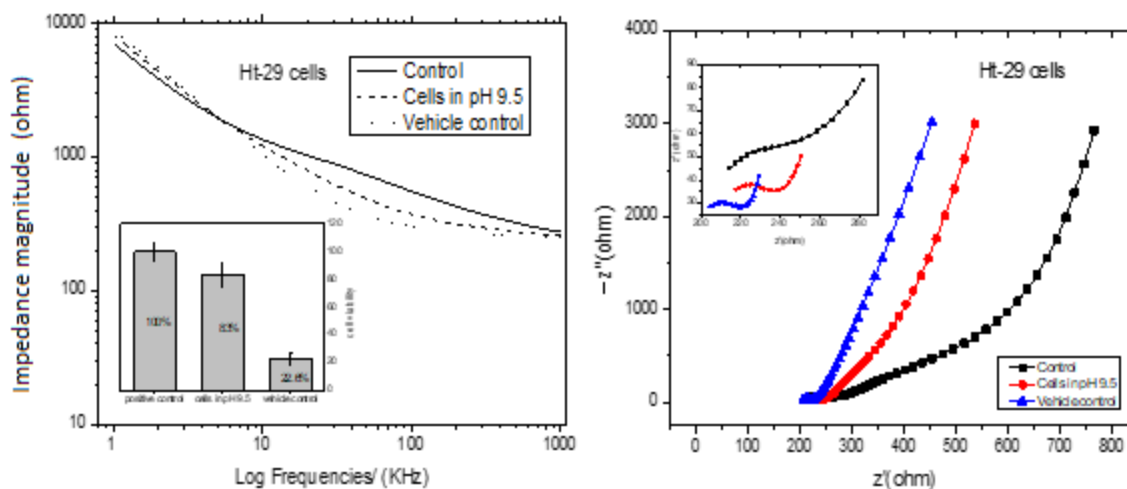


Figure 5. EIS results of the cells grew on the working electrode before and after exposure to DEA buffer. (A) Bode plots. In the insert, the resazurin assay. (B) Nyquist plots. In the insert, clarification of the semicircle of impedance response.

3.4 Real-time monitoring of ALP release

The impedance response of the cell line Ht-29 during differentiation was recorded via ECIS. The Ht-29 cell line indicated the highest quantity of ALP release, and, therefore, was used for further impedance detection [31], [45]. Sodium butyrate (NaBt), on the other hand, mediates differentiation in many kinds of colon cancer cells [31], [32]. Therefore, it was used specifically to induce the biomarker of ALP release in the culture media of Ht-29 cells [46] while attaching on ECIS. NaBt was mixed with routine media at two concentrations (0.5 mM) and (1mM) and incubated with cells for 14 hours. Figure 6 (A) shows the impedimetric responses of Ht-29 cell line in three cases: NaBt-non-treated cells, NaBt-treated cells at concentration of (0.5 mM) and (1mM)' and dead cells (vehicle control). The routine media with no cells was used as blank. The measurement was applied at the optimal frequency obtained in Figure (3) of 60 kHz. Real-time monitoring of the cells' monolayer was applied as cells were seeding, attaching and reaching the 70-90% confluence. The real-time monitoring was continued during differentiation with post-confluence and NaBt treatment. Normal exponential curve was observed from 1-72 hours. Cells were treated on day 3 and monitored for 14 hours. The media was changed, cells were incubated for another 72 hours and impedimetric signals were recorded. The impedance values illustrated slight decreases when low amounts of NaBt were applied compared to the positive control. A significant decline was shown when applying high amount of NaBt. This indicated a relationship between the amount of NaBt and cellular response.

This relationship needed more dilutions for optimizing the limit of detection. The significant differences between the values of differentiated cells and vehicle control indicated that the cells released ALP while alive. NaBt might inhibit the growth factor of Histone deacetylase (HDAC), which led to decrease the cell growth rapidly as seen in Figure 6(A). Microscope images (Figure 6 B) illustrated morphological changes in cells membrane. NaBt-non-treated cells appeared strongly attached to each other while NaBt-treated cells looked more likely to separate from each other. This results corresponding to the findings of Joseph et al (2004) [47]. NaBt affected cell-cell adhesion, which was seen in the changes in the monolayer shape [48].

The viability of cells was measured as shown in figure 6 (C). Untreated cells (positive control) had the highest viability (100 %) as cells maintained in their routine condition. The viability of NaBt-treated cells with (0.5 mM) and (1 mM) was (87.5%) and (82.3%). The viability of cells decreased as the concentration of NaBt increased. This might be the reason of for HDAC inhibition. There was no significant different for the viability values of NaBt-treated cells compared to the viability value of NaBt-non-treated cells (positive control). Vehicle control had the lowest level of viability (20.4%), because cells were already dead.

Real-time monitoring of ALP release from colon cancer cells lines (Ht-29) was performed using Amperometry (Figure 6 D). The current responses were applied in the media of NaBt-non-treated cells (positive control), the media of dead cells (vehicle control), and the media of NaBt- treated cells. It is noticeable that the current generated by the oxidation of pAP when using 1 mM of NaBt was 24.45 μ A, while 0.5 mM of NaBt allowed a generated current of 12.2 μ A. There was a small rise in NaBt-non-treated cells (control), which was approximately 7.5 μ A. The increase of the current density indicated that differentiation of Ht-29 cells with NaBt was enhanced. The vehicle control generated almost the lowest level of current at 0.9 μ A. Amperometric readings of the electroactive product pAP for all the four sample cells was calculated at 10 seconds and generated almost 800 μ L.

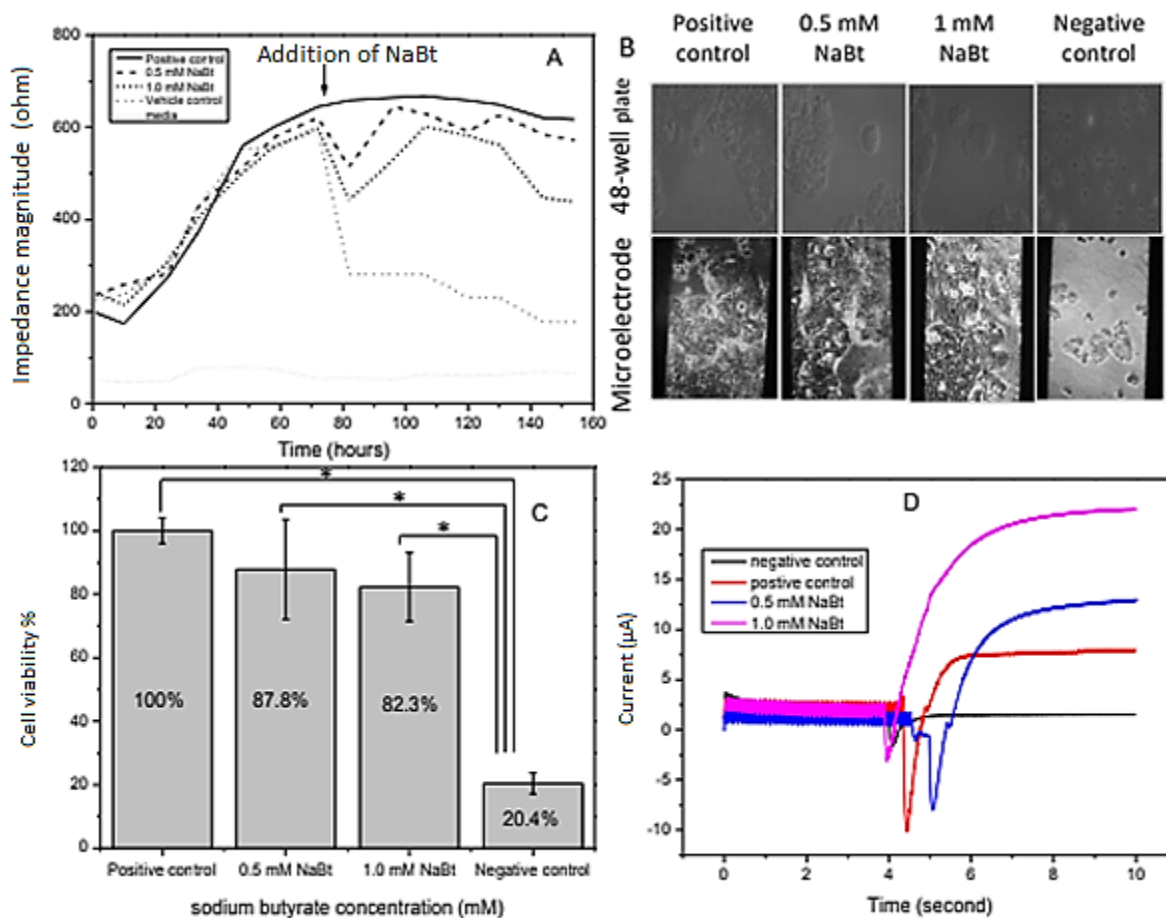


Figure 6. (a) Relative impedance changes of Ht-29 cells during ALP release. (b) Microscope images of cells adhesion on 48-well plate and microelectrode array after exposure to NaBt. (c) Resazurin-based assay for cells attached on microelectrode array after differentiation. (d) Amperometric current-time response curve of ALP release. Measurement was applied at a potential of 0.15 V and at assay buffer of DEA (9.5) in the presence of 10 mM pAPP.

4 Conclusion

In a summary, this paper reported a real-time impedance monitoring of ALP release utilizing microelectrode arrays. The impedance changes if there is any change in the interface between the attached cells and microelectrodes' surface during ALP release. Each cell line has membrane properties that differ from the other, which results in an optimal range of frequency. Ht-29 displayed different frequency ranges, which were (10-150) kHz and the highest impedance of the cells' membrane for Ht-29 cells was 60 kHz.

In order to verify the constancy of the assay, calibration curve was obtained, and the cell viability was monitored and compared to the resistance changes and was verified by resazurin assay and amperometry. The data clearly indicated a correlation between ALP activity and cell differentiation. This may suggest future studies on optimizing the relationship between the amount of NaBt and the cellular response by using microelectrode arrays.

Funding: This research was funded by the Ministry of Higher Education of Saudi Arabia.

Acknowledgments: The authors would like to acknowledge the financial support of the Ministry of Higher Education of Saudi Arabia.

Conflicts of Interest: The authors declare that there are no conflicts of interests from any parts.

Reference

- [1] E. E. Kim and H. W. Wyckoff, "Reaction mechanism of alkaline phosphatase based on crystal structures. Two-metal ion catalysis," *J. Mol. Biol.*, 1991, doi: 10.1016/0022-2836(91)90724-K.
- [2] E. Dirnbach, D. G. Steel, and A. Gafni, "Mg²⁺ binding to alkaline phosphatase correlates with slow changes in protein lability," *Biochemistry*, 2001, doi: 10.1021/bi011399m.
- [3] S. H. Kim et al., "Reassessment of alkaline phosphatase as serum tumor marker with high specificity in osteosarcoma," *Cancer Med.*, vol. 6, no. 6, pp. 1311–1322, 2017, doi: 10.1002/cam4.1022.
- [4] D. Heinrich, O. Bruland, T. A. Guise, H. Suzuki, and O. Sartor, "Alkaline phosphatase in metastatic castration-resistant prostate cancer: Reassessment of an older biomarker," *Future Oncology*. 2018, doi: 10.2217/fon-2018-0087
- [5] Mehrotra, S.; Rishishwar, P.; Sharma, R.K. Malnutrition and hyperphosphatemia in dialysis patients. *Clin. Queries Nephrol*. 2015, 4, 25–27.
- [6] B. Pavkovic, L. K. Nenadic, M. Brankovic, M. Zaric, and M. Brkic, "P-120 Serum alkaline phosphatase level as an early diagnostic tool in colorectal cancer," *Ann. Oncol.*, vol. 26, p. iv34, 2015, doi: 10.1093/annonc/mdv233.120.
- [7] H.-Y. Hung, J.-S. Chen, C.-Y. Yeh, R. Tang, P.-S. Hsieh, W.-S. Tasi, Y.-T. You, J.-F. You & J.-M. Chiang "Preoperative alkaline phosphatase elevation was associated with poor survival in colorectal cancer patients," *Int. J. Colorectal Dis.*, vol. 32, no. 12, pp. 1775–1778, 2017, doi: 10.1007/s00384-017-2907-4.
- [8] Zdrachek, E.; Bakker, E. Potentiometric Sensing. *Anal. Chem.* 2019, 91, 2–26.
- [9] Keyes, M.H. Electrochemical Potentiometric Method for Selectively Determining Alkaline Phosphatase Content in Aqueous Fluids. U.S. Patent 3896008A, 22 July 1975.
- [10] Zhang, L.; Hou, T.; Li, H.; Li, F. A highly sensitive homogeneous electrochemical assay for alkaline phosphatase activity based on single molecular beacon-initiated T7 exonuclease-mediated signal amplification. *Analyst* 2015, 14, 43–436
- [11] J. Berger Hauber, J., Hauber, R., Geiger, R. And Cullen, B. R., "Secreted placental alkaline phosphatase: a powerful new quantitative indicator of gene expression in eukaryotic cells," *Gene*, vol. 66, no. 1, pp. 1–10, 1988, doi: 10.1016/0378-1119(88)90219-3.
- [12] Winn, B., Tavares, R., Fanion, J., Noble, L., Gao, J., Sabo, E., & Resnick, M. (2009). Differentiating the undifferentiated: immunohistochemical profile of medullary carcinoma of the colon with an emphasis on intestinal differentiation. *Human Pathology*, 40(3), 398–404. doi: 10.1016/j.humpath.2008.08.014

Appendix

- [13] Kheirelseid, E. A.H., Miller, N., Chang, K. H., Nugent, M., and Kerin, M. J. (2013). Clinical applications of gene expression in colorectal cancer. *J Gastrointest Oncol*, 4(2): 144–157. doi: 10.3978/j.issn.2078-6891.2013.010
- [14] Ostendorff, H., Awad, A., Braunschweiger, K., Liu, Z., Wan, Z., Rothschild, K., & Lim, M. (2013). Multiplexed VeraCode bead-based serological immunoassay for colorectal cancer. *Journal Of Immunological Methods*, 400–401, 58–69. doi: 10.1016/j.jim.2013.09.013
- [15] Dressen, K., Hermann, N., Manekeller, S., Walgenbach-Bruenagel, G., Schildberg, F., & Hettwer, K. et al. (2017). Diagnostic Performance of a Novel Multiplex Immunoassay in Colorectal Cancer. *Anticancer Research*, 37(5), 2477–2486. doi: 10.21873/anticancer.11588
- [16] Ake, M.S.; Johnston, K.H.; Russell-Jones, G.J.; Gotschlich, E.C. A rapid, sensitive method for detection of alkaline phosphatase-conjugated anti-antibody on Western blots. *Anal. Biochem.* 1984, 136, 175–179.
- [17] Thiha, A.; Ibrahim, F. A Colorimetric Enzyme-Linked Immunosorbent Assay (ELISA) Detection Platform for a Point-of-Care Dengue Detection System on a Lab-on-Compact-Disc. *Sensors (Basel)* 2015, 15, 11431–11441.
- [18] Sussman, H.H.; Small, P.J.; Cotlove, E. Human alkaline phosphatase. Immunochemical identification of organ-specific isoenzymes. *J. Biol. Chem.* 1968, 243, 160–166.
- [19] Singh, I.; Tsang, K.Y. An in vitro production of bone specific alkaline phosphatase. *Exp. Cell Res.* 1975, 95, 347–358.
- [20] Ino, K.; Shiku, H.; Matsue, T. Bioelectrochemical applications of microelectrode arrays in cell analysis and engineering. *Curr. Opin. Electrochem.* 2017, 5, 146–151.
- [21] K. Wang et al., “Strategy for In Situ Imaging of Cellular Alkaline Phosphatase Activity Using Gold Nanoflower Probe and Localized Surface Plasmon Resonance Technique,” *Anal Chem*, vol. 90, no. 23, pp. 14056–14062, 2018, doi: 10.1021/acs.analchem.8b04179.
- [22] Y. C. Syu, W. E. Hsu, and C. T. Lin, “Review-Field-Effect Transistor Biosensing: Devices and Clinical Applications,” *ECS J. SOLID STATE Sci. Technol.*, vol. 7, no. 7, pp. Q3196–Q3207, 2018, doi: 10.1149/2.0291807jss.
- [23] A. Thammasittirong, M. Dechklar, S. Leetachewa, K. Pootanakit, and C. Angsuthanasombat, “Aedes aegypti Membrane-Bound Alkaline Phosphatase Expressed in Escherichia coli Retains High-Affinity Binding for Bacillus thuringiensis Cry4Ba Toxin,” *Am. Soc. Microbiol. Appl. Environ. Microbiol.*, vol. 77, no. 19, pp. 6836–6840, 2011, doi: 10.1128/AEM.05775-11.
- [24] J. Y. Lee, J. K. Ahn, K. S. Park, and H. G. Park, “An impedimetric determination of alkaline phosphatase activity based on the oxidation reaction mediated by Cu²⁺ bound to poly-thymine DNA,” *RSC Adv.*, vol. 8, no. 20, pp. 11241–11246, 2018, doi: 10.1039/c7ra13642k.
- [25] A. Ferancova et al., “Electrochemical Impedance Spectroscopy for Monitoring of Alkaline Phosphatase Reaction with Substrate,” *Procedia Technol.*, vol. 27, pp. 315–316, 2017, doi: 10.1016/j.protcy.2017.04.129.

Appendix

- [26] N. Mintz Hemed, A. Convertino, and Y. Shacham-Diamand, "Alkaline phosphatase detection using electrochemical impedance of anti-alkaline phosphatase antibody (Ab354) functionalized silicon-nanowire-forest in phosphate buffer solution," *Sensors Actuators B. Chem.*, vol. 259, pp. 809–815, 2018, doi: 10.1016/j.snb.2017.12.136.
- [27] I. Giaever and C. R. Keese, "Micromotion of mammalian cells measured electrically," *Proc. Natl. Acad. Sci. U. S. A.*, 1991, doi: 10.1073/pnas.88.17.7896.
- [28] I. Giaever and C. R. Keese, "Monitoring fibroblast behavior in tissue culture with an applied electric field," *Proc. Natl. Acad. Sci. U. S. A.*, 1984, doi: 10.1073/pnas.81.12.3761.
- [29] I. Giaever and C. R. Keese, "Electric cell-substrate impedance sensing concept to commercialization," *Cancer Metastasis - Biol. Treat.*, 2012, doi: 10.1007/978-94-007-4927-6_1.
- [30] Balbaied, T.; Moore, E. Resazurin-Based Assay for Quantifying Living Cells during Alkaline Phosphatase (ALP) Release. *Appl. Sci.* 2020, 10, 3840.
- [31] J. M. Harig, K. H. Soergel, R. A. Komorowski, and C. M. Wood, "Treatment of Diversion Colitis with Short-Chain-Fatty Acid Irrigation," *N. Engl. J. Med.*, 1989, doi: 10.1056/NEJM198901053200105.
- [32] A. Velcich and L. H. Augenlicht, "Regulated expression of an intestinal mucin gene in HT29 colonic carcinoma cells," *J. Biol. Chem.*, 1993.
- [33] S. P. Chiu, B. Batsaikhan, H. M. Huang, and J. Y. Wang, "Application of Electric Cell-Substrate Impedance Sensing to Investigate the Cytotoxic Effects of Andrographolide on U-87 MG Glioblastoma Cell Migration and Apoptosis," *Sensors (Basel)*, vol. 19, no. 10, p. 2275, 2019, doi: 10.3390/s19102275.
- [34] S. P. Chiu et al., "Application of ECIS to Assess FCCP-Induced Changes of MSC Micromotion and Wound Healing Migration," *Sensors (Basel)*, vol. 19, no. 14, p. 3210, 2019, doi: 10.3390/s19143210.
- [35] T. B. Tran, C. Baek, and J. Min, "Electric cell-substrate impedance sensing (ecis) with microelectrode arrays for investigation of cancer Cell - Fibroblasts interaction," *PLoS One*, 2016, doi: 10.1371/journal.pone.0153813.
- [36] F. Witzel, R. Fritsche-Guenther, N. Lehmann, A. Sieber, and N. Blüthgen, "Analysis of impedance-based cellular growth assays," *Bioinformatics*, 2015, doi: 10.1093/bioinformatics/btv216.
- [37] E. Moore, O. Rawley, T. Wood, and P. Galvin, "Monitoring of cell growth in vitro using biochips packaged with indium tin oxide sensors," *Sensors Actuators B Chem.*, vol. 139, no. 1, pp. 187–193, 2009, doi: <https://doi.org/10.1016/j.snb.2008.11.025>.
- [38] Z. L. Li, Z. J. Wang, G. H. Wei, Y. Yang, and X. W. Wang, "Changes in extracellular matrix in different stages of colorectal cancer and their effects on proliferation of cancer cells," *World J. Gastrointest. Oncol.*, 2020, doi: 10.4251/WJGO.V12.I3.267.
- [39] M. Hekmati, Y. Ben-Shaul, and S. Polak-Charcon, "A morphological study of a human adenocarcinoma cell line (HT29) differentiating in culture. Similarities to intestinal embryonic development," *Cell Differ. Dev.*, 1990, doi: 10.1016/0922-3371(90)90133-H.

Appendix

- [40] J. M. Biazik, K. A. Jahn, Y. Su, Y. N. Wu, and F. Braet, "Unlocking the ultrastructure of colorectal cancer cells *in vitro* using selective staining," *World J. Gastroenterol.*, 2010, doi: 10.3748/wjg.v16.i22.2743.
- [41] N. Mintz Hemed, A. Convertino, and Y. Shacham-Diamand, "Alkaline phosphatase detection using electrochemical impedance of anti-alkaline phosphatase antibody (Ab354) functionalized silicon-nanowire-forest in phosphate buffer solution," *Sensors Actuators B. Chem.*, vol. 259, pp. 809–815, 2018, doi: 10.1016/j.snb.2017.12.136.
- [42] B. A. Mei, O. Munteshari, J. Lau, B. Dunn, and L. Pilon, "Physical Interpretations of Nyquist Plots for EDLC Electrodes and Devices," *J. Phys. Chem. C*, 2018, doi: 10.1021/acs.jpcc.7b10582.
- [43] A. Allison, H.A. Andreas, (2019) Minimizing the Nyquist-plot semi-circle of pseudocapacitive manganese oxides through modification of the oxide-substrate interface resistance, *Journal of Power Sources*. <https://doi.org/10.1016/j.jpowsour.2019.04.029>
- [45] M. Kaatz, H. Schulze, I. Ciani, F. Lisdat, A. R. Mount, and T. T. Bachmann, "Alkaline phosphatase enzymatic signal amplification for fast, sensitive impedimetric DNA detection," *Analyst*, vol. 137, no. 1, pp. 59–63, 2012, doi: 10.1039/C1AN15767A.
- [46] R. A. Hodin, S. F. Meng, S. Archer, and R. Tang, "Cellular growth state differentially regulates enterocyte gene expression in butyrate-treated HT-29 cells," *Cell Growth Differ.*, vol. 7, no. 5, pp. 647–653, 1996,
- [47] J. Joseph, G. Mudduluru, S. Antony, S. Vashistha, P. Ajitkumar, and K. Somasundaram, "Expression profiling of sodium butyrate (NaB)-treated cells: Identification of regulation of genes related to cytokine signaling and cancer metastasis by NaB," *Oncogene*, 2004, doi: 10.1038/sj.onc.1207852.
- [48] A. S. Fiorino and I. Zvibel, "Disruption of cell-cell adhesion in the presence of sodium butyrate activates expression of the 92 kDa type IV collagenase in MDCK cells," *Cell Biol. Int.*, 1996, doi: 10.1006/cbir.1996.0064